OCS Study
MMS 96-0051

Louisiana/Texas Shelf Physical Oceanography Program: Eddy Circulation Study

Final Synthesis Report

Volume I: Technical Report

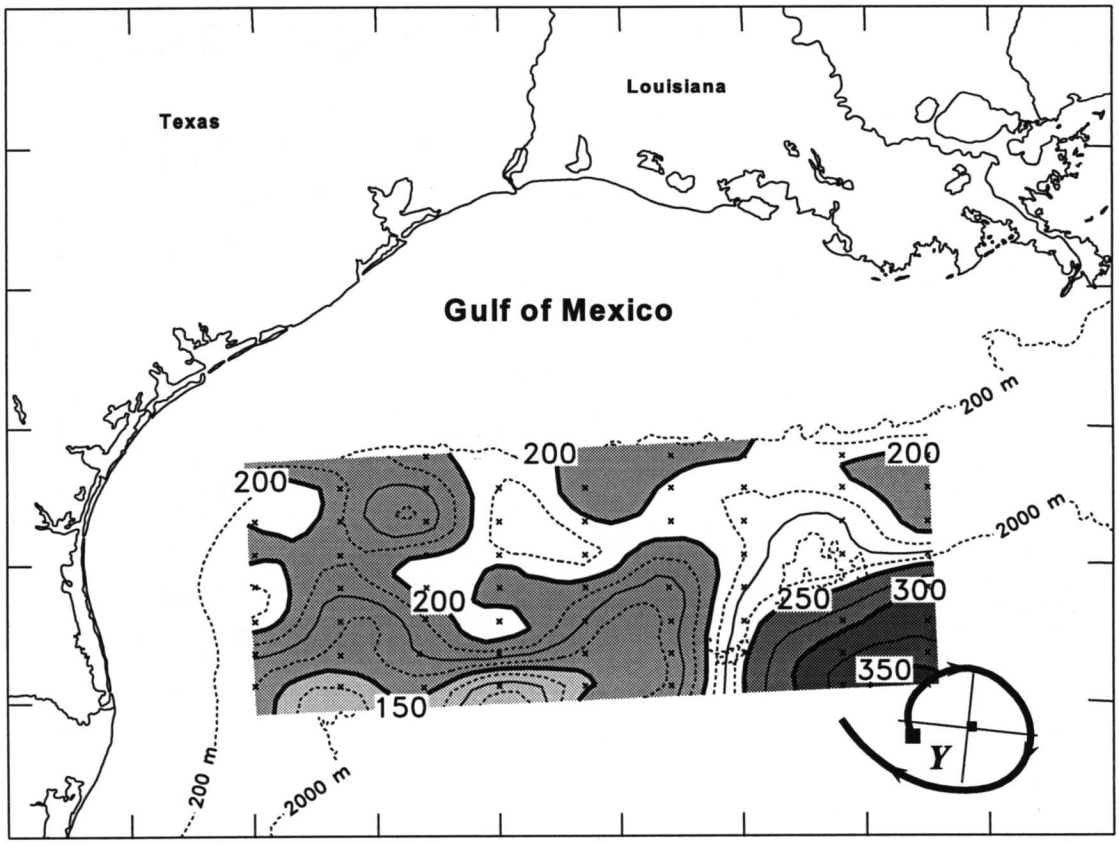

MMS U.S. Department of the Interior
Minerals Management Service
Gulf of Mexico OCS Region

OCS Study
MMS 96-0051

Louisiana/Texas Shelf Physical Oceanography Program: Eddy Circulation Study

Final Synthesis Report

Volume I: Technical Report

Authors

Thomas J. Berger
Peter Hamilton
James J. Singer
Science Applications International Corporation

Robert R. Leben
George H. Born
Chad A. Fox
University of Colorado

Prepared under MMS Contract
14-35-0001-30633
by
Science Applications International Corporation
615 Oberlin Road
Raleigh, North Carolina 27605

Published by

U.S. Department of the Interior
Minerals Management Service
Gulf of Mexico OCS Region

New Orleans
September 1996

DISCLAIMER

This report was prepared under contract between the Minerals Management Service (MMS) and Science Applications International Corporation (SAIC). This report has been technically reviewed by the MMS and approved for publication. Approval does not signify that the contents necessarily reflect the views and policies of the Service, nor does mention of trade names or commercial products constitute endorsement or recommendation for use. It is, however, exempt from review and compliance with MMS editorial standards.

REPORT AVAILABILITY

Extra copies of the report may be obtained from the Public Information Office (Mail Stop 5034) at the following address:

U.S. Department of the Interior
Minerals Management Service
Gulf of Mexico OCS Region
Public Information Office (MS 5034)
1201 Elmwood Park Boulevard
New Orleans, Louisiana 70123-2394

Telephone Number: 1-504-736-2519
1-800-200-GULF

CITATION

Suggested citation:

T.J. Berger, P. Hamilton, J.J. Singer, R.R. Leben, G.H. Born, and C.A. Fox. 1996. Louisiana/Texas Shelf Physical Oceanography Program: Eddy Circulation Study, Final Synthesis Report. Volume I: Technical Report. OCS Study MMS 96-0051. U.S. Department of the Interior, Minerals Management Service, Gulf of Mexico OCS Region, New Orleans, La. 324 pp.

COVER

The cover shows the depth of the 15°C isotherm on November 4, 1994 and the path of drifter 12376 (***Y***) during November 1-11, 1994. Arrow heads are at 3-day intervals (Volume I: Figure 5.6-5b).

TABLE OF CONTENTS

Section			Page
List of Figures			ix
List of Tables			xxvii
Acknowledgements			xxix
I.	INTRODUCTION		1
	1.1	Program Overview	1
	1.2	Program Elements	1
		1.2.1 Task C-1: Drifting Buoys Provided to Other Contractors	1
		1.2.2 Task C-2: Drifting Buoys in Loop Current Eddies	3
		1.2.3 Task C-3: Drifting Buoys in Other Meso-Scale Features	3
		1.2.4 Task C-4: Returned Buoys	4
		1.2.5 Task C-5: Buoy Quality Control	4
		1.2.6 Task C-6: Aerial Surveys	4
		1.2.7 Task C-7: Altimetry	5
		1.2.8 Task C-8: Ships-of-Opportunity	6
		1.2.9 Task C-9: Data Quality Control	6
		1.2.10 Task C-10: Analyses and Reports	6
		1.2.11 Task C-11: Information Transfer	6
		1.2.12 Task C-12: Government Furnished Equipment/Capital Equipment	7
	1.3	Principal Investigators and Primary Support Personnel	7
	1.4	Report Organization	8
	1.5	Scientific Background	8
		1.5.1 Loop Current Eddies	8
		1.5.2 Slope Eddies in the Central Gulf of Mexico	9
		1.5.3 Squirts and Jets	11
II.	DATA ACQUISITION AND PRESENTATION		15
	2.1	Introduction	15
	2.2	Drifting Buoy Data	15
		2.2.1 Introduction	15
		2.2.2 Drifter Descriptions and Argos Data Transmission	15
		2.2.3 Drifter Deployments and Performance	17

TABLE OF CONTENTS

Section		Page
2.2.4	Drifter Path Plots	19
2.3	Aerial Surveys	27
2.3.1	Introduction	27
2.3.2	Expendable Probes and Data Transmission	27
2.3.3	Survey Summaries and Probe Performance	28
2.3.4	Horizontal and Vertical Parameter Plots	28
2.4	GEOSAT Altimeter Data	36
2.4.1	Introduction	36
2.4.2	Historical Data	36
2.4.2.1	GEOSAT Geodetic Mission Data	36
2.4.2.2	GEOSAT Exact Repeat Mission Data	40
2.4.2.3	GEOSAT Global Wind/Wave Data	43
2.5	Ancillary Data	43
2.5.1	Introduction	43
2.5.2	LATEX A Current Meter Data	43
2.5.3	LATEX A Hydrographic and ADCP Data	46
2.5.4	LATEX B AVHRR Imagery Data	48
2.5.5	Ship-of-Opportunity XBT Data	48
2.5.6	GulfCet Hydrographic Data	49
2.5.7	SOOP/TIGER Hydrographic Data	51
2.5.8	SCULP Drifter Data	51
2.5.9	TOPEX and ERS-1 Altimeter Data	57
III.	DATA QUALITY ASSURANCE AND PROCESSING	59
3.1	Introduction	59
3.2	Drifting Buoys	59
3.2.1	Predeployment Testing	59
3.2.2	Generation of Smooth Trajectories	60
3.2.3	Drifter Track Analysis	60
3.3	Aerial Surveys	62

TABLE OF CONTENTS

Section		Page
3.3.1	Position Accuracy and Data Processing	62
3.3.2	AXBT Data and Expendable Probe Drop-Rate Equations	64
3.3.3	AXCP Data	69
3.3.4	AXCTD Data	72
3.4	GEOSAT Data	73
3.4.1	Introduction	73
3.4.2	Sea Surface Height	73
3.4.2.1	Wet and Dry Troposphere Correction	75
3.4.2.2	Ionosphere Correction	75
3.4.2.3	Tidal Corrections	76
3.4.2.4	Inverse Barometer Correction	76
3.4.2.5	Electromagnetic Bias Correction	76
3.4.2.6	Empirical Orbit Error Correction	77
3.4.2.7	Selection of a Mean Reference Surface	77
3.4.2.8	GM and ERM Data Processing	78
3.4.2.9	Data Quality Control	79
3.4.2.10	Interpolation of Cycle Data	79
3.4.2.11	Eddy/Buoy Statistics	81
3.4.2.12	Annual and Seasonal RMS Variability Statistics	84
3.4.3	Significant Wave Height	85
3.4.4	Wind Speed	86
3.5	Ancillary Data	87
3.5.1	Introduction	87
3.5.2	Current Meter Data	87
3.5.3	CTD Data	87
3.5.4	Imagery Data	87
3.5.5	XBT Data	88
3.5.6	Drifter Data	88
IV.	ANALYSIS OF GEOSAT DATA	89
4.1	Introduction	89

TABLE OF CONTENTS

Section			Page
4.2	Mean Sea Surface		89
4.3	Evaluation of Sea Surface Height Climatology		90
4.4	Loop Current Shedding Statistics		99
4.5	Eddy Tracking and Statistics		100
	4.5.1	Eddy B with Ghost Eddy Formation and Dissipation	102
	4.5.2	Eddy C and Eddy B Interaction	121
	4.5.3	Eddy D and Eddy C Interaction	134
	4.5.4	Eddy E, Unnamed Secondary Eddy and Eddy F	134
4.6	Estimates of Eddy Decay in the Western Gulf of Mexico		152
4.7	Mean Loop Current Eddy Statistics in the Western Gulf of Mexico		159
4.8	Eddy Statistics at 90°W Longitude		162
4.9	Eddy Variability Statistics		162
V.	ANALYSIS OF SURVEY AND DRIFTER DATA		169
5.1	Introduction		169
5.2	Eddy V Analysis		174
5.3	Eddy U Analysis		199
5.4	Eddy W Analysis		202
5.5	Eddy X Analysis		214
5.6	Eddy Y Analysis		215
5.7	Cyclones: Further Examples		234
	5.7.1	Introduction	234
	5.7.2	May 1994 Surveys	236
	5.7.3	December 1993 Surveys	243
	5.7.4	August 1992 Small Slope Cyclone	254
	5.7.5	Discussion	257
5.8	Miscellaneous Slope Anticyclones		257
5.9	Summary		270
	5.9.1	Loop Current Eddy Kinematics	270
	5.9.2	Ensemble Statistics	274
	5.9.3	Slope Eddies	279
VI.	SUMMARY AND CONCLUSIONS		283
VII.	REFERENCES		287

LIST OF FIGURES

Figure	Caption	Page
1.1-1.	Map of the Gulf of Mexico with the LATEX C study area indicated by shading	2
1.5-1.	Eddy B 1985-1986 showing a)approaching the slope, b)generation of anticyclone-cyclone pair, and c)migration of pair to the south	10
1.5-2.	The smoothed track for Argos drifter 3353	12
2.2-1.	Schematic of Clearwater Instrumentation, Inc. WOCE/SVP Drifter drogued at six meters	16
2.2-2.	Schematic of Horizon Marine, Inc. FHD/ Holey Sock Drifter drogued at 50 meters . .	18
2.2-3.	Time line for LATEX Argos drifters	20
2.2-4.	Composite path plot for all LATEX drifters	24
2.2-5.	Whole Gulf composite path plot for eight LATEX drifters: 2447 (C), 2448 (D), 6935 (O), 6937 (Q), 6938 (R), 7833 (W), 7835 (Y) and 7839 (b)	24
2.2-6.	Western Gulf composite path plot for nine LATEX drifters: 2449 (E), 2450 (F), 7838 (a), 7843 (f), 7844 (g), 12372 (h), 12374 (j), 12376 (m) and 12377 (n)	25
2.2-7.	Eastern Gulf composite path plot for three LATEX drifters: 2445 (A), 6934 (N) and 7841 (d)	25
2.2-8.	Northwestern Gulf composite path plot for 18 LATEX drifters: 2446 (B), 2451 (G), 3581 (H), 3582 (I), 3583 (J),3584 (K), 6932 (L), 6933 (M), 6936 (P), 6939 (S), 6940 (T), 6941 (U), 7832 (V), 7834 (X), 7837 (Z), 7842 (e), 12373 (i) and 12379 (q)	26

LIST OF FIGURES

Figure	Caption	Page
2.3-1(a-d).	Map showing station locations for: (a) F01SLOPE, (b) F02SLOPE, (c) F03SEDDY and (d) F04LEDDY aerial survey	30
2.3-1(e-h).	Map showing station locations for: (e) F05LEDDY, (f) F06SPECIAL, (g) F07SLOPE and (h) F08SLOPE aerial survey	31
2.3-1(i-l).	Map showing station locations for: (i) F09SEDDY, (j) F10SLOPE, (k) F11LEDDY and (l) F12SLOPE aerial survey	32
2.3-1(m-p).	Map showing station locations for: (m) F13SQUIRT, (n) F14LEDDY, (o) F15SLOPE and (p) F16SQUIRT aerial survey	33
2.3-1(q-t).	Map showing station locations for: (q) F17SLOPE, (r) F18LEDDY, (s) F19SEDDY and (t) F20SLOPE aerial survey	34
2.3-1u.	Map showing station locations for F21SQUIRT aerial survey	35
2.3-2.	Example of horizontal plot of the 15°C surface from AXBT data	37
2.3-3.	Example of vertical section plot of temperature from AXBT data	37
2.3-4.	Example of vertical section plot of (a) north-south component and (b) east-west component of relative velocity from AXCPs deployed in a Loop Current eddy . . .	38
2.3-5.	Example of an individual AXCP profile . . .	39
2.4-1.	Sample ground track/data coverage for the 23-day near repeat orbit used during the GEOSAT Geodetic Mission (GM)	41
2.4-2.	GEOSAT Exact Repeat Mission (ERM) 17-day exact repeat orbit ground track over the Gulf of Mexico	42

LIST OF FIGURES

Figure	Caption	Page
2.5-1.	Time line showing ancillary data and LATEX C data collection periods	44
2.5-2.	Map showing LATEX A shelf-edge current meter mooring locations	45
2.5-3.	Map showing an example of a typical LATEX A Louisiana-Texas shelf hydrographic survey	45
2.5-4.	Time line for LATEX A shelf-edge current meter levels	47
2.5-5.	Map showing GulfCet master station plan . .	50
2.5-6.	Schematic of Technocean Associates, Davis-type Argos drifter	53
2.5-7.	Map showing SCULP drifter deployment sites	55
3.2-1.	Example of (a) raw Argos drifter path plot and (b) smoothed Argos drifter path plot	61
3.3-1.	Plot of (a) raw AXBT data and (b) cleaned AXBT data from F12SLOPE survey, station 6, showing data dropouts corrected by interpolation	65
3.3-2.	Map showing F15SLOPE survey 8°C isotherm depth contours plotted through (a) all available AXBT probe data and (b) Hermes AXBT probe data only	70
3.3-3.	Map showing F16SQUIRT survey 8°C isotherm depth contours plotted through (a) all available AXBT probe data and (b) Hermes AXBT probe data only	71

LIST OF FIGURES

Figure	Caption	Page
3.3-4.	TS plots comparing AXCTD data from flight F21SQUIRT with historical CTD data from a cruise made through a Loop Current eddy in the western Gulf of Mexico	74
3.4-1.	Example of wiggle plot format of sea surface height anomaly with respect to mean sea surface	80
3.4-2.	Graphical User Interface for eddy/buoy tracking program used to automatically track Loop Current eddies observed by GEOSAT	82
4.2-1.	Ohio State University mean sea surface in the Gulf of Mexico	91
4.2-2.	Estimated standard deviation of the Ohio State mean sea surface based on the least squares collocation procedure statistics	92
4.2-3.	Magnitude of the gradient of the OSU mean sea surface	93
4.3-1.	Sample GEOSAT Geodetic Mission along-track sea surface height anomaly with respect to mean sea surface in wiggle plot format	94
4.3-2.	Sample GEOSAT Exact Repeat Mission along-track sea surface height anomaly with respect to mean sea surface in wiggle plot format	95
4.3-3.	Comparison of GEOSAT GM altimeter-derived estimates of geostrophic velocity anomalies with velocity estimates for drifter 3379 (February 1986 to September 1986)	97

LIST OF FIGURES

Figure	Caption	Page
4.3-4.	Comparison of GEOSAT ERM altimeter-derived estimates of geostrophic velocity anomalies with velocity estimates for drifter 3345 (June 1988 to March 1989)	98
4.5-1.	Composite of eddy-center locations determined from the centroid of the area contained within the 17-cm sea surface height anomaly contour	101
4.5-2.	Trajectory of eddy B center determined using GEOSAT altimeter data and an objective tracking program	103
4.5-3a.	Eddy tracking statistics for eddy B from May 1985 to January 1986 using GEOSAT altimetry: distance and velocity statistics	104
4.5-3b.	Eddy tracking statistics for eddy B from May 1985 to January 1986 using GEOSAT altimetry: maximum height anomaly, eddy area, areal averaged anomaly and ocean depth	105
4.5-3c.	Eddy tracking statistics for eddy B from May 1985 to January 1986 using GEOSAT altimetry: eccentricity, radius estimates, swirl speed, and Rossby number	106
4.5-3d.	Eddy tracking statistics for eddy B from May 1985 to January 1986 using GEOSAT altimetry: vorticity and circulation statistics	107
4.5-4.	Sea surface height anomaly with respect to mean sea surface for GEOSAT GM Cycle 6 (July 24 to August 15, 1985) showing eddy B and Ghost eddy	108

LIST OF FIGURES

Figure	Caption	Page
4.5-5.	Sea surface height anomaly with respect to mean sea surface for GEOSAT GM Cycle 1 (March 31 to April 22, 1985) showing early stages of eddy B and Ghost eddy . .	109
4.5-6.	Sea surface height anomaly with respect to mean sea surface for GEOSAT GM Cycle 2 (April 23 to May 15, 1985) showing early stages of eddy B and Ghost eddy . .	110
4.5-7.	Sea surface height anomaly with respect to mean sea surface for GEOSAT GM Cycle 3 (May 16 to June 7, 1985) showing eddy B and Ghost eddy	112
4.5-8.	Sea surface height anomaly with respect to mean sea surface for GEOSAT GM Cycle 4 (June 8 to 30, 1985) showing eddy B and Ghost eddy	113
4.5-9.	Trajectory of eddy O center determined using GEOSAT altimeter data and an objective tracking program	114
4.5-10.	Sea surface height anomaly with respect to mean sea surface for GEOSAT GM Cycle 7 (August 16 to September 7, 1985) showing eddy B and Ghost eddy	115
4.5-11.	Sea surface height anomaly with respect to mean sea surface for GEOSAT GM Cycle 8 (September 8 to 30, 1985) showing eddy B and Ghost eddy	117
4.5-12.	Sea surface height anomaly with respect to mean sea surface for GEOSAT GM Cycle 9 (October 1 to 23, 1985) showing eddy B and Ghost eddy	118
4.5-13.	Altimetric estimate of the average velocity magnitude as a function of the radial distance from the center of eddy B on November 12, 1985	119

LIST OF FIGURES

Figure	Caption	Page
4.5-14.	Sea surface height anomaly with respect to mean sea surface for GEOSAT GM Cycle 10 (October 24 to November 15, 1985) showing eddy B and Ghost eddy	120
4.5-15.	Trajectory of eddy C center determined using GEOSAT altimeter data and an objective tracking program	122
4.5-16.	Sea surface height anomaly with respect to mean sea surface for GEOSAT GM Cycle 17 (April 3 to 25, 1986) showing eddy C and eddy B	123
4.5-17.	Sea surface height anomaly with respect to mean sea surface for GEOSAT GM Cycle 18 (April 26 to May 18, 1986) showing interaction between eddy C and eddy B . .	124
4.5-18.	Sea surface height anomaly with respect to mean sea surface for GEOSAT GM Cycle 19 (May 19 to June 10, 1986) showing an elongated eddy C	125
4.5-19.	Sea surface height anomaly with respect to mean sea surface for GEOSAT GM Cycle 20 (June 11 to July 3, 1986) showing eddy C	126
4.5-20.	Sea surface height anomaly with respect to mean sea surface for GEOSAT GM Cycle 21 (July 4 to 26, 1986) showing eddy C .	127
4.5-21a.	Eddy tracking statistics for eddy C from January to September 1986 using GEOSAT altimetry: distance and velocity statistics	128
4.5-21b.	Eddy tracking statistics for eddy C from January to September 1986 using GEOSAT altimetry: maximum height anomaly, eddy area, areal averaged anomaly and ocean depth	129

LIST OF FIGURES

Figure	Caption	Page
4.5-21c.	Eddy tracking statistics for eddy C from January to September 1986 using GEOSAT altimetry: eccentricity, radius estimates, swirl speed, and Rossby number	130
4.5-21d.	Eddy tracking statistics for eddy C from January to September 1986 using GEOSAT altimetry: vorticity and circulation statistics	131
4.5-22.	Sea surface height anomaly with respect to mean sea surface for GEOSAT ERM Cycle 1 (November 8 to 24, 1986) showing eddy D and eddy C	133
4.5-23.	Trajectory of eddy D center determined using GEOSAT altimeter data and an objective tracking program	135
4.5-24.	Sea surface height anomaly with respect to mean sea surface for GEOSAT ERM Cycle 3 (December 12 to 28, 1986) showing eddy D and eddy C	136
4.5-25.	Sea surface height anomaly with respect to mean sea surface for GEOSAT ERM Cycle 4 (December 29, 1986 to January 24, 1987) showing eddy D and eddy C	137
4.5-26.	Sea surface height anomaly with respect to mean sea surface for GEOSAT ERM Cycle 5 (January 15 to 31, 1987) showing eddy D and eddy C	138
4.5-27.	Sea surface height anomaly with respect to mean sea surface for GEOSAT ERM Cycle 6 (February 1 to 17, 1987) showing eddy D and eddy C	139
4.5-28.	Sea surface height anomaly with respect to mean sea surface for GEOSAT ERM Cycle 7 (February 18 to March 6, 1987) showing eddy D and eddy C	140

LIST OF FIGURES

Figure	Caption	Page
4.5-29.	Sea surface height anomaly with respect to mean sea surface for GEOSAT ERM Cycle 8 (March 7 to 23, 1987) showing interaction between eddy D and eddy C . .	141
4.5-30.	Sea surface height anomaly with respect to mean sea surface for GEOSAT ERM Cycle 9 (March 24 to April 9, 1987) showing an elongated eddy D	142
4.5-31.	Sea surface height anomaly with respect to mean sea surface for GEOSAT ERM Cycle 10 (April 10 to 26, 1987) showing eddy D.	143
4.5-32.	The depth of the 15°C isothermal surface as constructed from XBT data collected during the period of April 5 to May 30, 1987	144
4.5-33a.	Eddy tracking statistics for eddy D from December 1986 through October 1987 using GEOSAT altimetry: distance and velocity statistics	145
4.5-33b.	Eddy tracking statistics for eddy D from December 1986 through October 1987 using GEOSAT altimetry: maximum height anomaly, eddy area, areal averaged anomaly and ocean depth	146
4.5-33c.	Eddy tracking statistics for eddy D from December 1986 through October 1987 using GEOSAT altimetry: eccentricity, radius estimates, swirl speed, and Rossby number	147
4.5-33d.	Eddy tracking statistics for eddy D from December 1986 through October 1987 using GEOSAT altimetry: vorticity and circulation statistics	148

LIST OF FIGURES

Figure	Caption	Page
4.5-34.	Sea surface height anomaly with respect to mean sea surface for GEOSAT ERM Cycle 28 (February 10 to 26, 1988) showing eddy E and an unnamed secondary anticyclonic eddy to the northwest . . .	149
4.5-35.	Sea surface height anomaly with respect to mean sea surface for GEOSAT ERM Cycle 29 (February 27 to March 14, 1988) showing eddy E and an unnamed secondary anticyclonic eddy to the northwest . . .	150
4.5-36.	Sea surface height anomaly with respect to mean sea surface for GEOSAT ERM Cycle 38 (July 29 to August 14, 1988) showing eddy F	151
4.5-37.	Trajectory of eddy F center determined using GEOSAT altimeter data and an objective tracking program	153
4.5-38a.	Eddy tracking statistics for eddy F from August 1988 to January 1989 using GEOSAT altimetry: distance and velocity statistics	154
4.5-38b.	Eddy tracking statistics for eddy F from August 1988 to January 1989 using GEOSAT altimetry: maximum height anomaly, eddy area, areal averaged anomaly and ocean depth	155
4.5-38c.	Eddy tracking statistics for eddy F from August 1988 to January 1989 using GEOSAT altimetry: eccentricity, radius estimates, swirl speed, and Rossby number	156
4.5-38d.	Eddy tracking statistics for eddy F from August 1988 to January 1989 using GEOSAT altimetry: vorticity and circulation statistics	157

LIST OF FIGURES

Figure	Caption	Page
4.5-39.	For drifter 3345, the (a) vorticity, normal deformation rate and shear deformation rate for eddy F, and (b) divergence for eddy F.	158
4.6-1.	Regression fits to anticyclonic circulation estimates for Loop Current eddies during the 120 days after transit across 90°W longitude	160
4.9-1.	The percent occurrence of positive sea surface height anomalies greater than 5 cm in the GEOSAT climatology	164
4.9-2.	The percent occurrence of negative sea surface height anomalies less than -5 cm in the GEOSAT climatology	165
4.9-3.	The percent occurrence of warm eddy water from monthly frontal analyses . . .	166
5.1-1.	Smoothed tracks for drifters 02447, 02449, 07493 and 07837	171
5.1-2.	Smoothed tracks for drifters 02448 and 06938	173
5.1-3.	Smoothed tracks for drifters 12376 and 12377	175
5.2-1.	Tracks of eddy center positions from ellipse-model fits to the paths of drifters 02447, 02451 and 06938	177
5.2-2.	Time series of ellipse parameters from model fits to the paths of drifters 02447 and 02451 for the period from September 16, 1992 to February 3, 1993 .	178
5.2-3.	Major axes every two days from ellipses fit to the path of drifter 02447	180
5.2-4.	Depth of the 20°C temperature surface from the GulfCet 03 survey	181

LIST OF FIGURES

Figure	Caption	Page
5.2-5.	Depth of the 20°C temperature surface from the F05LEDDY survey	182
5.2-6a.	Depth of the 20°C temperature surface from the F06SPECIAL survey	184
5.2-6b.	Depth of the 15°C temperature surface from the F06SPECIAL survey	185
5.2-6c.	Depth of the 8°C temperature surface from the F06SPECIAL survey	186
5.2-7.	Daily velocity vectors from drifter 07835 (beginning January 14, 1993) and drifters 02451 and 02447 (beginning January 15, 1993)	187
5.2-8a.	Stick plots of rotated 40-HLP currents from the 12-m and 100-m levels of the LATEX A shelf-break moorings for the period from January 1 to June 9, 1993 . .	189
5.2-8b.	Stick plots of rotated 40-HLP currents from the 12-m and 100-m levels of the LATEX A shelf-break moorings for the period from April 30 to October 7, 1993 .	190
5.2-9.	Depth of the 20°C temperature surface from the GulfCet 04 survey	191
5.2-10.	Daily velocity vectors from drifter 07835 beginning March 23, 1993	192
5.2-11.	Time series of ellipse parameters from the model fits to the path of drifter 06938	194
5.2-12a.	Depth of the 20°C temperature surface from the F08SLOPE and F09SEDDY surveys .	196
5.2-12b.	Depth of the 15°C temperature surface from the F08SLOPE and F09SEDDY surveys .	197

LIST OF FIGURES

Figure	Caption	Page
5.2-12c.	Depth of the 8°C temperature surface from the F08SLOPE and F09SEDDY surveys .	198
5.3-1.	Tracks of the center positions from the ellipse model fits of drifters 02449 and 02448 for eddies U and W_N, respectively .	200
5.3-2.	Time series of ellipse parameters from the model fits to the path of drifter 02449	201
5.4-1.	Time series of ellipse parameters from the model fits to the path of drifter 02448	203
5.4-2a.	Depth of the 20°C temperature surface from the F10SLOPE and F11LEDDY surveys .	205
5.4-2b.	Depth of the 15°C temperature surface from the F10SLOPE and F11LEDDY surveys .	206
5.4-2c.	Depth of the 8°C temperature surface from the F10SLOPE and F11LEDDY surveys .	207
5.4-3a.	Depth of the 20°C temperature surface from the GulfCet 06 survey	209
5.4-3b.	Depth of the 15°C temperature surface from the GulfCet 06 survey	210
5.4-3c.	Depth of the 8°C temperature surface from the GulfCet 06 survey	211
5.4-4.	Stick plots of rotated 40-HLP currents from LATEX A shelf-break moorings for the period from July 19, 1993 to October 27, 1993	212
5.6-1.	Tracks of center positions from the ellipse model fits to the paths of drifters 12376 and 12377	217

LIST OF FIGURES

Figure	Caption	Page
5.6-2.	Time series of ellipse parameters from model fits to the paths of drifters 12376 and 12377	218
5.6-3a.	Depth of the 20°C temperature surface from the F18LEDDY and F19SEDDY surveys .	220
5.6-3b.	Depth of the 15°C temperature surface from the F18LEDDY and F19SEDDY surveys .	221
5.6-3c.	Depth of the 8°C temperature surface from the F18LEDDY and F19SEDDY surveys .	222
5.6-4a.	North-south vertical-section plot of temperature, north velocity and east velocity from smoothed AXCP profiles from F18LEDDY survey (stations 1 to 12) .	223
5.6-4b.	West-east vertical-section plot of temperature, north velocity and east velocity from smoothed AXCP profiles from F18LEDDY survey (stations 20 to 11).	224
5.6-5a.	Depth of the 20°C temperature surface from the F20SLOPE survey	225
5.6-5b.	Depth of the 15°C temperature surface from the F20SLOPE survey	227
5.6-5c.	Depth of the 8°C temperature surface from the F20SLOPE survey	228
5.6-6a.	Depth of the 20°C temperature surface from the F21SQUIRT survey	229
5.6-6b.	Depth of the 15°C temperature surface from the F21SQUIRT survey	230
5.6-6c.	Depth of the 8°C temperature surface from the F21SQUIRT survey	231

LIST OF FIGURES

Figure	Caption	Page
5.6-7.	Vertical sections of temperature and north velocity component from the F21SQUIRT survey for (a) ~26.75°N latitude [stations 150 to 167] and (b) ~26.25°N latitude [stations 80 to 162] .	233
5.6-8.	Expanded vertical sections of temperature from the F21SQUIRT survey for (a) ~26.75°N latitude [stations 150 to 166] and (b) ~26.25°N latitude [stations 80 to 162]	235
5.7-1a.	Depth of the 20°C temperature surface from the F15SLOPE and F16SQUIRT surveys .	237
5.7-1b.	Depth of the 15°C temperature surface from the F15SLOPE and F16SQUIRT surveys .	238
5.7-1c.	Depth of the 8°C temperature surface from the F15SLOPE and F16SQUIRT surveys .	239
5.7-2.	North-south vertical section near 94°W longitude for the F16SQUIRT survey for (a) temperature to 1500 m depth [stations 1 to 9], (b) temperature to 400 m depth [stations 1 to 9], (c) north velocity to 1200 m depth [stations 64 to 69] and (d) east velocity to 1200 m depth [stations 64 to 69]	241
5.7-3.	Smoothed tracks from drifters 12372, 12373 and 12374 beginning May 27, 1994, and daily-averaged positions from SCULP drifters 20500, 20542 and 21661 beginning May 17, 1994	242
5.7-4a.	Smoothed track from drifter 12374 and daily-averaged positions from SCULP drifters 20555, 21707, 21708, 21763, 21767 and 21768 for the 28-day period beginning October 11, 1994	244

LIST OF FIGURES

Figure	Caption	Page
5.7-4b.	Smoothed tracks from drifters 12374 and 12376, and daily-averaged positions from SCULP drifters 20555, 21690, 21693, 21763 and 21768 for the 26-day period beginning November 2, 1994	245
5.7-5a.	Depth of the 20°C temperature surface from the F13SQUIRT and F14LEDDY surveys .	246
5.7-5b.	Depth of the 15°C temperature surface from the F13SQUIRT and F14LEDDY surveys .	247
5.7-5c.	Depth of the 8°C temperature surface from the F13SQUIRT and F14LEDDY surveys .	248
5.7-6.	Daily averaged positions for SCULP drifters 20396, 20440, 20465 and 20469 for a three-month period beginning December 1, 1993	250
5.7-7a.	Stick plots of rotated 40-HLP currents from the LATEX A shelf-break moorings for the period from December 6, 1993 to March 16, 1994	252
5.7-7b.	U and V components of the rotated 40-HLP currents from the LATEX A shelf-break moorings for the period from December 6, 1993 to March 16, 1994	253
5.7-8a.	Depth of the 15°C temperature surface from the F02SLOPE and F03SEDDY surveys .	255
5.7-8b.	Depth of the 8°C temperature surface from the F02SLOPE and F03SEDDY surveys .	256
5.7-9a.	Stick plots of rotated 40-HLP currents from the LATEX A shelf-break moorings for the period from April 30, 1994 to August 8, 1994	258

LIST OF FIGURES

Figure	Caption	Page
5.7-9b.	U and V components of the rotated 40-HLP currents from the LATEX A shelf-break moorings for the period from April 30, 1994 to August 8, 1994	259
5.8-1a.	Depth of the 20°C temperature surface from the F17SLOPE survey	261
5.8-1b.	Depth of the 15°C temperature surface from the F17SLOPE survey	262
5.8-1c.	Depth of the 8°C temperature surface from the F17SLOPE survey	263
5.8-2.	Stick plots of rotated 40-HLP currents from the LATEX A shelf-break moorings for the period from July 29, 1994 to December 6, 1994	264
5.8-3a.	Depth of the 20°C temperature surface from the F12SLOPE survey	265
5.8-3b.	Depth of the 15°C temperature surface from the F12SLOPE survey	266
5.8-3c.	Depth of the 8°C temperature surface from the F12SLOPE survey	267
5.8-4.	Vertical section of temperature from the F12SLOPE survey through the SLV for (a) the north-south section [stations 24 to 30] and (b) the west-east section [stations 41 to 35]	269
5.9-1.	Paths of eddy centers used for ensemble statistics	275
5.9-2.	Lagrangian time-lagged correlations of eddy translation velocity components for (a) means for paths east of 94°W longitude and (b) means for paths west of 94°W longitude	277

LIST OF TABLES

Table	Caption	Page
2.2-1.	Performance summary for LATEX drifters	19
2.2-2.	LATEX drifter data sets	21
2.2-3.	Off-shelf oceanic features tracked by LATEX drifters	23
2.3-1.	LATEX C aerial survey dates and expendable probe performance	29
2.5-1.	LATEX A shelf-edge current meter mooring locations and instrument levels (April 1992 - November 1994)	46
2.5-2.	LATEX A hydrographic cruises	48
2.5-3.	LATEX C XBT-7 and T-7 XBT shipments	49
2.5-4.	GulfCet hydrographic cruises	51
2.5-5.	SOOP/TIGER hydrographic cruises during LATEX field program	52
2.5-6.	SCULP drifter aerial and platform deployment sites	54
2.5-7.	Planned SCULP drifter deployment schedule	56
3.2-1.	Argos drifter thermistor specifications	60
3.3-1.	Aerial probe specifications	63
3.3-2.	Evolution of the Sippican AXBT probe drop-rate equation (1982-1989) from published sources	66
3.3-3.	Aerial probe drop-rate equations used to process data	67
3.3-4.	Comparison of AXBT probe drop-rate equation predictions	67
3.3-5.	Equations to convert Sippican-derived AXBT depth predictions (from EQN. 3) to each manufacturer's latest recommended equation result	69

LIST OF TABLES

Table	Caption	Page
3.4-1.	GEOSAT GM and ERM cycles used to compute annual and seasonal climatologies	85
4.3-1.	Comparison of GEOSAT topography with in situ measurements	99
4.4-1.	Major Loop Current eddy-separation times and shedding intervals during the GEOSAT period .	100
4.7-1.	Mean Loop Current eddy statistics in the western Gulf of Mexico from continuous altimetric tracking of four Loop Current eddies (B, C, D and F) for 120 days after transit across 90°W longitude	161
4.8-1.	Loop Current eddy statistics at 90°W longitude	163
5.9-1.	Summary statistics of ellipse model parameters	273
5.9-2.	Drifters in Loop Current eddies	276
5.9-3.	Lagrangian Mean Statistics of Gulf of Mexico Loop Current eddies	278

ACKNOWLEDGEMENTS

The Program Manager expresses particular thanks to Tim and Barbara Flynn of Aero-Marine Surveys, Inc., who did the flying and kept the data collection effort going through thick and thin; to Paul Higley and his staff at Specialty Devices, Inc., who responded with speed and good humor to a variety of logistics problems; and to Richard Fournet and his ground crews at Paul Fournet Air Services, who provided an outstanding operating base in Lafayette, Louisiana. The office staff in Raleigh, Ms. Susan Root, Ms. Stephanie Bowens, Mr. Jeff Brown, and Ms. Sharon Goodhart all contributed in untold ways throughout the course of the study including production of this report.

The continued support and encouragement of Dr. Walter R. Johnson and Dr. Murray Brown, the Contracting Officer's Technical Representative during the bulk of the Program, and the assistance of his successor, Dr. Alexis Lugo-Fernandez, are most gratefully acknowledged.

I. INTRODUCTION

1.1 Program Overview

This report documents completion of data collection and analysis activities, by Science Applications International Corporation (SAIC) and its subcontractors, in accomplishing the principal objectives of the Gulf of Mexico Eddy Circulation Study under Minerals Management Service (MMS) Contract 14-35-0001-30633. The study is also known as the C component of the Louisiana/Texas Shelf Physical Oceanography Program (LATEX Program). Briefly stated, the study objectives were:

- monitoring and characterizing three classes of mesoscale circulation patterns important in the open sea and slope waters of the northwestern Gulf of Mexico;
- providing efficient, centralized logistics support, including Service Argos liaison for drifting buoys, air deployed expendable bathythermograph (AXBT) and current profiler (AXCP) probes, and expendable bathythermograph (XBT) probes for a ship-of-opportunity program;
- disseminating information collected during this study to other investigators on a regular basis.

Monitoring Loop Current eddies and mesoscale features was accomplished in 21 aerial surveys, with AXBTs and AXCPs, to examine the instantaneous hydrographic and velocity structures of selected features. The general area covered by these surveys is shown in Figure 1.1-1. Continuous monitoring of features was done using air-deployed, satellite-tracked drifting buoys. Satellite altimetry was used to provide an historical perspective of conditions in the Gulf of Mexico from early 1985 through 1989. Through cooperative efforts with the University of Colorado, altimetry data from the ERS-1 and TOPEX/Poseidon satellites were available in near real-time during Years 2 and 3 of the Program as an aid in locating eddies for further study using AXBT and AXCP surveys.

1.2 Program Elements

The LATEX C program element comprised 12 tasks involving field activities, data quality control and analysis, and support activities identified in the contract as outlined below.

1.2.1 Task C-1: Drifting Buoys Provided to Other Contractors

Seventeen drifters "drogued at the surface" were ordered for subsequent distribution: 16 to TAMU, prime contractor for the

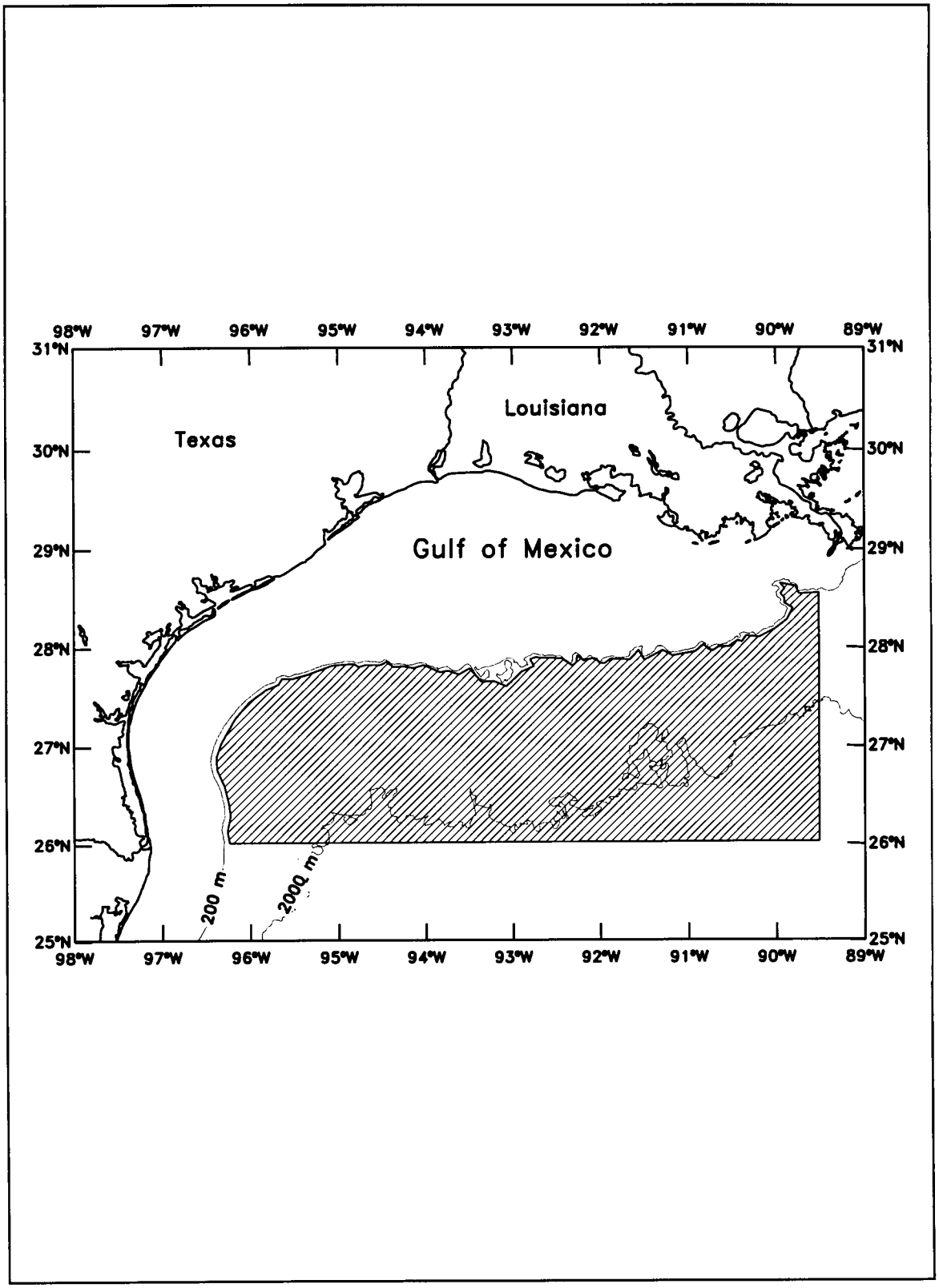

Figure 1.1-1. Map of the Gulf of Mexico with LATEX C study area indicated by shading.

Louisiana/Texas Shelf Circulation and Transport Processes (LATEX A) Study; and one to Louisiana State University (LSU), prime contractor for the Mississippi River Plume Hydrography (LATEX B) Study. The chosen configuration was a Clearwater Instrumentation, Inc., World Ocean Circulation Experiment (WOCE) type drifter with a 6x1 m holey sock drogue and approximate 3 m tether such that the bottom of the drogue was at 9 m.

Under this task Specialty Devices, Inc. of Plano, Texas maintained a central logistics facility and performed a variety of logistics tasks involving shipping and receiving drifters for this Task and Tasks C-2 and C-3, aerial expendable stores for Task C-6, and expendable stores and equipment for Task C-8.

1.2.2 Task C-2: Drifting Buoys in Loop Current Eddies

Six drifters were acquired for this task, which required that all eddies which separated form the Loop Current during the program were to be seeded with a drifter after being surveyed with AXBTs or were to be reseeded if a drifter were ejected from the eddy or failed to operate. The drifter configuration for this task was a Clearwater Instrumentation, Inc., WOCE type drifter with a 12x1 m holey sock drogue and approximate 88 m tether such that the bottom of the drogue was at 100 m.

After reprogramming funds originally budgeted for buoy refurbishment, two additional drifters were ordered from Horizon Marine, Inc. These drifters were packaged in a configuration approximating the dimensions of an A-size sonobuoy (0.9144 m [36 in] by 0.124 m [4.875 in] diameter) such that they could be launched from the same aircraft used for the aerial surveys, rather than from a leased air freighter. The drifters were configured with holey sock drogues and tethers to place the bottom of the drogue at 100 m.

1.2.3 Task C-3: Drifting Buoys in Other Meso-Scale Features

This task required tracking of meso-scale features such as slope cyclones and anticyclones and "squirts and jets" following location of such features by aerial surveys or other means. Two different air-deployable configurations of the Clearwater Instrumentation, Inc., WOCE type drifter were chosen: one set of four with the bottom of the drogue at 200 m for deployment in slope eddies, and one set of 10 with the bottom of the drogue at 50 m for deployment in squirts. Except for drogue tether length, these drifters were identical to the Loop Current eddy drifters.

Six additional drifters were later ordered from Horizon Marine, Inc. These drifters were packaged in a configuration approximating the dimensions of an A-size sonobuoy and were configured with holey sock drogues and tethers to place the bottom of the drogue at either 50 m (4) or 200 m (2).

1.2.4 Task C-4: Returned Buoys

This task provided for refurbishment of up to five buoys recovered and returned by third parties, as had occurred during previous MMS programs. No buoys were returned to the manufacturer for refurbishment during Year 1 or Year 2. Funds from this task were reprogrammed to allow purchase of Horizon Marine air-deployable drifters for use in Year 3.

1.2.5 Task C-5: Buoy Quality Control

Each of the drifters received by Specialty Devices, Inc., was turned ON, on receipt and again prior to shipment, and checked with a Telonics TSUR-B Satellite Uplink Receiver/ Analyzer System to verify correct operation of the Argos platform terminal transmitter (PTT). Each unit's operation was also verified through receipt of the signal through Service Argos.

1.2.6 Task C-6: Aerial Surveys

Five types of aerial survey were proposed to accomplish the objectives of the LATEX C program: Slope Surveys, Slope Eddy Surveys, Loop Current Eddy Surveys, Squirts and Jets Surveys, and Squirts and Jets Locator Surveys. These survey types are described below:

- Slope Survey - made over two days with 32 AXBTs on a regular hydrographic grid of five or six lines covering a portion of the upper slope between the 200 m and 2000 m isobaths. Three surveys were planned during each program year.

- Slope Eddy Location Survey - made with 16 AXBTs and five AXCPs on an as required basis if a slope eddy was discovered during a Slope Survey. Each survey was to be followed by aerial deployment of a drifter with a drogue at 200 m.

- Loop Current Eddy Survey - made with 16 AXBTs on an as required basis whenever the center of a Loop Current eddy was determined to have reached 90°W longitude after separating from the Loop Current. Each survey was to be followed by aerial deployment of a drifter with a drogue at 100 m.

- Squirts and Jets Survey - made over two days with 32 AXBTs and nine AXCPs whenever a 'squirt' was detected in satellite imagery. This survey was to be followed by a Squirts and Jets Location Survey (16 AXBTs) and deployment of two drifters with drogues at 50 m.

- Squirts and Jets Location Survey - made in one day with 16 AXBTs to determine the best locations in a 'squirt' for subsequent deployment of two drifters with drogues at 50 m.

The design of Loop Current eddy surveys and squirts and jets surveys was developed according to conditions existing just before the planned surveys. Slope surveys were conducted on a regular grid, one for each field year, and were repeated three times during each field year. The plans for the three Slope Survey grids were altered from those originally proposed to provide better coverage of the study area and to coordinate with the LATEX A shelf surveys.

1.2.7 Task C-7: Altimetry

The goal of this task was to use all publicly available U.S. Navy Geodetic Satellite (GEOSAT) data to provide an altimeter climatology consisting of the following elements:

- charts of the mean sea surface and mean slope;

- charts of sea surface topographic variability and slope variability for each year and season;

- charts of sea surface topography anomalies for each exact repeat cycle (ERC);

- charts of eddy paths, eddy size and shape, eddy decay and Loop Current penetration derived from the above; and

- wave height and wind speed analyses.

As originally proposed, this task was to use only the unclassified Exact Repeat Cycle data collected after the completion of the Navy's classified mission. Recently most of the Navy data have been declassified and have been incorporated in this analysis. The analysis has also benefitted from continuing efforts to generate the most accurate mean sea surface possible using the whole ensemble of altimetry missions flown during the 1980s and which continue with the ERS-1 and TOPEX/Poseidon satellites which are in orbit now.

1.2.8 Task C-8: Ships-of-Opportunity

Support of the Ships-of-Opportunity (SOOP) program involved distribution of T-7 XBT probes, in case lots, to investigators designated by the MMS Contracting Officer's Technical Representative (COTR). Probes were provided to the GulfCet Program (Dr. Giulietta Fargion) and to the TAMU Ship of Opportunity Program (Dr. Douglas Biggs). Data from these programs were shared among the various Principal Investigators. In each instance where probes were provided, they were used to augment other sources of data and so did not represent a separate 'contiguous' data set.

1.2.9 Task C-9: Data Quality Control

The goals of this task were to eliminate spurious or doubtful values in the data sets and to correct, where possible, values affected by identifiable and quantifiable sources of bias. Data collected or processed comprise three basic data types:

- Hydrographic Profile Data (XBTs/AXBTs/AXCPs),
- Lagrangian Data (Drifting Buoys), and
- Remotely Sensed Data (Altimetry).

Hydrographic profile data from AXBTs, AXCPs and drifter data were processed by SAIC, while quality control of altimetry data was performed by CCAR. Data from XBTs distributed under the SOOP Program were processed by the individual programs or investigators receiving the probes.

1.2.10 Task C-10: Analyses and Reports

This task specified generation of two annual progress reports (SAIC 1994, 1995) and this Final Synthesis Report. The two annual reports provide details of the data collection during the first two years of the program but without any data analysis. Analysis of the entire data set is covered in this report.

1.2.11 Task C-11: Information Transfer

This task included posting to the GULF.MEX Electronic Bulletin Board on OMNET, through the end of 1994, of the following types of messages:

- drifter tracks on a weekly basis, whenever a drifter was operational,

- cruise plans and reports before and after each set of surveys,
- inflection points from AXBTs after each aerial survey, and
- program schedule changes.

Additionally, data were shared with other program elements on an as requested basis.

1.2.12 Task C-12: Government Furnished Equipment/Capital Equipment

This task provided for refurbishment and return to MMS of government owned property at the end of the project. This property consisted of various small pieces of test equipment and miscellaneous other items which remained at the end of the field work. No expendable probes remained at the end of the program.

1.3 Principal Investigators and Primary Support Personnel

Principal Investigators for this program were Dr. Peter Hamilton of SAIC, who analyzed the drifter and hydrographic data as well as such ancillary data as shelf break and upper slope current meter data from the LATEX A program, and Drs. Robert Leben and George Born of CCAR who analyzed the GEOSAT data and provided altimetry support in near-real-time during Loop Current Eddy location surveys.

The 21 aerial surveys (including photography) and drifting buoy deployments were executed by an experienced subcontractor, Aero-Marine Surveys, Inc., under the direct supervision of an SAIC scientist. All survey operations, except in January 1993, were conducted from the Paul Fournet Air Services facility at Lafayette Regional Airport in Lafayette, Louisiana. The support provided by this fixed base operator was exceptional and included shipping and receiving activities before each survey and storage of materials, at no additional cost to the program.

Centralized storage and shipping of drifting buoys and air and ship launched expendable probes were provided in a thoroughly professional manner by Specialty Devices, Inc., from their facility in Plano, Texas. The operator of the facility was responsible for checkout of the satellite uplink transmitter in each drifting buoy procured under this program.

1.4 Report Organization

The remainder of this chapter summarizes the knowledge about the studies processes at the beginning of the program. Chapter II provides an overview of data collection and data presentation methods. Chapter III documents data quality control and quality assurance techniques and results and data processing methodologies. Chapter IV provides results of the analysis of the GEOSAT data. Chapter V documents analysis of the survey and drifter data and supporting data from the LATEX A program. Chapter VI provides the Summary and Conclusions. Chapter VII contains the References.

1.5 Scientific Background

Prior to this project, extensive work had been done on the Loop Current eddy shedding cycle and the paths of Loop Current eddies across the central and western Gulf of Mexico. A summary of this prior knowledge is presented below.

1.5.1 Loop Current Eddies

Major warm eddies, after shedding from the Loop Current, have diameters on the order of 200-400 km and propagate westward or southwestward at between three and six $km \cdot day^{-1}$ (Kirwan et al. 1984a, Lewis et al. 1989). After the eddies pass through a relatively narrow region of deep water between the Mississippi delta and the Yucatan shelf, there appear to be two preferred paths into the western Gulf of Mexico: one parallel to the northern slope (SAIC 1988; Lewis et al. 1989) and one southwestward towards the Bay of Campeche. Surface swirl velocities generally range from about 75 to 100 $cm \cdot s^{-1}$, though higher speeds have been measured (Cooper et al. 1990), and the period of rotation is usually about 8 to 10 days (Kirwan et al. 1984a). Rings are usually elliptical with eccentricities of between 1.2 and 2. The orientation of the major axis varies considerably as the ring propagates into the western basin, which gives rise to the characteristic oscillations in the paths of drifters deployed in rings.

As the Loop Current eddies move into the western Gulf, they seem to remain vigorous with little change in size or in the depression of the isotherms, indicating only small losses of energy from friction and topographic interaction. As the eddies approach the south Texas-Mexican slope they begin to feel the topography of the slope and/or interact with remnants of earlier rings. The former case for the decay of Eddy B was quite well documented by an extensive set of hydrographic surveys, drifter tracks, and a current meter array in Year III of the MMS Gulf of Mexico Physical Oceanography

Program (SAIC 1988; Lewis et al. 1989). The sequence for Eddy B was roughly as follows: the eddy approached the slope around 25°N latitude, became more elongated in the east-west direction and began generating secondary cyclonic perturbations on the periphery (Figure 1.5-1a). This set of features evolved into a cyclone-anticyclone pair of similar magnitude eddies, (Figure 1.5-1b) which were individually about half the size of Eddy B. The pair slowly migrated southward along the slope (Figure 1.5-1c) with indications from drifters that the eddy pair may have moved eastward off the slope between February and April 1986 (SAIC 1988). A result of this process was strong offshore transport between the anticyclone and cyclone around 25°N latitude. This kind of feature often seems to move upper-slope and shelf water across the isobaths into the deep Gulf. A distinct plume of cold water is often observed leaving the Mexican coast around 25°N latitude in winter and spring satellite AVHRR imagery. Earlier hydrographic studies (Merrell and Morrison 1981; Brooks and Legeckis 1982; Brooks 1984) have observed similar eddy structures in the region of 25°N latitude though the connection to Loop Current anticyclones was not made. Brooks (1984) indicated that the geostrophic transport in the offshore jet was equivalent to transport in the Loop Current (~30 Sv).

Drifter studies (Kirwan et al. 1984a, Lewis and Kirwan 1985) and numerical model results (Hurlburt and Thompson 1982) have suggested that remnants of eddies that collide with the shelf around 23°N latitude migrate northward along the slope resulting in a weak, warm eddy in the northwest corner region of the slope. A warm feature in this corner region is often observed in satellite imagery and may have an important influence on slope circulation and shelf-slope exchange processes off Texas. The apparent differences between northward migration of intact but weakening anticyclones and the southward movement along the slope of strong cyclone-anticyclone eddy pairs resulting from topographic interaction of a LC eddy with the slope indicate that the complex behavior of eddies in this region has not been completely resolved. Numerical models support both kinds of behavior (Smith 1986; Hurlburt and Thompson 1982) and it seems likely that both processes can exist at differing times depending on the characteristics of the approaching major LC eddies and the eddy field existing along the Mexican slope.

1.5.2 Slope Eddies in the Central Gulf of Mexico

During the Gulf of Mexico Physical Oceanography Program a strong cold eddy was detected over the lower slope just north of Eddy F. It was about 150 km in diameter and elongated in the east-west direction, though this may have been an effect

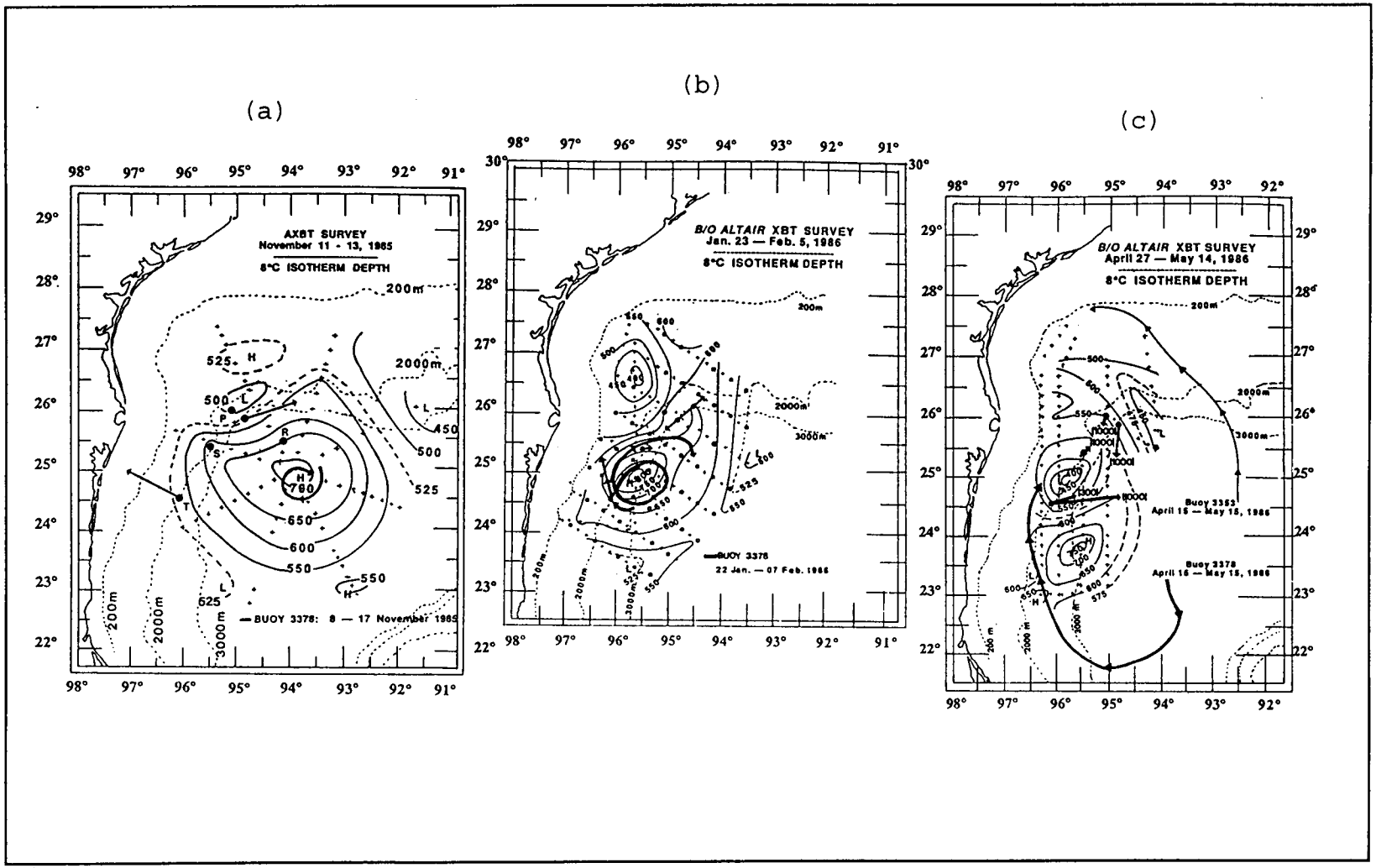

Figure 1.5-1. Eddy B 1985-1986 showing a) approaching the slope, b) generation of anticyclone-cyclone pair, and c) migration of pair to the south (from SAIC 1988).

of the lack of synopticity in the surveys. This cyclone was tracked from its first appearance in imagery (May 7, 1988) in deep water east of the mooring transect along 92°W longitude (SAIC 1989). Over the next three months, the cyclone underwent a number of small displacements in deep water including passing, both westward and eastward, through the mooring transect, eventually ending up on the lower slope as Eddy F propagated to the west. The cyclone remained in the vicinity of 92°W longitude until at least November 1988, undergoing two rapid northwestward displacements followed by a slow return drift to the east (Hamilton 1992; SAIC 1989).

Further evidence of the quasi-stationary nature of this cyclone on the lower slope is given by the drifter track in Figure 1.5-2. The drifter made both clockwise and counterclockwise loops as it progressed eastward along the slope, passing through both anticyclones and cyclones. The position of the cyclone detected in an October 1988 survey had not substantially changed a month later. The existence of small scale quasi-stationary cyclones and anticyclones on the lower slope explains the characteristics of the currents on the slope (SAIC 1989; Hamilton 1992). They usually show long periods of several weeks to months of sustained flows that are strongly sheared and coherent in the upper layers. Cross-slope, and by implication along-slope, coherences between moorings separated by more than 50-100 km are weak or not significant. The existence of both cyclones and anticyclones indicates that there will be strong cross-isobath flows, which are likely to affect the upper slope and shelf break region, causing outflows and inflows in regions between the eddies. These effects are sometimes observed in imagery; however, cyclones are not usually directly observable in AVHRR imagery since there is little thermal contrast in the upper 100 m.

The existence of small cyclones in both the deep basin and lower Louisiana slope waters seems to be a relatively common occurrence as documented by hydrography, inverted echo sounder (IES) and current meter records and drifters over a two-year period (Hamilton 1992; SAIC 1989). Their relationship to major LC eddies is at present uncertain, since they occur both in proximity to and distant from major warm eddies.

1.5.3 Squirts and Jets

The shelf break and upper slope of the LATEX region has been studied very little. There are indications from winter AVHRR imagery of small scale (~10-20 km) interleavings of warm offshore water with cooler shelf water, as well as larger scale offshore flows probably resulting from the occurrence of

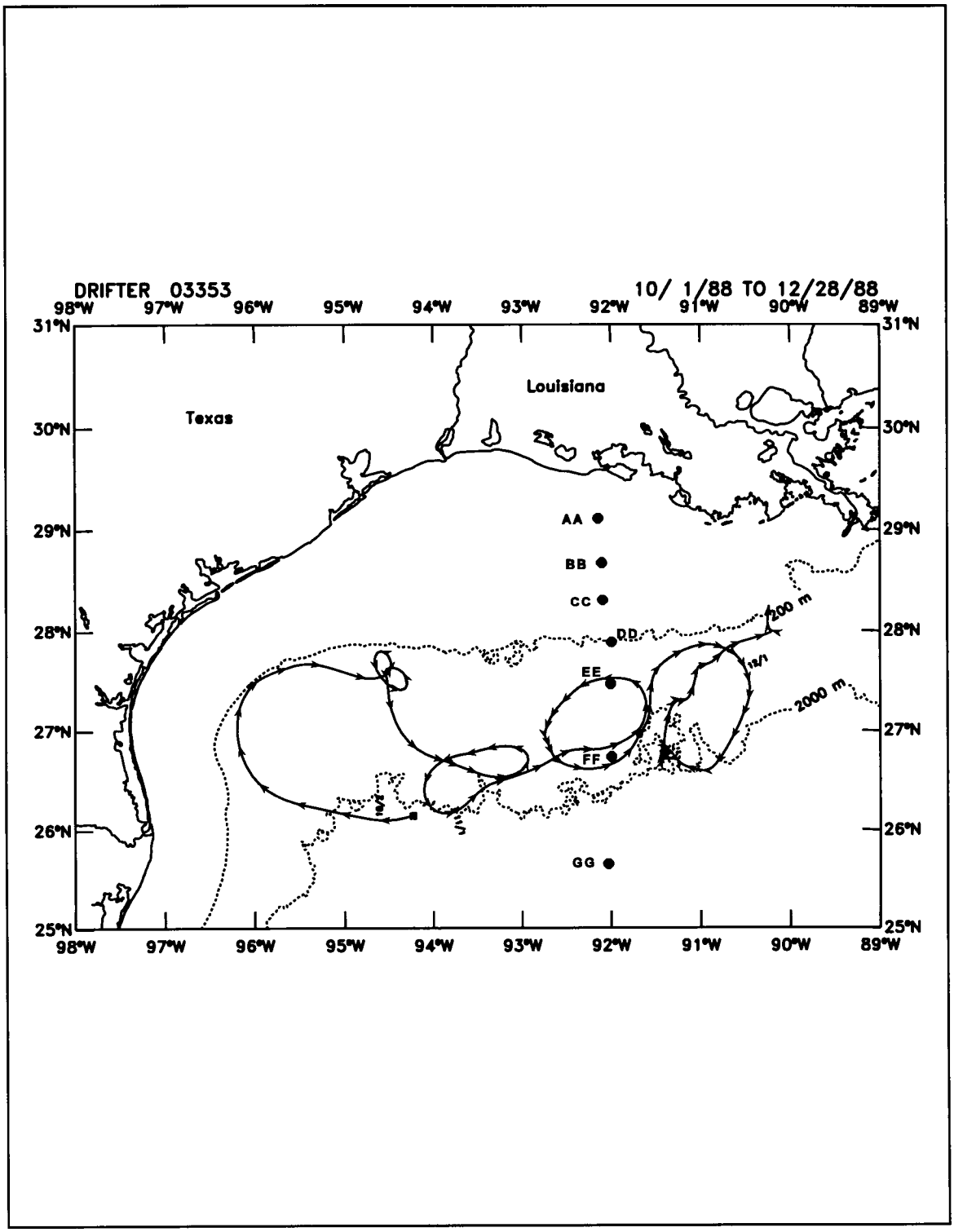

Figure 1.5-2. The smoothed track for ARGOS drifter 3353. The arrows mark 00 hours GMT for each day. Dots mark postion of moorings deployed during the Gulf of Mexico, Year 5, Physical Oceanography Program (plotted from SAIC 1989).

pairs of slope eddies, as discussed previously. Measurements in the shelf-break region are very sparse and include a few hydrographic sections that cover the outer shelf and upper slope current meter moorings along 92°W longitude (SAIC 1989), and at the Flower Gardens, ~27.6°N latitude, 93.5°W longitude, though little information can be gleaned from this latter data since the flows are overwhelmingly dominated by topographic effects of the Flower Garden Banks. There is also a limited number of industry current meter moorings from the early 1980s on the upper slope ranging from East Breaks in the west to the Mississippi Canyon in the east (Hamilton 1987b). There have been oil company current measurements and ship-mounted ADCP surveys around the Mississippi Delta and Green Canyon. Some evidence is available that shelf-slope exchange processes differ by geographical region.

In the vicinity of the Mississippi Canyon and Green Canyon, major warm eddies, or perhaps the Loop Current itself, are more likely to impinge on the upper slope (SAIC 1989) because the delta region intrudes upon the westward passage of the eddies. Thus, large extrusions of shelf and upper slope surface water that may contain Mississippi plume water are sometimes observed to be wrapped around the outer part of a Loop Current eddy. Similar extrusions are sometimes observed along the Mid-Atlantic Bight shelf when Gulf Stream warm core rings are present in slope waters (Churchill et al. 1986).

In the central part of the slope, LC eddies rarely intrude on the upper slope and the circulation is more likely to be dominated by slope cyclones and anticyclones as discussed previously. However, upper slope circulations appear to be more complex, with moorings showing two, three, or four separate layers moving at different velocities (Hamilton 1987b). The dynamics are not understood, nor indeed the phenomena well described. A number of mechanisms can be proposed such as wind-driven exchange, small scale (~20 km) upper slope eddies such as found in the Mid-Atlantic Bight (Houghton et al. 1988; Garvine et al. 1988), or eddy-driven bottom intrusions such as found in the South-Atlantic Bight (Atkinson et al. 1987; Hamilton 1987a).

In the northwest corner of the Gulf of Mexico, the presence of a weak anticyclone, along with a narrow shelf which brings the coastal boundary layer closer to the shelf break, creates stronger cross-shelf density and velocity gradients in wintertime. The spring peak in Mississippi River flow takes several months to reach the southwest Texas coast. In AVHRR imagery, this region seems particularly active in producing small scale (1-10 km) fingers, or squirt jets, which may imply that instability processes are important.

II. DATA ACQUISITION AND PRESENTATION

2.1 Introduction

LATEX C data collection included the deployment and tracking of Argos drifters, the deployment of air-deployed expendable probes to collect vertical profiles of temperature, current shear and salinity, some aerial photography, and the acquisition of historical Geosat altimetry data. In addition, ancillary data, including subsurface current measurements, AVHRR imagery, CTD and XBT profiles, additional surface-drogued Argos drifter data, and TOPEX/Poseidon and ERS-1 altimetry data, collected by other investigators, were made available as part of complimentary programs coincident in time with the LATEX C field effort.

2.2 Drifting Buoy Data

2.2.1 Introduction

A total of forty-five Argos drifters were deployed and tracked as part of this program. Thirty-seven of these were WOCE compatible and were designed, where possible, with drogue drag area ratios of approximately forty-to-one to keep buoy slip to a minimum (one to two $cm \cdot s^{-1}$). They were also designed to improve drifter survivability per the latest heavy weather test information from the WOCE program investigators. Eight additional non-WOCE type drifters were acquired, however, and deployed late in the program when it was apparent that drifter refurbishment funds would not be consumed and that sufficient Argos system processing funds remained to permit additional drifter tracking. The selection of the eight, additional drifters was made primarily based on air-deployment survivability criteria rather than WOCE compatability, though ease of deployment and cost were also considered.

2.2.2 Drifter Descriptions and Argos Data Transmission

Thirty-seven Clearwater WOCE-type drifters were deployed during the first two years of the field program. Each was configured with an eleven inch diameter surface float, an eight inch diameter subsurface float, a tether and a holey-sock drogue (see Figure 2.2-1). The subsurface float served to provide low tether tension at the surface element. Its purpose was to reduce or significantly uncouple the influence of surface wind and wave dynamics on the transmitting buoy at the surface from the current following characteristics of the drogue at depth. The holey-sock was typically on the order of one meter in diameter by six or seven meters in length while the tether length varied depending on the type of oceanic

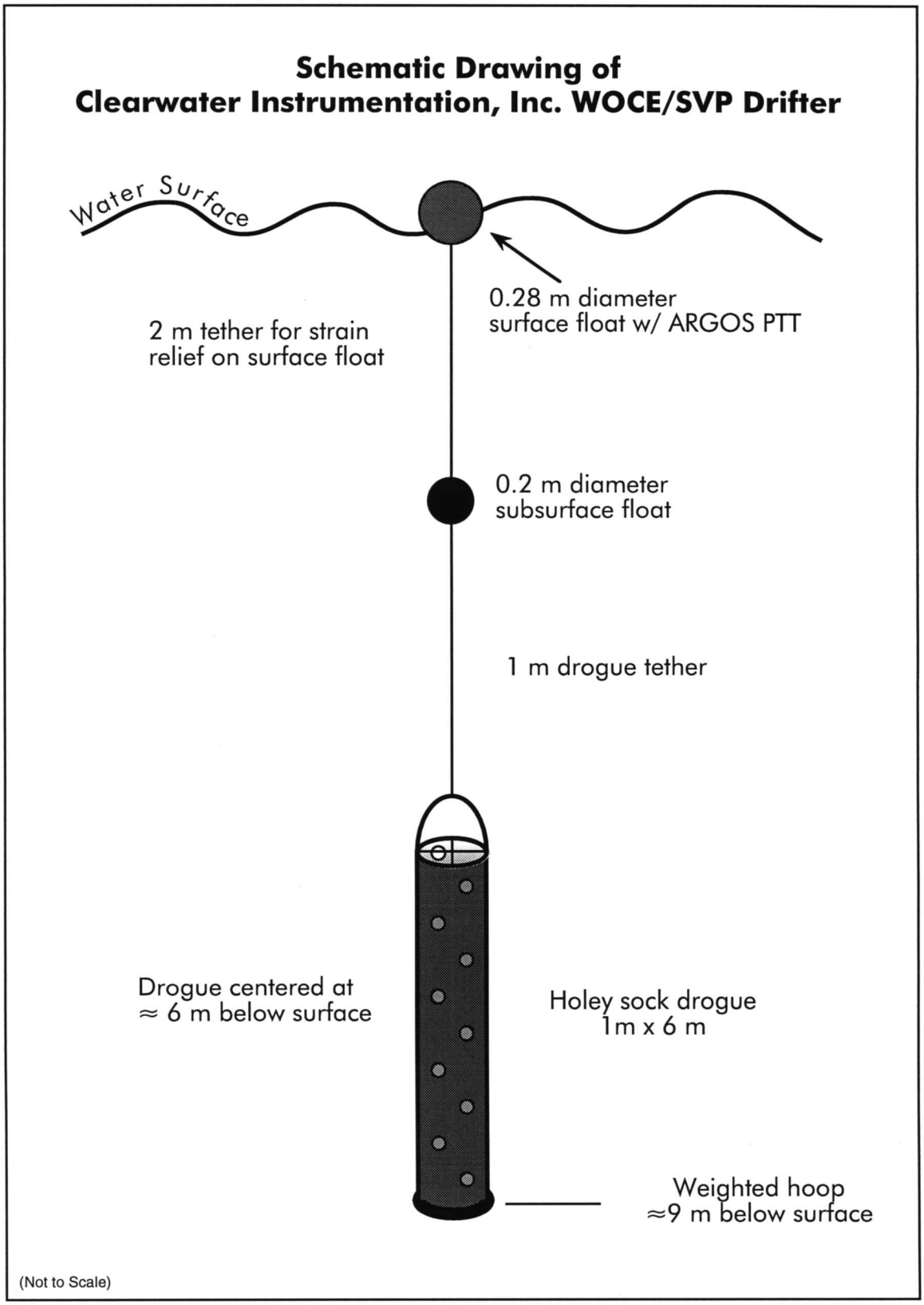

Figure 2.2-1. Schematic of Clearwater Instrumentation, Inc. WOCE/SVP drifter drogued at six meters.

feature the drifter was expected to follow (i.e. the drogue was centered at six meters for near-surface circulation on the shelf, 50 meters for squirts and jets, 100 meters for Loop Current eddies, and 200 meters for small cyclonic and anti-cyclonic eddies along the shelf break). Each drifter was also equipped to measure surface temperature, to detect the presence or absence of the drogue, and was programmed to provide continuous service for one year with a total shutdown after 365 days.

Eight Horizon FHD/Holey Sock drifters were deployed during Year three of the program. Each of these was configured so as not to exceed the standard "A" size sonobuoy dimensions in launch configuration. They were 4.75 inches in diameter and 38.25 inches long. Each had a tether and was drogued with a 0.10 meter diameter by 10 meter long holey sock (at 50 meters, 100 meters or 200 meters) (see Figure 2.2-2). They were equipped with a thermistor to measure surface temperature and were powered to transmit for one year with a total shutdown after 365 days.

Drifter sensor data were transmitted through built-in Argos Platform Transmitter Terminals (PTTs) to NOAA polar orbiting spacecraft. These data were then separated, time-coded, formatted and retransmitted by the spacecraft to the Global Processing Center (GPC) ground stations at Toulouse, France and Landover, Maryland. Drifter position was determined at each GPC from the relative motion between the drifter and the satellite in its orbital track which produced a Doppler shift in the frequency of the RF link. These processed data were then obtained from the GPC (often referred to as Service Argos) via Internet.

2.2.3 Drifter Deployments and Performance

The drifters were deployed by both ship and by air. Seventeen Clearwater drifters were initially deployed by ship as part of the LATEX A and B components of the study. In addition, twenty more of these same type drifters were scheduled for air deployment as part of LATEX C following aerial expendable bathythermograph surveys. However, because of air-deployment survivability problems, primarily due to parachute failures (see SAIC 1994 and 1995), this number was reduced to ten. Subsequently, four additional Clearwater drifters were deployed by ship as part of the LATEX A hydrographic effort, after reducing their drogue tether length, and six more were deployed by ship, without drogue tether modification, as part of the LATEX C Ship-of-Opportunity Program. Four each of the Horizon drifters were deployed by air and by ship, respectively.

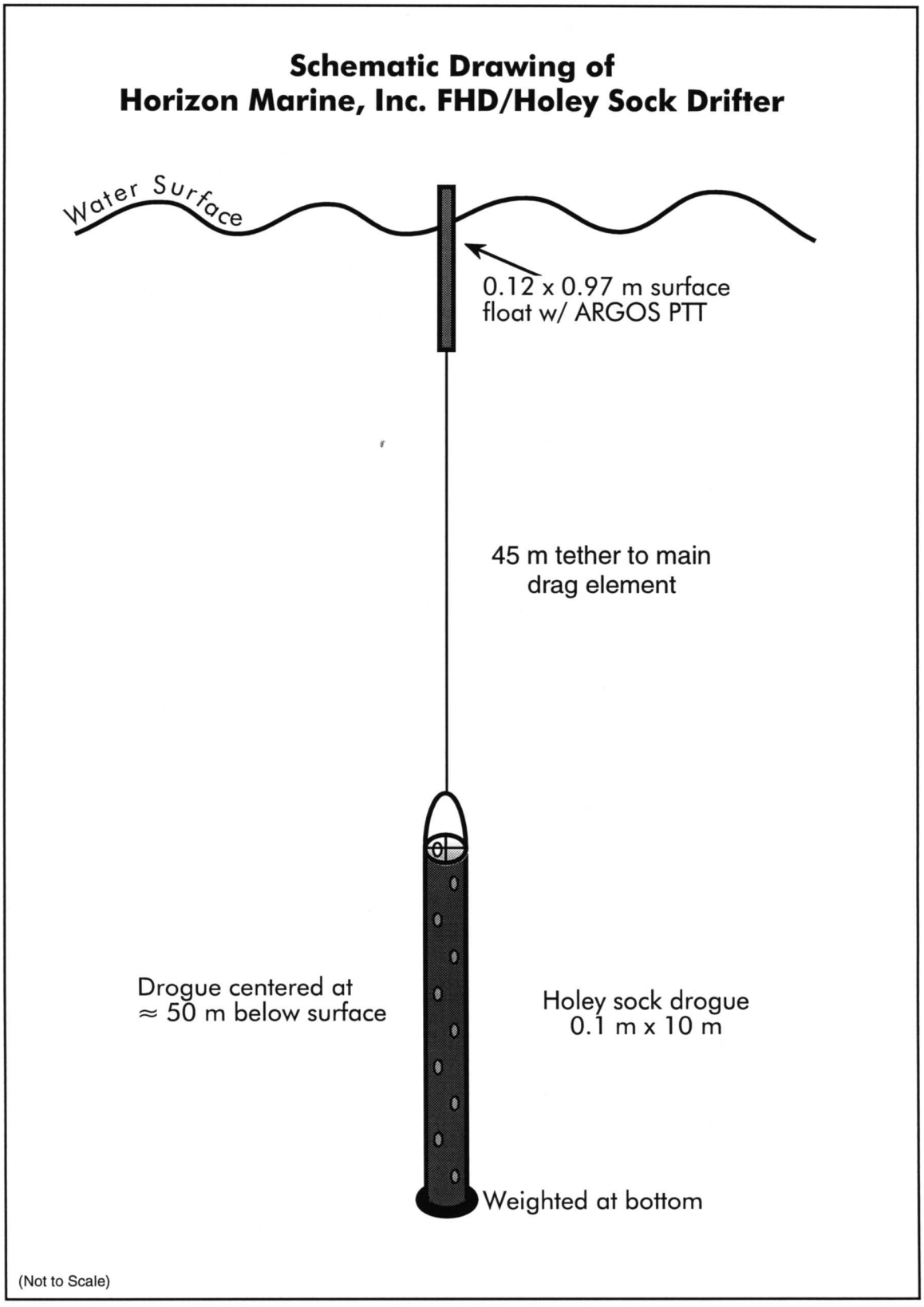

Figure 2.2-2. Schematic of Horizon Marine, Inc. FHD/Holey Sock drifter drogued at 50 meters.

Table 2.2-1 summarizes the average, maximum and minimum "days-of-data" performance for all LATEX drifters. Figure 2.2-3 provides a time line for the periods during which each drifter provided useful drifting data, and Table 2.2-2 summarizes each drifter's deployment period including the number of drifting days. Not suprisingly, the LATEX A and B shelf drifters were more susceptable to interference by other offshore interests. This is reflected in their lower average number of days of drifting data. They averaged approximately 68 days of drifting data versus 114 days for the 24 drifters deployed further offshore as part of LATEX C. In fact, four of the LATEX C drifters were still operational beyond 30 April 1995 when data were last considered for inclusion in this report. Table 2.2-3 summarizes the "off-shelf" oceanic features tracked by these drifters.

Table 2.2-1. Performance summary for LATEX drifters.

Program Component	Drifter Type	Number of Drifters	Deployment Method	Average No. Drifting Days of Data	Max. No. Days	Min. No. Days
LATEX A	Clearwater	16(+4)	Ship	68	251	0(3X)
LATEX B	Clearwater	1	Ship	61	61	61
LATEX C	Clearwater	6	Ship	207*	348*	58
	Clearwater	10	Air	83	203	0(2X)
	Horizon	4	Ship	91**	200**	0(1X)
	Horizon	4	Air	77	199	0(1X)

* Three units still transmitting as of 4/30/95.
** One unit still transmitting as of 4/30/95.

2.2.4 Drifter Path Plots

Each individual drifter's location was updated and plotted a number of times during its transmitting life. A composite path plot for all available LATEX drifter data is presented in Figure 2.2-4 and path plots for four subsets of these drifter tracks, for various regions of the Gulf, are presented in Figures 2.2-5 through 2.2-8. The whole Gulf composite (Figure 2.2-5) was compiled for eight drifters that drifted in both the western and eastern Gulf (as defined by 88°W longitude) during their transmitting lifetimes. The western Gulf composite is for nine drifters that reported locations only in the western Gulf with excursions south of 25°N latitude. The eastern Gulf composite is for three drifters that reported locations only in the eastern Gulf, and the northwestern Gulf composite is for eighteen drifters that reported locations

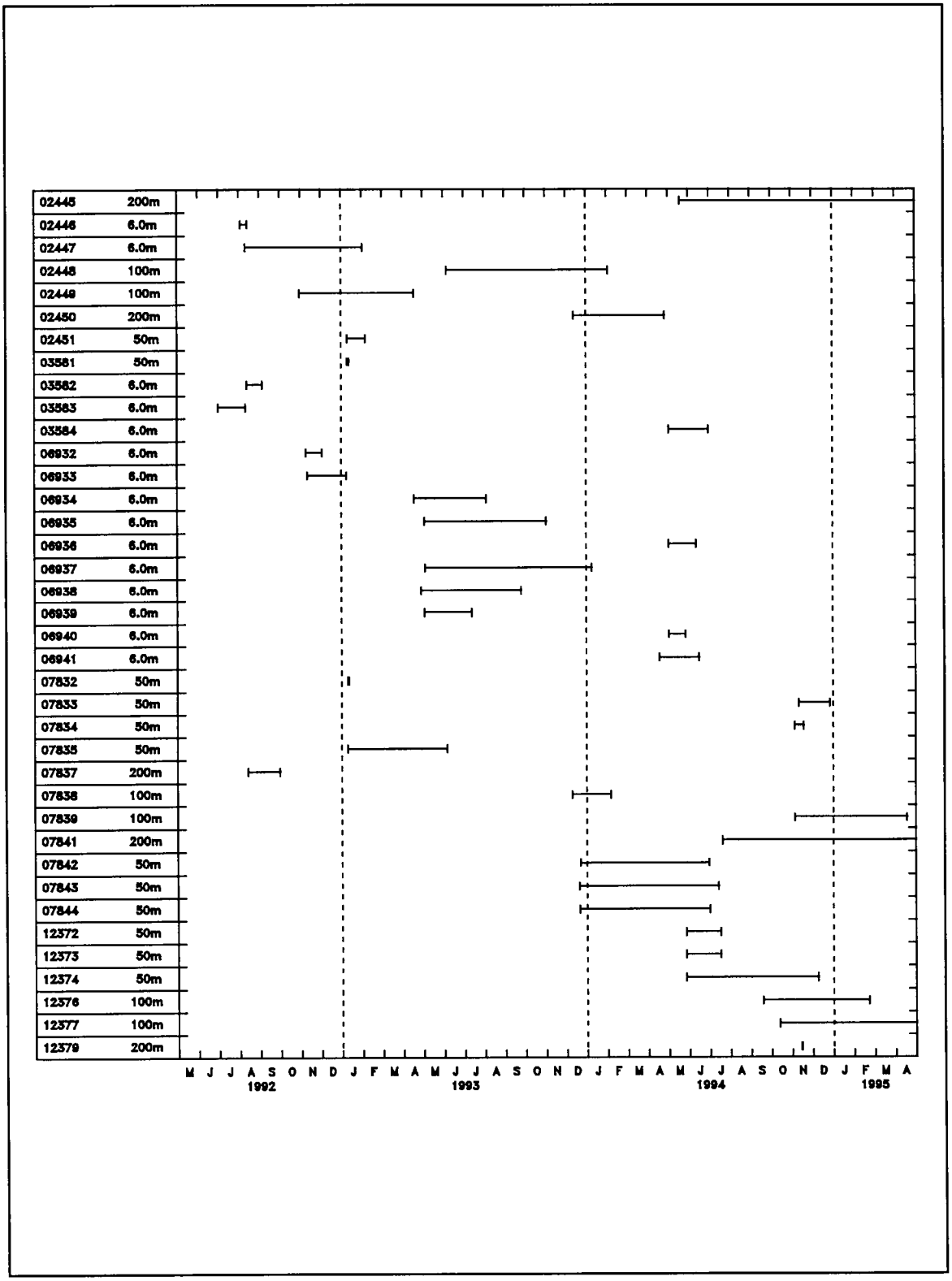

Figure 2.2-3. Time line for LATEX Argos drifters.

Table 2.2-2. LATEX drifter data sets.

Drifter ID	Drogue Depth (m)	LATEX Component	Begin Date	End Date	No. Drifting Days
02445 (A)	200	C	05/17/94	04/30/95**	348**
02446 (B)	6	A	08/03/92	08/13/92	10
02447 (C)	6	A	08/04/92	02/09/93	189
02448 (D)	100	C	06/02/93	02/02/94	245
02449 (E)	100	C	10/30/92	04/17/93	169
02450 (F)	200	C	12/12/93	04/25/94	134
02451 (G)	50	C	01/09/93	02/05/93	27
03581 (H)	50	C	01/09/93	01/12/93	3
03582 (I)	6	A	08/03/92	09/04/92	32
03583 (J)	6	A	08/03/92	08/09/92	6
03584 (K)	6	A	05/01/94	06/29/94	59
03585 (*)	6	A	11/12/92	11/12/92	0
06931 (*)	6	A	11/12/92	11/12/92	0
06932 (L)	6	A	11/08/92	12/02/92	24
06933 (M)	6	A	11/10/92	01/08/93	59
06934 (N)	6	A	04/17/93	08/02/93	107
06935 (O)	6	A	05/02/93	11/02/93	184
06936 (P)	6	A	05/01/94	06/11/94	41
06937 (Q)	6	A	05/02/93	01/08/94	251
06938 (R)	6	A	05/02/93	10/17/93	168
06939 (S)	6	A	05/02/93	07/12/93	71
06940 (T)	6	A	05/01/94	05/26/94	25
06941 (U)	6	B	04/15/94	06/15/94	61
07832 (V)	50	C	01/09/93	01/11/93	2
07833 (W)	6	A (from C)	11/10/94	12/26/94	46
07834 (X)	6	A (from C)	11/04/94	11/17/94	13
07835 (Y)	50	C	01/09/93	06/29/93	171

Table 2.2-2. LATEX drifter data sets (continued).

Drifter ID	Drogue Depth (m)	LATEX Component	Begin Date	End Date	No. Drifting Days
07836 (*)	100	C	10/12/92	10/12/92	0
07837 (Z)	200	C	08/13/92	09/29/92	47
07838 (a)	100	C	12/09/93	02/05/94	58
07839 (b)	6	A (from C)	11/04/94	04/30/95**	177**
07840 (*)	6	A (from C)	08/28/94	08/28/94	0
07841 (d)	200	C	07/19/94	04/30/95**	285**
07842 (e)	50	C	12/22/93	06/29/94	189
07843 (f)	50	C	12/22/93	07/13/94	203
07844 (g)	50	C	12/22/93	06/30/94	190
07845 (*)	50	C	12/22/93	12/22/93	0
12372 (h)	50	C	05/23/94	07/16/94	54
12373 (i)	50	C	05/23/94	07/16/94	54
12374 (j)	50	C	05/23/94	12/08/94	199
12375 (*)	50	C	05/23/94	05/23/94	0
12376 (m)	100	C	09/17/94	02/26/95	162
12377 (n)	100	C	10/12/94	04/30/95**	200**
12378 (*)	200	C	11/29/94	11/29/94	0
12379 (q)	200	C	11/13/94	11/14/94	1

* Not assigned.
** Still transmitting as of 4/30/95.

Note:

Clearwater Instrumentation, Inc. Drifter IDs: 2445-7845.
Horizon Marine, Inc. Drifter IDs: 12372-12379.

Table 2.2-3. Off-shelf oceanic features tracked by LATEX drifters.

Drifter ID	Dates	Tracked Off-shelf Oceanic Feature(s)
2445	05/17/94 - 04/30/95	Loop Current
2447	08/04/92 - 02/09/93	Eddy U, Eddy V
2448	06/02/93 - 02/02/94	Eddy Wn, Eddy W
2449	10/30/92 - 04/17/93	Eddy U, Eddy T
2450	12/12/93 - 04/25/94	NW Gulf cyclone, meandering, old anticyclone
2451	01/09/93 - 02/05/93	Eddy V
6934	04/17/93 - 08/02/93	Loop Current
6935	05/02/93 - 11/02/93	Loop Current
6937	05/02/93 - 01/08/94	Eastern Gulf cyclones
6938	05/02/93 - 10/17/93	Eddy V, cyclone, meandering
7833	11/10/94 - 12/26/94	Mid-Gulf meandering, Loop Current
7835	01/09/93 - 06/29/93	Eddy V, old anticyclone, Loop Current
7837	08/13/92 - 09/29/92	NW Gulf cyclone
7838	12/09/93 - 02/05/94	Mid-Gulf meandering, Eddy X
7839	11/04/94 - 04/30/95	Western gulf cyclone, meandering, Loop Current
7841	07/19/94 - 04/30/95	Loop Current
7842	12/22/93 - 06/29/94	NW Gulf cyclone, meandering
7843	12/22/93 - 07/13/94	Mid-Gulf cyclone, meandering
7844	12/22/93 - 06/30/94	Old anticyclone, meandering
12372	05/23/94 - 07/16/94	NW Gulf cyclone
12374	05/23/94 - 12/08/94	Western Gulf meandering
12376	09/17/94 - 02/26/95	Eddy Y
12377	10/12/94 - 04/30/95	Eddy Y

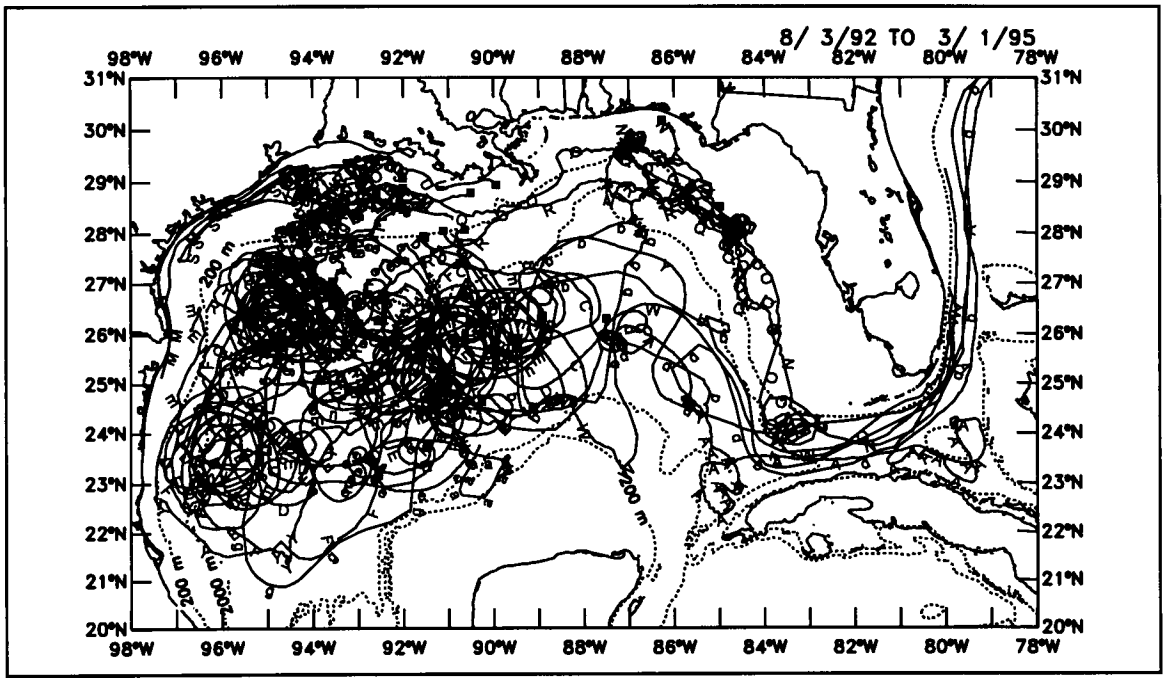

Figure 2.2-4. Composite path plot for all LATEX drifters.

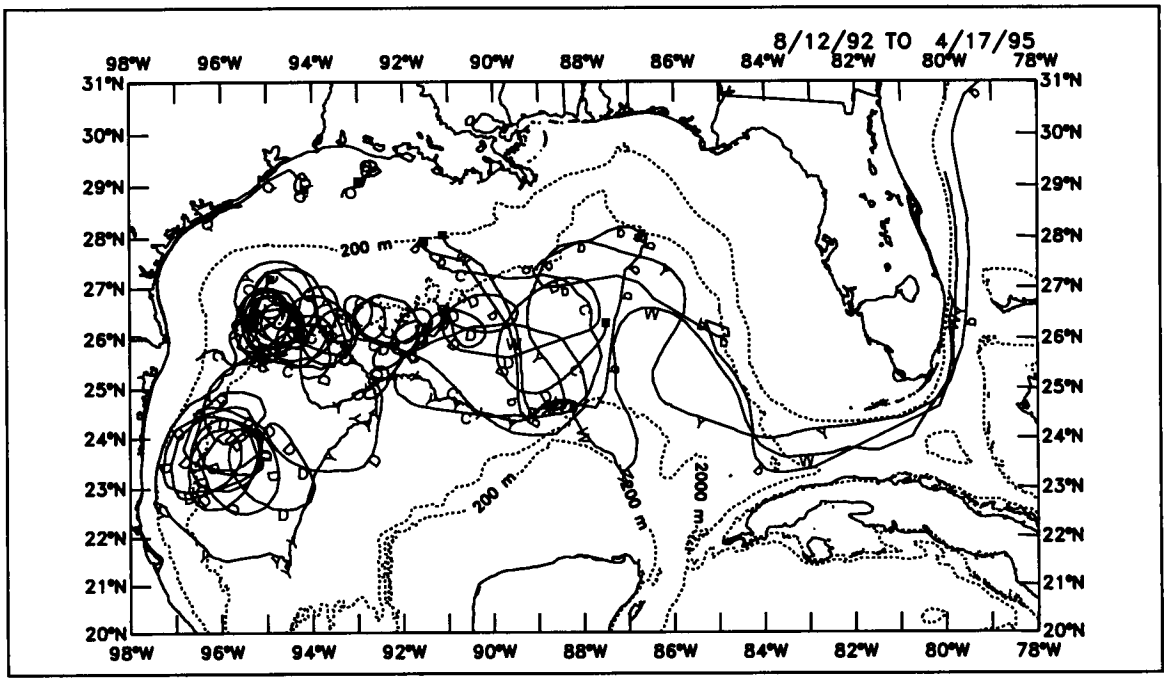

Figure 2.2-5. Whole Gulf composite path plot for eight LATEX drifters: 2447(C), 2448(D), 6935(O), 6937(Q), 6938(R), 7833(W), 7835(Y) and 7839(b).

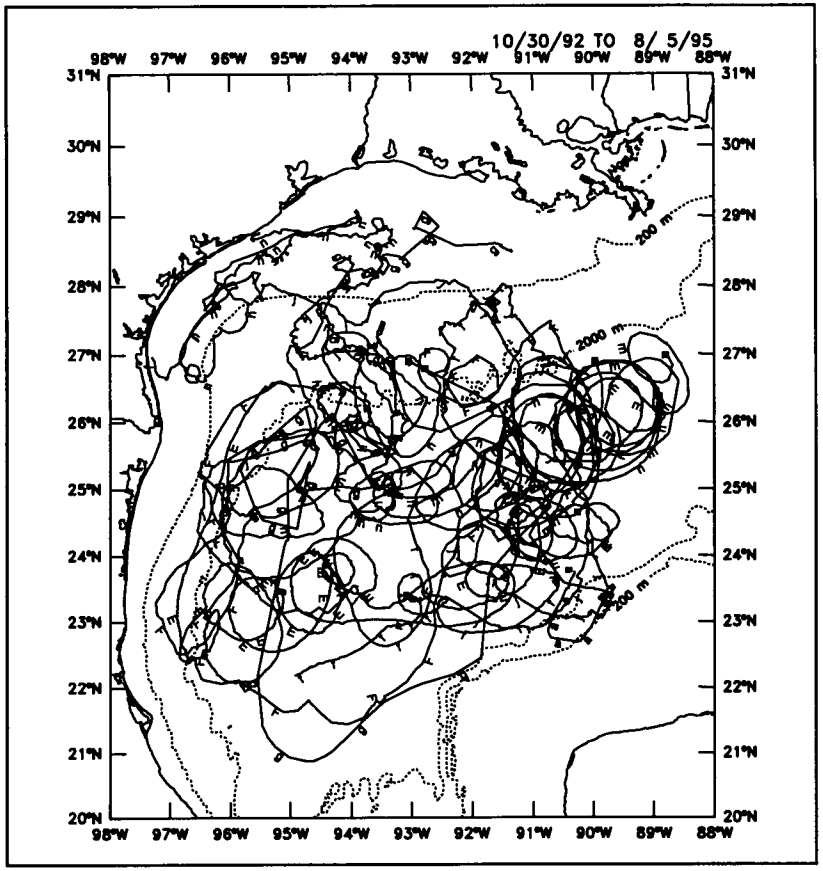

Figure 2.2-6. Western Gulf composite path plot for nine LATEX drifters: 2449(E), 2450(F), 7838 (a), 7843(f), 7844(g), 12372 (h), 12374(j), 12376(m) and 12377(n).

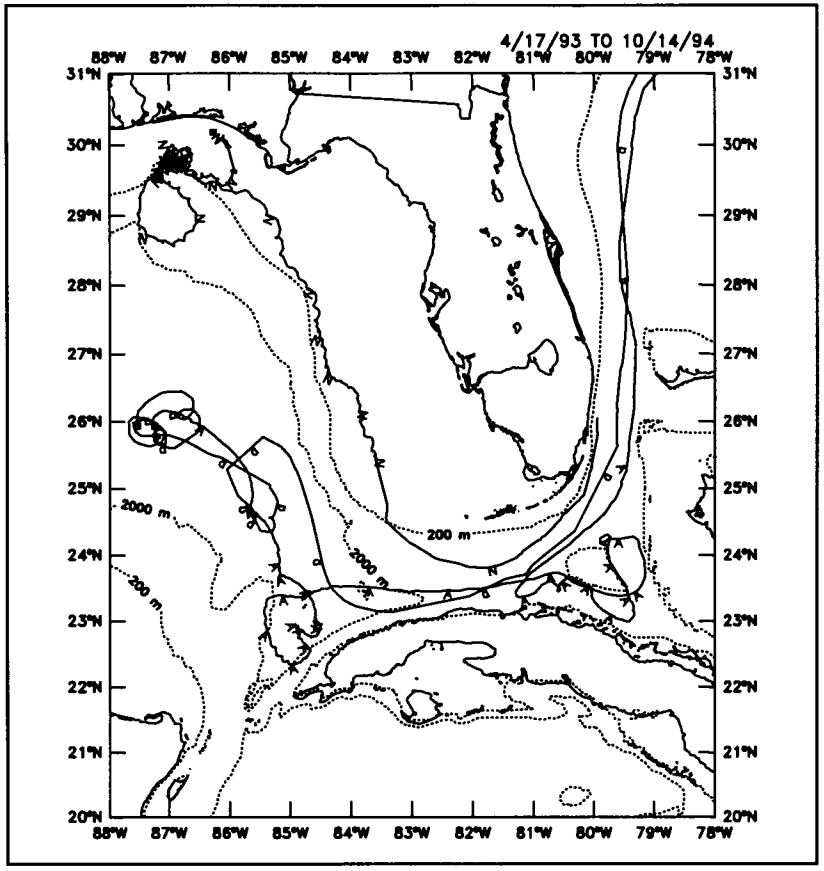

Figure 2.2-7. Eastern Gulf composite path plot for three LATEX drifters: 2445(A), 6934(N) and 7841(d).

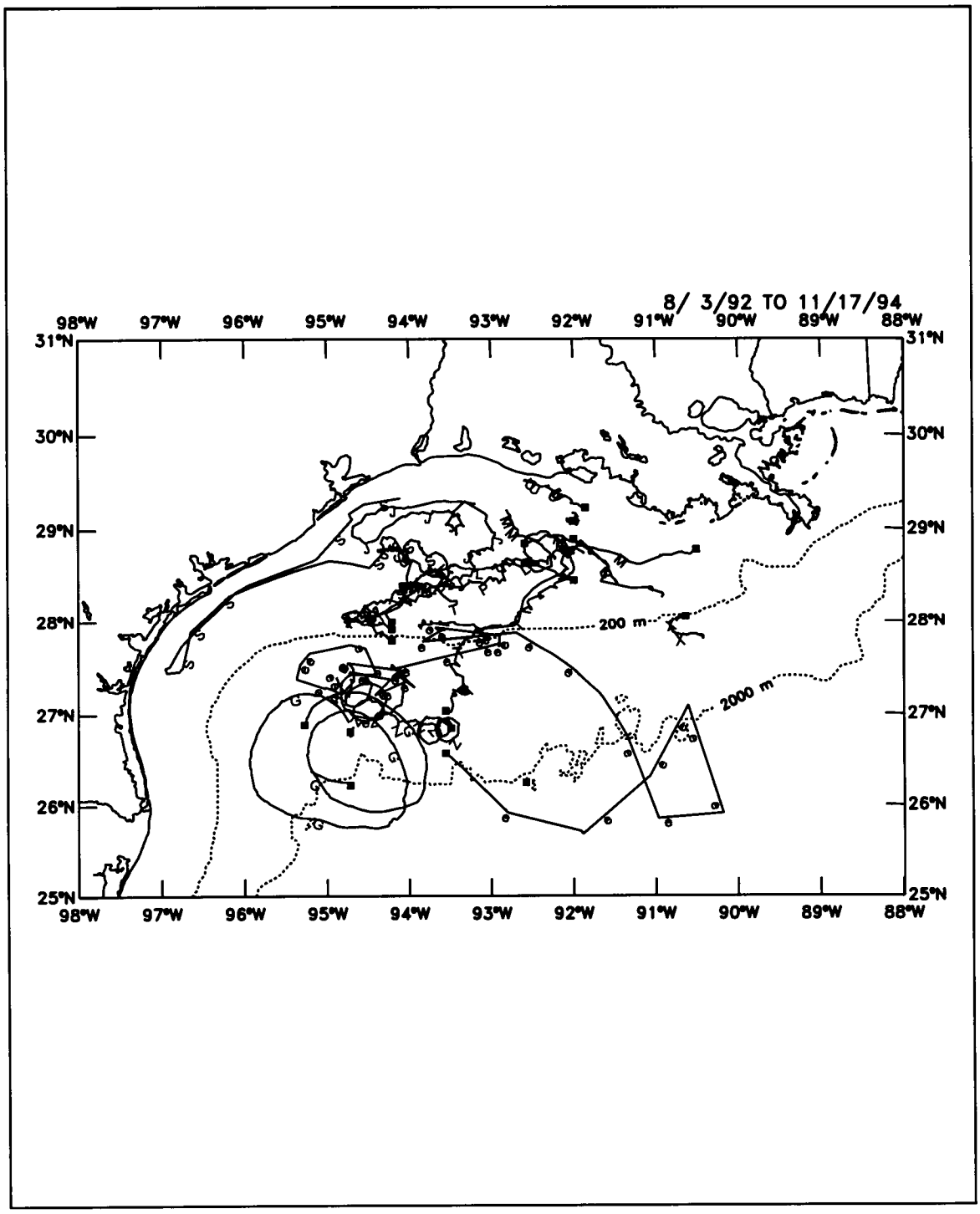

Figure 2.2-8. Northwestern Gulf composite path plot for 18 LATEX drifters: 2446(B), 2451(G), 3581(H), 3582(I), 3583(J), 3584(K), 6932(L), 6933(M), 6936(P), 6939(S), 6940(T), 6941(U), 7832(V), 7834(X), 7837(Z), 7842(e), 12373(i) and 12379(q).

only in the western Gulf, north of 25°N latitude. Only seven of the forty-five drifters exited the Gulf through the Florida Straits while still transmitting.

2.3 Aerial Surveys

2.3.1 Introduction

Twenty-one aerial surveys were conducted over the 2.7 year period of the field effort. During this time, nine slope surveys, three slope eddy surveys, five Loop Current Eddy surveys, and four combined squirts and jets surveys were completed. A total of 759 aerial expendable bathythermographs (AXBTs), 84 aerial expendable current profilers (AXCPs) and six aerial expendable conductivity/ temperature/depth probes (AXCTDs) were deployed. All but one of these surveys was conducted out of the Paul Fournet Air Services facility at Lafayette Regional Airport in Lafayette, Louisiana. The remaining survey was flown out of Galveston, Texas.

Each survey was originally planned to include sea surface photography using a 70 mm format camera with black and white film, with emphasis on oceanic fronts. However, after the first series of photographs was evaluated and found to be inadequate (because they were taken at low altitude), discussions were initiated among MMS, SAIC, Aero-Marine Surveys and the Principal Investigator to define more fully the exact requirements for the photographic component of the program. It was decided that the stated altitude requirement (~3,000 m) for useful photographs was incompatible with safety requirements imposed by dropping expendable probes from an aircraft and that photography would be limited to occasions when the altitude requirement could be met without compromising the main part of the program. An opportunity to provide a substantial number of photographs was developed and was carried out successfully during the F08SLOPE survey in May 1993. No further photographic surveys were undertaken during the program.

2.3.2 Expendable Probes and Data Transmission

All of the AXCPs and AXCTDs were manufactured by Sippican, Inc., and the AXBTs were provided by two different manufacturers: Sparton of Canada, Ltd. and Hermes Electronics, Ltd. (now called Devtek Applied Electronics Inc.). The initial Sparton AXBTs (also known by the military designation AN/SSQ-36) were the same size deployment package as the standard "A-size" sonobuoy. Later shipments of probes received from both Hermes and Sparton were "A/3" or "F" in size. This change amounted to a 2/3 reduction in the overall

probe-package size carried on board the deployment aircraft. The reduction in size, however, did not affect the manufacturers' probe dimensions, shape and weight, but only the dimensions of the electronics component of the deployment package. Probe depth capabilities were 1500 meters for AXCPs, 1000 meters for AXCTDs and 800 meters for AXBTs. Each probe was equipped to broadcast data on one of three possible frequency channels and all three types of broadcast data (AXCP, AXCTD and AXBT) were received by an FM multi-channel sonobuoy receiving set (AN/ARR-75) on board the deployment aircraft.

2.3.3 Survey Summaries and Probe Performance

The twenty-one aerial surveys are listed in Table 2.3-1 and are shown in Figures 2.3-1a through 2.3-1u. Two of the surveys (F02SLOPE and F07SLOPE) included southerly excursions to drop AXBTs at the deep (3130 meter) LATEX A inverted echo sounder (IES) site (Mooring 43) along 92°W longitude. This was to provide calibration data in support of the mooring program. AXCPs were deployed during eight of the surveys and AXCTDs were deployed only during the last survey (F21SQUIRT).

Individual probe type performances were monitored and are also summarized in Table 2.3-1. Generally, the probes performed well with the exception of the first flights using A/3 (F-size) probes from Sparton (surveys F15SLOPE and F16SQUIRT). The data return for these particular probes during these two surveys was only 61.4 percent. All of the remaining Sparton A/3 probes were returned to the manufacturer for repair, and these re-worked probes, plus 15 additional replacement probes, were again provided by the manufacturer for later use. Subsequent surveys using the re-worked probes had a 97.0 percent data return.

The overall AXBT data return was 92.8 percent and that of the AXCPs was 84.5 percent. All six (100 percent) of the AXCTDs provided useful data. The AXCTDs had been provided by Sippican for use and evaluation as part of their AXCTD development program.

2.3.4 Horizontal and Vertical Parameter Plots

Horizontal plots of the twenty, fifteen and eight degree isotherm levels were contoured for each survey. These were used to clearly define the extent of the various cyclonic and anticyclonic features found in the study area. In addition, vertical section plots to 200 meters and to 800 meters depth were generated for all north-south temperature sections. Additional east-west vertical sections were only occasionally

Table 2.3-1. LATEX C aerial survey dates and expendable probe performance.

Flight ID	Dates		AXBTs		AXCPs	
	From	To	Used	Good	Used	Good
F01SLOPE	05/06/92	05/08/92	34*	34	-	-
F02SLOPE	08/07/92	08/09/92	35*	35	-	-
F03SEDDY	08/10/92	08/11/92	17*	17	5	4
F04LEDDY	10/11/92	10/12/92	16*	16	-	-
F05LEDDY	12/19/92	12/19/92	16*	16	-	-
F06SPECI	01/04/93	01/09/93	42*	41	10	7
F07SLOPE	01/21/93	01/22/93	35*	35	-	-
F08SLOPE	05/14/93	05/17/93	36**	36	-	-
F09SEDDY	05/18/93	05/19/93	15**	13	5	4
F10SLOPE	08/03/93	08/04/93	36**	35	-	-
F11LEDDY	08/05/93	08/05/93	16*	16	-	-
F12SLOPE	10/28/93	11/01/93	50**	42	-	-
F13SQURT	12/16/93	12/21/93	62**	56	16	15
F14LEDDY	12/23/93	12/23/93	16*	15	-	-
F15SLOPE	05/18/94	05/19/94	29**/10***	26**/7***	-	-
F16SQURT	05/20/94	05/24/94	22**/47***	18**/28***	11	8
F17SLOPE	08/13/94	08/14/94	23*/10***	22*/8***	-	-
F18LEDDY	10/15/94	10/15/94	3***	3	17	13
F19SEDDY	10/16/94	10/17/94	48***	46	-	-
F20SEDDY	11/04/94	11/08/94	69***	68	2	2
F21SQURT	11/11/94	11/16/94	72***	71	18	18
Total			**759**	**704**	**84**	**71**
Percent good			**92.8%**		**84.5%**	

* Sparton A
** Hermes A/3
*** Sparton A/3 (F-size)

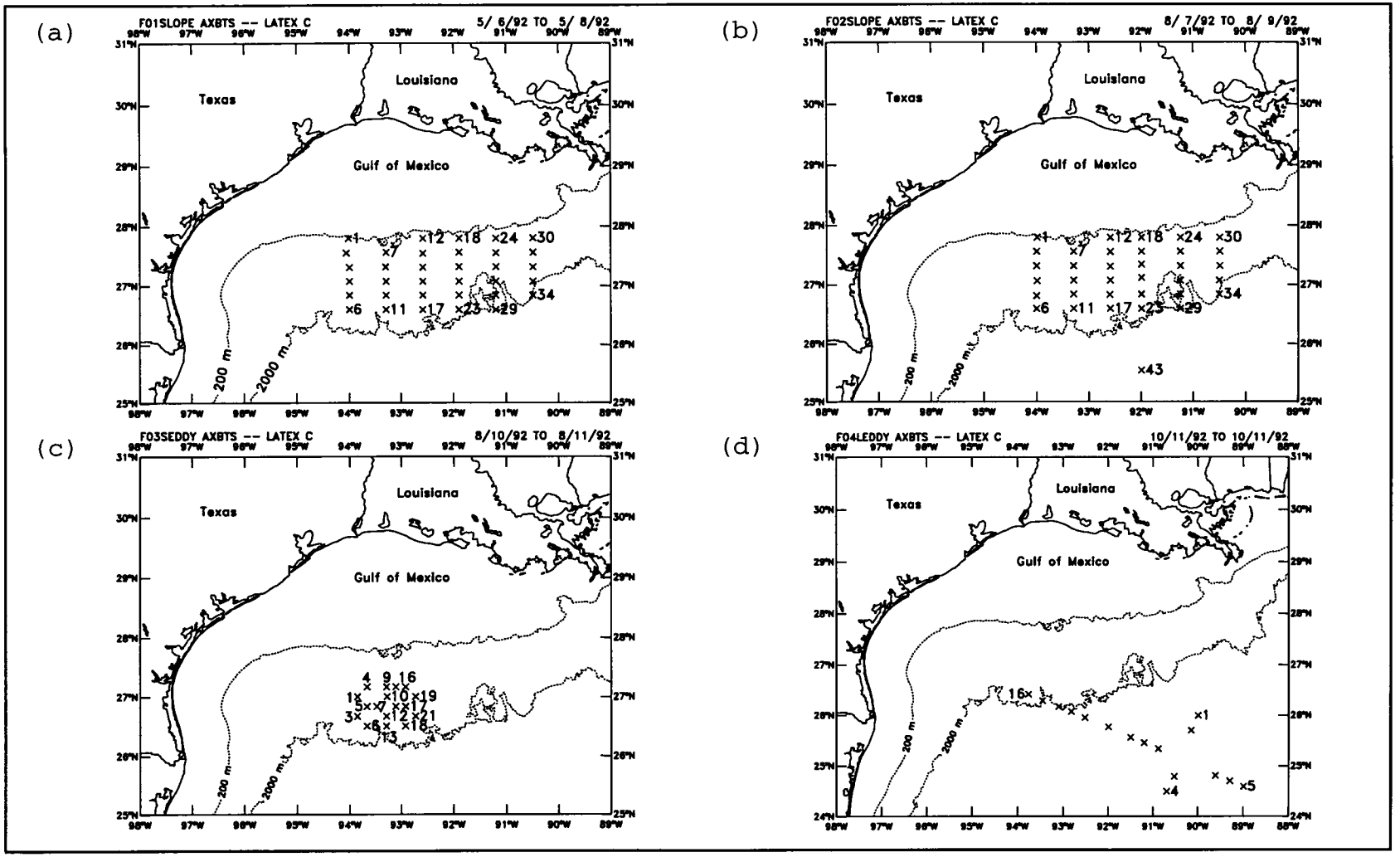

Figure 2.3-1a, b, c, d. Map showing station locations for: (a) F01SLOPE, (b) F02SLOPE, (c) F03SEDDY and (d) F04LEDDY aerial survey.

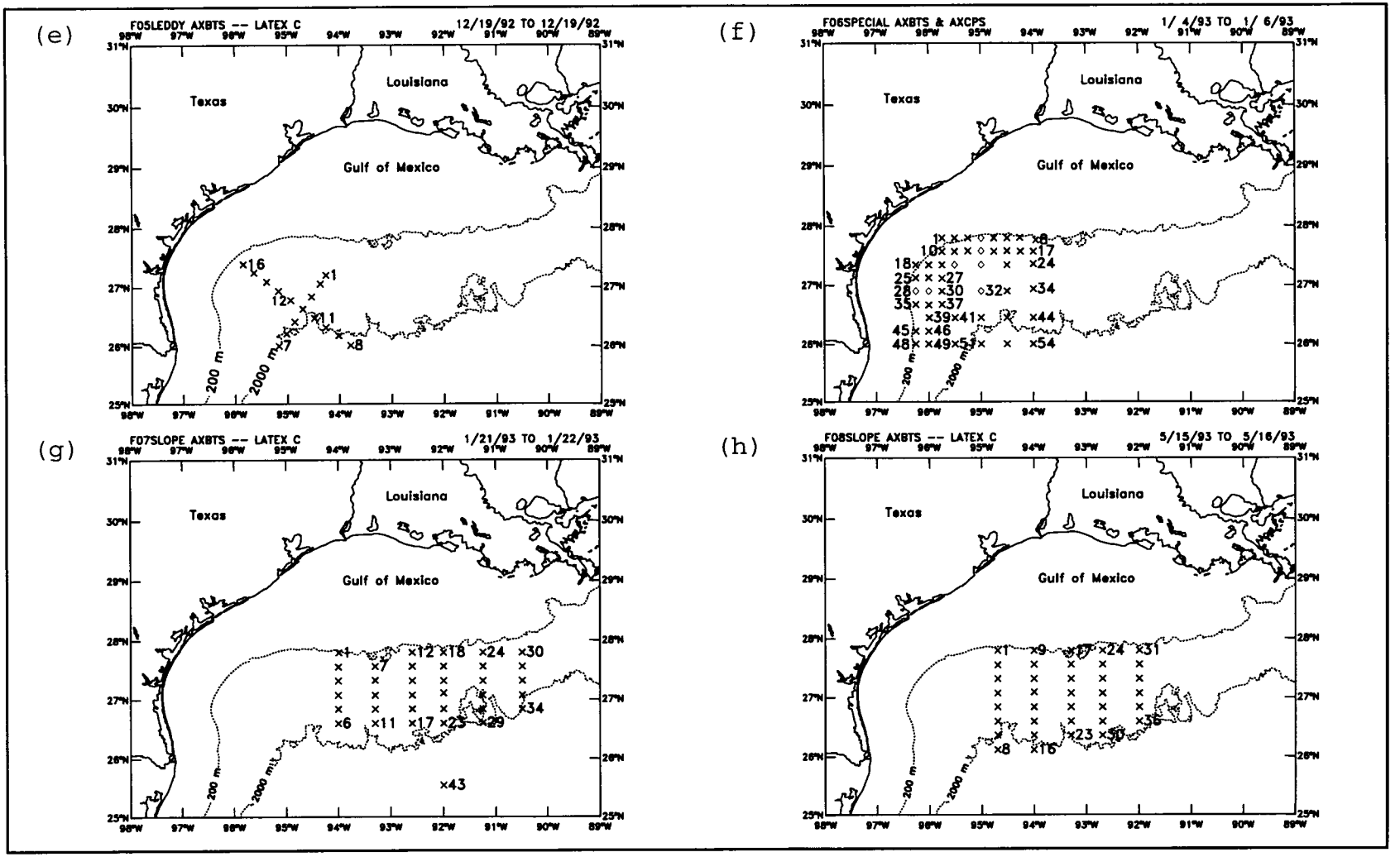

Figure 2.3-1e, f, g, h. Map showing station locations for: (e) F05LEDDY, (f) F06SPECIAL, (g) F07SLOPE and (h) F08SLOPE aerial survey.

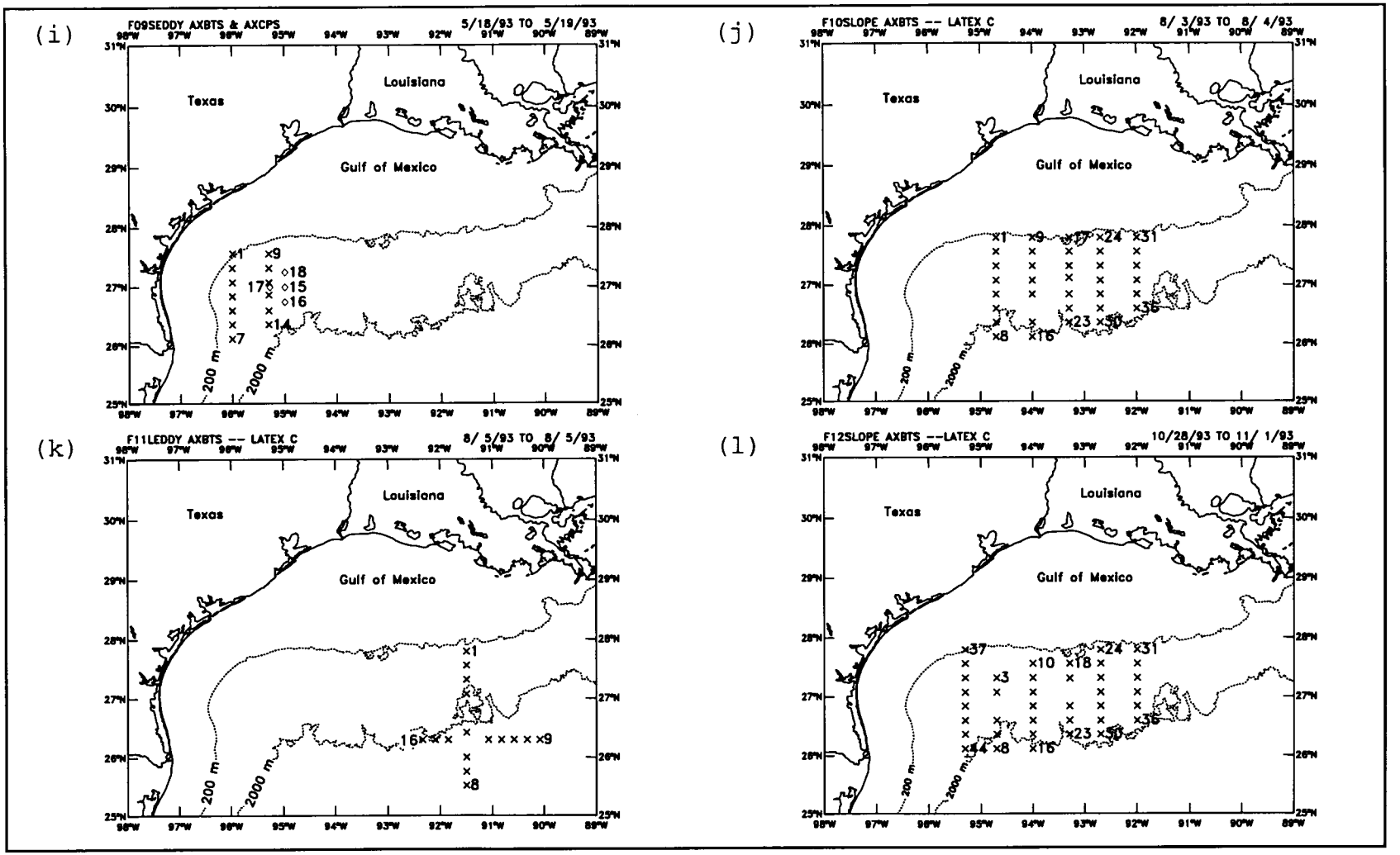

Figure 2.3-1i, j, k, l. Map showing station locations for: (i) F09SEDDY, (j) F10SLOPE, (k) F11LEDDY and (l) F12SLOPE aerial survey.

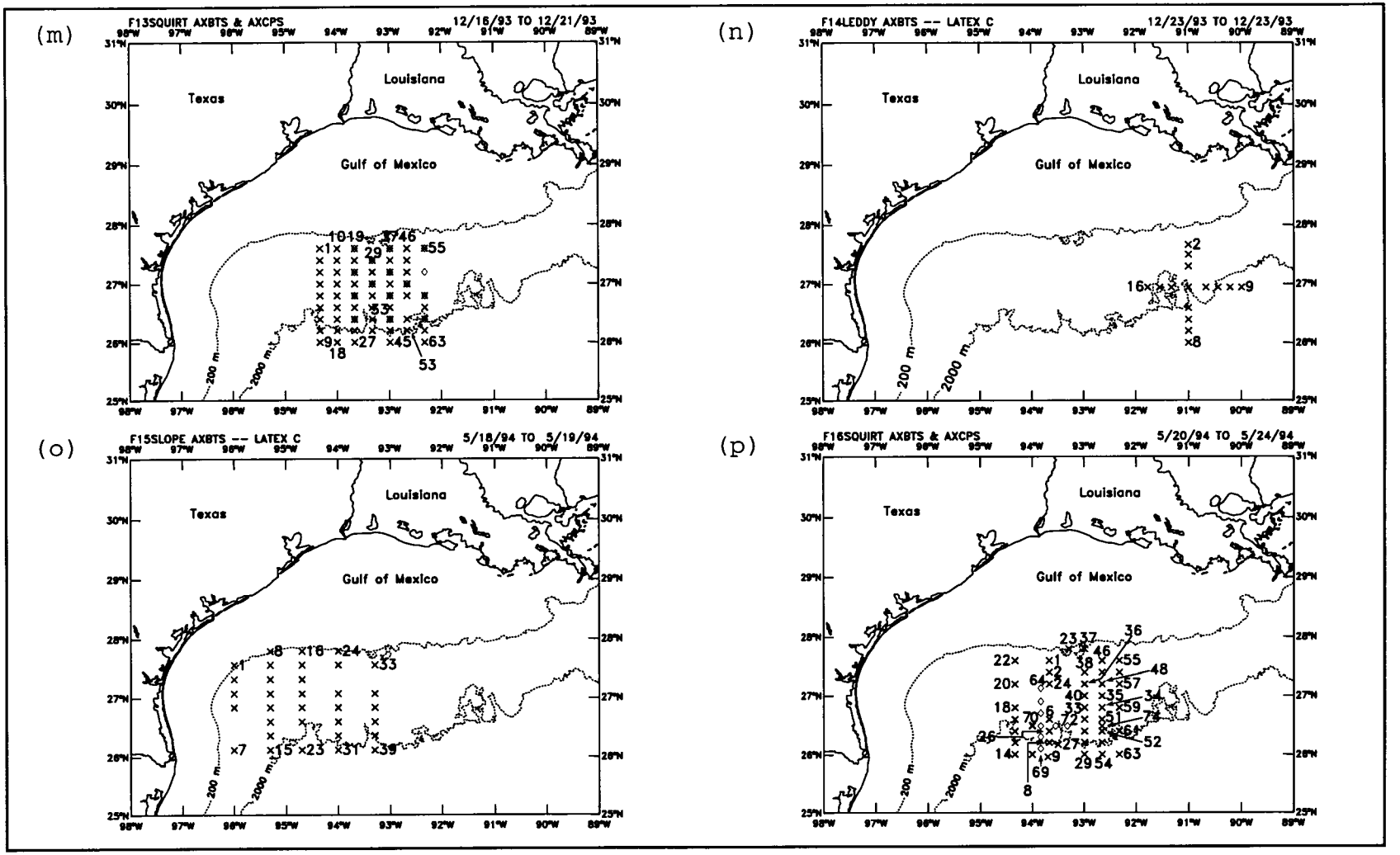

Figure 2.3-1m, n, o, p. Map showing station locations for: (m) F13SQUIRT, (n) F14LEDDY, (o) F15SLOPE and (p) F16SQUIRT aerial survey.

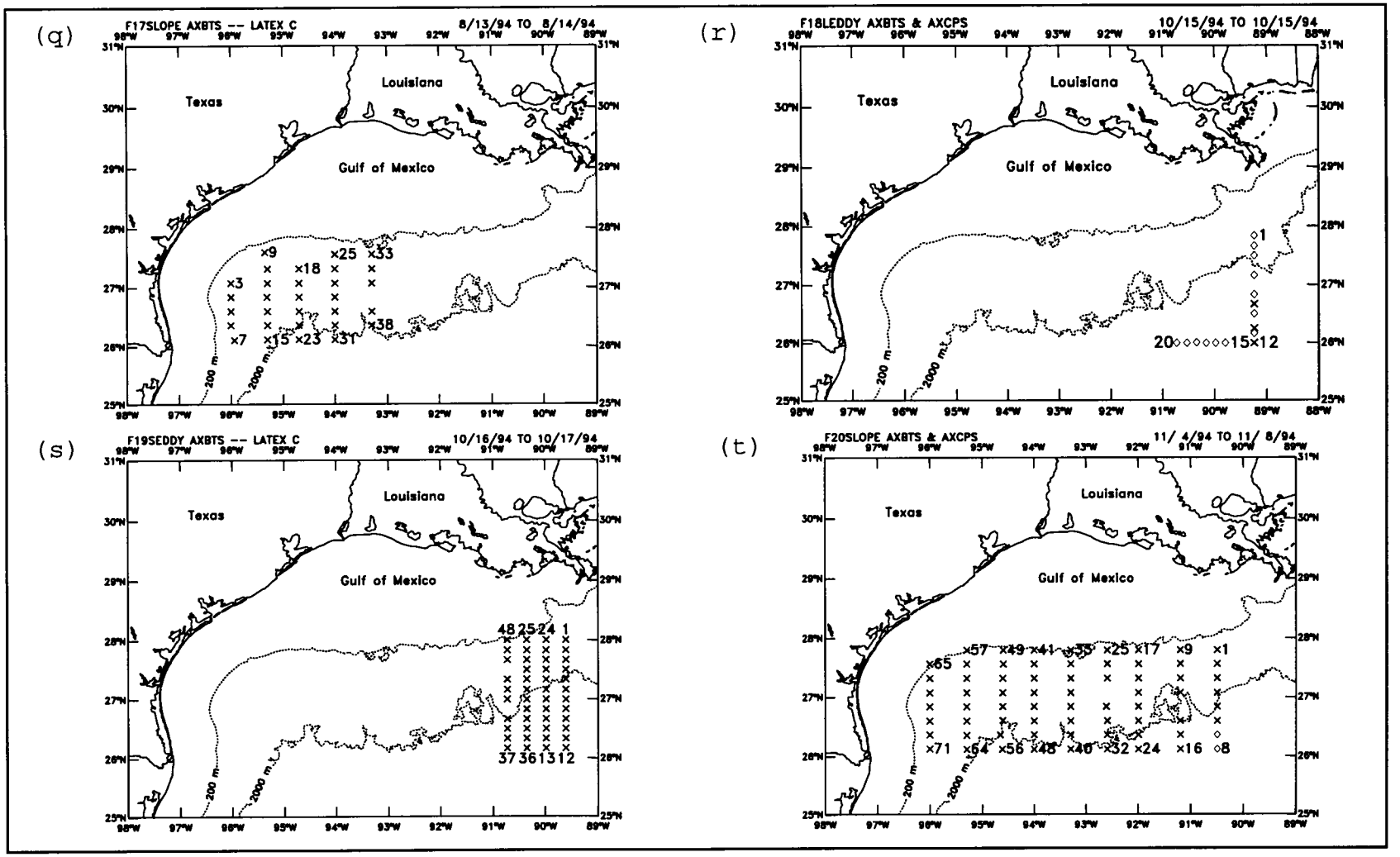

Figure 2.3-1q, r, s, t. Map showing station locations for: (q) F17SLOPE, (r) F18LEDDY, (s) F19SEDDY and (t) F20SLOPE aerial survey.

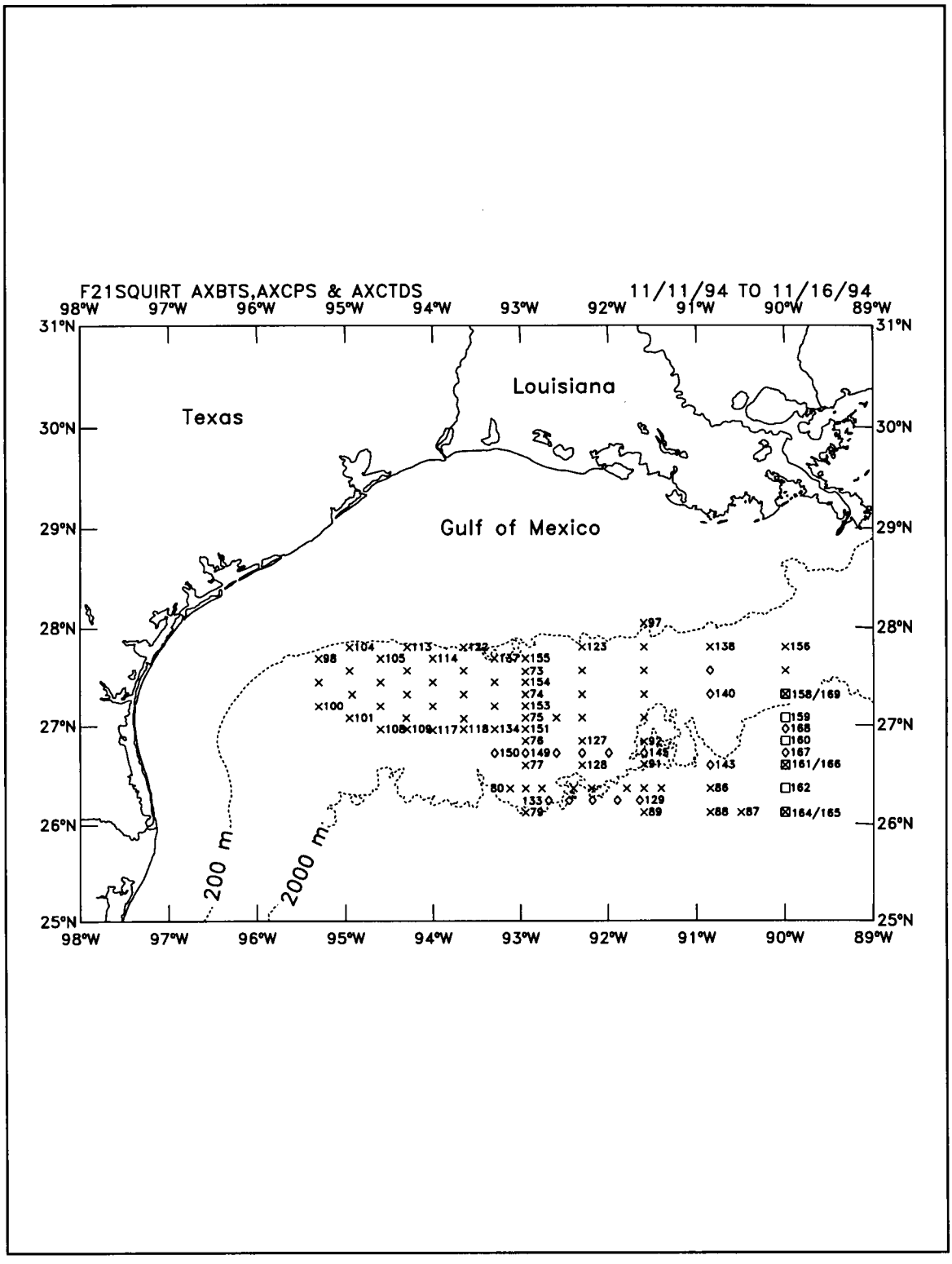

Figure 2.3-1u. Map showing station locations for F21SQUIRT aerial survey.

generated. Vertical section plots were also generated for current shear data when reasonable useful sections could be assembled from the small number of probes deployed on each applicable survey. Otherwise, individual current shear profile plots were generated. Representative examples of these type plots are presented in Figures 2.3-2 through 2.3-5.

2.4 GEOSAT Altimeter Data

2.4.1 Introduction

From March 1985 to January 1990 the U. S. Navy altimeter satellite GEOSAT collected observations of the global oceans at unprecedented spatial and temporal resolution. The acronym GEOSAT was derived from *geodetic satellite* because the primary mission of the satellite was to map the marine geoid at high spatial resolution. This mission was completed during the first 18 months (March 30, 1985 to September 30, 1986) of satellite operation and is referred to as the Geodetic Mission (GM). In October 1986 the satellite was maneuvered into a 17-day exact repeat orbit to collect data along the previously sampled Seasat ground tracks. This so-called Exact Repeat Mission (ERM) began on November 8, 1986 and continued until the satellite ultimately failed in January 1990.

Necessary information to use GEOSAT data for oceanographic research is contained in geophysical data records (GDRs) released by the National Oceanographic Data Center (NODC) on CD-ROM. These data have been acquired and include the complete historical data set collected during GEOSAT's operational lifetime from March 30, 1985 to December 31, 1989.

2.4.2 Historical Data

2.4.2.1 GEOSAT Geodetic Mission Data

The goal of the primary mission of GEOSAT, the Geodetic Mission (GM), was to map the global ocean mean sea surface topography by altimetric sampling along a high spatial resolution nonrepeating ground track. This mission lasted from March 30, 1985 to September 30, 1986. Absolute height measurements from these data were originally classified because of the military significance of the data, and initially only crossover differences of the altimetric height were released. The entire GEOSAT GM data set was declassified in the summer of 1995, due in large part to the public availability of altimeter observations from the European Space Agency satellite ERS-1. The ERS-1 altimeter had just completed the geodetic phase of its mission in March 1995, completing two cycles of a 168-day repeat orbit for mapping

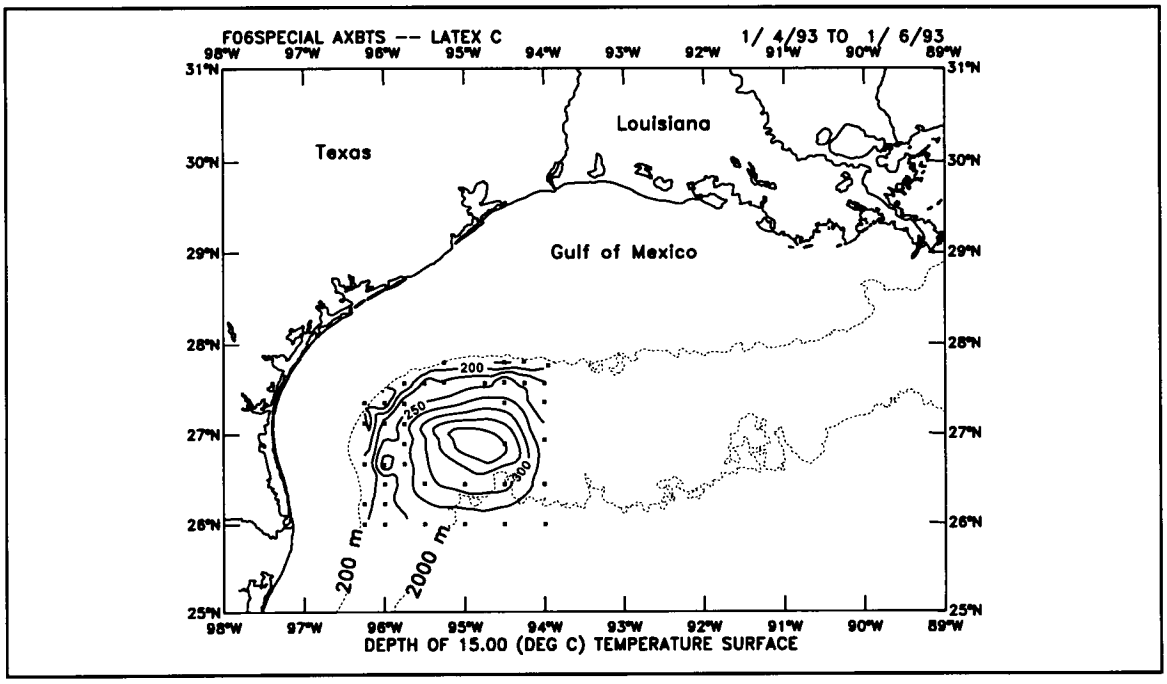

Figure 2.3-2. Example of horizontal plot of the 15°C surface from AXBT data (plot shows a Loop Current eddy centered near 27°N lat., 95°W long.).

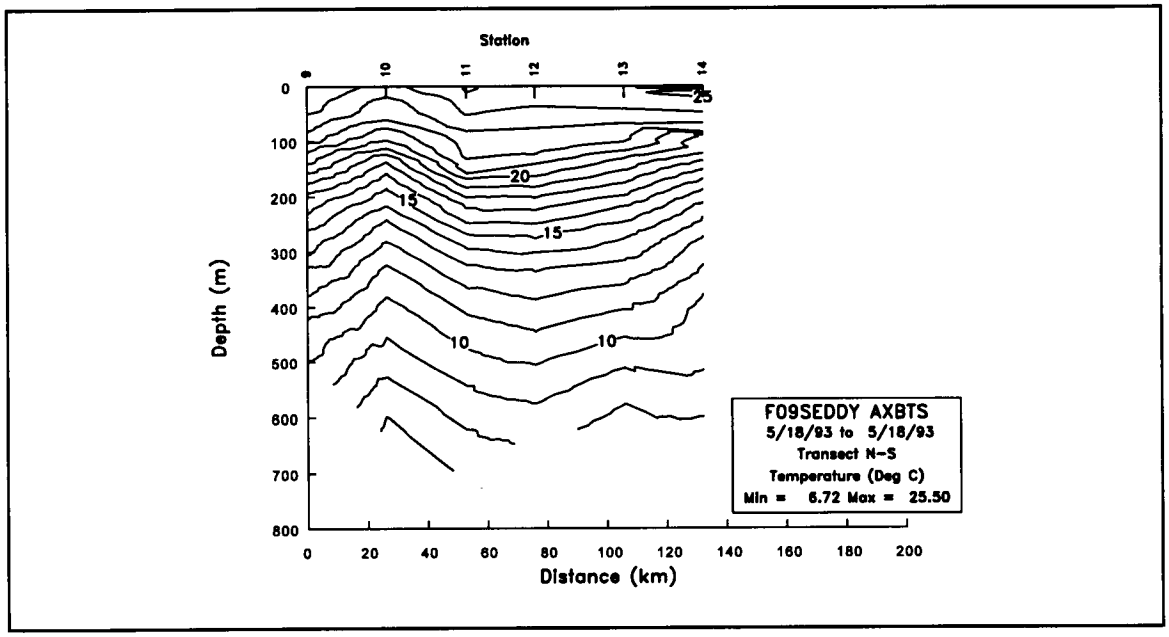

Figure 2.3-3. Example of vertical section plot of temperature from AXBT data (plot shows a cyclonic slope eddy centered at station 10 and an anticyclonic Loop Current eddy centered at station 12 along this section). See Figure 2.3-1i for survey location.

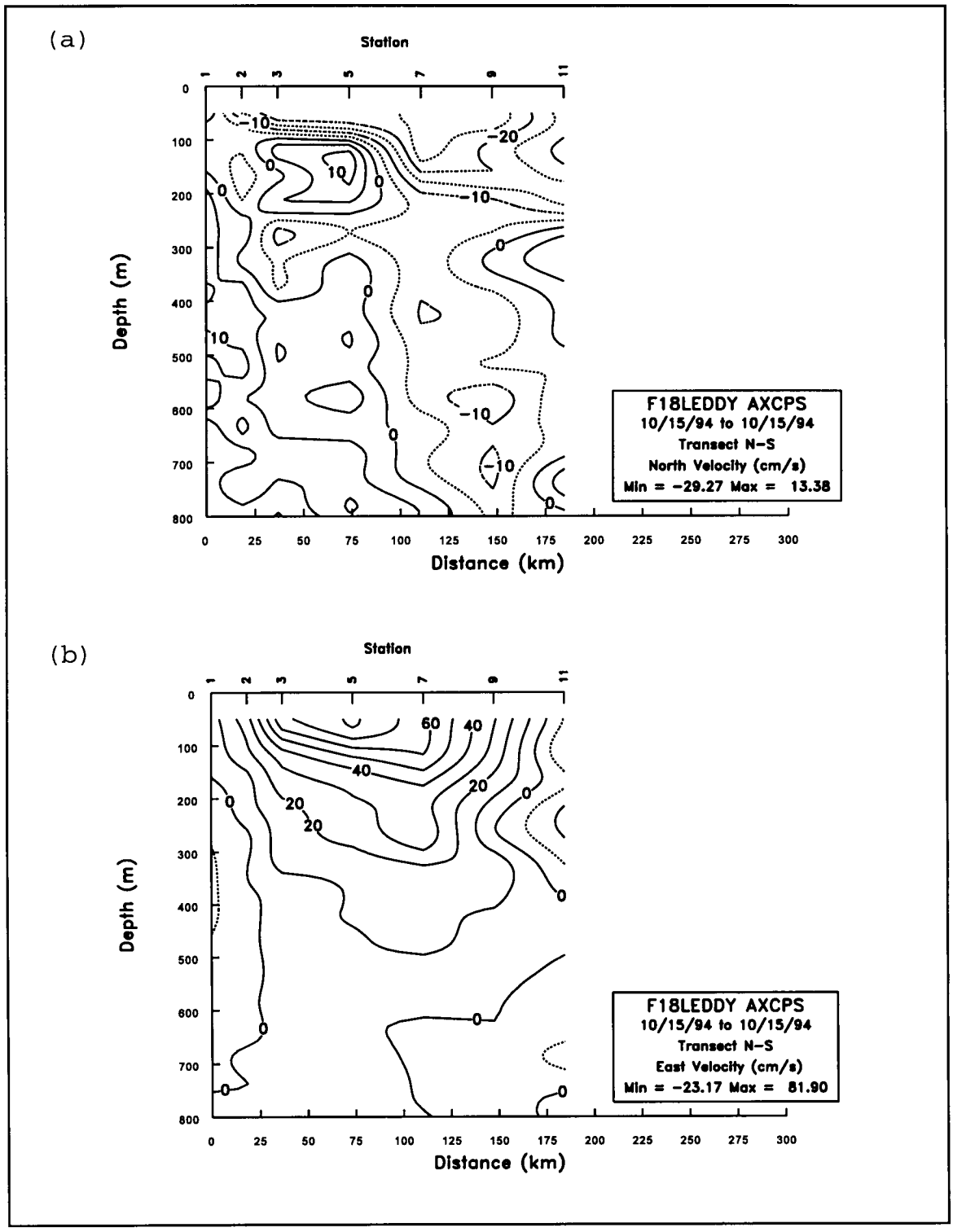

Figure 2.3-4. Example of vertical section plot of (a) north-south component and (b) east-west component of relative velocity from AXCPs deployed in a Loop Current eddy. See Figure 2.3-1r for survey location.

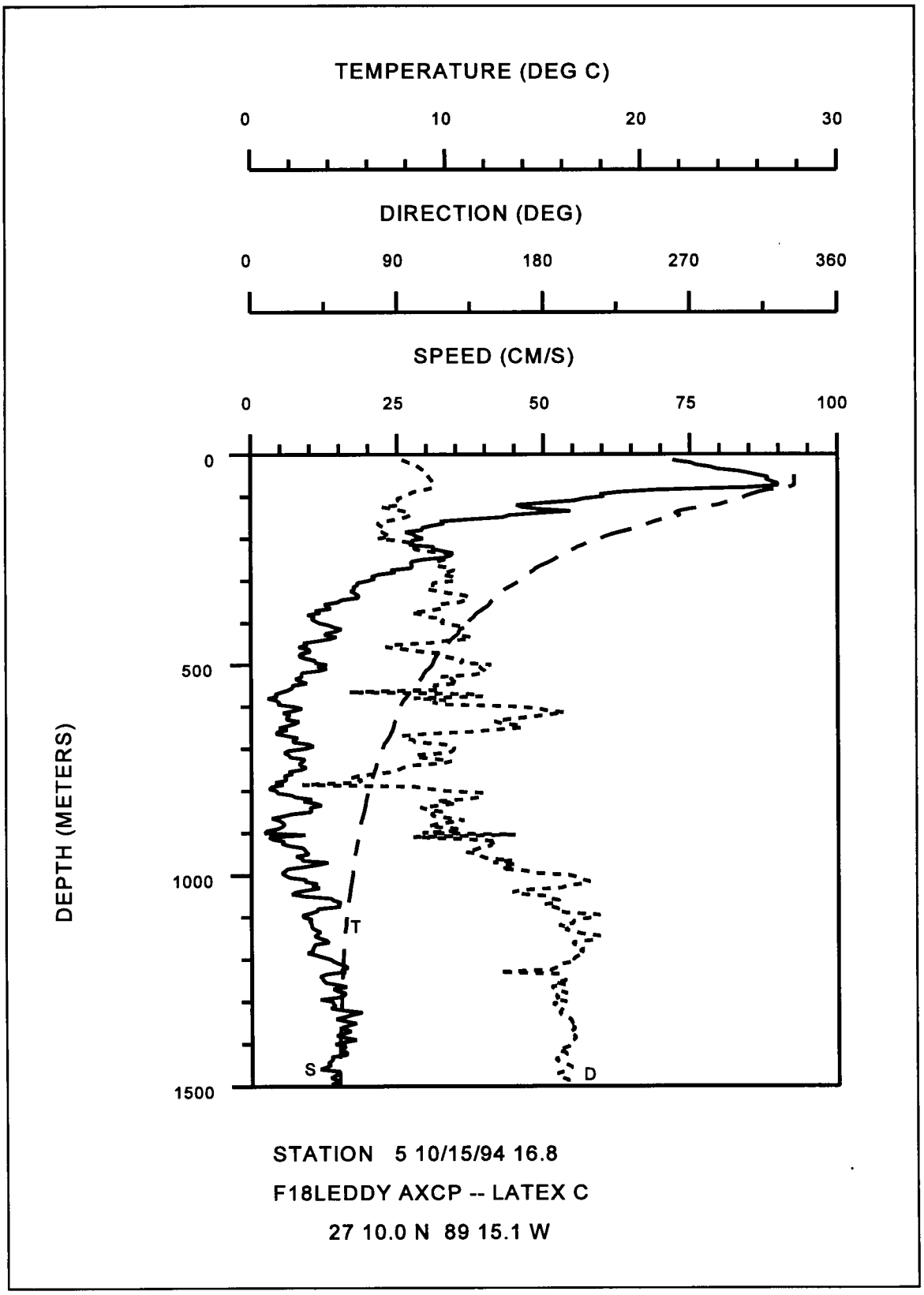

Figure 2.3-5. Example of an individual AXCP profile.

the ocean topography. The declassified GEOSAT data were processed into a standard GEOSAT altimeter geophysical data record (GDR) format and released by the National Oceanographic Data Center on CD-ROMs in October 1995.

In order to produce a high resolution map of the marine geoid, the GM was based on a 23-day near-repeat orbit which was permitted to drift, ultimately producing a dense spatial sampling of the global ocean topography. This 23-day near-repeat period is the cycle interval used for the mapping of oceanic circulation variability during the GM. A sample GM cycle is shown in Figure 2.4-1. In all, 24 cycles of data were collected during the time period from March 30, 1985 to September 30, 1986. Ground track/data coverage maps for each 23-day near-repeat cycle can be found in Cheney et al. (1991a).

Two GM altimeter data sets have been released by NODC: 1) GEOSAT altimeter crossover differences geophysical data records (XGDRs) from the GM and the first year of the ERM, and 2) GEOSAT Geodetic Mission GDRs. The declassification of along-track GM GDRs has made it possible to reference GM data relative to an existing mean surface, allowing consistent along-track analysis and comparison of the sea surface height variability observed by GEOSAT in the Gulf of Mexico (Leben and Born 1995). This obviates the use of crossover data for the retrospective analysis of GEOSAT altimeter data presented in this report. The four NODC CD-ROMs titled "U.S. Navy GEOSAT Geodetic Mission Altimeter Data (GDRs) Geodetic Mission" were acquired (CD-ROMs NODC-60 through NODC-63). These contain the complete GEOSAT GM GDRs which include sea surface heights, backscatter coefficients (from which wind speed is derived) and wave heights. GEOSAT GM crossover data were also acquired from NODC which released the data on CD-ROMs titled "U.S. Navy GEOSAT Altimeter Crossover Differences from the Geodetic Mission." The crossover data in the Gulf of Mexico (CD-ROMs NODC-11 & 12) were used for initial analyses performed before the along-track data became declassified (Leben and Born 1993).

2.4.2.2 GEOSAT Exact Repeat Mission Data

In October 1986, GEOSAT was maneuvered into a 17-day exact repeat orbit to begin the ERM on November 8, 1986. The ERM ground track over the Gulf Of Mexico is shown in Figure 2.4-2. GEOSAT completed 62 exact repeat cycles before the on-board tape recorder failed in October 1989. A limited amount of data in the Gulf of Mexico was subsequently collected by direct broadcast. Degradation of the altimeter output power eventually ended the GEOSAT Mission by January 1990. Ultimately 68 cycles of ERM data were collected. Ground track/

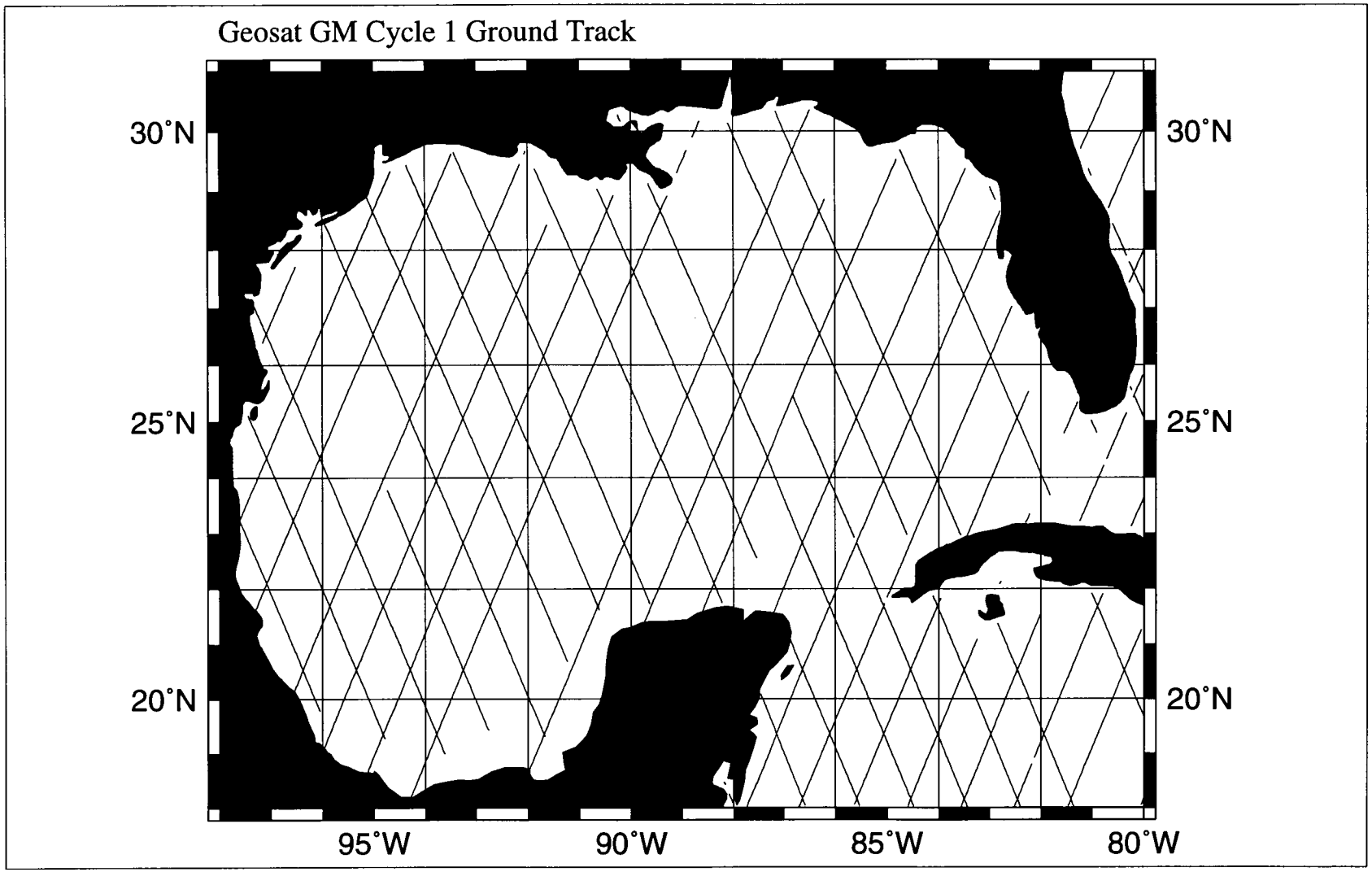

Figure 2.4-1. Sample ground track/data coverage for the 23-day near repeat orbit used during the GEOSAT Geodetic Mission(GM). GM Cycle 1 is shown.

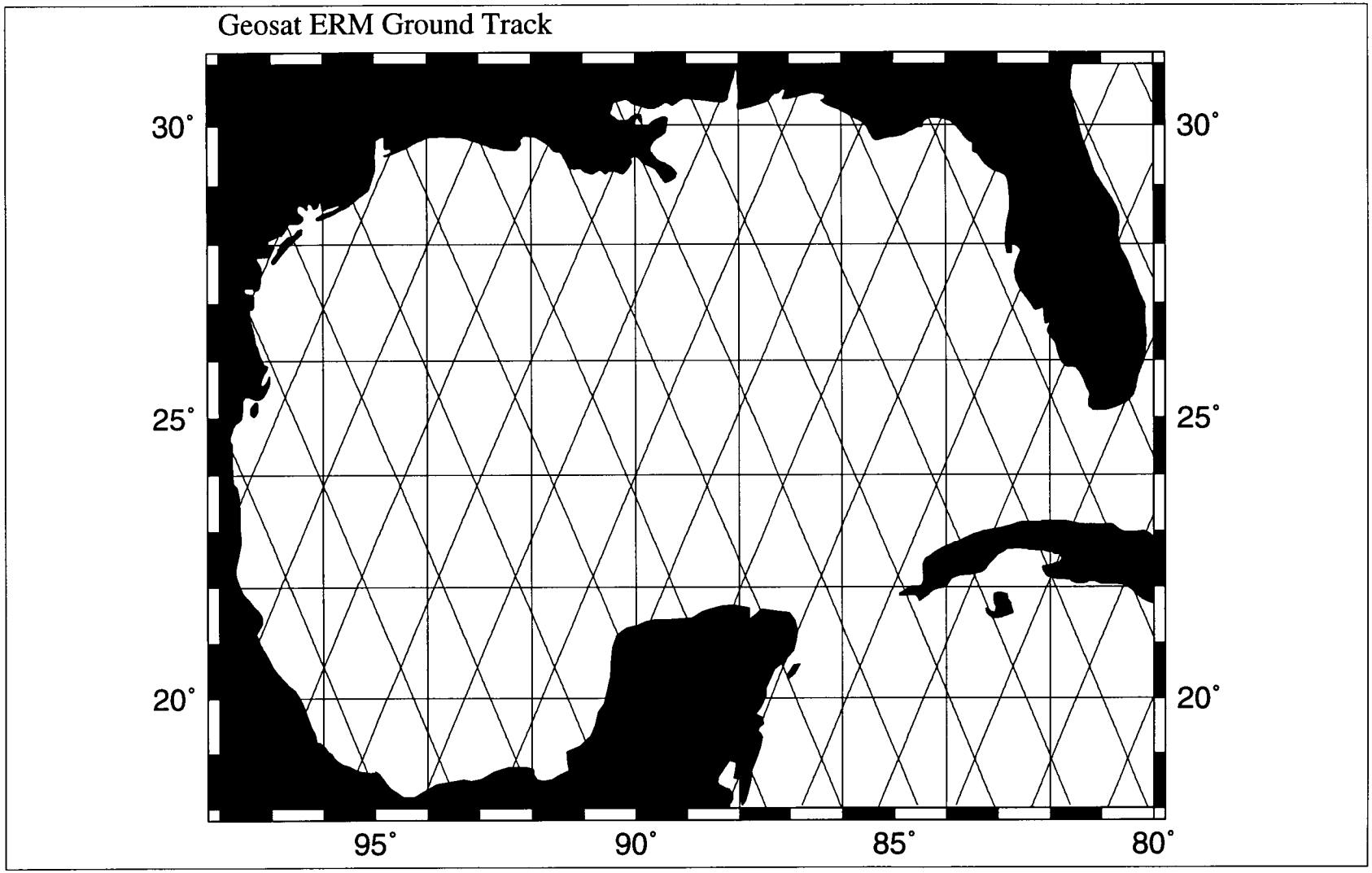

Figure 2.4-2. GEOSAT Exact Repeat Mission (ERM) 17-day exact repeat orbit ground track over the Gulf of Mexico.

data coverage maps for each 17-day repeat cycle can be found in Cheney et al. (1991b).

The complete GEOSAT ERM data set is contained on six NODC CD-ROMs titled "U.S. Navy GEOSAT Altimeter Data (T2 GDRs) from the Exact Repeat Mission" (CD-ROMs NODC-04 through NODC-09). These were acquired for subsequent processing to determine sea surface heights, wind speed and wave heights during the ERM.

2.4.2.3. GEOSAT Global Wind/Wave Data

In 1988 the U. S. Navy released the backscatter coefficient, σ_0 (from which wind speed is derived) and the significant wave height data collected during the Geodetic Mission. These data were released by NODC on a CD-ROM titled "U.S. Navy GEOSAT Global Wind/Wave Data" (CD-ROM NODC-36) and were acquired for initial processing of wind speed and wave height. Radar backscatter and significant wave height were also included on the GM GDRs later released by NODC. The wind speed and wave height analyses in this report are based on the data from the GM and ERM GDRs.

2.5 Ancillary Data

2.5.1 Introduction

A number of sources of ancillary data were available from complimentary programs coincident in time with the LATEX C field effort. Many of these programs were supported, at least in part, by the U.S. Department of the Interior, Minerals Management Service, as part of, or supplemental to, the Louisiana/Texas Shelf Physical Oceanography Program. These programs and the applicable data are discussed below. A time line is presented in Figure 2.5-1.

2.5.2 LATEX A Current Meter Data

Current meter measurements were made at fourteen different shelf-edge sites over the course of the LATEX A field program (see Figure 2.5-2 and Table 2.5-1). At most sites, measurements were made near surface (approximately 12 meters), mid-depth (100 meters) and near bottom (190 or 495 meters). Endeco Type 174 current meters were used at the near-surface level and Aanderaa RCM 4,5,7 and 8s were used at the lower levels. Two of the mooring locations (45 and 47) were discontinued part way through the program. In addition, two IESs, at stations 42 and 43 (not shown), were expected to, but did not, provide useful eddy tracking data at two deeper offshore sites along 92°W longitude. A time line for each of the mooring instrument levels is presented in Figure 2.5-4.

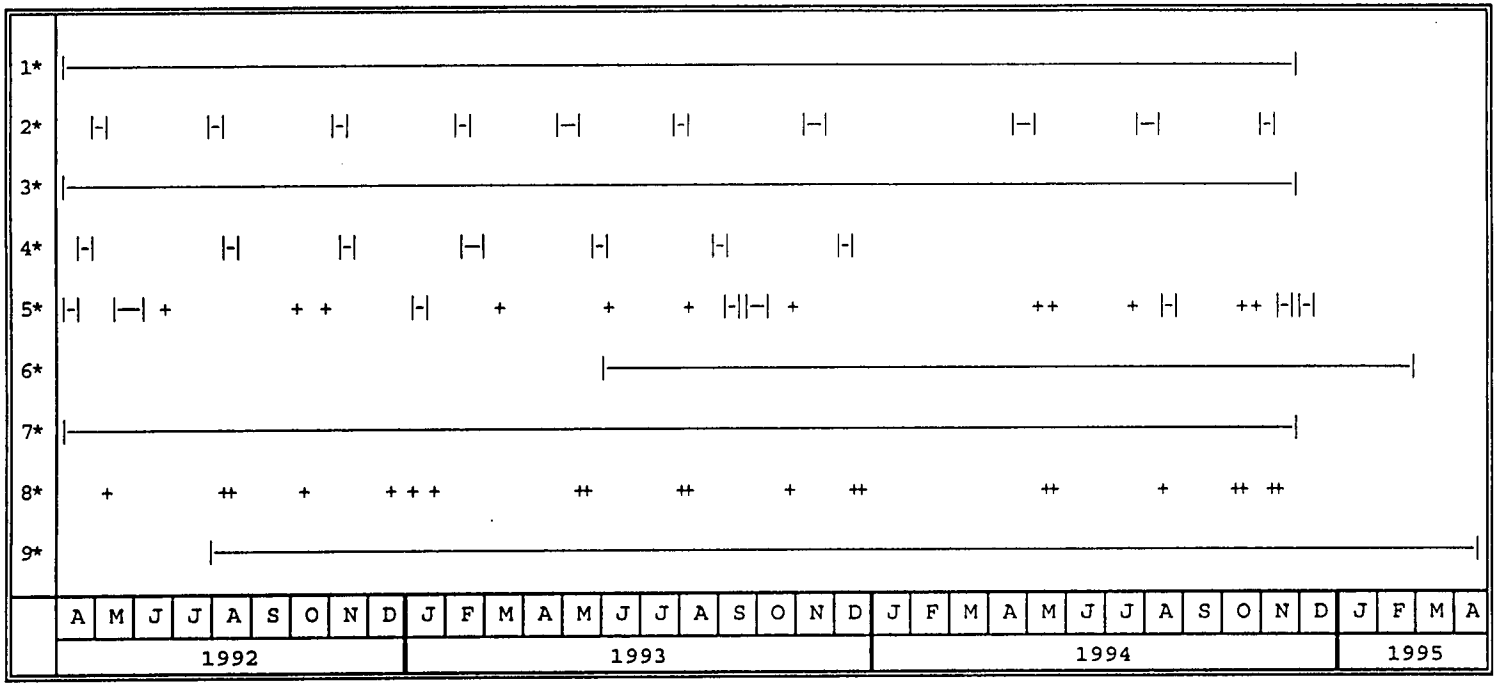

1* LATEX A (CMS)
2* LATEX A (HYDRO)
3* LATEX B (AVHRR)
4* GULFCET (HYDRO)
5* SOOP/TIGER (HYDRO)
6* SCULP (DRIFTERS)
7* TOPEX/ERS-1 (ALTIMETRY)
8* LATEX C (FLIGHTS)
9* LATEX C (DRIFTERS)

Figure 2.5-1. Time line showing ancillary data and LATEX C data collection periods.

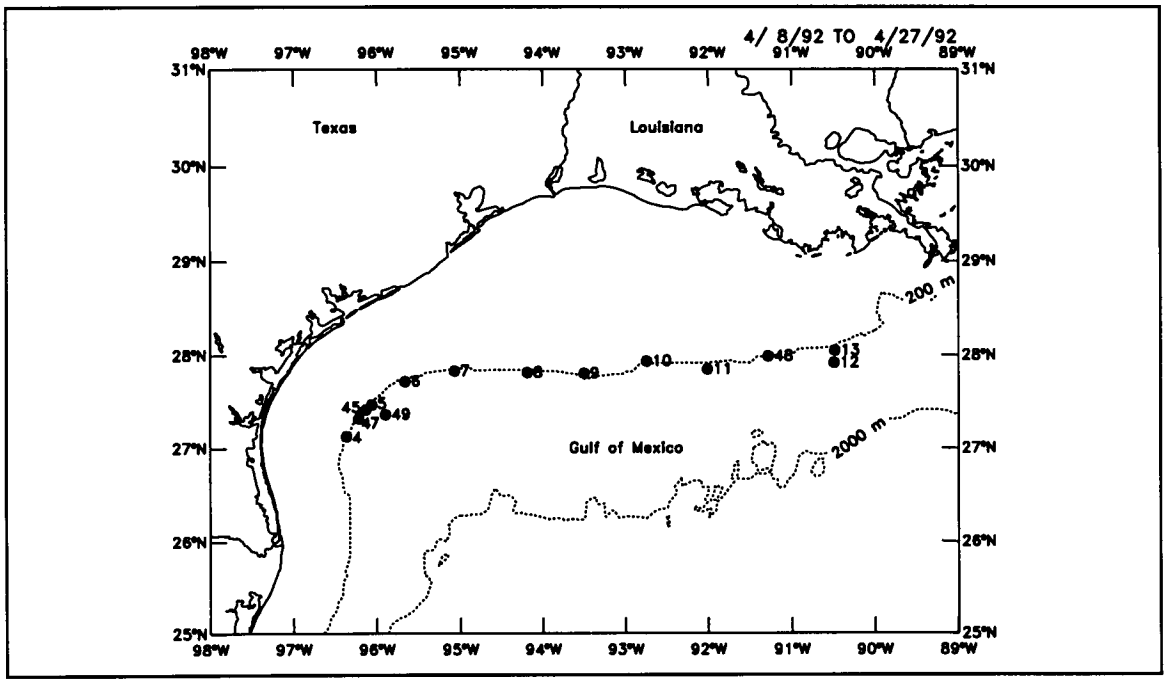

Figure 2.5-2. Map showing LATEX A shelf-edge current meter mooring locations.

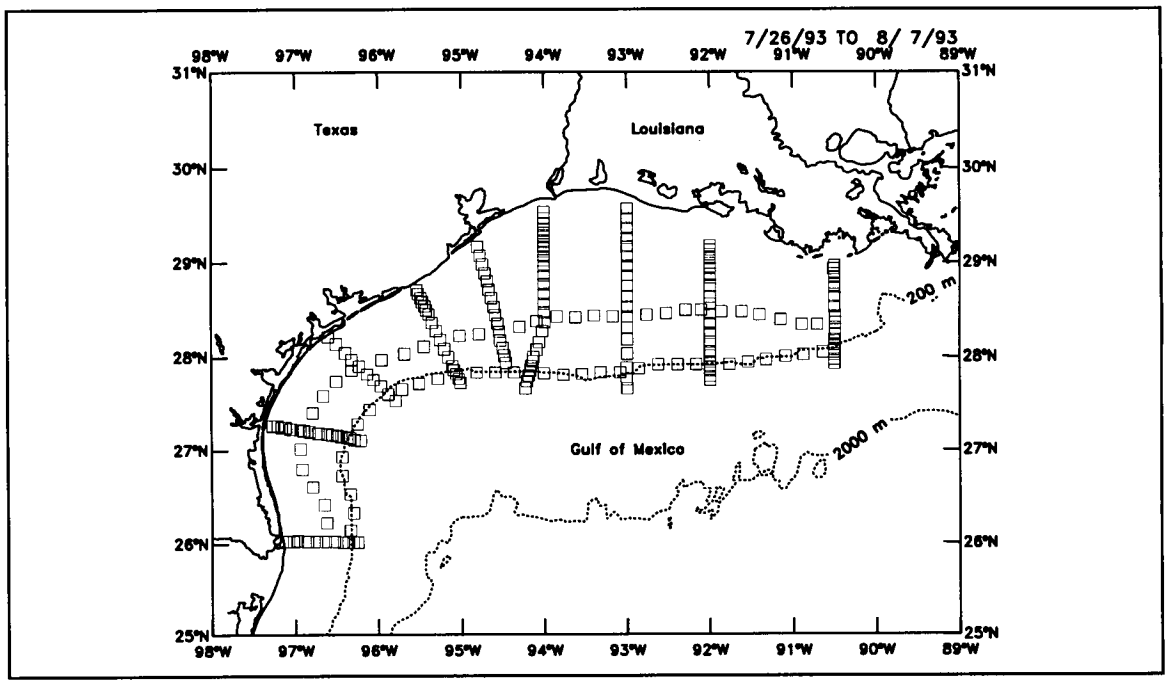

Figure 2.5-3. Map showing an example of a typical LATEX A Louisiana-Texas shelf hydrographic survey [station locations are plotted for cruise H06CPW9311 (26 July - 8 August 1993)].

Table 2.5-1. LATEX A shelf-edge current meter mooring locations and instrument levels (April 1992 - November 1994).

Mooring No.	Water Depth (m)	Location		Instrument Levels (m)
		Latitude (N)	Longitude (W)	
04	201	27° 07.76'	96° 21.63'	12, 100, 190
05	199	27° 27.82'	96° 04.12'	12, 100, 190
06	201	27° 42.59'	95° 39.76'	12, 100, 190
07	199	27° 50.12'	95° 04.19'	12, 100, 190
08	200	27° 49.47'	94° 10.77'	12, 100, 190
09	200	27° 48.92'	93° 31.91'	12, 100, 190
10	200	27° 56.07'	92° 44.70'	12, 100, 190
11	200	27° 50.64'	92° 00.45'	12, 100, 190
12	505	27° 55.76'	90° 29.64'	12, 100, 495
13	200	28° 03.48'	90° 29.18'	12, 100, 190
45*	200	27° 25.09'	96° 07.59'	12, 190
47*	200	27° 19.30'	96° 12.77'	12, 100, 190
48	200	27° 58.98'	91° 16.99'	12, 100, 190
49	505	27° 23.13'	95° 53.96'	12, 100, 495

* Mooring location discontinued part way through the field program.

2.5.3 LATEX A Hydrographic and ADCP Data

Ten shelf hydrographic surveys were conducted as part of the LATEX A field program. A Sea-Bird SBE-911*plus* CTD and a hull-mounted RD Instruments acoustic Doppler current profiler (ADCP) were used on each cruise. The first four of these cruises (ending in February 1993) were made only on the Louisiana shelf (extending as far west as 94°W longitude) and the last six cruises (ending in November 1994) were made on both the Louisiana and Texas shelves. The survey periods are identified in Table 2.5-2, and an example of a typical hydrographic/ADCP cruise track with station locations for one of the more extensive Louisiana-Texas surveys is presented in Figure 2.5-3 (see page 39). Four of the ten surveys were coincident in time with LATEX C aerial surveys conducted off the shelf break.

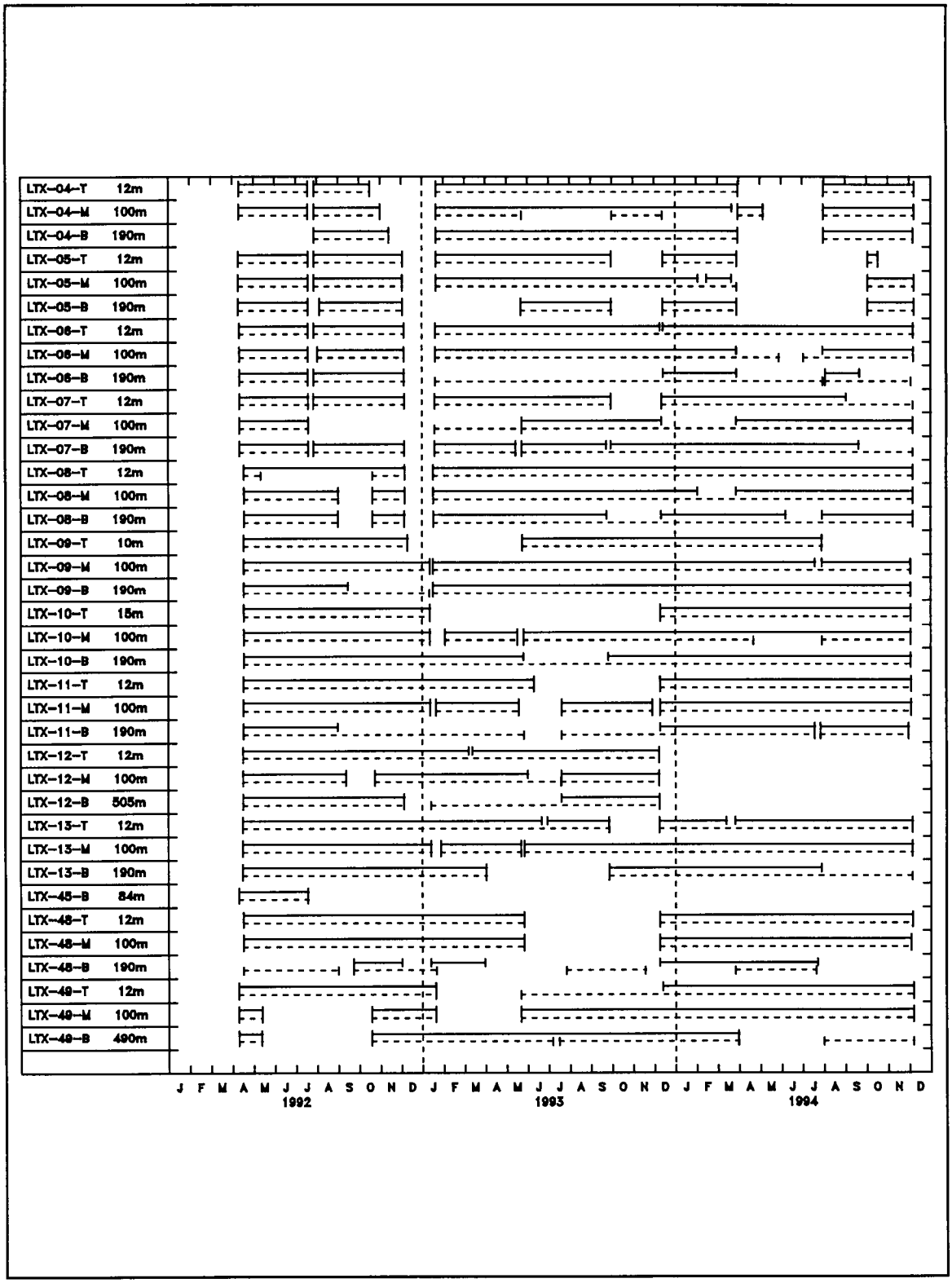

Figure 2.5-4. Time line for LATEX A shelf-edge current meter levels.

Table 2.5-2. LATEX A hydrographic cruises.

Cruise ID	Dates		CTDs
	From	To	
H01CGY9205*	04/30/92	05/09/92	114
H02CGY9211*	07/31/92	08/09/92	124
H03CPW9210	11/04/92	11/13/92	114
H04CGY9302	02/04/93	02/13/93	119
H05CPW9306	04/26/93	05/11/93	215
H06CPW9311*	07/25/93	08/07/93	215
H07CPW9314	11/06/93	11/22/93	238
H08CGY9401	04/23/94	05/07/94	170
H09CPW9410	07/26/94	08/07/94	171
H10CGY9409*	11/01/94	11/14/94	170

* Coincident in time with LATEX C aerial survey.

2.5.4 LATEX B AVHRR Imagery Data

Periodically, over the course of the LATEX C field effort, imagery were obtained on an as-needed basis from the LATEX B component to aid in scheduling and planning the AXBT surveys. These images were helpful in locating the specific features (i.e. Loop Current eddies, squirts and jets and slope eddies) to be surveyed. No record was maintained, however, of the time and ID of the various images that were used, though, as a general rule, images were reviewed a few days before each survey.

2.5.5 Ship-of-Opportunity XBT Data

Fifty-six cases of XBT-7 or T-7 XBT probes (672 probes) were shipped to various investigators over the course of the field effort. Most of the resulting data contributed to other ancillary data sets such as the GulfCet and SOOP/TIGER hydrographic programs described below. Table 2.5-3 summarizes the probe shipments. Twenty-eight cases each of Sparton (XBT-7) and Sippican (T-7) probes were provided.

Table 2.5-3. LATEX C XBT-7 and T-7 XBT shipments.

No. Cases	Manufacturer	Date Shipped	Consignee	Program
4	Sparton	04/09/92	G. Fargion (TAMU)	GulfCet
4	Sparton	04/20/92	M. Dagg (LUMCON)	NECOP*
3	Sparton	05/05/92	D. Biggs (TAMU)	SOOP/TIGER
2	Sparton	07/08/92	W. Nowlin (TAMU)	LATEX-A (Hydro)
1	Sparton	09/31/92	D. Biggs (TAMU)	SOOP/TIGER
1	Sparton	10/12/92	D. Biggs (TAMU)	SOOP/TIGER
2	Sparton	03/01/93	D. Biggs (TAMU)	SOOP/TIGER
1	Sparton	03/23/93	G. Fargion (TAMU)	GulfCet
6	Sparton	10/27/93	D. Wiesenburg (TAMU)	LATEX-A (Hydro)
4	Sparton	11/22/93	G. Fargion (TAMU)	GulfCet
3	Sippican	04/02/94	D. Biggs (TAMU)	SOOP/TIGER
1	Sippican	07/05/94	B. Hamilton (EH)	LATEX-A (Mooring)
4	Sippican	09/26/94	D. Biggs (TAMU)	SOOP/TIGER
5	Sippican	10/12/94	C. Neuhard (TAMU)	LATEX-A (Hydro)
2	Sippican	10/12/94	D. Biggs (TAMU)	SOOP/TIGER
3	Sippican	10/13/94	D. Biggs (TAMU)	SOOP/TIGER
10	Sippican	11/08/94	D. Biggs (TAMU)	SOOP/TIGER
56	**TOTAL NO. CASES**			

* NECOP = Nutrient Enrichment Coastal Ocean Program.

2.5.6 GulfCet Hydrographic Data

Seven hydrographic surveys, beginning in April 1992 and ending in December 1993, were conducted as part of the GulfCet program. This effort was funded by the Minerals Management Service to study the "Distribution and Abundance of Marine Mammals in the North-Central and Western Gulf of Mexico". Each survey was conducted over parts of a master station plan consisting of a total of 143 possible stations distributed along 14 north-south sections (see Figure 2.5-5). The sections extended from the 100 to 2000 m isobaths and from approximately 96°10'W longitude to 87°30'W longitude. CTD casts were made using a Sea-Bird SBE-911*plus* CTD at the 100

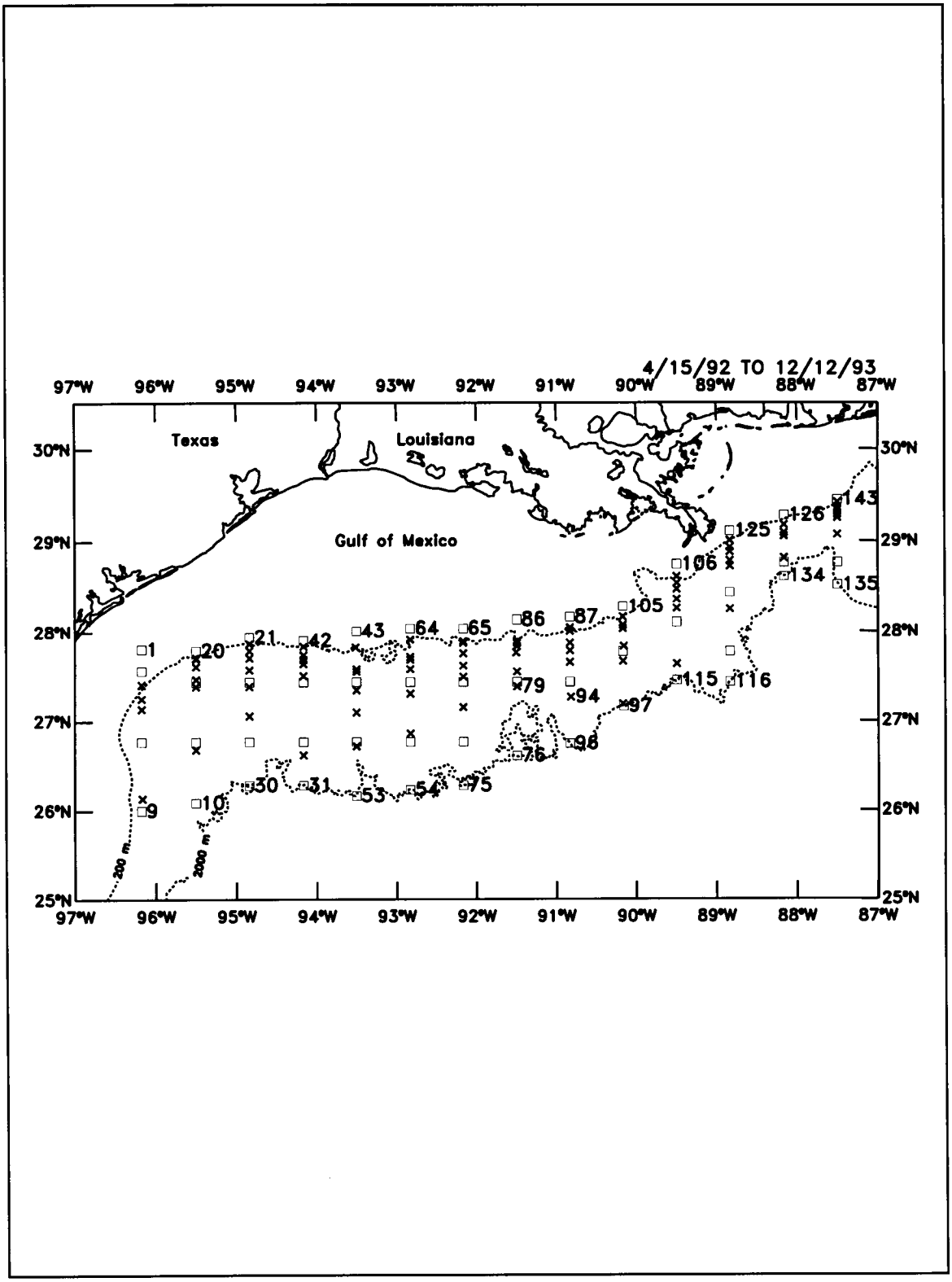

Figure 2.5-5. Map showing GulfCet master station plan. CTDs are indicated by squares and XBTs by crosses.

and 2000 m isobaths and at 40 nautical mile intervals along each section. XBTs manufactured by Sparton of Canada, Ltd. were deployed at the 200, 350, 500, 800, 1000 and 1500 m isobaths along these same sections. Table 2.5-4 summarizes the cruise dates and the number of stations occupied during each cruise. One of the seven cruises coincided in time with LATEX C aerial surveys.

Table 2.5-4. GulfCet hydrographic cruises.

Cruise ID	Dates		CTDs	XBTs
	From	To		
GulfCet 01	04/15/92	05/01/92	19**	95
GulfCet 02*	08/10/92	08/24/92	44	78
GulfCet 03	11/08/92	11/22/92	39	76
GulfCet 04	02/12/93	02/27/93	46	83
GulfCet 05	05/23/93	06/05/93	42	71
GulfCet 06	08/28/93	09/05/93	38	92
GulfCet 07	12/03/93	12/14/93	32	73

* Coincident in time with LATEX C aerial survey.
** CTD system failed; data questionable.

2.5.7 SOOP/TIGER Hydrographic Data

Twenty hydrographic cruises aboard the R/V GYRE were conducted between April 1992 and December 1994 as part of the Texas Institutions Gulf Ecosystem Research (TIGER) initiative. These state-sponsored training and research cruises focused primarily on the continental margin of the northwestern Gulf of Mexico, but periodically collected data in the vicinity of the Loop Current during transits between Galveston and the Yucatan Channel or Florida. Table 2.5-5 summarizes the cruise dates and the types of data collected. Four of these cruises were coincident in time with LATEX C aerial surveys.

2.5.8 SCULP Drifter Data

The Minerals Management Service sponsored the Surface Current and Lagrangian-Drift Program (SCULP). It was designed to measure the statistical patterns of circulation in the upper meter on the Louisiana-Texas shelf and included the deployment of 341 Technocean Associates Davis-type Argos drifters (see Figure 2.5-6). However, since some of these were recovered and redeployed once or twice, the total number of deployments

Table 2.5-5. SOOP/TIGER hydrographic cruises during LATEX field program.

Cruise ID	Dates		CTDs	XBTs
	From	To		
92G-04	04/01/92	04/09/92	√	---
92G-06	05/17/92	06/07/92	---	√
92G-07	06/20/92	06/25/92	√	---
92G-10	10/02/92	10/06/92	√	---
92G-13	10/28/92	10/31/92	√	√
93G-01*	01/06/93	01/12/93	√	---
93G-03	03/10/93	03/14/93	√	√
93G-05	06/02/93	06/04/93	√	√
93G-09	08/06/93	08/09/93	√	√
93G-10	09/10/93	09/21/93	√	---
93G-11	09/24/93	10/09/93	√	√
93G-12*	10/28/93	11/03/93	√	---
94G-02	05/09/94	05/14/94	√	---
94G-03*	05/16/94	05/19/94	√	√
94G-05	07/17/94	07/21/94	√	√
94G-07*	08/09/94	08/22/94	√	√
94P-12	10/09/94	10/14/94	√	√
94G-08	10/19/94	10/25/94	√	√
94G-10	11/17/94	11/26/94	---	√
94G-11	11/30/94	12/07/94	---	√

* Coincident in time with LATEX C aerial survey.

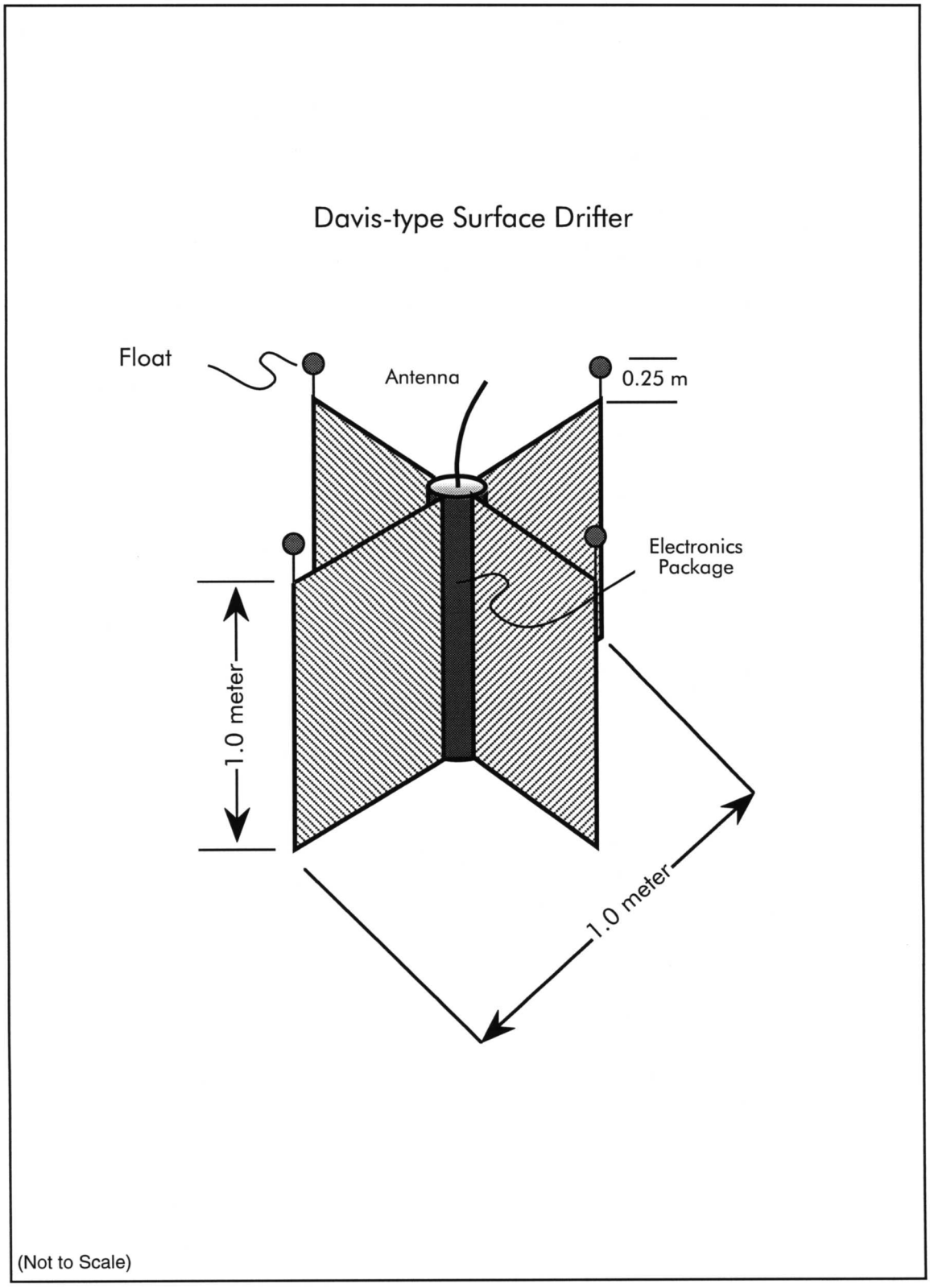

Figure 2.5-6. Schematic of Technocean Associates, Davis-type ARGOS drifter.

was approximately 383, with 246 deployed by air and approximately 137 deployed from platforms. The deployment grid sites, centered at 28°45.0'N latitude, 93°00.0'W longitude on the Louisiana shelf, and three nearby platform locations are presented in Table 2.5-6 and Figure 2.5-7. The planned deployment schedule is summarized in Table 2.5-7. The drifters consisted of three groups with IDs ranging from 20008 to 20023, from 20346 to 20559, and from 21643 to 21802. Each drifter was set to transmit for 127 days.

Table 2.5-6. SCULP drifter aerial and platform deployment sites.

Site	Location	
	Latitude (N)	Longitude (W)
A	29°15.0'	93°30.0'
B	29°15.0'	93°00.0'
C	29°15.0'	92°30.0'
D	29°00.0'	93°30.0'
E	29°00.0'	93°00.0'
F*	29°00.0'	92°30.0'
G	28°45.0'	93°30.0'
H*	28°45.0'	93°00.0'
I	28°45.0'	92°30.0'
J	28°27.0'	93°30.0'
K	28°27.0'	93°00.0'
L	28°27.0'	92°30.0'
M*	28°12.0'	93°30.0'
N	28°12.0'	93°00.0'
O	28°12.0'	92°30.0'

* Near a platform deployment site:

F - BT Operations (Vermilion 119D) ..... 29°05.4'N lat., 92°34.2'W long.
H - UNOCAL (West Cameron 280) ..... 28°48.0'N lat., 93°01.8'W long.
M - Shell Oil (West Cameron 565) ..... 28°15.6'N lat., 93°22.2'W long.

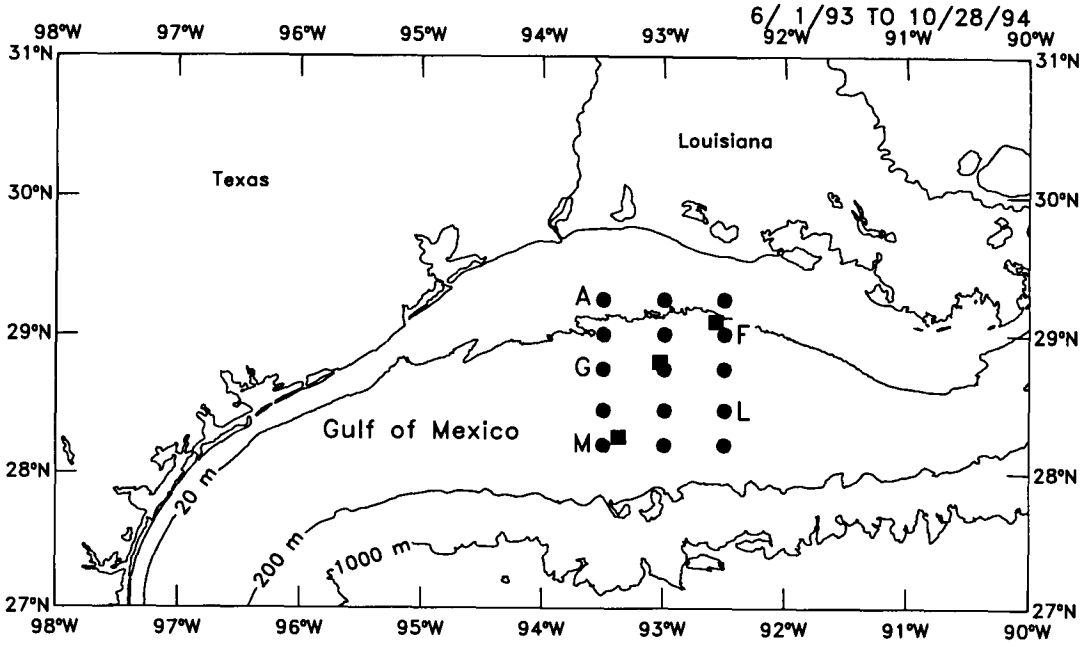

Figure 2.5-7. Map showing SCULP drifter deployment sites.

Table 2.5-7. Planned SCULP drifter deployment schedule.

Date	Quantity (aerial/rig)	Date	Quantity (aerial/rig)	Date	Quantity (aerial/rig)
06/01/93	13/0	02/17/94	3/3	06/29/94	0/2
10/14/93	15/0	02/25/94	0/2	07/08/94	0/2
10/22/93	15/1	03/04/94	12/3	07/12/94	20*/1
10/28/93	15/2	03/10/94	0/3	07/14/94	0/3
11/06/93	8/2	03/17/94	0/3	07/21/94	0/3
11/10/93	8/3	03/23/94	5/3	07/28/94	0/3
11/18/93	12/3	03/31/94	0/3	08/04/94	12/3
11/24/93	8/3	04/07/94	0/3	08/12/94	0/2
12/01/93	12/3	04/13/94	12/3	08/18/94	0/2
12/09/93	5/3	04/22/94	0/3	08/25/94	0/3
12/16/93	2/3	05/02/94	0/3	09/02/94	0/3
12/28/93	3/3	05/05/94	12/3	09/08/94	0/2
01/07/94	6/3	05/13/94	0/3	09/16/94	0/2
01/10/94	5/2	05/20/94	0/3	09/23/94	13/1
01/20/94	5/2	05/26/94	0/2	09/29/94	0/1
01/28/94	5/3	06/02/94	12/1	10/07/94	0/3
02/04/94	4/3	06/10/94	0/3	10/13/94	0/3
02/10/94	0/2	06/16/94	0/3	10/20/94	0/2
02/11/94	4/0	06/24/94	0/3	10/28/94	0/2

* Deployed near Galveston; not in the standard box grid centered at 28°45.0'N lat., 93°00.0'W long.

The first deployment of 13 drifters occurred in June 1993 and the intensive deployment period ran from October 1993 through October 1994. Platform deployments (54 of them) occurred approximately every seven days, beginning 22 October 1993 and ending on 28 October 1994. Aerial deployments (27 of them) were generally made on a weekly basis between 14 October 1993 and 17 February 1994 and then shifted to a once-a-month schedule (except for two flights in March 1994) through 23 September 1994 when the last aerial deployment was made. Not all grid sites were occupied during each flight.

One hundred seven (107) of the drifters left the shelf region and collected data over the shelf break and/or further offshore in the study area. Some became entrained in cyclonic and/or anticyclonic features or drifted through the Gulf until they ceased operation or became entrained in the Loop Current. Sixty-six (66) were affected by cyclonic flow, fourteen (14) by anticyclonic flow, and six (6) by both. Only a small number of the drifters continued to transmit beyond October 1994.

2.5.9 TOPEX and ERS-1 Altimeter Data

A complete archive of TOPEX interim GDRs (IGDRs) and GDRs has been acquired from the Physical Oceanography Distributed Active Archive Center (PO.DAAC) at the Jet Propulsion Laboratory. IGDR data were collected in near real-time (within 10 days of overflight) by file transfer over the Internet. TOPEX GDR data were provided later by PO.DAAC on 8mm tape. A complete archive of ERS-1 IGDRs and real-time GDRs (RGDRs) product provided by NOAA (Cheney and Lillibridge 1992) have also been collected by file transfer. All of these data are archived on 8mm tapes. Archival ERS-1 Altimeter Ocean (ALTOPR) data were acquired from the European Space Agency on CD-ROM.

III. DATA QUALITY ASSURANCE AND PROCESSING

3.1 Introduction

Data quality assurance and processing techniques are discussed in this chapter. Where possible, detailed calibration and/or processing methods are described. Applicable methods for ancillary data are presented from the point in processing at which data were obtained. In some instances LATEX C PIs were significantly involved in the ancillary programs which permitted their involvement in all aspects of data handling.

3.2 Drifting Buoys

3.2.1 Predeployment Testing

Upon receipt from the manufacturer, each Argos drifter was activated and tested with a Telonics TSUR-B Satellite Uplink Receiver/Analyzer. This permitted a quick (within minutes) verification of proper message length, bit format, format synchronization, initialization and identification. Furthermore, each drifter was activated in an unobstructed "clear-sky" environment to permit an operational test through Service Argos. This provided a further check of drifter operation and permitted verification that the drifter ID was properly registered under the program account number. No unit failed these "initial" predeployment tests.

After the above testing and temporary storage, each drifter was repackaged and shipped to its respective deployment mobilization point. It then became the responsibility of each user to do a further operational check and properly deploy the drifter. Depending on the circumstances, this was accomplished either as a through-system check involving Service Argos or by use of the TSUR-B.

One drifter was returned to the manufacturer following this second set of operational tests as there appeared to be some noise in the quality of the position data (actual position accuracy, typically on the order of 350 meters, is a function of the PTT oscillator stability). However, the manufacturer was unable to duplicate the symptoms and the drifter was returned for deployment.

The manufacturers' stated drifter thermistor specifications are presented in Table 3.2-1. No additional effort was made to verify the accuracy of each individual drifter's built-in temperature sensor other than to confirm the receipt of reasonable temperature values.

Table 3.2-1. Argos drifter thermistor specifications.

Drifter Type	Clearwater WOCE/SVP	Horizon FHD/Holey Sock
Temperature Range	0 to 37°C	-5 to 45°C
Temperature Accuracy	± 0.1°C	± 0.15°C

3.2.2 Generation of Smooth Trajectories

The raw position data, as determined by Service Argos, were extracted and separated from other on board sensor data such as battery condition, drogue presence or absence and sea water temperature. After extraction, the position data were plotted on a high resolution map of the study area containing bathymetry and coastline. Generally, anywhere from three to eight position fixes were obtained each day. Duplicate positions were removed from the time series and spurious changes in the drifter's movement were identified. Since a number of drifters were recovered by vessels operating in the study area and were then transported to port, the data for these drifters were truncated at the last free-drifting fix before the drifter appeared to have been picked up. Once these preliminary cleanup activities had been completed, the data were reprocessed and replotted.

Some of the drifter position data were filtered and smoothed using a modification of the method of successive corrections and Gaussian filters given by Pedder (1993). The modification calculates smoothed and interpolated latitudes and longitudes of the positions as a function of time rather than a constructed gridded field in two dimensional space. The influence time scale for the drifter tracks is usually 28 hours. Thus, motions with time scales less than about three days were filtered out of the smoothed drifter tracks. The positions were resampled at six hour intervals. Figure 3.2-1 presents examples of raw and smoothed drifter tracks.

3.2.3 Drifter Track Analysis

The drifter tracks were analyzed by least squares fitting of a diverging, translating ellipse to the smoothed position data. The method follows Glenn et al. (1990). The equations fit to a drifter orbit were:

$$x(t) = x_o + ut + (1+Dt)\,[a \cos\theta \cos(-\omega t + \phi) - b \sin\theta \sin(-\omega t + \phi)] \quad (1)$$

$$y(t) = y_o + vt + (1+Dt)\,[a \sin\theta \cos(-\omega t + \phi) + b \cos\theta \sin(-\omega t + \phi)] \quad (2)$$

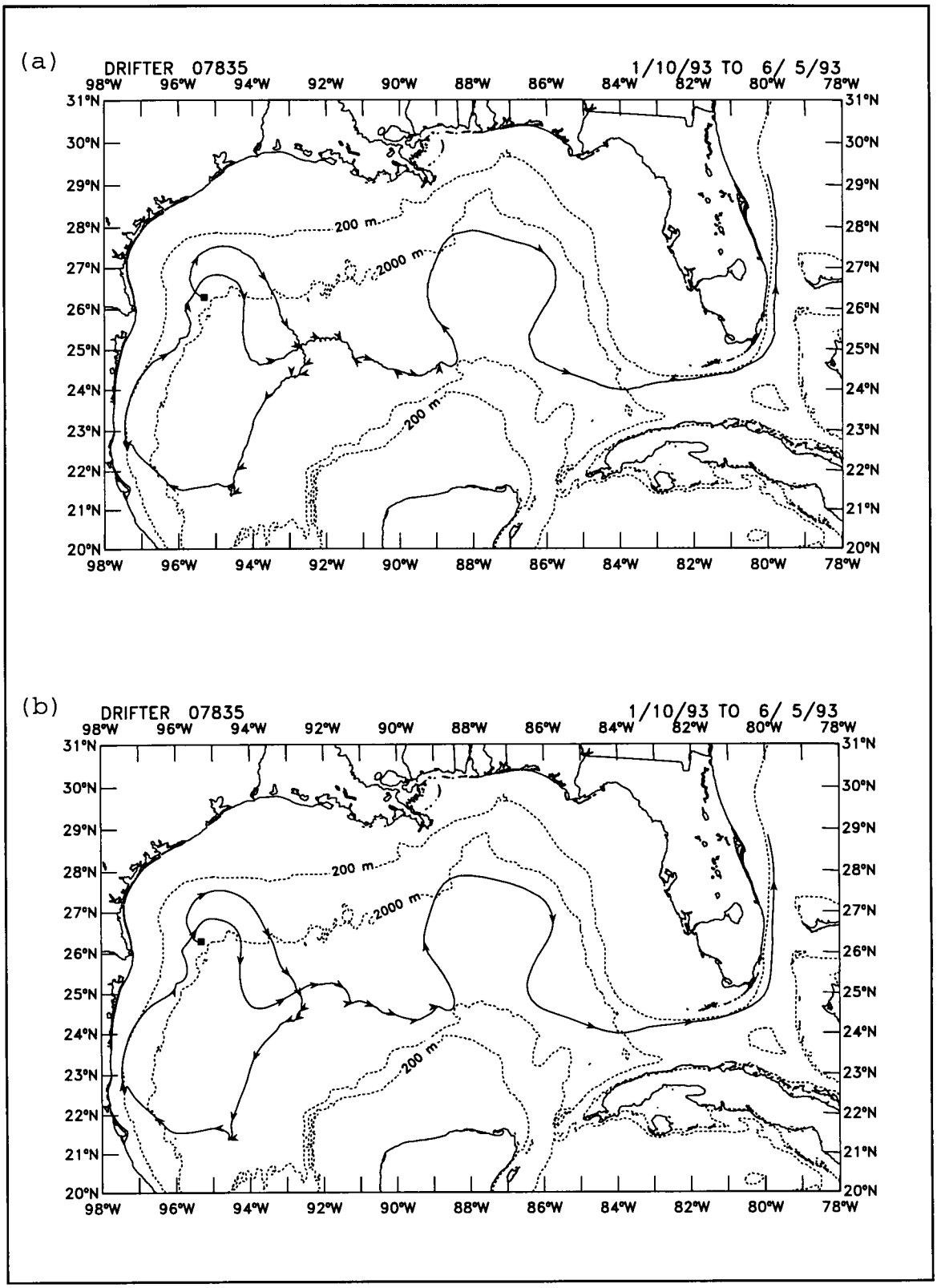

Figure 3.2-1. Example of (a) raw Argos drifter path plot and (b) smoothed Argos drifter path plot.

where:

x,y	are the coordinates of the modeled buoy track,
x_o,y_o	is the t = o center position of the ellipse,
u,v	are the x and y components of the center translation velocity,
a,b	are the major and minor axes of the ellipses,
θ	is the inclination of the major axis to the east or x axis,
ω	is the orbital frequency,
ϕ	is the t = o phase of the orbit,

and

D	is the divergence.

Latitudes and longitudes were transformed into the (x,y) coordinate system using standard f-plane projections. Minor differences from the Glenn et al. (1990) method of least squares fitting of equations (1) and (2) to buoy positions are that smoothed equally spaced tracks are used, (u, v) are constrained to be (dx_o/dt, dy_o/dt), and that the period T, over which the orbit is fit, adapts by iteration so that $T^{(k)} = 2\pi/\omega^{(k-1)}$, where $\omega^{(k)}$ is given by the least squares solution to equations (1) and (2). Thus, all that was required was an estimate of $T^{(o)}$ for the first orbit of the drifter track. T was then allowed to change by daily increments between sets of iterations until convergence.

The estimations of the parameters proceed by daily increments, with the results of the previous least squares fit providing the initial estimates for the subsequent calculation. The adaption of T to the calculated orbit frequency was found to improve the χ^2 of the fit in almost all cases, as opposed to assuming a constant period for the orbit fits. Thus, it was not necessary to segment a drifter track into sections where different orbit periods (found by trial and error) predominated as in Glenn et al. (1990). The model fits worked satisfactorily only when there were data points in all four quadrants of the elliptical orbit.

3.3 Aerial Surveys

3.3.1 Position Accuracy and Data Processing

The aircraft's position was determined using a Teledyne Systems Company TDL-711 Micro-Navigator. It is a fully automatic area navigation system based on LORAN-C that is functional at all altitudes and in all weather conditions. It has a typical location accuracy on the order of ±500 meters. These data were automatically interfaced into the on-board micro-computer and data loggers along with the expendable probe data.

The combined probe and navigation data were then recorded on both nine-track analog tape and on DAT cassettes from separate channels of the receiver in the aircraft. The AXBT and AXCTD data were processed through a Sippican Mk-12 Oceanographic Data Aquisition System, and the AXCP data were processed through a Sippican Mk-10 Digital Data Interface. These systems converted the data to ASCII files containing a header with information about each drop and the corresponding depth/parameter pairs. Depth was calculated from the fall time of the probe through the water column by application of a drop-rate equation, temperature was measured from the probe thermistor, current velocity and direction were measured from the probe electrodes and compass coil, and conductivity was measured from the probe conductivity cell. Table 3.3-1 summarizes the manufacturers' specifications for the various probes and their respective parameters. No effort was made to confirm that the probes met these specifications other than a general evaluation of the reasonableness of the data. Additional discussion follows in the next section regarding drop-rate equations.

Table 3.3-1. Aerial probe specifications.

Probe Type	**AXBT**		**AXCP**	**AXCTD**
Manufacturer	Hermes	Sparton	Sippican	Sippican
Depth Range	0 to 800 m	0 to 800 m	0 to 1500 m	0 to 1000 m
Depth Accuracy*	± 2% of depth	± 5% of depth	± 5 m or 2% of depth	± 5 m or 2% of depth
Depth Res.	0.15 m	0.15 m	0.3 m	0.8 m
Temp. Range	-2 to 36°C	-2 to 35°C	0 to 30°C	-2.2 to 30°C
Temp. Accuracy	± 0.18°C	± 0.15°C	± 0.18°C	± 0.035°C
Cond. Range	NA	NA	NA	20 to 75 $mS \cdot cm^{-1}$
Cond. Accuracy	NA	NA	NA	± 0.035 $mS \cdot cm^{-1}$
Vel. Accuracy	NA	NA	± 1 $cm \cdot s^{-1}$ rms	NA

* Using manufacturer's recommended drop-rate equation.

After acquisition and the initial processing described above, the data were uploaded into the Physical Oceanographic Data Base Management System (PODBMS) and inspected for spikes, large data gaps and the total number of points. This permitted the user to clip bad/noisy drops and to apply a spline to noisy or gappy data (a common problem with aerial probe data) in an attempt to smooth the data or supply missing

data. This smoothing can be applied to an entire cast, or over a particular depth range of a cast, or over one parameter of a multi-parameter cast (e.g. AXCPs and AXCTDs). Bad casts were deleted from the PODBMS. Figure 3.3-1 presents examples of 'raw' and 'cleaned up' AXBT data.

3.3.2 AXBT Data and Expendable Probe Drop-Rate Equations

Expendable probe drop rates are primarily dependent on probe weight and shape. Sippican, Inc., the only known manufacturer of AXCPs and AXCTDs, provides unique drop-rate equations for each type probe. The stated depth accuracy of these equations is ±5 meters or 2% of depth where the maximum depth is 1500 meters for the AXCP and 1000 meters for the AXCTD. These equations (Equations 1 and 2) are presented in Table 3.3-3.

The appropriate drop-rate equations for the two different manufacturers' AXBTs are less obvious. Hermes acquired the original Sippican AXBT production line in 1993 and produced the same AXBT probe that had been produced by Sippican except that it increased the depth capability by 40 meters (from 760 m to 800 m). This was accomplished by adding 19 grams of wire and reducing the probe nose weight by 20 grams (to 360 grams). Sparton developed its own probes independently. Neither manufacturer, however, provided its own drop-rate equation at the time the probes were acquired for this program (Sparton in April 1992 and Hermes in June 1993). Subsequently, the original Sippican (1985) 760 meter AXBT drop-rate equation identified in Tables 3.3-2 and 3.3-3 (Equation 3) was used for all AXBT data acquisition and processing. Later (in 1995), after the field work had been completed and the data processed, both Hermes and Sparton provided new and different drop-rate equations. These are presented as Equations 4, 5 and 6 in Table 3.3-3.

In addition to the unavailability of the appropriate drop-rate equations from the probe manufacturers, the Sippican (1985) equation, which was initially selected for data acquisition and processing, was found to be just one of many equations that Sippican and others had published over the years. These equations are presented in Table 3.3-2. Subsequently, not knowing which of the Sippican equations would be most appropriate, but knowing that none was determined for the newer, deeper, Hermes and Sparton probes, use of the Sippican (1985) equation was maintained for consistency in data collection.

The latest manufacturer-provided Sparton equation was finally derived from actual field tests, using 46 near-simultaneous pairs of CTD and AXBT profiles, conducted by the Naval

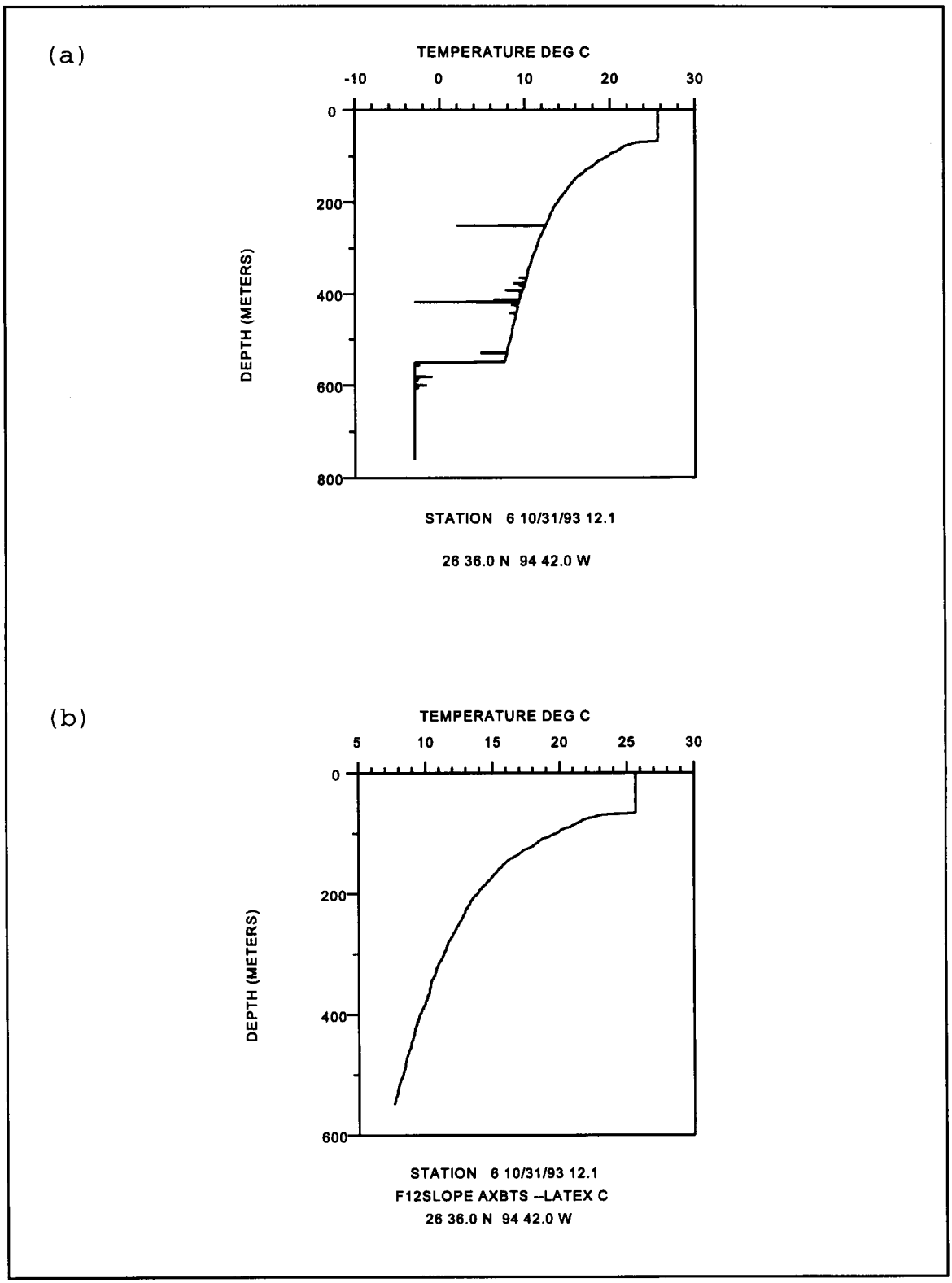

Figure 3.3-1. Plot of (a) raw AXBT data and (b) cleaned AXBT data from F12SLOPE survey, station 6, showing data dropouts corrected by interpolation.

Research Laboratory (Boyd and Linzell 1993); whereas the Hermes' equation was derived mathematically by Hermes by recalculating the equation coefficients in the original (1982) Sippican 305 meter baseline drop-rate equation for the newer 800 meter probe characteristics (Sue Ann Healy, Hermes/Devtek Applied Electronics (DAE), and Alan Hudson, formerly of Sippican; personal communication).

Table 3.3-2. Evolution of the Sippican AXBT probe drop-rate equation (1982-1989) from published sources.

Year	Equation	Depth (m)	Reference
1982	$Z = 1.559t - 1.63 \times 10^{-4}t^2$	305	Original Sippican equation (per Alan Hudson)
1985*	$Z = 1.554602t - 1.634 \times 10^{-4}t^2$	760	Sippican MK-9 manual
1987	$Z = 1.63249t - 2.15 \times 10^{-4}t^2$	760	Boyd (1987) for Sippican probe
1989	$Z = 1.6753t - 2.2745 \times 10^{-4}t^2$	760	Sippican MK-12 manual (Revision 2.2)

* Equation used to acquire and process LATEX C AXBT data.

The general form of this equation is:

$$Z=V_0t-\tfrac{1}{2}at^2$$

where:
- Z is the depth of the probe at time t
- V_0 is the maximum velocity achieved at the start of the descent
- t is the time in seconds

and a is the de-acceleration of the probe.

The first term can also be expressed as:

$$V_0t=(2T_0/C_dA\rho)^{\frac{1}{2}}t$$

where:
- T_0 is the thrust due to the initial in-water weight of the probe
- C_dA is the drag coefficient of the probe *x* the cross sectional area

and ρ is the sea water density.

Table 3.3-3. Aerial probe drop-rate equations used to process data.

Probe Type	Probe Manufacturer	Sippican Equation Used For Processing Data	Manufacturer's Latest Recommended Equation
AXCP	Sippican	(EQN. 1) $Z = 4.276t - 6.30 \times 10^{-4}t^2$	(EQN. 1)
AXCTD	Sippican	(EQN. 2) $Z = 3.254t - 5.30 \times 10^{-4}t^2$	(EQN. 2)
AXBT	Hermes (DAE)	(EQN. 3) $Z = 1.554602t - 1.634 \times 10^{-4}t^2$ (see Table 3.3-2)	(EQN. 4)* $Z = 1.6103t - 1.63 \times 10^{-4}t^2$ *or* (EQN. 5)** $Z = 1.5985t - 2.15 \times 10^{-4}t^2$
AXBT	Sparton	(EQN. 3) $Z = 1.554602t - 1.634 \times 10^{-4}t^2$	(EQN. 6)*** $Z = 1.620t - 2.2384 \times 10^{-4}t^2 + 1.291 \times 10^{-7}t^3$

* Derived by Hermes by mathematically adjusting the original (1982) Sippican 305m baseline equation ($Z = 1.559t - 1.63 \times 10^{-4}t^2$) for the deeper (800m) depth capability (more wire and lower nose weight).
** Derived by Hermes by mathematically adjusting the Boyd (1987) 760m equation ($Z = 1.63249t - 2.15 \times 10^{-4}t^2$) for Sippican probes for the deeper (800m) depth capability (more wire and lower nose weight).
*** Determined by Boyd and Linzell (1993) for Sparton 800m probes.

Table 3.3-4. Comparison of AXBT probe drop-rate equation predictions.

Time(s)	[EQN. 3] Sippican Depth (m)	[EQN. 4] Herm./Sipp. Depth (m)	[EQN. (4-3)] Depth (m) Difference	[EQN. 5] Hermes/Boyd Depth (m)	[EQN. (5-3)] Depth (m) Difference	[EQN. 6] Sparton Depth (m)	[EQN. (6-3)] Depth (m) Difference
100	153.826	159.400	+ 5.574	157.700	+ 3.874	159.891	+ 6.065
200	304.384	315.540	+ 11.156	311.100	+ 6.716	316.078	+ 11.694
300	451.675	468.420	+ 16.745	460.200	+ 8.525	469.337	+ 17.662
400	595.697	618.040	+ 22.343	605.000	+ 9.303	620.442	+ 24.745
500	736.451	764.400	+ 27.949	745.500	+ 9.049	770.165	+ 33.714

The second term can be expressed as:

$$\frac{1}{2}at^2=\frac{1}{2}(dT/dZ/C_dA\rho)t^2$$

where:

dT/dZ is the change in thrust with depth due to loss of wire, the effect on weight due to changes in sea water density and signal cable payout tension.

The mathematical solution of these equations for the newer 800 meter probe specifications produces Equation 4 in Table 3.3-3. Hermes also mathematically adjusted the Boyd (1987) equation which was experimentally determined for the original 760 meter Sippican probe by comparing near-simultaneous CTD casts and AXBT drops. The result is presented as Equation 5 in this same table. Hermes states that both of these recalculated equations (Equations 4 and 5) satisfy the depth accuracy specifications for the probe (±2%). It is emphasized, however, that no new deployment data were collected by the manufacturer to verify these conclusions. Subsequently, it is not clear as to which equation should be preferred and how accurate these calculated equations really are.

Predicted depth differences at selected time intervals due to use of the original Sippican (1985) 760 meter equation instead of the Hermes or Sparton equations are presented in Table 3.3-4. As an example, after 500 seconds, the Hermes-adjusted Sippican equation (Equation 4) predicts a depth which would be deeper than the Sippican depth prediction by nearly 28 meters, whereas the Hermes-adjusted Boyd equation (Equation 5) predicts a depth which would be deeper than the Sippican depth prediction by only nine meters, a nineteen meter difference between the two Hermes-derived equations. The Sparton equation (Equation 6) predicts a depth which would be deeper by nearly 34 meters. Subsequently, the relative depth differences between the two probes' equations could be as little as six meters, or as much as 25 meters.

Clearly, probe drop-rate differences are significant and emphasize the problems associated with comparing/combining data from one probe type and/or manufacturer with other expendable probe or CTD data sets. Fortunately, however, these differences are not critical in identifying oceanographic features (e.g. Loop Current eddies and small cyclonic and anticyclonic eddies), particularly if the different manufacturers' probes and probe types are not mingled during each survey, which was the case for 19 of the 21 surveys. Unfortunately, probes were mixed during two of the surveys (F15SLOPE and F16SQUIRT) when variable availability and a large number of probe failures occurred. However, it is

apparent from depth contours of the 8°C surface, which would be most affected by drop-rate differences, that the effects of probe mixing were minimal with respect to feature identification for these two surveys (see Figures 3.3-2 and 3.3-3). Subsequently, no effort has been made to reprocess any of the data for the 'latest', reported drop-rate equations. Conversion equations have been calculated, however, and are presented in Table 3.3-5.

Table 3.3-5 Equations to convert Sippican-derived AXBT depth predictions (from EQN. 3) to each manufacturer's latest recommended equation result.

Manufacturer's Equation	Conversion Equation
Hermes/Sippican (EQN. 4)	$Z_{EQN.4} = 1.0375\ Z_{EQN.3}$
Hermes/Boyd (EQN. 5)	$Z_{EQN.5} = 1.0290\ Z_{EQN.3} - 2.26 \times 10^{-5} (Z_{EQN.3})^2$
Sparton (EQN. 6)	$Z_{EQN.6} = 1.0326\ Z_{EQN.3} + 1.65 \times 10^{-5} (Z_{EQN.3})^2$

3.3.3 AXCP Data

Each AXCP is provided with five calibration constants (Gcca, Gcora, Gefa, Gevfa and Gcvfa) which must be programmed into the Mk-10 Digital Data Interface. These coefficients refer to compass voltage gain, correction voltage gain, electric field voltage gain, electric field deviation, and compass deviation, respectively. They are measured by the manufacturer and provided as calibration information with each individual probe prior to use. Nominal values for these coefficients for the first fifty probes obtained from Sippican were 1847.37, 920.01, 25244.20, 499.53, and 495.42, respectively. These averaged values could be applied instead of the probe-specific values, but their use would reduce the accuracy of the measurement. Data from the first five AXCPs deployed (during the F03SEDDY survey) were discarded because there were no visible serial numbers on the probes (a manufacturing error) to permit use of the calibration coefficients. The remaining probes were returned to Sippican for re-work and were replaced with numbered probes, each with a unique calibration sheet.

The probes measure velocity relative to a reference velocity which is constant with depth. This was estimated by averaging the smoothed velocity components between 750 and 1500 meters depth on the assumption that the deep currents were small. The removed velocities often had magnitudes of 10 to 12 $cm \cdot s^{-1}$, which is about twice the maximum reported by Sanford et al. (1987) and Glenn et al. (1990) using similar procedures. However, smoothing was accomplished by a least squares fitting

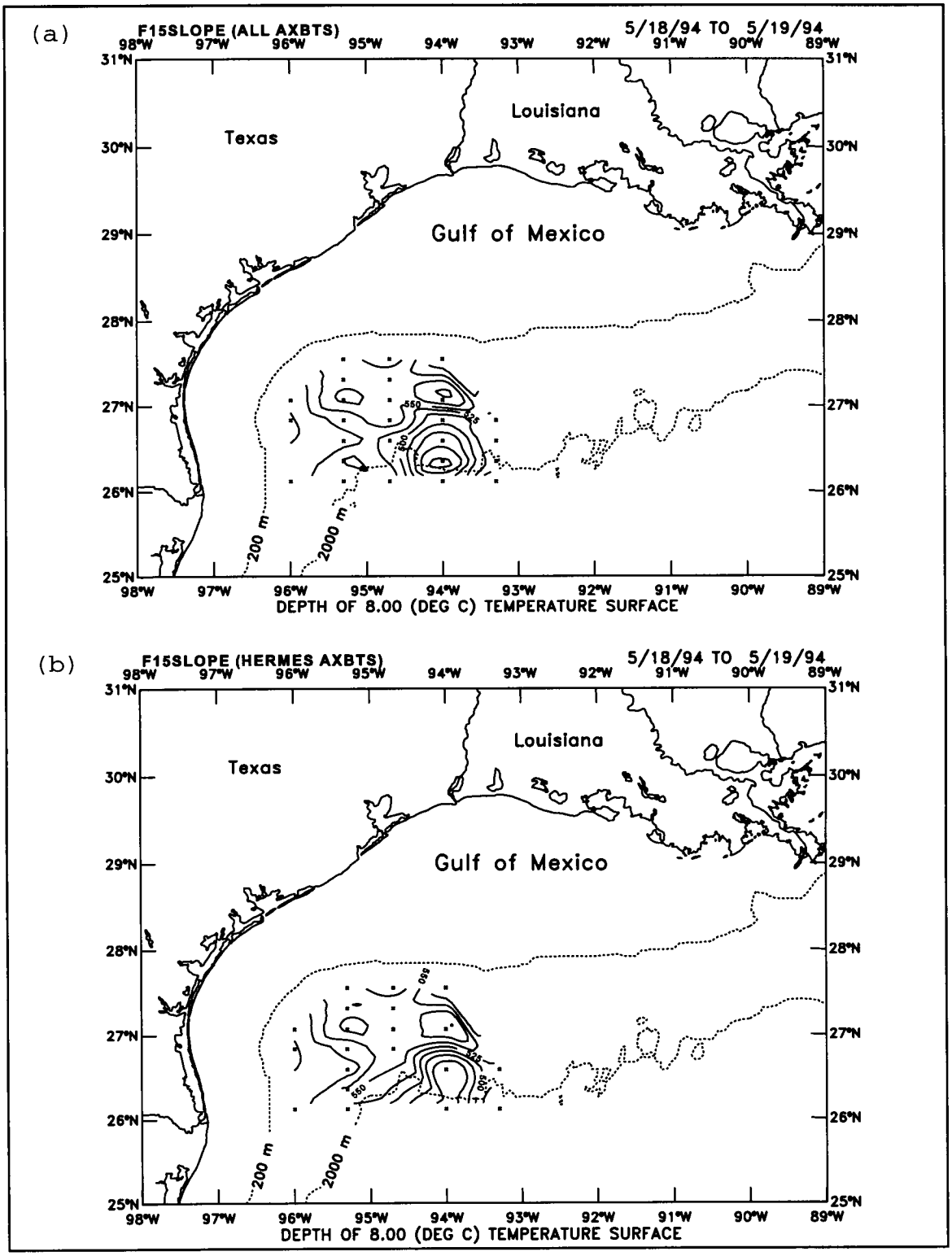

Figure 3.3-2. Map showing F15SLOPE survey 8°C isotherm depth contours plotted through (a) all available AXBT probe data and (b) Hermes AXBT probe data only.

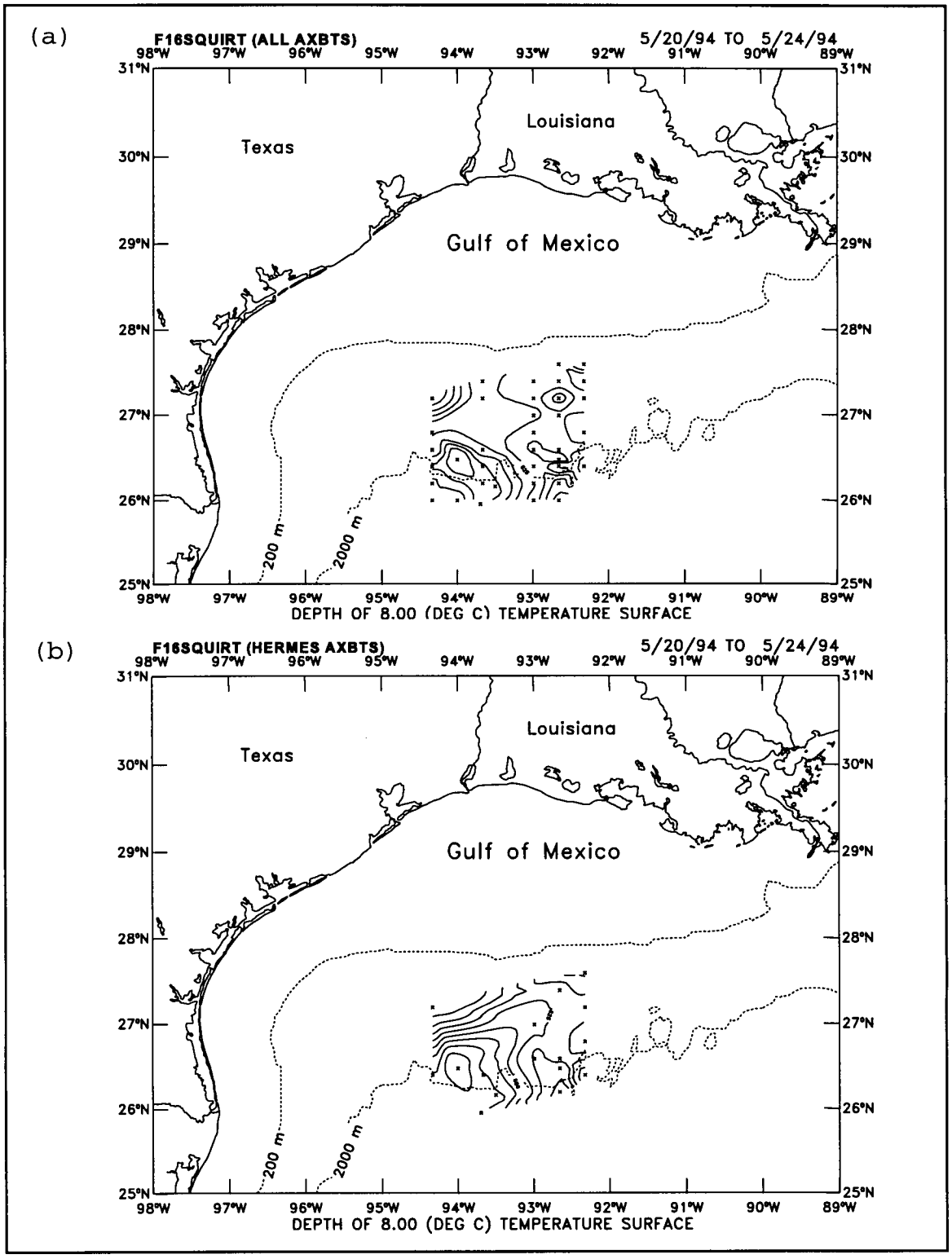

Figure 3.3-3. Map showing F16SQUIRT survey 8°C isotherm depth contours plotted through (a) all available AXBT probe data and (b) Hermes AXBT probe data only.

of cubic splines to the u and v components. This removed most of the high frequency fluctuations with wave numbers greater than ~20-50m^{-1}. When comparisons were possible, the resulting near-surface velocities were found to agree well with velocities estimated from drifters and current meters.

In the upper 50 m of the water column, velocity shears measured by AXCPs are likely to be aliased by orbital surface wave velocities. This is because the fall time through the surface layer is comparable to typical surface wave periods of 5 to 20 seconds. This aliasing decreases rapidly with depth and depends upon the surface sea state (significant wave height and period) at the time of the probes' deployment. Fifty meters is a conservative estimate of the depth where aliasing of wave velocities may be significant. In general, the sea state was small, particularly in summer, for most of the AXCP deployments. In the data processing the 0-10 m part of the shear profiles are discarded and in the section plots of velocity the upper 50 m are excluded. However, in a few cases, the depth-averaged velocities for 10 to 50 m from the AXCPs are included for comparison with drifter and current meter-derived velocities. These are expected to be less reliable than depth-averaged velocities below 50 m.

3.3.4 AXCTD Data

The performance of the AXCTD probes was evaluated by the manufacturer (Sippican, Inc. 1995) as part of their probe development program. The quality of the data was considered to be good, but following an initial round of processing by the manufacturer, all probes were found to have experienced a noise signature on the order of ±0.3°C or ±0.3 $mS \cdot cm^{-1}$. The noise was an order of magnitude greater than the expected accuracy of the probe. However, Sippican found that the noise could be successfully averaged without a significant loss of resolution by using the post-processing capabilities of the Mk-12 recorder. The noise was initially thought to be due to electromagnetic interference generated either in the aircraft or in the environment where the probes were deployed. However, no other probes dropped either prior to or following these deployments experienced this noise problem. Later, it was discovered that the noise was in some way linked to the recording equipment which had been provided by Sippican for the deployments. Backup recording equipment was found to have produced much less noisy data.

No coincidental CTD casts were made in the vicinity of the AXCTD drops for comparison to examine the drop-rate equation or to check the accuracy of the temperature and salinity data. However, the data were compared with available historical

temperature/salinity (TS) data from CTD profiles which had been made in the same general region in 1985. These comparisons revealed an excellent fit to the tight TS envelope, particularly at temperatures below 18°C (see Figure 3.3-4). The mean salinity difference ($\overline{CTD} - \overline{AXCTD}$) between the two data sets for each whole and half degree Celsius from 18°C to 5°C was -5.67×10^{-3} psu with a standard deviation of 7.17×10^{-3} psu. The maximum difference was -1.90×10^{-2} psu at 18°C.

Earlier work by Sy (1993) suggests that XCTD probes (and by inference AXCTD probes), like XBT and AXBT probes, fall faster than specified by the manufacturer. The effect is thought to be on the order of 30 meters at 900 meters depth (or about 3.3%) for the XCTD. No comprehensive study, however, is known to have been completed to establish a revised drop-rate equation for the XCTD or to check the drop-rate equation for the AXCTD. Sy (1995) and Elgin (1994) have both reported on a slow start of the conductivity measurement in the upper 50 to 60 meters of the profile, possibly due to air bubbles remaining in the conductivity cell. This results in low salinity values outside the reported accuracy range of the probe for this upper part of the water column.

3.4 GEOSAT Data

3.4.1 Introduction

The goal of the GEOSAT data quality assurance and processing was to derive accurate climatologies of sea surface height, wind speed and wave height observed by altimetry during the GEOSAT Geodetic and Exact Repeat missions, the GM and ERM. To achieve this goal the GDRs from the GM and ERM were processed in a consistent manner based on recommendations in the GDR Handbook (Cheney et al. 1991b) and the scientific literature. Processing also benefited from personal communication with the NOAA personnel who produced the GDRs and with scientists working with data from the TOPEX/Poseidon and ERS-1&2 missions. The following sections describe the processing and quality control of the GDR data used to determine sea surface height, wave height and wind speed.

3.4.2 Sea Surface Height

The estimation of sea surface height from a satellite altimeter is conceptually quite simple. A microwave pulse is transmitted to and reflected from the ocean surface, allowing the travel time of the pulse to be used to estimate the range from the satellite to the ocean surface. Accurate knowledge of the position of the satellite can then be used to determine the absolute height of the ocean relative to a fixed reference

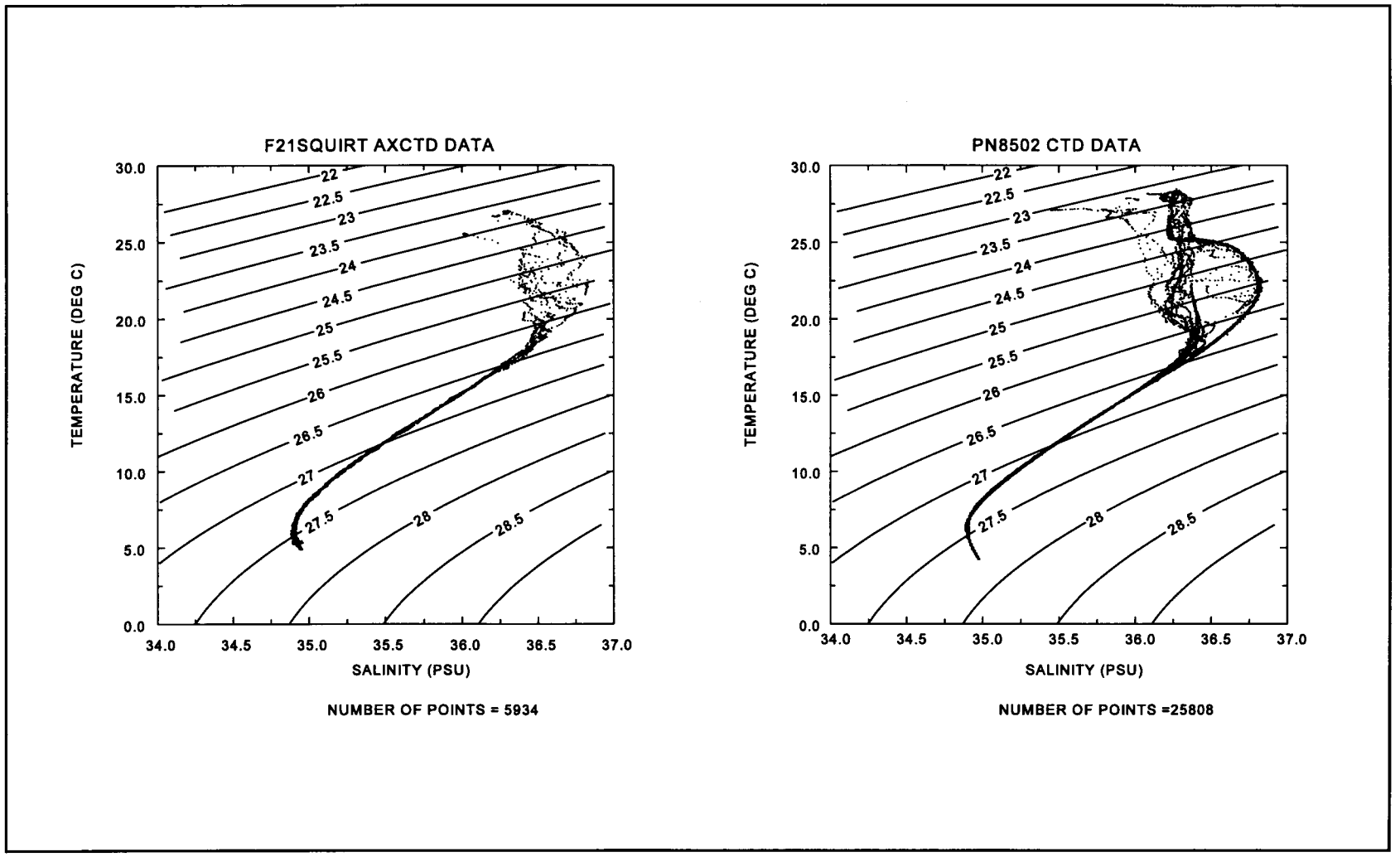

Figure 3.3-4 TS plots comparing AXCTD data from flight F21SQUIRT with historical CTD data from a cruise made through a Loop Current eddy in the western Gulf of Mexico in 1985.

surface. However, the measurement is complicated by a host of possible error sources independent of the precision of the altimeter, which on GEOSAT was able to measure range to within five cm rms. These errors arise from a number of path-length corrections which must be applied to the data to infer the height of the ocean surface, independent of the surface response to tidal and inverse barometric effects. The nature of these corrections and the processing applied to the sea surface height data in this report are discussed below.

3.4.2.1 Wet and Dry Troposphere Correction

Water and air molecules in the troposphere refract the radar pulse and increase the travel time between the altimeter and the ocean surface. Path-length corrections caused by these delays are included in the GDRs. The formulae used to compute the corrections are presented in the GDR Handbook (Cheney et al. 1991b).

The dry troposphere correction is based on the surface atmospheric pressure from operational models. The dry troposphere correction applied to the GM data is based on the Fleet Numerical Oceanographic Center (FNOC) model. Because the FNOC model changed in 1988, the corrections applied to the ERM data are based on the European Center for Medium-range Weather Forecasting (ECMWF) model as recommended in the GDR Handbook. The ECMWF correction was not included on the GM GDRs.

Since GEOSAT carried no radiometer, the wet troposphere correction must be determined by using estimates of the vertically integrated water vapor from an atmospheric model or by using estimates from satellite radiometer measurements. The GM data were corrected for wet troposphere using the FNOC model rather than the NIMBUS 7 scanning multichannel microwave radiometer (SMMR) monthly climatology, because of limited coverage of the Gulf of Mexico in the SMMR monthly climatology. The ERM data were corrected using satellite radiometer measurements from the TIROS operation vertical sounder (TOVS) (Emery et al. 1990), and the special sensor microwave imager (SSMI) (Wentz 1989). TOVS was used to correct for wet troposphere from the beginning of the GEOSAT ERM to July 8,1987, and SSMI was used for the remainder of the ERM.

3.4.2.2 Ionosphere Correction

Free electrons in the ionosphere refract the radar pulse and increase the travel time between the altimeter and the ocean surface. No direct measure of this delay was made by the single frequency altimeter on GEOSAT, thus the path-length

corrections are based on an ionospheric model. Both the GM and ERM data were corrected based on the Klobuchar (1987) model.

3.4.2.3 Tidal Corrections

The same solid earth and ocean tide models were used to correct the GM and ERM data. The solid earth tide correction was based on Cartwright and Taylor (1971) and Cartwright and Edden (1973). The Schwiderski (1980) model was used to correct for ocean tides. This model is a linear hydrodynamic model based on the inversion of tide gauge data. During 1994 alone, 12 new global ocean tide models were released (Anderson et al. 1995). These models are based on high precision altimetry from the TOPEX/POSEIDON mission; a mission designed specifically to enable development of accurate global tide models. TOPEX-derived corrections to the Schwiderski (1980) model have been reported by Schrama and Ray (1994). For the dominant tide in the Gulf of Mexico, M2, corrections to the in-phase and quadrature components of the Schwiderski (1980) model are less than 2.5 cm in absolute value over the deep basin. Some residual tidal signal in the "tide-corrected sea surface height data are reduced by the empirical orbit error correction, which filters basin-scale signals from along-track data.

3.4.2.4 Inverse Barometer Correction

The ocean surface rises and falls with changes in the atmospheric pressure as an inverse barometer with approximately one cm of height change per millibar of pressure change. This correction was applied to the data using pressure determined from the dry troposphere range correction, so the FNOC and ECMWF operational model surface atmospheric pressures were used to compute the correction. The formulae used for the correction may be found in the GDR Handbook (Cheney et al. 1991b).

3.4.2.5 Electromagnetic Bias Correction

Qualitatively, the sea-state bias, or the electromagnetic (EM) bias, is caused by crests and troughs of surface ocean waves differentially reflecting the altimeter wave forms, with the troughs of the wave reflecting more of the transmitted power. This biases the estimates of mean sea level within the altimeter footprint toward the wave troughs. Typical values of the EM bias are a percentage of significant wave height (2% for GEOSAT), which is subtracted from the altimeter range to account for this error. No EM bias was applied to the GEOSAT sea surface height data because it was found that the quality

and coverage of the significant wave height (SWH) measurements was poor from GEOSAT over the Gulf of Mexico.

3.4.2.6 Empirical Orbit Error Correction

Orbits included on the GM and ERM GDRs are based on satellite ephemerides computed using different gravity models and tracking data. However, the accuracy of the orbits is comparable. The GM GDR orbits are based on Naval Surface Weapons Center (NSWC) orbits with an accuracy estimated at approximately 60 cm rms (Cheney et al. 1991a). ERM GDR orbits are based on the GEM-T2 orbits, with an estimated accuracy of 10-25 cm early in the ERM, which grew to 40-60 cm as the solar activity increased later in the mission due to mismodeling of the accompanying atmospheric drag (Haines et al. 1990).

The accuracy of orbits provided on the GEOSAT GDRs required that an empirical orbit correction be applied to the data for oceanographic studies. A least absolute deviation detrending of the along-track data was performed. A tilt and bias (line) was fit to the sea surface height anomaly along each track and removed. The tilt and bias were estimated by minimizing the absolute deviation (Press et al. 1992). This procedure gives a robust estimate of the tilt and bias, independent of large blunders or outliers in the data, and was applied to the along-track data before editing.

The degree to which a tilt and bias removes orbit error along arcs over the Gulf of Mexico can be estimated for a standard least squares fit (Tai 1989). For 15-degree arc lengths, 0.25% of the rms orbit error would remain in the detrended data. Assuming orbit accuracy of 50 cm, the rms residual orbit error would be less than one cm rms for detrended altimeter data in the Gulf of Mexico. Detrending of the data also has the added advantage of removing other residual long-wavelength errors in the data, such as the EM bias which was not applied.

3.4.2.7 Selection of a Mean Reference Surface

Before the release of the GM GDRs, altimetric studies of the Loop Current eddies in the Gulf of Mexico, using the GM data, had to rely on crossover analysis techniques (Johnson et al. 1992, Leben and Born 1993). Crossovers from the GM were not classified because they contained no absolute height information from which to construct the ocean surface. Unfortunately, this lack of an absolute reference system also makes consistent referencing of data between the Geodetic mission and other altimeter missions difficult, especially in areas with large interannual variability such as the Gulf of Mexico.

With the release of the declassified along-track data, the non-repeat GEOSAT GM could be referenced to an existing mean sea surface (Leben and Born 1995). Accurate surfaces based on the TOPEX/Poseidon, ERS-1 and GEOSAT ERM data first became available in the spring of 1995. An evaluation of these surfaces to select a mean reference surface for reprocessing of TOPEX/Poseidon GDRs was performed in the early summer of 1995 by the TOPEX Science Working Team. A 1/16-degree resolution mean surface (OSUMSS95) produced at the Ohio State University (OSU) (Yi 1995) was recommended and accepted as the best candidate. Both the GM and ERM sea surface heights were referenced to this mean surface. Interpolation of the gridded mean surface to subsatellite points was done using software provided by OSU with the surface.

3.4.2.8 GM and ERM Data Processing

The GM GDRs acquired from NODC contained no $1 \cdot s^{-1}$ averages of the $10 \cdot s^{-1}$ sea surface height data. NOAA software (J. Lillibridge and R. Agreen, personal communication) used to calculate and edit the $1 \cdot s^{-1}$ values included on the ERM GDRs was used to compute $1 \cdot s^{-1}$ averages from the GM GDR $10 \cdot s^{-1}$ values. To be consistent with the ERM GDRs, the one-degree land mask used on the GM GDRs was replaced with a 1/12-degree land mask based on the 1/12-degree ETOP05 digital gridded bathymetry data set (NOAA 1986). The GM sea surface height data were directly differenced relative to OSUMSS95 at the $1 \cdot s^{-1}$ subsatellite points, with no referencing of the data to a nominal ground track because of the nonrepeating nature of the mission. Corrections discussed in the previous sections were applied to determine the sea surface height anomaly with respect to the mean sea surface.

All GEOSAT ERM T2 GDR data and corrections were interpolated to a 17-day reference orbit using linear interpolation in the along-track direction. This provided an accurate and easily manipulated data set for subsequent processing. The reference orbit was based on the ground track of ERM cycle 2, since no satellite maneuvers occurred during this period. A statistical orbit propagation program was used to perform a least squares fit of the reference orbit to the cycle 2 ground track. This resulted in a reference orbit which comes within 100 m cross track of the actual cycle 2 data. The reference orbit for the interpolation consists of points along the orbit-solution ground track spaced at one second intervals. Ocean points were identified based on the 1/12-degree ETOP05 digital gridded bathymetry data set (NOAA 1986), and the corrections discussed in the previous sections were applied to determine the sea surface height anomaly with respect to the mean sea surface.

3.4.2.9 Data Quality Control

An iterative editing procedure was developed to edit the along-track GM and ERM GDR $1 \cdot s^{-1}$ sea surface heights, based on the sea surface slope computed from the sea surface height after detrending. Most sea surface outliers appeared as localized blunders or as unreasonably large values located at the end of arcs or next to points where the sea surface height was flagged as bad. Forward, backward and central differences of the along-track sea surface height were used to calculate estimates of the rate-of-change of sea surface height along track at each $1 \cdot s^{-1}$ point. The spacing of the along-track $1 \cdot s^{-1}$ points are such that sea surface height rate-of-changes of 5 $cm \cdot s^{-1}$ correspond to cross-track geostrophic velocities of 1.2 $m \cdot s^{-1}$. Central difference slopes with absolute values less than 5 $cm \cdot s^{-1}$, at points with forward and backward slopes greater than 5 $cm \cdot s^{-1}$ in absolute value, were flagged as bad. Three iterations were performed to flag remaining points with forward or backward slopes greater than 2.5 $cm \cdot s^{-1}$ next to previously flagged values. Finally, all points greater than 70 cm (GM) and 80 cm (ERM) absolute value were flagged. These ranges were determined by examination of the largest reasonable values observed in Loop Current eddies by GEOSAT.

3.4.2.10 Interpolation of Cycle Data

Each cycle of GM and ERM sea surface height anomaly data was interpolated to a 1/4-degree grid over the Gulf of Mexico using a two-dimensional objective analysis procedure (Cressman 1959). The method used an iterative difference-correction scheme to update an initial guess field and converge to a final gridded map. A multigrid procedure was used to provide the initial guess. The complete multigrid preconditioned Cressman algorithm is described in an appendix to Hendricks et al. (1996). Five Cressman iterations were used with radii of influences of 200, 175, 150, 125 and 100 km, employing a 100 km spatial de-correlation length scale in the isotropic Cressman weighting function. No temporal weighting of the data within a cycle was used. Maps of the sea surface height anomaly for each GM and ERM cycle are presented in Appendix A of this report. Cycles for which there were insufficient data to objectively map are shown in an along-track wiggle plot format (see Figure 3.4-1). The magnitude of the sea surface height anomaly is proportional to the width of the swath according to the scale shown on the plot, with black and white representing positive and negative anomalies, respectively.

3.4.2.11 Eddy/Buoy Statistics

A matrix-oriented language with a graphical user interface (GUI) was used to develop an interactive eddy/buoy tracking program. This program was used to automatically track and derive statistics on Loop Current eddies from the mapped sea surface height anomaly fields, and to compare satellite-tracked drifting buoy and altimeter estimates of the surface velocity along the buoy trajectories.

An example of the GUI interface for eddy tracking is shown in Figure 3.4-2. In eddy tracking mode, the user selects the initial cycle map, a given eddy contour and interpolation interval for eddy tracking, and selects an eddy by clicking on a point within the eddy contour. Linear interpolation in time of the sea surface height anomaly maps is used to estimate the analysis field at each tracking time step. Grid points within the eddy contour are found and a mask is formed to identify these points in the gridded data field. An average of the latitude and longitude pairs within the contour is used to estimate the eddy center. This eddy center is used to advance the tracking to the next time step.

The sea surface height anomaly fields are also used to calculate gridded geostrophic velocity anomalies and relative vorticity fields, based on an f-plane approximation fixed on the eddy center latitude. Geostrophic velocity anomalies are computed by central finite differencing of the equations for geostrophic velocities u and v, given by:

$$u = -\frac{g}{f}\frac{\partial h}{\partial y} \qquad \text{and} \qquad v = \frac{g}{f}\frac{\partial h}{\partial x}$$

where g is the acceleration due to gravity, and f is the local Coriolis parameter.

The relative vorticity, ζ, is computed from the gridded velocity fields by central finite differencing of the equation:

$$\zeta = \frac{\partial v}{\partial x} - \frac{\partial u}{\partial y}.$$

Total vorticity and potential vorticity are also calculated. Total vorticity is the sum of the relative vorticity and the planetary vorticity:

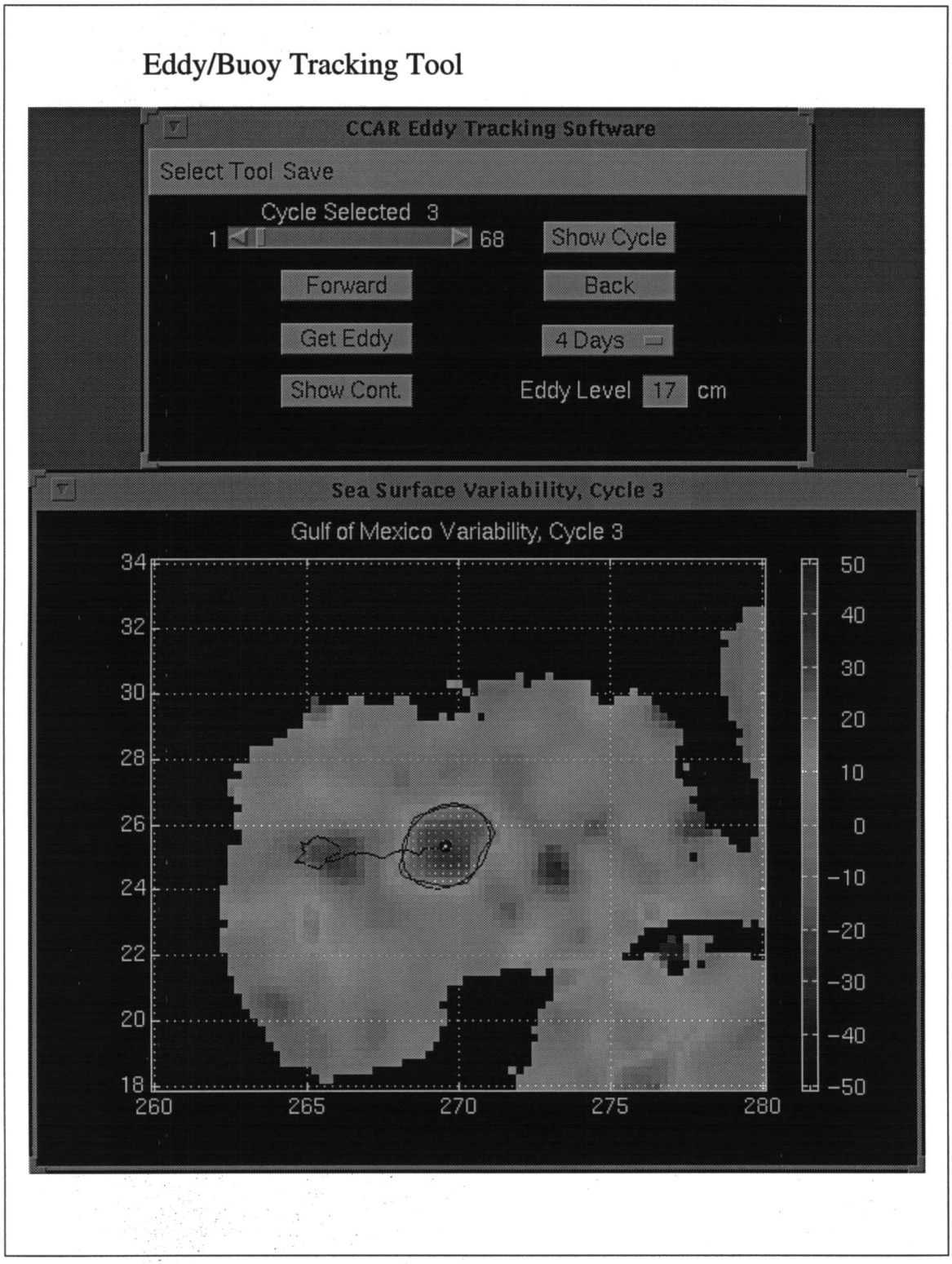

Figure 3.4-2. Graphical User Interface for eddy/buoy tracking program used to automatically track Loop Current eddies observed by GEOSAT. Eddy B tracking shown.

$$\textit{Total Vorticity} = \zeta + f$$

where f is the Coriolis parameter. We define the potential vorticity as:

$$\textit{Potential Vorticity} = (\zeta + f)/H$$

where H is the depth of the water column. This is the potential vorticity of a homogenous rotating fluid.

An ellipse is least squares fit to the tracking contour to estimate the semi-major and minor axes, A and B, of the eddy, and their ratio which, is a measure of the eccentricity of the eddy. The mean radius of the ellipse is calculated using

$$R_{ellipse} = \sqrt{AB}.$$

The maximum swirl speed, V_{swirl}, is found by averaging velocity magnitudes in 25 km bins radially from the eddy center. The bin associated with the maximum swirl speed determines the swirl radius, R_{swirl}. The Beta Rossby number defined by these quantities is:

$$\textit{Beta Rossby Number} = V_{swirl} / \beta (R_{swirl})^2$$

where β is the northward gradient of the Coriolis parameter. This is also the ratio of the Rossby numbers associated with nonlinear advection and linear wave propagation, and is a measure of the nonlinearity of the eddy. When eddies are governed by linear dynamics they disperse by radiating energy away in the form of Rossby waves. Nonlinearity, thus, implies longevity of an eddy.

Two circulation estimates are derived from the eddy tracking statistics and are based on the equivalent integrals given by Stoke's Theorem:

$$\textit{Circulation} = \iint \zeta dA = \oint \vec{V} \cdot ds.$$

The area integral is evaluated by the areal sum of the relative vorticity within the tracking contour. The line integral is approximated by the swirl velocity statistics as:

$$Circulation = 2\pi R_{swirl} V_{swirl}.$$

Other statistics calculated during eddy tracking include: 1) the north-south, east-west, and total distance of the current eddy center relative to its original center location, 2) the north-south, east-west, and total magnitude of the center velocity in the current time step, 3) the maximum sea surface height anomaly within the eddy, 4) the area bounded by the eddy contour, 5) areal averaged sea surface height anomaly within the eddy contour, and 6) areal averaged ocean depth of the eddy contour.

In buoy-tracking mode, a buoy trajectory is read into the program and finite differenced to compute the buoy velocities. Altimetric geostrophic velocity anomalies at the buoy location are interpolated from the gridded velocity fields at the buoy observation time. The velocities are computed in the same manner as described above for the eddy-tracking mode. East-west velocity, north-south velocity, and velocity magnitude time series are plotted. The vector correlation between the buoy and altimeter times series are computed using the definition of vector correlation proposed by Crosby et al. (1993), which is a generalization of the standard scalar correlation.

3.4.2.12 Annual and Seasonal RMS Variability Statistics

Annual and seasonal root mean square (RMS) variability maps for the sea surface height and geostrophic velocity anomalies were computed for each year and season. GM and ERM cycles used for these statistics are given in Table 3.4-1. Sea surface height RMS variability was computed on a 1/4 grid using sea surface height anomaly data within a one degree radius of each grid point. Geostrophic velocity RMS variability was computed in a similar manner, after first estimating the cross-track velocity anomaly, v, from the along-track slope of the sea surface height anomaly, h, using the geostrophic relationship:

$$v = \frac{g}{f}\frac{\partial h}{\partial x}$$

where g is the acceleration due to gravity, f is the local Coriolis parameter, and x is the along-track distance. The

along-track slope was estimated by a linear regression over an 80 km window, because the along-track slope was contaminated by instrument noise at wavelengths less than 40 km, and residual mean surface errors in the GM data at wavelengths less than approximately 75 km. A least-absolute deviation regression was used for this estimate (Press et al. 1992). Maps of the annual and seasonal RMS sea surface height anomalies and geostrophic velocity anomalies may be found in Appendix A.

Table 3.4-1. GEOSAT GM and ERM cycles used to compute annual and seasonal climatologies.

YEAR	CYCLES	
	GM	ERM
1985	1-12	———
1986	13-24	1-3
1987	———	4-25
1988	———	26-46
1989	———	47-68
SEASON		
WINTER	13-16	4-9,26-30,47-51
SPRING	1-4,17-20	10-14,31-35,52-57
SUMMER	5-8,21-24	15-19,36-41,58-62
FALL	9-12	1-3,20-25,42-46

3.4.3 Significant Wave Height

Significant wave height is estimated by satellite altimetry from the leading edge slope of the reflected microwave altimeter pulse. These estimates were derived on board GEOSAT and included in the GEOSAT GDRs. Initial comparisons of GEOSAT estimates with measurements from buoys showed that the accuracy was within the design specification of 0.5 m, or 10%, of significant wave height (whichever is greater), but suggested that GEOSAT values were biased low by about 0.4 meters (Dobson et al. 1987). A later study comparing GEOSAT values with buoy data concluded that there was a scaling error, recommending that GEOSAT values be multiplied by 1.13 to obtain agreement with the buoy data (Carter et al. 1992).

Gulf of Mexico significant wave height values at $1 \cdot s^{-1}$ along-track spacing were extracted from the GEOSAT GM and ERM GDRs. To remove outliers from the data set, the along-track values were smoothed by fitting a least-absolute deviation tilt and bias to the along-track data centered on a 150 km window and replacing the measured value with the regression estimate. At least 12 points were required to be within the window and the distance between the first and last good points was required to be at least 110 km, or the data point was flagged as bad. The smoothed values were multiplied by 1.13 as recommended by Carter et al. (1992).

Maps of the annual and seasonal means of the significant wave height were computed for each year and season. GM and ERM cycles used to compute the means are given in Table 3.4-1. The maps were computed on a 1/4 grid using significant wave height data within a two degree radius of each grid point. These maps may be found in Appendix B.

3.4.4 Wind Speed

Altimetric estimates of wind speed are derived from the strength of the returned power of the reflected microwave pulse given by the backscatter coefficient, σ_0. There is no simple physical relationship between wind speed and σ_0, however, and physical arguments and comparisons between measurements of σ_0 and wind speeds from buoys have both been used to develop algorithms. There is general agreement in the literature that the modified Chelton and Wentz (1986) algorithm (Witter and Chelton 1991) is preferred for deriving wind speed from GEOSAT σ_0 (Carter et al. 1992), although one study concluded that the modified algorithm was not as good as the original Chelton and Wentz (1986) algorithm (Etcheto and Banege 1992). A comparison of wind speeds from 119 NDBC buoys with GEOSAT altimeter-derived wind speeds computed using the modified Chelton and Wentz algorithm give an rms difference of 1.9 $m \cdot s^{-1}$ and an average difference of 0.45 $m \cdot s^{-1}$ (Witter and Chelton 1991). Three of the 119 NDBC buoys used in that comparison are in the Gulf of Mexico.

To estimate wind speed, $1 \cdot s^{-1}$ along-track σ_0 values were extracted from the GEOSAT GM and ERM GDRs for the Gulf of Mexico. All data for which the measured σ_0 was outside the range 4 to 19.7 dB were eliminated. The modified Chelton and Wentz (1986) algorithm (Witter and Chelton 1991) was used to estimate the wind speed at 10 m. The algorithm is given in the form of a table. To avoid discontinuities in deriving the wind speed as a function of σ_0, a cubic spline was fit to these tabular data. Wind speeds for σ_0 values less than seven

dB were estimated by linearly extrapolating the first two entries in the table.

Maps of the annual and seasonal mean wind speed at 10 meters above the ocean surface were computed for each year and season. GM and ERM cycles used to compute the means are given in Table 3.4-1. The maps were computed on a 1/4 grid using significant wave height data within a two-degree radius of each grid point. These maps may be found in Appendix C.

3.5 Ancillary Data

3.5.1 Introduction

Most of the data contributed by the various ancillary programs were provided in final calibrated form and entered into the PODBMS for further processing. Standard procedures were then followed from the point in processing at which the data were received. These procedures are described below.

3.5.2 Current Meter Data

Current meter data were obtained from the LATEX A program and were filtered with three-hour and 40-hour low pass Lanczos kernels. The resulting 40-HLP records were decimated to six hour intervals and rotated clockwise so that the v-component was aligned with the general trend of the isobaths at the mooring site. This is indicated by the notation Rθ, where θ is the direction of the v-component, after the instrument ID which consists of the mooring number appended with T, M or B (for top, middle or bottom). Actual calibration of current speed and direction, temperature, and conductivity for the different instruments was carried out under LATEX A per Nowlin et al. (1991).

3.5.3 CTD Data

CTD data were obtained from the LATEX A, GulfCet and SOOP/TIGER programs. These data were adjusted to one meter increments, as necessary, before being contoured for presentation. The data were collected with various Sea-Bird CTDs that were frequently returned to the manufacturer for calibration checks.

3.5.4 Imagery Data

AVHRR imagery were obtained from the LATEX B program and were used 'as is' with no additional navigational processing to locate oceanic features in the study area.

3.5.5 XBT Data

Sippican T-7 and Sparton XBT-7 data were obtained from the GulfCet and SOOP/TIGER programs. Similar to the case for AXBT data, the established Sippican T-7 drop-rate equation ($Z_{Sipp.} = 6.472t - 2.16 \times 10^{-3}t^2$), which was used to collect data from both Sippican and Sparton probes, is known to underestimate probe depth with time by three to five percent. Subsequently, when possible, an appropriate adjustment was calculated for the data by the GulfCet and SOOP/TIGER program investigators by comparing with nearly coincidental CTD casts in a manner similar to that presented in Singer (1990).

More recently, the Integrated Global Ocean Services System (IGOSS) Task Team on Quality Control for Automated Systems (TT/QCAS) has proposed a new equation for the Sippican T-7 probe ($Z_{IGOSS} = 6.691t - 2.25 \times 10^{-3}t^2$). This equation, derived by a temperature-error-free method, is presented and discussed in Hanawa et al. (1995). It reveals that the mean depth error is about +25 meters (3.33%) at the Sippican equation-predicted 750-meter level (after 120.75 seconds) for Sippican probes. Subsequently, an approximate linear formula for correcting depths recorded using the original Sippican drop-rate equation is: $Z_{IGOSS} = 1.0336 \times Z_{Sipp.}$. In addition, one study (from 40 probes) indicates that the same IGOSS equation identified above is suitable for Sparton XBT-7 data collected from probes manufactured beginning in 1992 (Rual et al. 1995). However, in February 1995, Sparton provided a different XBT-7 probe drop-rate equation: $Z_{Spart.} = 6.7000t - 1.638 \times 10^{-3}t^2$ (Colin McCrae, Sparton, personal communication). This equation predicts that the mean depth error is about +35 meters (4.67%), not the +25m predicted by the IGOSS equation. A subsequent polynomial expression for adjusting depths recorded using the original Sippican drop-rate equation to the new Sparton equation result is: $Z_{Spart.} = 1.0348 \times Z_{Sipp.} + 1.60 \times 10^{-5}(Z_{Sipp.})^2$. The difference in predicted depths, at the deepest depths, for the two different correcting equations is 10 meters.

3.5.6 Drifter Data

Argos drifter data were obtained from the SCULP drifter program as time series of daily-average positions and velocities for each buoy. These averages were generated from each day's available position data, generally on the order of five fixes per day.

IV. ANALYSIS OF GEOSAT DATA

4.1 Introduction

An updated climatology of Gulf of Mexico sea surface height has been produced using the complete GEOSAT altimeter time series, including declassified along-track data from the Geodetic Mission released in the summer of 1995. All along-track data are referenced relative to an accurate high-resolution mean surface, based on altimeter data collected from the TOPEX/Poseidon, ERS-1 and GEOSAT Exact Repeat Missions. By referencing these data with respect to an independent altimetric mean, the climatology can be extended to include present and future altimeter data in a consistent reference frame. Re-referencing of the GEOSAT climatology can also be achieved with a minimum of effort when more altimeter observations, such as those from the GEOSAT Geodetic Mission, are added to improve estimates of the mean sea surface topography.

The dominant oceanographic signal observed by an altimeter over the Gulf of Mexico is the sea surface height variability associated with the shedding of large anticyclonic eddies from the Loop Current. During the GEOSAT time period, April 1985 to December 1989, six major Loop Current eddies were observed. The updated climatology provides a benchmark for inter-comparison of the surface topography of these eddies and will allow comparisons with Loop Current eddies observed in the 1990s by altimeters aboard the ongoing TOPEX/Poseidon, ERS-1 and ERS-2 missions.

This report concentrates on the evaluation and synthesis of the GEOSAT Geodetic Mission (GM) and Exact Repeat Mission (ERM) sea surface climatology. The complete sea surface topography climatology is included in Appendix A. Wave height climatology is presented in Appendix B, and wind speed climatology is presented in Appendix C.

4.2 Mean Sea Surface

Both the GEOSAT GM and ERM once-per-second along-track altimeter data were referenced to a 1/16-degree resolution mean sea surface (OSUMSS95) produced at the Ohio State University (OSU) by Richard Rapp and Yuchan Yi. This mean surface is based on one-year means of sea surface height from the exact repeat TOPEX, ERS-1 and GEOSAT data, and the first cycle of 168-day repeat ERS-1 data (Yi 1995). It is believed that this is the first attempt to reference nonrepeat-track altimeter data to existing mean surfaces.

The mean sea surface height over the Gulf of Mexico is shown in Figure 4.2-1. A measure of the accuracy of the mean surface is the standard deviation of the height estimated during the least squares collocation (optimal interpolation) procedure used to estimate the mean. A map of the mean sea surface height standard deviation over the Gulf of Mexico is shown in Figure 4.2-2. Estimated standard errors of mean sea surface are approximately 2 cm along repeat ground tracks from the GEOSAT ERM. This is below the precision of the $1 \cdot s^{-1}$ measurements by the GEOSAT altimeter (estimated at 5 cm rms). Thus, the mean sea surface is ideally suited to accurately reference the along-track ERM data. The magnitude of the gradient of the surface was computed and is shown in Figure 4.2-3 to identify regions of steep mean sea surface topography which may not be well represented in the mean, especially along the nonrepeat GM ground tracks.

4.3 Evaluation of Sea Surface Height Climatology

Qualitative and quantitative comparisons have been made to determine the efficacy of referencing the GEOSAT data to the OSUMSS95 mean sea surface. Both the along-track data and the interpolated maps of sea surface height anomalies were evaluated. A detailed description of the processing of altimeter data is found in Section 3.4.

Qualitative comparisons were made of the along-track data from representative cycles of GEOSAT GM and ERM altimeter data. GM cycle 3 (Figure 4.3-1) and ERM cycle 3 (Figure 4.3-2) are shown in a wiggle plot format. This format plots the sea surface height anomaly along track so that the ground-track width is proportional to the absolute anomaly. The track is colored black or white to indicate positive and negative anomalies. The width scale is shown in the lower right hand corner of each plot. These plots show that the GM data are noticeably noisier along track than the ERM data, a result of contamination by residual geoid signal in the mean surface. Systematic errors in the OSU mean reference surface are larger along the GM ground tracks. This is primarily a result of having used only GEOSAT ERM data in the estimation of the OSU mean surface, since the GM data were classified at the time. Residual errors in the GM along-track sea surface height anomalies caused by referencing to OSUMSS95 are below 5 cm rms, the precision of the GEOSAT altimeter.

Quantitative evaluation of the interpolated GM and ERM climatology was performed by comparing buoy and altimeter estimates of the surface velocity along satellite-tracked drifting-buoy trajectories in the Gulf of Mexico during the GEOSAT time period. These statistics were computed using the

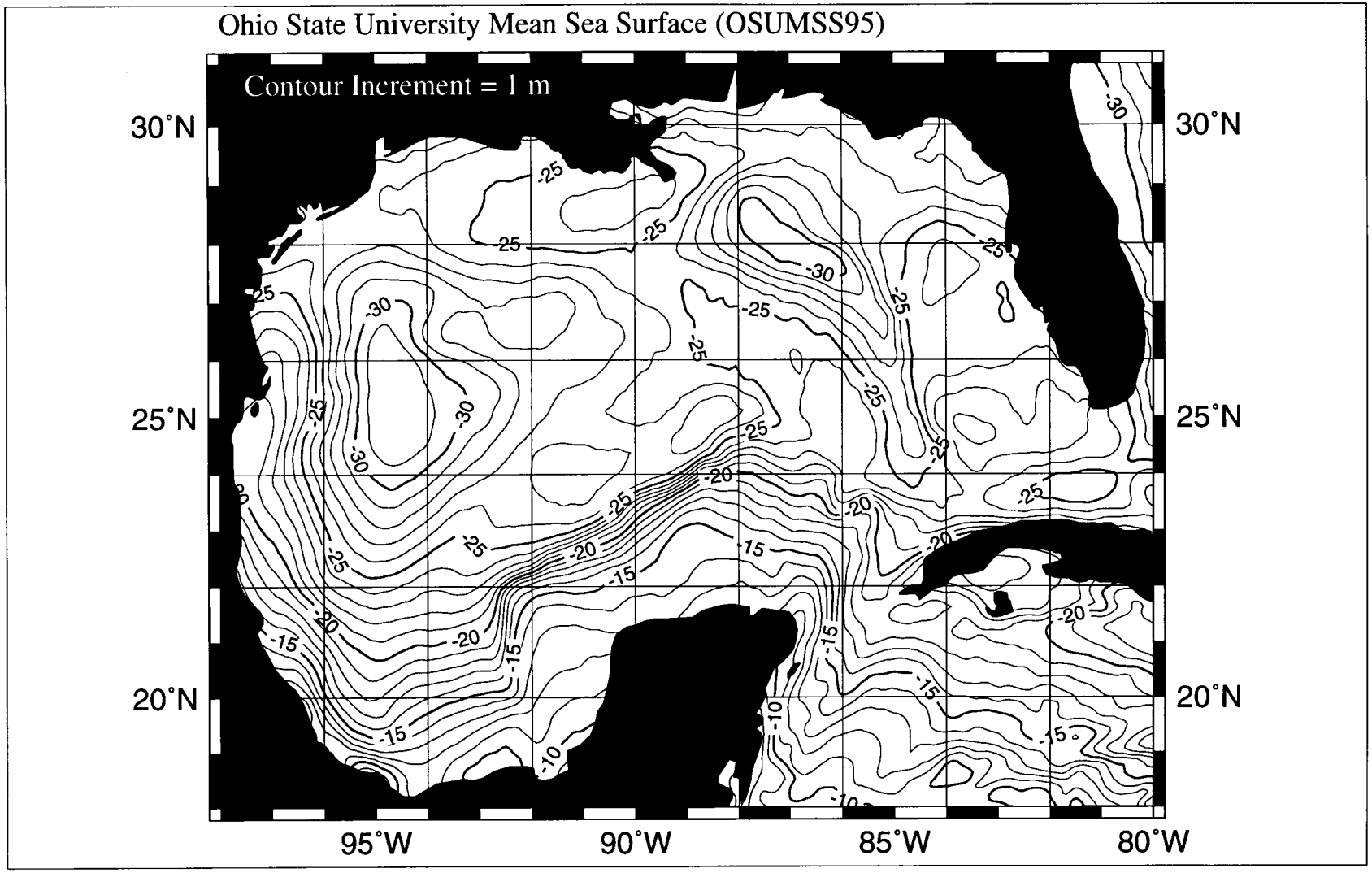

Figure 4.2-1. Ohio State University mean sea surface (OSUMSS95) in the Gulf of Mexico.

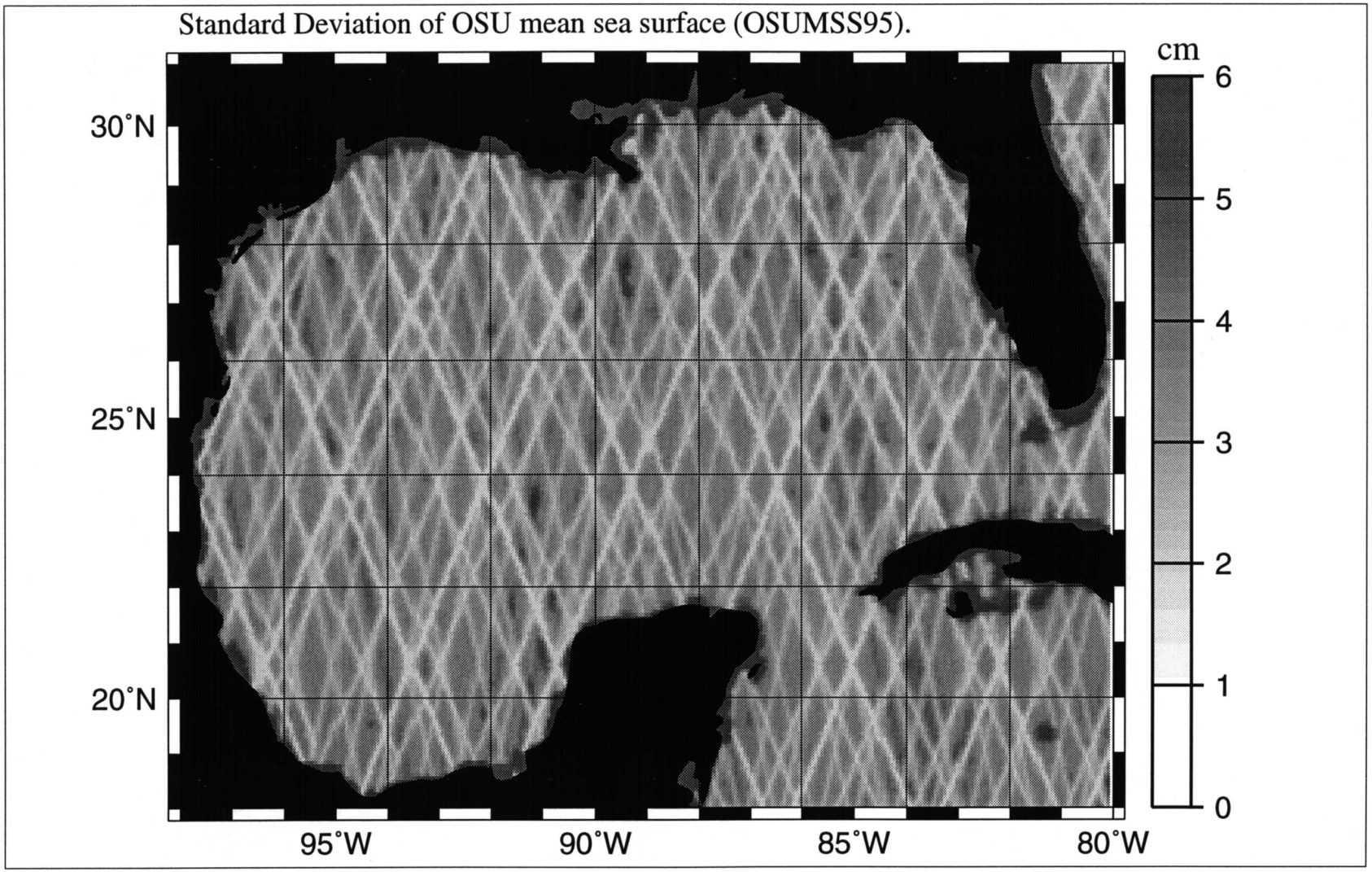

Figure 4.2-2. Estimated standard deviation of the Ohio State mean sea surface(OSUMSS95) based on the least squares collocation procedure statistics (Yi 1995).

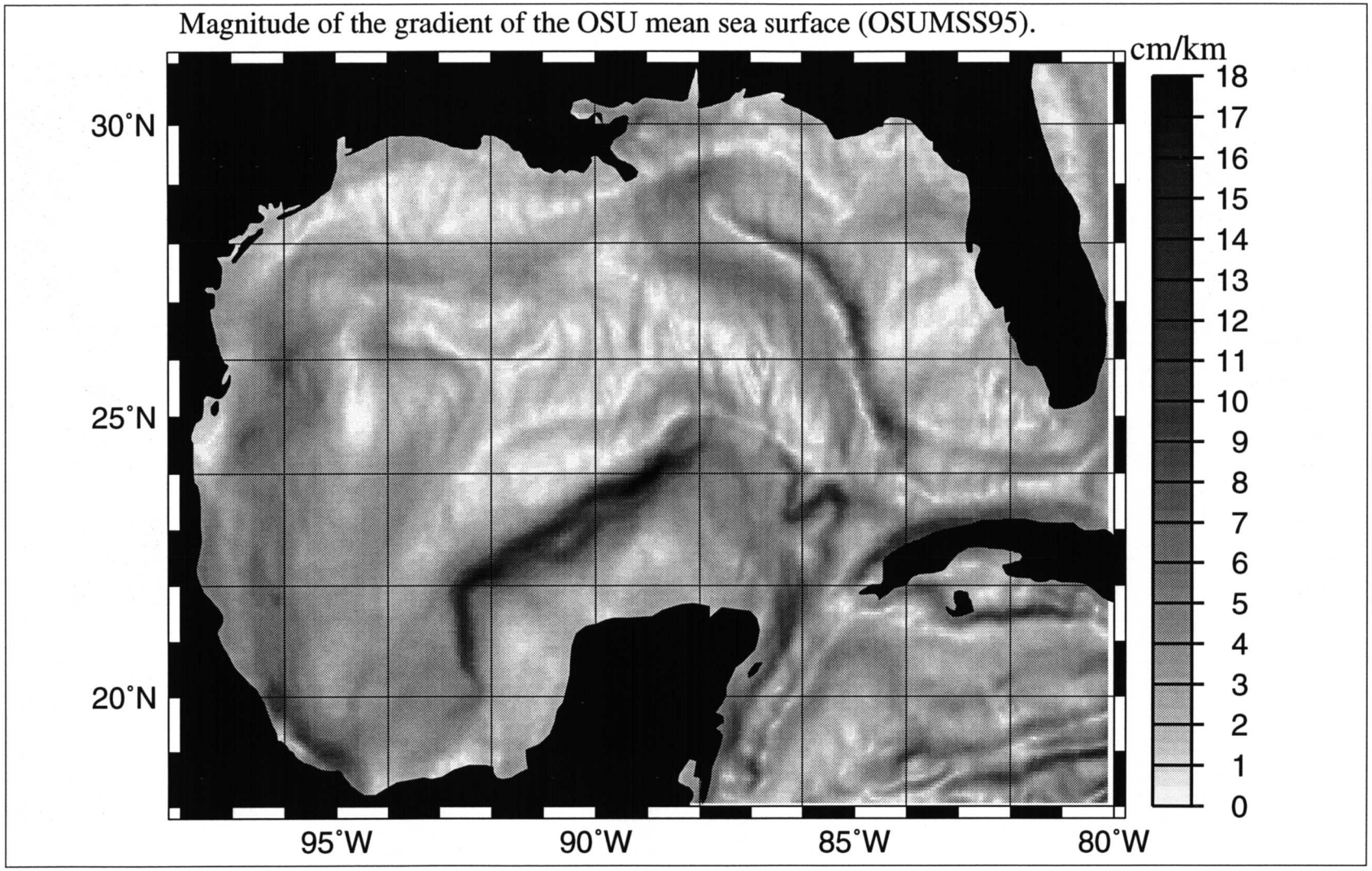

Figure 4.2-3. Magnitude of the gradient of the OSU mean sea surface (OSUMSS95).

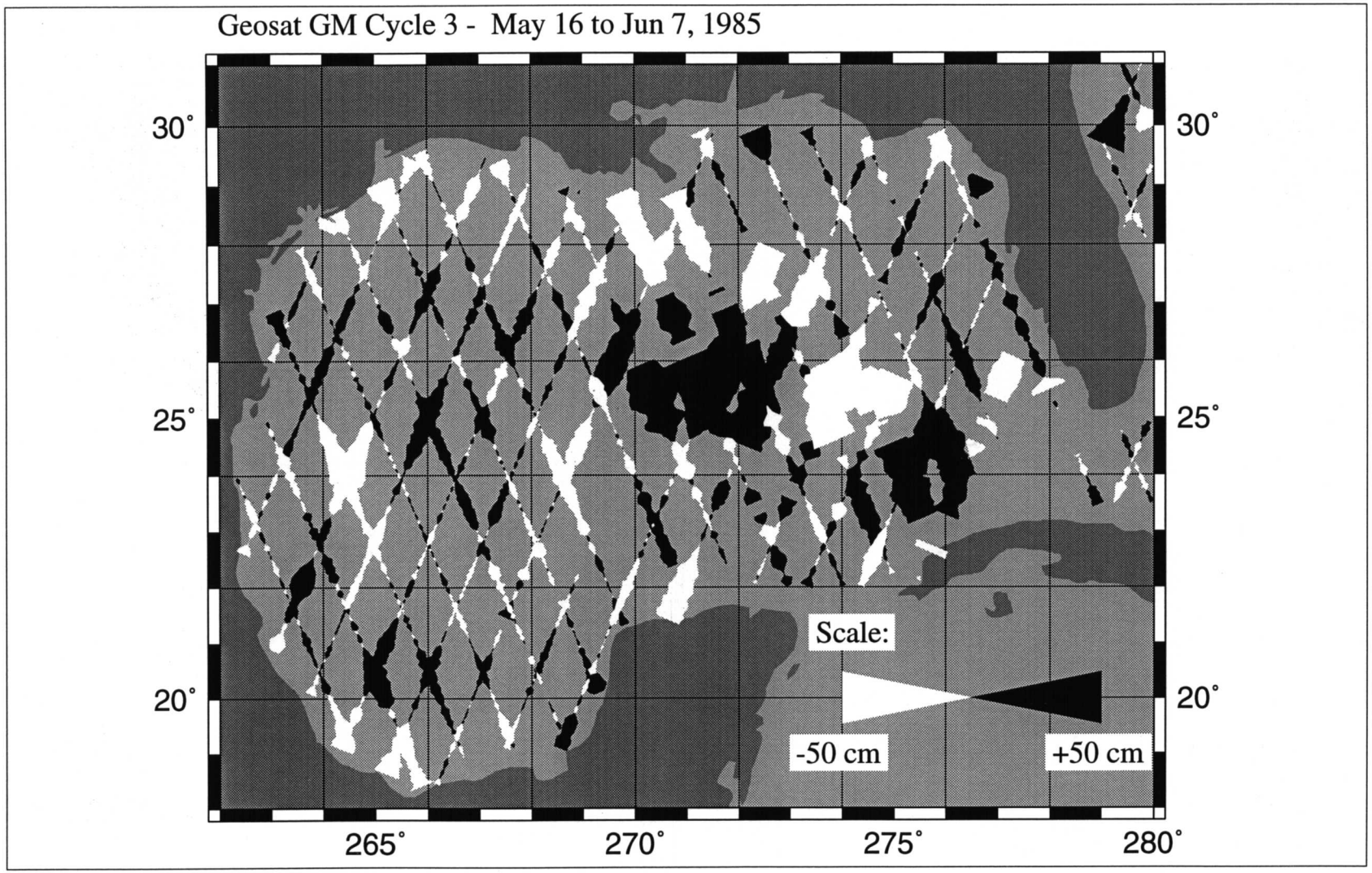

Figure 4.3-1. Sample GEOSAT Geodetic Mission along-track sea surface height anomaly with respect to mean sea surface (OSUMSS95) in wiggle plot format.

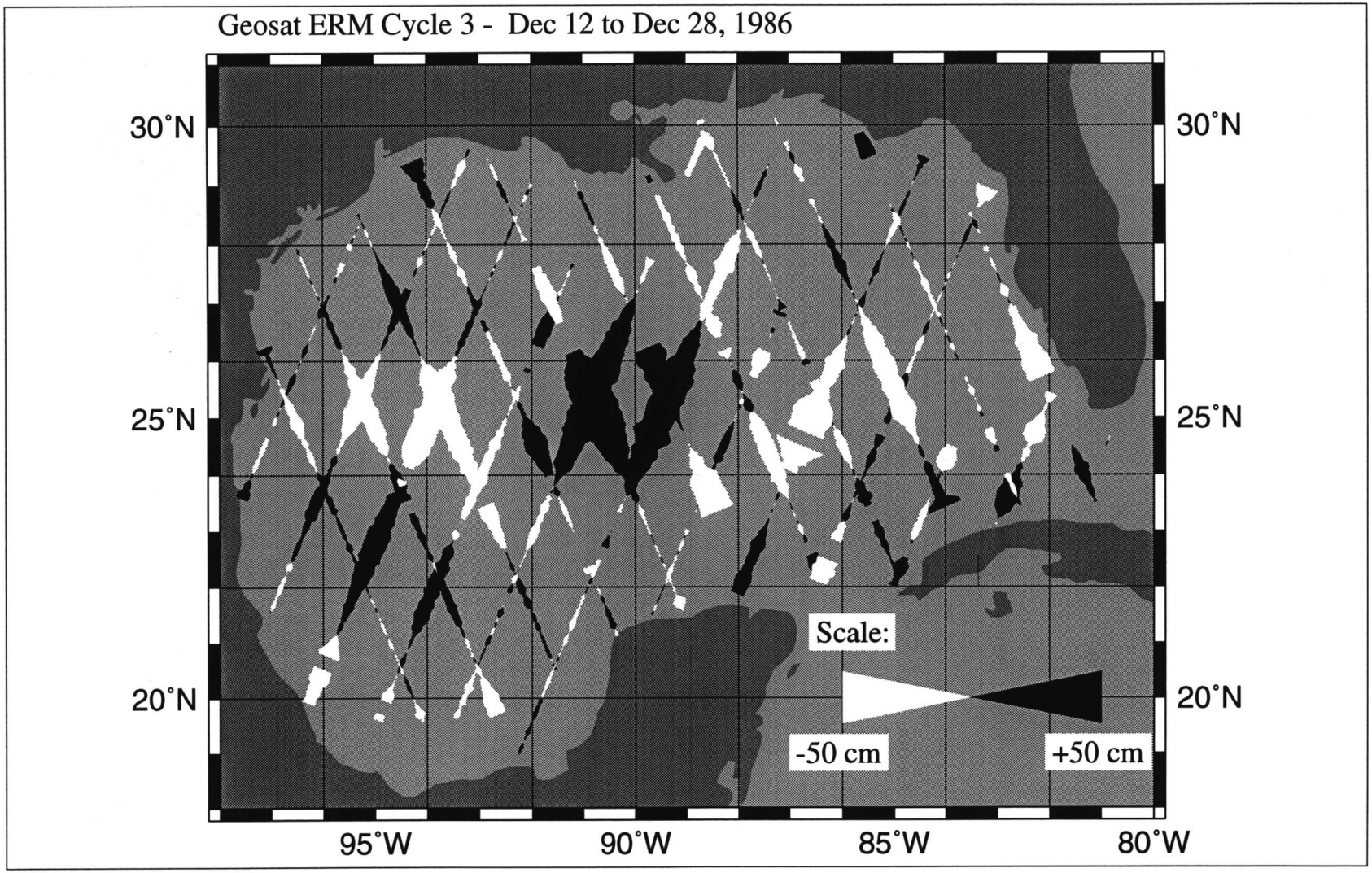

Figure 4.3-2. Sample GEOSAT Exact Repeat Mission along-track sea surface height anomaly with respect to mean sea surface (OSUMSS95) in wiggle plot format.

program described in Section 3.4.2.11. To evaluate the climatology, Argos drifters tracked during both the GM (drifter 3379) and the ERM (drifter 3345) were selected. These drifters were tracked in Loop Current eddies for over six months. Comparisons of the altimeter-derived velocities with the drifter velocities are shown in Figures 4.3-3 and 4.3-4, and agree quite well in both magnitude and direction. The vector correlations of the time series exceed 0.70 for both the GM and ERM time periods. This comparison is a stringent test of the accuracy of the altimeter-derived ocean topography. Errors in sea surface topography maps due to removal of the mean, data errors, outages, or undersampling should significantly affect the correlation statistics. The good correlations found with both GM and ERM data imply that the derived climatology is consistent throughout the GEOSAT mission. The 23-day and 17-day sampling of Loop Current eddies by the GM and ERM orbits appears to be as good as tandem sampling by TOPEX and ERS-1 in 10-day and 35-day repeat orbits. These GEOSAT correlations are as good as have been found in similar buoy/altimeter comparisons with altimetric analyses based on combined TOPEX and ERS-1 altimeter data (Jochens et al. 1996).

Quantitative comparisons were also made between GEOSAT-derived sea surface height topography and topography derived from in situ measurements collected during the Gulf of Mexico Physical Oceanography Program (SAIC 1988; SAIC 1989). When maps of sea surface height topography were unavailable, maps of the depth of the 8°C isotherm were used to estimate the sea surface height topography, assuming a density contrast of 2×10^{-3} g·cm^{-3} (Johnson et al. 1992). Eddy-center height anomalies relative to eddy-perimeter anomalies were estimated from the coincident altimeter cycle and composite survey maps. The summary of these comparisons is shown in Table 4.3-1.

GEOSAT estimates were approximately 150% of the in situ estimates, which is reasonable given that altimeter measurements include the additional baroclinic contribution from depths below the 8°C isotherm, and the barotropic contribution to which the hydrography is insensitive. These contributions could be substantial, given the deep penetration of the eddy flow field found in hydrographic (Hofmann and Worley 1986) and current meter (Hamilton 1990) data. This is in contrast to earlier comparisons of GM altimetry with in situ measurements, which found a significant reduction in the amplitude of the sea surface topography as well as inferred current speeds (Johnson et al. 1992). This was an artifact of excessive smoothing and poor spatial resolution required by the crossover analysis technique employed in that study. Along-track detrending of the nonrepeat-track altimetry from the GM to an accurate mean sea surface makes such processing

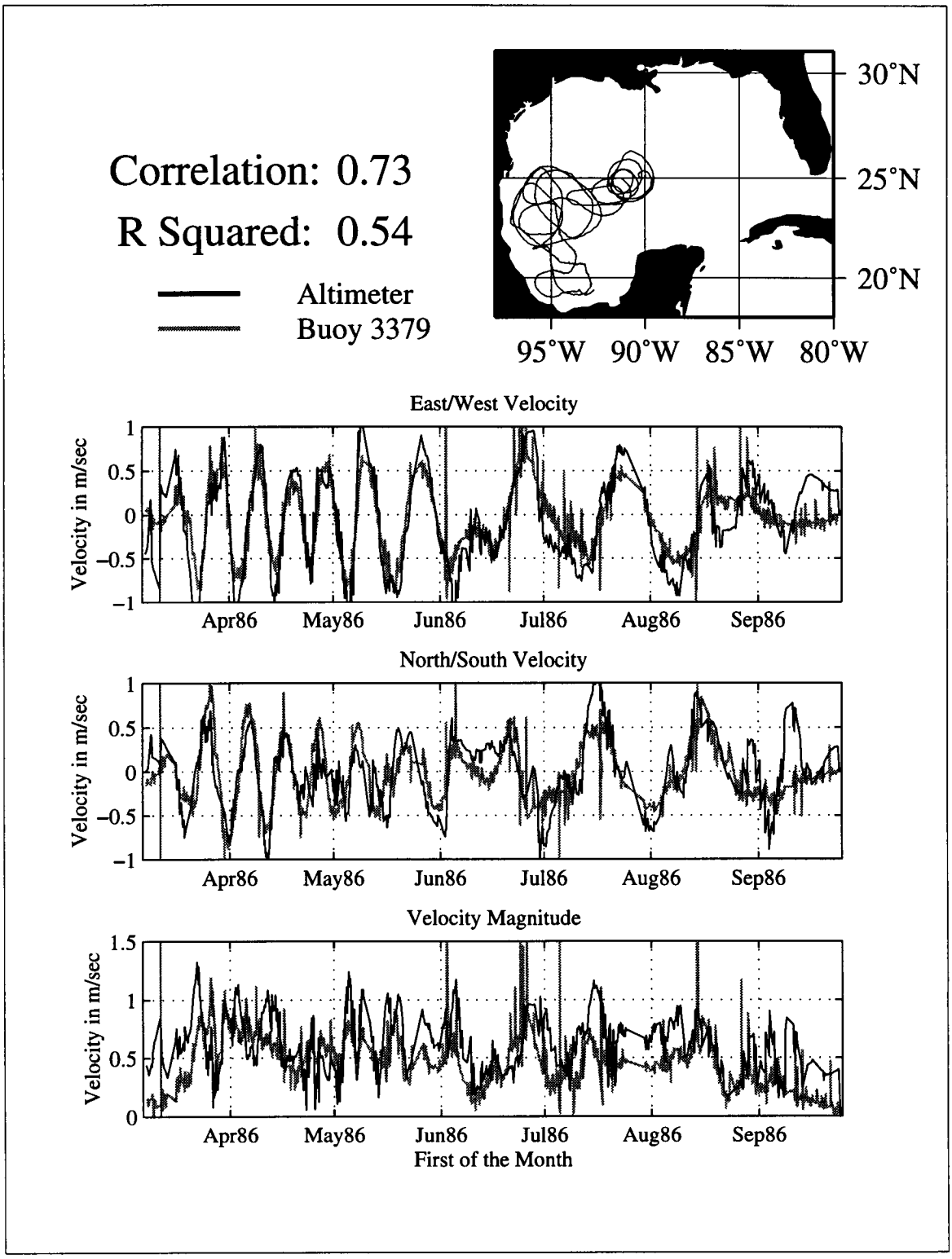

Figure 4.3-3. Comparison of GEOSAT GM altimeter-derived estimates of geostrophic velocity anomalies with velocity estimates for drifter 3379 (February 1986 to September 1986).

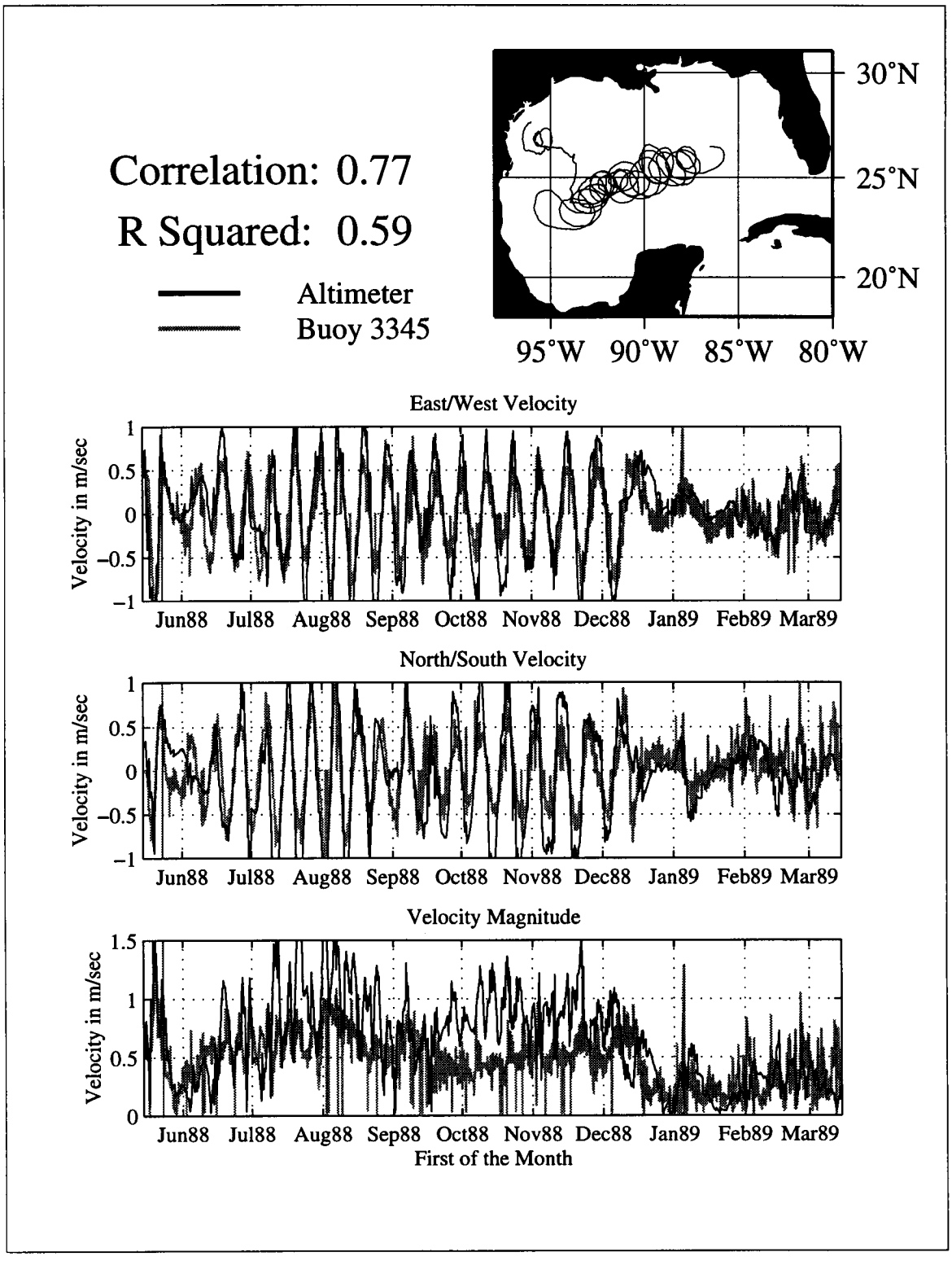

Figure 4.3-4. Comparison of GEOSAT ERM altimeter-derived estimates of geostrophic velocity anomalies with velocity estimates for drifter 3345 (June 1988 to March 1989).

Table 4.3-1. Comparison of GEOSAT topography with in situ measurements.

GEOSAT Cycle No.	Eddy Center Height (cm)		Date	Source
	Altimetry	In situ		
GM 5	65	40	07/85	SAIC 1988, Fig. 4.3-22
GM 10	45	28	11/85	SAIC 1988, Fig. 4.4-12
GM 14	15	20	01/86	SAIC 1988, Fig. 4.4-20a
GM 17	20	23	04/86	SAIC 1988, Fig. 4.5-7
ERM 21	20	12	10/87	SAIC 1989, Fig. 4.3-13
ERM 38	50	30	07/88	SAIC 1989, Fig. 4.3-18
ERM 43	40	20	10/88	SAIC 1989, Fig. 4.3-22

unnecessary and retains a majority of the topographic height signal measured by the altimeter.

It can be concluded, based on quantitative comparisons with both drifter and hydrographic data, that the altimetric analyses presented in this report preserve both the sea surface height signal and surface slope. This validates the utility of the mean surface used in this study (OSUMSS95) for referencing altimeter data for climatological studies of the Gulf of Mexico.

4.4 Loop Current Shedding Statistics

Maps of the sea surface height anomaly in the Gulf of Mexico (Appendix A) were used to determine the eddy shedding interval during the GEOSAT time period. Separation of eddies from the Loop Current is difficult to determine using sea surface height anomaly data alone, since the mean topography defining attachment or separation is absent from the measurements. Consequently, using altimeter observations, it was decided to arbitrarily define shedding times as when the eddy center transited across 90°W longitude. This was based on historical observations of Loop Current eddies, which showed that if an eddy center reached 90°W longitude, reattachment would be unlikely. Table 4.4-1 shows the major eddy separation times and shedding intervals based on transit across 90°W longitude. The names for the Loop Current eddies presented in Table 4.4-1 follow the convention used in the earlier MMS studies, with a cross-reference to names used by the private sector Eddy Joint Industry Project (EJIP). However, there is no MMS name for one of the eddies, Nelson eddy.

Table 4.4-1. Major Loop Current eddy-separation times and shedding intervals during the GEOSAT period.

Loop Current Eddy	Date of Separation*	Interval (days)
B (Fast Eddy)	July 1985	--
C (Hot Eddy)	February 1986	185
D (Krazy Eddy)	December 1986	300
E (Lazy Eddy)	January 1988	425
F (Eddy Murphy)	August 1988	195
N (Nelson Eddy)	September 1989	365
Mean time between eddy shedding events:		**294 days (9.8 months)**

* Defined as transit across 90°W longitude.

The average period between transit across 90°W longitude was 9.8 months, with individual separation intervals ranging from 6 to 14 months. This compares favorably with the 11.1 month average shedding period (6 to 17 month range) determined from an analysis of a 22-year data set of satellite imagery (Vukovich 1995). Sturges (1992 and 1994) determined that the fundamental period of Loop Current variability is about 8.5 months, using approximately 12 years of IR and ship-of-opportunity transects to obtain estimates of the northernmost position of the Loop Current front. The GEOSAT analysis falls midway between these two estimates.

4.5 Eddy Tracking and Statistics

A matrix oriented program with a graphical user interface described in Section 3.4.2.11 was used to objectively track Loop Current eddies and derive statistics from the GEOSAT climatological sea surface height anomaly fields. A composite of Loop Current eddy tracks from the GEOSAT time period is shown in Figure 4.5-1. The 17-cm contour was selected for eddy tracking after initial tests showed that this contour closely matched the location of maximum gradients in the topography and allowed continuous tracking of eddies during their translation through the western Gulf of Mexico. The eddy centers were determined from the centroid of the area enclosed by the tracking contour. Four major Loop Current eddies [B (Fast), C (Hot), D (Krazy) and F (Murphy)], and one secondary eddy, (eddy O), were continuously tracked for extended periods in the western Gulf of Mexico. Tracking statistics for these major Loop Current eddies are presented below

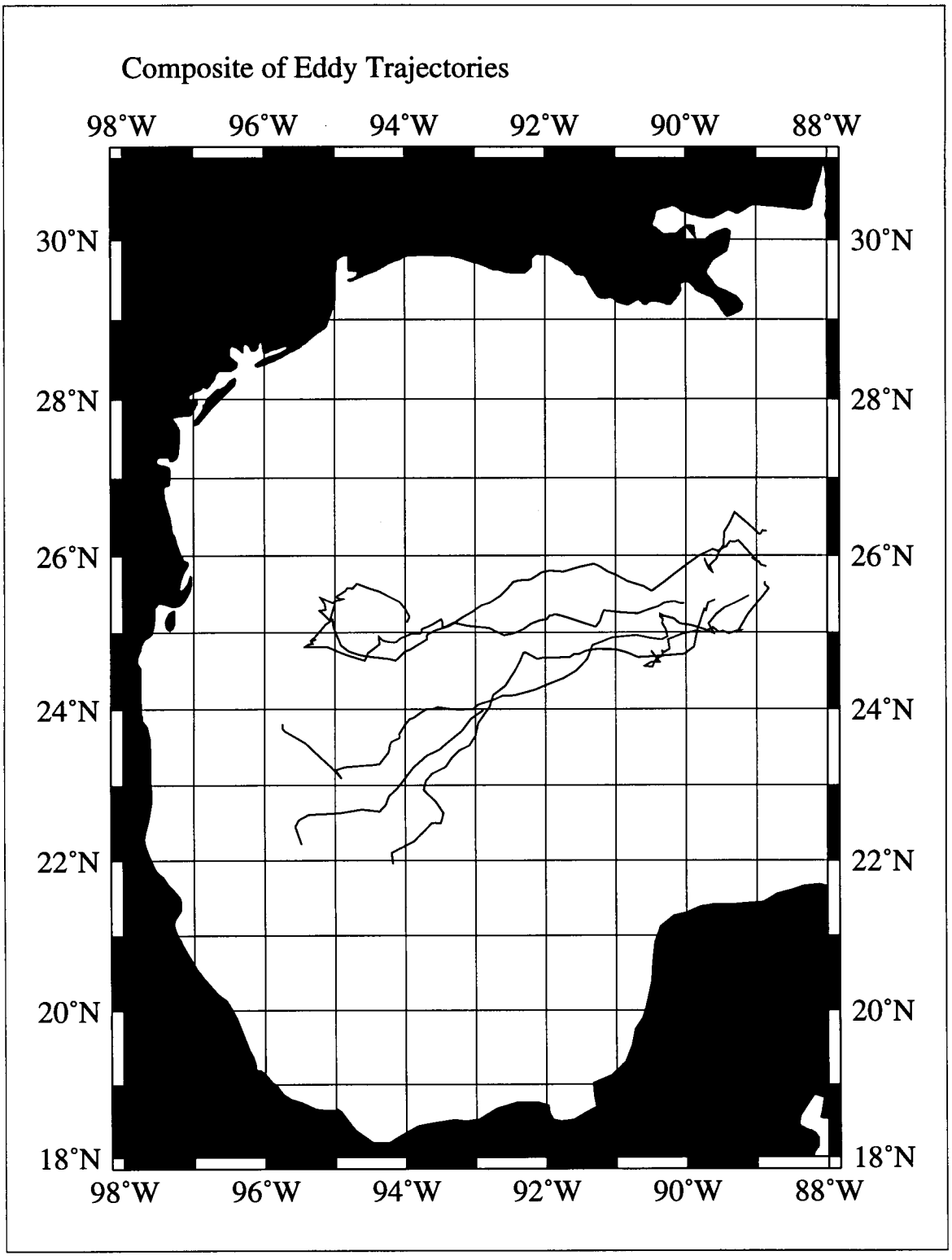

Figure 4.5-1. Composite of eddy-center locations determined from the centroid of the area contained within the 17-cm sea surface height anomaly contour.

with a description and interpretation of the dynamical events observed in light of the updated altimeter climatology.

4.5.1 Eddy B with Ghost Eddy Formation and Dissipation

A large anticyclone, referred to as eddy B, separated from the Loop Current in July 1985 (Lewis and Kirwan 1987; Forristall et al. 1992). The primary events during the westward propagation of this eddy through the eastern Gulf of Mexico were its movement onto the slope in mid-August 1985, and its subsequent rapid movement southwestward into deeper water in mid-September 1985 (Lewis et al. 1989). Altimetric tracking of eddy B, using the GEOSAT climatology, is shown in Figure 4.5-2, and the derived statistics are presented in Figures 4.5-3a, b, c and d. The areal-averaged ocean depth within the tracking contour (Figure 4.5-3b) highlights the movement of eddy B into and away from the shallower depths over the continental slope in August and September 1985, resulting from the north-south displacement of the eddy center (Figure 4.5-3a). Lewis et al. (1989) noted that there are no internal mechanisms that would cause a ring to migrate onto the continental slope, and hypothesize that unobserved external flow features such as cyclones, anticyclones or shelf-slope circulation could have influenced the path of the eddy. The altimeter climatology presented in this report provides additional observations to assess the role of external forcing mechanisms on the anomalous movement of eddy B.

One of the observed circulation features in the western Gulf of Mexico at this time was a secondary eddy, Ghost eddy (Forristall et al. 1992), which was discovered when a drifter left eddy B and began circulating in a previously unobserved eddy to the southwest (Figure 4.5-4). There is some controversy over the origin of this feature. Forristall et al. (1992) presented evidence that suggested that a large elongated eddy separated from the Loop Current and later split into two smaller eddies, eddy B and Ghost eddy. Johnson et al. (1992) noted in their analysis of GEOSAT crossover data that there was a growing high in sea surface topography in the southwestern Gulf of Mexico at the time Ghost eddy was detected, possibly forced by the presence of a maximum in the negative wind stress curl over the western Gulf of Mexico. The new altimeter climatology presented in this report does not support wind forcing as the primary mechanism for the formation of this eddy. While a weak anticyclonic circulation was present in the western Gulf of Mexico in April and May 1985 (Figures 4.5-5 and 4.5-6), the first indication of Ghost eddy was observed after eddy B approached, and cyclones intensified to both the east and west of, a coherent positive anomaly in the sea surface topography at 25°N latitude, 93°W

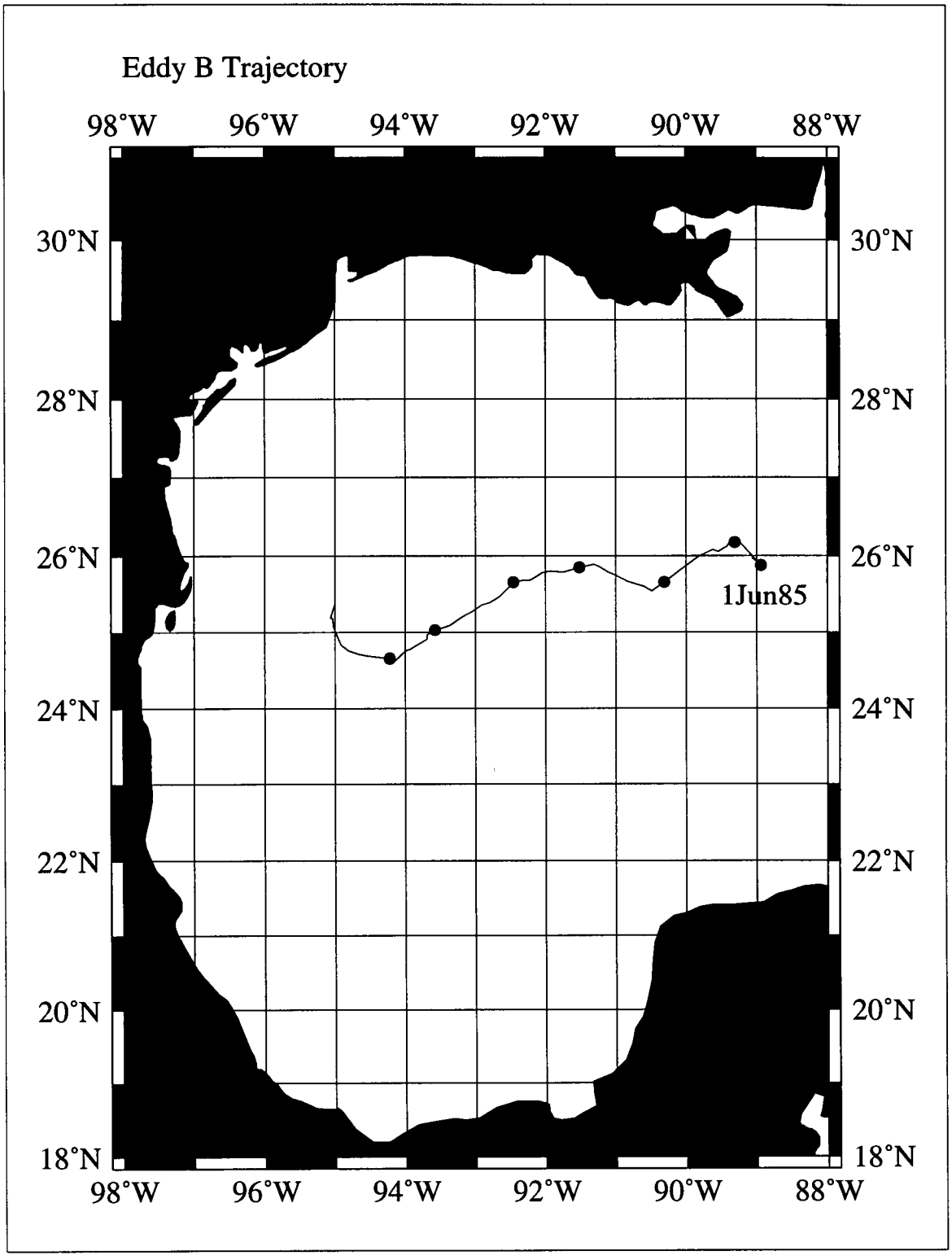

Figure 4.5-2. Trajectory of eddy B center determined using GEOSAT altimeter data and an objective tracking program. Dots show center location on the first of each month.

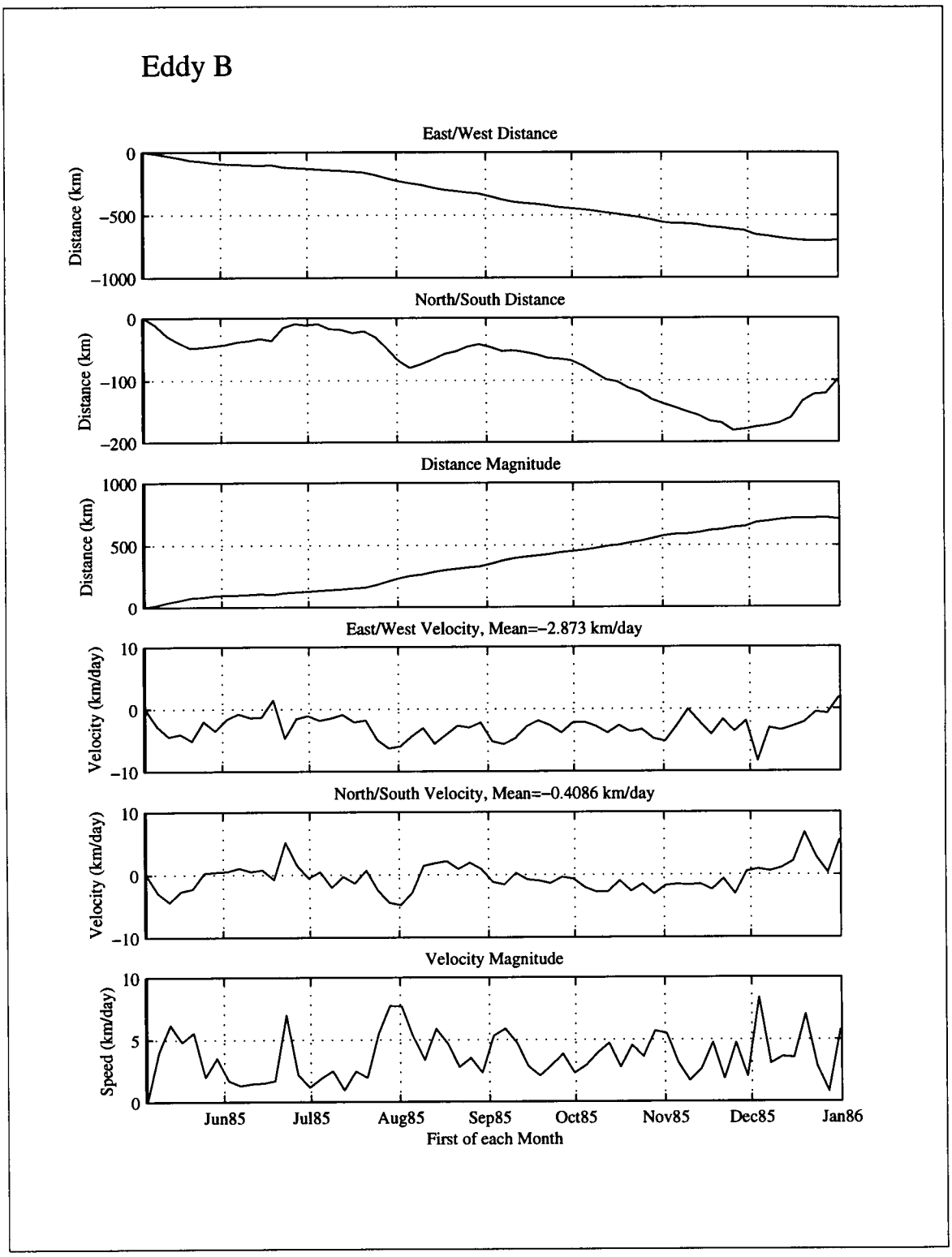

Figure 4.5-3a. Eddy tracking statistics for eddy B from May 1985 to January 1986 using GEOSAT altimetry: distance and velocity statistics.

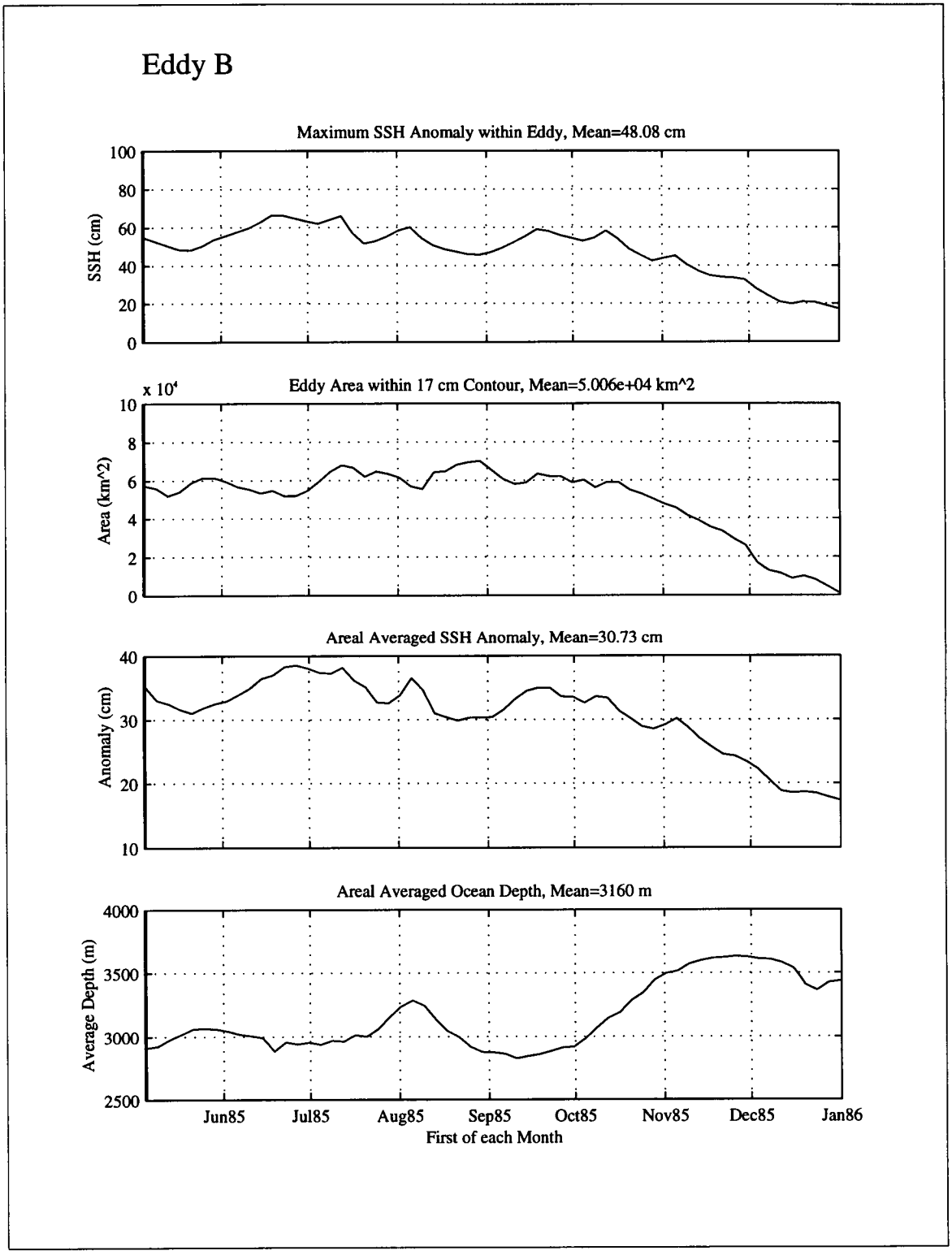

Figure 4.5-3b. Eddy tracking statistics for eddy B from May 1985 to January 1986 using GEOSAT altimetry: maximum height anomaly, eddy area, areal averaged anomaly and ocean depth.

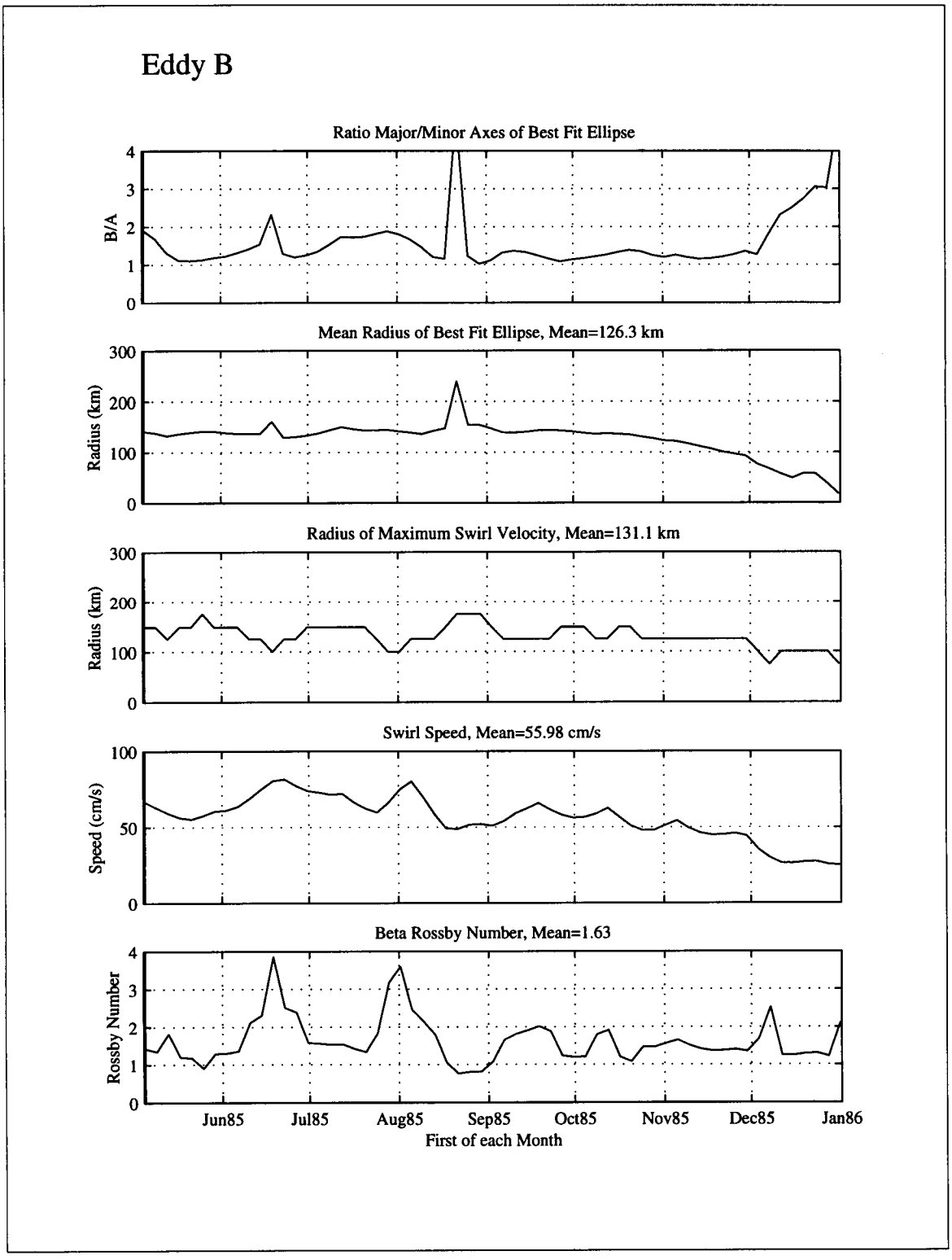

Figure 4.5-3c. Eddy tracking statistics for eddy B from May 1985 to January 1986 using GEOSAT altimetry: eccentricity, radius estimates, swirl speed, and Rossby number.

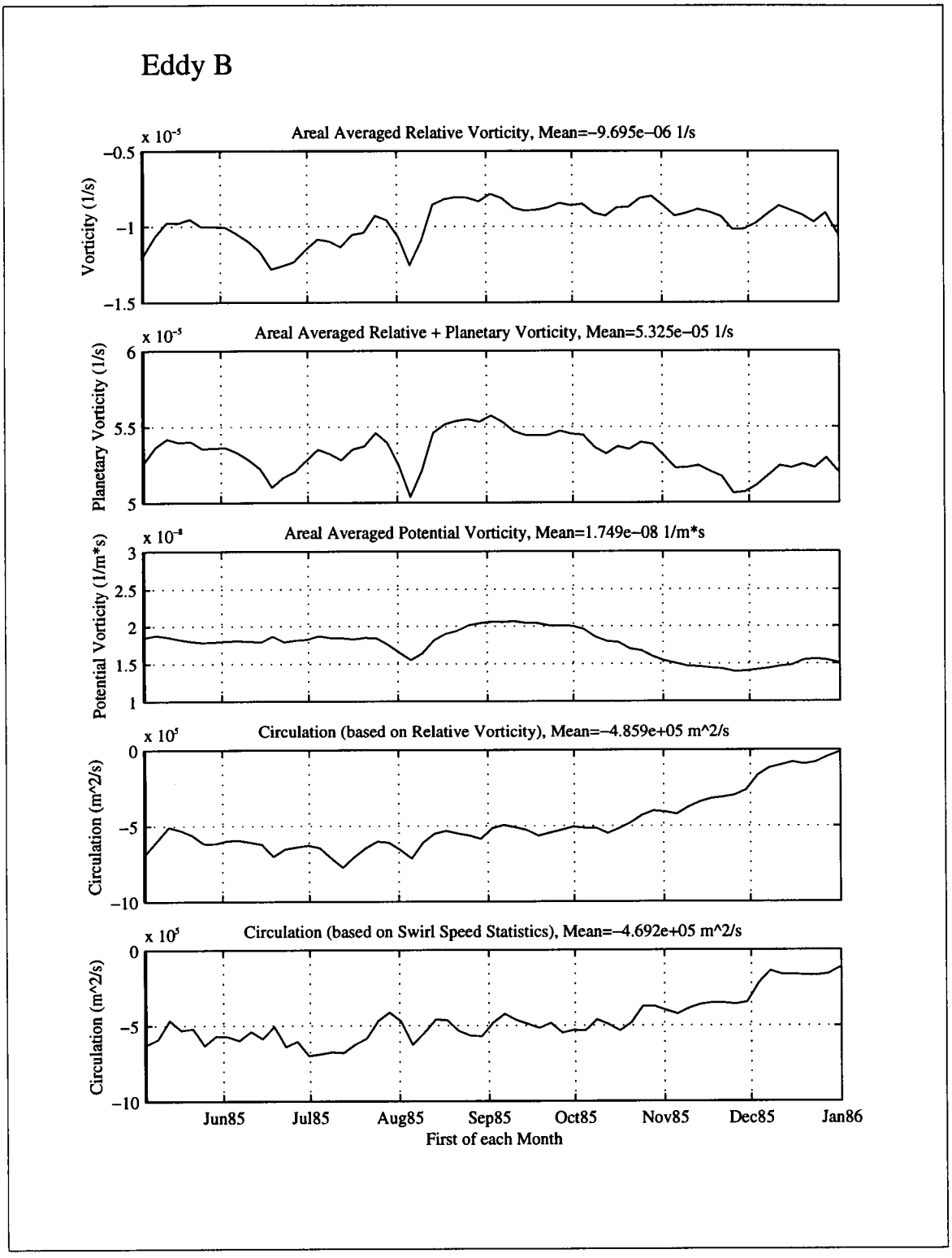

Figure 4.5-3d. Eddy tracking statistics for eddy B from May 1985 to January 1986 using GEOSAT altimetry: vorticity and circulation statistics.

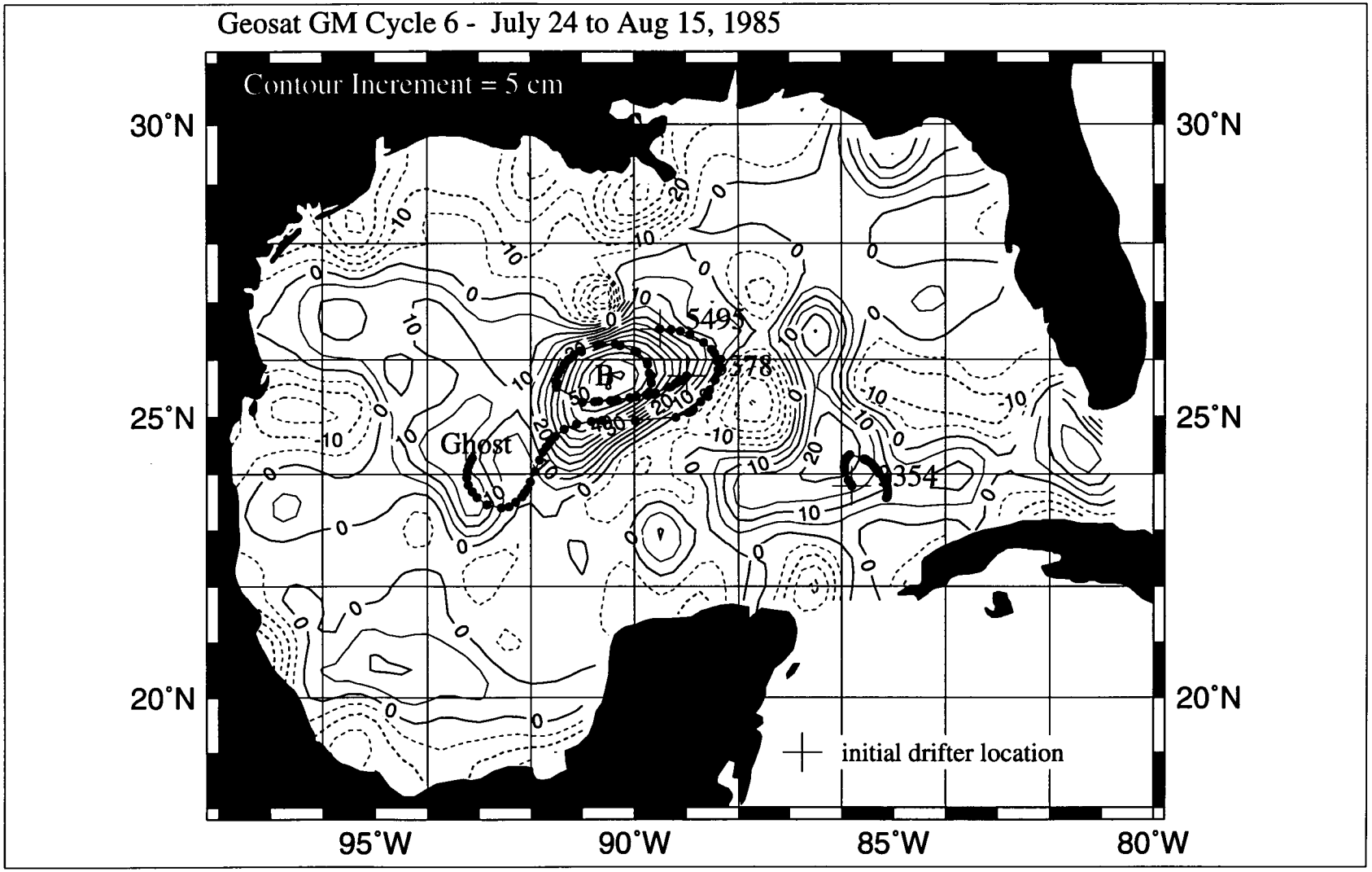

Figure 4.5-4. Sea surface height anomaly with respect to mean sea surface (OSUMSS95) for GEOSAT GM Cycle 6 (July 24 to August 15, 1985) showing eddy B and Ghost eddy. Drifter locations within five days of the midpoint of the cycle are shown.

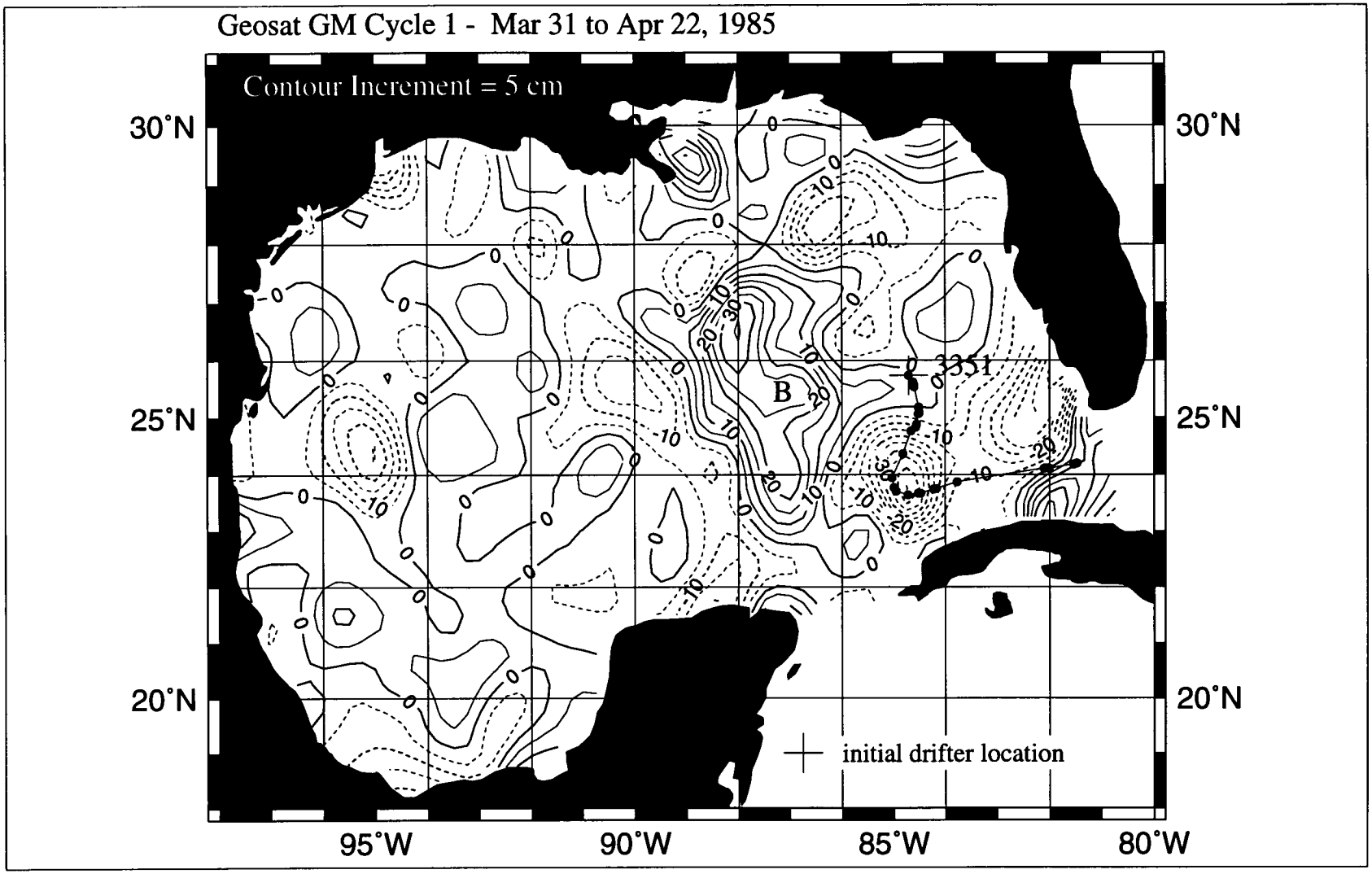

Figure 4.5-5. Sea surface height anomaly with respect to mean sea surface (OSUMSS95) for GEOSAT GM Cycle 1 (March 31 to April 22, 1985) showing early stages of eddy B and Ghost eddy. Drifter locations within five days of the midpoint of the cycle are shown.

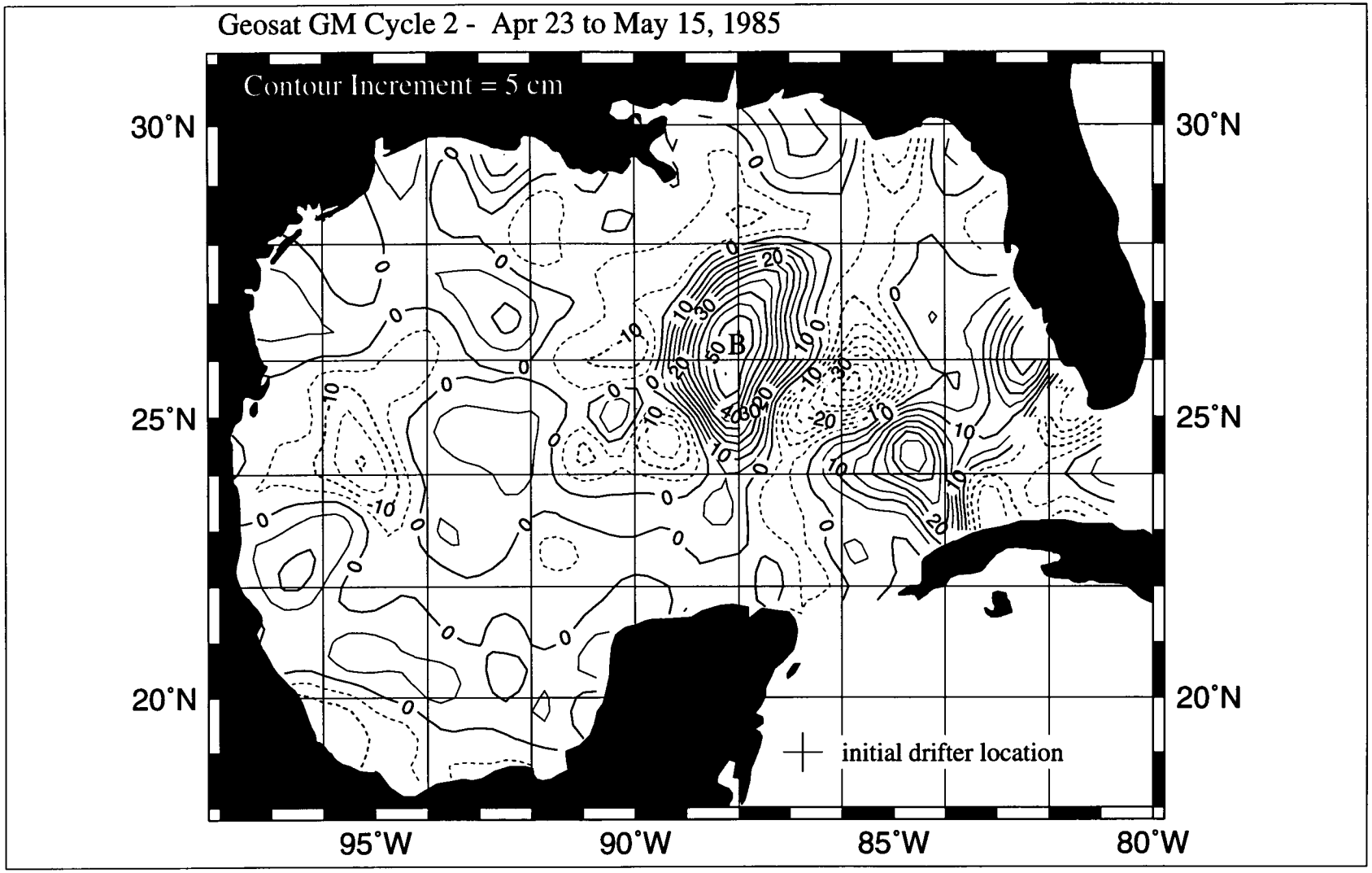

Figure 4.5-6. Sea surface height anomaly with respect to mean sea surface (OSUMSS95) for GEOSAT GM Cycle 2 (April 23 to May 15, 1985) showing early stages of eddy B and Ghost eddy.

to 94°W longitude (Figures 4.5-7 and 4.5-8). The cyclone at 25°N latitude, 91°W longitude was located near cyclonic turns of the warm fronts detected on the far western boundary of eddy B in the last clear satellite infrared image of the Gulf of Mexico charted by the National Environmental Satellite Service on June 4, 1985 (see Figure 3 in Forristall et al. 1992). Ghost eddy appears to have formed from the interaction of this cyclone with the western perimeter of eddy B, and may have been further enhanced by the far western cyclone.

The splitting scenario of Forristall et al. (1992) is difficult to support, given the near-constant geometric and kinematic statistics of eddy B derived from the altimetry during the formation of Ghost eddy. A splitting of the primary eddy into two smaller pieces should show a reduction in the size and circulation of eddy B during this time period; however, these statistics remain relatively constant (Figures 4.5-3a and d). Ghost eddy appears to be a minor secondary anticyclone which formed on the perimeter of eddy B, due in large part to the cyclonic circulation on the southwest boundary of eddy B. A much stronger secondary eddy, eddy O, was observed later in the GEOSAT climatology associated with the extended penetration of the Loop Current into the Gulf of Mexico during the Nelson eddy event in 1989, and followed a path similar to Ghost eddy. The track of eddy O from July to September 1989 is shown in Figure 4.5-9. Eddy O had a maximum height anomaly which averaged over 35 cm during this time period, compared with the relatively weak Ghost eddy, which rarely showed maximum values over 20 cm.

The cyclones to the south and west of eddy B, after the formation of Ghost eddy, provide a viable mechanism for the movement of eddy B onto the northern Gulf of Mexico slope in mid-August 1985 (Figure 4.5-10). The cyclones were positioned so that their interaction with eddy B would have forced eddy B to the northwest (Hooker 1987). Lewis et al. (1989) proposed such a scenario when they speculated that a cyclone had formed in the wake of Ghost eddy (by Rossby wave dispersion) and interacted with eddy B. However, it is doubtful that the cyclonic circulation produced by the dispersive decay of a minor eddy such as Ghost eddy could be the primary mechanism for the observed movement of eddy B. A more likely source of the cyclonic circulation necessary to cause this movement would have been cyclonic vorticity produced by lateral shear as eddy B interacted with the abrupt topography of the Campeche escarpment. Similar dynamics have been proposed for the formation of the vortex pairs and triads observed in the western Gulf of Mexico resulting from the interaction of Loop Current eddies with the continental shelf (Vidal et al. 1992; Vidal et al. 1994).

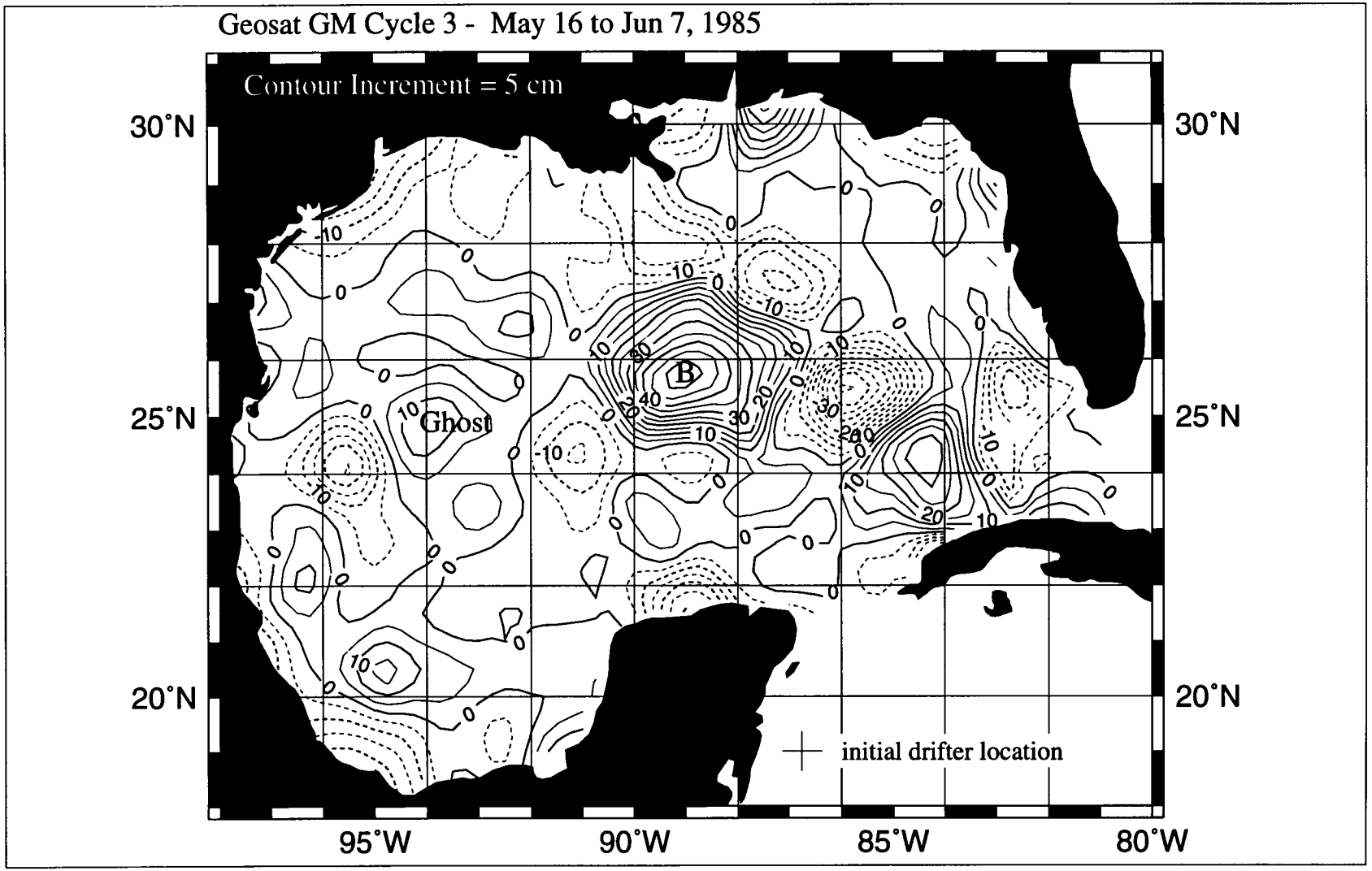

Figure 4.5-7. Sea surface height anomaly with respect to mean sea surface (OSUMSS95) for GEOSAT GM Cycle 3 (May 16 to June 7, 1985) showing eddy B and Ghost eddy.

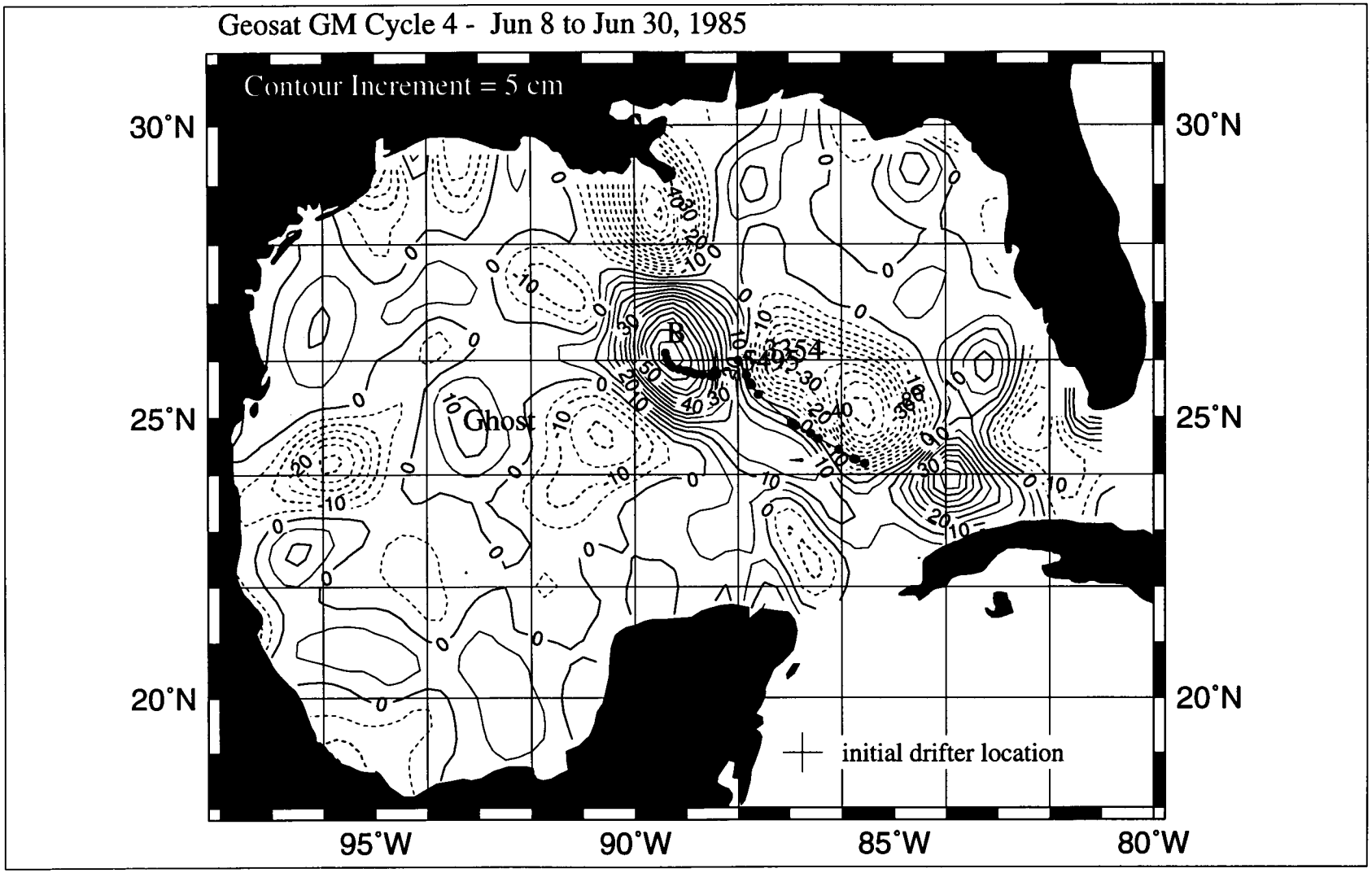

Figure 4.5-8. Sea surface height anomaly with respect to mean sea surface (OSUMSS95) for GEOSAT GM Cycle 4 (June 8 to 30, 1985) showing eddy B and Ghost eddy. Drifter locations within five days of the midpoint of the cycle are shown.

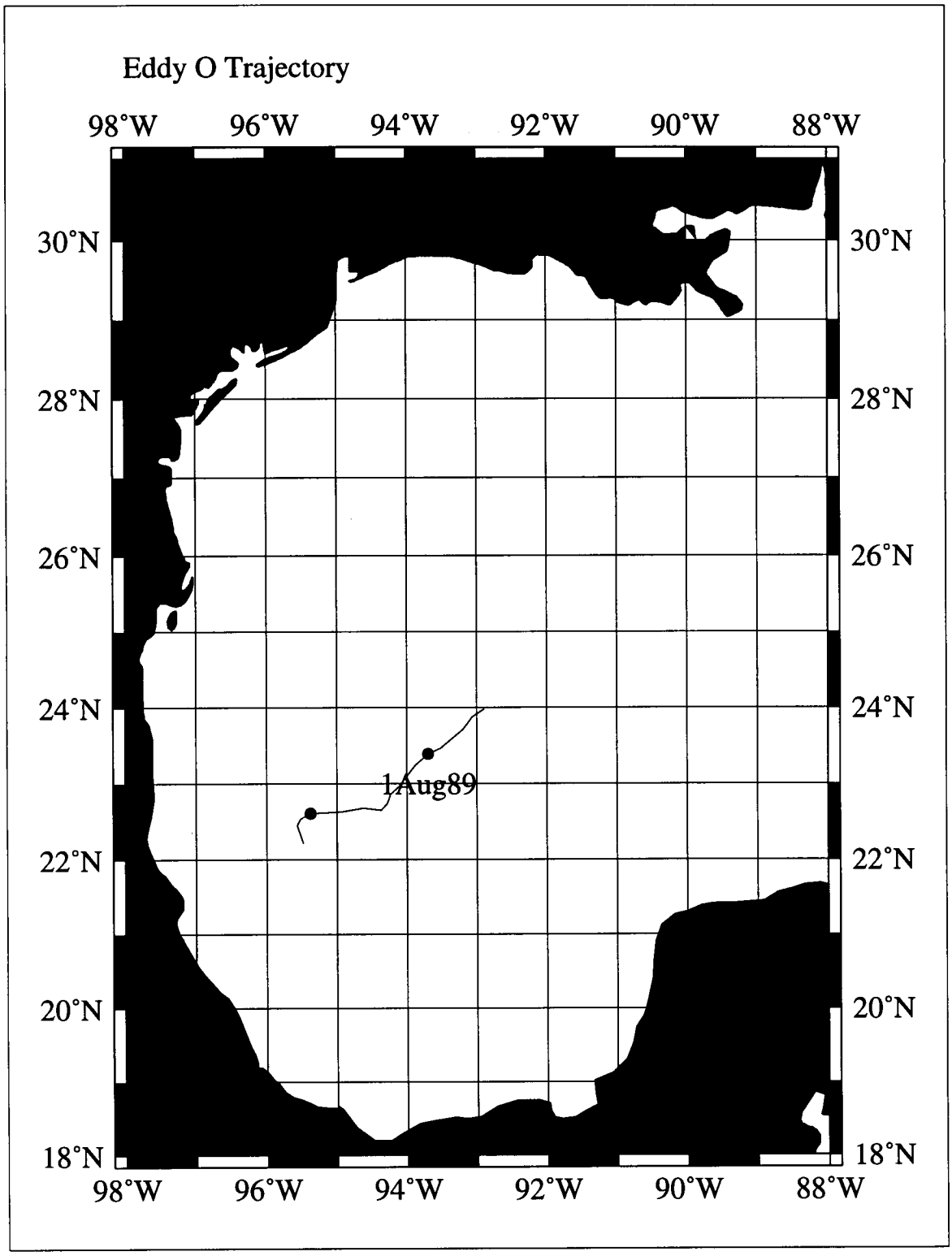

Figure 4.5-9. Trajectory of eddy O center determined using GEOSAT altimeter data and an objective tracking program. Dots show center location on the first of each month.

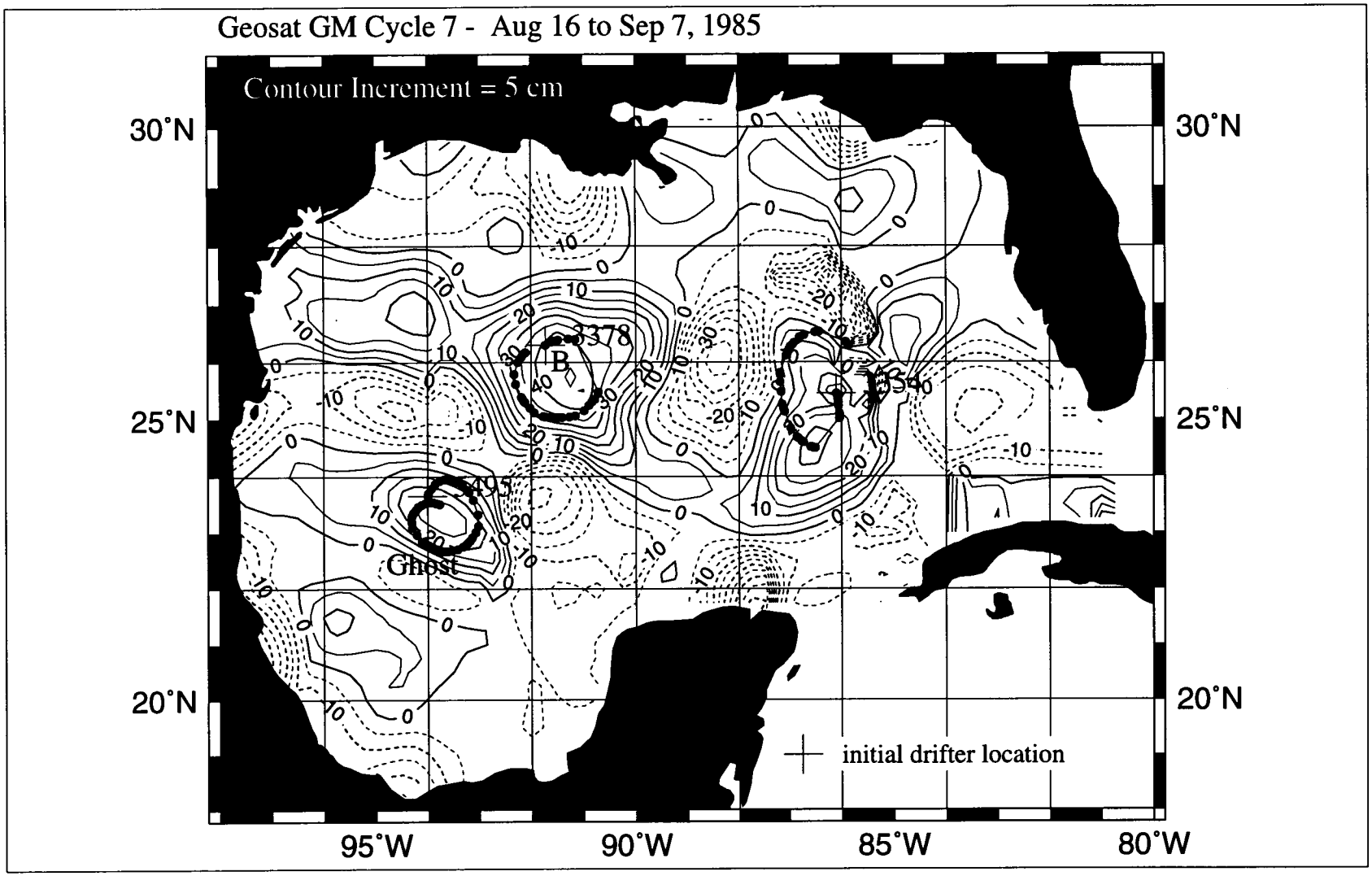

Figure 4.5-10. Sea surface height anomaly with respect to mean sea surface (OSUMSS95) for GEOSAT GM Cycle 7 (August 16 to September 7, 1985) showing eddy B and Ghost eddy. Drifter locations within five days of the midpoint of the cycle are shown.

Further verification of the importance of the southern cyclone is confirmed by the abrupt southward motion of eddy B in September-October 1985 (Figures 4.5-11 and 4.5-12). As the southern cyclone dissipated, the western cyclone and eddy B interacted and the pair rotated anticyclonically, as would be predicted for the interaction of a vortex pair composed of a weak cyclone and a strong anticyclone. This caused the center of eddy B to move quickly to the southwest. This is in contrast to the dynamical argument proposed by Lewis et al. (1989) that the entrainment of fluid by eddy B, as inferred from the convergence in the upper layer observed in the buoy trajectory, caused movement into deeper water. Glenn and Ebbesmeyer (1993) refuted this interpretation based on the fact that the swift propagation into deep water occurred in mid-September 1985, while the rapid decrease in the buoy radius occurred in early October 1985, approximately 20 days later. Lewis et al. (1989) also estimated the amount of entrainment based on volumetric estimates of the water between the 8°C and 15°C isotherms from selected eddy surveys, which showed an increase of approximately 60% from mid-July to mid-October 1985. Altimetric estimates of eddy area and areal-averaged sea surface height anomaly showed only small decreases over this time period (Figure 4.5-3b, page 105). Thus, the most consistent argument for the apparent motion of eddy B onto and away from the continental slope is the external flow field produced by cyclones present near the eddy during its transit of the western Gulf of Mexico.

Several of the statistics presented for the tracked eddies rely on altimetry-derived swirl speed as a function of radial distance from the eddy center. Figure 4.5-13 shows an example of estimated swirl speed based on the average velocity magnitude as a function of the radial distance from the center of eddy B on November 12, 1985, the midpoint of the November 11-13 AXBT survey (SAIC 1988). The altimetric eddy center (25°N latitude, 94°W longitude) agrees well with the eddy center determined from the survey (24.8°N latitude, 94°W longitude). At this time, eddy B was nearly circular, with a weak cyclone on its northwest perimeter (Figure 4.5-14). The near-solid-body rotation of the eddy, out to the radius of maximum velocity, is clearly seen in the altimetric analysis. The maximum geostrophic velocity found in the synthetic dynamic-height field, estimated from the survey temperatures (SAIC 1988), was 52 $cm \cdot s^{-1}$. This agrees well with the 46 $cm \cdot s^{-1}$ swirl velocity estimated from altimetry. The 125 km radius is well below the 200 km radius estimated from drifter trajectories by Lewis et al. (1989), but appears to be in good agreement with the mean radius, out to the maximum gradients in the AXBT-derived synthetic dynamic-height field.

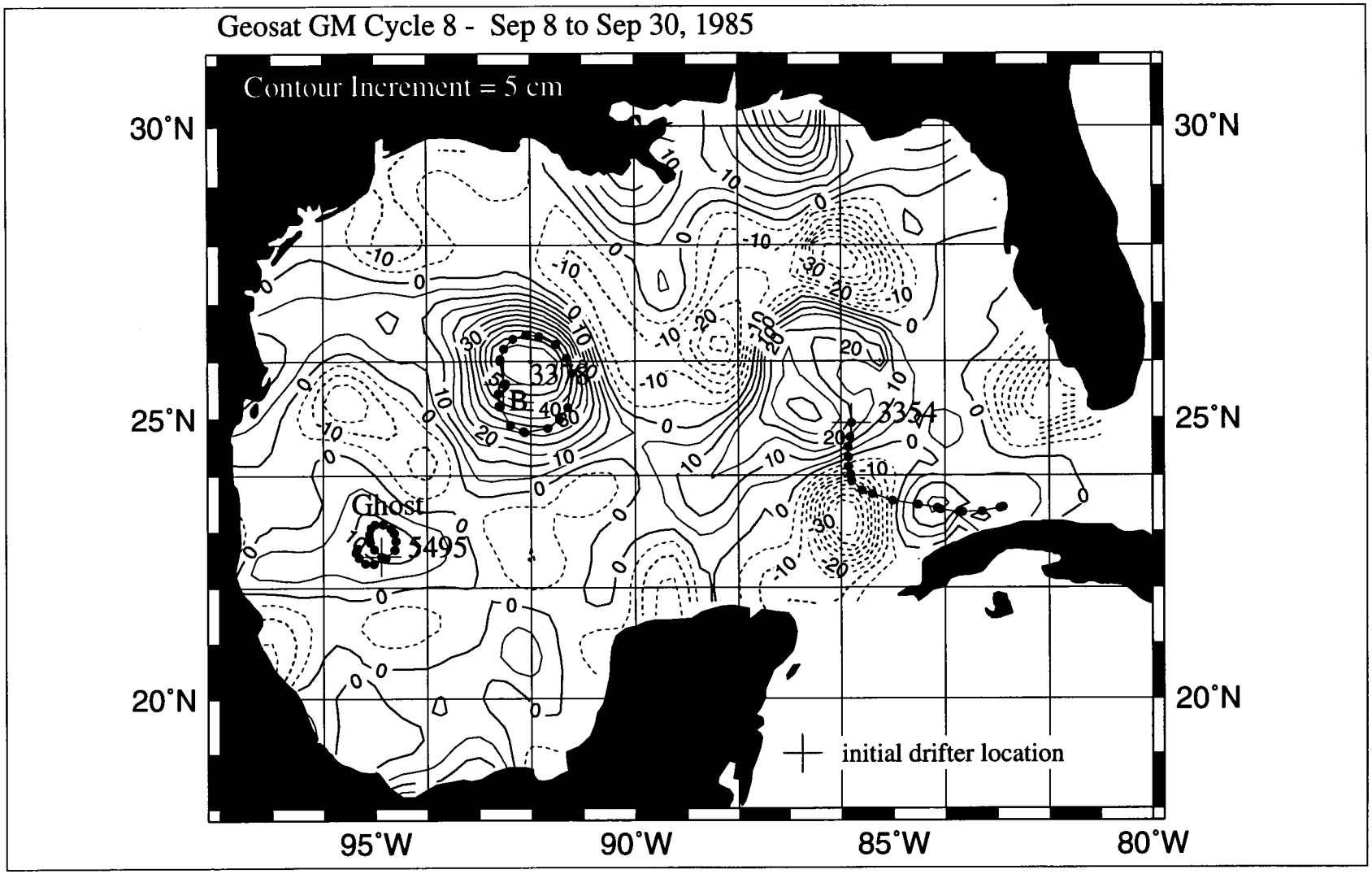

Figure 4.5-11. Sea surface height anomaly with respect to mean sea surface (OSUMSS95) for GEOSAT GM Cycle 8 (September 8 to 30, 1985) showing eddy B and Ghost eddy. Drifter locations within five days of the midpoint of the cycle are shown.

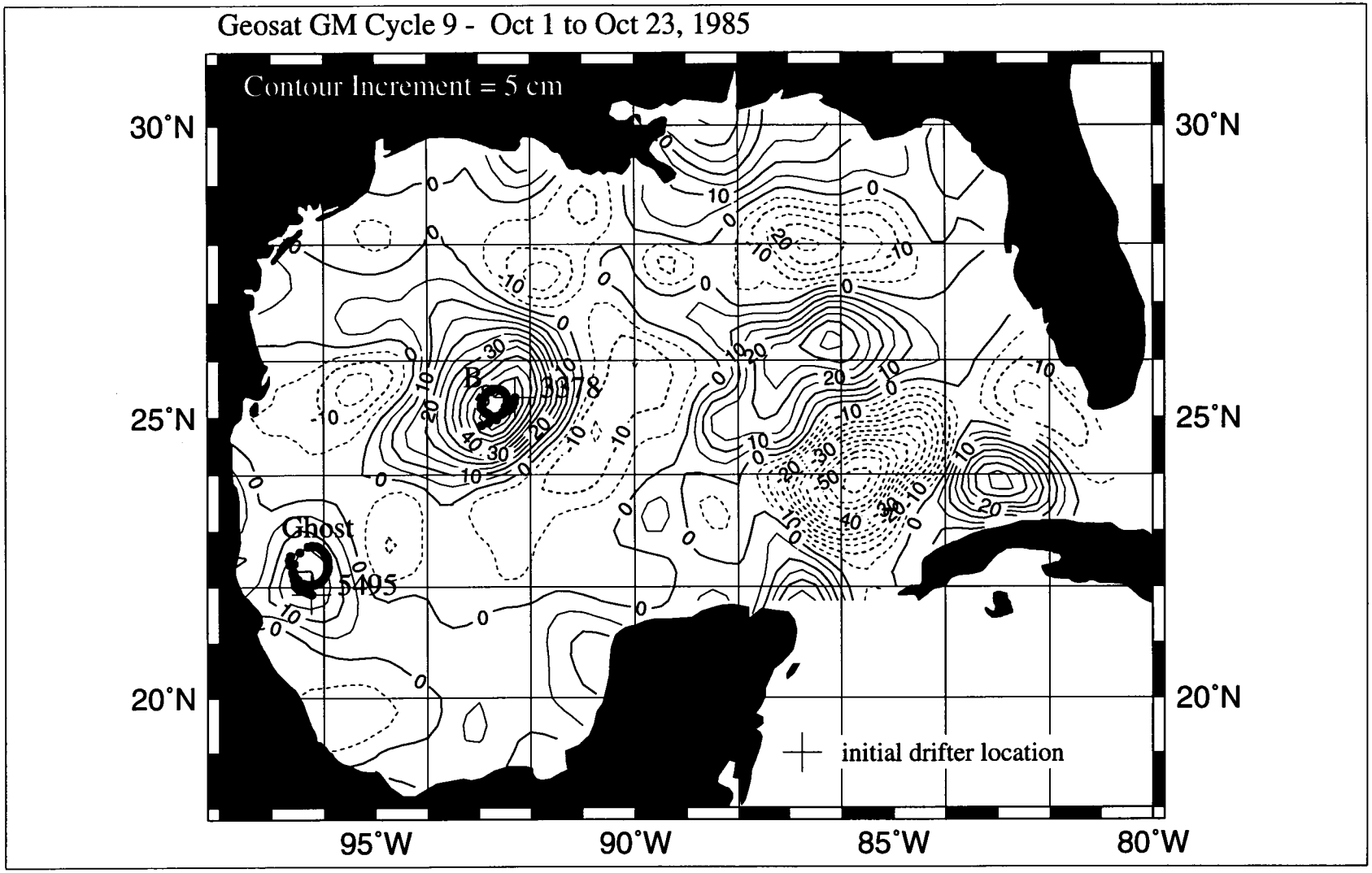

Figure 4.5-12. Sea surface height anomaly with respect to mean sea surface (OSUMSS95) for GEOSAT GM Cycle 9 (October 1 to 23, 1985) showing eddy B and Ghost eddy. Drifter locations within five days of the midpoint of the cycle are shown.

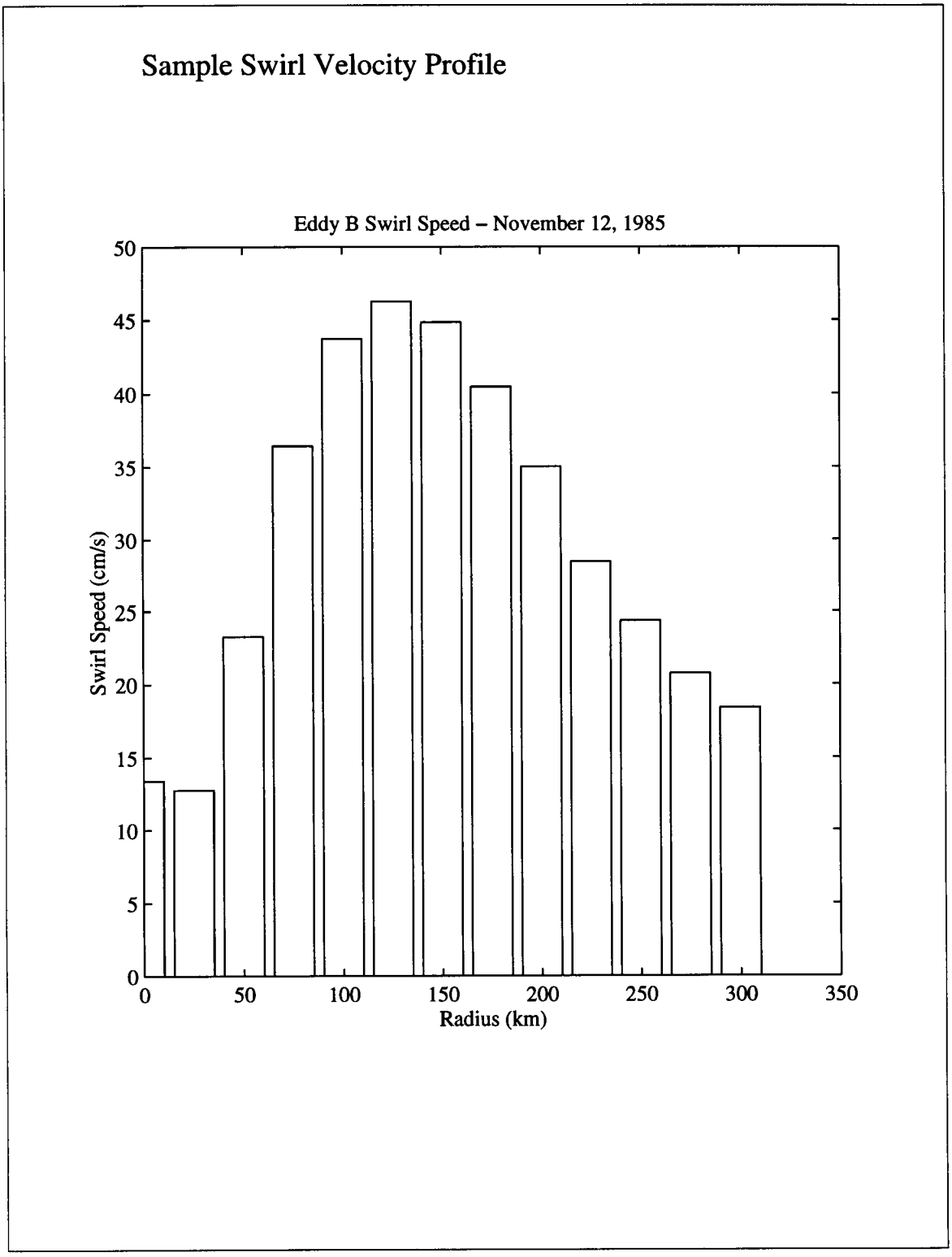

Figure 4.5-13. Altimetric estimate of the average velocity magnitude as a function of the radial distance from the center of eddy B on November 12, 1985.

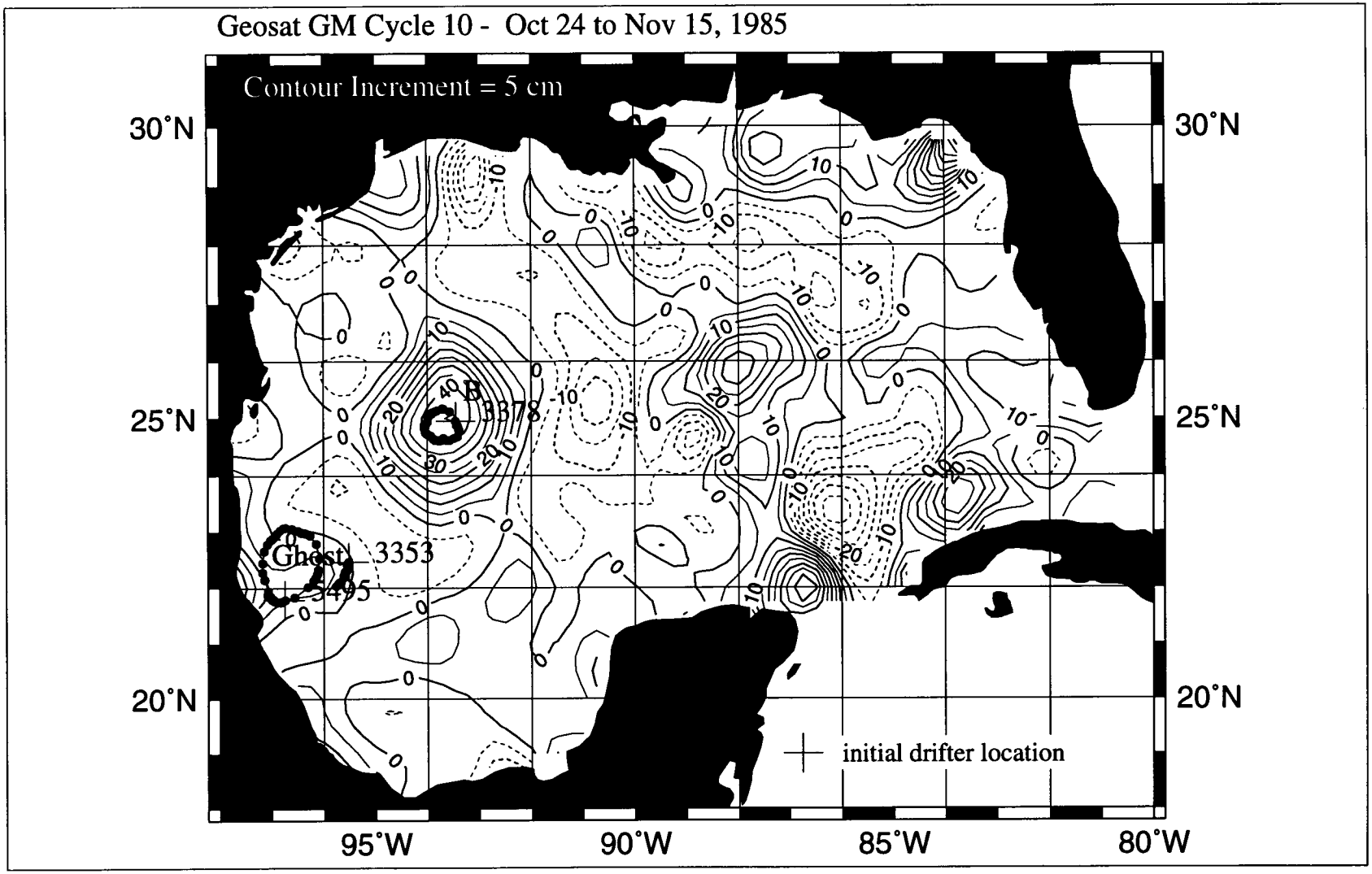

Figure 4.5-14. Sea surface height anomaly with respect to mean sea surface (OSUMSS95) for GEOSAT GM Cycle 10 (October 24 to November 15, 1985) showing eddy B and Ghost eddy. Drifter locations within five days of the midpoint of the cycle are shown.

4.5.2 Eddy C and Eddy B Interaction

Eddy C crossed 90°W longitude in February 1986, just six months after the transit of eddy B. The short time interval between the shedding of these eddies from the Loop Current allowed two energetic anticyclones to interact in the western Gulf of Mexico before the older of the two had dissipated. The trajectory of the eddy center of eddy C tracked by altimetry (Figure 4.5-15) shows that the eddy followed the more common southwestern propagation path. In the late spring of 1986, eddy C merged with the remnant of eddy B in the southwestern Gulf of Mexico to form a large anticyclone covering over four degrees in latitude and longitude, as inferred from the anticyclonic loops of a drifter circling the feature in the summer of 1986 (Lewis et al. 1989). Unfortunately, surveys during the coalescence of these two eddies did not provide a complete enough data set to determine how the two anticyclones merged. GEOSAT climatology, however, provides a continuous data set for investigation of the inter-action of this young, energetic Loop Current eddy with the residual circulation field of the older eddy. This merging event was observed during GM cycles 17 through 21 (Figures 4.5-16, 4.5-17, 4.5-18, 4.5-19 and 4.5-20). The comparison of GEOSAT-derived estimates of geostrophic velocity with drifter 3379 velocities, while orbiting eddy C during this time period (Figure 4.3-3, page 97), further validates the continuity and accuracy of the altimeter data during the merging event.

The sea surface height anomaly map for GM cycle 17 (Figure 4.5-16) shows the two eddies in early April 1986, just before the merging process began. Tracking statistics for eddy C derived from the GEOSAT climatology are shown in Figures 4.5-21a, b, c and d. The statistics for the remnant of eddy B during cycle 17 were also determined (based on the 10-cm contour) and showed that the eddy was approximately 150 km in diameter on April 15, and was located at 23°N latitude, 95°W longitude, with an anticyclonic circulation of approximately 1.5×10^5 $m^2 \cdot s^{-1}$. The two altimetric estimates of the eddy circulation were in good agreement. The coalescence of the eddies began in mid-April 1986, as streamlines surrounding the eddies gradually merged along an axis parallel to 24°N latitude, to produce a nearly circular eddy by mid-July 1986 (Figure 4.5-20). Thus, the entire merging process was completed in approximately 90 days. A small amount of clockwise rotation of the vortex pair was observed in the early stages of coalescence (to move eddy B to 24°N latitude); however, this rotation stopped as the merging process proceeded. The characteristic peanut shape of the merging streamlines can be seen in the cycle maps (Figures 4.5-17, 4.5-18 and 4.5-19), and was also seen in the drifter paths (Lewis et al. 1989).

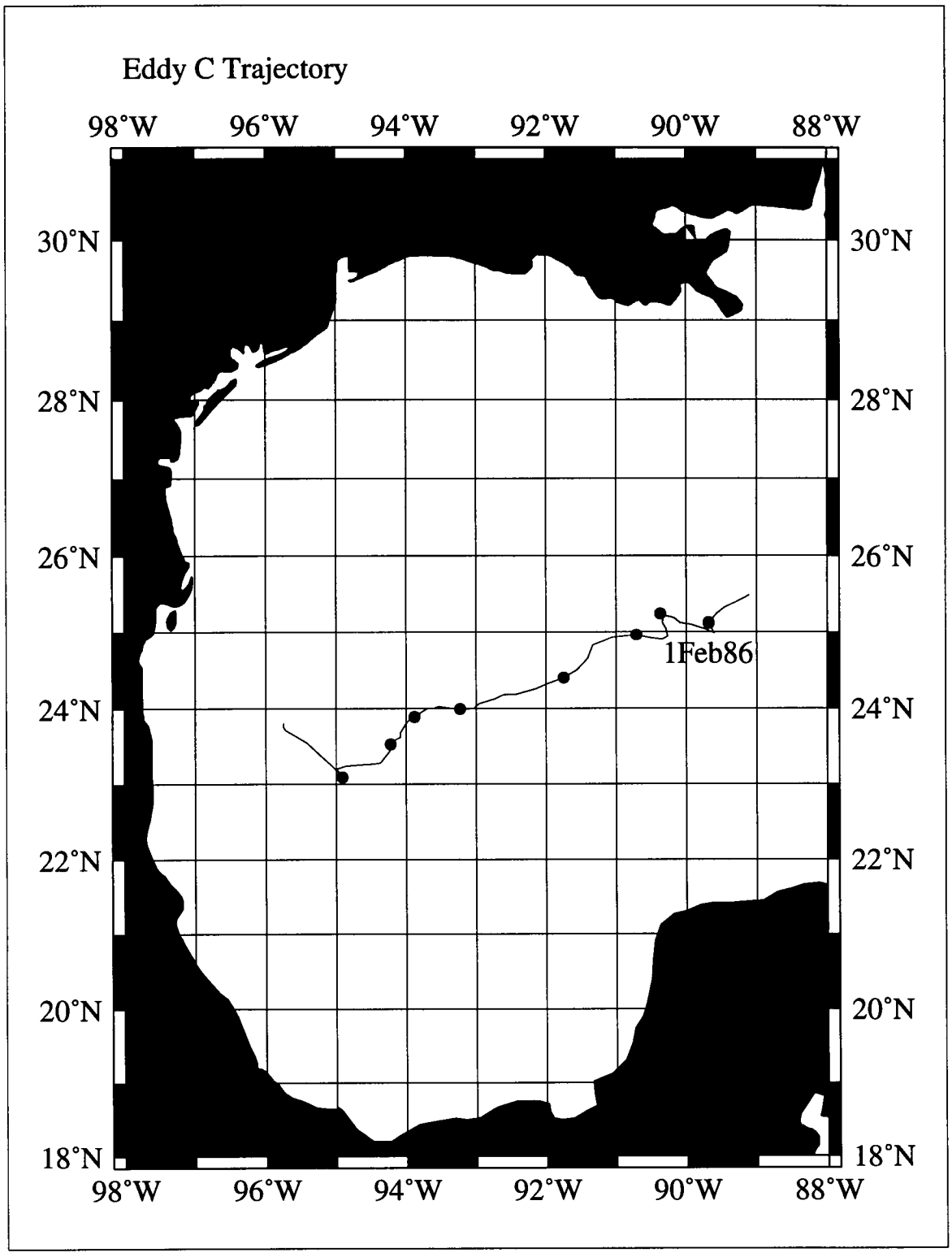

Figure 4.5-15. Trajectory of eddy C center determined using GEOSAT altimeter data and an objective tracking program. Dots show center location on the first of each month.

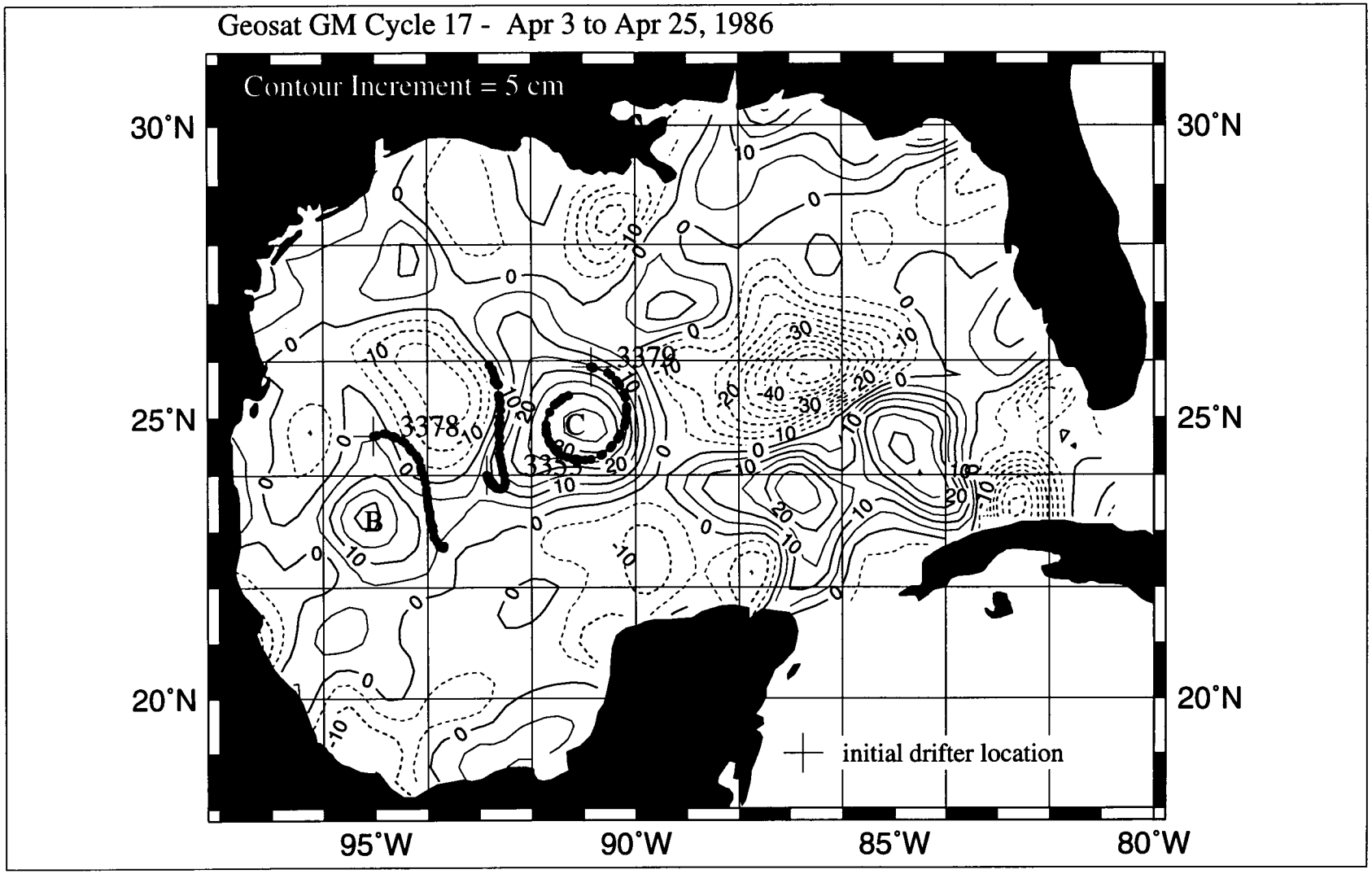

Figure 4.5-16. Sea surface height anomaly with respect to mean sea surface (OSUMSS95) for GEOSAT GM Cycle 17 (April 3 to 25, 1986) showing eddy C and eddy B. Drifter locations within five days of the midpoint of the cycle are shown.

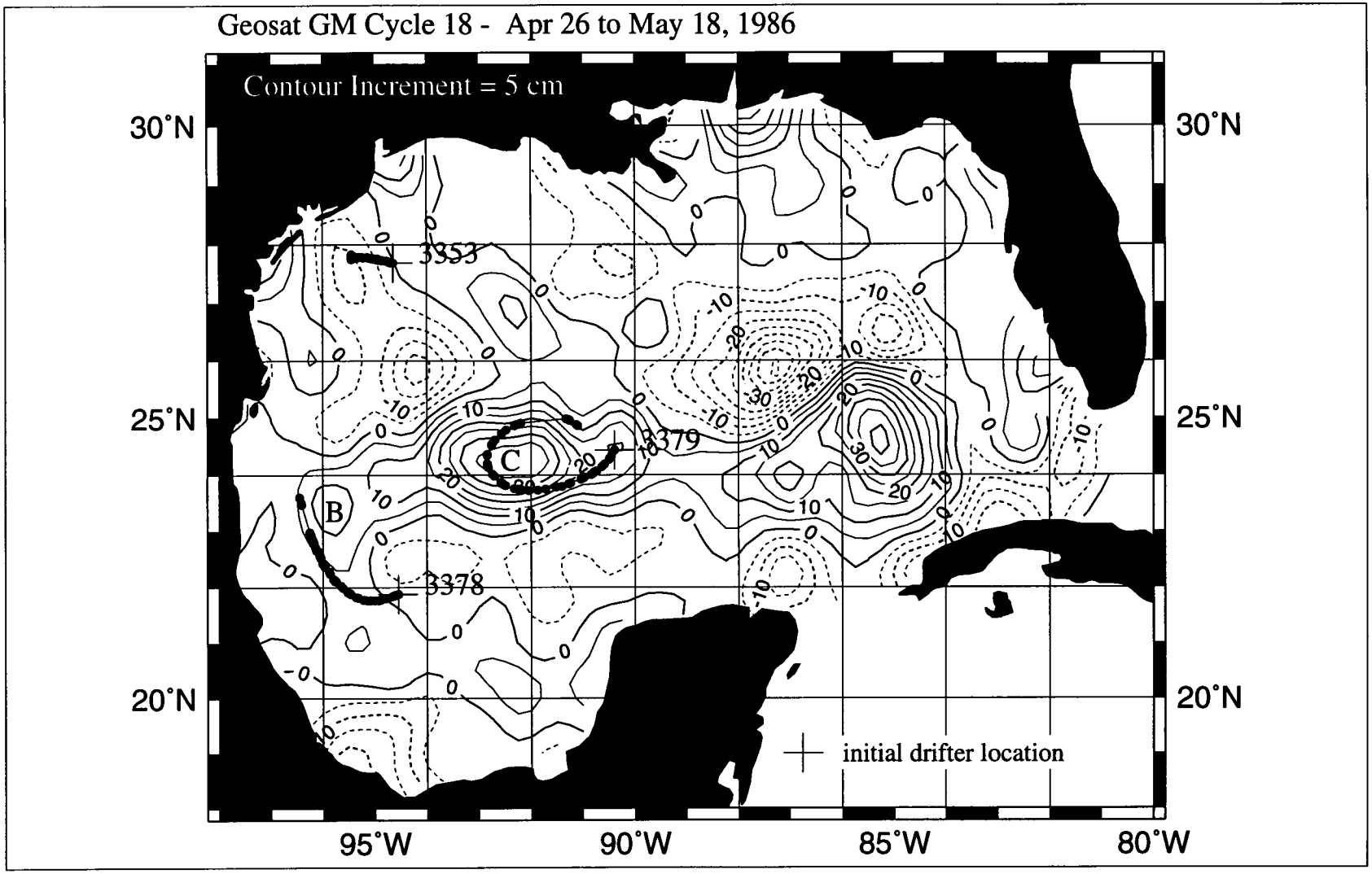

Figure 4.5-17. Sea surface height anomaly with respect to mean sea surface (OSUMSS95) for GEOSAT GM Cycle 18 (April 26 to May 18, 1986) showing interaction between eddy C and eddy B. Drifter locations within five days of the midpoint of the cycle are shown.

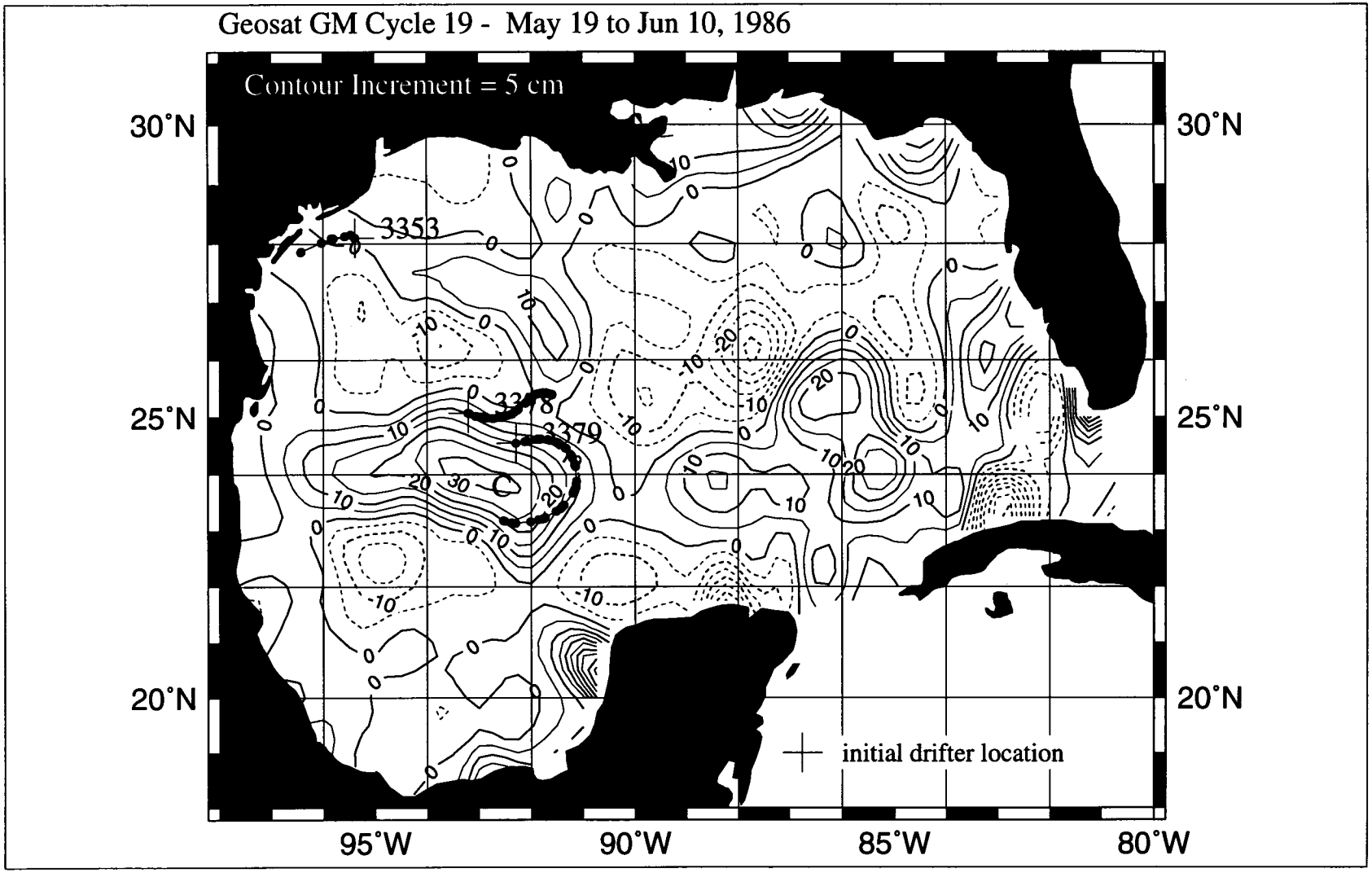

Figure 4.5-18. Sea surface height anomaly with respect to mean sea surface (OSUMSS95) for GEOSAT GM Cycle 19 (May 19 to June 10, 1986) showing an elongated eddy C. Drifter locations within five days of the midpoint of the cycle are shown.

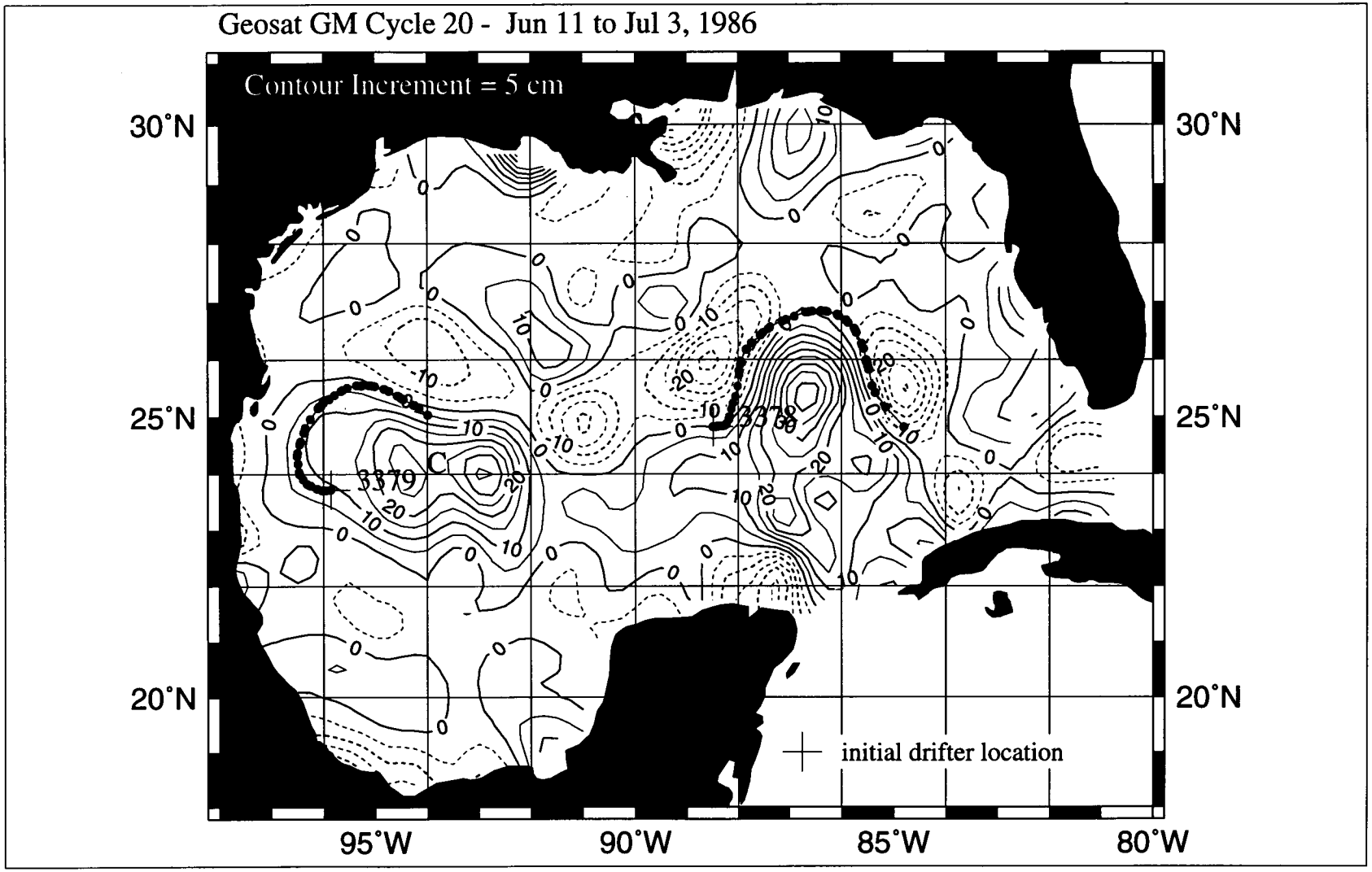

Figure 4.5-19. Sea surface height anomaly with respect to mean sea surface (OSUMSS95) for GEOSAT GM Cycle 20 (June 11 to July 3, 1986) showing eddy C. Drifter locations within five days of the midpoint of the cycle are shown.

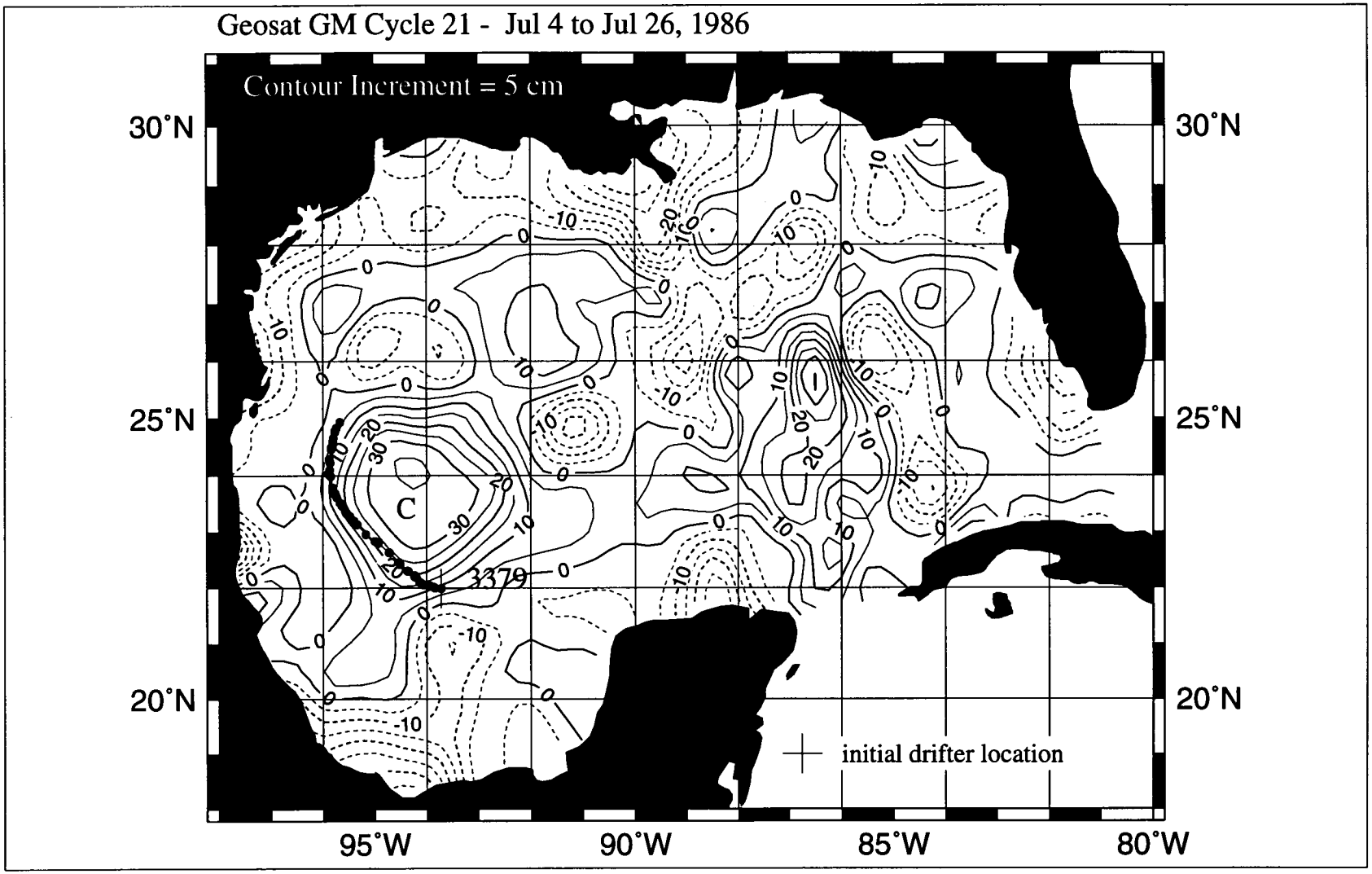

Figure 4.5-20. Sea surface height anomaly with respect to mean sea surface (OSUMSS95) for GEOSAT GM Cycle 21 (July 4 to 26, 1986) showing eddy C. Drifter locations within five days of the midpoint of the cycle are shown.

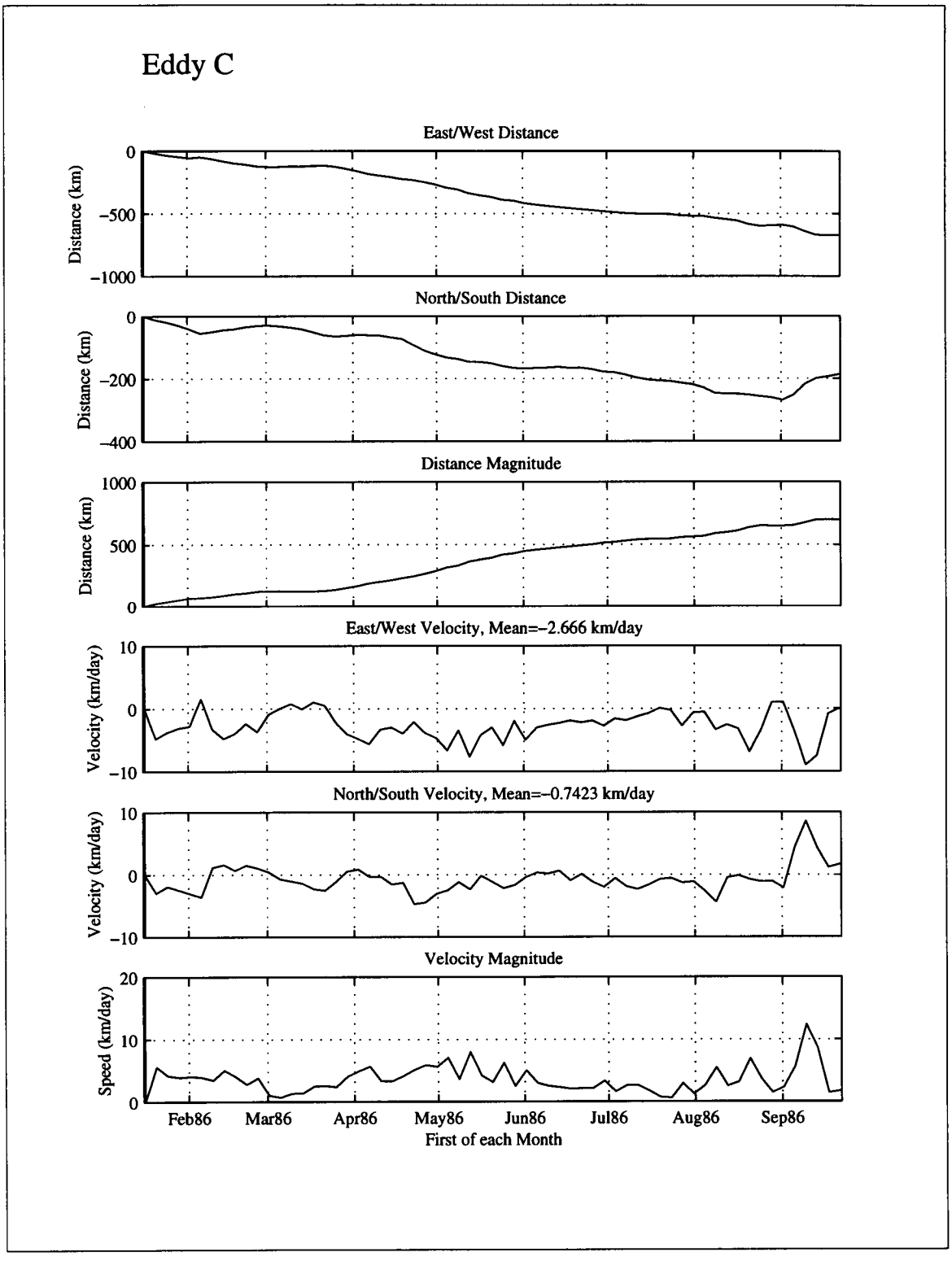

Figure 4.5-21a. Eddy tracking statistics for eddy C from January to September 1986 using GEOSAT altimetry: distance and velocity statistics.

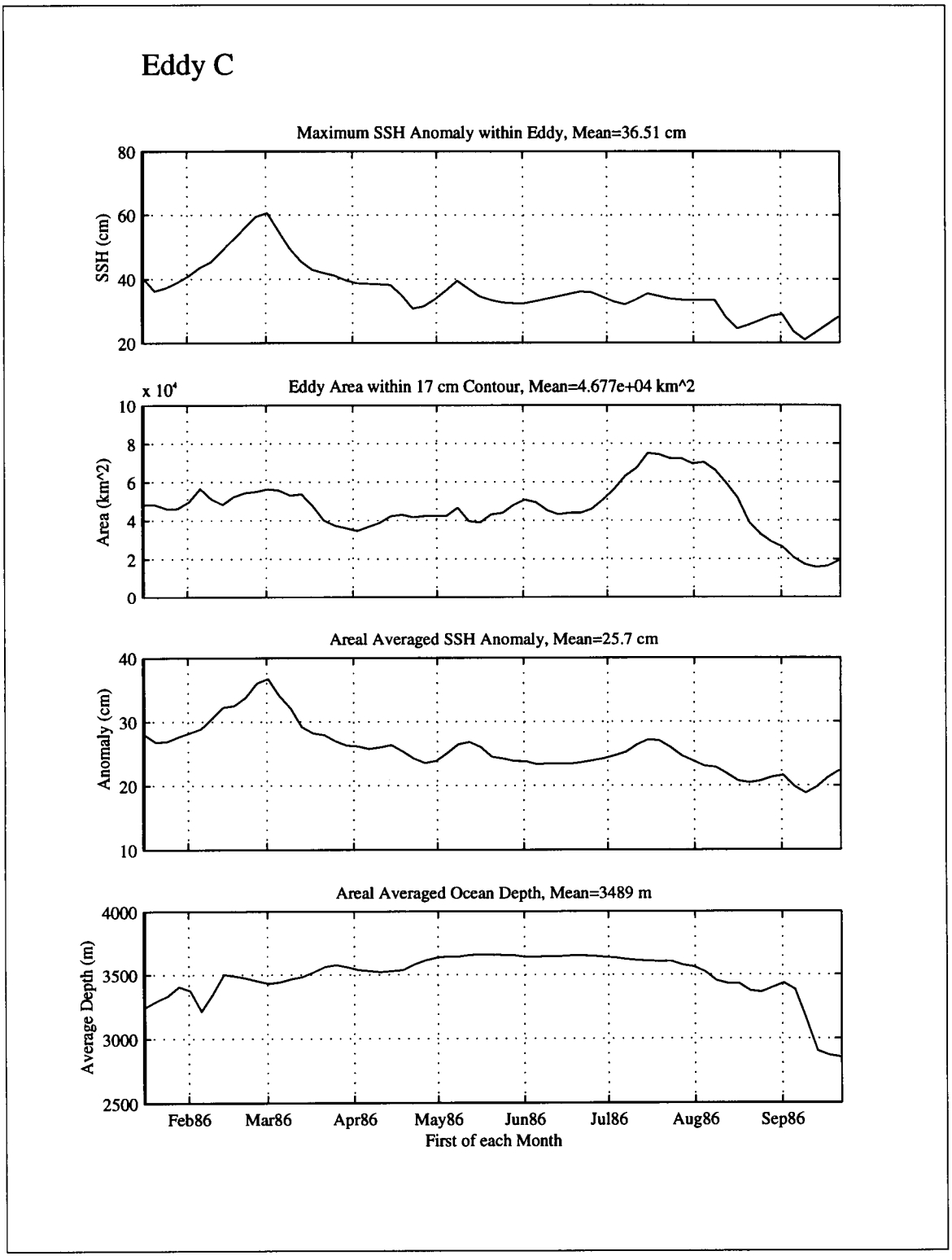

Figure 4.5-21b. Eddy tracking statistics for eddy C from January to September 1986 using GEOSAT altimetry: maximum height anomaly, eddy area, areal averaged anomaly and ocean depth.

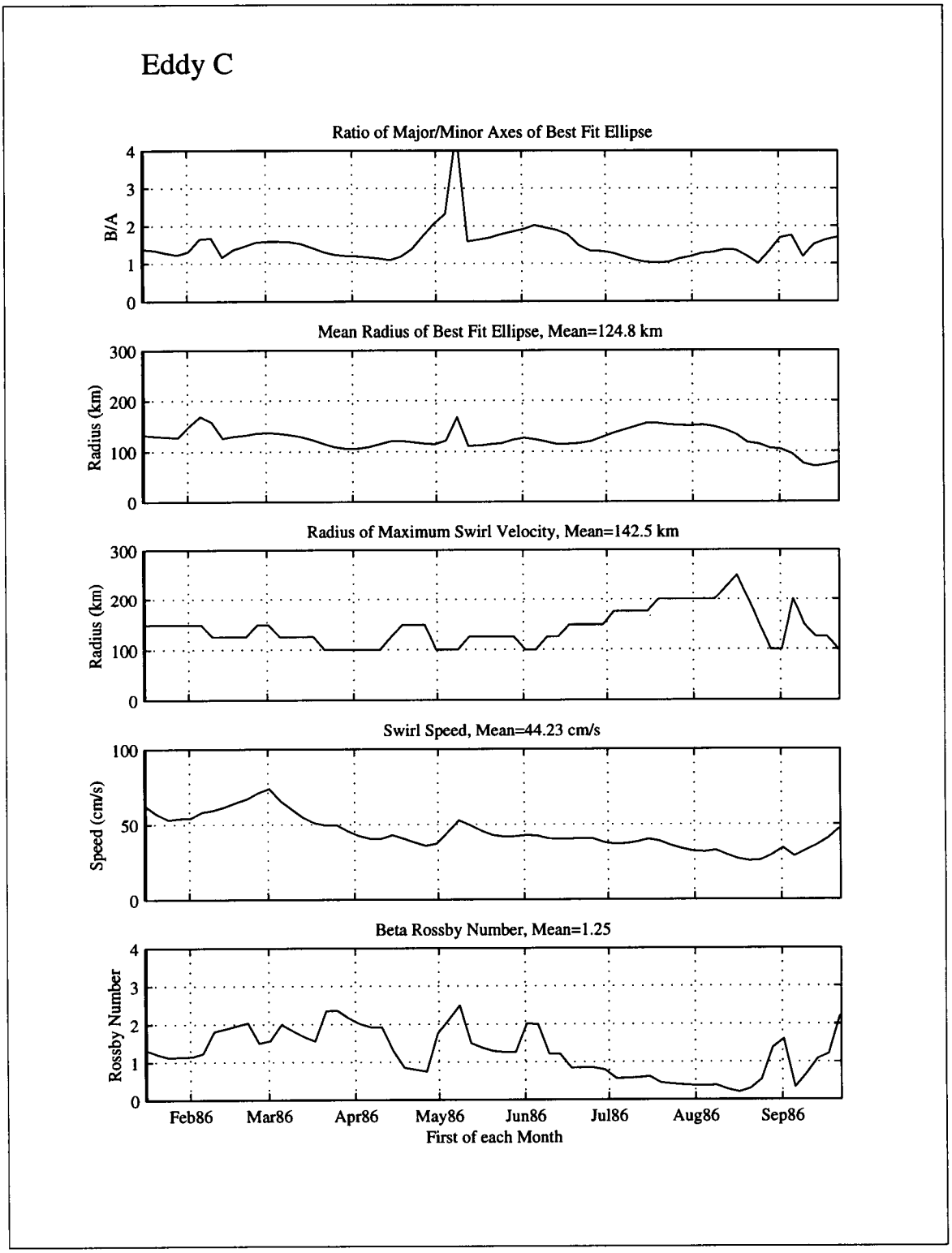

Figure 4.5-21c. Eddy tracking statistics for eddy C from January to September 1986 using GEOSAT altimetry: eccentricity, radius estimates, swirl speed, and Rossby number.

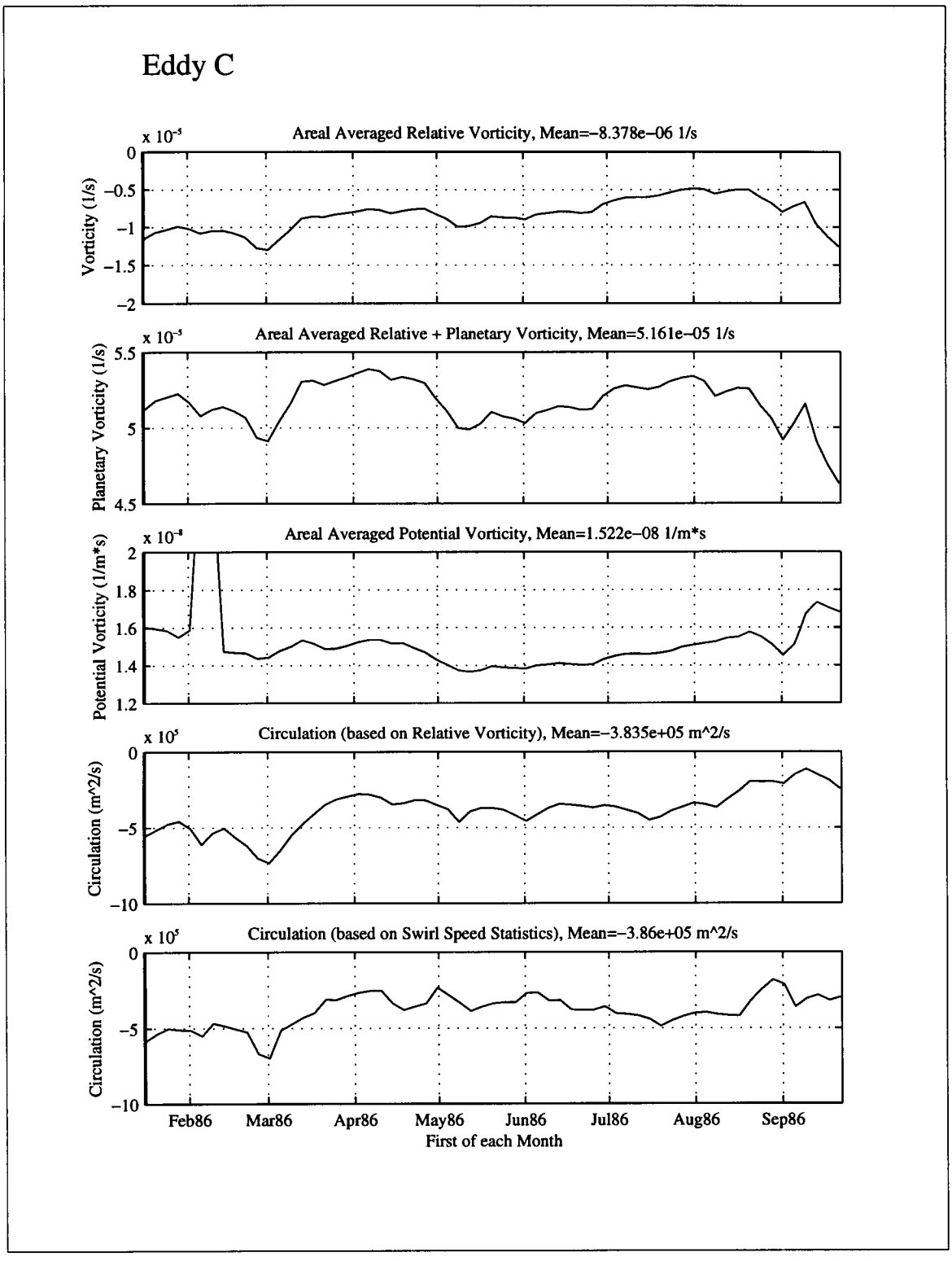

Figure 4.5-21d. Eddy tracking statistics for eddy C from January to September 1986 using GEOSAT altimetry: vorticity and circulation statistics.

The tracking statistics for eddy C highlight several interesting features of this merging event. A large increase in the areal extent occurred in July 1986, as the merging of the eddy was completed (Figure 4.5-21b). This increase in area was confirmed by drifter 3379, and was also evident in the altimetric estimate of the radius of maximum swirl velocity (Figure 4.5-21c). It appears that the entire mass of the two eddies merged, given the great increase in area and the fact that no positive height anomalies were ejected during the merging process. Anticyclonic circulation gradually increased from mid-April to mid-July 1986 over the time period of the merging (Figure 4.5-21d). The amount of anticyclonic circulation increase during the merging process is in good agreement with the total circulation present in eddy B just before merging. After merging was complete, the eddy began to decay and eventually resulted in the cyclonic-anticyclonic-cyclonic ring triad described in detail by Vidal et al. (1994). This triad is also seen in the map from the first cycle of the ERM (Figure 4.5-22).

Thus, the altimetric observations support the conclusion that both the circulation and mass of the eddies were conserved during the merging process. Further work is necessary to synthesize these altimetric observations with the enigmatic literature on theoretical, experimental and numerical studies of the merging of anticyclonic eddies and lenses. Conservation of both mass and circulation are precluded by a number of the theories by preventing merger because of energy considerations (Gill and Griffiths 1981), or requiring modification of the potential vorticity by shocks if mass is conserved (Nof 1988), or ejecting mass in thin filaments to conserve energy and momentum (Cushman-Roisin 1989). Griffiths and Hopfinger (1987) suggest a possible scenario consistent with the altimetric observations by suggesting that additional energy may be supplied by a cyclonic flow of fluid around the merging eddies. A strong cyclonic circulation (which is confirmed by the path of drifter 3353 in Figure 4.5-16) was positioned between the vortex pair in April 1986 and dissipated to the north as the eddies merged. This cyclone may have added the necessary energy to allow the eddies to merge without ejecting mass. It is estimated that 13% of the mass of the combined system would have been ejected, without an energy input, based on the eddy-center height anomalies and the theory of Cushman-Roisin (1989). Ejection of this amount of mass and its associated circulation should have been observable in the altimetry.

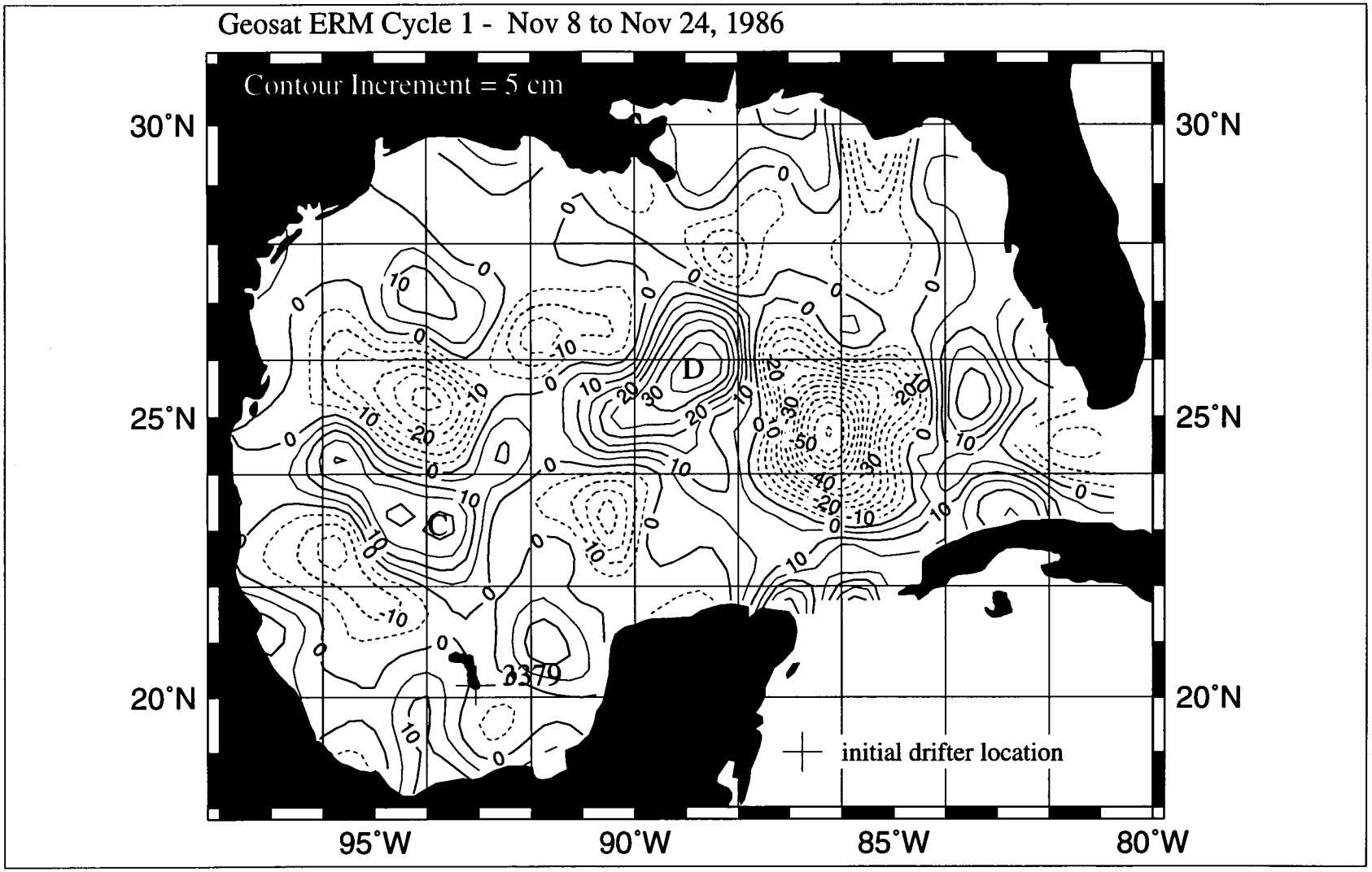

Figure 4.5-22. Sea surface height anomaly with respect to mean sea surface (OSUMSS95) for GEOSAT ERM Cycle 1 (November 8 to 24, 1986) showing eddy D and eddy C. Drifter locations within five days of the midpoint of the cycle are shown.

4.5.3 Eddy D and Eddy C Interaction

Eddy D transited across 90°W longitude in December 1986 and took a direct westward path along 25°N latitude through the western Gulf of Mexico (Figure 4.5-23), similar to the track of eddy B, but without the northward excursion onto the continental slope. A possible explanation for the fact that there was not a northward excursion of eddy D was the absence of a Campeche slope cyclone, which had been observed during eddy B's northward excursion. The westward path of eddy D may be explained by the cyclone which was positioned just west of the translating eddy (Figures 4.5-24 through 28). A cyclone in this position would have induced a northward component to the eddy translation, counteracting the nonlinear self-advection tendency to the south. This would result in the eddy propagating directly to the west due to planetary β (Smith and O'Brien 1983). During March through May, 1987, the anticyclone-cyclone pair rotated clockwise (Figures 4.5-29, 4.5-30 and 4.5-31), which moved the cyclone to the north of eddy D, as confirmed by the hydrography shown in Figure 4.5-32.

Outages during ERM cycles 9 and 10 preclude a detailed examination of the merging of eddy D with the remnant of eddy C in March and April, 1987. However, the tracking statistics for eddy D (Figures 4.5-33a, b, c, and d) were quite good, highlighting the slow decay of the anticyclonic circulation within the eddy, and the tendency of the eddy to conserve potential vorticity while remaining over relatively constant topography of the deep northwestern abyssal basin.

4.5.4 Eddy E, Unnamed Secondary Eddy and Eddy F

Eddy E crossed 90°W longitude in January 1988 and was a relatively weak Loop Current eddy, which may have been a result of the earlier shedding of an unobserved secondary anticyclone during the summer of 1987 (Hamilton 1992). This unnamed secondary eddy may have merged with the remnants of eddy D to form an anticyclonic feature seen to the northwest of eddy E in February 1988, during ERM cycles 28 and 29 (Figures 4.5-34 and 4.5-35). Continuous tracking of eddy E and the weak secondary eddy was hampered by severe data outages which affected GEOSAT during this time period. However, by August 1988 (Figure 4.5-36) there was very little anticyclonic circulation in the western Gulf of Mexico, indicating that eddy E and the secondary anticyclonic eddy had dissipated.

Eddy F crossed 90°W longitude in August 1988, approximately 6½ months after the transit of eddy E. The short period between these eddy sheddings could have provided another chance to observe Loop Current eddies merging. However, the rapid

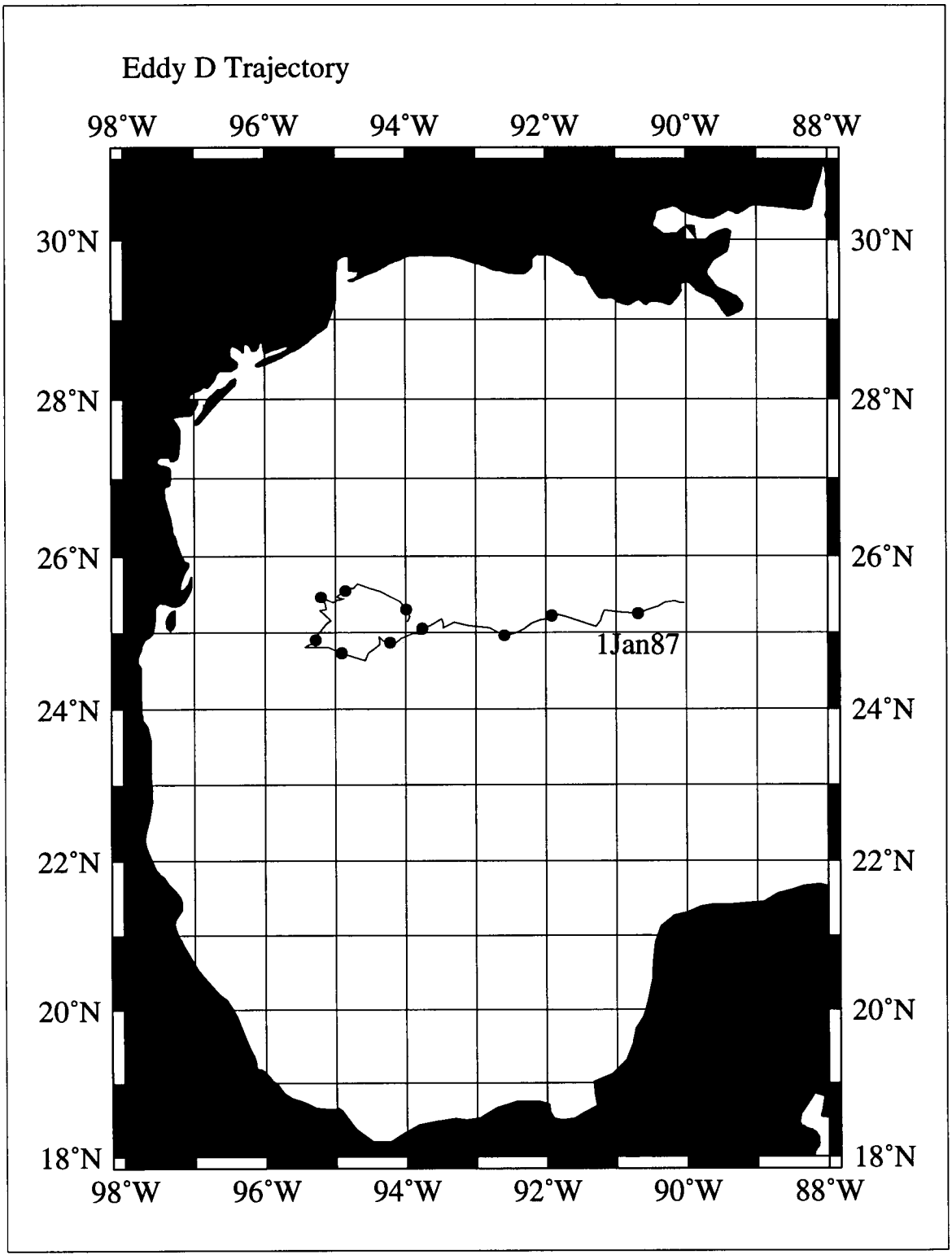

Figure 4.5-23. Trajectory of eddy D center determined using GEOSAT altimeter data and an objective tracking program. Dots show center locations on the first of each month.

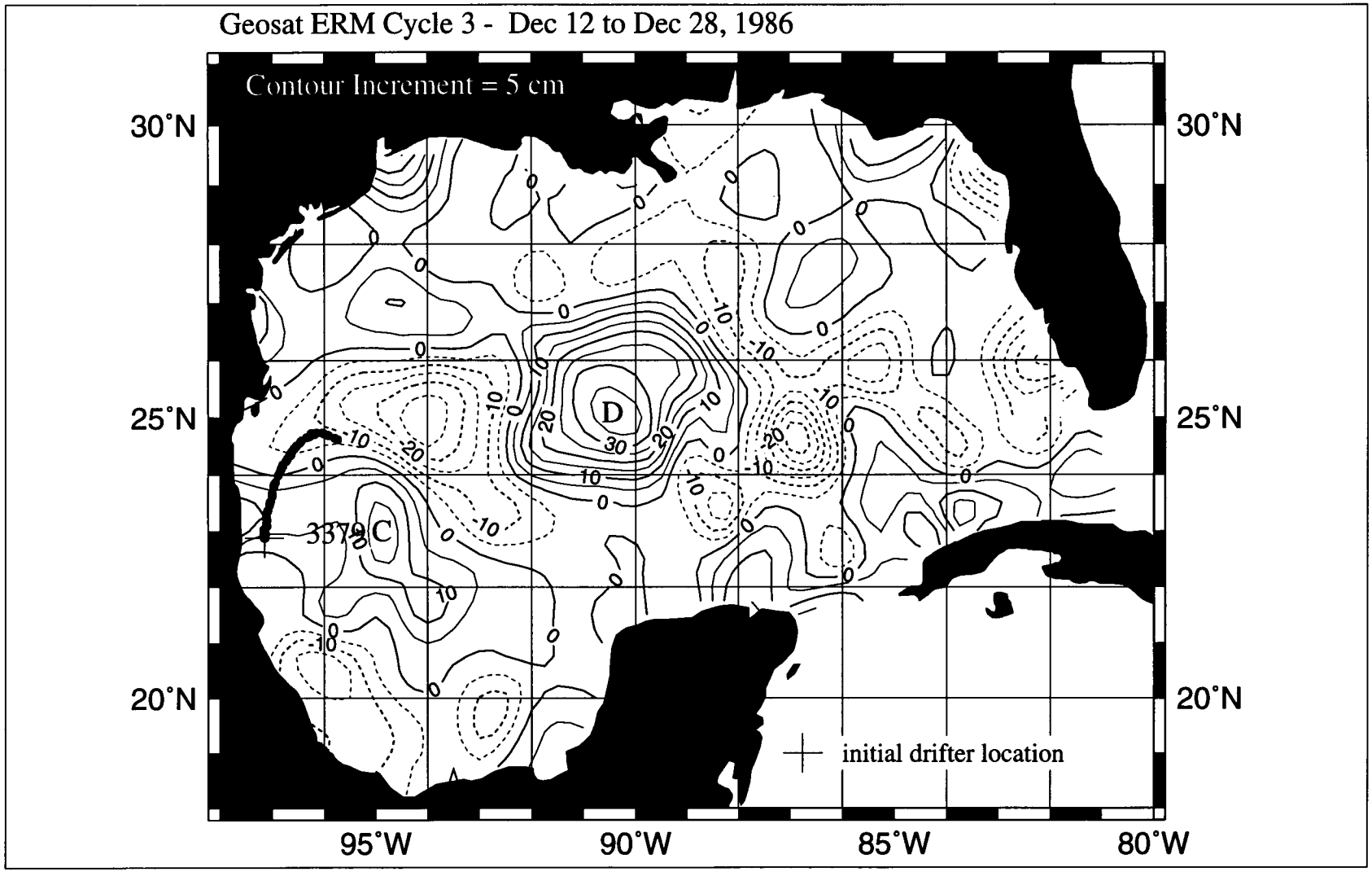

Figure 4.5-24. Sea surface height anomaly with respect to mean sea surface (OSUMSS95) for GEOSAT ERM Cycle 3 (December 12 to 28, 1986) showing eddy D and eddy C. Drifter locations within five days of the midpoint of the cycle are shown.

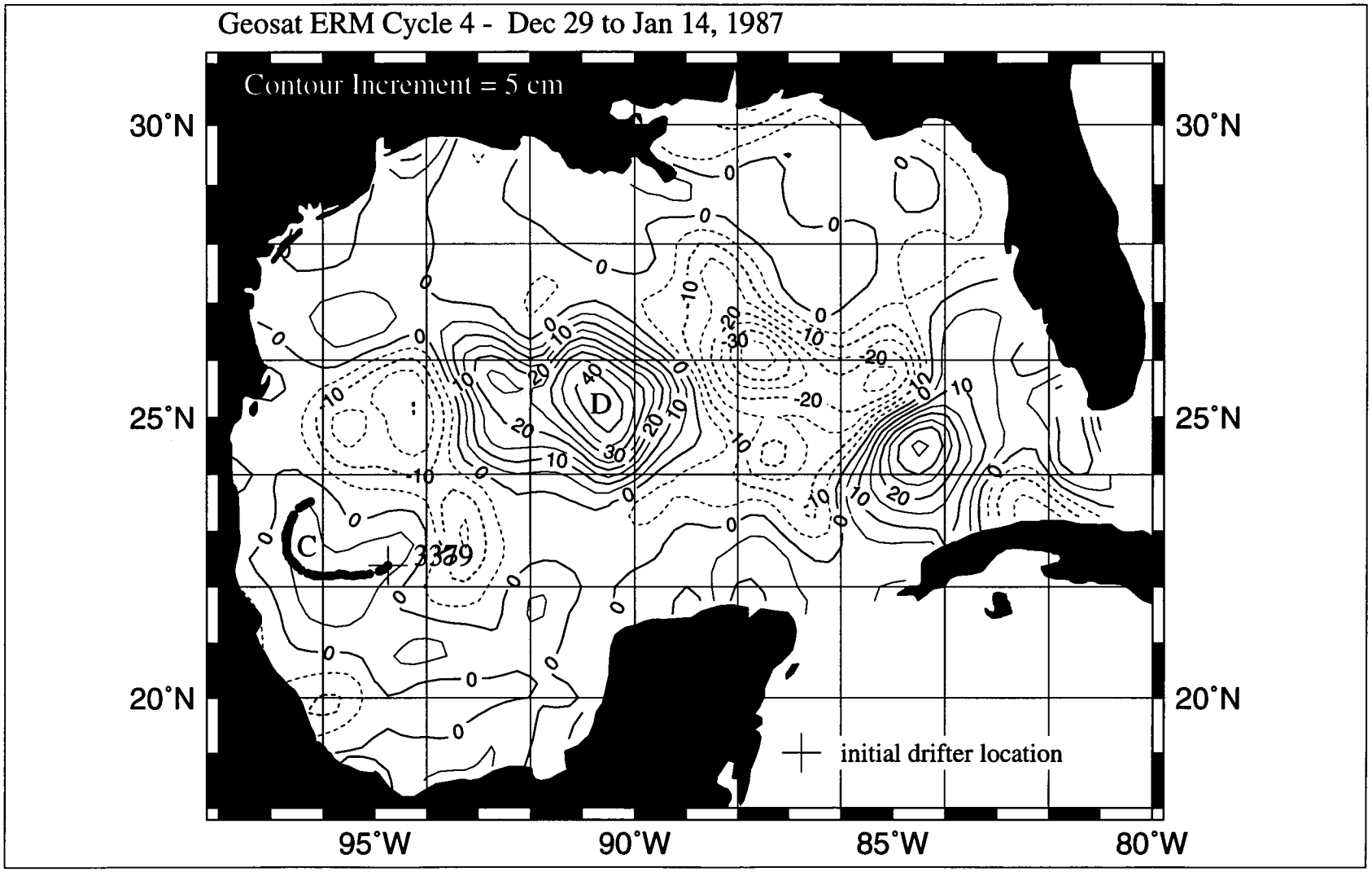

Figure 4.5-25. Sea surface height anomaly with respect to mean sea surface (OSUMSS95) for GEOSAT ERM Cycle 4 (December 29, 1986 to January 24, 1987) showing eddy D and eddy C. Drifter locations within five days of the midpoint of the cycle are shown.

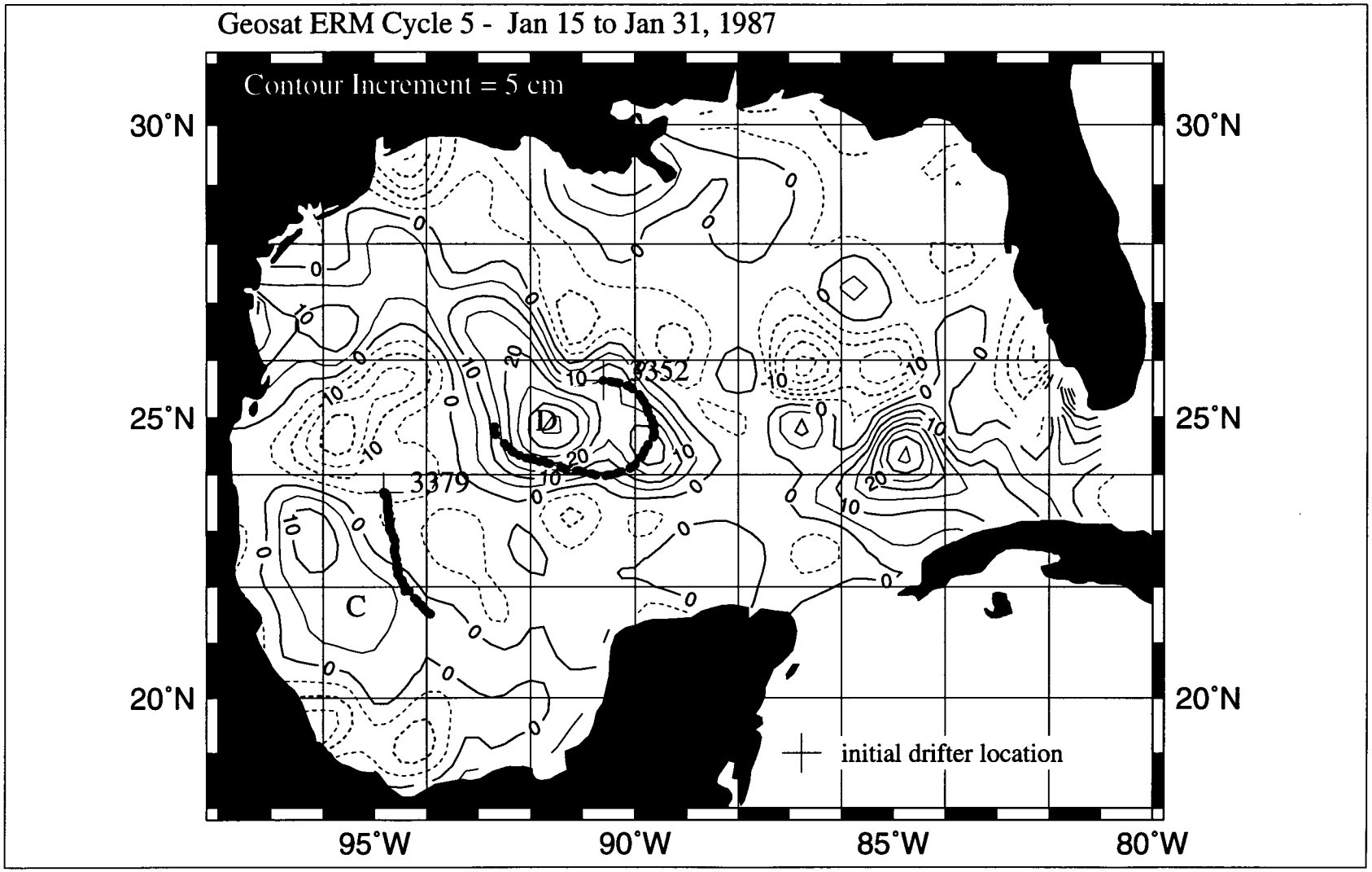

Figure 4.5-26. Sea surface height anomaly with respect to mean sea surface (OSUMSS95) for GEOSAT ERM Cycle 5 (January 15 to 31, 1987) showing eddy D and eddy C. Drifter locations within five days of the midpoint of the cycle are shown.

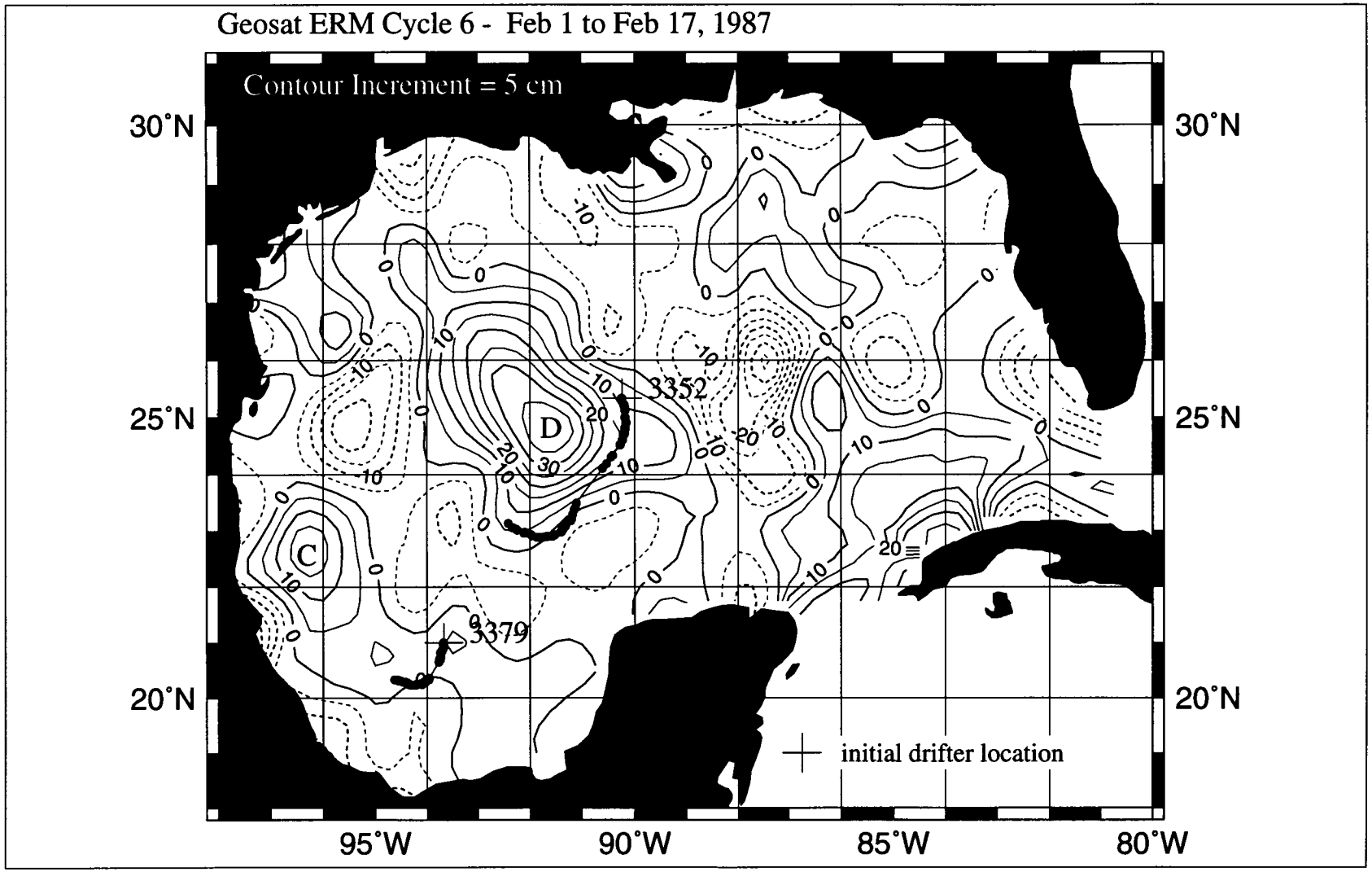

Figure 4.5-27. Sea surface height anomaly with respect to mean sea surface (OSUMSS95) for GEOSAT ERM Cycle 6 (February 1 to 17, 1987) showing eddy D and eddy C. Drifter locations within five days of the midpoint of the cycle are shown.

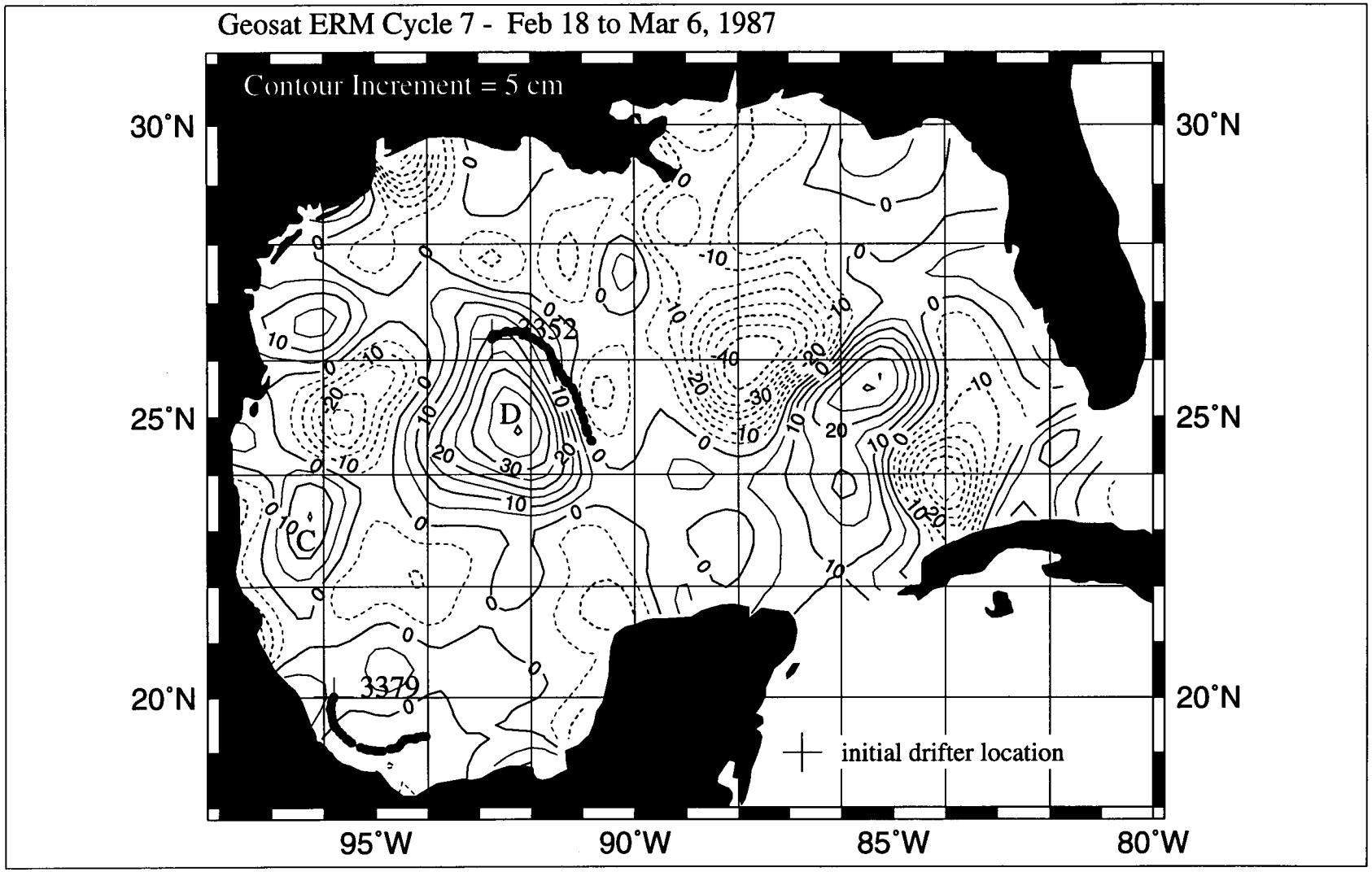

Figure 4.5-28. Sea surface height anomaly with respect to mean sea surface (OSUMSS95) for GEOSAT ERM Cycle 7 (February 18 to March 6, 1987) showing eddy D and eddy C. Drifter locations within five days of the midpoint of the cycle are shown.

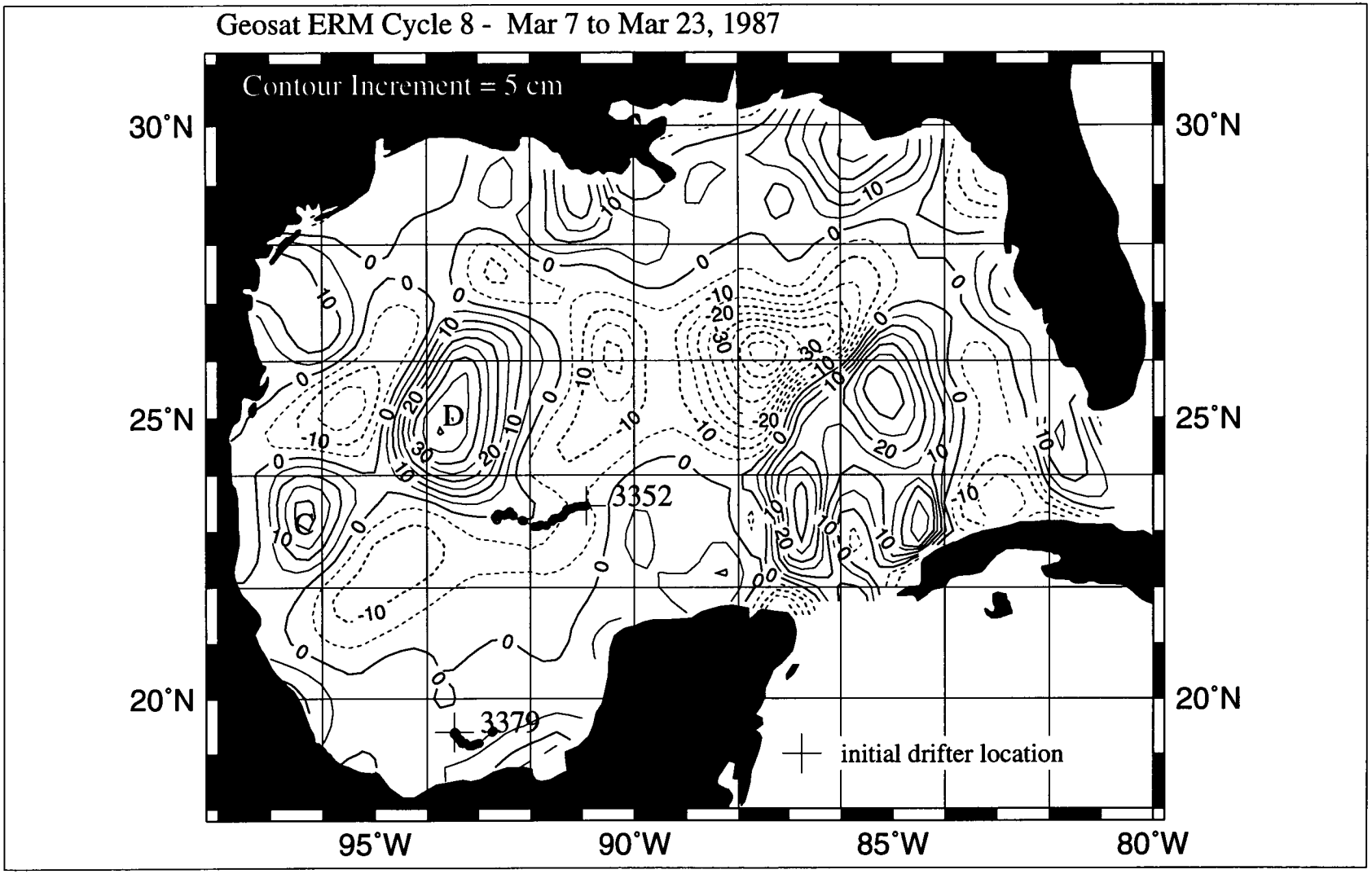

Figure 4.5-29. Sea surface height anomaly with respect to mean sea surface (OSUMSS95) for GEOSAT ERM Cycle 8 (March 7 to 23, 1987) showing interaction between eddy D and eddy C. Drifter locations within five days of the midpoint of the cycle are shown.

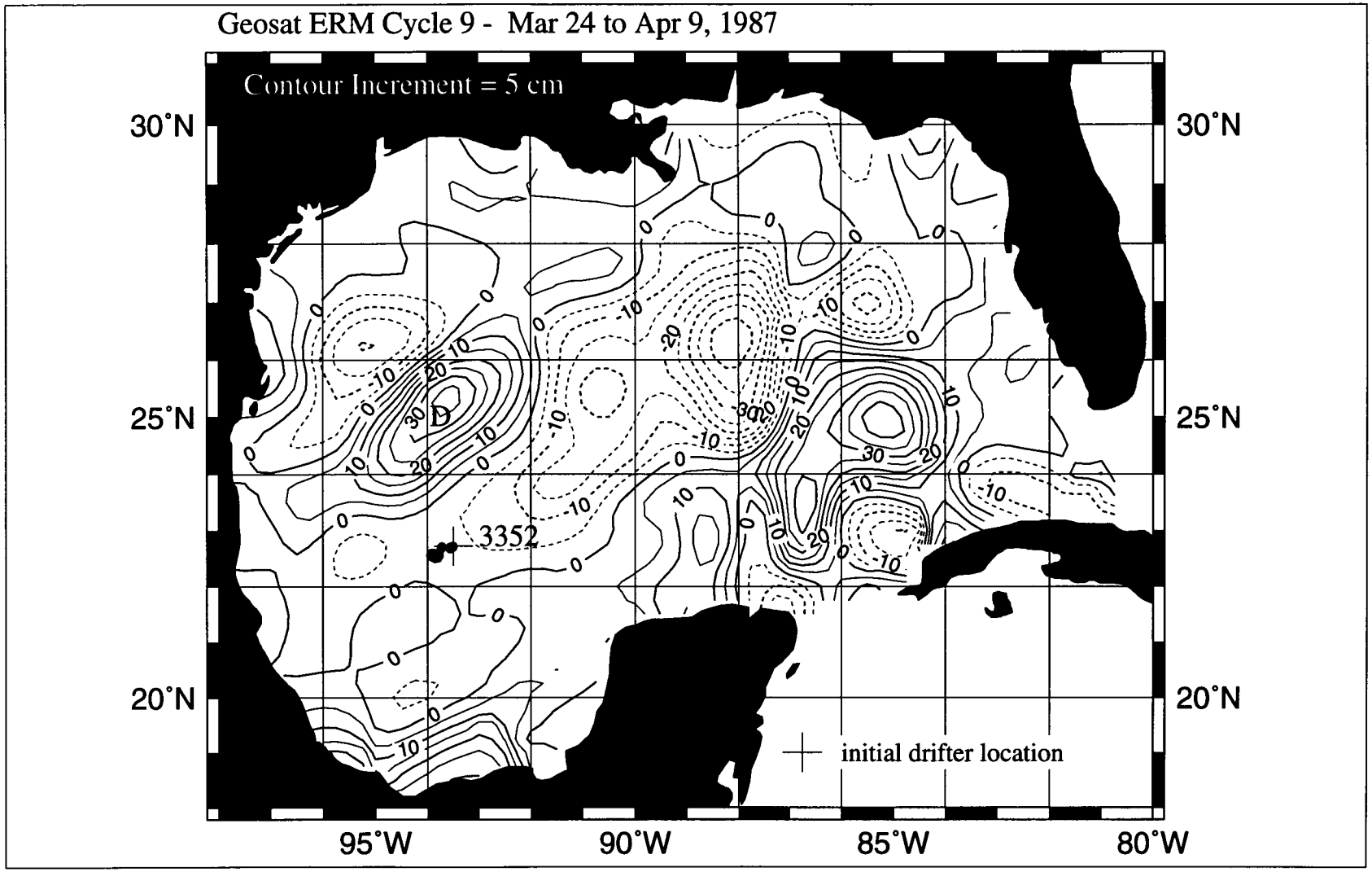

Figure 4.5-30. Sea surface height anomaly with respect to mean sea surface (OSUMSS95) for GEOSAT ERM Cycle 9 (March 24 to April 9, 1987) showing an elongated eddy D. Drifter locations within five days of the midpoint of the cycle are shown.

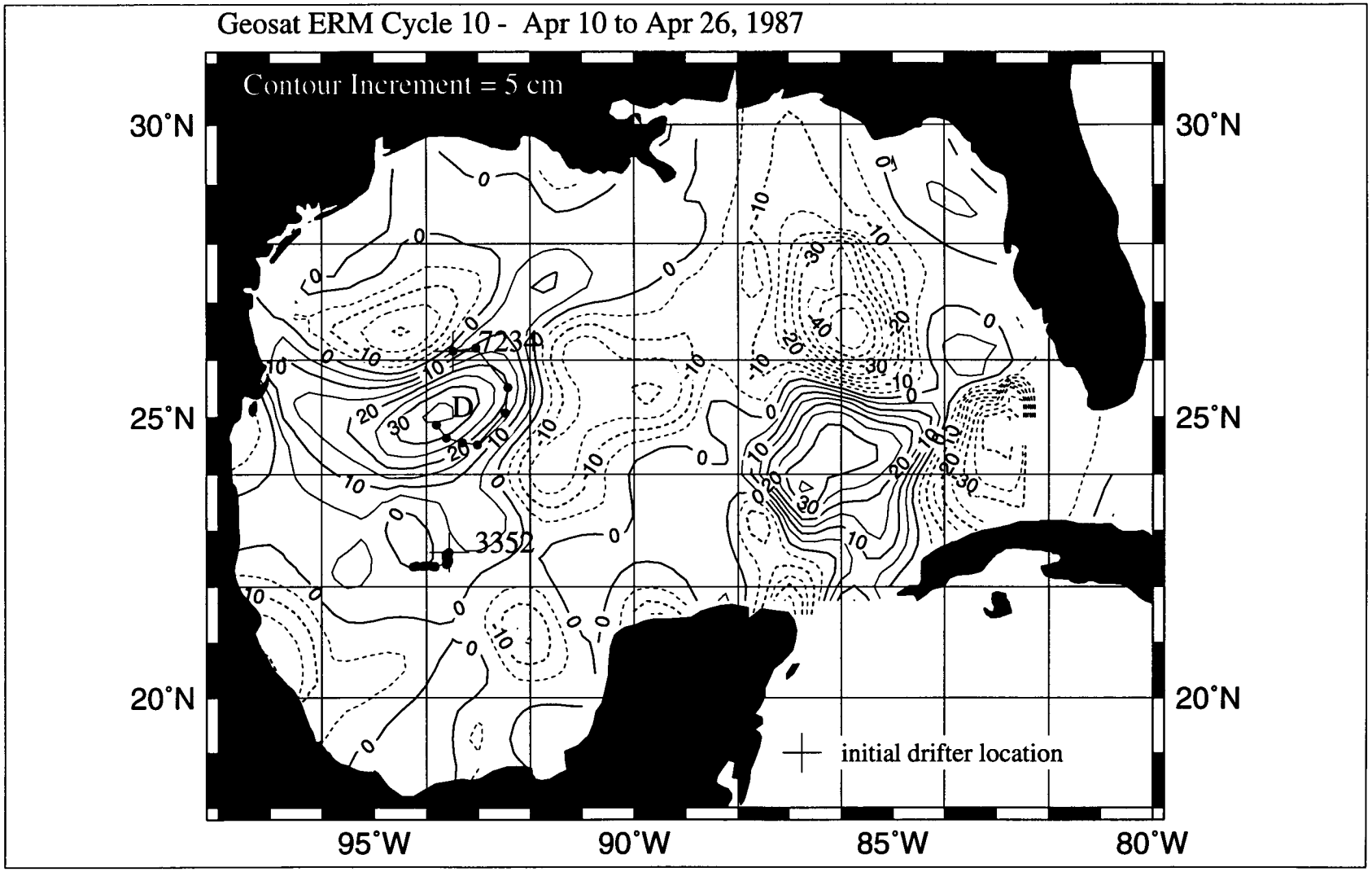

Figure 4.5-31. Sea surface height anomaly with respect to mean sea surface (OSUMSS95) for GEOSAT ERM Cycle 10 (April 10 to 26, 1987) showing eddy D. Drifter locations within five days of the midpoint of the cycle are shown.

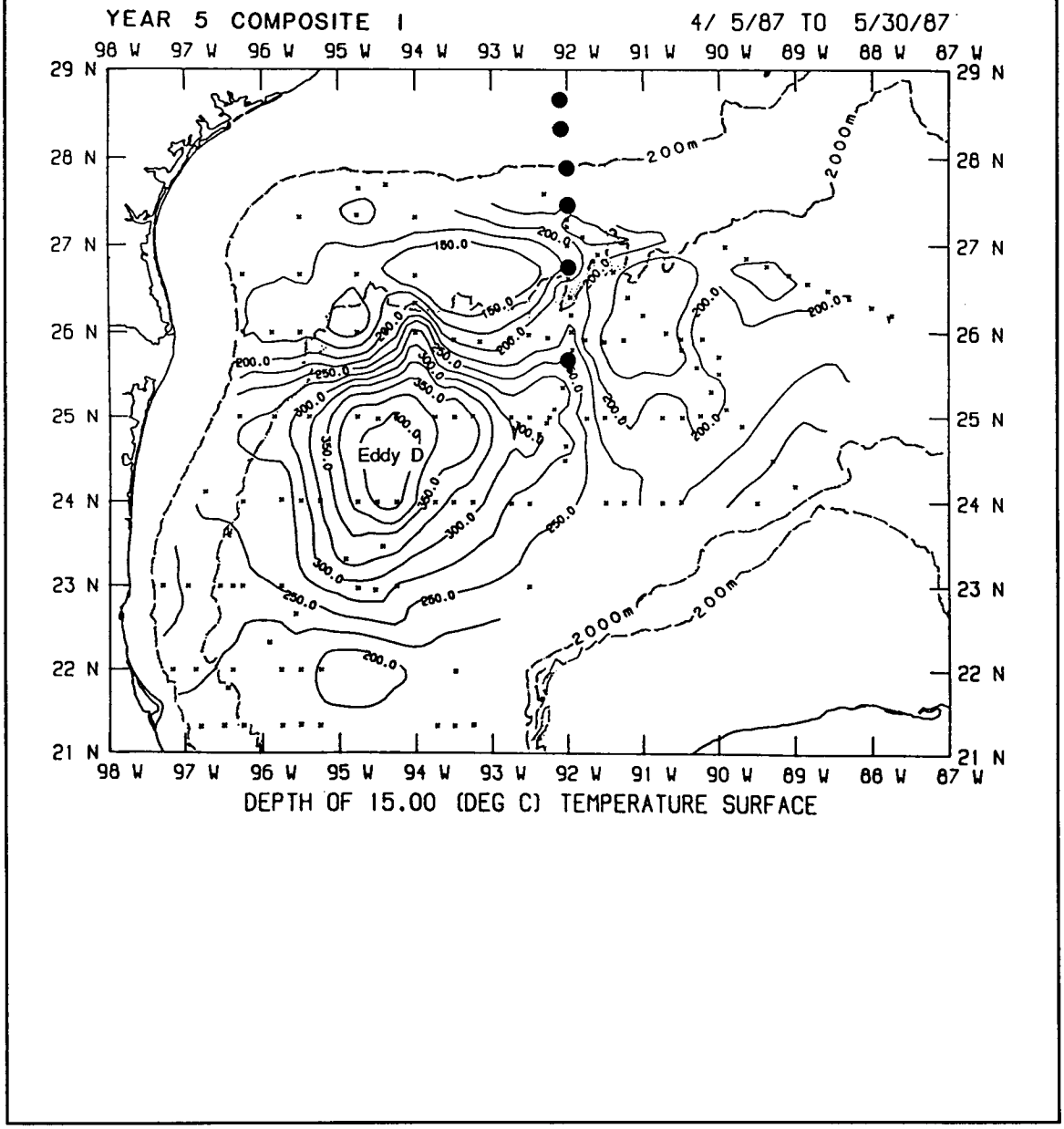

Figure 4.5-32. The depth of the 15°C isothermal surface as constructed from XBT data collected during the period of April 5 to May 30, 1987 (from SAIC 1989, Figure 4.3-10).

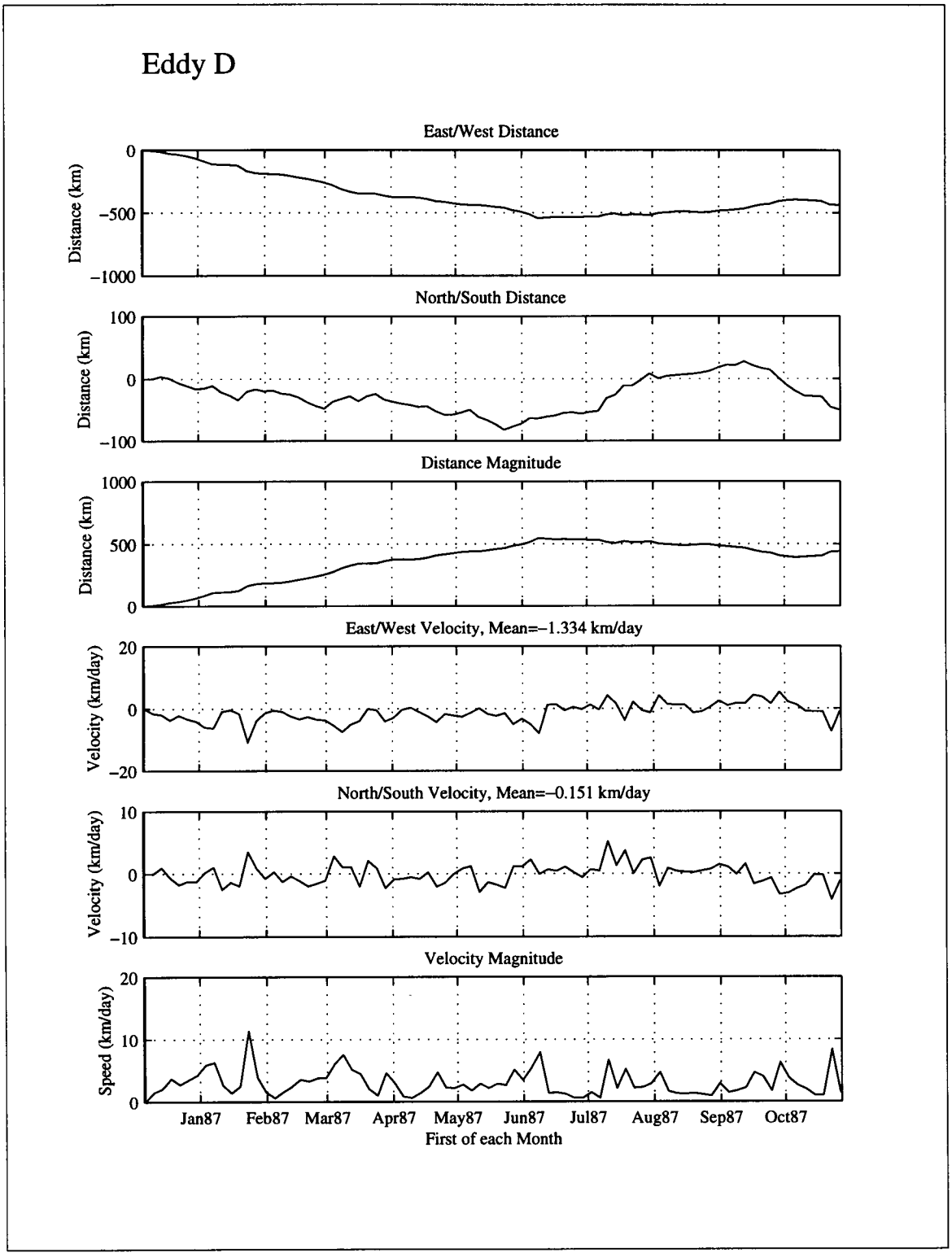

Figure 4.5-33a. Eddy tracking statistics for eddy D from December 1986 through October 1987 using GEOSAT altimetry: distance and velocity statistics.

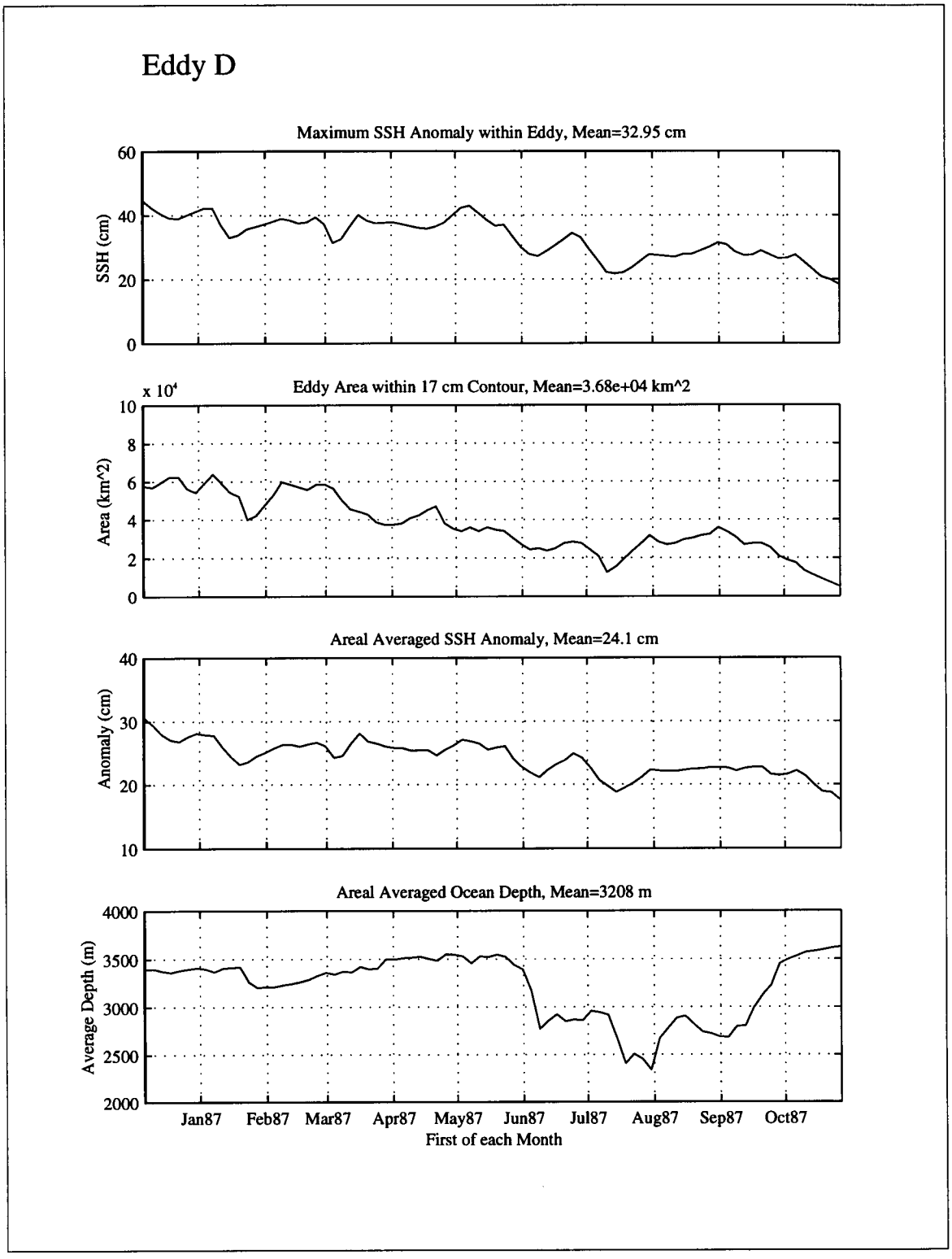

Figure 4.5-33b. Eddy tracking statistics for eddy D from December 1986 through October 1987 using GEOSAT altimetry: maximum height anomaly, eddy area, areal averaged anomaly and ocean depth.

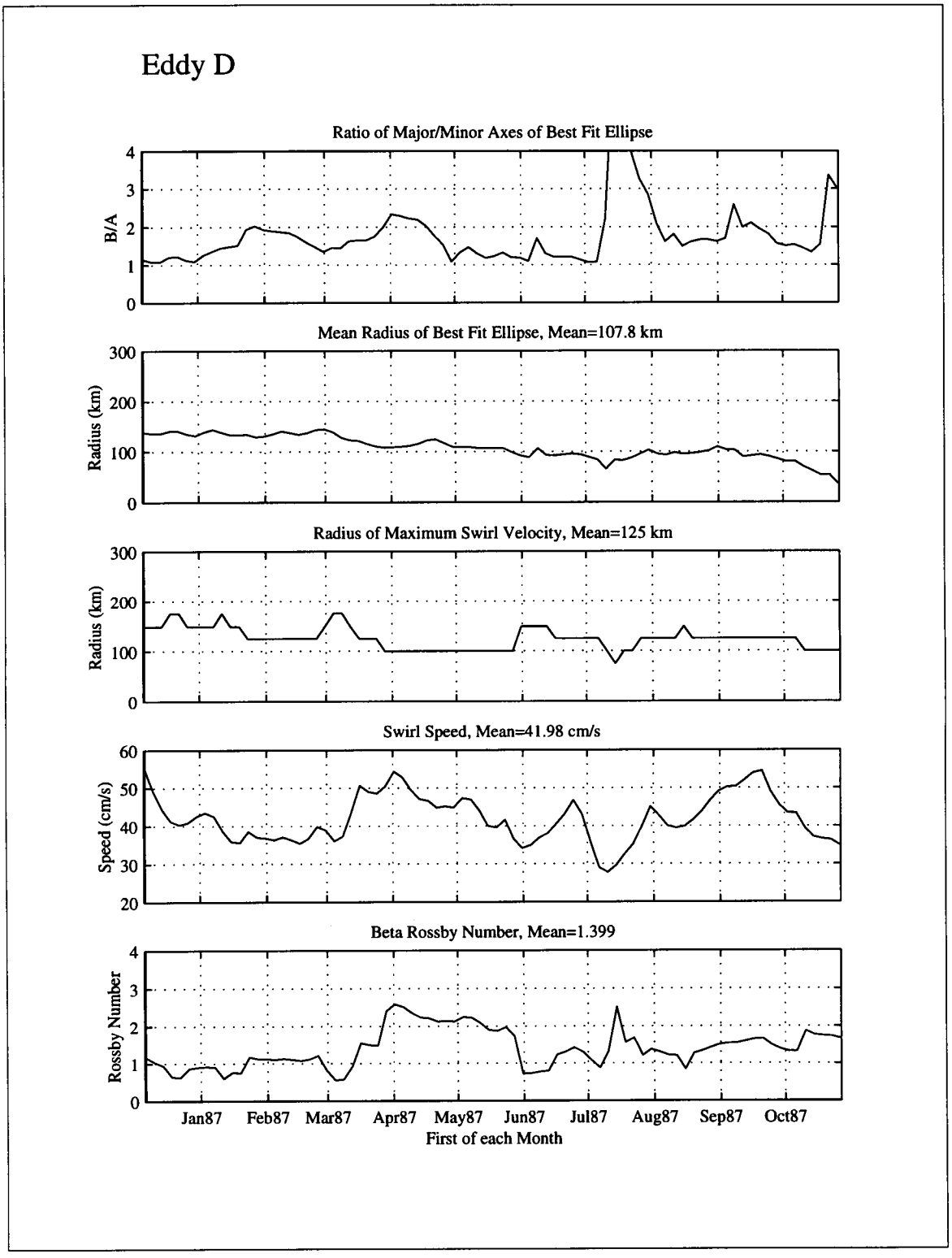

Figure 4.5-33c. Eddy tracking statistics for eddy D from December 1986 through October 1987 using GEOSAT altimetry: eccentricity, radius estimates, swirl speed, and Rossby number.

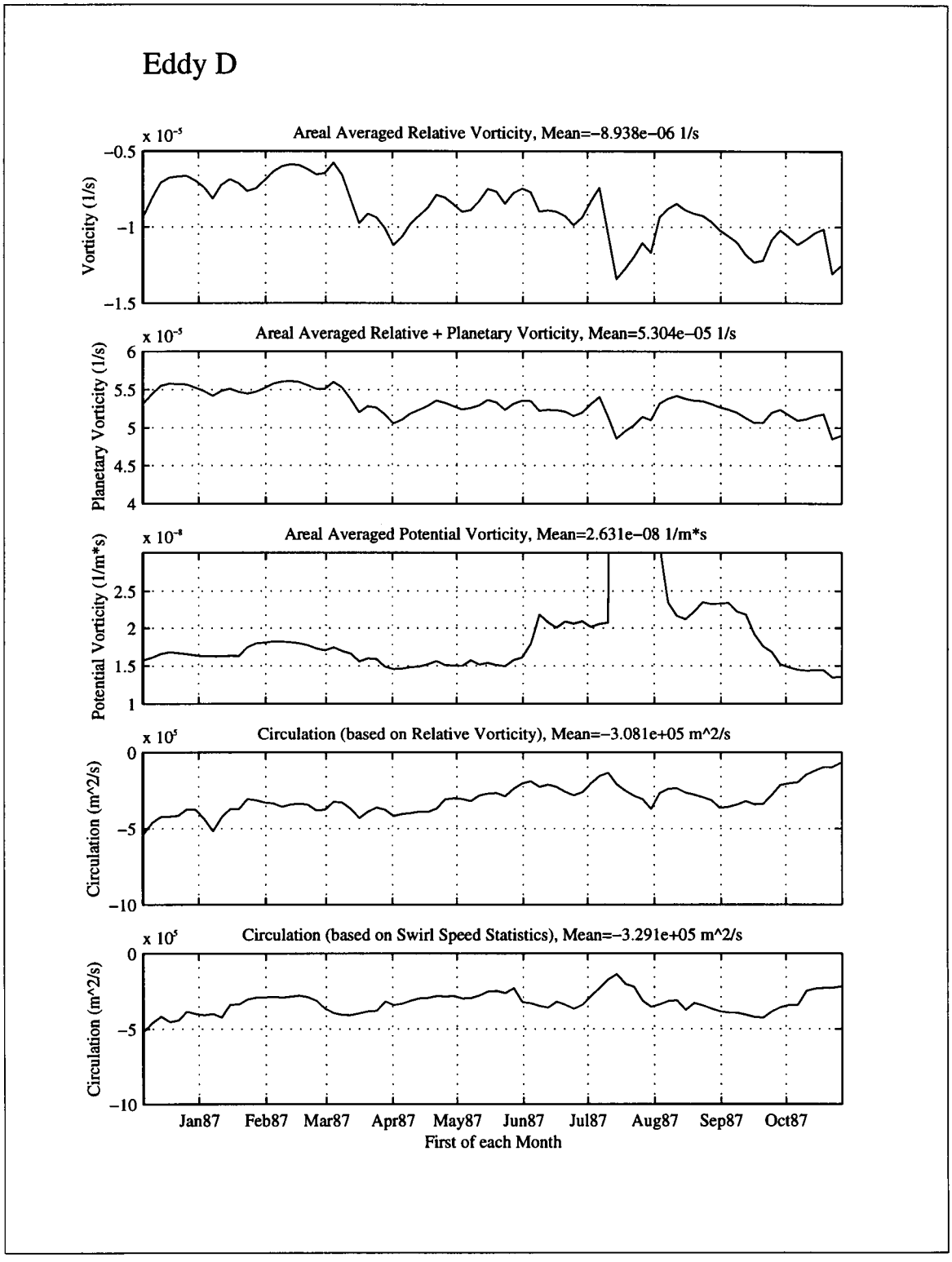

Figure 4.5-33d. Eddy tracking statistics for eddy D from December 1986 through October 1987 using GEOSAT altimetry: vorticity and circulation statistics.

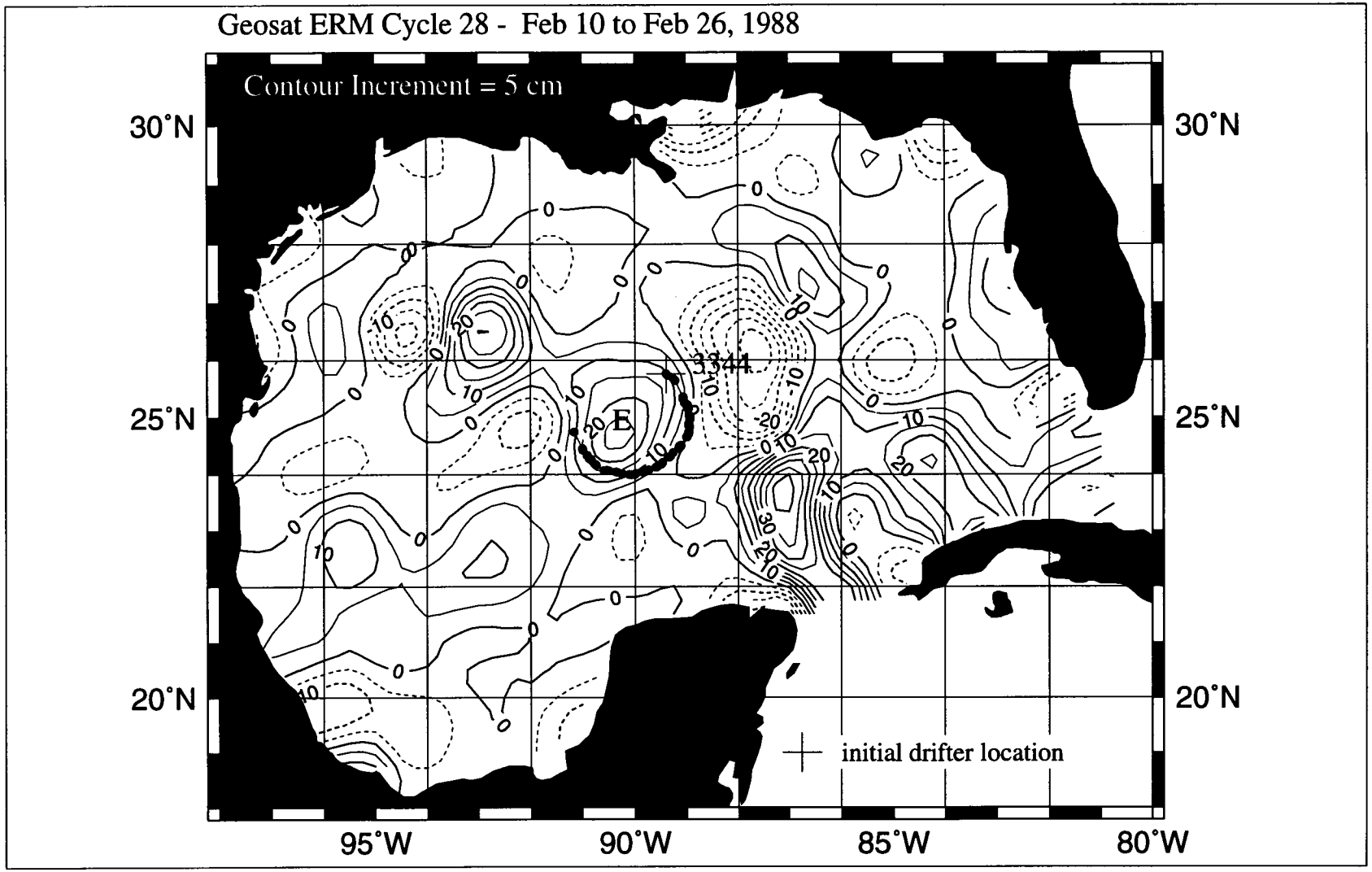

Figure 4.5-34. Sea surface height anomaly with respect to mean sea surface (OSUMSS95) for GEOSAT ERM Cycle 28 (February 10 to 26, 1988) showing eddy E and an unnamed secondary anticyclonic eddy to the northwest. Drifter locations within five days of the midpoint of the cycle are shown.

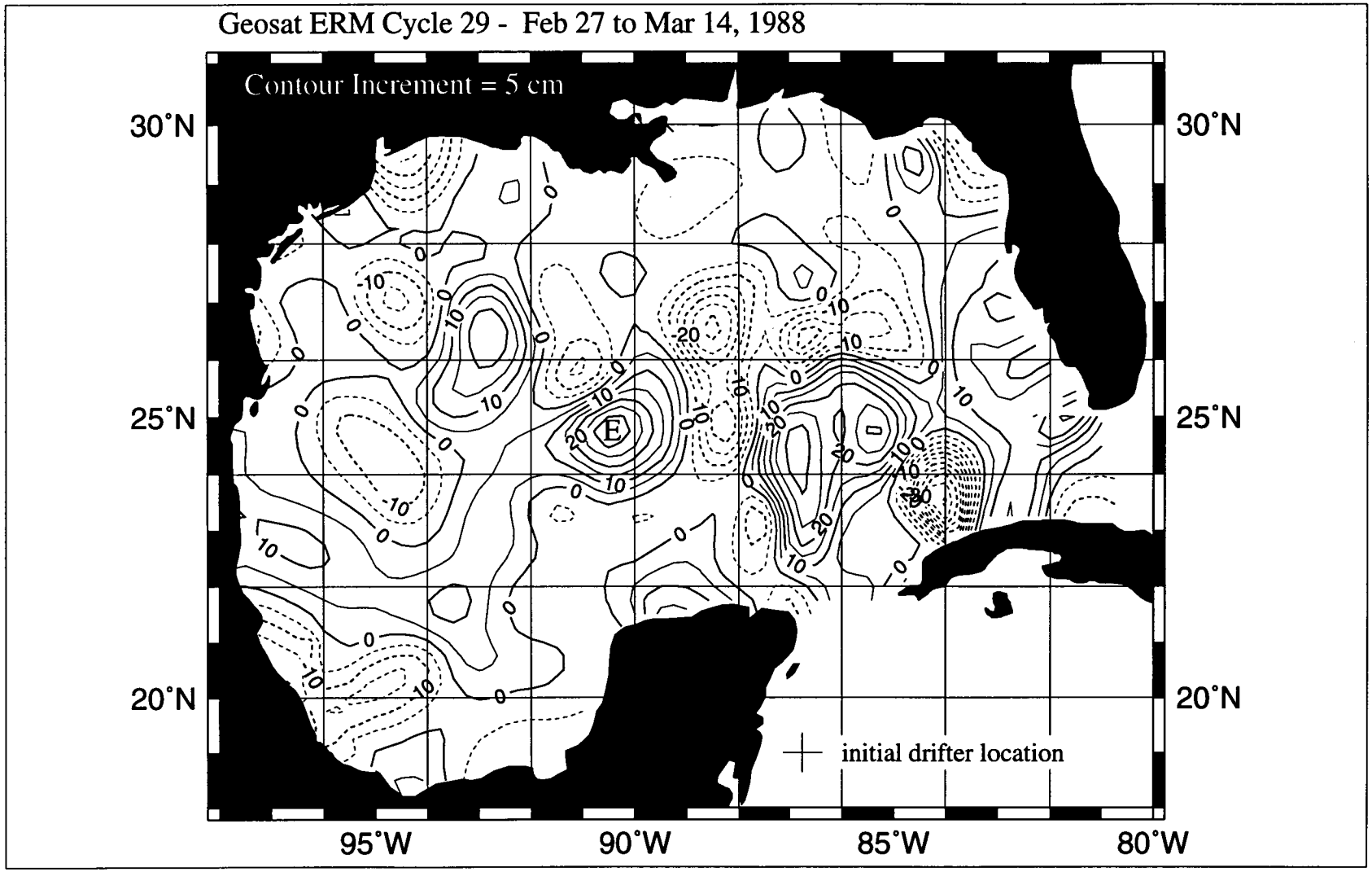

Figure 4.5-35. Sea surface height anomaly with respect to mean sea surface (OSUMSS95) for GEOSAT ERM Cycle 29 (February 27 to March 14, 1988) showing eddy E and an unnamed secondary anticyclonic eddy to the northwest.

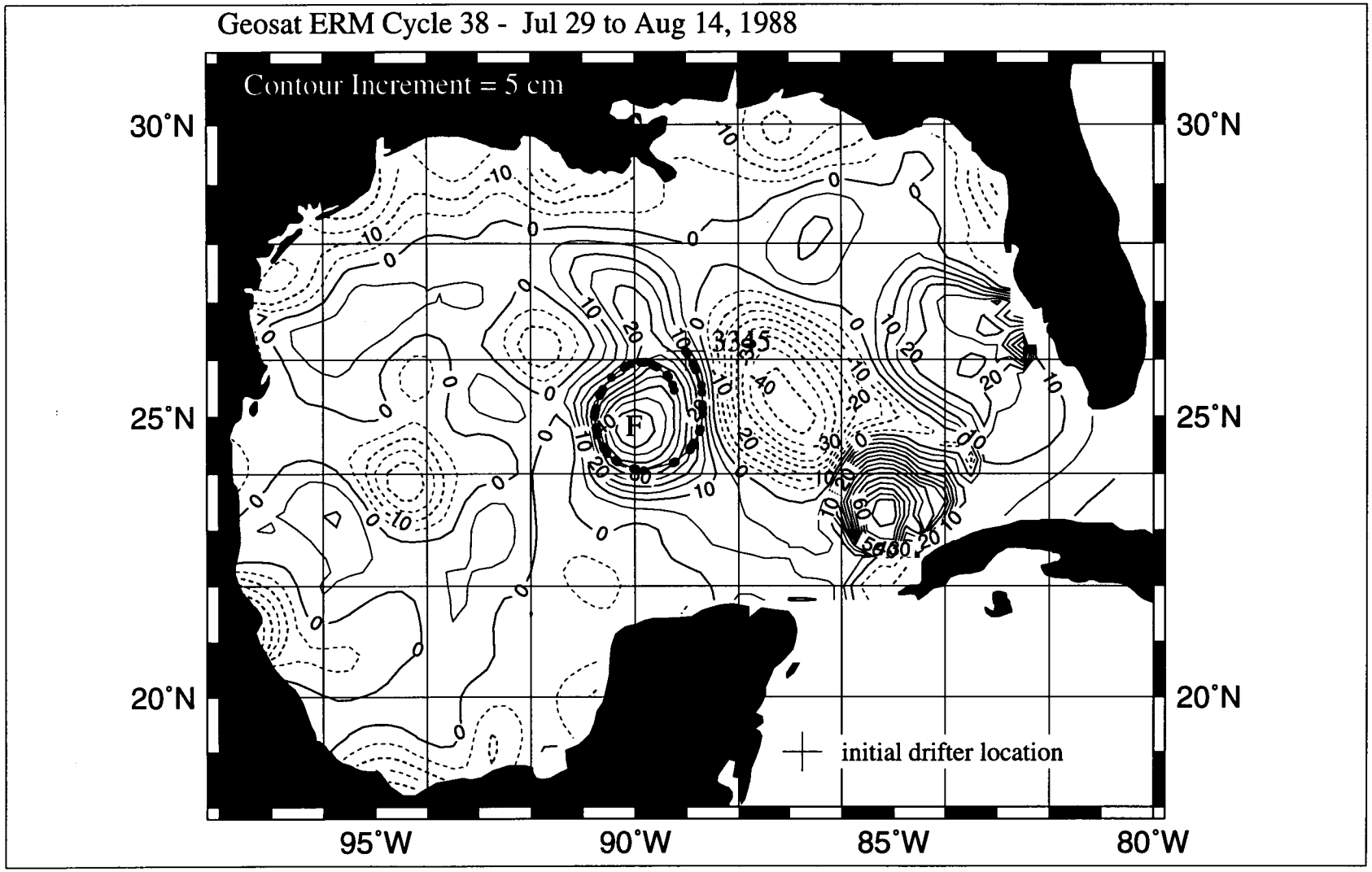

Figure 4.5-36. Sea surface height anomaly with respect to mean sea surface (OSUMSS95) for GEOSAT ERM Cycle 38 (July 29 to August 14, 1988) showing eddy F. Drifter locations within five days of the midpoint of the cycle are shown.

dissipation of eddy E allowed eddy F to propagate without any major interaction with other circulation features. Data outages affecting the GEOSAT altimeter abated and eddy F could be continuously tracked throughout its life span in the western Gulf of Mexico. The eddy took a characteristic southwestward path (Figure 4.5-37), which seems to be the preferred path in the absence of external forcing. The eddy was continuously tracked by both altimetry and an Argos-tracked drifter (3345), which remained in the eddy for over 200 days. Comparisons of altimetry-derived estimates of the geostrophic velocity with the velocity of drifter 3345 (Figure 4.3-4, page 98) verified the accuracy of the climatological sea surface height fields during this time period.

Tracking statistics for eddy F are shown in Figures 4.5-38a, b, c, and d. Because drifter 3345 remained in the eddy for an extended period, it is possible to compare the drifter-derived relative vorticity (Figure 4.5-39) with the altimetric estimate (Figure 4.5-38d). The mean vorticity derived from the drifter trajectory was approximately -1.4×10^{-5} rad·s^{-1}, which was somewhat larger than the -0.9×10^{-5} rad·s^{-1} determined for the areal-averaged relative vorticity derived from the altimetry. The time history of the change of relative vorticity for the two estimates agrees closely, with both showing a comparable slow decrease in magnitude over the time period. This is additional verification of the temporal accuracy of the velocity and vorticity fields derived from the altimetry. The good agreement in the time rate-of-change of vorticity between the drifter and altimetry is important because it directly influences the accuracy of the altimetric estimate of the time rate-of-decrease of circulation, which is a measure of eddy decay.

4.6 Estimates of Eddy Decay in the Western Gulf of Mexico

The decay of Loop Current eddies was studied using circulation estimates from the tracking statistics of four Loop Current eddies (B, C, D and F) over the first 120 days after transit across 90°W longitude. During these four months the eddies were propagating through the western Gulf of Mexico and had not yet made contact with the western margin. Only four months of data were used to avoid the later time period in eddy life when interaction with topography, and residual Loop Current eddies along the western margin, could significantly affect the time history of the eddy circulation (Lewis and Kirwan 1985; Vidal et al. 1992). A curve of the form:

$$Circulation = A\ exp(-Bt)$$

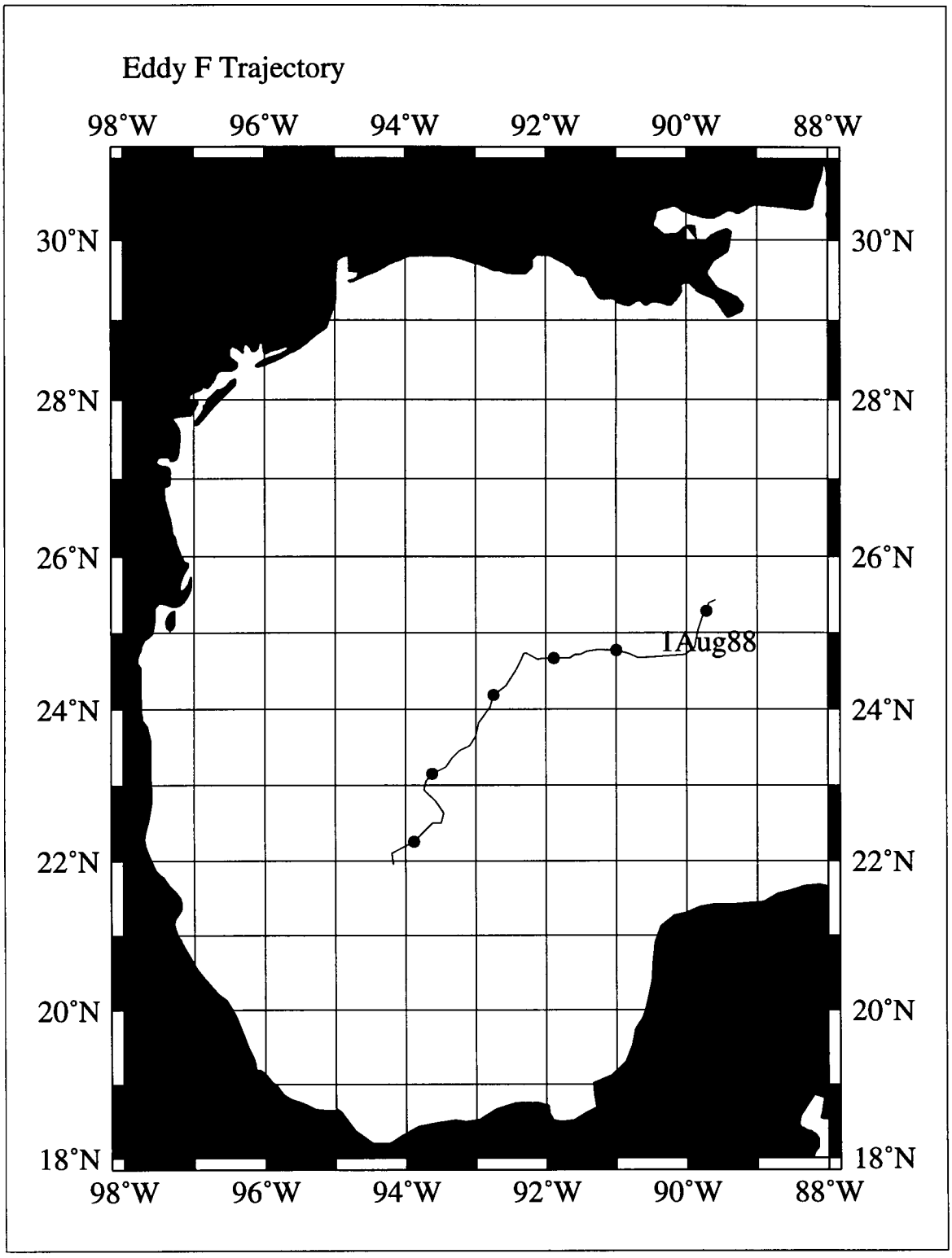

Figure 4.5-37. Trajectory of eddy F center determined using GEOSAT altimeter data and an objective tracking program. Dots show center location on the first of each month.

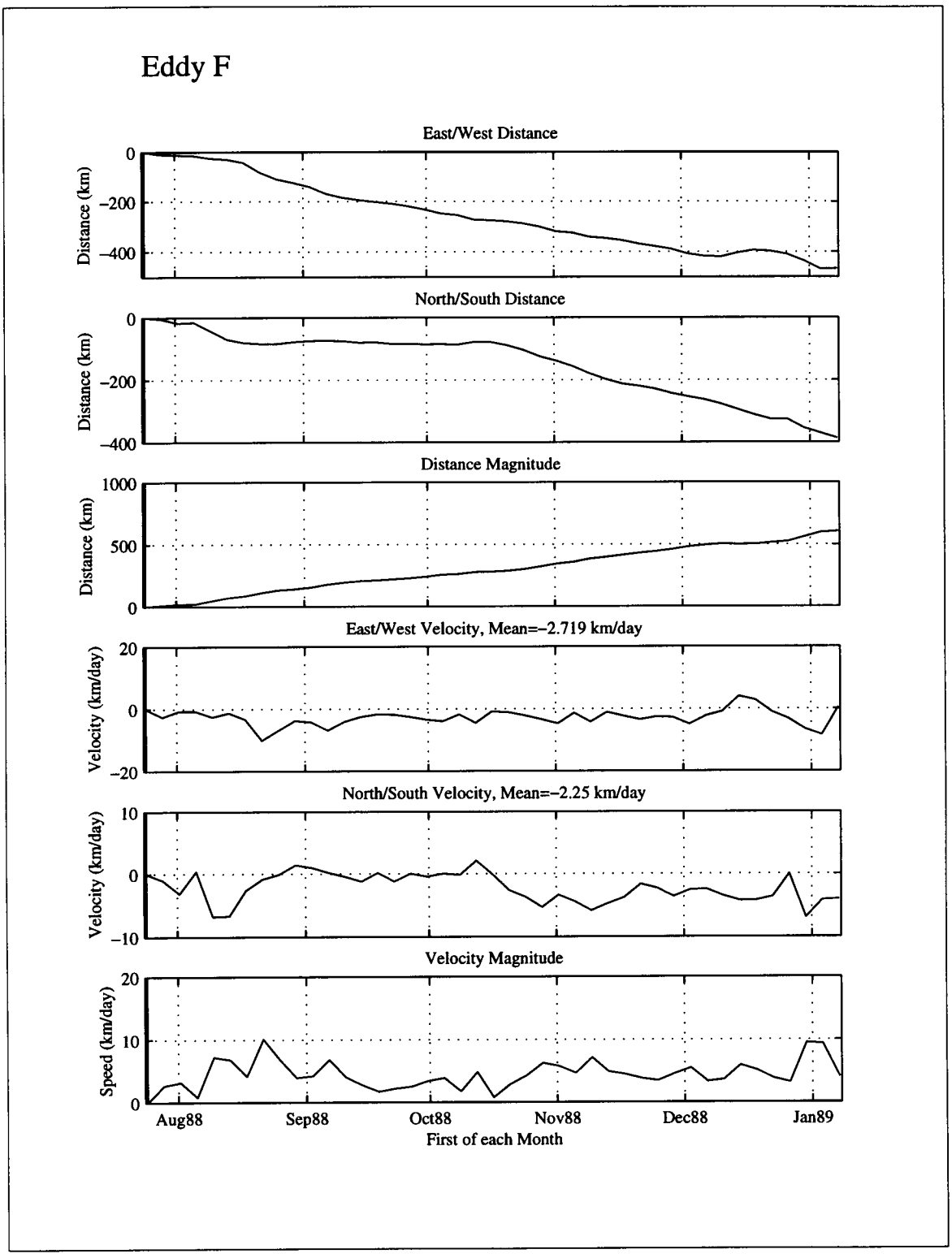

Figure 4.5-38a. Eddy tracking statistics for eddy F from August 1988 to January 1989 using GEOSAT altimetry: distance and velocity statistics.

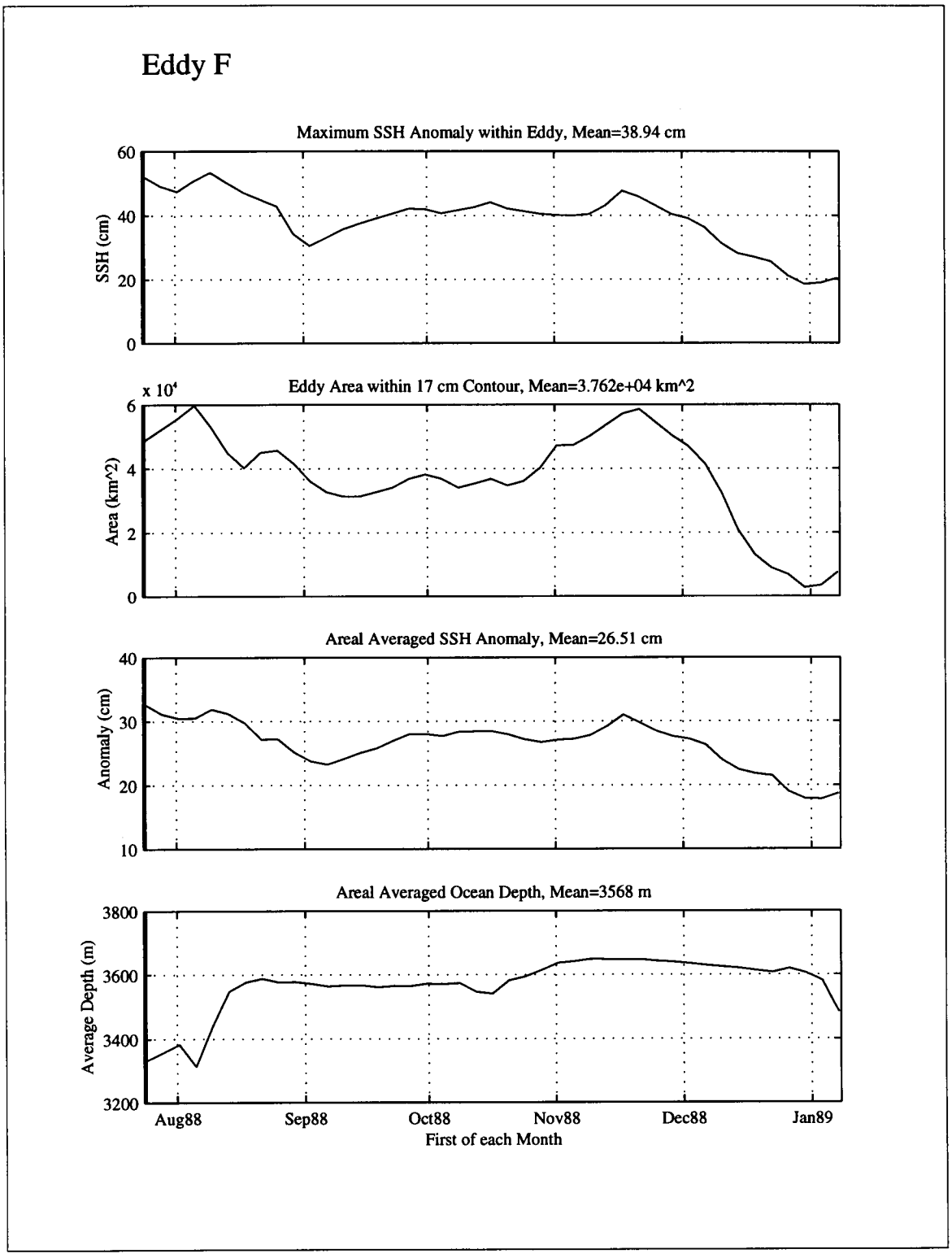

Figure 4.5-38b. Eddy tracking statistics for eddy F from August 1988 to January 1989 using GEOSAT altimetry: maximum height anomaly, eddy area, areal averaged anomaly and ocean depth.

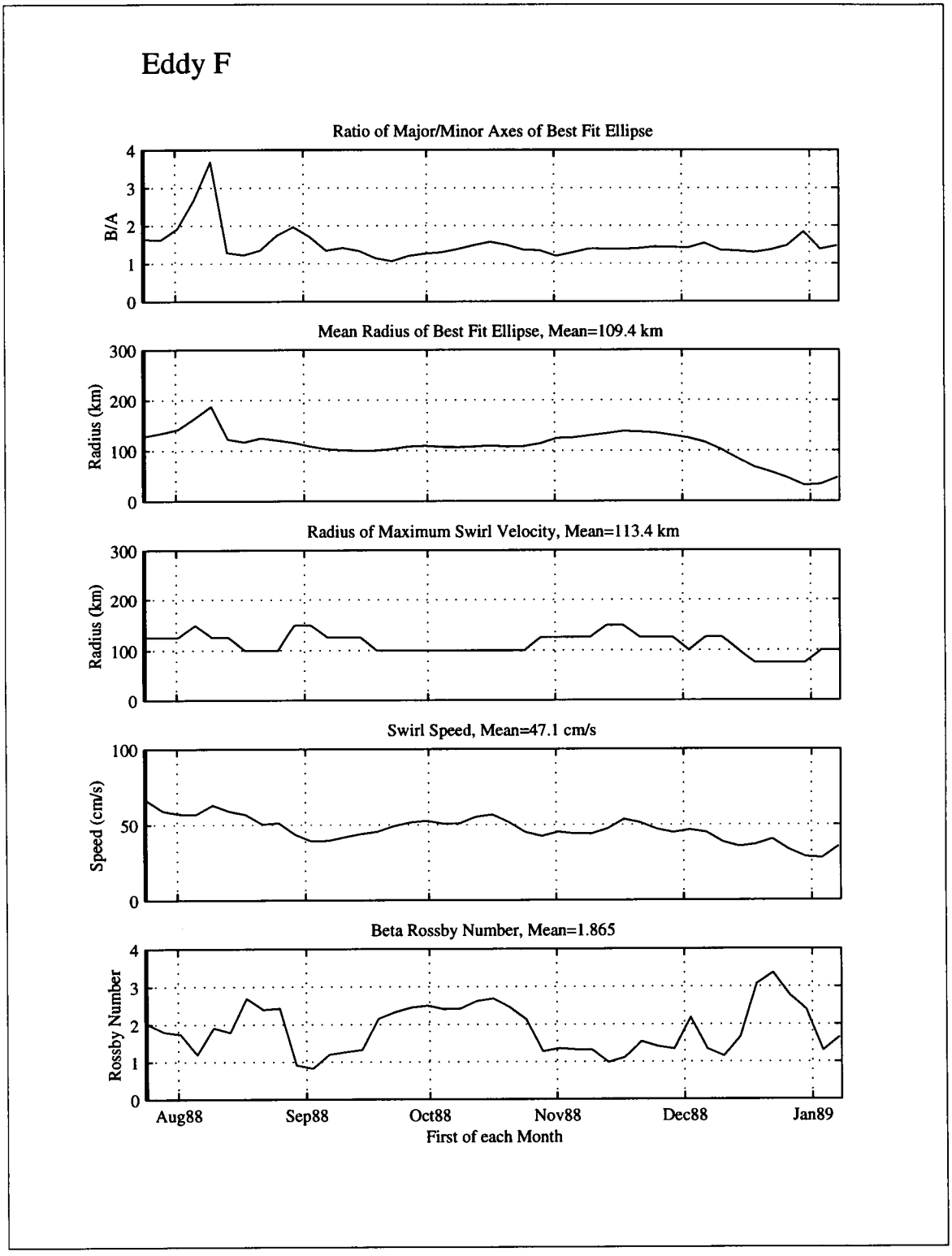

Figure 4.5-38c. Eddy tracking statistics for eddy F from August 1988 to January 1989 using GEOSAT altimetry: eccentricity, radius estimates, swirl speed, and Rossby number.

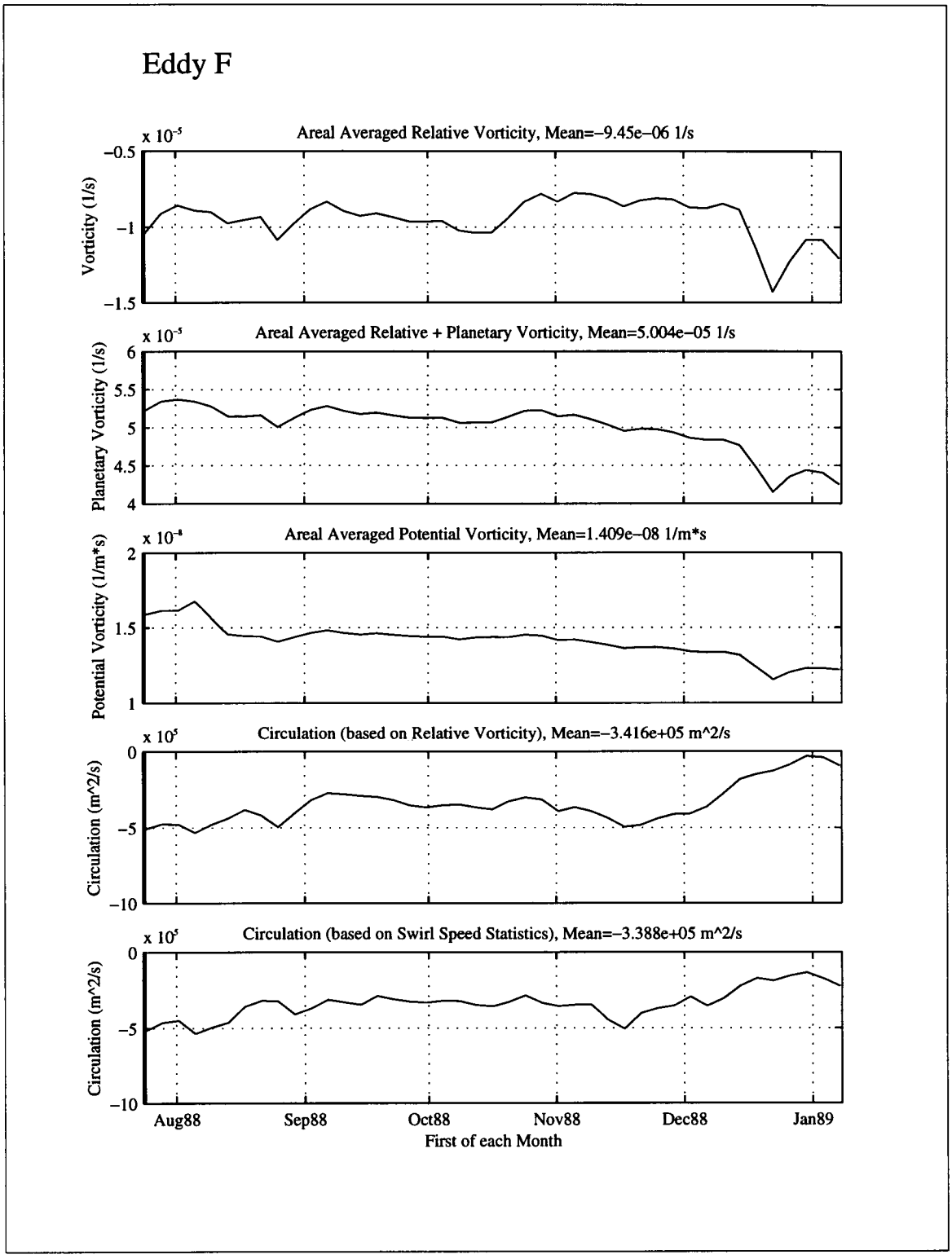

Figure 4.5-38d. Eddy tracking statistics for eddy F from August 1988 to January 1989 using GEOSAT altimetry: vorticity and circulation statistics.

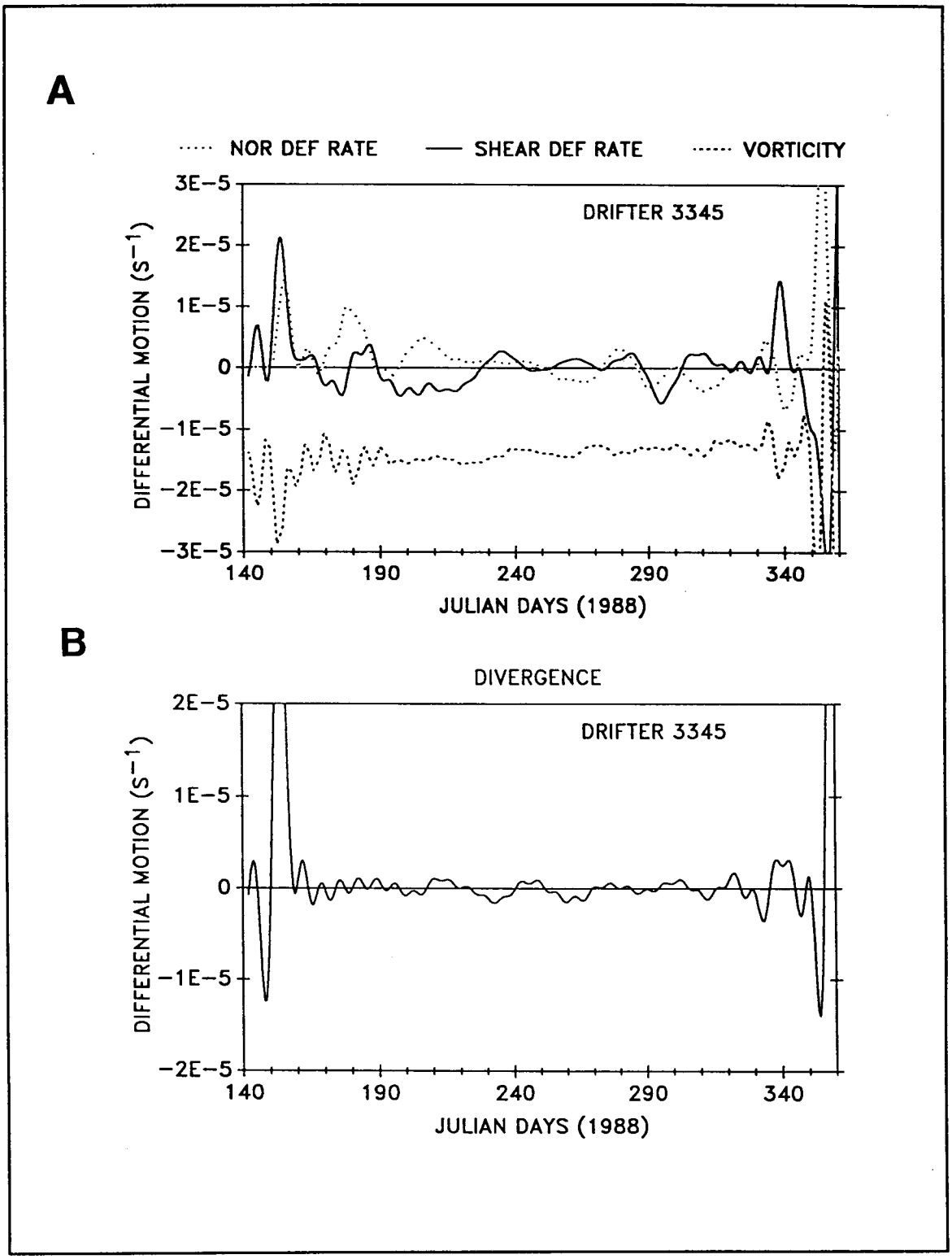

Figure 4.5-39. For Drifter 3345, the (a) vorticity, normal deformation rate and shear deformation rate for eddy F, and (b) divergence for eddy F (from SAIC 1989, Figure 4.3-29).

was fit to anticyclonic circulation estimates based on relative vorticity and the swirl speed statistics. Section 3.4.2.11 contains details on the circulation calculations and the objective eddy-tracking program used to make the estimates. B is a decay coefficient with units of $1 \cdot day^{-1}$. The regression fits and raw data are shown in Figure 4.6-1. The values for B were found to be $438 \cdot day^{-1}$ and $427 \cdot day^{-1}$, for circulations based on relative vorticity and swirl speed, respectively. This indicates an average e-folding time of approximately 1.2 years for the observed eddies. This agrees with a one-year estimate of eddy decay based on isotherm rising rates determined from hydrographic surveys of a Loop Current eddy in 1966 (Elliot 1982).

4.7 Mean Loop Current Eddy Statistics in the Western Gulf of Mexico

Mean eddy statistics were also computed for the four major Loop Current eddies which were continuously tracked for 120 days after transit across 90°W longitude. These statistics are shown in Table 4.7-1.

These mean values have been compared with similar estimates which have appeared in the literature and show good agreement, given the uncertainty in determining these statistics from the different data sources. The altimetric estimate of a mean eddy area of 48,961 km^2 is comparable to the mean eddy area of 43,041 km^2 derived from 10 years of monthly frontal analysis maps derived from satellite infrared imagery (SAIC 1989). The consistency of the two mean radius estimates from the altimeter data is remarkable, given the different estimation techniques. A 127 km mean radius was found based on averages of the best fit to the tracking contour, and a 128 km mean radius was determined for averages of the radial bin relative to the eddy center containing the maximum mean velocity magnitude. The altimeter-derived mean-radius estimates are similar to the 117 km radius estimated from monthly frontal analysis maps (SAIC 1989), and to estimates from hydrography by Elliot (1982). These latter estimates found a mean radius of 183 km in the eastern Gulf of Mexico and 133 km in the western Gulf of Mexico (from a limited sampling of eddies).

The mean propagation speed and direction of the eddy center determined from altimetry ($3.4\ km \cdot day^{-1}$ at 251 degrees true north) are also similar to the estimates by Elliot (1982), who found a vector mean velocity of $2.1\ km \cdot day^{-1}$ at 279 degrees true north, with mean translation velocities ranging from 2.2 to $4.9\ km \cdot day^{-1}$. Vukovich and Crissman (1986) found a $5\ km \cdot day^{-1}$ mean translation speed of Loop Current eddies, based on continuous tracking of eddies using satellite imagery.

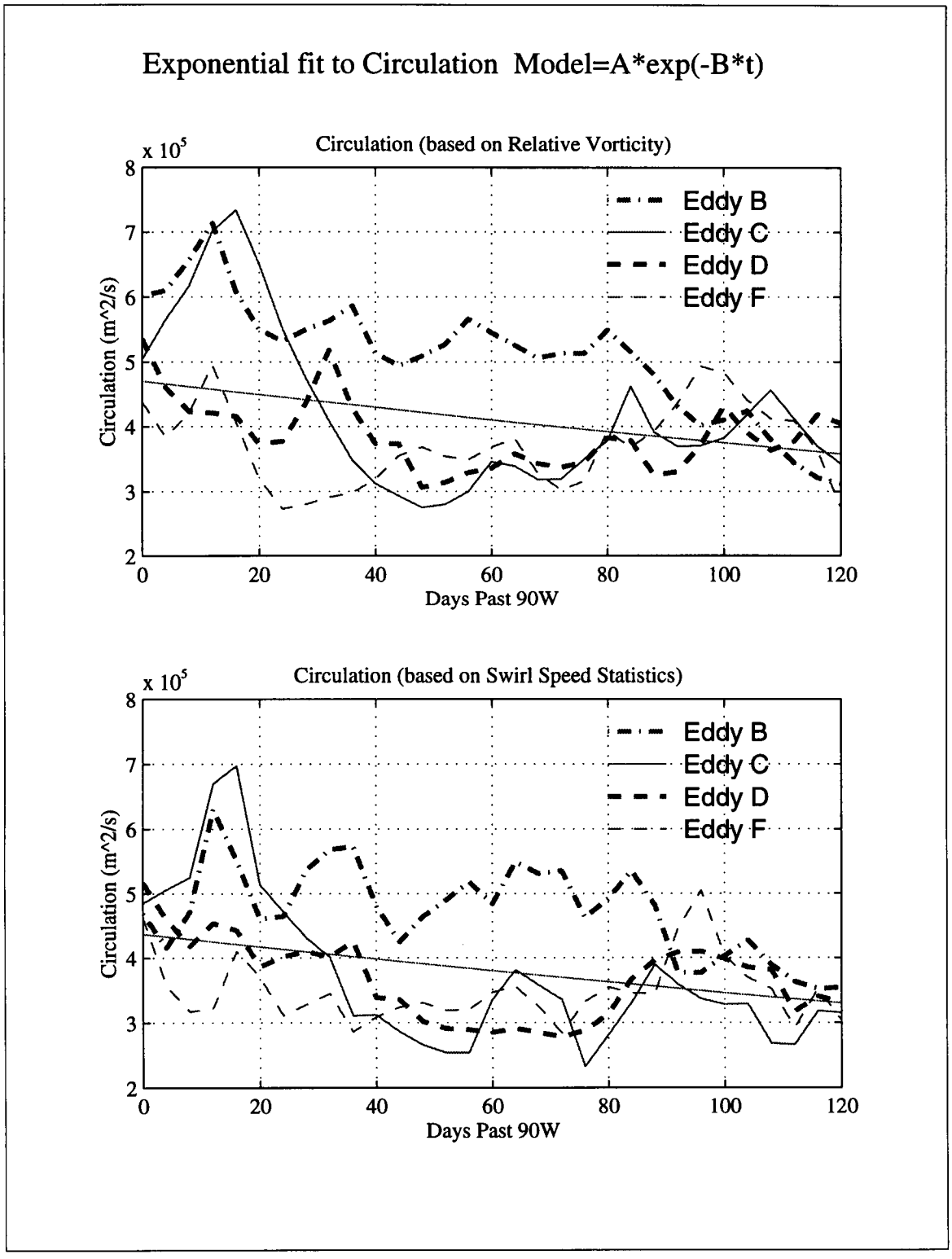

Figure 4.6-1 Regression fits to anticyclonic circulation estimates for Loop Current eddies during the 120 days after transit across 90°W longitude.

Table 4.7-1. Mean Loop Current eddy statistics in the western Gulf of Mexico from continuous altimetric tracking of four Loop Current eddies (B, C, D and F) for 120 days after transit across 90°W longitude.

Eddy Statistic	Mean
Area	48,961 km^2
Radius	127 km* 128 km**
Propagation Speed	3.4 $km \cdot day^{-1}$
Propagation Direction	251°T
Maximum SSH Anomaly	42 cm
Swirl Speed	49 $cm \cdot s^{-1}$
Major/Minor axes (a/b)	1.5
Beta Rossby number	1.55

* Estimated from best fit ellipse to 17-cm contour.
** Estimated from the radial bin containing the maximum mean velocity magnitude.

Drifter observations have shown eddy-center translation velocities of 3 to 6 $km \cdot day^{-1}$ and swirl speeds of about 50 $cm \cdot s^{-1}$ (Kirwan et al. 1984b), comparable to the altimetric results. Altimetry cannot observe the ageostrophic velocity component of the swirl velocity which is observed in the translation of the drifters. Assuming a steady cyclogeostrophic balance within the eddies observed in the Gulf of Mexico, this would increase the mean maximum swirl velocity estimate from the altimeter by 7% (Didden and Schott 1993).

The altimetry estimate of the mean eccentricity of the eddies was 1.55, and was defined as the mean of the ratios of the major to minor axes of the best fit ellipse to the tracking contour. This is in good agreement with the eccentricity estimates by Elliot (1982) for eddies in the western Gulf of Mexico, which ranged from 1.5 to 2.3, with a mean of 1.75. Eddy eccentricities have also been estimated from drifter trajectories (SAIC 1986; SAIC 1989) and typically range from 1.1 to 2.0 in the western Gulf of Mexico. The altimeter-derived mean β Rossby number of 1.55 is consistent with the theory of Hurlburt and Thompson (1982) which predicts $\mathcal{O}(1)$ β Rossby numbers for eddy shedding by the Loop Current in the Gulf of Mexico.

4.8 Eddy Statistics at 90°W Longitude

Referencing of the altimeter data from the GM and ERM to the same mean surface allows a consistent comparison of eddy statistics during transit across 90°W longitude. Table 4.8-1 shows a compilation of these statistics. The largest Loop Current eddy observed during the GEOSAT time period was Nelson eddy, which had a maximum sea surface height anomaly in excess of 70 cm and covered an area over 76,000 km^2 (within the 17-cm contour). Unfortunately, excessive outages during the end of the GEOSAT mission prevented a detailed study of this unique eddy event. The limited sampling of Loop Current eddies by GEOSAT supports the conclusion that large energetic Loop Current eddies, such as eddy B and Nelson eddy, do penetrate farther into the northern Gulf of Mexico.

4.9 Eddy Variability Statistics

Annual and seasonal sea surface height and geostrophic velocity variability maps are found in Appendix A of this report. Because Gulf of Mexico circulation is dominated by the aperiodic shedding of anticyclonic eddies from the Loop Current, both the annual and seasonal variability are a reflection of the eddy shedding events that happen to occur in a particular year or season.

Additional analyses were performed to isolate the contribtions from positive and negative anomalies to the sea surface topographic variability observed during the GEOSAT mission. The sea surface height anomaly maps (Appendix A) were used to determine the percent occurrence of height anomalies greater than 5 cm (Figure 4.9-1) and less than 5 cm (Figure 4.9-2).

The patterns of percent occurrence of positive anomalies are in good qualitative agreement with the percent occurrence of warm eddy water determined from monthly frontal analyses, reported in SAIC (1989) [see Figure 4.9-3]. Both analyses show a region of highest probability in the western Gulf of Mexico near 25°N latitude, 93°W longitude, where the eddy trajectories are still tightly bunched after shedding from the Loop Current (see Figure 4.5-1, page 101). The contours of equal probability follow continental slope isobaths around the perimeter of the western basin. The patterns of areas of high probability within the interior of the western basin show paths of high probability consistent with the characteristic eddy paths determined by Vukovich and Crissman (1986). A region of high probability (>40%) is found in the northwest corner of the Gulf of Mexico near 27°N latitude, 92°W to 96°W longitude on the Texas-Louisiana slope, the location of the so-called "eddy graveyard."

Table 4.8-1. Loop Current eddy statistics at 90°W longitude.

Eddy	GEOSAT cycle	Lat. (°N)	SSH (cm)	Area (km^2)	$\bar{h}$ (cm)	Z (m)	a/b axes	Equiv. Radius R_{ab} (km)	V_s ($cm \cdot s^{-1}$)	R_s (km)	β
B (Fast)	GM 5	26.08	64	68,072	38	2874	1.73	149	71	150	1.52
C (Hot)	GM 15	25.24	62	57,016	37	3428	1.58	138	76	150	1.60
D (Krazy)	ERM 2	25.37	46	58,310	31	3396	1.15	141	58	150	1.23
E (Lazy)	ERM 28	24.88	28	16,339	22	3556	1.45	74	36	100	1.69
F (Murphy)	ERM 39	24.68	43	45,684	27	3577	1.74	120	51	100	2.43
N (Nelson)	ERM 62	25.87	70	76,297	40	3082	1.28	158	77	175	1.21

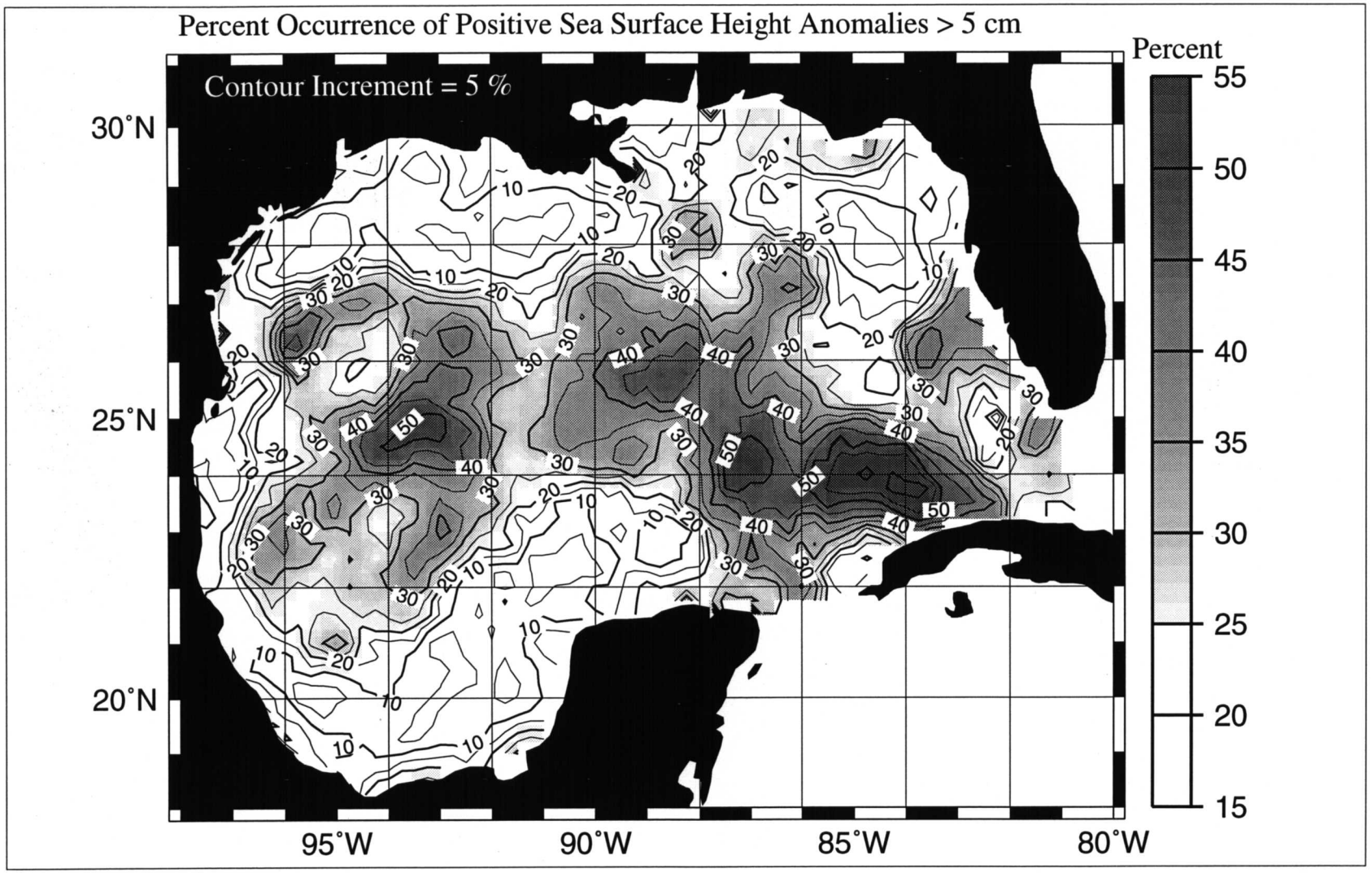

Figure 4.9-1. The percent occurrence of positive sea surface height anomalies greater than 5 cm in the GEOSAT climatology.

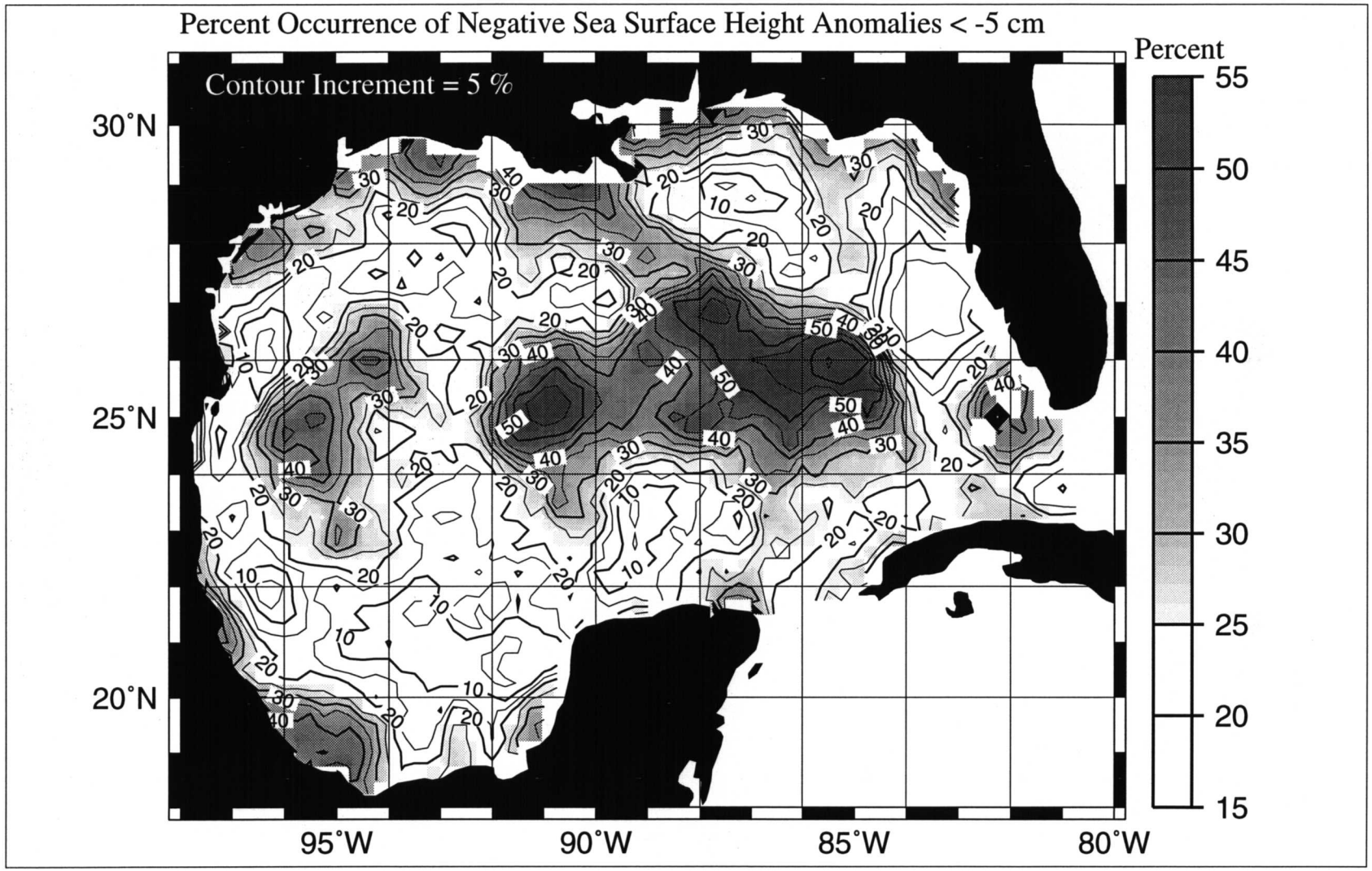

Figure 4.9-2. The percent occurrence of negative sea surface height anomalies less than -5 cm in the GEOSAT climatology.

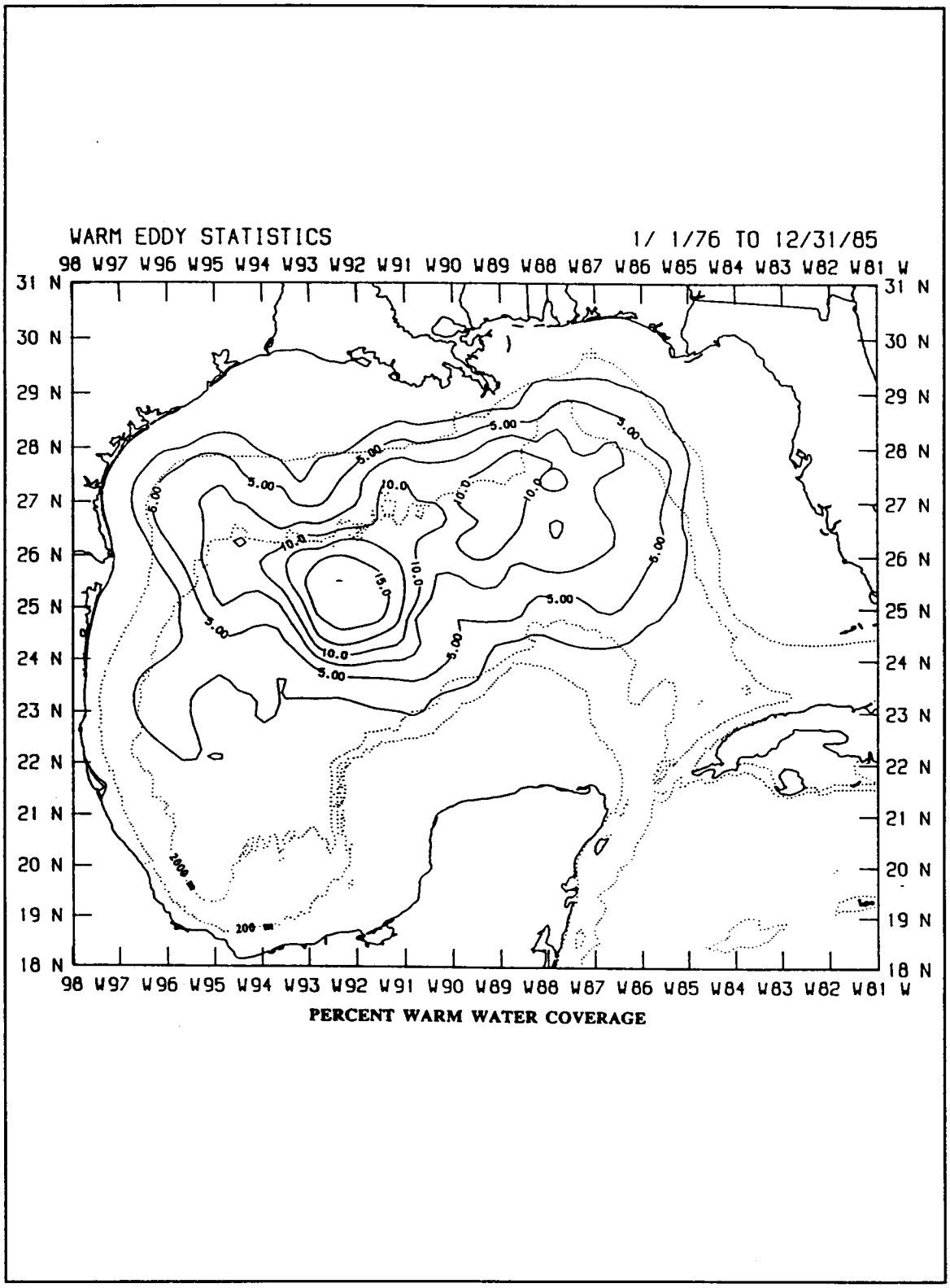

Figure 4.9-3. The percent occurrence of warm eddy water from monthly frontal analyses (from SAIC 1989, Figure 4.2-10).

The patterns of percent occurrence of negative anomalies show a region of highest probability at 25°N latitude, 91°W longitude, where cyclones have been observed before and after the passage of Loop Current eddies (Hamilton 1992). The other area of high percent occurrence is along the western margin of the deep basin (near 25°N and 26°N latitude), possibly associated with the collision between Loop Current eddies and the Mexican shelf, and the generation of secondary cyclonic eddies. A peculiar result of this analysis is the low probability of negative anomalies over the northwestern continental slope, where cyclonic eddies were observed during the GEOSAT time period (Hamilton 1992). This may have been a result of undersampling of these small scale features by the GEOSAT altimeter.

V. ANALYSIS OF SURVEY AND DRIFTER DATA

5.1 Introduction

This chapter is organized as follows: First, the behavior of five major Loop Current eddies is analyzed, paying attention to each ones' influence on slope eddies (Sections 5.2 through 5.6). Then, Sections 5.7 and 5.8 concentrate on slope cyclones and anticyclones, and their relationships to smaller peripheral eddies that were found in hydrographic surveys. Finally, the major results are discussed and summarized in Section 5.9.

Significantly, the most interesting data occurred in the last year of the study, when a number of strong flows between eddies were documented with AXCPs. This period also had the advantage that many drifters from the SCULP program revealed interrelationships among the many surveyed slope eddies. Unfortunately, however, it was almost impossible to follow the complete evolution of a slope eddy, and therefore, the analyses concentrate on the events shown by the surveys. It will also be shown that the eddy fields on the slope strongly influenced the currents at the shelf break.

Between August 1992 and December 1994, five Loop Current anticyclonic eddies were tracked across the central and western parts of the Gulf of Mexico. These eddies, named U, V, W, X and Y, were surveyed by air-deployed AXBTs and AXCPs, and ship-deployed CTDs and XBTs. In addition, all but one were seeded with satellite tracked Argos drifters. These eddies had markedly different life histories, with differing interactions with secondary eddies over the slope. One purpose in this report is to compare and contrast the evolution of these eddies, using drifter orbits as the principal data source, with additional information on the hydrographic and velocity structures derived from the surveys, and a number of current meter moorings deployed along the shelf break. A second objective is to describe the multitude of smaller cyclones and anticyclones that were mapped on the northern Gulf of Mexico slope, which was the focus of the majority of the aircraft-based surveys. The relationships of these smaller eddies to the major Loop Current anticyclones are explored.

Drifter paths of Loop Current anticyclones in the western Gulf of Mexico have been analyzed for orbit period, translation and swirl velocities, and orbit ellipse parameters by Kirwan et al. (1984a), Kirwan et al. (1988) and Lewis et al. (1989). They found that the orbits were elliptical, with clockwise rotations of the major axes. Translation speeds were between about 3 and 6 km·day^{-1}. In the first two papers, two different

eddies were examined in 1980-1981 and 1982-1983, respectively. They both moved southwestward across the central Gulf of Mexico before colliding with the Mexican continental slope at about 23°N latitude. This behavior is similar to that of eddy U in the present study. Lewis et al. (1989) analyzed a vigorous eddy that travelled due west along the base of the northern continental slope in 1985. This eddy (eddy B) was also discussed in Hamilton (1990) and its track was about 1° further south than a principal subject of this study, eddy V. When it reached the western continental slope, eddy B formed a cyclone-anticyclone pair (Lewis et al. 1989) which then drifted southward along the slope and generated a complex system of secondary cyclonic features by the summer of 1985 (Vidal et al. 1992). Eddy V, on the other hand, moved northward up onto the slope in the corner region between Galveston and the U.S.-Mexican border. Eddy W also translated westward along the base of the northern slope, similar to the path followed by eddy V. However, it then interacted with a slope cyclone at about 93°W longitude, after which eddy W moved rapidly into deep water to the south-southwest. Eddy Y took a path between that of eddies U and V; it passed further south than eddy V, and took a more westerly path than eddy U. Eddy X was only intermittently detected by the surveys, and therefore little is known about its history. The drifter paths of these eddies are analyzed by using the method of Glenn et al. (1990), where the drifter tracks are least squares fit to a translating ellipse model.

Eddy U was initially a large (~300 km diameter), vigorous Loop Current eddy that formed in the early summer of 1992. In Figure 5.1-1, drifter 02447 made one circuit of the eddy in late August 1992 and then was entrained in a smaller anticyclonic eddy, located to the northwest over the base of the slope at about 92.5°W longitude. This smaller anticyclone, named eddy V, appears to have cleaved from eddy U during August and September 1992. Eastward flow, along the periphery of the still-combined eddies U and V, was observed between 27.5°N and 26.5°N latitude at hydrographic stations over the lower slope in mid-August 1992 (F02SLOPE and GulfCet 02 surveys). A separation (at Station 11, Figure 5.1-1) between eddies U and V was evident in an AXBT transect (F04LEDDY) on October 11, 1992, and was confirmed by a Ship-of-Opportunity Program (SOOP) hydrographic transect about a month later, when eddy U was seeded with drifter 02449. Thus, between August and November 1992, eddy U remained in much the same position at about 91°W longitude (Figure 5.1-1). Eddy U subsequently moved to the southwest as tracked by drifter 02449, eventually merging with eddy T in the western Gulf of Mexico. Eddy T had been shed from the Loop Current about 11 months earlier than eddy U (Biggs et al. 1996).

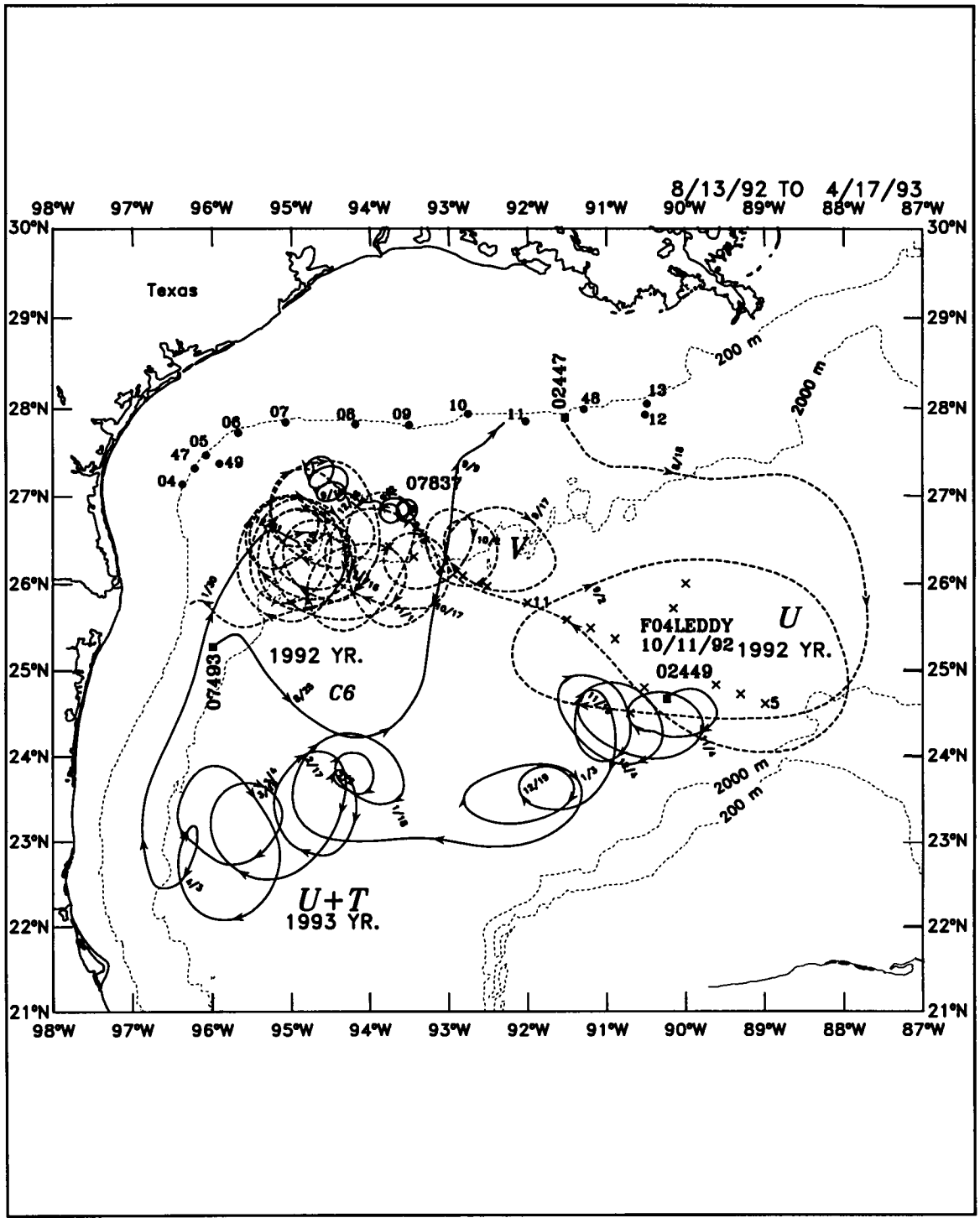

Figure 5.1-1. Smoothed tracks for drifters 02447, 02449, 07493 and 07837. Arrow heads are every five days. Station positions for the F04LEDDY AXBT survey of eddies U and V are indicated with small crosses. LATEX A shelf-break moorings are marked with dots.

During September to November 1992, eddy V moved westward along the base of the slope. At the same time, a cold cyclonic eddy that was observed on the middle to lower slope at about 93.5°W longitude (from hydrographic and AXBT surveys in August 1992) was seeded with drifter 07837 (Figure 5.1-1). This cyclone moved to the west preceding the advance of eddy V. There was also a large cold cyclone centered about 25°N latitude, 94.5°W longitude. It is indicated by the track of drifter 07493 (Figure 5.1-1), which skirted its periphery before moving northward over the slope under the influence of eddy V's swirl currents. This cyclone, also observed in the October 1992 altimetry, is probably responsible for the fairly rapid westward translation of both eddy V and the small slope cyclone (drifter 07837). Eddy V was surveyed a number of times between mid-November 1992 and May 1993, after its arrival at the base of the slope (2000 m isobath) in the northwestern corner of the Gulf of Mexico at about 95°W longitude. In the latter half of December 1992, eddy V made an abrupt excursion northward onto the lower slope. Between February and April 1993, the eddy remained in the northwest corner, strongly affecting currents along the shelf break. During May 1993, drifter 06938 left the shelf near 94°W longitude and became entrained in eddy V (Figure 5.1-2). Its track shows that eddy V was over the middle of the slope and was drifting westward towards 96°W longitude. The long-lived nature (November 1992 to June 1993) of the eddy circulation in the northwest corner of the Gulf of Mexico slope region is confirmed by satellite altimetry (Biggs et al. 1996).

Eddy W was shed from the Loop Current in June 1993. Satellite AVHRR Imagery indicate that, within a month, the initially large eddy split into two eddies (Walker et al. 1993), and drifter 02448 (Figure 5.1-2) remained with the northern portion (eddy W_N). Drifter 02448 revealed that this part of the eddy moved westward along the base of the slope to about 92°W longitude. At this point, at the beginning of August 1993, the eddy and the surrounding slope were surveyed with AXBTs. The survey showed a relatively small, elongated eddy with drifter orbits similar in size to those of eddy V, but with much less vigorous swirl velocities (compare Figures 5.1-1 and 5.1-2). The AXBT survey showed the anticyclone interacting with a cyclonic cold eddy (C1) on the lower slope at about 93°W longitude. Drifter 06938 made counterclockwise (cyclonic) circuits of this cold eddy between mid-June and mid-August 1993 (Figure 5.1-2). The AXBT survey suggests that the interaction caused the deeper sections of eddy W_N to be forced up onto the middle slope. Immediately after the interaction, eddy W_N moved rapidly away from the slope in a south-southwest direction. This is a completely different track from that of eddy V, which remained close to the northern

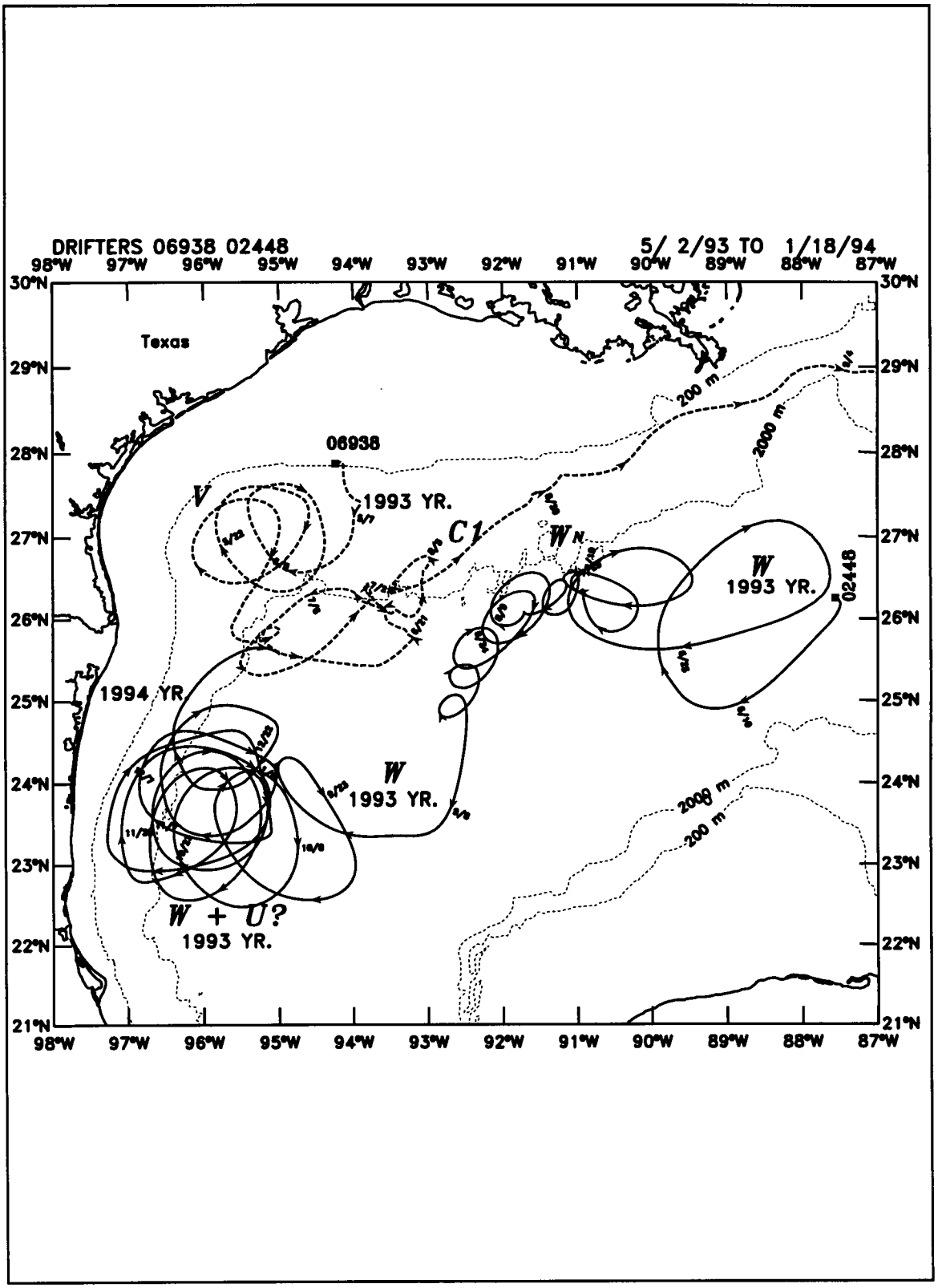

Figure 5.1-2. Smoothed tracks for drifters 02448 and 06938. Arrow heads are every five days.

slope in its journey across the Gulf of Mexico (compare Figures 5.1-1 and 5.1-2). Drifter 02448 was later entrained in a large anticyclone that was adjacent to the slope at about 23.5°N latitude. This circulation was probably the southern part of the original eddy W, which could have moved fairly rapidly westward while the northern portion (W_N) remained stalled on the lower northern slope. The TOPEX/ERS-1 altimetry maps indicate that eddy U probably dissipated earlier in the summer of 1993 in the southwestern Gulf of Mexico. Therefore, it appears that drifter 02448 (Figure 5.1-2) was re-entrained into eddy W at about 23.5°N latitude, 94°W longitude, in September 1993 and tracked its interaction with the Mexican slope until January 1994. Throughout this five-month period, eddy W moved slowly north-ward along the base of the Mexican slope with little evidence of any decrease in size or vigor of its circulation.

Eddy X was shed from the Loop Current in the fall of 1993. Unfortunately, it was, not successfully seeded with a drifter and thus the details of its life history are rather limited.

Eddy Y detached from the Loop Current during the summer of 1994. It was seeded with two drifters, 12376 and 12377, in September 1994, and was surveyed once in October and twice in November of that same year. The eddy was of moderate size and was tracked as it moved west-southwestward, seaward of the 2000 m isobath, until it reached about 94°W longitude in February 1995 (Figure 5.1-3). At this point, the drifters moved out of the eddy and indicate interactions with a large slope cyclone (C2) to the north, and an anticyclone (probably the remnants of eddy X) to the west, against the Mexican slope (Figure 5.1-3). Because two drifters were simultaneously tracking eddy Y for about four months, they provide an opportunity to compare the results of the ellipse model for the two tracks and thus, the representativeness of the analysis when performed using a path from a single drifter. The LATEX field program ended in December 1994 and therefore only the early stage of eddy Y's life history was surveyed. However, the October and November 1994 surveys showed specific interactions with cyclones on eddy Y's northern and western peripheries, respectively. The late-November 1994 surveys provide a clear example that the clockwise circulation of Loop Current eddies can be effective in moving deep-water cyclones northward onto the Louisiana-Texas slope.

5.2 Eddy V Analysis

The diverging ellipse model was applied to the track of drifter 02447 (drogued at 6 m) after it exited eddy U and was entrained into eddy V on September 15, 1992, and until it left

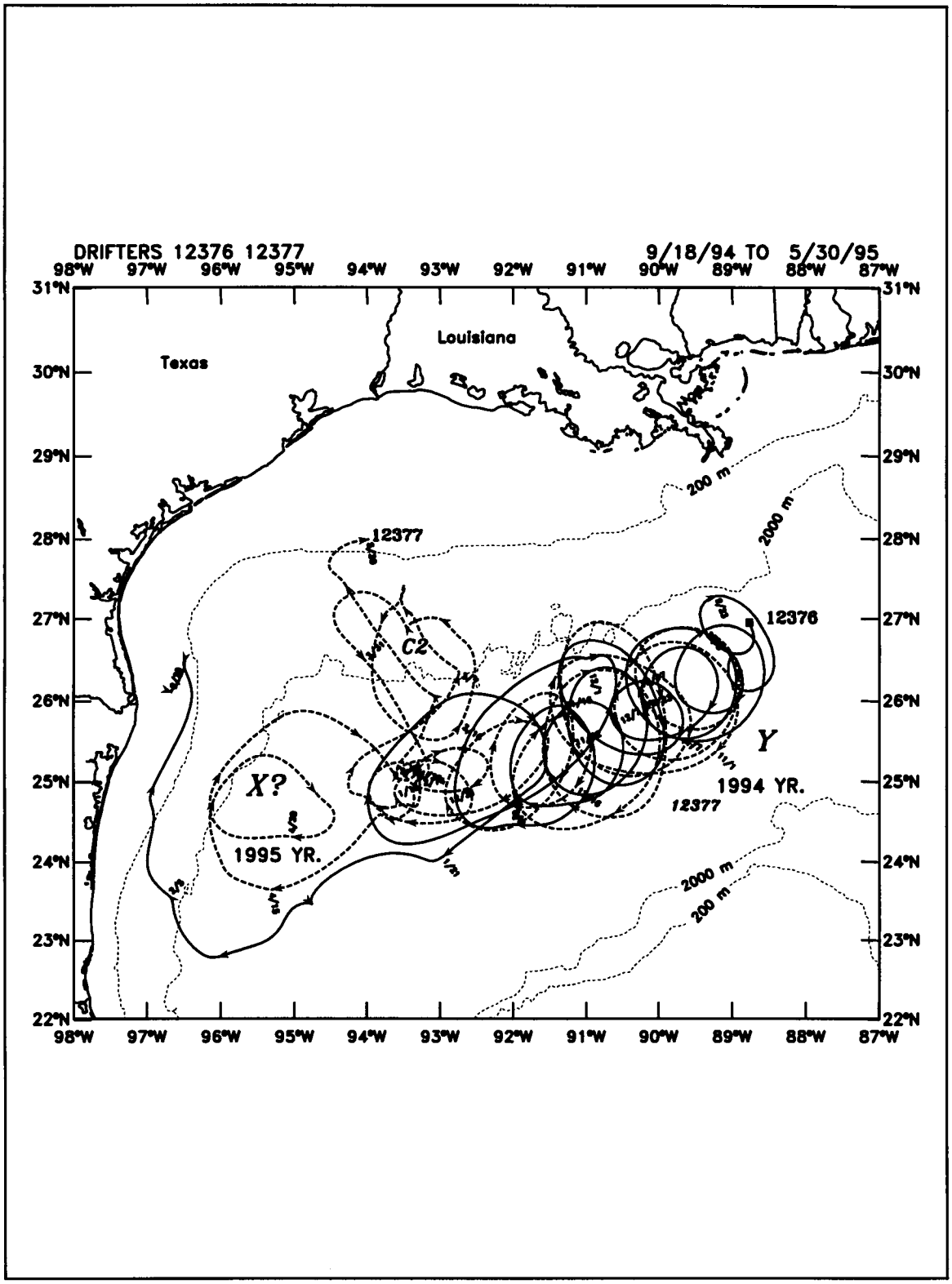

Figure 5.1-3. Smoothed tracks for drifters 12376 (solid) and 12377 (dashed). Arrow heads are every five days.

eddy V on about January 26, 1993 (Figure 5.1-1). The analysis continued with drifter 02451 (drogued at 50 m) until the beginning of February 1993. The resulting tracks of the ellipse centers (x_o, y_o) are given in Figure 5.2-1. There is a six-day overlap in January 1993 between the two tracks. The separation of the near-surface and 50 m centers over this six-day overlap period will be discussed in more detail when the ellipse model fits are combined with the January 1993 AXBT surveys and moored current meter records. Time series plots of the ellipse parameters are given in Figure 5.2-2. They include the mean swirl velocity ($r\omega$), where 'r' is the geometric mean radius $(ab)^{\frac{1}{2}}$, and the angular momentum ($ab\omega$), assuming the divergence (D) can be neglected (Glenn et al. 1990).

Eddy V initially moved fairly rapidly westward, following the trend of the 2000 m isobath, between September 20 and November 10, 1992 (see Figure 5.2-1). This westward translation may have been assisted by the westward flows of the northern part of the cyclone (C6), revealed by the track of drifter 07493 (Figure 5.1-1). The altimetry maps for October 1992 through January 1993 suggest that this cyclone was squeezed between eddy V and the remnants of eddy T, which were against the Mexican slope around 24°N to 25°N latitude. Part of the cyclone split off and moved onto the slope east of eddy V. The F07SLOPE survey on January 21, 1993 indicates that a weak cyclonic feature was located on the slope at about 93.5°W longitude. This helps to confirm the fate of the cyclone as suggested by the altimetry. Eddy V had two excursions shoreward of the 2000 m isobath, and two seaward in the September to November period. Through most of November and December 1992 the eddy was stalled around 95°W longitude at the base of the slope. Towards the end of December 1992 there was an abrupt movement northward onto the slope, whereupon it drifted slowly eastward, eventually returning to the 2000 m isobath around January 15, 1993. Until the end of drifter 02451 data in eddy V at the beginning of February 1993, the eddy again drifted westward with its center returning to a position similar to that occupied previously, at the beginning of its northward excursion, in the middle of December 1992. Maps of sea-level anomalies derived from satellite altimetry indicate that eddy V interacted with eddy U at the end of January 1993 when eddy U (Figure 5.1-1) was approaching 95°W longitude at about 23.5°N latitude (Jochens et al. 1996).

In the first westward translation phase of the track, prior to November 10, 1992, the ellipse parameters underwent some notable changes. During the eddy's first deep water excursion around 93.5°W longitude, at the beginning of October 1992, the period increased from 6.5 to 8 days and then decreased again, and 'a', 'b' and 'r' increased along with the mean swirl velo-

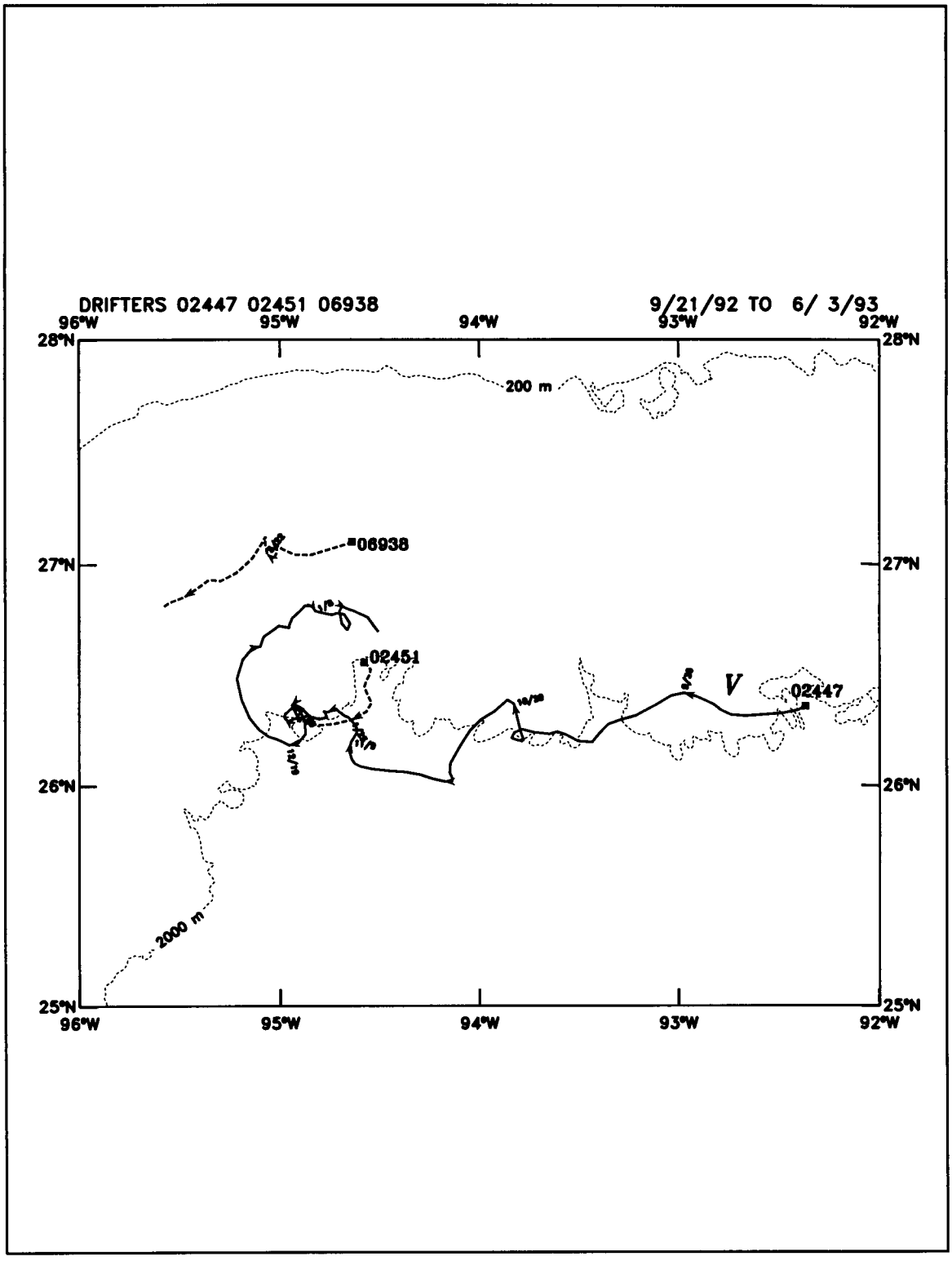

Figure 5.2-1. Tracks of eddy center positions from ellipse-model fits to the paths of drifters 02447 (solid), 02451 (short-dashed) and 06938 (long-dashed). Arrow heads are every 10 days.

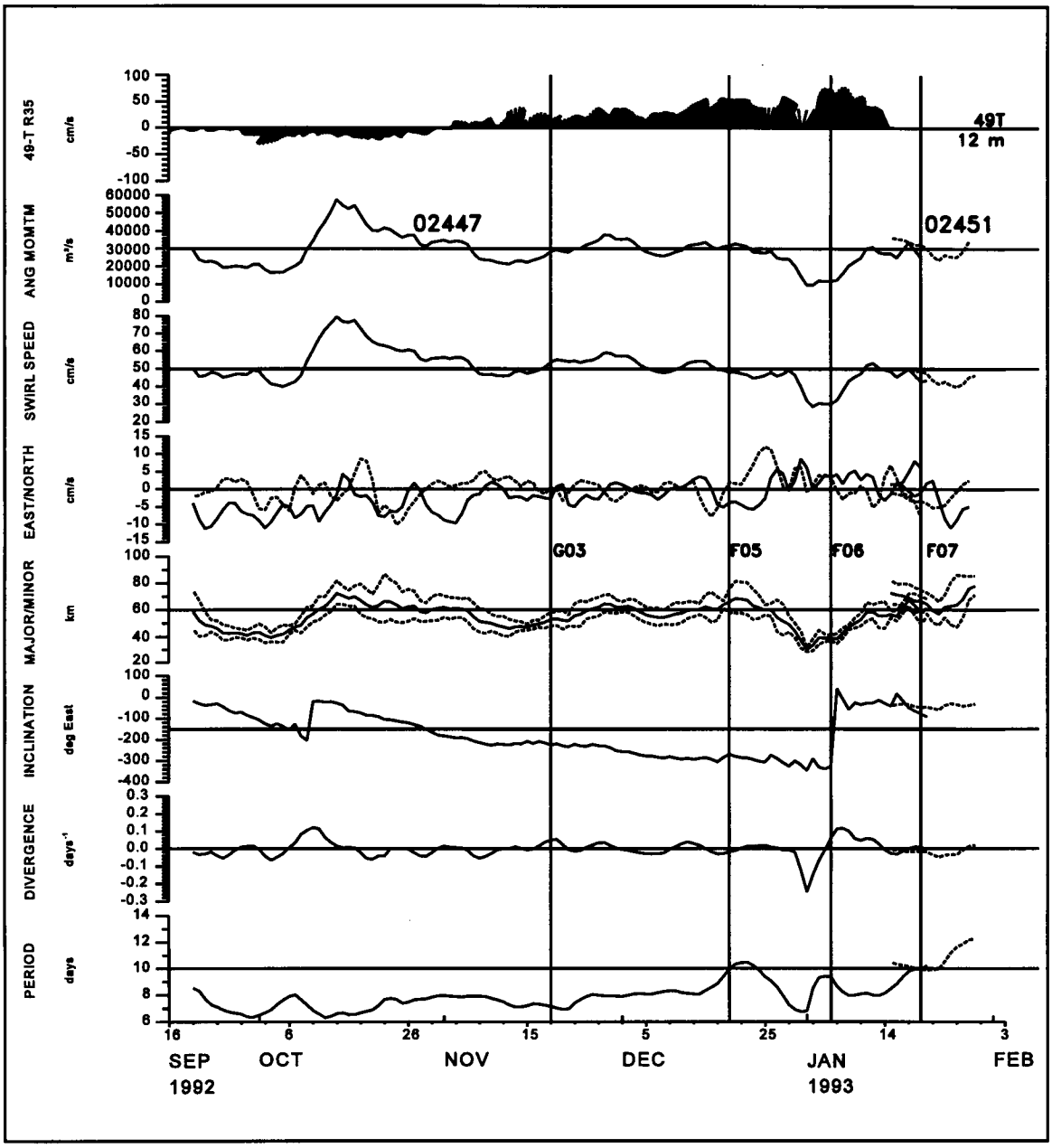

Figure 5.2-2. Time series of ellipse parameters from model fits to the paths of drifters 02447 (solid) and 02451 (dashed) for the period from September 16, 1992 to February 3, 1993. Top panel shows the rotated 40-HLP sticks from the 12-m level of mooring 49. Up is the along-isobath direction towards the east. The fifth panel shows semi-major and minor axes (dashed) and mean radii (solid). Vertical lines mark the start of the GulfCet 03, F05LEDDY, F06SPECIAL and F07SLOPE surveys.

city to about 75 $cm \cdot s^{-1}$ on October 14, 1992 (Figure 5.2-2). There are indications from satellite altimetry that these increases may have resulted from an interaction with eddy U, which was centered about 350 km to the southeast (Figure 5.1-1). There followed a slow decrease of the mean radius and swirl velocity until the next shoreward excursion, when these parameters remained fairly steady until the end of October 1992. The increase in radius and swirl speed was in accordance with the eddy being in approximately solid-body rotation and the drifter moving further out from the center.

During this phase, the major axis of the ellipse rotated at a fairly steady rate (mean of $8° \cdot day^{-1}$). The sharp jump in the inclination on October 10, 1992 (Figure 5.2-2) was caused when 'a' and 'b' switched. The code always assigns 'a' to the larger axis and makes adjustments to the inclination and phase if an axis switch occurs between time steps. Fast axis rotation rates correspond to the short orbital periods and high translation speeds as noted by Glenn et al. (1990) for ring 82-E in the northwest Atlantic. Cushman-Roisin et al. (1985) indicate that about $9° \cdot day^{-1}$ is typical for warm rings. The rotation rate and its slowing after the eddy stalled is illustrated by plots of the major axis on the eddy track (Figure 5.2-3).

While eddy V was stalled at the base of the slope during November and December 1992, the rotational period, mean radius, and swirl velocity remained fairly steady at 7-8 days, 60 km, and 50-55 $cm \cdot s^{-1}$, respectively. During this period, two snapshots were available from hydrographic surveys which were centered on November 19 and December 19, 1992, respectively. Figure 5.2-4 shows the daily averaged drifter velocities, the ellipse axes from the model, and daily averaged currents from the moored instruments. The drifter track is approximately the same as the 200 m depth contour for the 20°C surface. Eddy currents were clearly affecting the flow at the shelf break, though they were outside the area where the ring was in near solid-body rotation. For Loop Current eddies, a good measure of the position of maximum velocity is where the 20°C isotherm crosses 125 m depth.

A month later (Figure 5.2-5), the eddy was in nearly the same position, but the radius had increased and the drifter had moved out over the 175 m contour of the 20°C surface. Interestingly, the swirl velocities were about the same as in Figure 5.2-4, even though the radius had grown. Current velocities had also increased at the near-surface current meter (12 m depth) on mooring 49, over the 500 m isobath. Time series of 40-HLP sticks from the 12 m level of mooring 49 are included in Figure 5.2-2. Eddy V began to influence

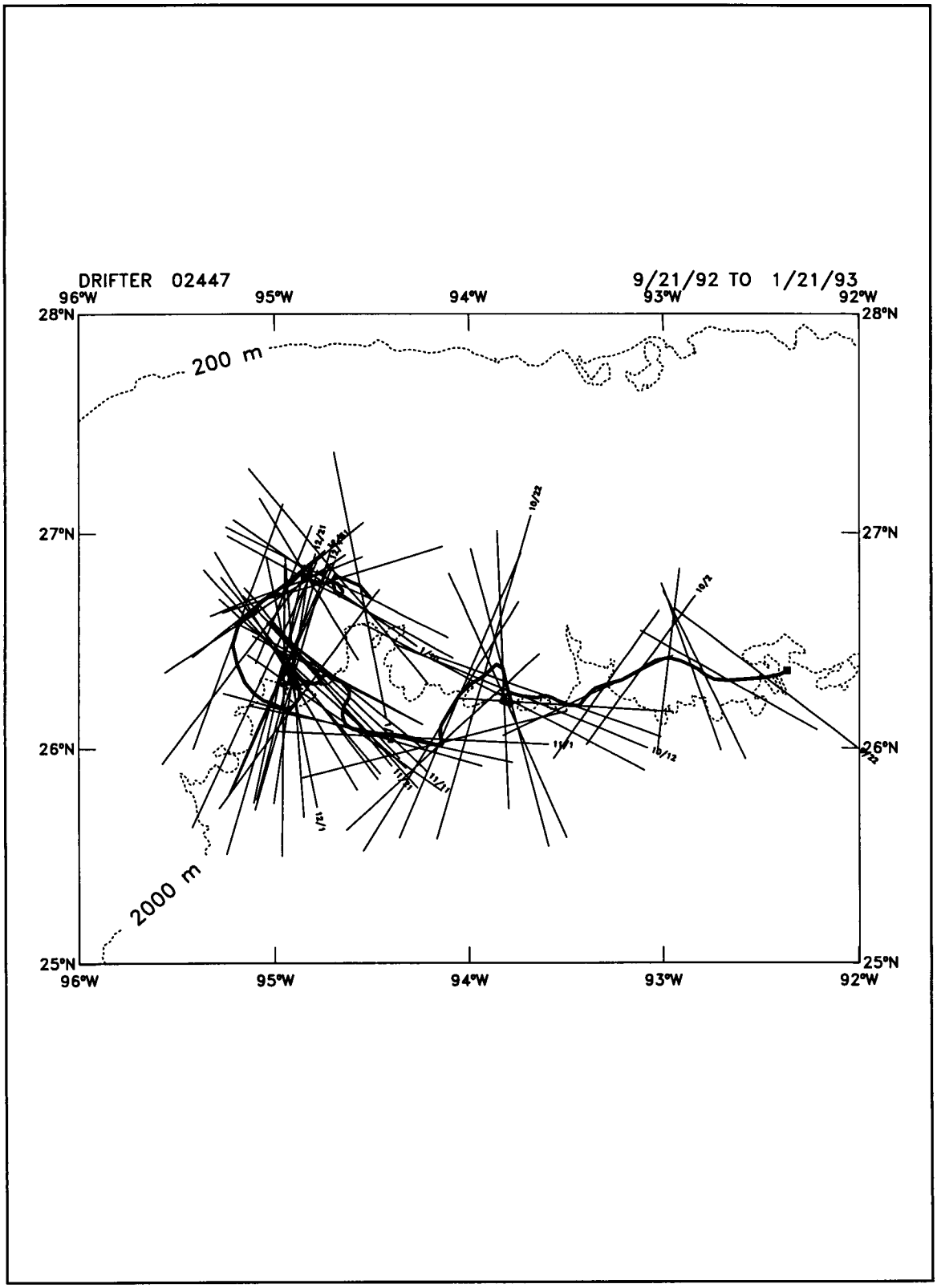

Figure 5.2-3. Major axes every two days from ellipses fit to the path of drifter 02447.

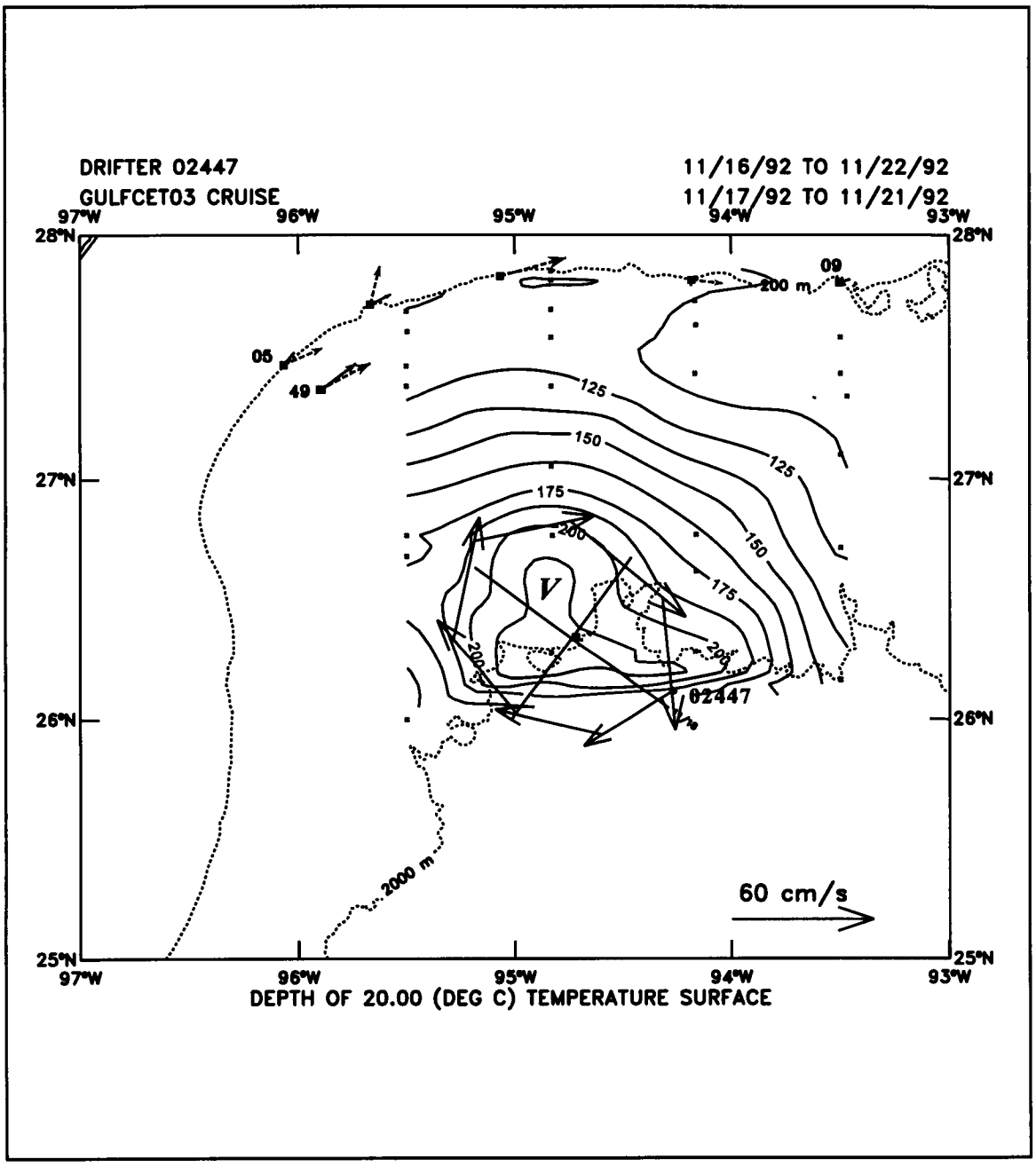

Figure 5.2-4. Depth of the 20°C temperature surface from the GulfCet 03 survey. Daily velocity vectors from drifter 02447 are overlaid beginning November 16, 1992. Dashed and solid arrows emanating from squares represent the 12-m and 100-m daily mean 40-HLP currents, respectively, from the LATEX A shelf-break moorings for November 19, 1992. Ellipse axes are given for this same date and the solid square in the eddy marks the ellipse center 24 hours earlier.

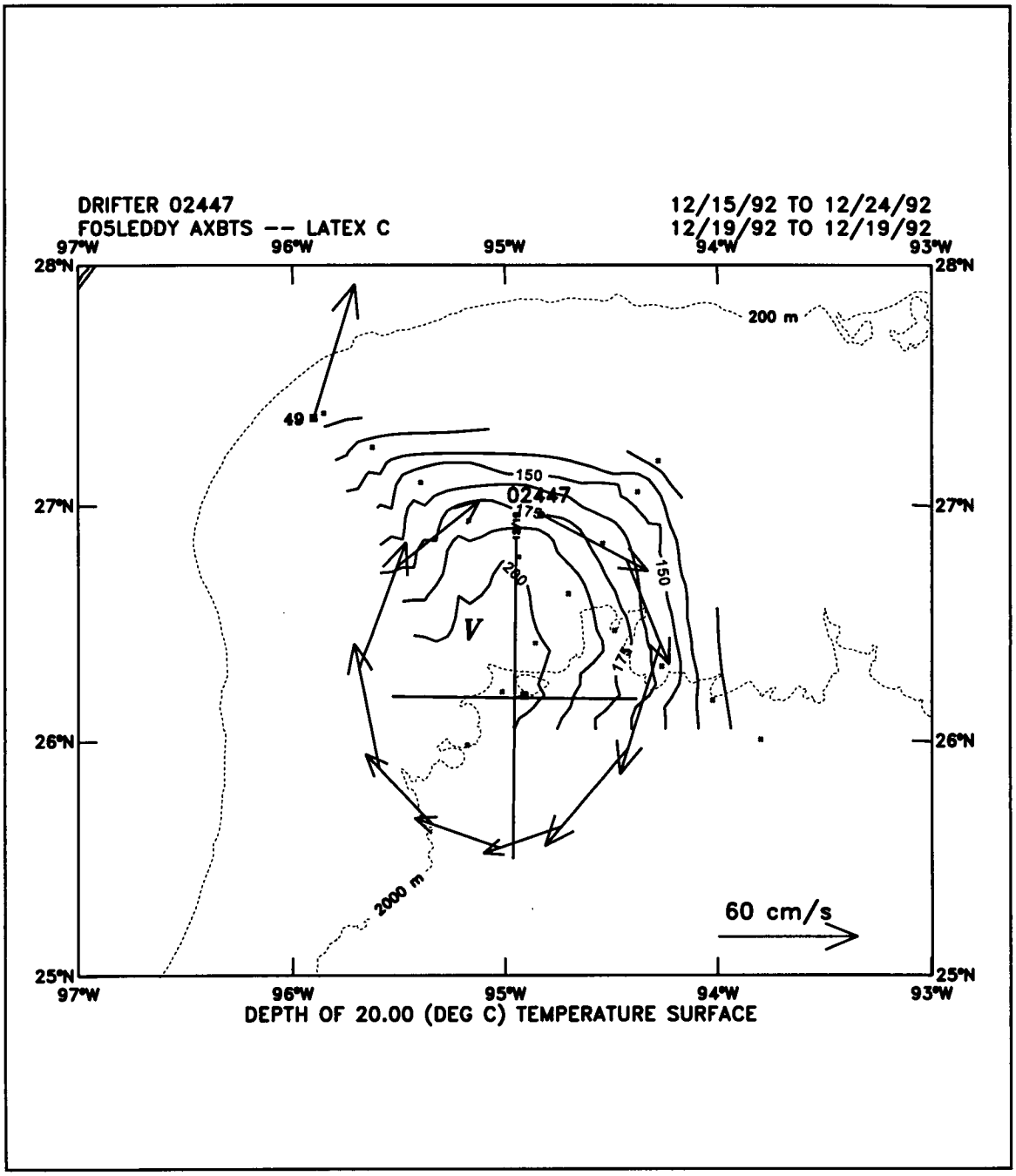

Figure 5.2-5. Depth of the 20°C temperature surface from the F05LEDDY survey. Daily velocity vectors from LATEX drifter 02447 are overlaid beginning December 15, 1992. The daily mean 40-HLP current vector from the 12-m level of LATEX A mooring 49, and the ellipse axes are given for December 19, 1992. The solid square in the eddy marks the ellipse center 24 hours earlier.

currents at this position as early as the beginning of November 1992. The hydrography indicates that on December 19, 1992 the ring was of similar size to that of November 19. The increase in the rotational period began on about December 16, 1992, reaching about 10.5 days on December 20-21, and rapidly decreased to seven days at the beginning of January 1993, as the eddy moved northward over the slope. There was also a corresponding contraction of 'a', 'b' and 'r', and a decrease in swirl speed as the eddy moved northward between about December 25, 1992 and January 1, 1993 (Figure 5.2-2). Thus, the drifter track experienced a weak divergence followed by a strong convergence in moving into shallower water. This convulsion also affected the currents at the 12 m level of mooring 49, where there was an anticyclonic rotation of the current vectors (Figure 5.2-2). This is even more marked at the 100 m level for this same mooring (not shown).

The eddy recovered rapidly and by the time of the next survey on January 5, 1993 (Figure 5.2-6), the rotational period was about eight days and the drifter was again approximately following the 200 m contour of the 20°C surface. Surface-layer velocities from AXCPs (Figure 5.2-6a) agreed well with the drifter and the daily averaged current vector at the 12 m level of mooring 49. The AXCP vectors were also parallel to the isotherm contours and agreed in magnitude with the eddy being in solid-body rotation. The eddy was roughly circular, with high surface velocities over the 500 m isobath. The situation was similar for the 200-325 m AXCP averaged velocities and the 15°C surface (Figure 5.2-6b), except that the center, as indicated by the isotherm depths, appeared to be displaced eastward of the center determined from the surface drifter track. This was also the case for the 8°C surface (Figure 5.2-6c). The deep AXCP currents were weak and eastward along 95°W longitude.

The suggestion that the deeper center of the eddy was displaced from the near-surface center is born out for the period around January 20, 1993, when there were three drifters in the eddy (Figure 5.2-7). Two drifters, drogued at 50 m (02451 and 07835), followed parallel tracks, and the analysis of one of these (drifter 02451) placed the center on the 2000 m isobath. The analysis of the near-surface drogued drifter (02447) for January 20, 1993 places the center about 30 km north with similar-size axes, but rotated clockwise by 30° relative to the axes for drifter 02451. The separation of the 50 m and surface centers between January 15 and 21, 1993 is clearly indicated in Figure 5.2-1. The other parameters in Figure 5.2-2 agree fairly well between the two drifters during the overlap period. The rotational period was about 10 days and increased to 12 days by the end of January 1993. There was no

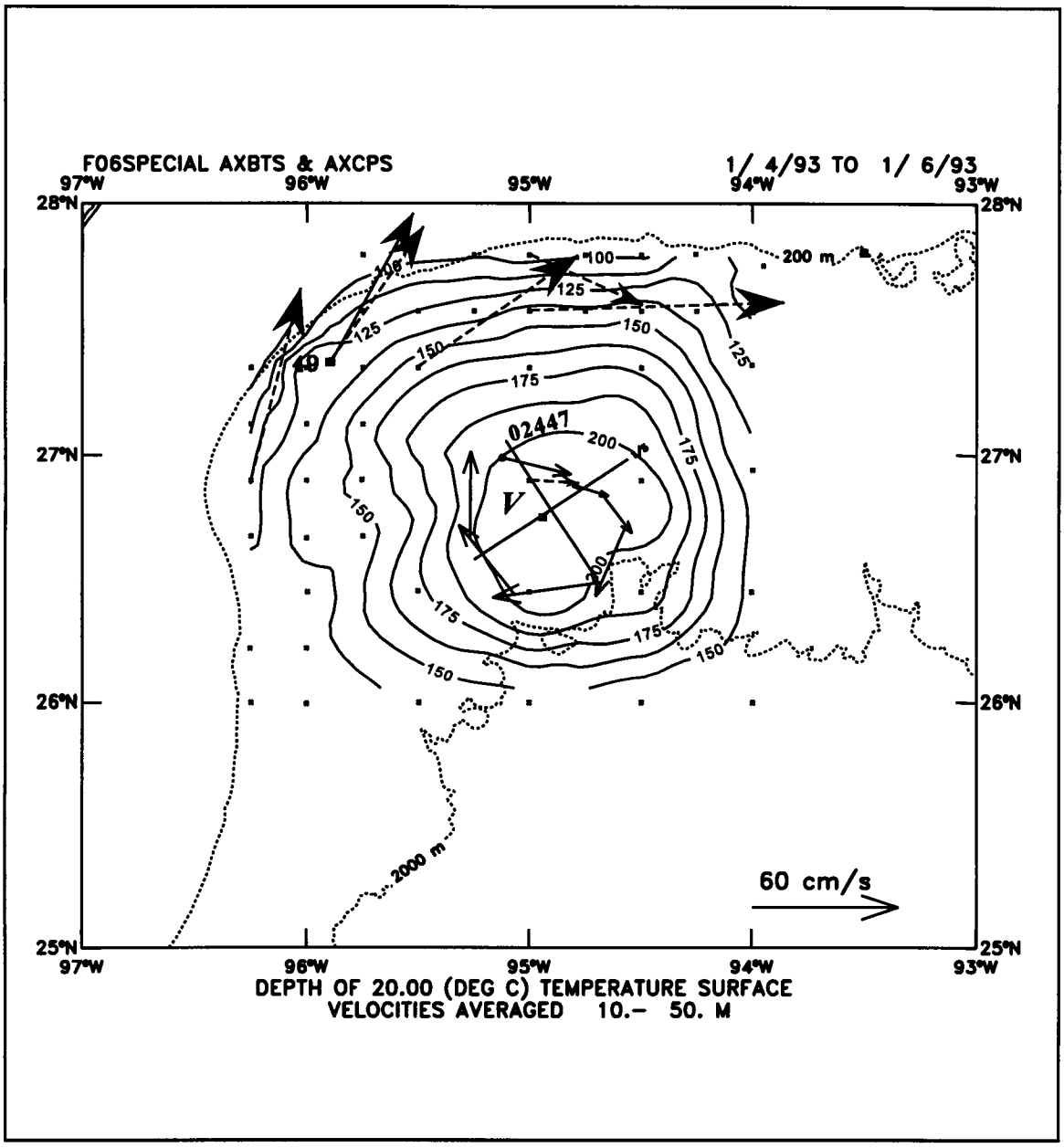

Figure 5.2-6a. Depth of the 20°C temperature surface from the F06SPECIAL survey. Daily velocity vectors from drifter 02447 are overlaid beginning January 1, 1993. Dashed arrows emanating from crosses are 0-50 m averaged-smoothed velocities from AXCP profiles. Dashed and solid arrows emanating from the square labeled 49 represent the 12-m and 100-m daily mean 40-HLP currents, respectively, from LATEX A shelf-break mooring 49 for January 5, 1993. The ellipse axes are given for this same date and the solid square in the eddy marks the ellipse center 24 hours earlier.

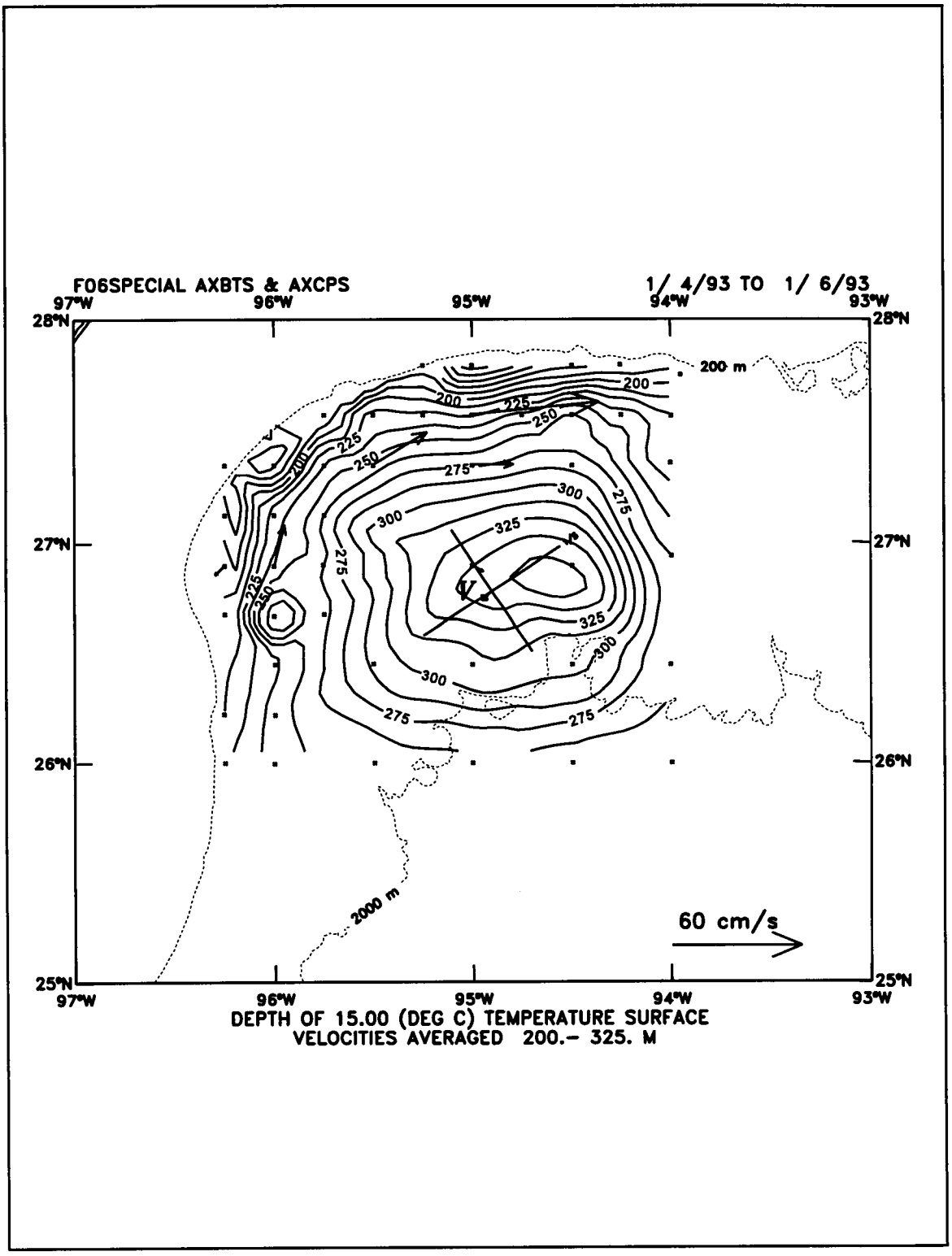

Figure 5.2-6b. Depth of the 15°C temperature surface from the F06SPECIAL survey. Dark arrows emanating from crosses are 200-325 m averaged-smoothed velocities from AXCP profiles.

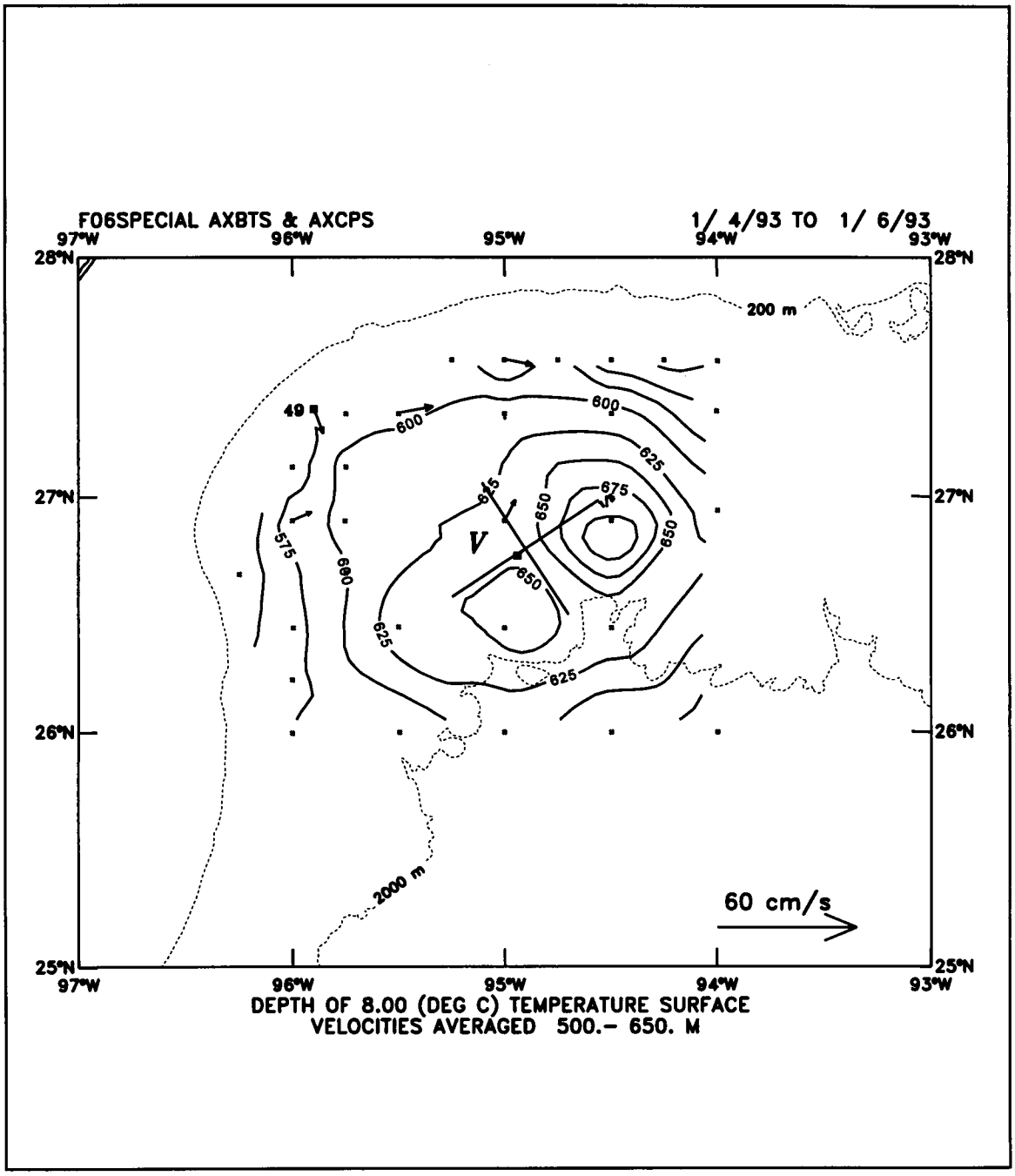

Figure 5.2-6c. Depth of the 8°C temperature surface from the F06SPECIAL survey. Dark arrows emanating from crosses are 550-650 m averaged-smoothed velocities from AXCP profiles. The dark arrow emanating from the square labeled 49 represents the 495 m daily mean 40-HLP current vector from LATEX A shelf-break mooring 49 for January 5, 1993.

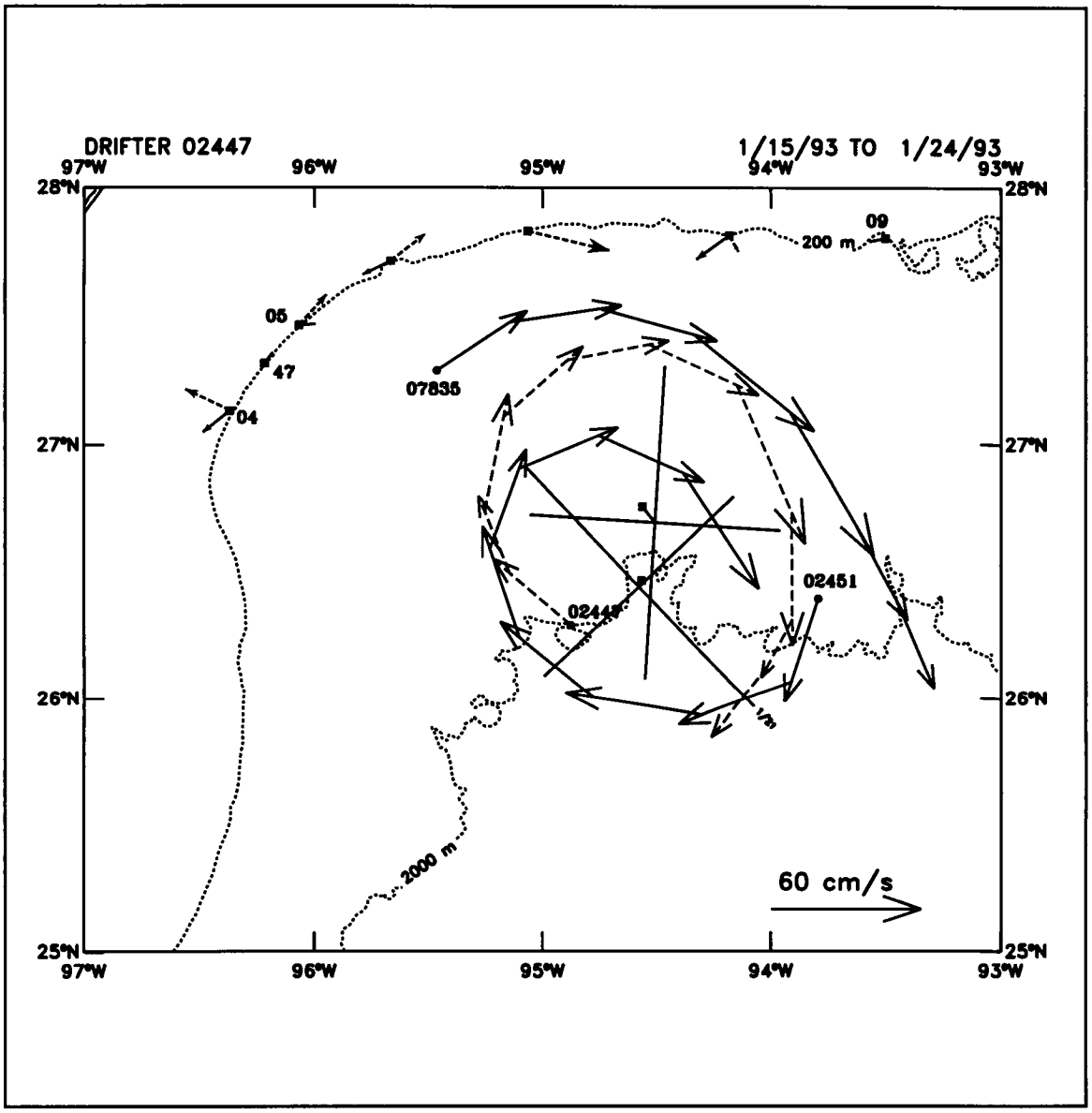

Figure 5.2-7. Daily velocity vectors from drifter 07835 (beginning January 14, 1993) and drifters 02451 and 02447 (beginning January 15, 1993). Dashed and solid arrows emanating from squares represent the 12-m and 100-m daily mean 40-HLP currents, respectively, from the LATEX A shelf-break moorings for January 25, 1993. The ellipse axes are given for January 21, 1993 and the solid squares in the eddy mark the ellipse centers 24 hours earlier. Dashed arrows represent near-surface velocities (drifter 02447 and the 12-m level of the moorings), and the solid arrows represent drifters 02451 and 07835, or the 100-m current meter velocities, respectively.

indication from the 15°C and 8°C surfaces from the surveys in November and December 1992 that, prior to the northward movement onto the slope, there was any displacement of the eddy center with depth. It is noteworthy that eddy currents were strongly felt at the 12 m level of mooring 07, at the shelf break at 95°W longitude, and that there was a suggestion of entrainment into the eddy at the 100 m level at the shelf break to the east of 95°W longitude (moorings 08 and 09, Figure 5.2-7).

The path of the eddy center derived from drifter 02451 indicates a slow westward movement along the 2000 m isobath for the latter part of January 1993. Examination of near-surface current stick plots for January and February 1993 (Figure 5.2-8a) indicates that anticyclonic eddy currents were first felt at the 12 m level of mooring 04 on February 9. The eddy event propagated clockwise around the shelf break to mooring 07 by about February 16. There was a hydrographic survey (GulfCet 04, Figure 5.2-9) between February 20 and 24 that showed the eddy center to be close to 95°W longitude and perhaps a little north of the 2000 m isobath. The eddy was elongated in the north-south direction and therefore strong currents were observed at moorings 06 and 07, but nowhere else along the shelf break. The southwestward and onshore flows at moorings 04, 47 and 05 suggest that a small cyclone may have been situated between eddy V and the shelf break to the northwest. Similar small cyclones on the periphery of on-slope eddies were surveyed in more detail in 1994 (Section 5.7). This survey confirmed that the eddy center remained in the vicinity of 95°W longitude and the 2000 m isobath at least until the end of February 1993.

The current meter records in early March 1993 (Figure 5.2-8a) show a similar sequence of events to that of February. Again there was a clockwise propagation of anticyclonic flows from the 12 m levels of moorings 04 to 08. The events showed slightly weaker maximum currents than in February 1993, but they lasted longer. There was a slow decrease in current magnitudes, lasting through most of March 1993, at all of the moorings except the 12 m level of mooring 08. Drifter 07835 exited eddy V on January 21, 1993 (Figure 5.2-7). It then moved into the southwestern Gulf of Mexico, reaching 21.5°N latitude, before returning to the northwest corner by rapidly transiting northward along the Mexican continental slope during March 1993. Figure 5.2-10 shows the velocity vectors from the drifter and daily averaged current vectors from the moorings for March 26, 1993. The center was at about 26°N latitude, 95°W longitude, a little further south than during the February 20-24, 1993 survey of Figure 5.2-9. Consequently, the flows at the shelf break were weakly anticyclonic

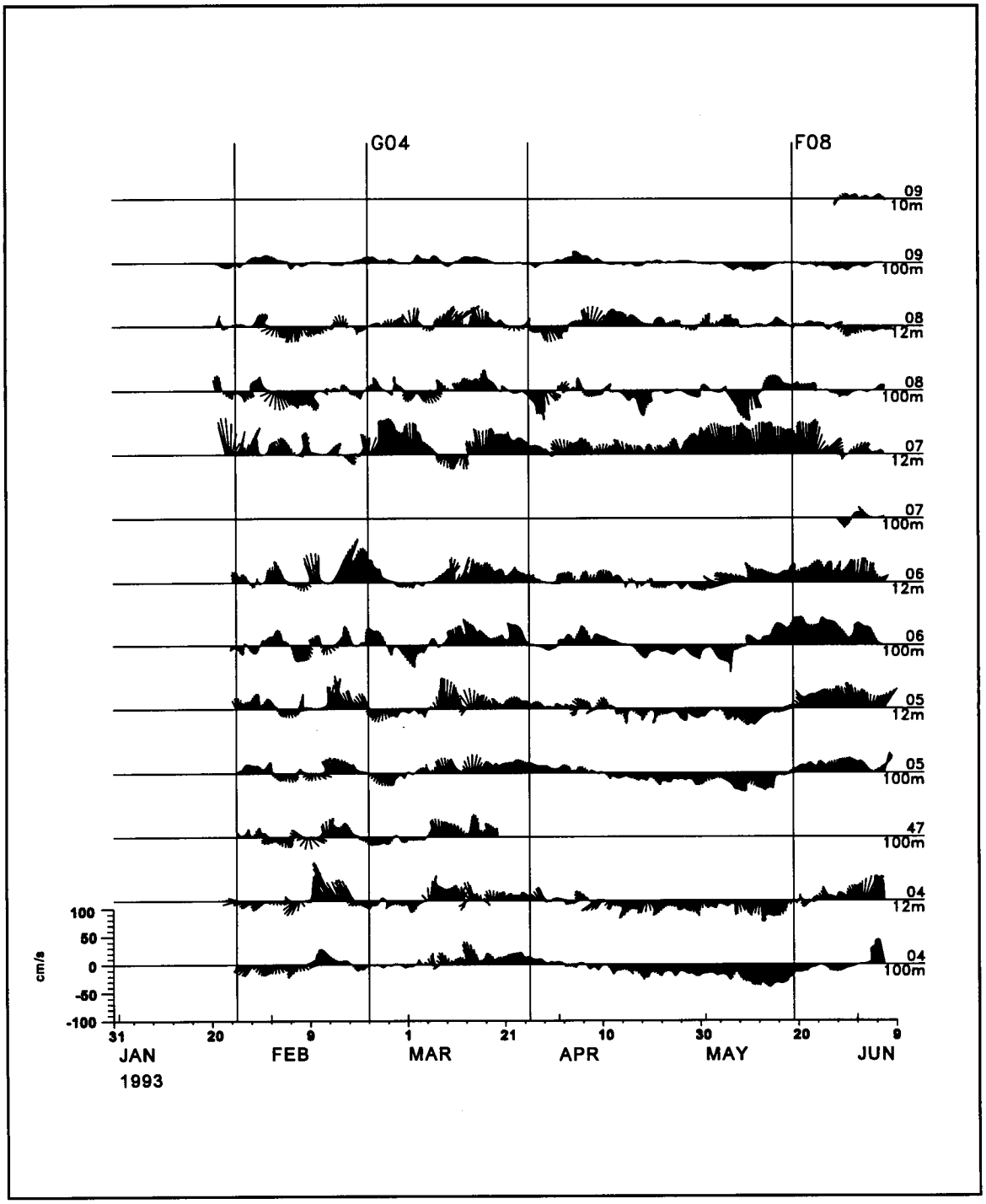

Figure 5.2-8a. Stick plots of rotated 40-HLP currents from the 12-m and 100-m levels of the LATEX A shelf-break moorings for the period from January 1 to June 9, 1993. Up is the along-isobath direction towards the east. Vertical lines mark the start of the period in Figure 5.2-7, the GulfCet 04 survey, the period in Figure 5.2-10 and the F08SLOPE survey.

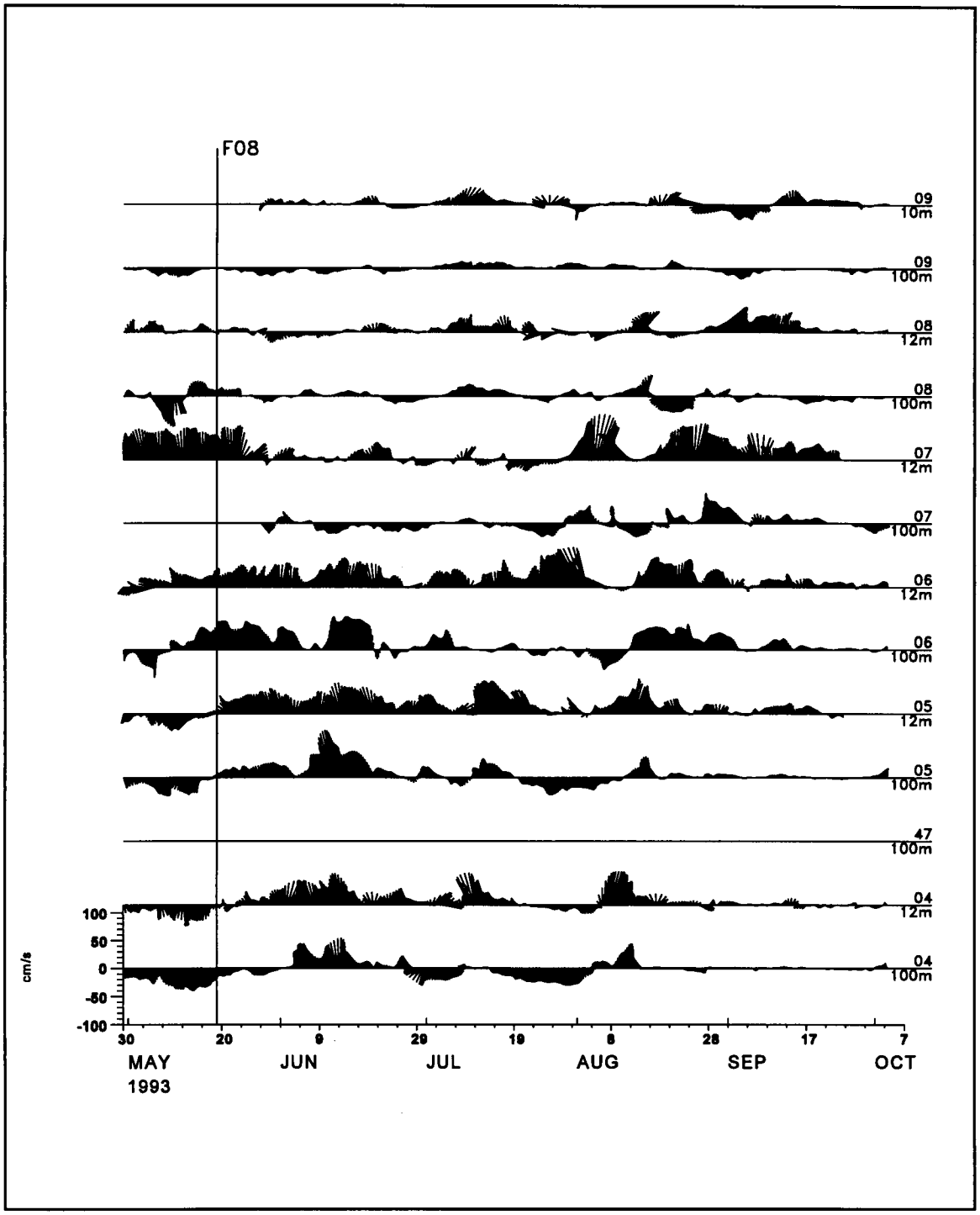

Figure 5.2-8b. Stick plots of rotated 40-HLP currents from the 12-m and 100-m levels of the LATEX A shelf-break moorings for the period from April 30 to October 7, 1993. Up is the along-isobath direction towards the east. A vertical line marks the start of the F08SLOPE survey.

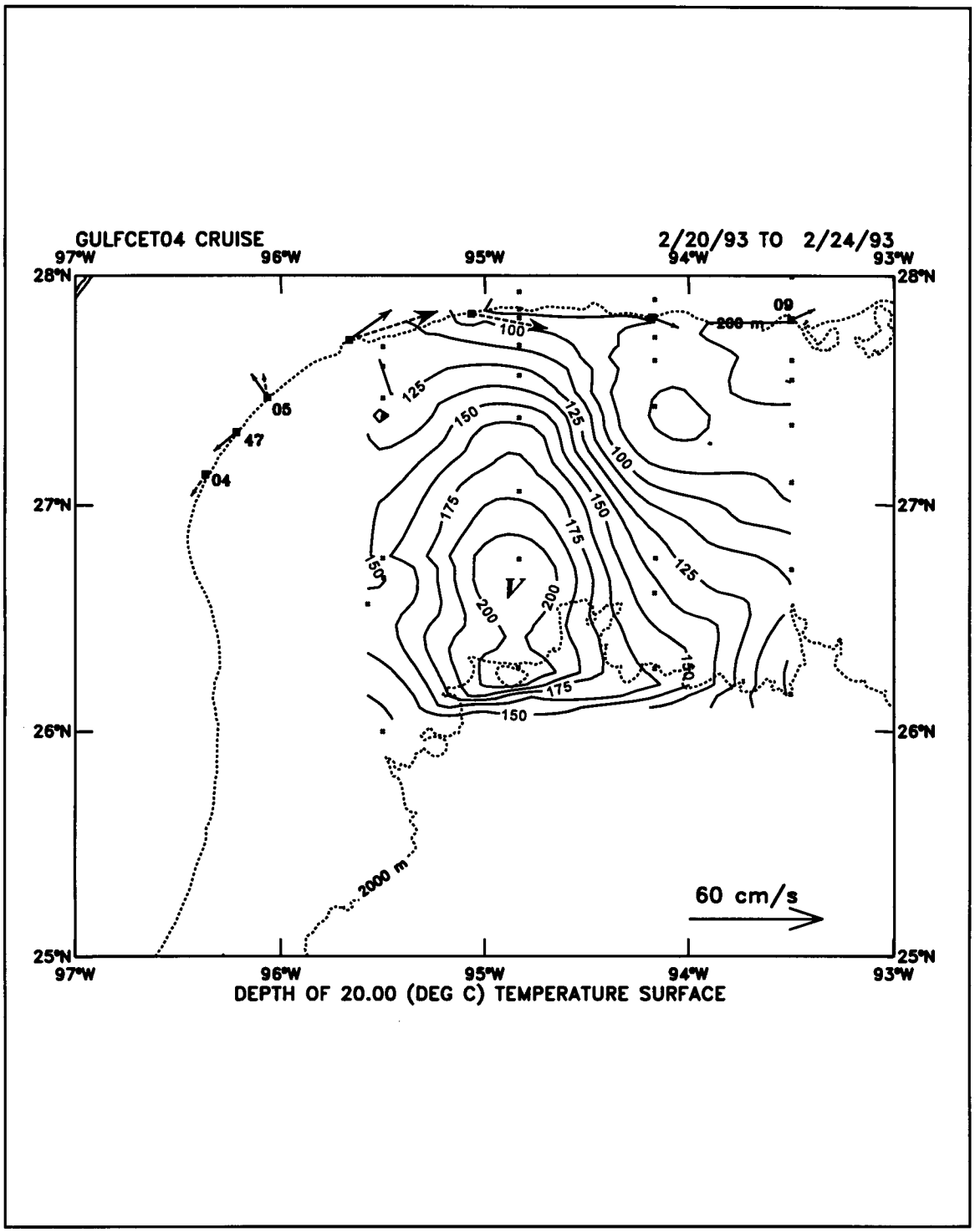

Figure 5.2-9. Depth of the 20°C temperature surface from the GulfCet 04 survey. Dashed and solid arrows emanating from squares represent the 12-m and 100-m daily mean 40-HLP currents, respectively, from the LATEX A shelf-break moorings for February 21, 1993.

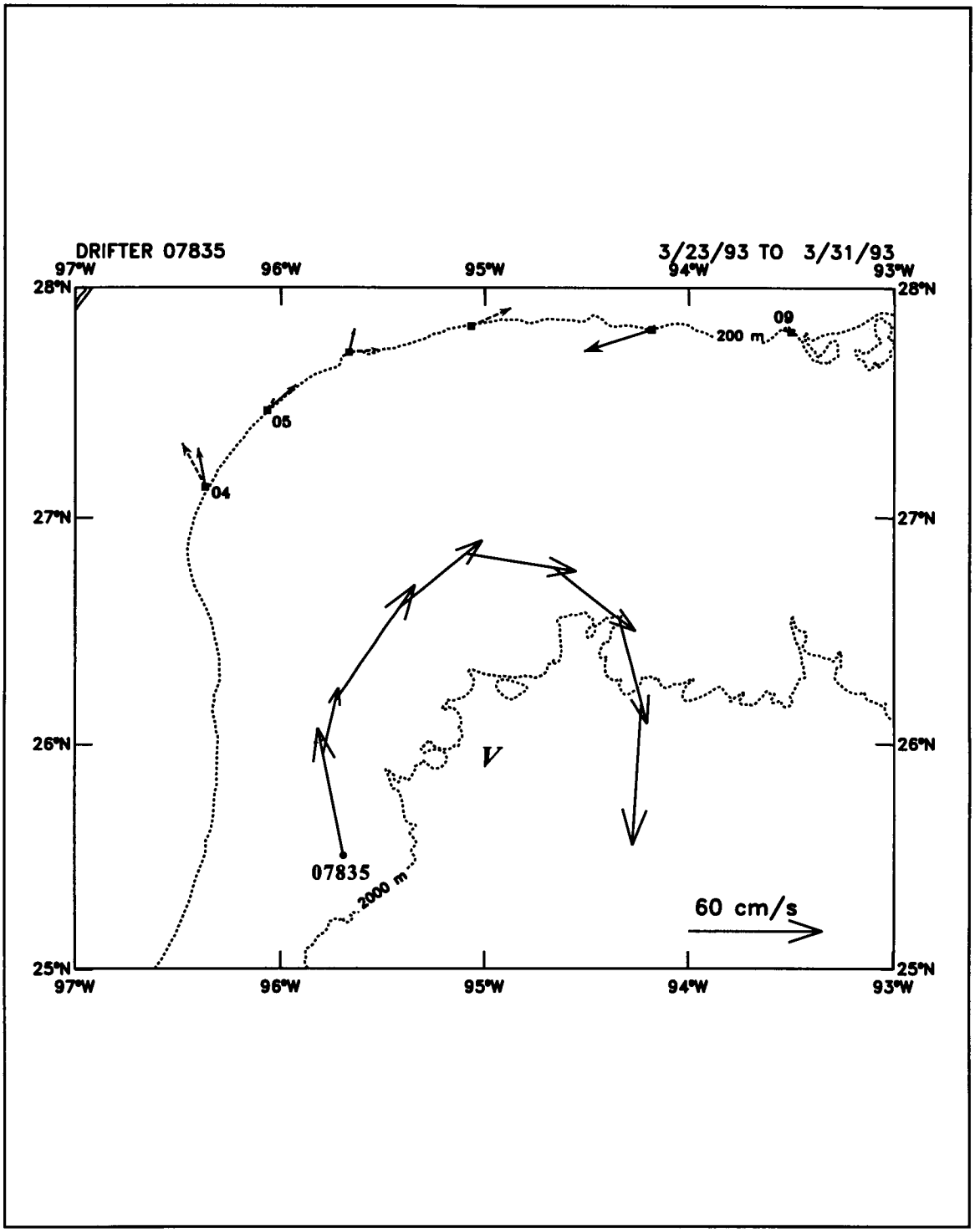

Figure 5.2-10. Daily velocity vectors from drifter 07835 beginning March 23, 1993. Dashed and solid arrows emanating from squares represent the 12-m and 100-m daily mean 40-HLP currents, respectively, from the LATEX A shelf-break moorings for March 26, 1993.

(10-20 $cm \cdot s^{-1}$) at the moorings west of the 95°W longitude meridian. Daily averaged currents from the drifter, however, had a maximum of 65 $cm \cdot s^{-1}$, very similar to the drifter eddy currents observed in January 1993 (Figure 5.2-7).

Eastward flows on the order of 20 $cm \cdot s^{-1}$ at the 12 m level of mooring 07, shown in Figure 5.2-8, continued without break until about April 25, 1993, when the currents increased to about 60 $cm \cdot s^{-1}$. The very end of the track of drifter 02449 (Figure 5.1-1) shows an anticyclonic turn between April 14 and 17, 1993 in almost the same position as that shown by drifter 07835 in Figure 5.2-10. It is during this time period that altimetry data suggest that eddy V partially coalesced with another anticyclone to the south (Jochens et al. 1996). However, drifters 07835 (Figure 5.2-10) and 02449 (Figure 5.1-1), and the current meter time series, suggest that the eddy was not absent from the lower slope for any substantial period of time during April and May 1993. During this period, there is a suggestion from the track of drifter 07835 that a vigorous cyclone was centered at about 25.5°N latitude, 93.5°W longitude (not shown in Figure 5.2-10). Eddy V seems to have remained a distinct circulation, and by May 1993 had separated from the anticyclone to the south (eddy U) and moved northward onto the lower slope. The cyclone indicated by the track of drifter 07835 (not shown) was observed south of the dissipated eddy V in early July 1993 and is shown by the track of drifter 06938 (Figure 5.1-2). This cyclone may have been responsible for keeping eddies U and V from completely coalescing (Jochens et al. 1996).

The last surveys of eddy V and the adjacent slope were obtained in May 1993. During a hydrographic survey of the shelf, surface drifter 06938 was deployed at the shelf break and moved off-shelf into eddy V in early May 1993. There were two AXBT/AXCP surveys between May 12 and 19, 1993, followed by a ship survey (GulfCet 05) at the end of May. However, the entire eddy was west of the westernmost transect (along 95°W longitude) by the time of the ship survey. The track of drifter 06938 is shown in Figure 5.1-2 and the path of the eddy center, obtained from the model fits, is shown in Figure 5.2-1. From early May through early June 1993, Figure 5.2-1 shows that the eddy translated quite rapidly westward around 27°N latitude with a mean translation speed of 6.5 $cm \cdot s^{-1}$.

The ellipse parameters for drifter 06938 are given in Figure 5.2-11. The ellipse rotational periods, semi-major and minor axes and mean swirl speeds were not greatly different than in January 1993 (Figure 5.2-2). There was little rotation of the ellipse axes and, based solely on the drifter track, the eddy had similar characteristics to those of four months earlier.

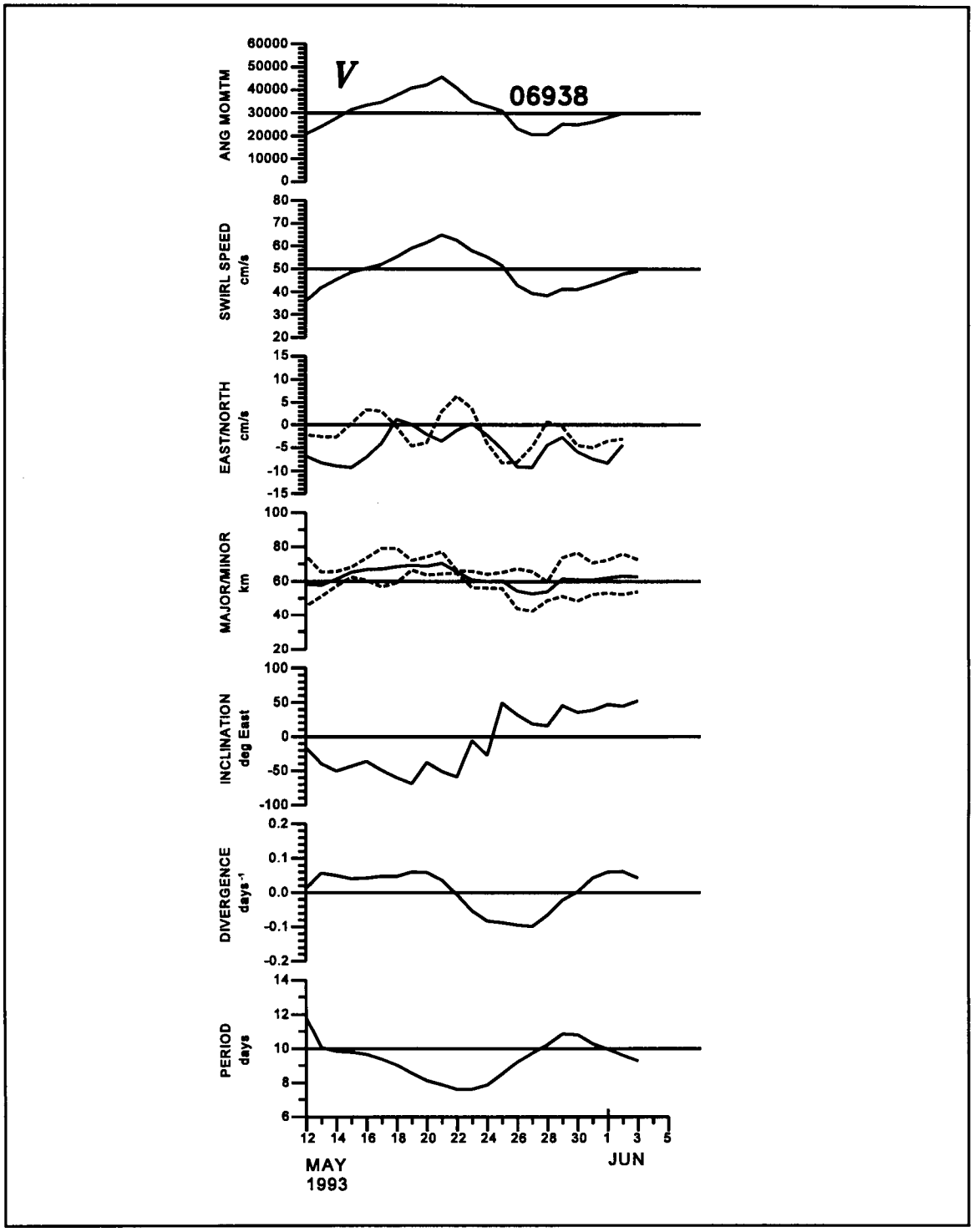

Figure 5.2-11. Time series of ellipse parameters from the model fits to the path of drifter 06938. The third panel shows the north (dashed) and east (solid) translation velocity components. The fourth panel shows the semi-major and minor axes (dashed) and mean radii (solid).

However, a comparison of the January and May 1993 current and hydrographic fields shows conclusively that, during this five-month period, eddy V decreased ~15 cm in dynamic height.

Figure 5.2-12a shows the May 1993 drifter, AXCP and current meter velocities superimposed on the depth of the 20°C surface. The drifter track approximately overlies the 125 m depth contour, the region of maximum velocities. The AXCP surface layer averaged velocities are all in the central part of the eddy and are again consistent with solid-body rotation around the indicated center. Interestingly, all of the AXCP velocities in Figure 5.2-12a have positive radial components, which is consistent with the positive divergence calculated by the model fits for May 12-22, 1993 (Figure 5.2-11). In contrast, the near-surface current meter velocities at the shelf break are all less than their adjacent drifter-calculated currents, indicating that they are in the cyclonic shear zone outside the eddy front. The eddy appears to be forcing on-shore surface flow at mooring 05. Therefore, the drifter mean radius, on the order of 70 km, is close to the true size of the eddy. In January 1993, the drifter radius was smaller and less than half of the size of the maximum radius (~100 km) of the region of solid-body rotation (Figure 5.2-6a).

The deepest depressions of isotherms for the 20°C and 15°C surfaces were much less (by about 50 and 100 m, respectively) in May 1993, than their January 1993 counterparts (Figures 5.2-6a,b and 5.2-12a,b). The 8°C surface (Figure 5.2-12c) shows a complex pattern which seems to indicate that the lower layers of the eddy were collapsing into a number of smaller-scale features. Flows at these depths, measured by the AXCPs, were generally westward under the eddy center. Thus, it appears that this eddy had spun down during May 1993 while at its most northerly position. Indeed, summer hydrographic surveys (in August 1993) found no sign of an eddy over the northwest slope. However, the AXBT flights and a ship survey (GulfCet 06) did not sample west of 95°W longitude. The shelf-break current meter records (moorings 04 to 09) between May and October 1993 are given in Figure 5.2-8b. They show strong anticyclonic surface currents at the 12 m levels of moorings 05 and 06, persisting for most of the summer. The altimetry suggests that eddy V dissipated by the end of June. However, suggestions of a weak warm feature are observable in most of the summer 1993 map products. The altimetry had difficulties in distinguishing eddy V from the background between March and May 1993 and this may be because of the complex, rapidly varying, slope topography of this northwest corner of the Gulf of Mexico. The October 30, 1993 survey (F12SLOPE), discussed in section 5.8, suggests that a slope cyclone was west of 95°W longitude at this time. Thus, based

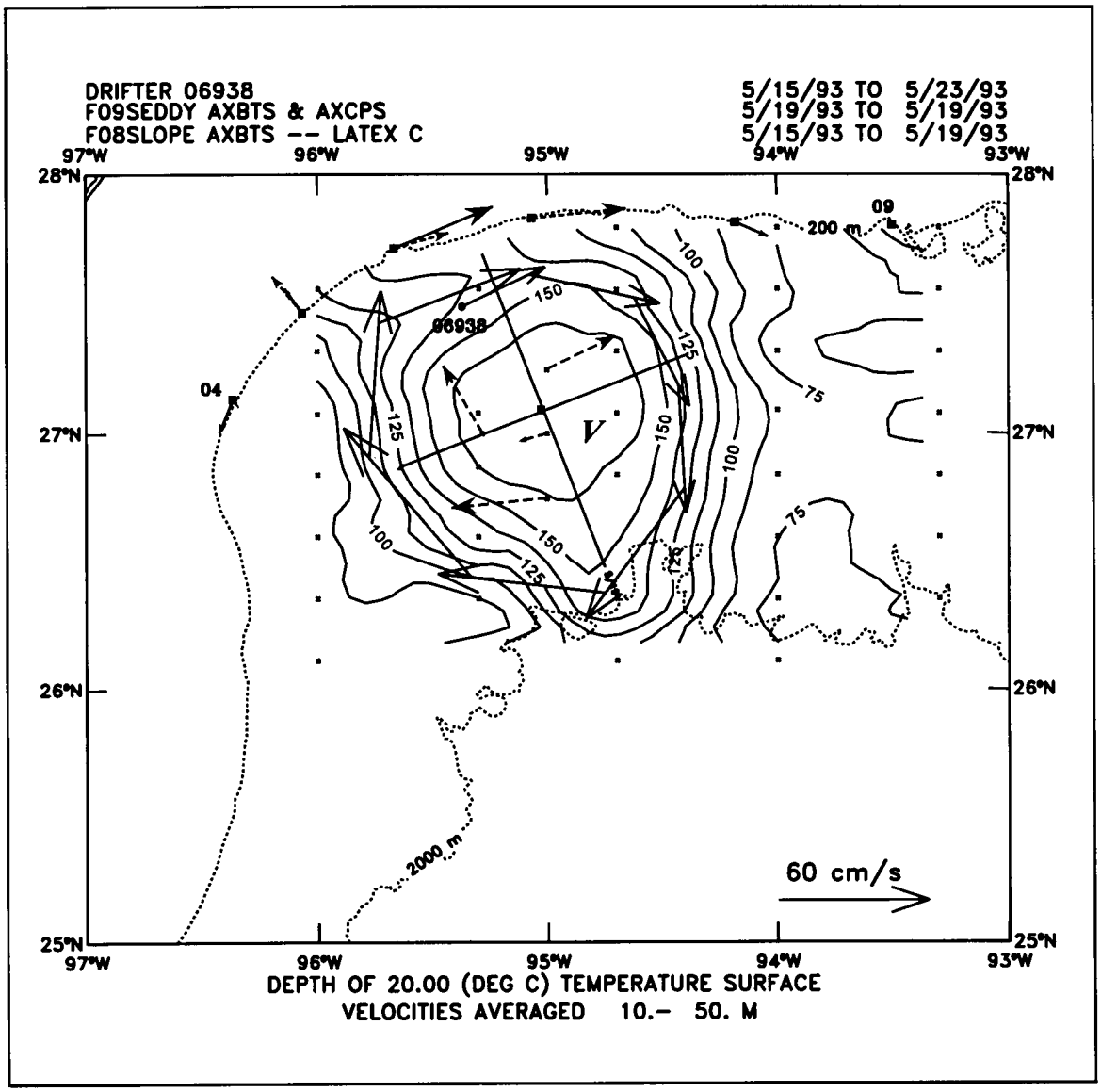

Figure 5.2-12a. Depth of the 20°C temperature surface from the F08SLOPE and F09SEDDY surveys. Daily velocity vectors from drifter 06938 are overlaid beginning May 15, 1993. Dark arrows emanating from crosses are 0-50 m averaged-smoothed velocities from AXCP profiles for May 19, 1993. Dark and light arrows emanating from squares represent the 12-m and 100-m, respectively, daily mean 40-HLP currents from LATEX A shelf-break moorings for May 19, 1993. The ellipse axes are given for May 19, 1993 and the solid square in the eddy marks the ellipse center 24 hours earlier.

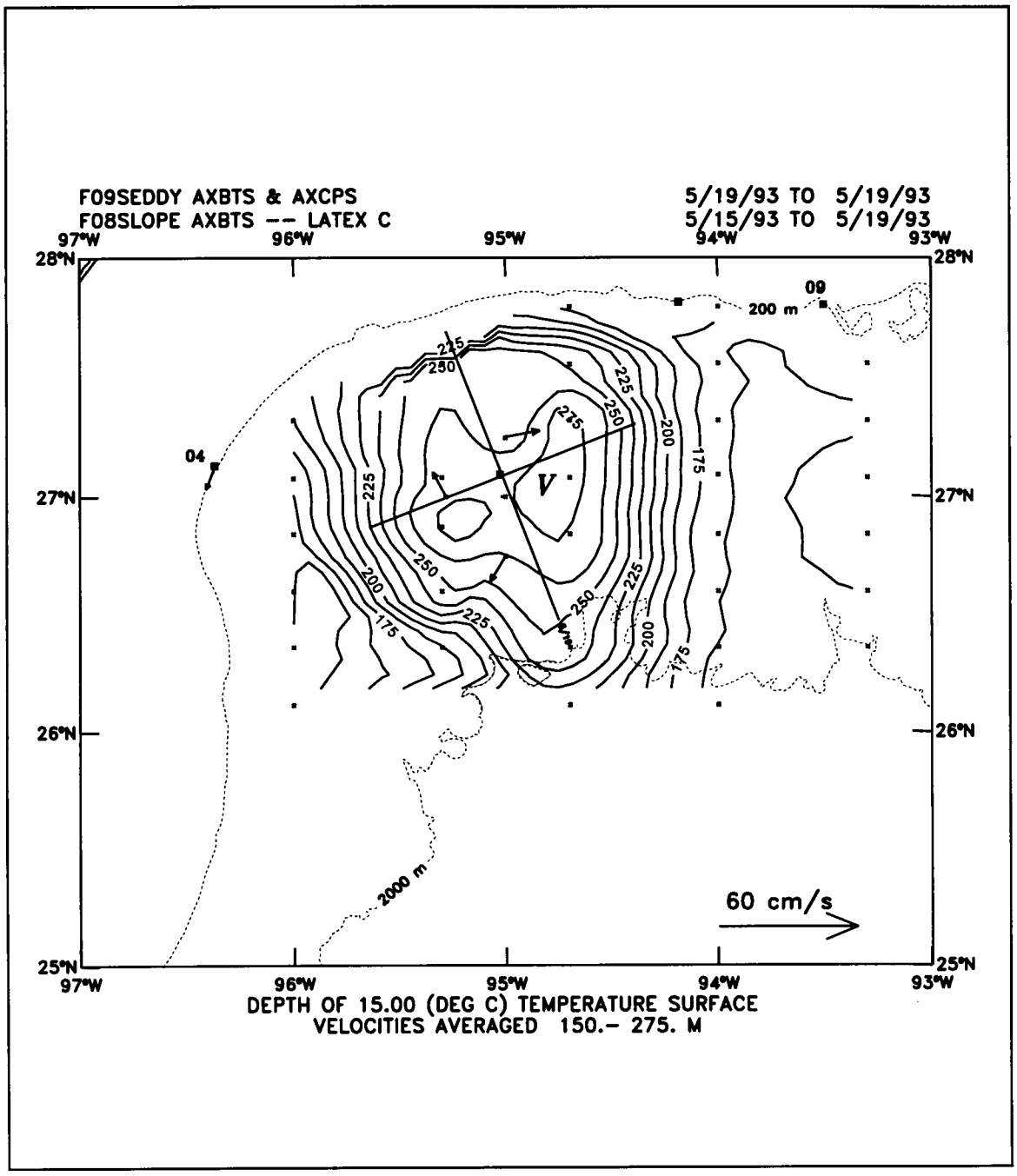

Figure 5.2-12b. Depth of the 15°C temperature surface from the F08SLOPE and F09SEDDY surveys. Dark arrows emanating from crosses are 150-275 m averaged-smoothed velocities from AXCP profiles for May 19, 1993. The dark arrow emanating from the square labeled 04 represents the ~200 m daily mean 40-HLP current vector from LATEX A mooring 04 for May 17, 1993.

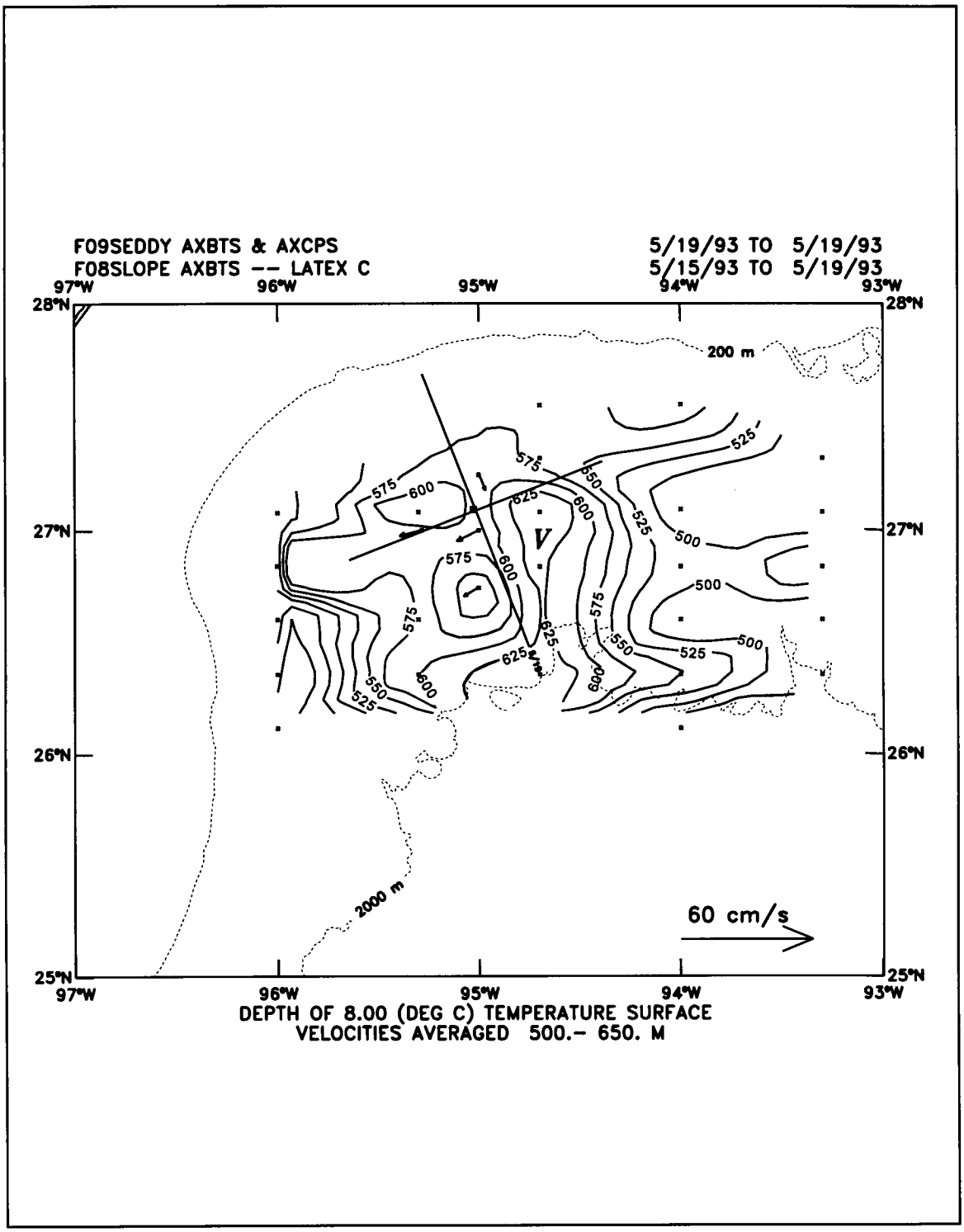

Figure 5.2-12c. Depth of the 8°C temperature surface from the F08SLOPE and F09SEDDY surveys. Dark arrows emanating from crosses are 500-650 m averaged-smoothed velocities from AXCP profiles for May 19, 1993.

on the current meter records, anticyclonic circulations that may have originated with eddy V could have remained in the northwest corner of the Gulf of Mexico until the beginning of October 1993. However, it is also likely that another anticyclone replaced the remnants of eddy V sometime in July or August and generated the vigorous eastward flows observed at moorings 05, 06 and 07 (Figure 5.2-8b). This in turn was replaced by a cyclone by the end of October 1993.

5.3 Eddy U Analysis

After shedding eddy V, the path of eddy U more closely conformed to those of previously studied eddies in the western Gulf of Mexico (Kirwan et al. 1984a). Figure 5.1-1 shows the path of drifter 02449, which was deployed within eddy U at the end of October 1992. The AXBT survey, F04LEDDY, which was flown two weeks earlier in October, shows that eddy U was very large, with semi-major axes greater than 150 km, and was in a similar position to that indicated by the early September 1992 track of drifter 02447. In contrast, eddy V's mean radius was just 60 to 70 km at the beginning of October 1992 (Figure 5.2-2).

The path of the center of eddy U, and the time series of the ellipse parameters derived from the model fits are shown in Figures 5.3-1 and 5.3-2, respectively. The model analysis of the track of drifter 02449 was split, at the end of December 1992, when the drifter was expelled from eddy U, moved rapidly westward, and interacted with the remnants of eddy T. Eddy T had detached from the Loop Current about 11 months prior to eddy U, and in April-May 1992 had collided with the Mexican slope around 23°N latitude (Biggs et al. 1996). It appears that eddy U absorbed the remnants of eddy T in January 1993 and then continued to drift west-southwestward through March 1993 (Figures 5.1-1 and 5.3-1). This interpretation of drifter 02449's track is consistent with the altimetry data from December 1992 and January 1993 (Leben and Born 1994).

During the November to December 1992 part of the track of drifter 02449, the parameters are relatively uniform (Figure 5.3-2). The eddy initially moved slowly westward at about 5 $cm \cdot s^{-1}$, stalled at the beginning of December 1992, and then moved rapidly with a translation speed on the order of 10 $cm \cdot s^{-1}$ to the southwest. Mean radii were quite uniform around 50 km and swirl speeds averaged 30 to 40 $cm \cdot s^{-1}$, much smaller than for eddy V during the same period (Figure 5.2-2). However, drifter 02449 was drogued at 100 m, rather than near-surface as for drifter 02447. The clockwise rotation of the major axis was also relatively uniform (~3°·day^{-1}) through the middle of December 1992, when the major axis aligned east-west prior to

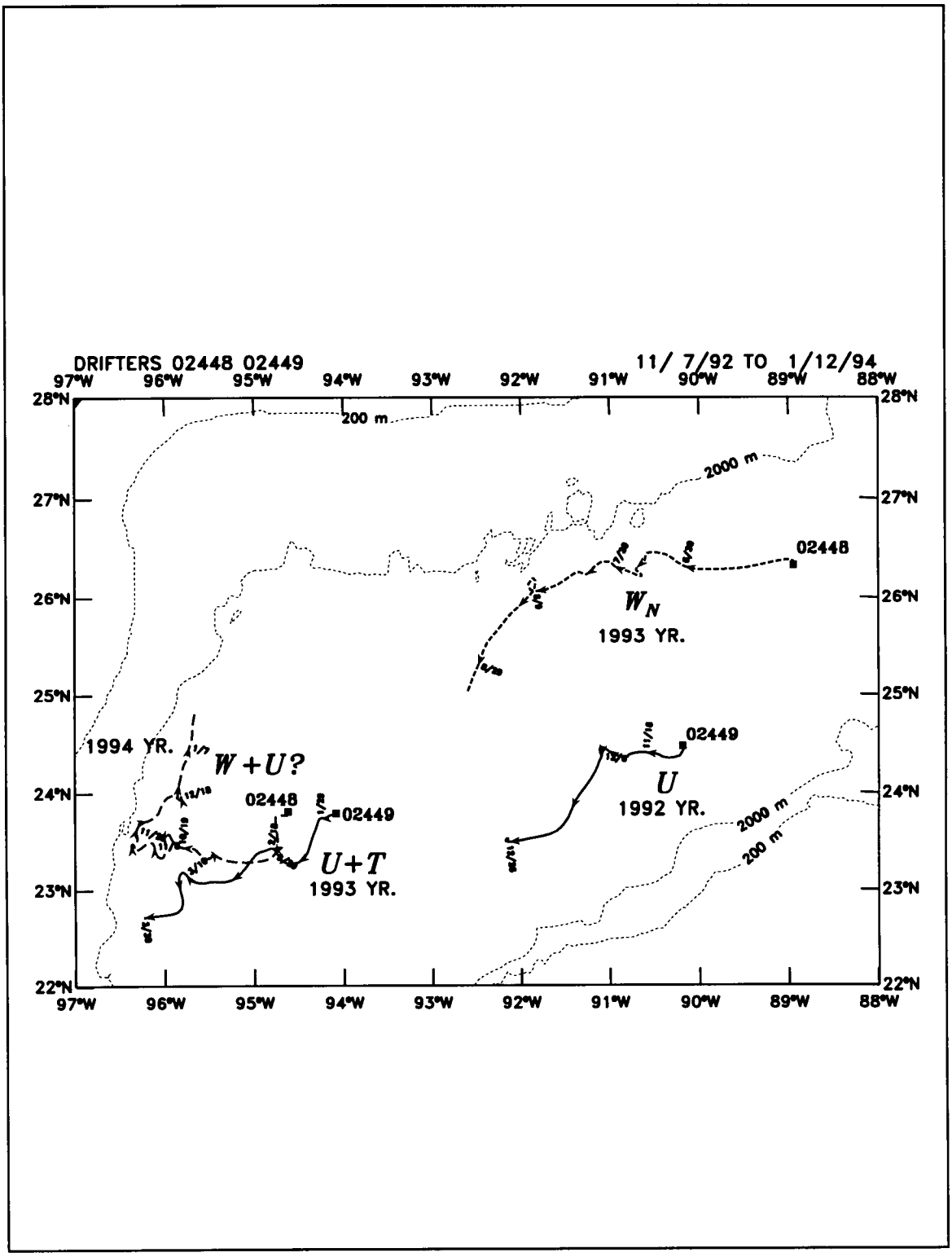

Figure 5.3-1. Tracks of the center positions from the ellipse model fits of drifters 02449 (solid) and 02448 (short-dashed and long-dashed) for eddies U and W_N, respectively.

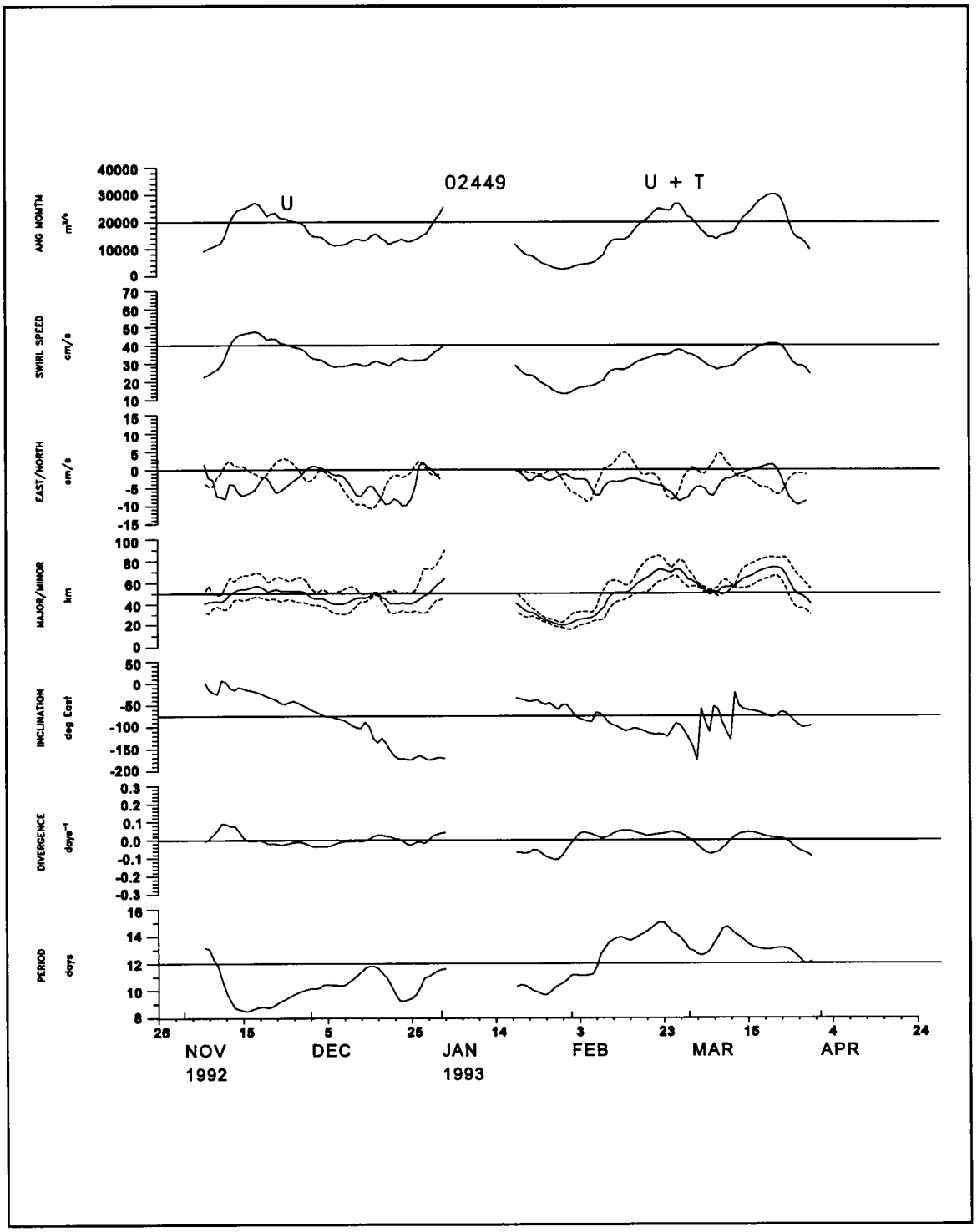

Figure 5.3-2. Time series of ellipse parameters from the model fits to the path of drifter 02449. The third panel shows north (dashed) and east (solid) translation velocity components. The fourth panel shows the semi-major and minor axes (dashed) and mean radii (solid).

interaction with the remnants of eddy T. Eddy rotation periods ranged from 8 to 12 days, longer than those for eddy V in November 1992.

In the second half of the record (Figure 5.3-2), after the drifter was entrained into the remnant of eddy T to the west, the center coordinates moved from 94°W to 96°W longitude. There was an increase in the rotation period to 14 days, along with an increase in the mean radius on the order of 60 km. It is noteworthy that the eddy U and T interaction in January 1993 was coincident with the abrupt northward motion of eddy V onto the slope (Figures 5.1-1 and 5.2-1) and its return to the 2000 m isobath at the end of January 1993. Through March and April 1993, while eddy U moved slowly westward and southwestward towards the Mexican slope, there was a distinct periodicity of 20 to 25 days in the axes lengths, southward translation velocity components and swirl speeds. This periodicity is also clear in the path of the eddy center shown in Figure 5.3-1. Presumably, this 20-25 day pulsing was a reaction to the earlier absorption event.

5.4 Eddy W Analysis

Drifter 02448 was deployed within the Loop Current at the beginning of June 1993, just as eddy W was separating. Shortly thereafter, eddy W cleaved (Walker et al. 1993), and by the end of June, this drifter was moving clockwise in the northern, smaller portion of the two pieces of eddy W. A second drifter, deployed in the main part of eddy W in late June 1993, showed a closed circulation separate from that of drifter 02448 (K. Schaudt, personal communication). Thus, it is concluded that drifter 02448 spent July through September 1993 in a relatively weak anticyclone, which will be referred to as W_N to distinguish it from the main portion of eddy W. The formation of eddy W and its subsidiaries from a well-extended Loop Current in May and June 1993 was complex, and it is difficult to arrive at a complete picture with the available drifter data. Accordingly, the focus of this section will be on the interaction of eddy W_N with a cyclone on the lower slope.

Figure 5.4-1 shows the results of ellipse model fits for the track of drifter 02448. The record was split into two sections, with the break in early September 1993. The first section of the path has two cusps (July 21 and August 6, 1993) where the drifter slowed and made a sharp ~90° turn to the left. These cause the model fit ellipse to contract and expand rapidly and thus generate large changes in the divergence (D). Because the second cusp, on August 6, 1993, occurred while W_N was interacting with a cyclone, the rapid changes in

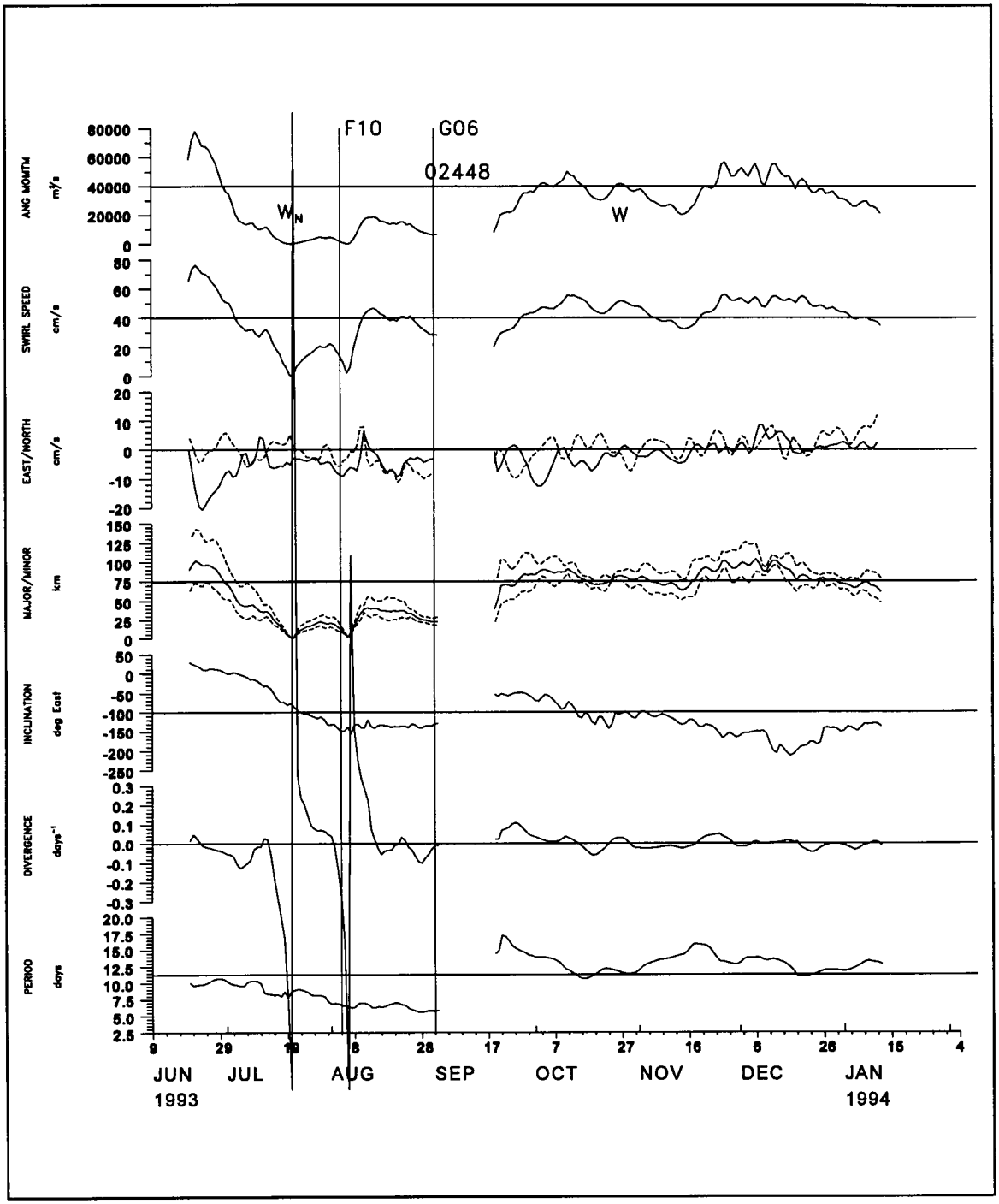

Figure 5.4-1. Time series of ellipse parameters from the model fits to the path of drifter 02448. The third panel shows north (dashed) and east (solid) translation velocity components. The fourth panel shows the semi-major and minor axes (dashed) and mean radii (solid). Vertical lines mark the start of the F10SLOPE and GulfCet 06 surveys.

the ellipse parameters appear to be a true indication of a perturbation in the eddy's circulation.

There are no distinct transitions (Figure 5.4-1) up to the first cusp. Rather, the swirl speed, angular momentum, axis lengths and rotational periods all show steadily decreasing values with time. This suggests eddy decay. The major axis rotated clockwise at an average rate of about $4°\cdot day^{-1}$, similar to that exhibited by eddy U, but slower than the early stages of eddy V's history. By August 6, 1993, the eddy was quite weak and was moving slowly southwestward, just seaward of the 2000 m isobath (Figures 5.3-1 and 5.4-1).

The path of drifter 06938 (Figure 5.1-2) documents the presence of a small (50 km diameter) cyclone (C1) centered near 26.5°N latitude, 93.5°W longitude on the lower slope. Figure 5.4-2 shows the depths of the 20°C, 15°C and 8°C isothermal surfaces from AXBT surveys of this cyclone and eddy W_N. The 15°C isotherm maximum depression is at about 300 m for eddy W_N, compared to ~350 m for eddy V in January 1993 (Figure 5.2-6b). The track of drifter 02448 approximately overlies the 175 m depth contour for the 20°C surface (Figure 5.4-2a). However, because of the complexity of the track, the ellipse axes are shown for the August 2 and August 12, 1993 model fits. The northern edge of eddy W_N (20°C at 125 m) extends to mid-slope. While the cyclone barely shows up in the 20°C surface, it is more defined by the doming of the deeper isotherms, as has been previously observed for the Gulf of Mexico (Hamilton 1992). Surface velocities for drifter 06938 were about 20 $cm\cdot s^{-1}$ and there appears to be no influence from the surface field of eddy W_N. The cyclone ellipse axes correspond reasonably well with the center, as defined by the 150 m contour of the 15°C surface (Figure 5.4-2b). However, there is some indication in the 15°C surface of eddy W_N, particularly the 250 and 275 m contours, that the deeper cyclonic circulation was advecting warm eddy water northward over the slope. This is even more evident for the deepest layers of eddy W_N, represented by the 8°C surface (Figure 5.4-2c). The deepest contours (600 m) are elongated northward over the slope and the center is a little west of that indicated by drifter 02448 and the 20°C surface (Figure 5.4-2a). The deep center of the cyclone was also displaced to the northeast of its surface by more than 50 km. Therefore, this interaction caused the vertical axes of the centers of rotation to be tilted away from each other, and the cyclone's tilt was the larger of the pair of the two eddies.

Following this interaction, the anticyclone appears to have been reinvigorated, and moved rapidly off the slope towards the south-southwest. Swirl speeds and axis lengths increased

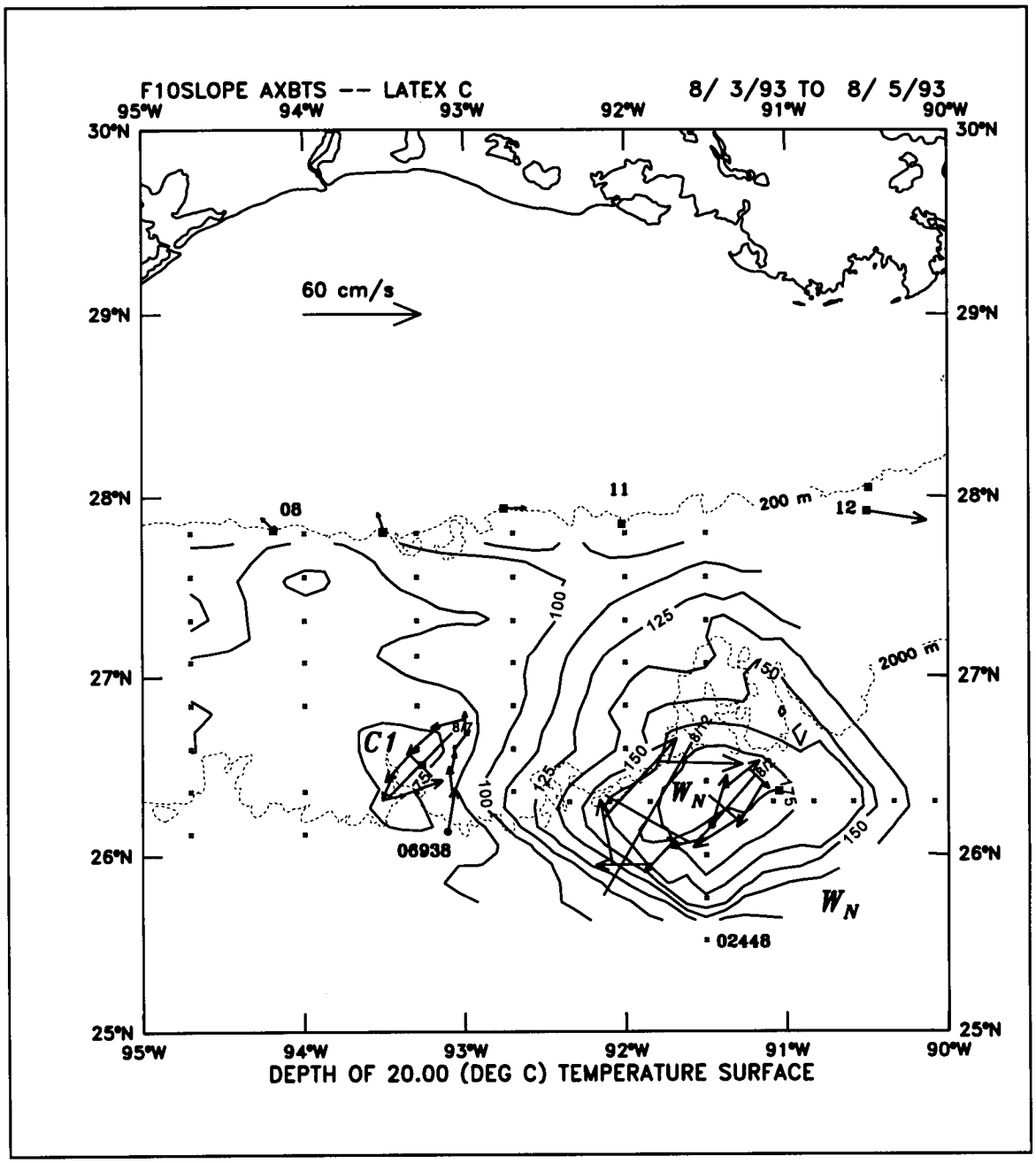

Figure 5.4-2a. Depth of the 20°C temperature surface from the F10SLOPE and F11LEDDY surveys. Daily velocity vectors from drifters 06938 and 02448 are overlaid beginning July 30, 1993. Dark arrows emanating from squares represent the 12-m daily mean 40-HLP currents from LATEX A shelf-break moorings for August 4, 1993. Ellipse axes are shown for August 2 and 12, 1993 (for drifter 02448) and August 7, 1993 (for drifter 06938). The solid squares in the eddies mark the ellipse centers 24 hours earlier.

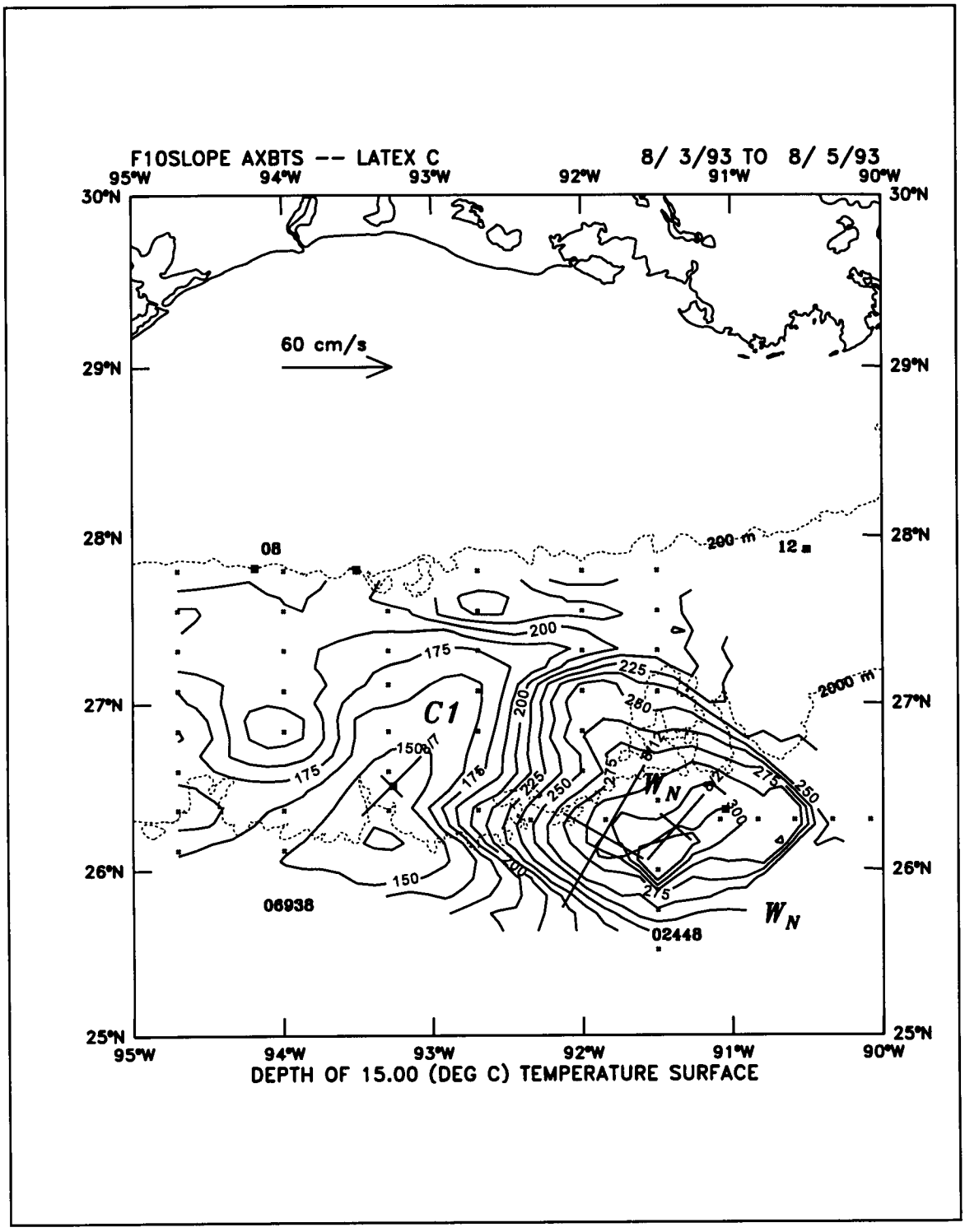

Figure 5.4-2b. Depth of the 15°C temperature surface from the F10SLOPE and F11LEDDY surveys. Dark arrows emanating from squares represent the 200-m daily mean 40-HLP currents from LATEX A shelf-break moorings for August 4, 1993.

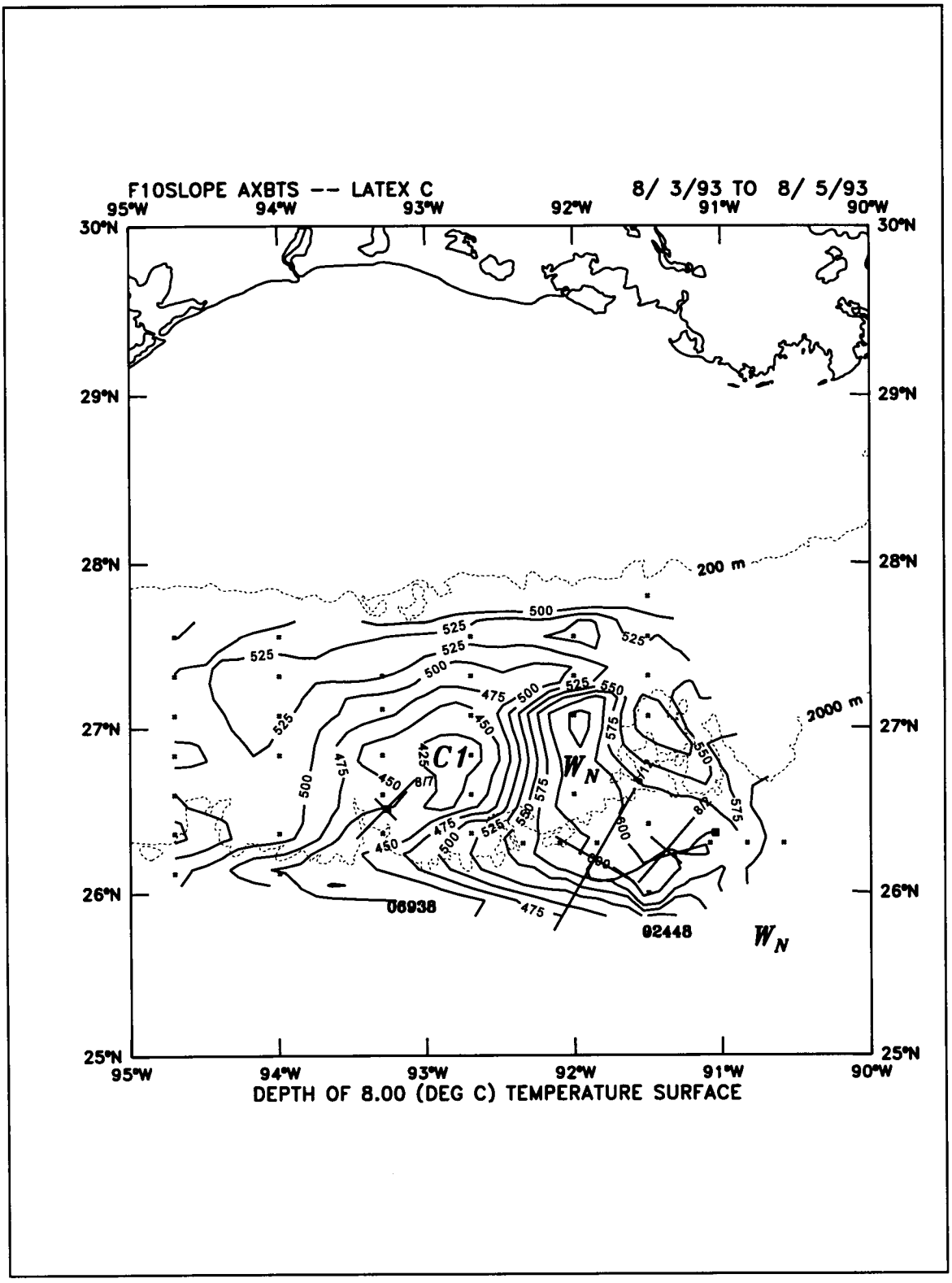

Figure 5.4-2c. Depth of the 8°C temperature surface from the F10SLOPE and F11LEDDY surveys.

and the rotational period remained fairly constant at about six days. The ellipse's major axis did not rotate, being directed NE-SW. The drifter data indicate that the center of eddy W_N was at about 25°N latitude, 92.6°W longitude at the beginning of September 1993. At this time, there was another hydrographic survey of the slope (GulfCet 06). The 8°C surface (Figure 5.4-3c) shows that the cold slope eddy (C1) had moved further eastward and northward to ~27°N latitude, 92°W longitude, apparently displacing the warmer water from eddy W_N southward and offshore. Note that seaward of about 1800 m, there is a hint of deepening of the isotherms at the southeast edge of the grid, corresponding to the northern edge of the rapidly departing anticyclone. Thus, any warm deep water that was previously located over the slope associated with eddy W_N appears to have been removed along with the eddy.

The shelf-break currents at the times of the two surveys are superimposed on Figures 5.4-2 and 5.4-3. At the beginning of August 1993 (Figure 5.4-2a),neither eddy W_N nor the cyclone appeared to have much effect on the shelf break, except for strong flows at mooring 12, to the east of eddy W_N. There is a suggestion in the 20°C and 15°C surfaces that flows at moorings 08, 09 and 10 may have been related to small eddy-like features just south of the 200 m isobath. This is much more evident in the GulfCet 06 survey (Figures 5.4-3a and b), where a pair of cold and warm upper-layer eddies is found between 93.5°W and 94°W longitude on the upper and mid slope, respectively. Strong cyclonic flow is observed at the surface at mooring 09 (Figure 5.4-3a) and there is a suggestion that the strong southeastward flow at mooring 08 is caused by an interaction between these eddies, and can be considered an offshore exchange event (e.g. a "squirt"). The cold eddy that interacted with eddy W_N and is now at mid slope had no discernable signature in the currents at the shelf-break moorings (10 and 11) to the north. Therefore, not all mid-slope eddies are observable in the shelf-break current records. It is noted that the GulfCet 06 station spacing barely resolves these smaller (~50 km diameter) upper slope features.

Forty-HLP current vectors for the moorings in Figure 5.4-2, for the period between the August and September 1993 surveys, are shown in Figure 5.4-4. The strong eastward surface flows at moorings 12 and 13, prior to GulfCet 06, can be attributed to eddy W_N. Cyclonically rotating vectors followed by westward flows beginning about August 14, 1993 at mooring 08 is repeated about a week later at mooring 09. This kind of pattern could be explained by a warm and cold pair of eddies moving eastward along the upper slope. There is some suggestion of a weak warm feature east of the cold eddy at 93.5°W longitude in the 20°C and 15°C surfaces in Figure 5.4-3.

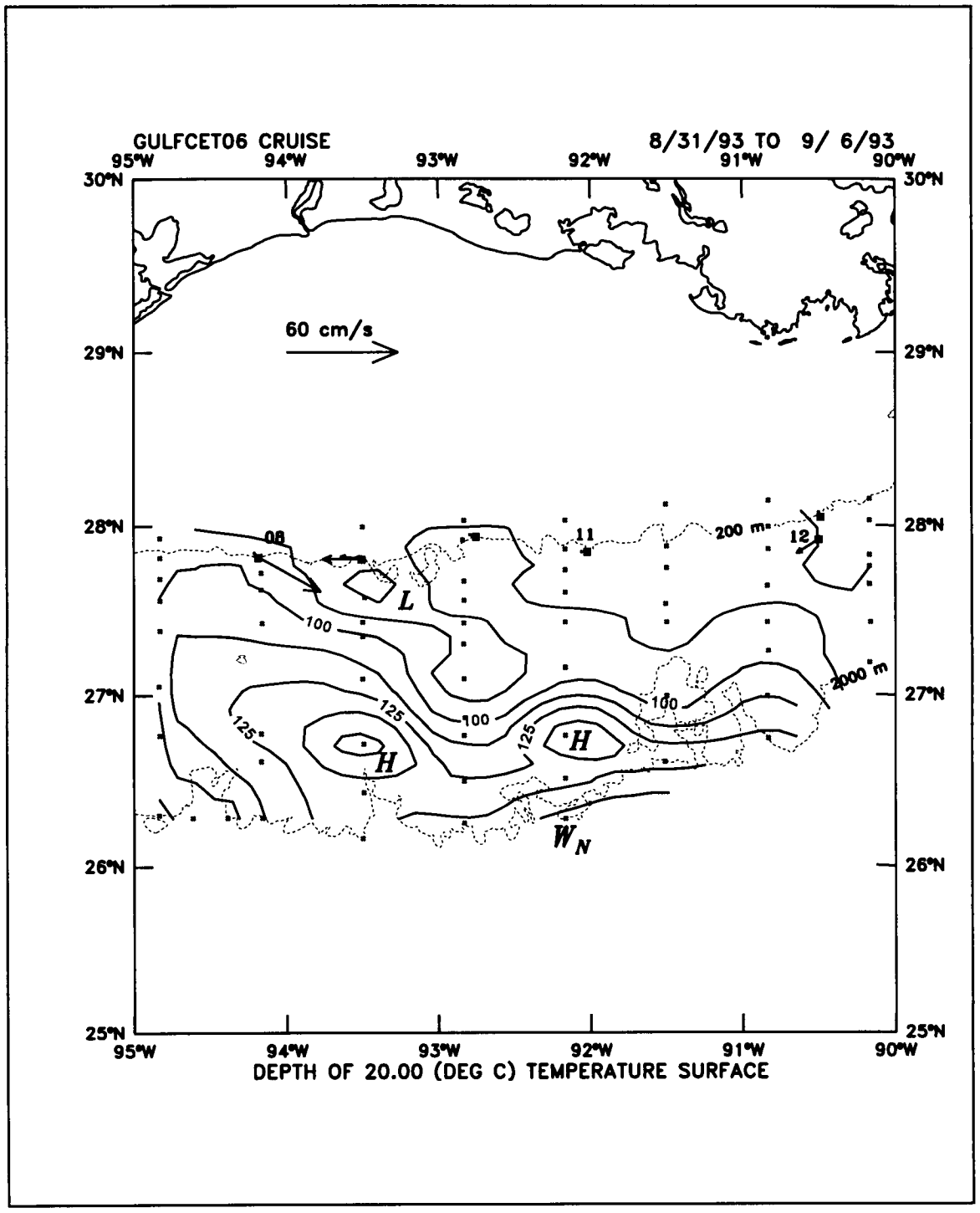

Figure 5.4-3a. Depth of the 20°C temperature surface from the GulfCet 06 survey. Dark arrows emanating from squares represent the 12-m daily mean 40-HLP currents from LATEX A shelf-break moorings for September 2, 1993. Anticyclonic and cyclonic features are identified with an H or an L, respectively.

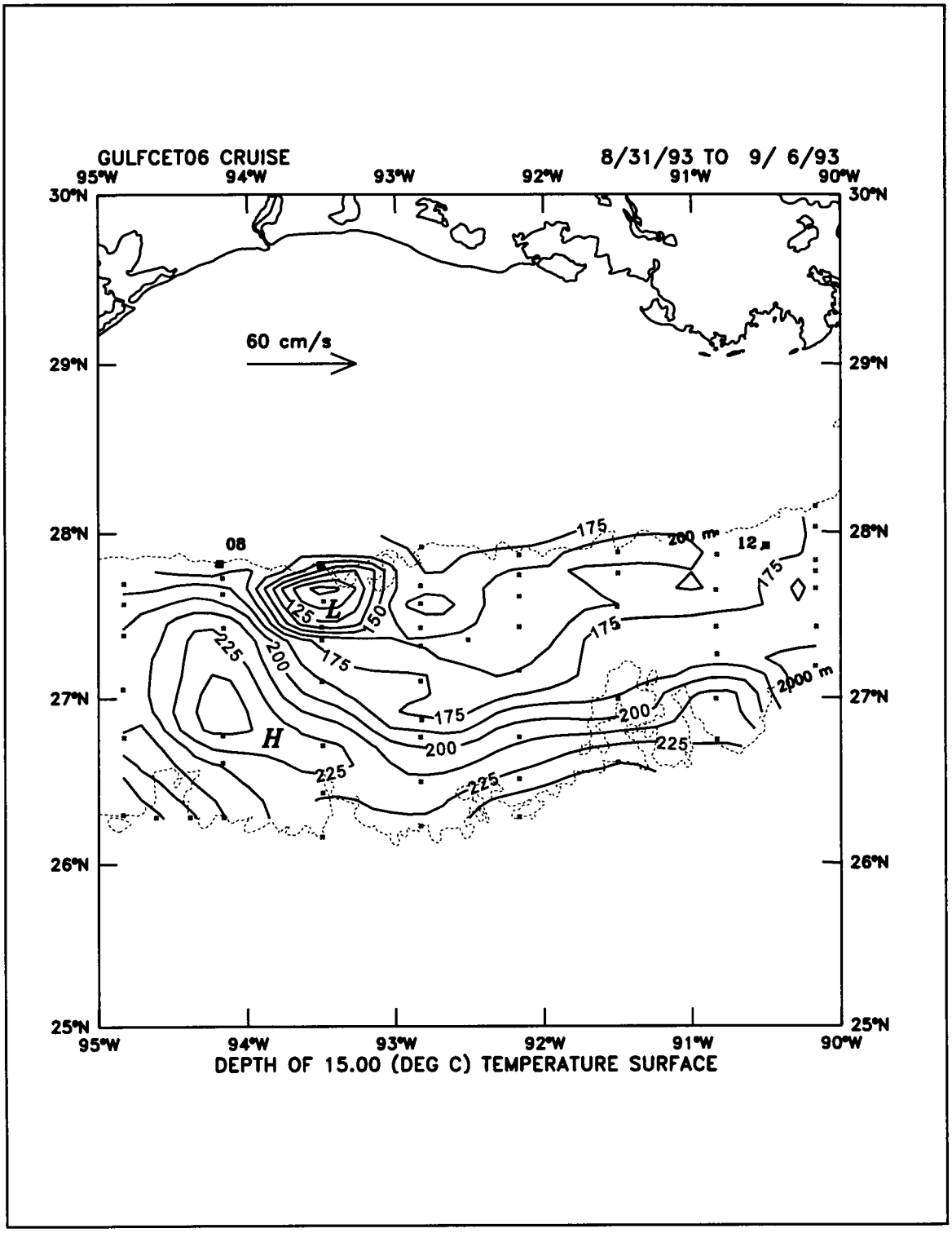

Figure 5.4-3b. Depth of the 15°C temperature surface from the GulfCet 06 survey. Dark arrows emanating from squares represent the 200-m daily mean 40-HLP currents from LATEX A shelf-break moorings for September 2, 1993.

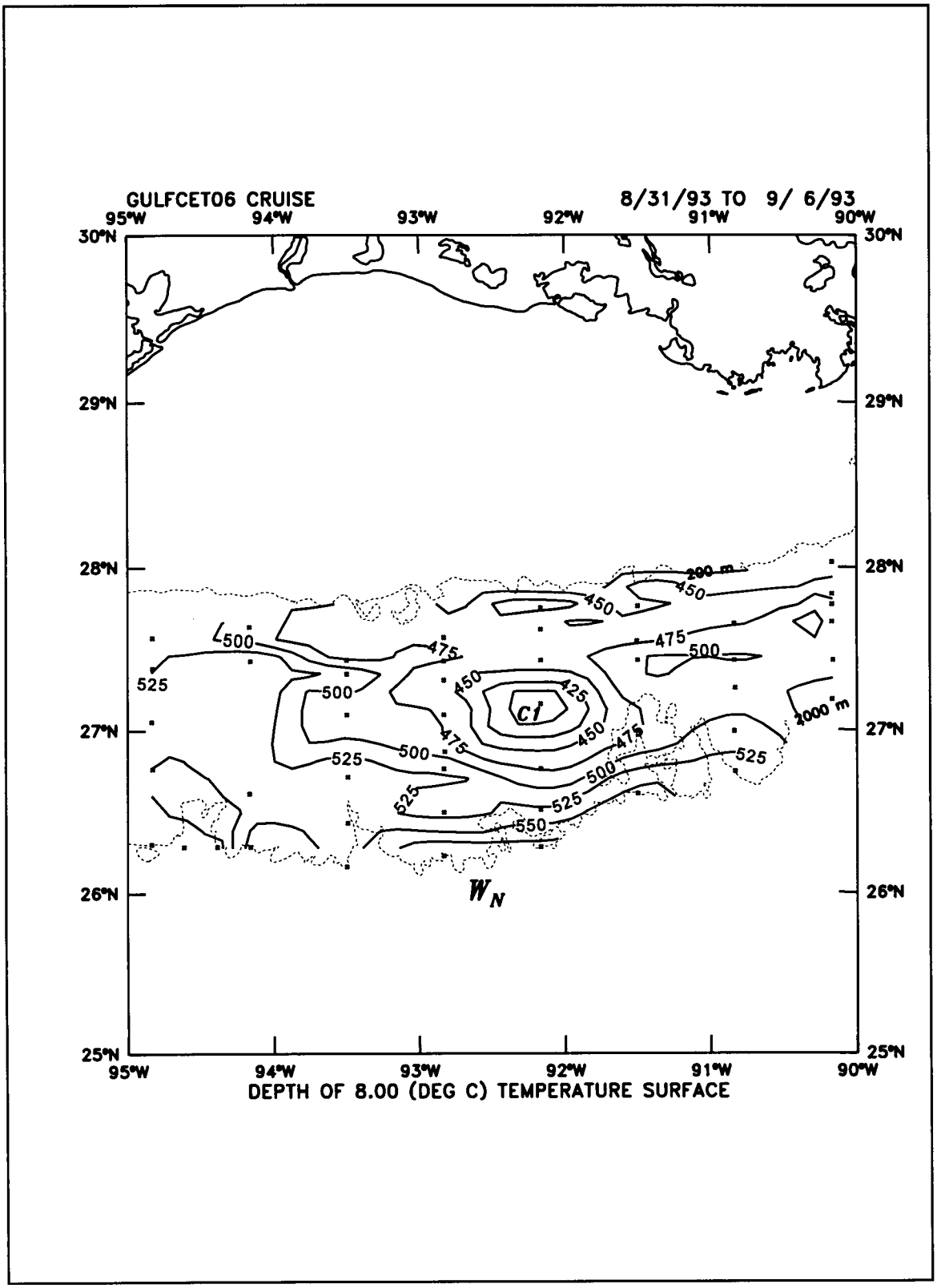

Figure 5.4-3c. Depth of the 8°C temperature surface from the GulfCet 06 survey.

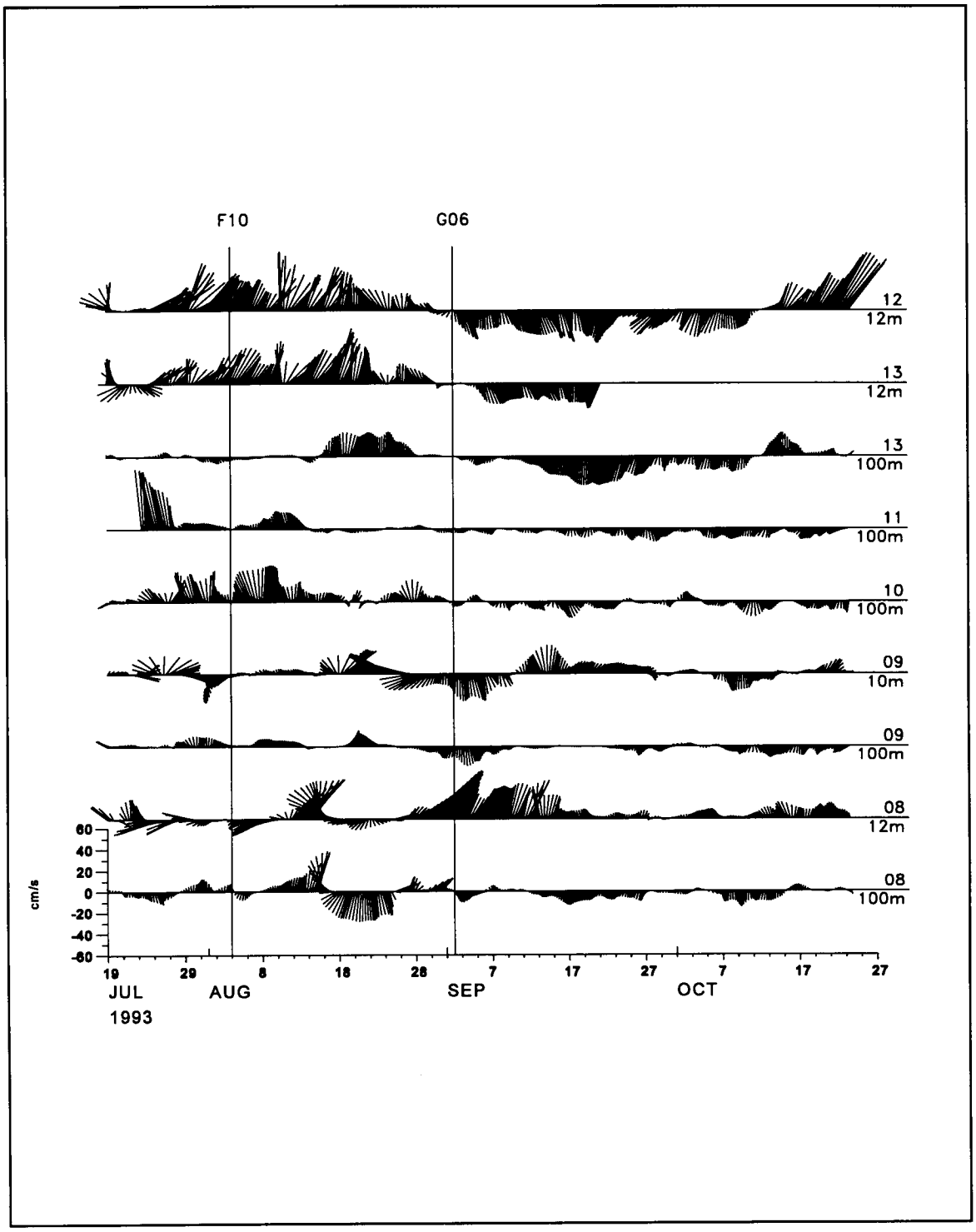

Figure 5.4-4. Stick plots of rotated 40-HLP currents from LATEX A shelf-break moorings for the period from July 19, 1993 to October 27, 1993. Up is the along-isobath direction towards the east. Vertical lines mark the start of the F10SLOPE and GulfCet 06 surveys.

Thus, if this is the warm feature observed at moorings 08 and 09, on about August 14 and 20, 1993 respectively, it apparently dissipated quite rapidly. More examples of these small upper-slope eddies will be discussed in Section 5.7 using higher resolution hydrographic data and the many SCULP drifter tracks that help to better define the events and their associated scales.

In the final part of the track of drifter 02448, the drifter left eddy W_N, making a large anticyclonic turn, and was entrained into a large, slowly rotating (period ~15 days) anticyclone (Figures 5.1-2 and 5.4-1). The most plausible explanation, and one consistent with altimeter data, is that the drifter (and eddy W_N) coalesced back into the major (or southern) part of the original eddy W, which had moved southwestward across the deep Gulf of Mexico in July and August 1993, while eddy W_N was stalled on the lower slope. Thus, it is probable that the southward movement of eddy W_N in August 1993 was driven by the influence of this larger anticyclonic circulation to the southwest, as well as by its interaction with a slope cyclone.

For the period after drifter 02448 became re-entrained in eddy W, the drifter track can be divided into three parts (Figures 5.3-1 and 5.4-1): *1*) September 1 - October 14, 1993, characterized by rapid southward and westward translation towards the western slope, until the center reached the 3000 m isobath; *2*) October 15 - November 30, 1993, when the eddy seemed to stall and meandered only slowly towards the slope; and *3*) December 1 - 31, 1993, when the center reached its closest approach to the western shelf (though it did not cross the 2000 m isobath). After this time, drifter 02448 moved fairly rapidly northward, with some movement away from the slope towards the 3000 m isobath. The drifter was expelled from the eddy on about January 18, 1994.

From September 1 to October 14, 1993, the center translation speeds (mean ~7.3 $cm \cdot s^{-1}$) were high and the path had a similar shape (two sharp turns) to that of eddy U (drifter 02449) as it approached the western slope (Figure 5.3-1). The drifter track began this segment being strongly elliptical, but became more circular as it approached the coast. From October 15 to November 30, 1993, while the eddy was stalled against the western slope, the mean radius remained fairly constant at ~75 km. The rotational period increased from 11 to 16 days on about November 20, 1993, and then decreased as the center moved slowly away from its farthest west position. The eccentricity of the ellipse also increased and decreased over the same period. The inclination remained constant with the major axis being directed approximately north-south as the eddy

approached the slope. A more east-west major axis became prevalent in December 1993 as the eddy drifted northward and eastward from the 2000 m isobath (Figure 5.4-1). In this third stage, mean translation speeds were ~5.6 $cm \cdot s^{-1}$ and there was again a small increase in the rotation period, coupled with decreasing mean radii, resulting in decreasing swirl speeds.

Perhaps the most notable characteristics of the ellipse parameters, as eddy W approached the shoaling continental margin, were the relative robustness of the values, indicating that dissipation of eddies in this region is small and/or slow. Although there are two periods in the records, October 15 to November 20, 1993, and December 20, 1993 to January 12, 1994, where rotational periods increased (causing a small slowing of the swirl speeds with no corresponding decrease in mean radius [which implies decay]), on the whole, the swirl speeds were on the order of 40 to 50 $cm \cdot s^{-1}$ and the rotational periods were about 13 days. The latter are comparable to those exhibited by drifter 02449 in eddy U + T in February and March 1993. Finally, both eddies U + T and W showed significantly longer rotational periods, during their approach to the Mexican slope, than earlier in their life histories in the central Gulf of Mexico. The significance of this in terms of eddy decay is discussed in Section 5.9.1.

5.5 Eddy X Analysis

Eddy X was the least documented Loop Current anticyclone during the LATEX program. Eddy X was shed from the Loop Current in October - November 1993. The origins of eddy X were a well-extended Loop Current in August and September 1993. The GulfCet 06 cruise, at this time, showed a large warm anticyclonic circulation intruding onto the slope and shelf just south of the Mississippi River delta at 89°W longitude. The TOPEX/ERS-1 altimetric maps show that the birth of eddy X was complex and that the eddy may have attached and detached from the Loop Current several times before breaking free. The next set of surveys, in December 1993 comprised of GulfCet 07, F13SQUIRT and F14LEDDY. The former showed eddy X intruding well onto the mid-slope just east of 91°W longitude. The latter survey, about 10 days later, showed that the eddy had moved a little off the slope and was centered at about 26°N latitude, 91W° longitude. Since only the northern part was surveyed, it is difficult to estimate its size and vigor. However, the survey suggests that eddy X was relatively small (~200 km in diameter) and had weak circulation (8°C isotherm was depressed to less than 625 m in the center). Drifter 07838, deployed at this time, only skirted the eastern side of the eddy and did not become entrained.

Eddy X was not observed again in any of the subsequent slope surveys of drifter tracks and is presumed to have moved southwestward across the Gulf of Mexico, encountering the Mexican slope in the summer of 1994. In October of 1994, SCULP drifters 21708 and 20555 showed the presence of a warm eddy at about 24.5°N latitude and 95°W to 96°W longitude. This anticyclone is a possible candidate for the remnants of eddy X.

5.6 Eddy Y Analysis

Eddy Y detached from the Loop Current during the late summer of 1994. Drifter 12374 skirted the edge of an extended Loop Current (or eddy Y) in August 1994, and the path indicates that the center was near 26°N latitude, 89°W longitude. Drifter 12376 was seeded into the eddy on September 17, 1994 with the eddy centered at about 27°N latitude, 89°W longitude, and drifter 12377 was seeded on October 12 with the center at about 26.2°N latitude, 89.5°W longitude. Both were drogued at 100 meters depth. The smoothed tracks of these two drifters are shown in Figure 5.1-3. The eddy diameter was about 200 km, and thus, was a moderate-sized, rather slow-moving Loop Current anticyclone. Eddy Y moved west-southwestward (Figure 5.1-3) and the drifters remained seaward of the 2000 m isobath. This is a more conventional behavior than that exhibited by eddies U, V and W, which were discussed earlier. Drifter 12376 was spun out of the eddy in January 1995 and moved rapidly towards the Mexican slope. Drifter 12377 was entrained into a cyclone (C2) situated on the lower slope at about 93.5°W longitude, immediately north of the position of eddy Y in early February 1995. This drifter made two circuits of the cyclone, returned briefly to eddy Y, and then was apparently expelled from eddy Y and entrained into another anticyclone to the west. This latter anticyclone may have been the remnants of eddy X. Eddy Y may have been in the process of merging with this older anticyclone in the April 1995 time period (Figure 5.1-3). Drifter 12377 then moved rapidly northward across the slope in May 1995 and remained on the western Louisiana-Texas shelf until August 1995.

The translating ellipse model was applied to the tracks of drifters 12376 and 12377 until the drifters were expelled from eddy Y. The existence of two drifters in the same eddy for an extended period of time allows comparison of the analyses, and therefore some indication of the reliability of the parameter estimates. Kirwan et al. (1984b) used a similar ellipse model for the simultaneous analysis of three drifters that tracked a single Loop Current anticyclone in the western Gulf of Mexico. They found that there were, at times, quite large differences between the estimated parameters from the three drifter paths. The largest differences occurred for estimates

of the translation and swirl velocities. However, the overall trends and magnitudes were, in general, quite similar. Figure 5.6-1 shows the paths of the center of eddy Y derived from the analyses of the two drifters. The two paths coincide quite well, except for the large north-south fluctuation for drifter 12376 at the end of December 1994. This occurred just prior to that drifter being expelled from the eddy when its orbits were rapidly expanding. At the same time, drifter 12377's orbits were contracting. It is concluded that unstable orbits of the drifter around the periphery of an eddy can cause fluctuations in the indicated position of the center.

A comparison of other ellipse parameters derived from the two model fits is given in Figure 5.6-2. Rotation periods steadily increased from six days in September 1994, to 14 days in January 1995. There was a large convulsion in most of the parameters for drifter 12377 at the end of January 1995 as the eddy interacted with the cyclone to the north. Inclinations were mostly identical [the difference of almost exactly 180° in Figure 5.6-2 indicates that the major axes were practically parallel], and the clockwise rotation rate was about $2°\cdot day^{-1}$ for most of the record. Like the other eddies discussed in this report, this rate is slower than the $8°\cdot day^{-1}$ that is calculated by the theory of Cushman-Roisin et al. (1985). Mean radii ranged from 50 to 100 km for most of the record. Also, the paths were reasonably circular before the middle of December 1994. Mean radii from drifter 12377 showed a general decrease with time, whereas radii from drifter 12376 were relatively steady until the large increase at the end of December 1994 as the drifter moved to the periphery of the eddy. The divergence for drifter 12376 was small but positive at this time, though the drifter track did become highly elliptical. As was found by Kirwan et al. (1984b), the largest instantaneous differences between analyses of multiple drifter tracks were for the velocity parameters. The translation velocity component differences are directly related to the differences in the paths of the center (Figure 5.6-1). Mean swirl velocities showed the same general decreasing trend until the end of December 1994, when drifter 12376 started to move out of the eddy circulation. Swirl speeds were similar to the other eddies analyzed and the decrease, along with increasing period over most of the record, indicates that the eddy was becoming less energetic as it moved across the central and western Gulf of Mexico.

Early in the life of eddy Y, the LATEX C program performed extensive surveys of the eddy and adjacent slope waters. In October 1994, surveys F18LEDDY and F19SEDDY were able to map the temperature and velocity structure of the anticyclone and a companion mid-slope cyclone. In November 1994, two compre-

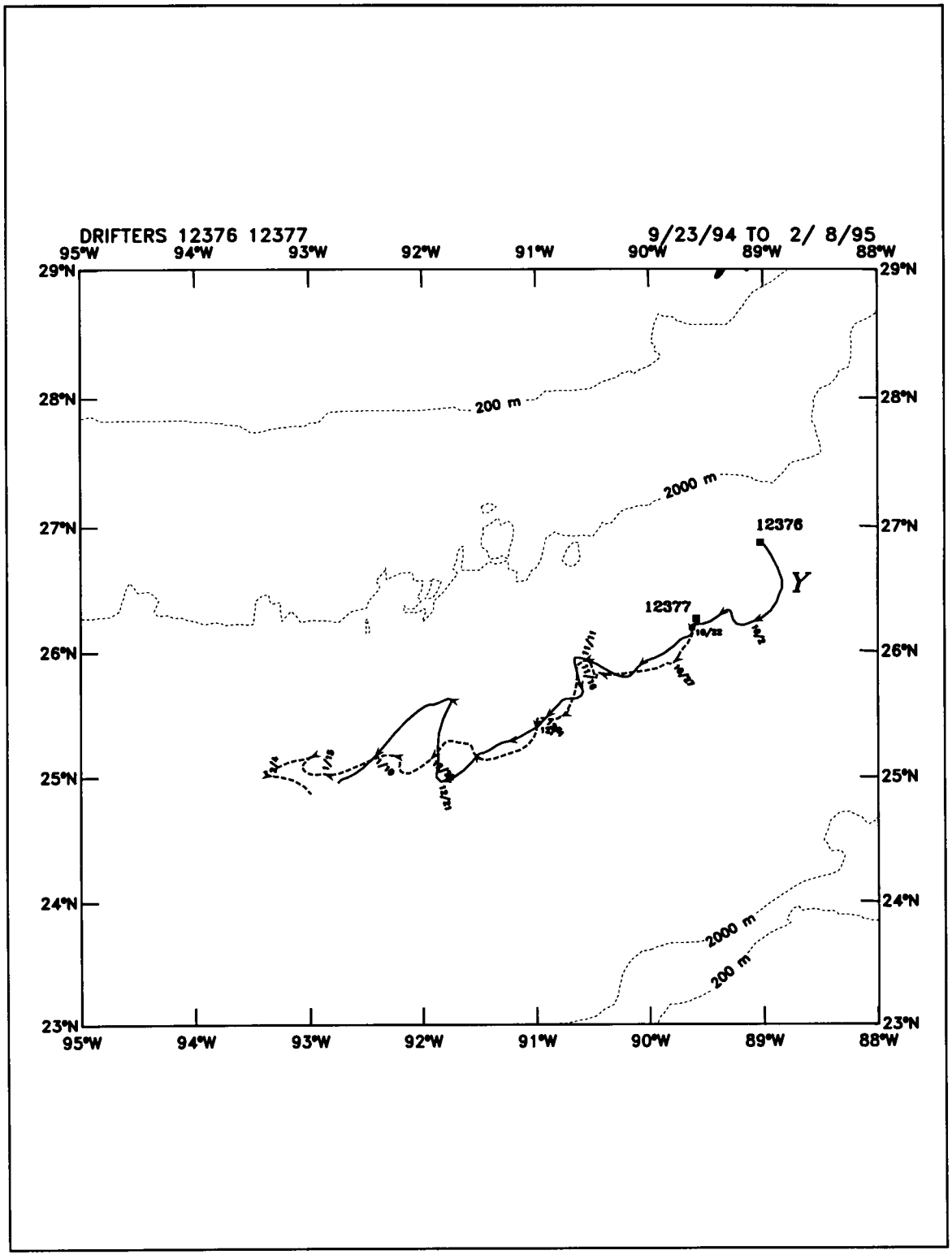

Figure 5.6-1. Tracks of center positions from the ellipse model fits to the paths of drifters 12376 (solid) and 12377 (dashed). Arrow heads are every 10 days.

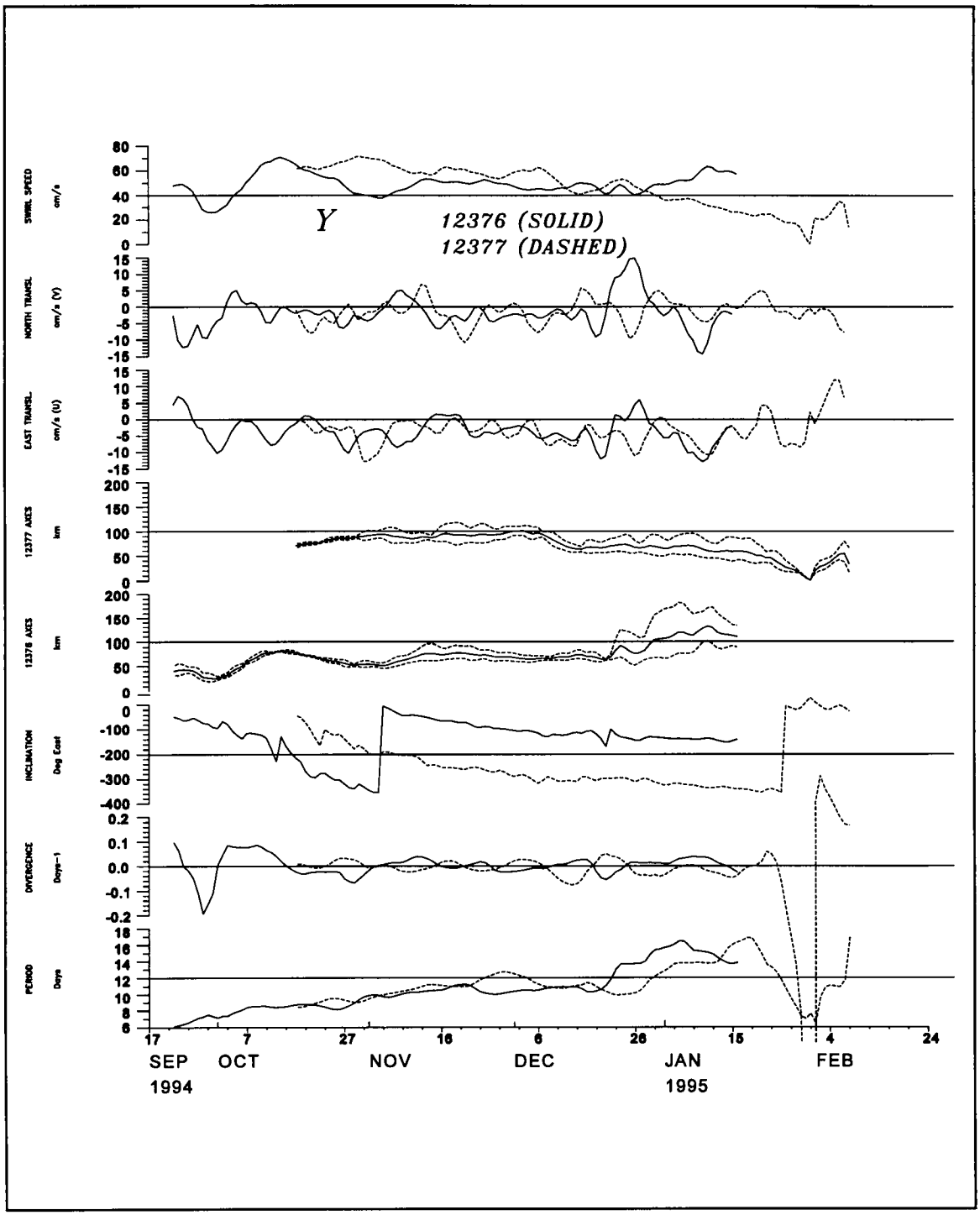

Figure 5.6-2. Time series of ellipse parameters from model fits to the paths of drifters 12376 (solid) and 12377 (dashed). The fourth and fifth panels show the semi-major and minor axes (dashed) and mean radii (solid) for drifters 12377 and 12376, respectively.

hensive surveys, F20SLOPE and F21SQUIRT, about a week apart, showed a strong interaction between eddy Y and another lower slope cyclone.

Figure 5.6-3 shows maps of the 20°C, 15°C and 8°C surfaces, along with appropriately averaged and smoothed AXCP velocities, and daily velocity vectors from drifter 12376 (drogued at 100 m). The eddy was translating westward at less than 4.32 km·day^{-1} during the period of these surveys. Drifter velocities were consistent with the averaged upper layer AXCP velocities and show that solid-body rotation was largely confined to the area inside the 150 m contour for the 20°C surface (Figure 5.6-3a). [The 125 m contour is usually a good estimate of the position of the surface front and maximum surface velocities]. On the north-south AXCP transect, the cyclonic shear zone north of the front was about 50 km wide. The rather weak cyclone on the middle slope was most clearly seen in the 15°C surface, and evidence of cyclonic flows is observed in the northernmost three or four AXCP velocity vectors in Figure 5.6-3c. At the deepest level, the small, and therefore more uncertain, velocities indicate convergence towards the center of the eddy (Figure 5.6-3c). The maximum depth of the 8°C surface was about 725 m and is comparable to eddy V, but is less than the 750 m (estimated) attained by eddy U in October 1992 at a similar early stage (see F04LEDDY station locations in Figure 5.1-1).

The north-south and east-west AXCP transects were to the east and south of eddy Y's center (Figure 5.6-3a). The temperature, and north-south and west-east velocity components for these two transects, are shown in the vertical sections of Figure 5.6-4. The anticyclonic circulation extends down to about 600 m in the north-south section (Figure 5.6-4a, station 7) and about 800 m in the west-east section (Figure 5.6-4b, station 19). The region of near solid-body rotation extends about 50 km from the center, and shoals towards the edges from a maximum depth on the order of 300 to 400 m. There is, however, some indication of more complex structures imposed on these relatively uniform shear profiles at stations 15, 16 and 17. Maximum speeds approached 110 cm·s^{-1} and occurred at about 25 to 50 m below the surface (e.g. stations 5 and 20). Thus, the velocity fields were similar to those observed previously for moderate-sized Loop Current eddies (Cooper et al. 1990; Forristall et al. 1992).

About a month after the October 1994 survey, another slope survey (F20SLOPE) was carried out. Eddy Y was about one degree of longitude further west (Figure 5.6-5a) and was intruding more onto the slope in its northwest quadrant. There was no sign of the upper slope cyclone, though the survey did

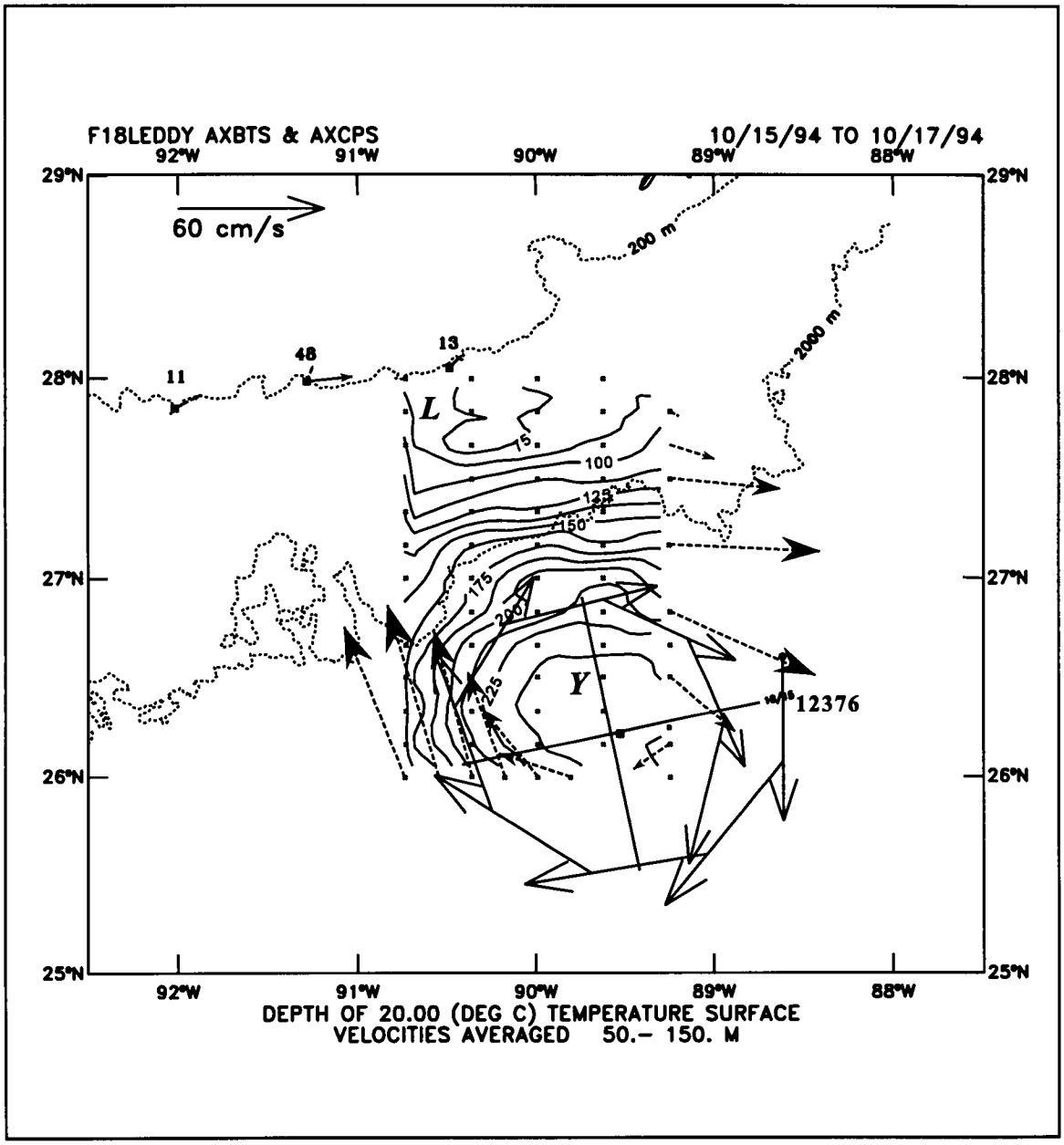

Figure 5.6-3a. Depth of the 20°C temperature surface from the F18LEDDY and F19SEDDY surveys. Daily velocity vectors from drifter 12376 are overlaid beginning October 10, 1994. Dark arrows emanating from crosses are 50-150 m averaged-smoothed velocities from AXCP profiles. Dashed and solid arrows emanating from squares represent the 12-m and 100-m daily mean 40-HLP currents, respectively, from the LATEX A shelf-break moorings for October 16, 1994. The ellipse axes are shown for October 15, 1994 and the solid square in the eddy marks the ellipse center 24 hours earlier.

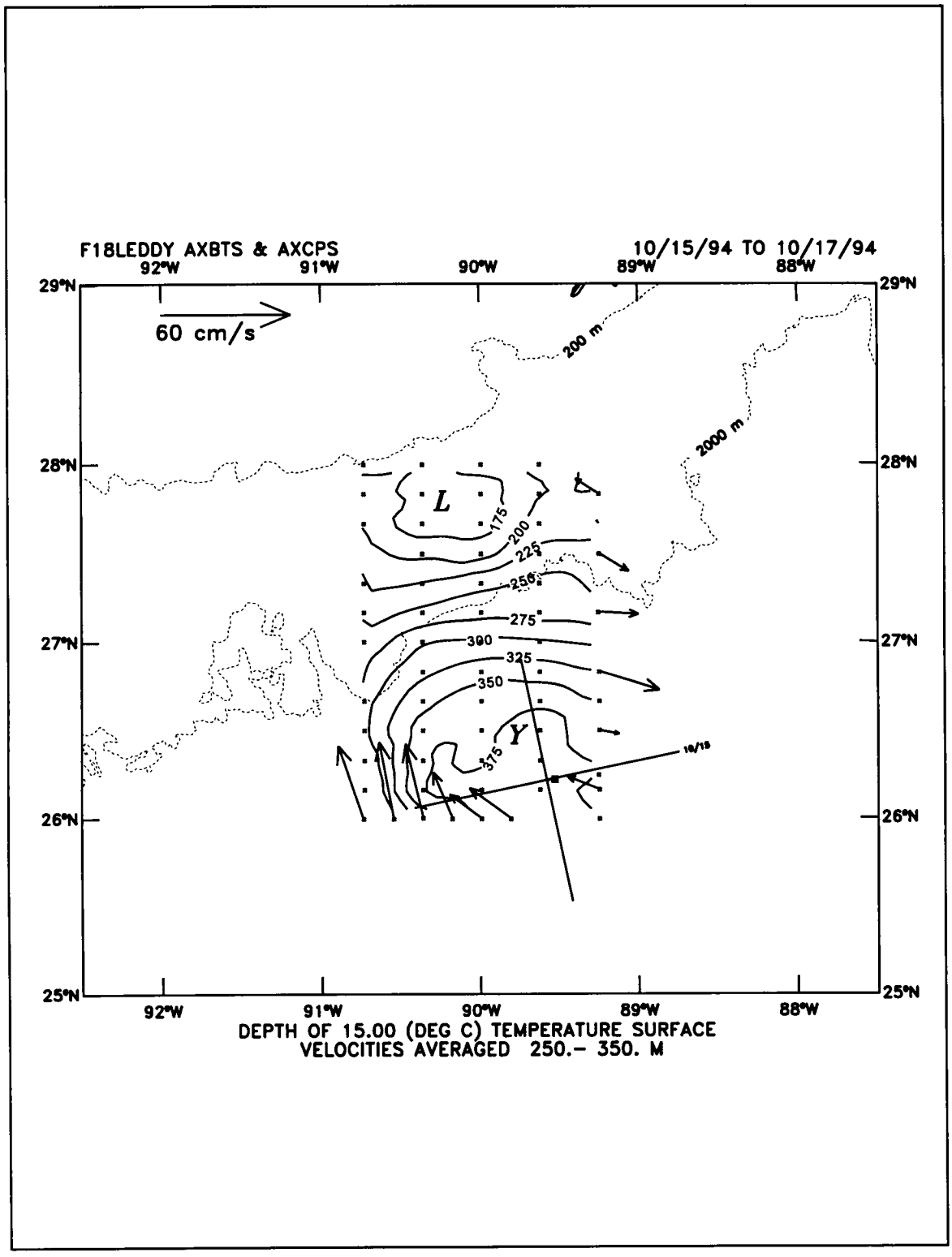

Figure 5.6-3b. Depth of the 15°C temperature surface from the F18LEDDY and F19SEDDY surveys. Dark arrows emanating from crosses are 250-350 m averaged-smoothed velocities from AXCP profiles.

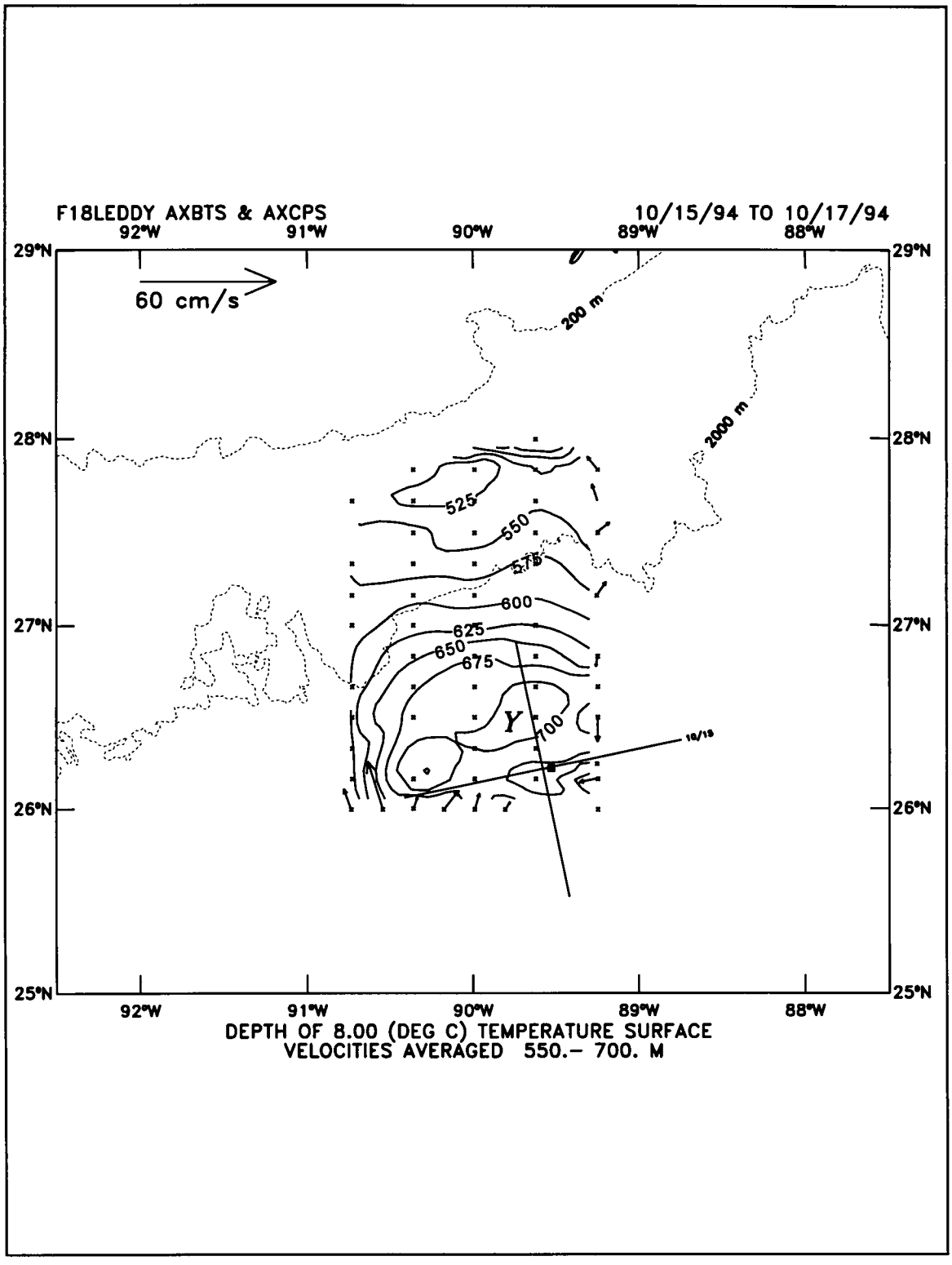

Figure 5.6-3c. Depth of the 8°C temperature surface from the F18LEDDY and F19SEDDY surveys. Dark arrows emanating from crosses are 550-700 m averaged-smoothed velocities from AXCP profiles.

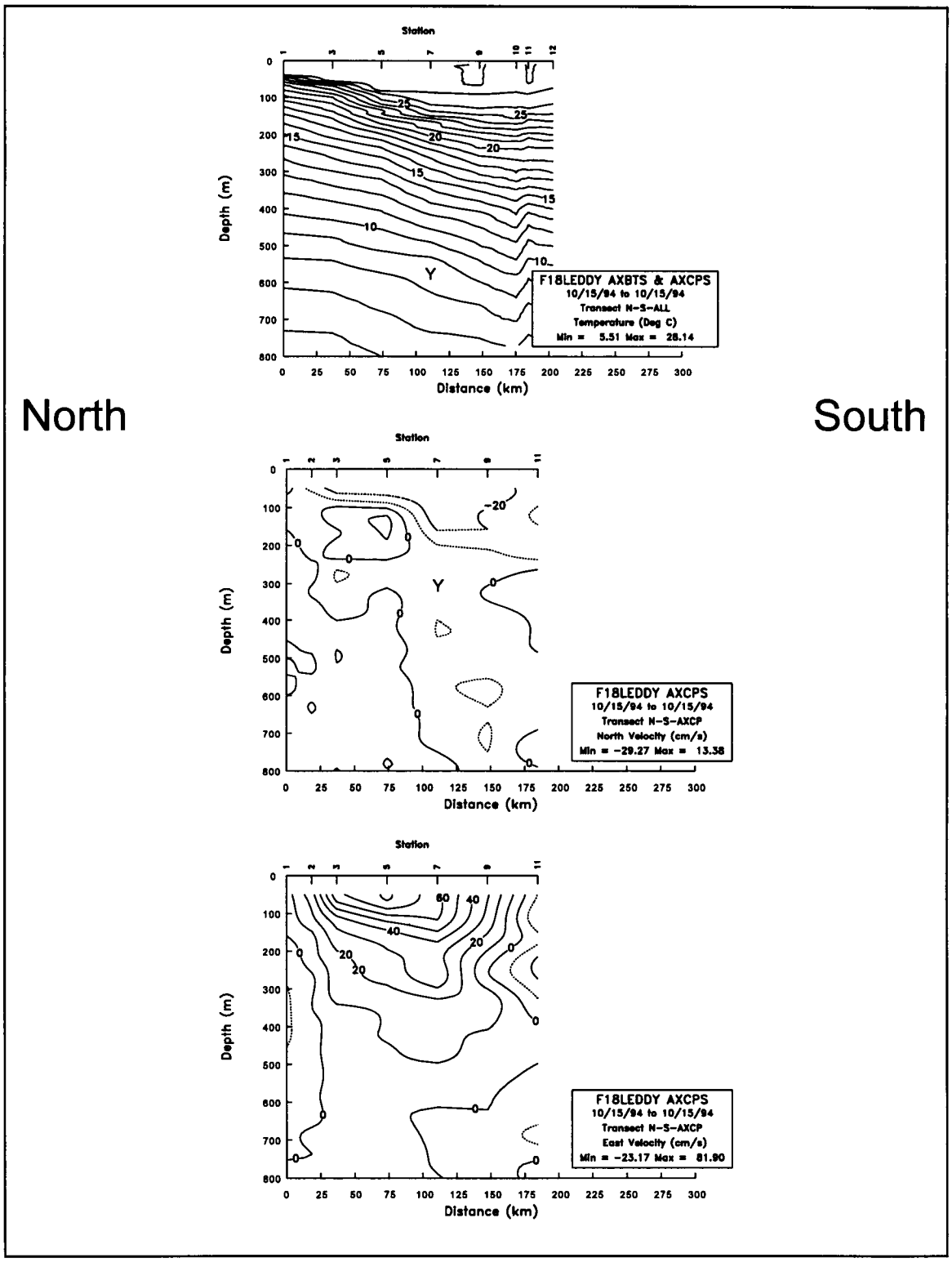

Figure 5.6-4a. North-south vertical-section plot of temperature (top), north velocity (middle) and east velocity (bottom) from smoothed AXCP profiles from F18LEDDY survey (stations 1 to 12).

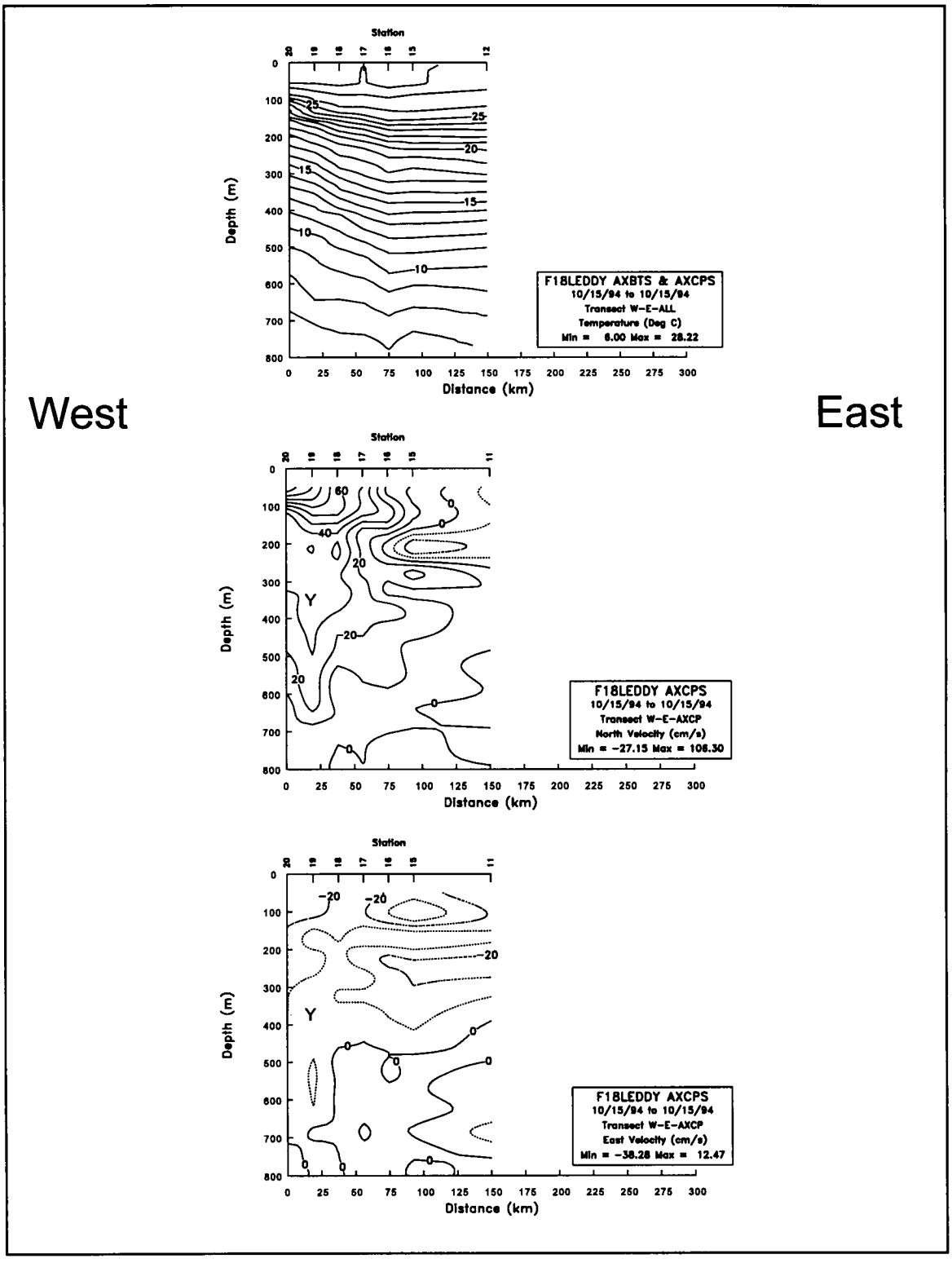

Figure 5.6-4b. West-east vertical-section plot of temperature (top), north velocity (middle) and east velocity (bottom) from smoothed AXCP profiles from F18LEDDY survey (stations 20 to 11).

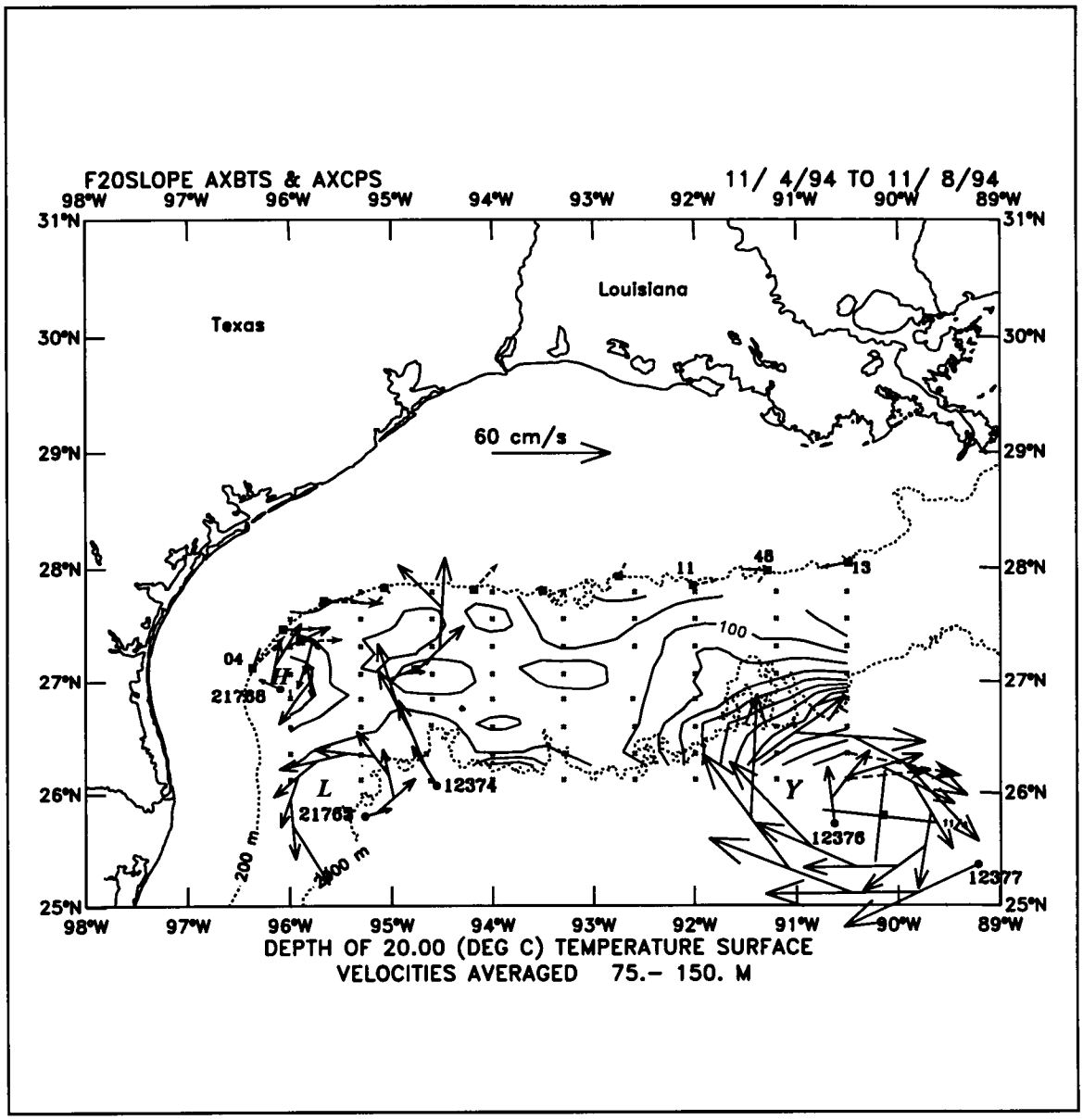

Figure 5.6-5a. Depth of the 20°C temperature surface from the F20SLOPE survey. Daily velocity vectors from drifters 12374, 12376 and 12377, and SCULP drifters 21763 and 21768 are overlaid beginning November 1, 1994. Dashed arrows emanating from crosses are 75-150 m averaged-smoothed velocities from AXCP profiles. Dashed and solid arrows emanating from squares represent the 12-m and 100-m daily mean 40-HLP currents, respectively, from the LATEX A shelf-break moorings for November 4, 1994. The ellipse axes are shown for this same date and the solid square in the eddy marks the ellipse center 24 hours earlier.

not extend east of 90.5°W longitude. However, the deeper temperature surfaces (Figures 5.6-5b, c) reveal that a strong cold cyclonic anomaly (C2) was present at the base of the slope (near 26.2°N latitude, 92.8°W longitude), partially blocking the westward translation of eddy Y. The northward distortion of the eddy's 20°C surface (e.g. 100 m contour) may have been caused by the upper advective velocities of the cyclone. There was a complex field of two cyclones and an anticyclone in the western part of the slope. These will be discussed in Section 5.7.

The next survey (F21SQUIRT), about a week later, used closely spaced stations and 16 AXCPs, and concentrated on the interaction between eddy Y and its adjacent cyclone. This survey achieved some of the most detailed measurements of a cyclone-anticyclone interaction in the Gulf of Mexico to date. Figure 5.6-6 shows the 20°C, 15°C and 8°C surfaces overlaid with appropriately averaged velocities from AXCPs. Eddy Y had moved further west and the major axis had rotated clockwise from the east-west direction a week earlier. Strong near-surface velocities were observed between the cyclone (C2, centered at about 26.5°N latitude, 93°W longitude) and eddy Y (Figure 5.6-6a). There was a convergence in the flows towards the east side of the cyclone. The transition between the cyclonic and anticyclonic shear zones of the warm eddy and the cyclone occurred approximately on the 100 m contour of the 20°C surface. The transition, with a minimum in velocity, moved eastward with increasing depth, corresponding to the general bowl shape of the temperature surfaces (Figures 5.6-6b and c). As observed for warm anticyclones and expected from geostrophy, eddy Y's velocities decreased in magnitude with increasing depth. In the cyclone, the currents maintained their strength, so at depth, velocity magnitudes were greater than in the warm eddy. A comparison of the velocity vectors in the cyclone between the 100 m and 300 m depths (Figures 5.6-6a and b) shows little change in magnitude.

The center of the cyclone was well defined in the 15°C and 8°C surfaces and coincided with one of the AXCP profiles (station 149). The velocities suggest that the center was moving northward at about 25.9 $km \cdot day^{-1}$ (at the 20°C and 15°C levels), and at about half that speed at the 8°C level. The implication is that strong surface-layer velocities (of eddy Y) were advecting the cyclone northward onto the slope. If the position of the center of the cyclone is compared with the survey a week earlier (Figure 5.6-5c), then indeed, the center had moved 50 km to the north, and thus at a speed of approximately 5.18 $km \cdot day^{-1}$. This compares favorably with the 450 m to 600 m depth-averaged velocity from station 149 (Figure 5.6-6c). The northward cyclone movement is also less

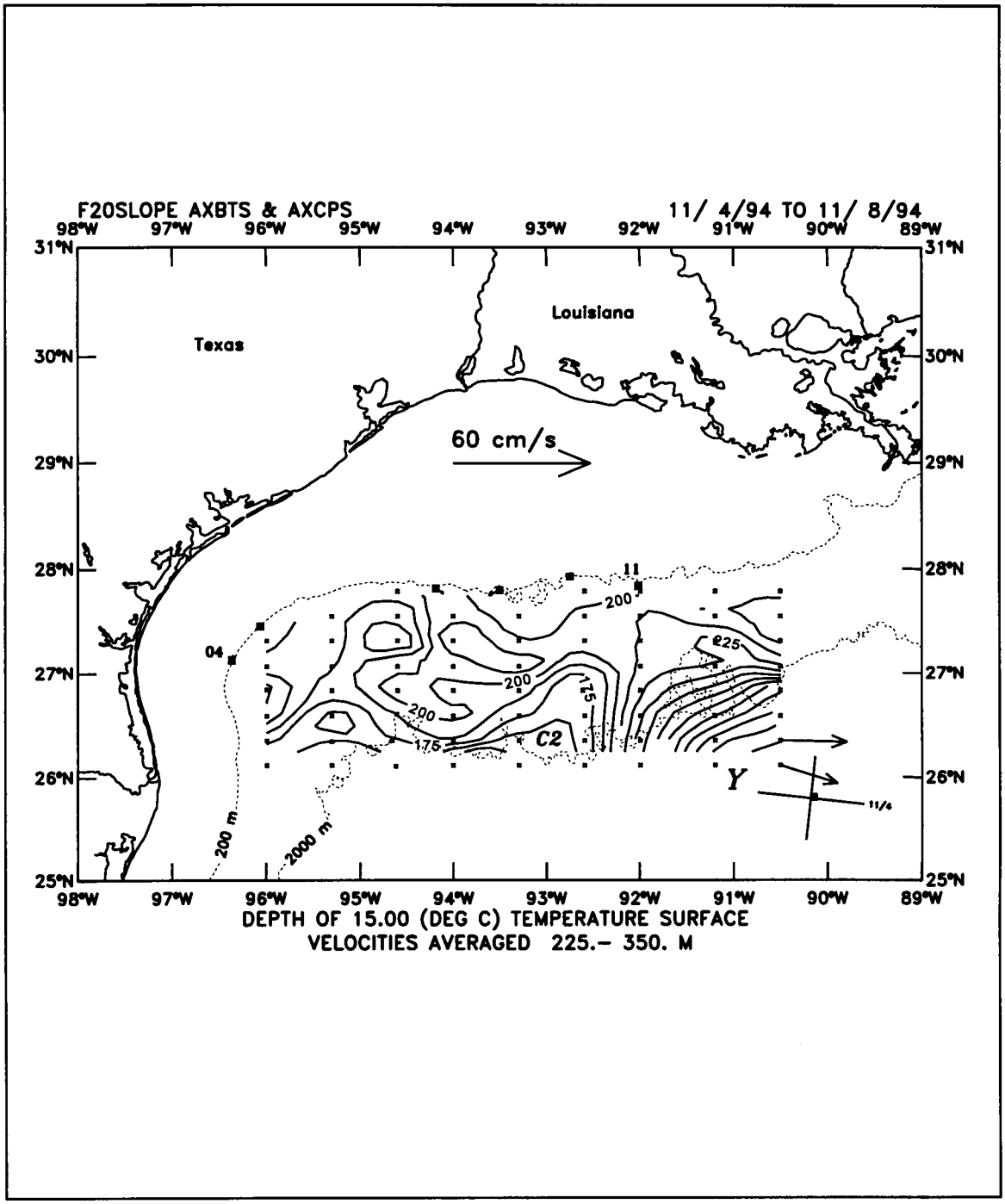

Figure 5.6-5b. Depth of the 15°C temperature surface from the F20SLOPE survey. Dark arrows emanating from crosses are 225-350 m averaged-smoothed velocities from AXCP profiles. Arrows emanating from squares represent bottom level (~200 m) daily mean 40-HLP currents from the LATEX A shelf-break moorings for November 4, 1994.

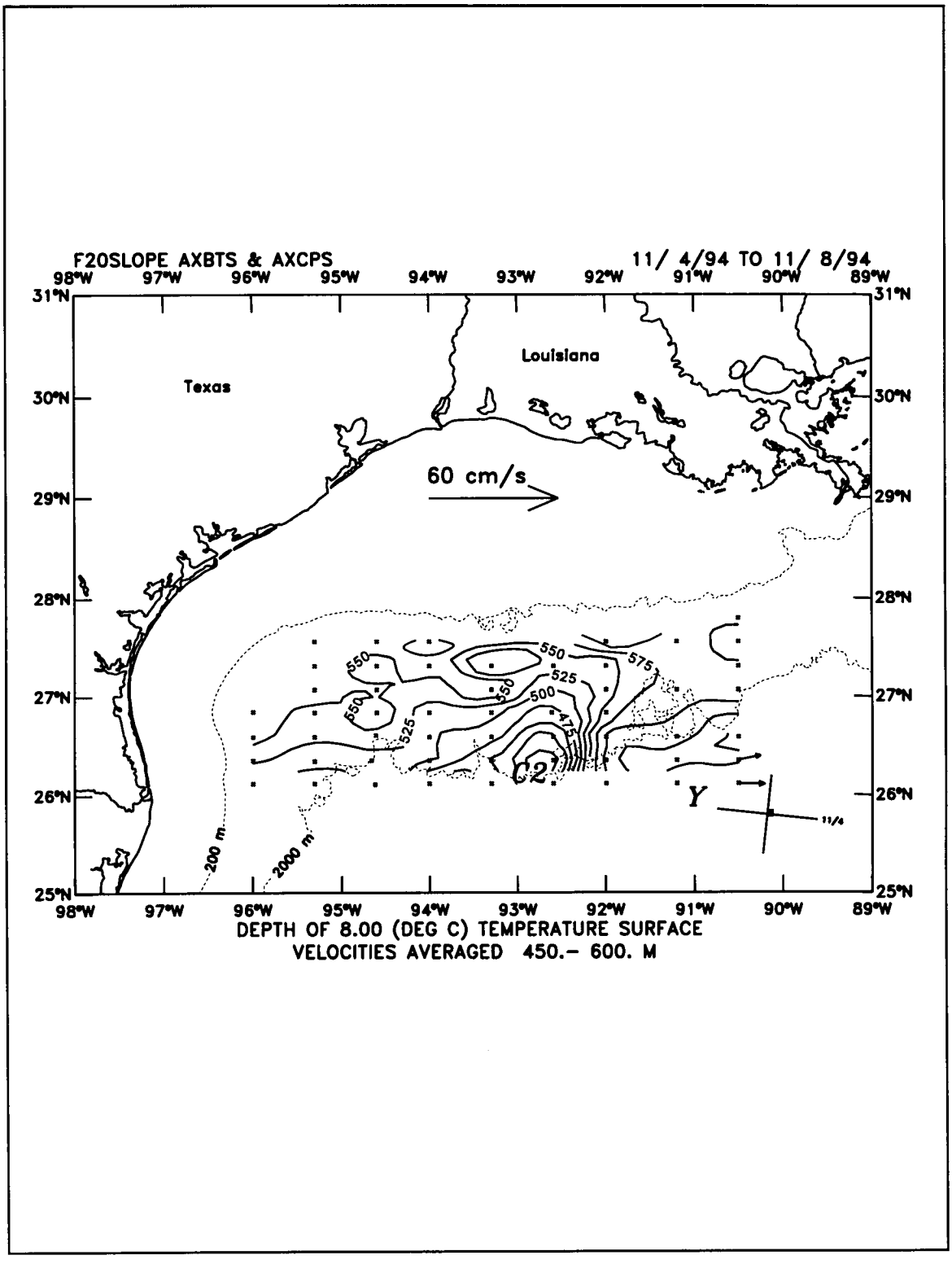

Figure 5.6-5c. Depth of the 8°C temperature surface from the F20SLOPE survey. Dark arrows emanating from crosses are 450-600 m averaged-smoothed velocities from AXCP profiles.

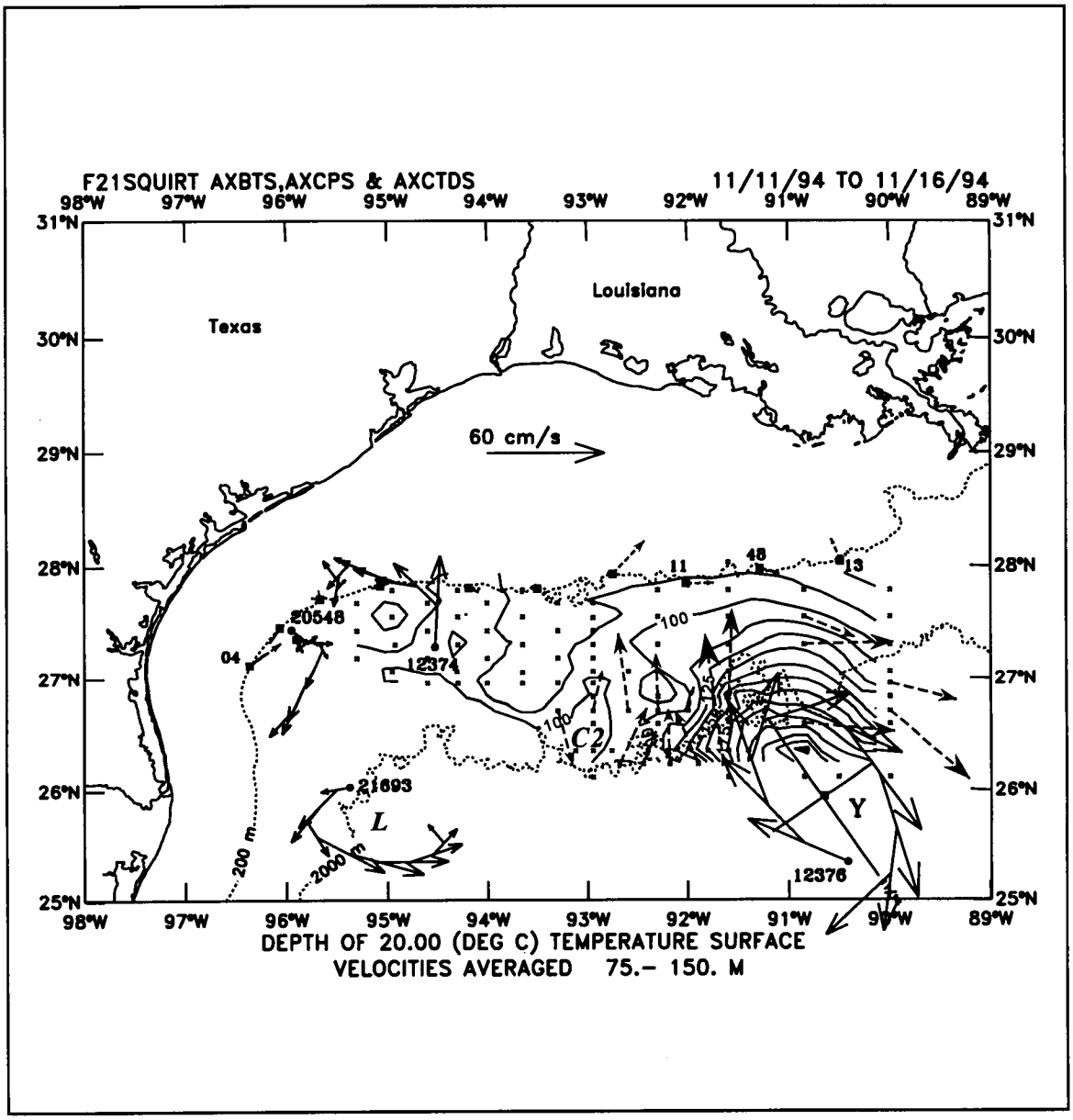

Figure 5.6-6a. Depth of the 20°C temperature surface from the F21SQUIRT survey. Daily velocity vectors from drifters 12374 and 12376, and SCULP drifters 20548 and 21693 are overlaid beginning November 9, 1994. Dashed arrows emanating from crosses are 75-150 m averaged-smoothed velocities from AXCP profiles. Dashed and solid arrows emanating from squares represent the 12-m and 100-m daily mean 40-HLP currents, respectively, from the LATEX A shelf-break moorings for November 14, 1994. The ellipse axes are shown for this same date and the solid square in the eddy marks the ellipse center 24 hours earlier.

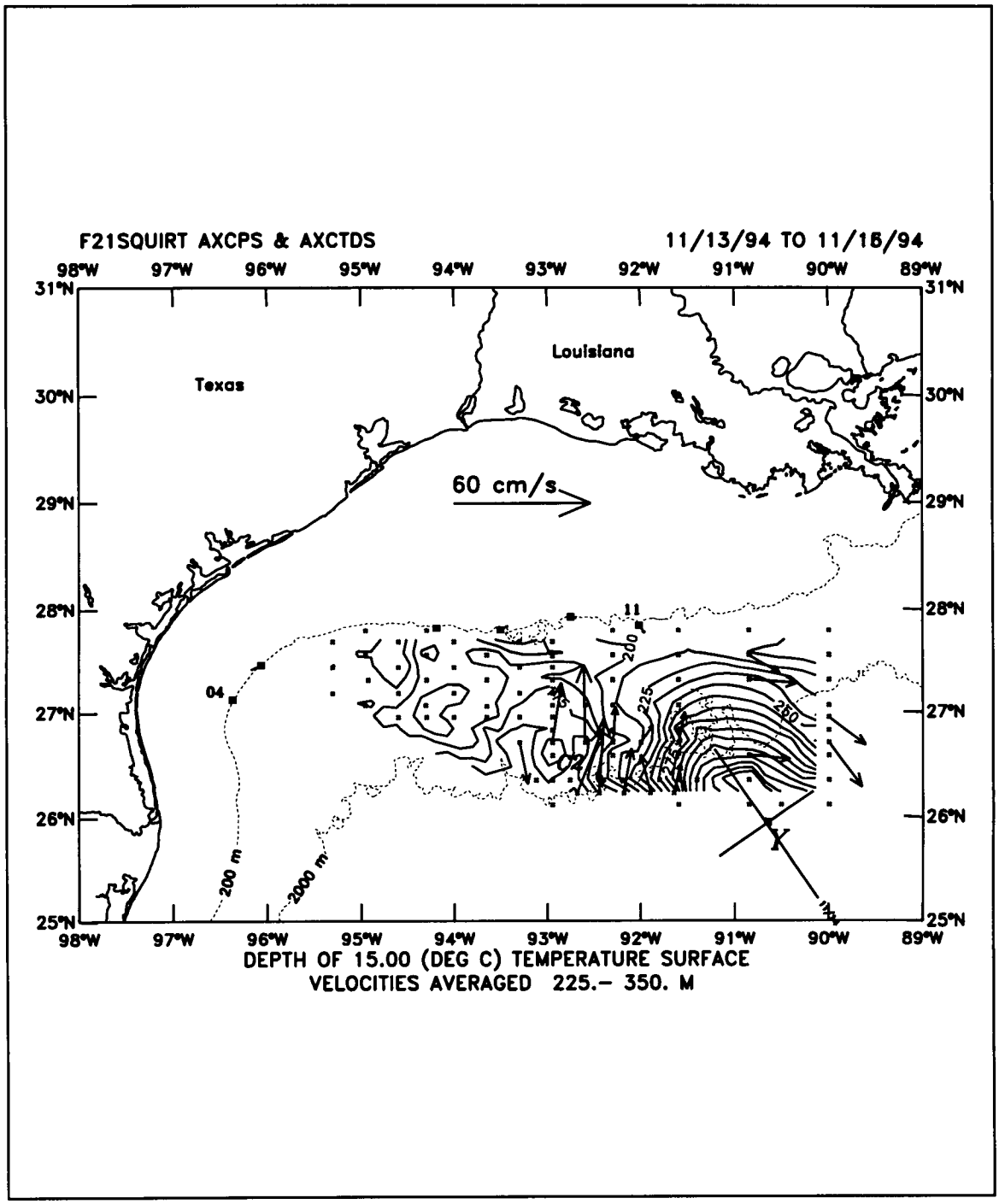

Figure 5.6-6b. Depth of the 15°C temperature surface from the F21SQUIRT survey. Dark arrows emanating from crosses are 225-350 m averaged-smoothed velocities from AXCP profiles. Arrows emanating from squares represent bottom level (~200 m) daily mean 40-HLP currents from the LATEX A shelf-break moorings for November 14, 1994.

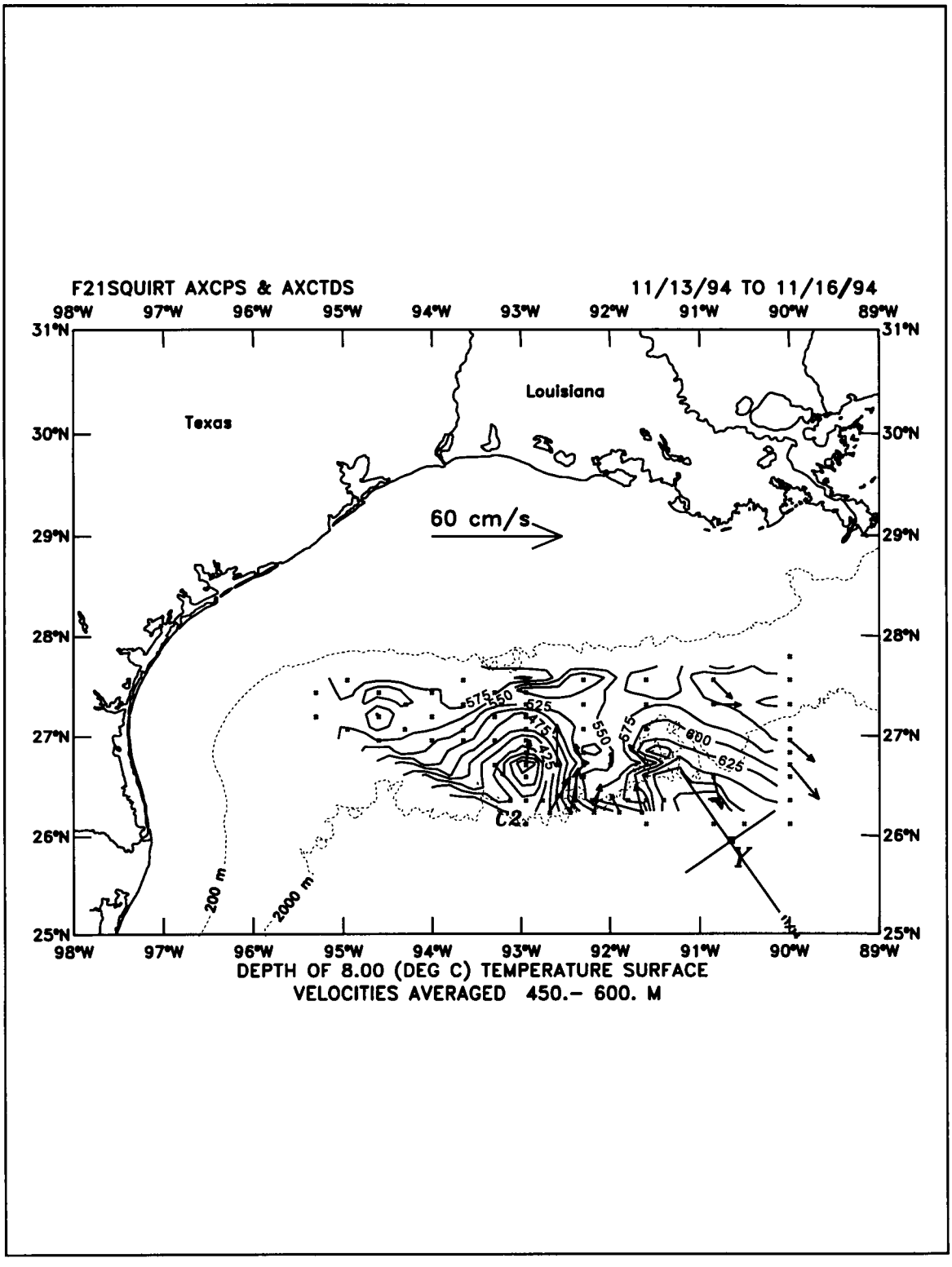

Figure 5.6-6c. Depth of the 8°C temperature surface from the F21SQUIRT survey. Dark arrows emanating from crosses are 450-600 m averaged-smoothed velocities from AXCP profiles.

than the clockwise rotation of the eddy's major axis, as can be seen by comparing the positions of the model-fitted ellipse axes from drifter 12376 in Figures 5.6-5 and 5.6-6, respectively. The cyclone is situated at approximately the westward extremity of the semi-major axis of the elliptical eddy Y in the earlier (November 4, 1994) survey. It is also noted that the deeper temperature gradients were stronger on the north side than on the south side of the cyclone. Significantly steeper gradients in the direction of propagation are not observed for Loop Current eddies in deep water. Therefore, it is expected that the shoaling bathymetry is contributing to this effect.

The existence of two east-west AXCP transects through the cyclone and into the western part of eddy Y permits a comprehensive look at the velocity and temperature fields down to depths greater than the 800 m limit of AXBTs. Vertical temperatures and northward velocity components are contoured for these two vertical sections in Figure 5.6-7. On the southernmost section (Figure 5.6-7b), which only samples the southeast quadrant of the cyclone, velocities are relatively uniform below 50 m to depths of ~800 m with, however, a distinct subsurface maximum (~35 $cm \cdot s^{-1}$) between 200 and 300 m depth. The other section (Figure 5.6-7a) is north of the center of eddy Y but close to the center of the cyclone, as indicated by the 8°C isotherm (Figure 5.6-6c). In this section, the influence of the anticyclone's velocities is further from the center of the cyclone than in the southern transect. There are relatively depth-independent flows up to about 50 km from the center, with a distinct subsurface jet-like structure with a maximum of ~40 $cm \cdot s^{-1}$ at a depth of 150 m at station 148.

Higher velocity currents in the cyclone were above the 600 m to 700 m level, but weaker currents (<10 $cm \cdot s^{-1}$) were observed to 1200 m depth (there is some uncertainty in deriving absolute deeper currents from AXCPs because of the way the unknown barotropic component is estimated and removed from the velocity profiles [see Section 3.3.3]). In this vertical section, eddy Y's velocities were less than 10 $cm \cdot s^{-1}$ below about 300 m. The zero-velocity contour was displaced westward of station 149, where the deep isotherms were shallowest. The cyclone was moving northward around the periphery of the anticyclone at speeds similar to those measured at station 149 below 600 m, and at neither the 17 to 28 $km \cdot day^{-1}$ speeds measured above 600 m, nor at higher speeds related to direct advection by the surface layer velocities of the outer parts of the anticyclone. However, the interaction of the two eddies clearly caused the cyclone to move northward. These data also show that the energetic currents in a cyclone are at 600 m to 800 m depth, which is comparable to the central parts

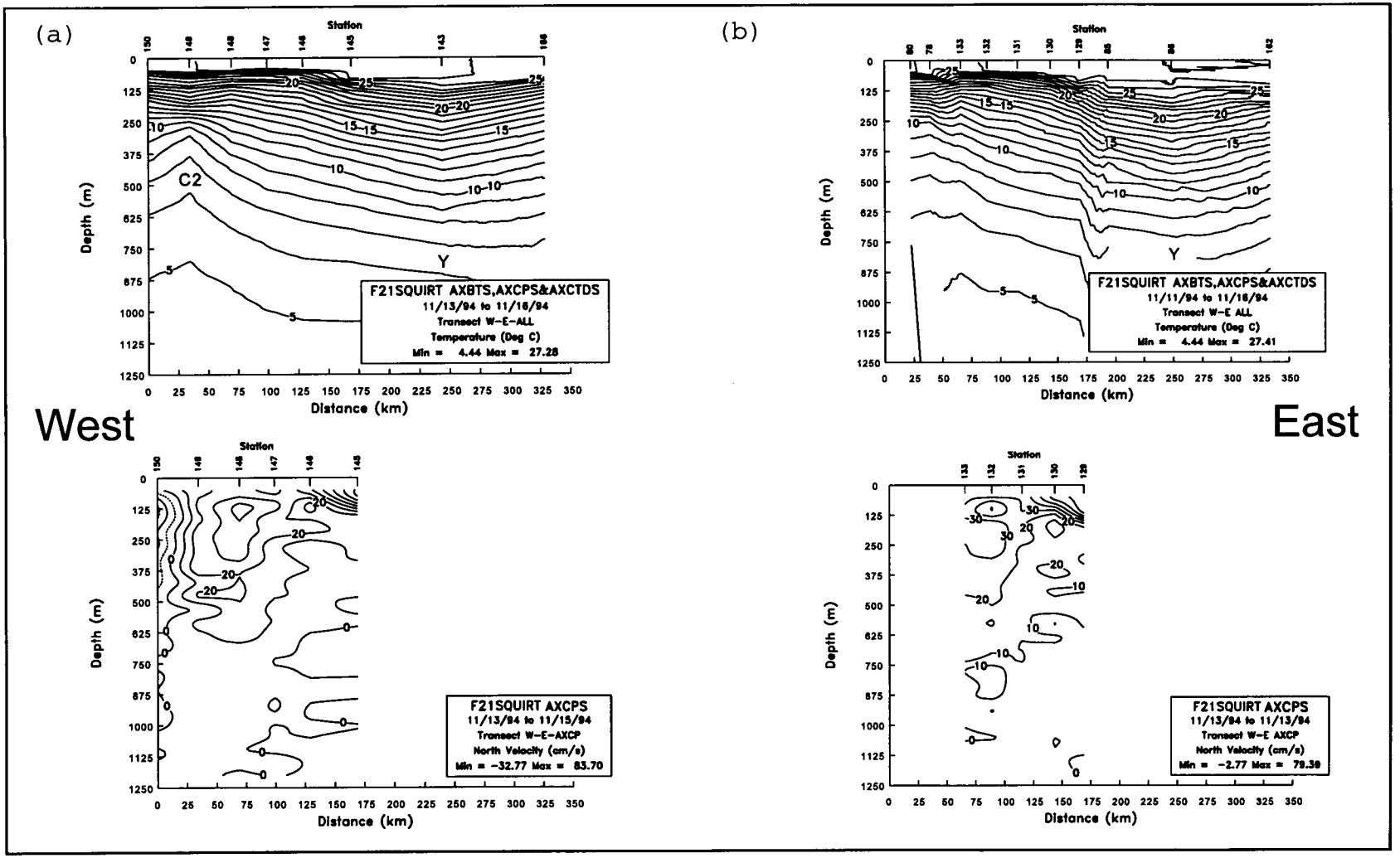

Figure 5.6-7. Vertical sections of temperature and north velocity component from the F21SQUIRT survey for (a) ~26.75°N latitude [stations 150 to 167] and for (b) ~26.25°N latitude [stations 80 to 162].

of a Loop Current eddy. In a study of a small cyclone (diameter ~20 km) on the periphery of a Gulf Stream warm-core ring (82-B) in the northwest Atlantic, Kennelly et al. (1985) estimated that the ringlet was advected around the anticyclone at about 20 $cm \cdot s^{-1}$. This is four times the estimate from the changes in the center position of this larger Gulf of Mexico cyclone.

Figure 5.6-7 shows that above 200 m the isotherms were relatively level in both sections. A more detailed examination of the upper layer temperature structure shows that the upper layer isotherms were slightly depressed and that the coldest temperatures in the upper 200 meters were found about one station east of the center position given by the 8°C or 10°C isotherms (Figure 5.6-8). This displacement of the weak upper-layer cold dome towards eddy Y indicates a rather complex interaction, with eddy Y water possibly being mixed into the cyclone's upper layers. On the other hand, the slightly depressed isotherms could also indicate downwelling in the center of the cyclone and therefore convergence of the upper layer azimuthal flows. This latter conjecture is more likely because of the isolated nature of the warm patch at the center of the cyclone. The apparent tilt of the cyclone's vertical axis, as shown by these temperature sections, is not observed in the vertically coherent structures of the velocity fields. There is some indication of a small eastward tilt in the 0 $cm \cdot s^{-1}$ contour in Figure 5.6-7a. Thus, the dynamics of the interaction of a westward-propagating Loop Current eddy with a cyclone in deep water or on the lower slope are not clear. It is noted, however, that the interaction of eddy W_N with a lower-slope cyclone also appeared to tilt the axis of the cyclone away from the eddy.

5.7 Cyclones: Further Examples

5.7.1 Introduction

The previous sections have discussed the behavior of the major Loop Current eddies that moved into the western Gulf during the period of the LATEX program. A number of the surveys captured some aspects of the interaction of these eddies with cyclones on the lower slope. There were also extensive surveys of the slope during December 1993 and May 1994, which were able to map at least one vigorous cyclone during each period. In these cases there were no obvious interactions with anticyclones and/or other smaller eddies. Because of the similarities to the eddy Y cyclone discussed immediately above, the May 1994 surveys (F15SLOPE and F16SQUIRT) will be discussed first.

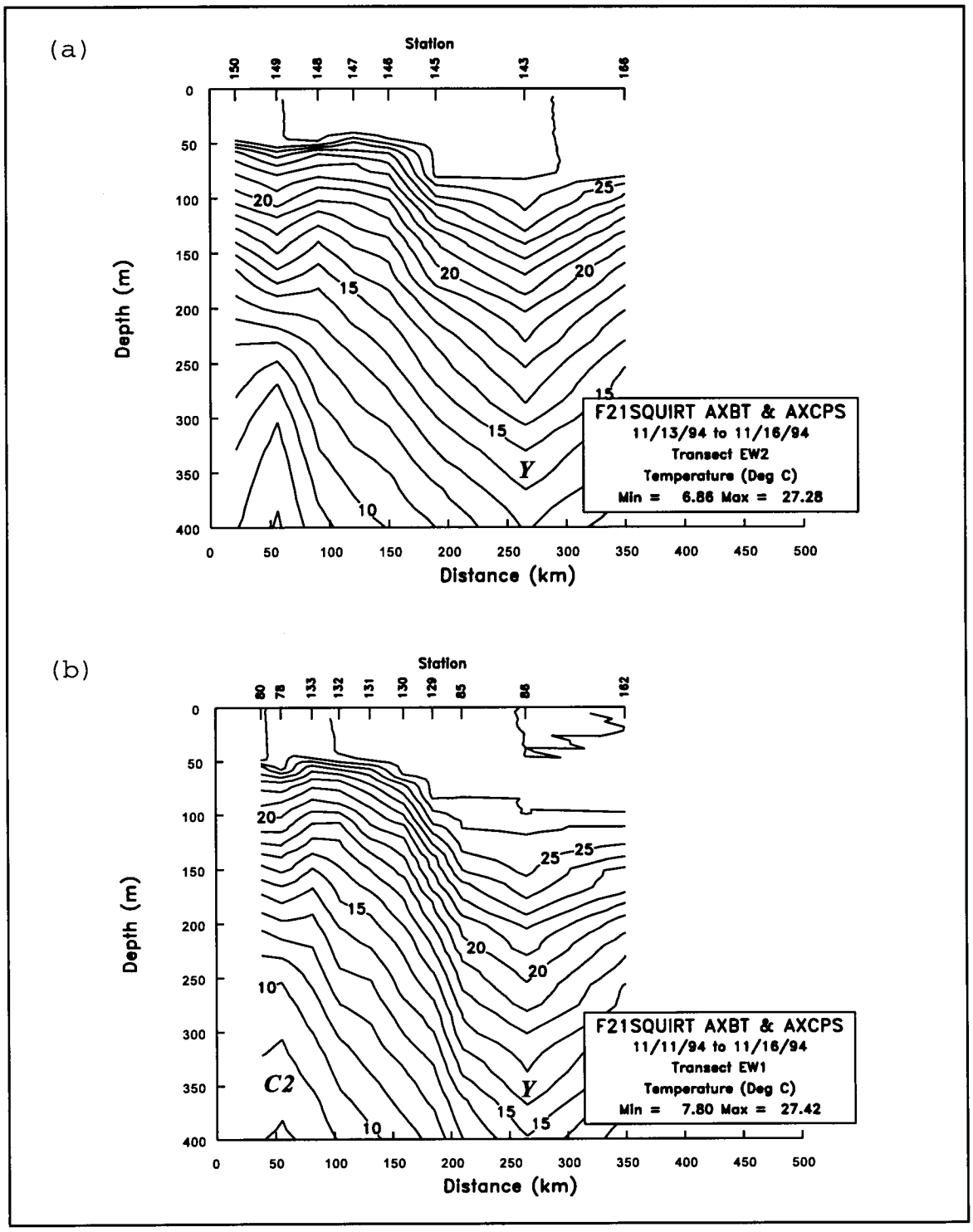

Figure 5.6-8. Expanded vertical sections of temperature (plotted to 400 m depth) from the F21SQUIRT survey for (a) ~26.75°N latitude [stations 150 to 166] and (b) ~26.25°N latitude [stations 80 to 162].

5.7.2 May 1994 Surveys

Figure 5.7-1 shows plots of the 20°C, 15°C and 8°C temperature surfaces overlaid with appropriate velocity vectors from drifters, AXCPs, and shelf-break current meters. A vigorous cyclone (C3) is centered on the 2000 m isobath at 94°W longitude with two small warm eddies on the upper slope, and possibly two more at the shelf-break, and a large deep-water anticyclone to the southwest (drifter 20500). Because of its size and the elapsed time since it was last definitively observed (December 1993), at 91°W longitude, the latter is thought to be eddy X approaching the Mexican slope. Typical Loop Current eddy propagation speeds would allow eddy X to be in this position at this time. The cyclone entrained a number of SCULP drifters which remained with it for a few circuits. Ten days of velocity vectors show that the cyclone center given by the drifters was a little west of the north-south AXCP transect. However, the cyclonic eddy (C3) appears to have moved southeastward, in the general direction of the flow of the deep water anticyclone. The velocity vectors also indicate a broad band of enhanced flow between the cyclone and a small anticyclone to the northeast, which appears to have rather weak surface currents.

The two slope anticyclones had rather different depth structures. The one to the east had greater displacements in the 15°C surface, whereas the one in shallower water to the west had greater displacements in the 8°C surface. The latter eddy also appears to have been more diffuse, with the deeper parts displaced southeast of the surface layers. However, a lack of resolution in the spacing of the AXBTs may be distorting the picture.

One-day averaged 40-HLP currents from the LATEX A shelf-edge moorings are shown in Figure 5.7-1a for the same day (May 24, 1994) as the AXCP survey. Surface flows were generally eastward, with differing magnitudes ranging from about 6 to 25 $cm \cdot s^{-1}$. The direction and magnitudes are consistent with the effects of the three small upper-slope anticyclones shown in the 20°C temperature surface between 93°W and 96°W longitude. These anticyclones are also indicated by drifter tracks, one of which (drifter 21652) is shown in Figure 5.7-1a. Thus, this particular lower-slope cyclone (C3) could not influence the shelf-break currents, because of the presence of the smaller upper-slope anticyclones. This is similar to the slope cyclone (C1) that interacted with eddy W_N in August 1993 (Figures 5.4-2 and 5.4-3). That cyclone also appeared to have minimal influence on the shelf-break currents. Indeed, it could be argued that the shelf-break currents were part of a coherent shelf gyre, as postulated by Cochrane and Kelly

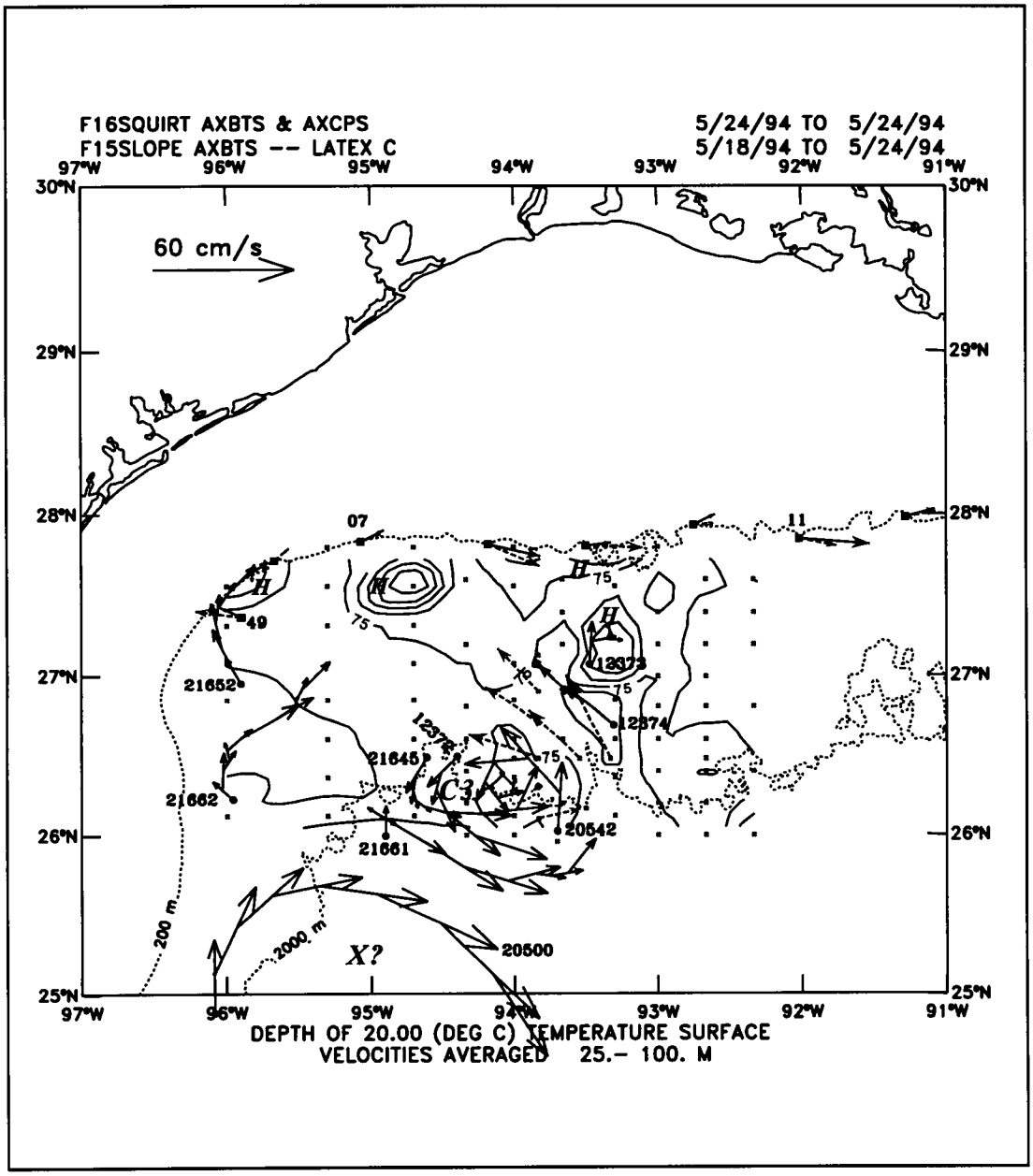

Figure 5.7-1a. Depth of the 20°C temperature surface from the F15SLOPE and F16SQUIRT surveys. Daily velocity vectors from drifters are overlaid. SCULP drifters (20500, 20542, 21645, 21652, 21661 and 21662) begin on May 20, 1994 and LATEX drifters (12372, 12373 and 12374) begin on May 27, 1994. Dark arrows emanating from crosses are the 25-100 m averaged-smoothed velocities from AXCP profiles. Dark and light arrows emanating from squares represent the 12-m and 100-m, respective daily mean 40-HLP currents from the LATEX A shelf-break moorings for May 24, 1994.

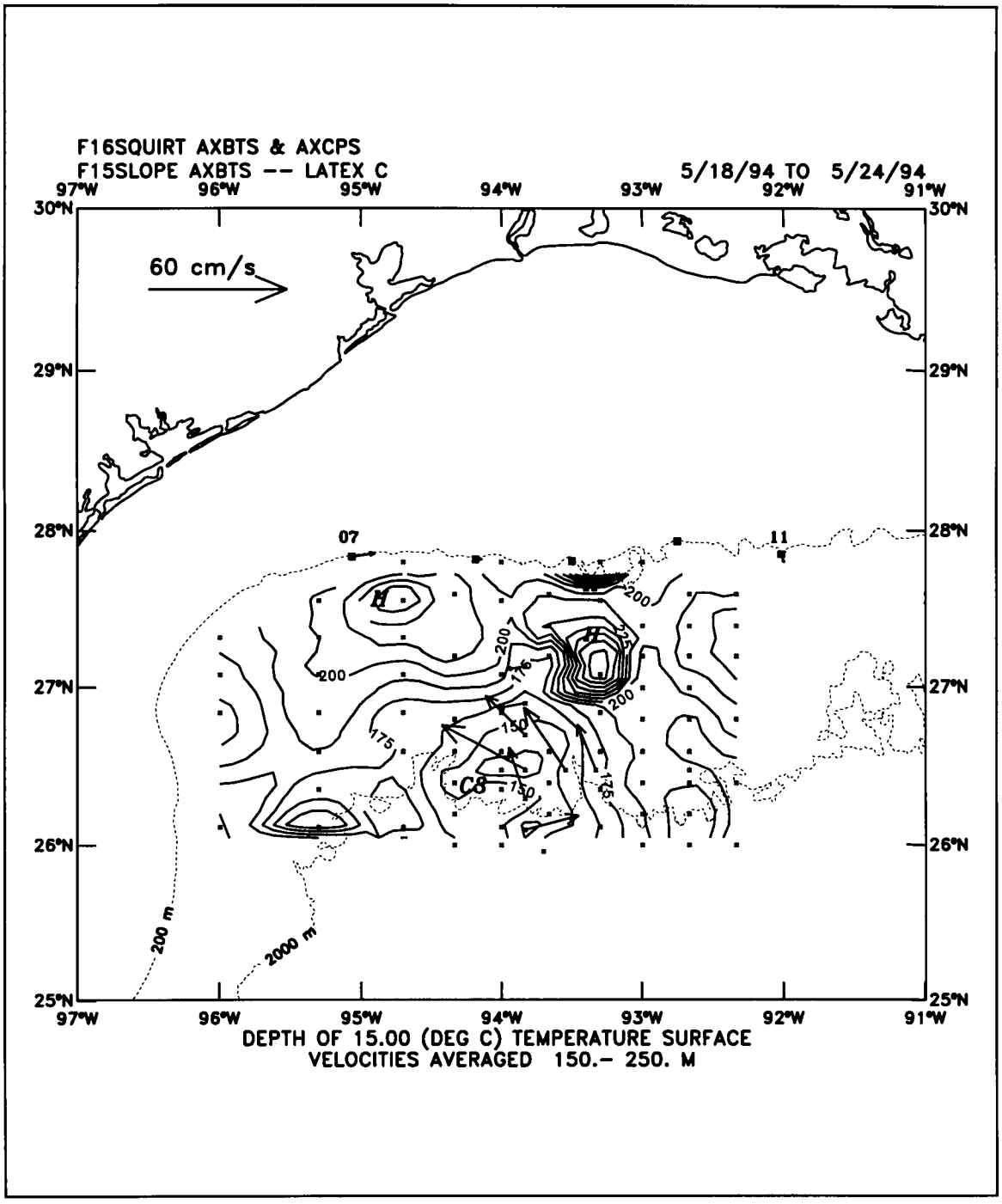

Figure 5.7-1b. Depth of the 15°C temperature surface from the F15SLOPE and F16SQUIRT surveys. Dark arrows emanating from crosses are 150-250 m averaged-smoothed velocities from AXCP profiles. Arrows emanating from squares represent bottom level (~200 m) daily mean 40-HLP currents from the LATEX A shelf-break moorings for May 24, 1994.

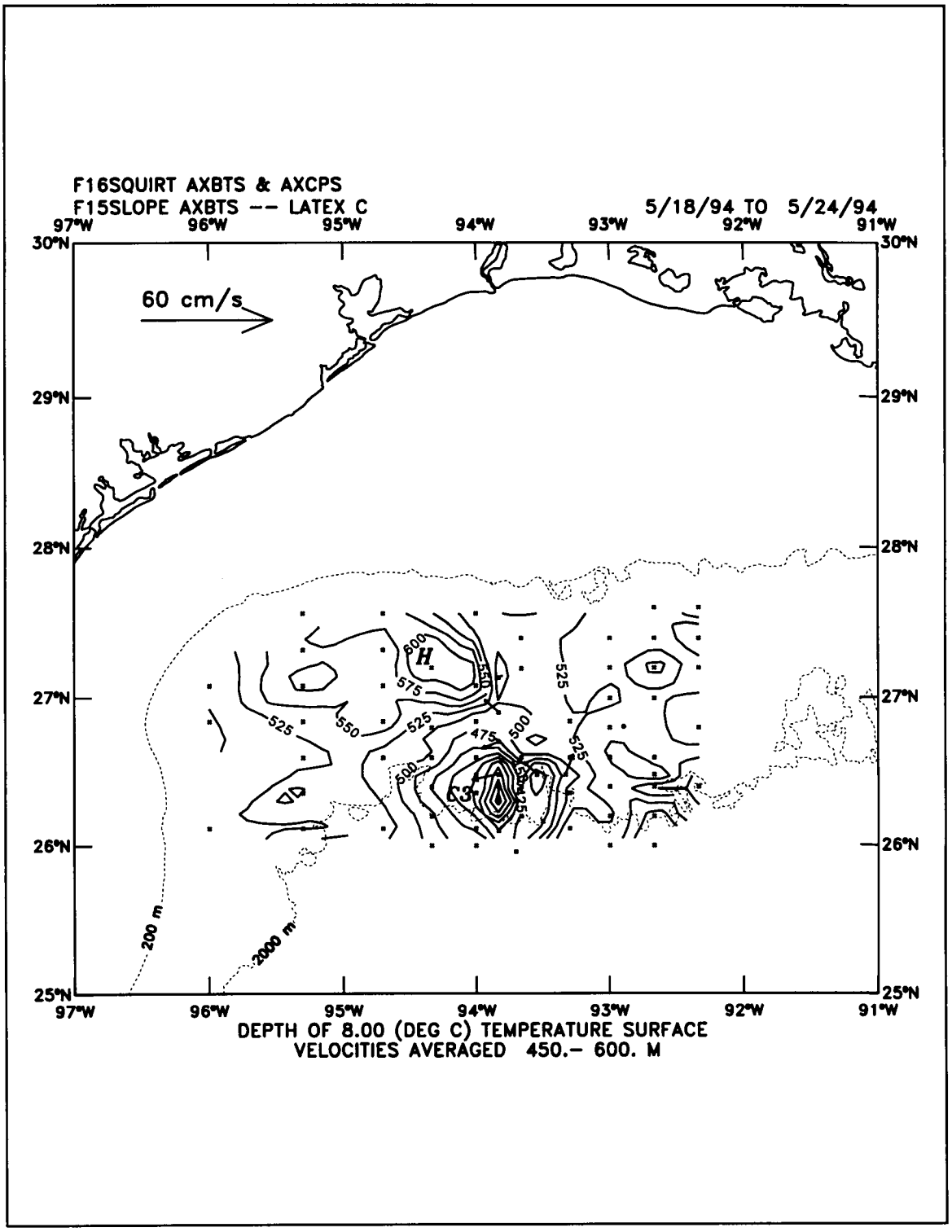

Figure 5.7-1c. Depth of the 8°C temperature surface from the F15SLOPE and F16SQUIRT surveys. Dark arrows emanating from crosses are 450-600 m averaged-smoothed velocities from AXCP profiles.

(1986). However, more evidence will be presented later that the slope eddies were strongly forcing the observed shelf-break current field.

The north-south transect of AXCPs that passed almost through the center of the cyclone (C3) permits a detailed examination of the temperature and velocity structure, similar to that for transects for eddy Y (Figures 5.6-7 and 5.6-8). The results for this cyclone are given in Figure 5.7-2. The azimuthal velocities (Figure 5.7-2c) reveal a very similar distribution to those in Figure 5.6-7. The region of solid-body rotation and small vertical shears shows a horizontal extent of about half that of eddy Y's cyclone (radius ~25 km), and extends to 800 m to 1000 m depth. Thus, this cyclone was more compact than eddy Y's cyclone, but the deep isotherms (5°C) were about 100 m shallower. Maximum velocities were about the same (~40 $cm \cdot s^{-1}$), as was the subsurface maximum and the jet-like structure at the outer edge (station 67) of the cyclone. The 1500 m depth of the AXCP drops permits examination of the deep temperature structure and shows that the cyclone still had relatively strong gradients and a cold core at 1500 m, even though velocities were quite weak below 1000 m depth. The expanded-scale temperature plot (Figure 5.7-2b) shows slight depressions of the isotherms above the center in the upper layers, similar to the cyclone in F21SQUIRT (Figure 5.6-8b). There is also an indication that there was a small tilt to the south of the cyclone's axis between the deep (center station 67) and upper (center station 68) layers. The tilt, like that of eddy Y's cyclone, was towards the adjacent major anticyclone. In both cases, the cyclone was moving in the direction of the swirl velocities of the anticyclone.

The relationship of the May 1994 cyclone to the surrounding eddies is shown by drifter tracks plotted over a longer period (Figure 5.7-3). The cyclone moved to the south-southeast at less than 2 $km \cdot day^{-1}$, with an average rotational period of about 12 days. It was clearly moving towards the large anticyclone indicated by SCULP drifter 20500. Drifter 20542 was spun out of the cyclone and followed a similar path to drifter 12374 by moving clockwise around the small anticyclone on the upper slope and then up onto the shelf. The other anticyclone, to the northeast of the C3 cyclone, influenced the paths of drifters 12373 and 21661. The latter was influenced by flows from the large anticyclone, the cyclone, and lastly, the small mid-shelf anticyclone, in its passage to the outer shelf.

This type of drifter behavior, moving around the periphery of several eddies, and being transported across the slope from deep water to the shelf, is quite common. The October and

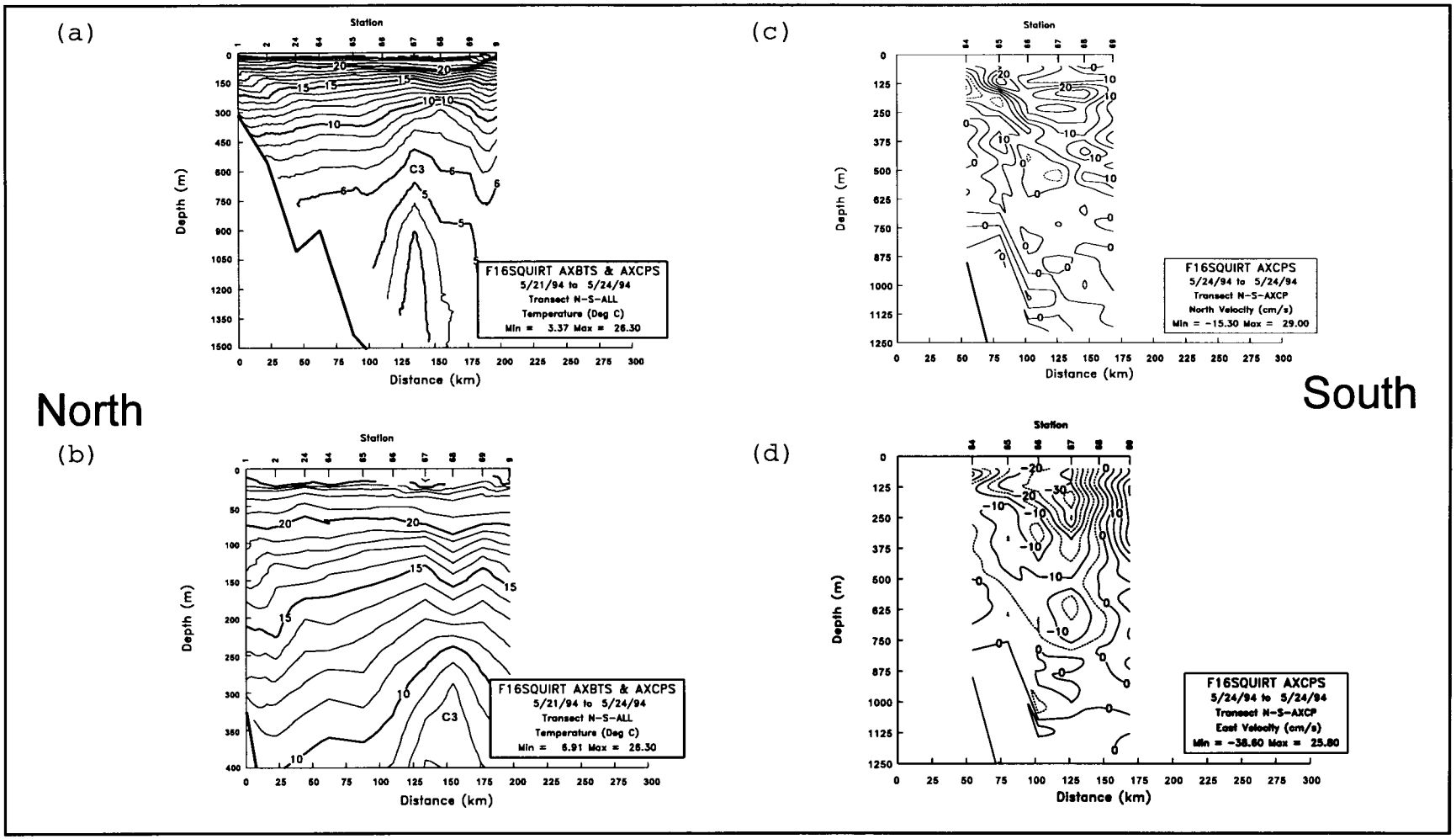

Figure 5.7-2. North-south vertical section near 94°W longitude for the F16SQUIRT survey for (a) temperature to 1500 m depth [stations 1 to 9], (b) temperature to 400 m depth [stations 1 to 9], (c) north velocity to 1200 m depth [stations 64 to 69] and (d) east velocity to 1200 m depth [stations 64 to 69].

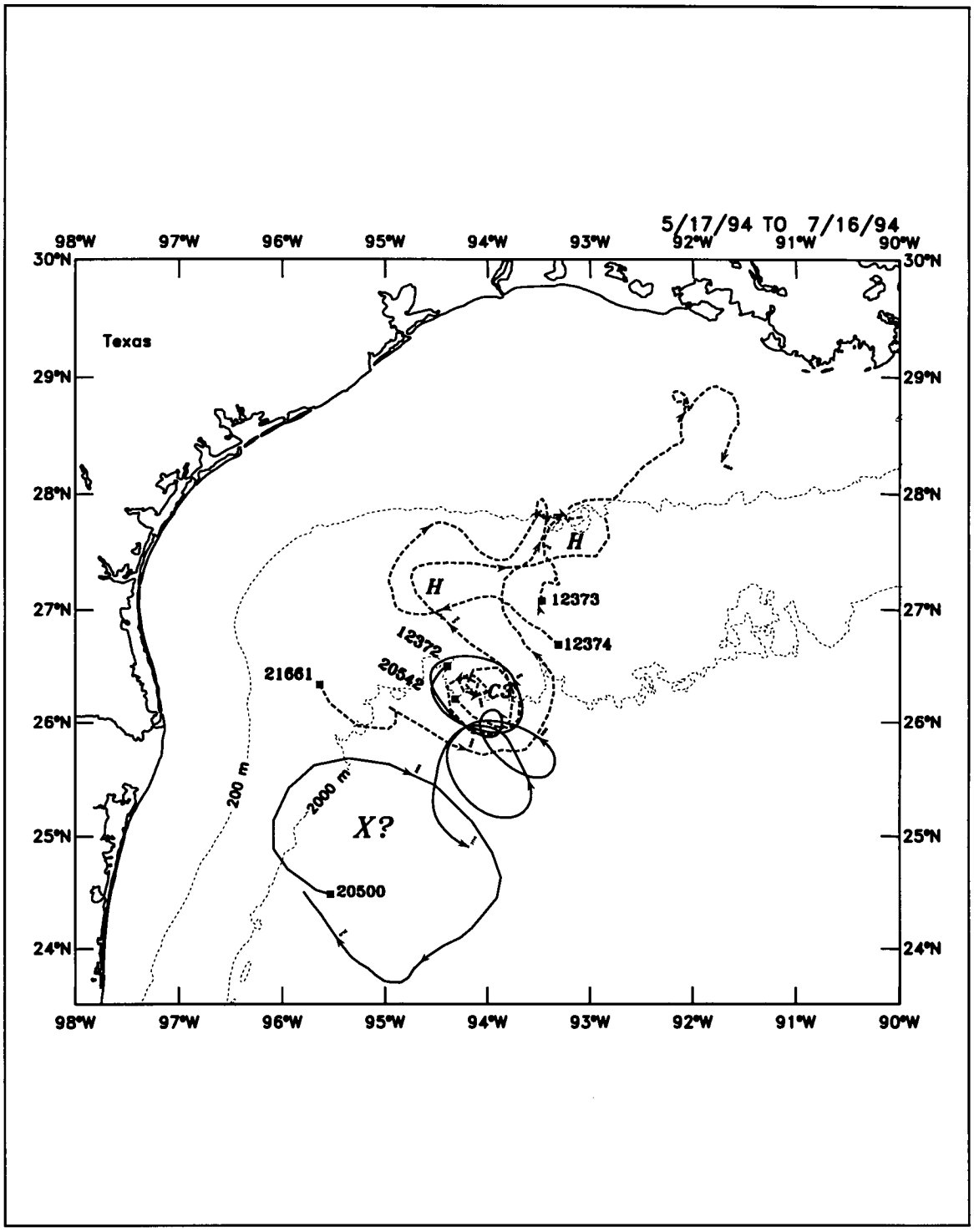

Figure 5.7-3. Smoothed tracks from drifters 12372, 12373 and 12374 beginning May 27, 1994, and daily-averaged positions from SCULP drifters 20500, 20542 and 21661 beginning May 17, 1994. Arrow heads are every 10 days. Small anticyclonic features are identified with an H.

November 1994 surveys are good examples. Figure 5.6-5a shows the velocity vectors from drifters that moved around lower and upper-slope cyclones, as well as a small shelf-break anti-cyclone on the western part of the slope. The two cyclones were much weaker features than the vigorous cyclone associated with eddy Y at 93°W longitude. SCULP and LATEX drifters place these eddies in a larger scale context by showing their relationships to other eddy circulations. Figure 5.7-4 shows selected drifter tracks for the months of October and November 1994. In October 1994, prior to the F20SLOPE survey (Figure 5.7-4a), the drifters showed a large anticyclone centered at about 24.75°N latitude, 95.5°W longitude with a cyclone (C4) to the north. The anticyclone may have been the same feature that was observed in May 1994 in much the same position, and thus could be related to eddy X. North of the cyclone there was a small upper-slope anticyclone which moved westward, in the same direction as the counterclockwise flow of the cyclone. It is the small feature delineated by drifter 21768. By the beginning of November 1994 (Figure 5.7-4b), the lower slope cyclone (C4) and large anticyclone were in much the same position as in October 1994. However, another small cyclone had moved into the upper-slope waters formerly occupied by the small anticyclone. Also in November 1994, the lower slope cyclone (C4) began to move eastward, apparently propagating clockwise around the major warm eddy. This is very similar to the movement of the C3 cyclone in May 1994 (Figure 5.7-3). It is noted that cyclone-anticyclone pairs adjacent to the western slope appear to be a fairly common phenomenon, and that the offshore flow between eddy pairs can be significant (as shown by the drifters in Figure 5.7-4). It is often the mechanism for exporting shelf water into deeper Gulf of Mexico waters between 25°N and 26°N latitude. Model studies (Smith 1986) indicate that such a cyclone can be formed by insta-bilities in a Loop Current eddy as it approaches the western slope. This was also documented for eddy B by Lewis et al. (1989) and SAIC (1988).

5.7.3 December 1993 Surveys

The December 1993 cyclone (C5) was a feature that occupied most of the slope to the west of the approaching eddy X. Figure 5.7-5 shows the temperature surfaces and velocity vectors from drifters and AXCPs. The AXCPs mapped most of the western part of the cyclone, and both these velocities and the drifters show a rather intense southeastward flow across the slope between the cyclone and an anticyclone in deep water around 94°W longitude. The drifters moved south of the C5 cyclone and then northeastward around eddy X. Eddy X was, at this time, a relatively weak Loop Current anticyclone with the

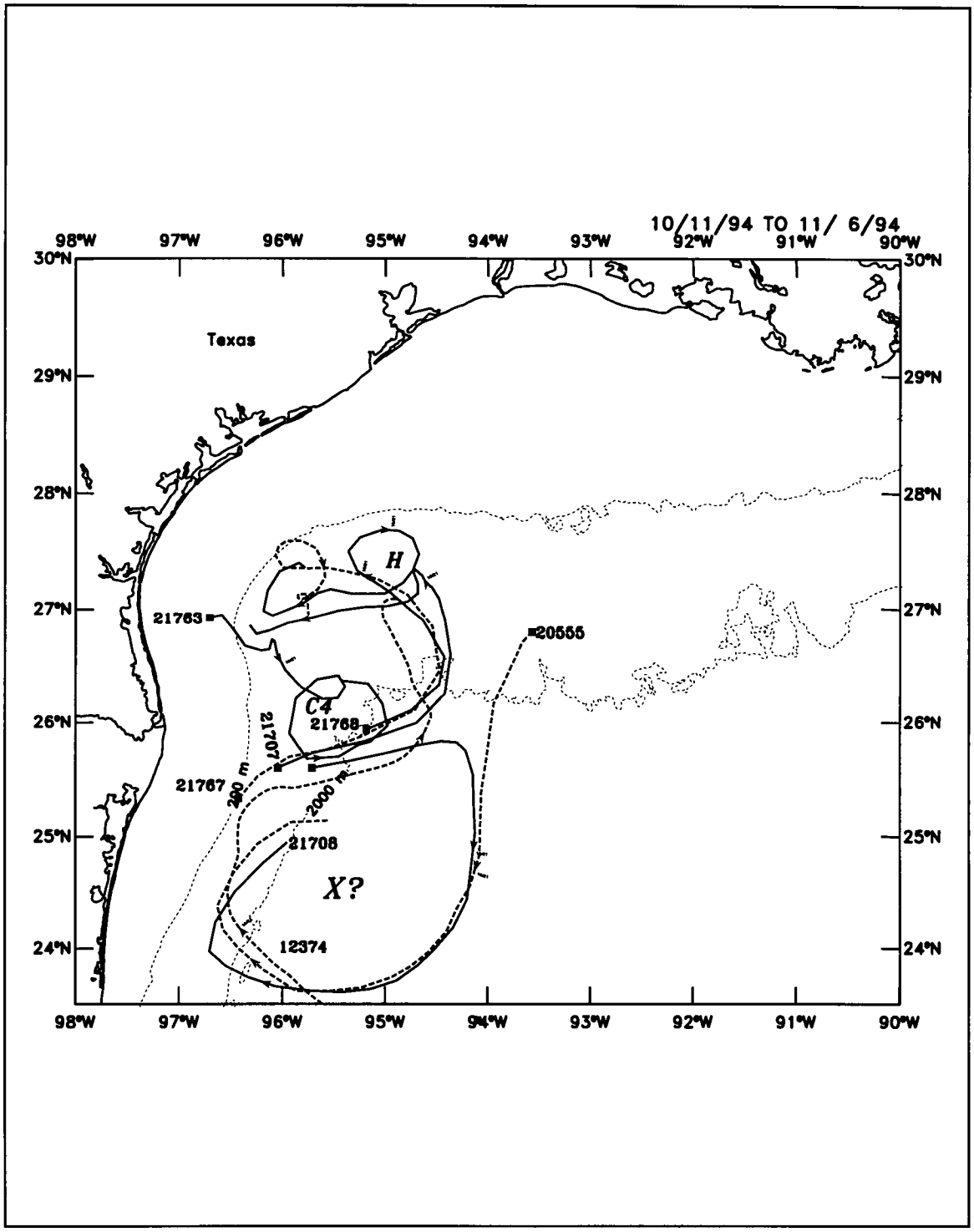

Figure 5.7-4a. Smoothed track from drifter 12374 and daily-averaged positions from SCULP drifters 20555, 21707, 21708, 21763, 21767 and 21768 for the 28-day period beginning October 11, 1994. Small anticyclonic features are identified with an H.

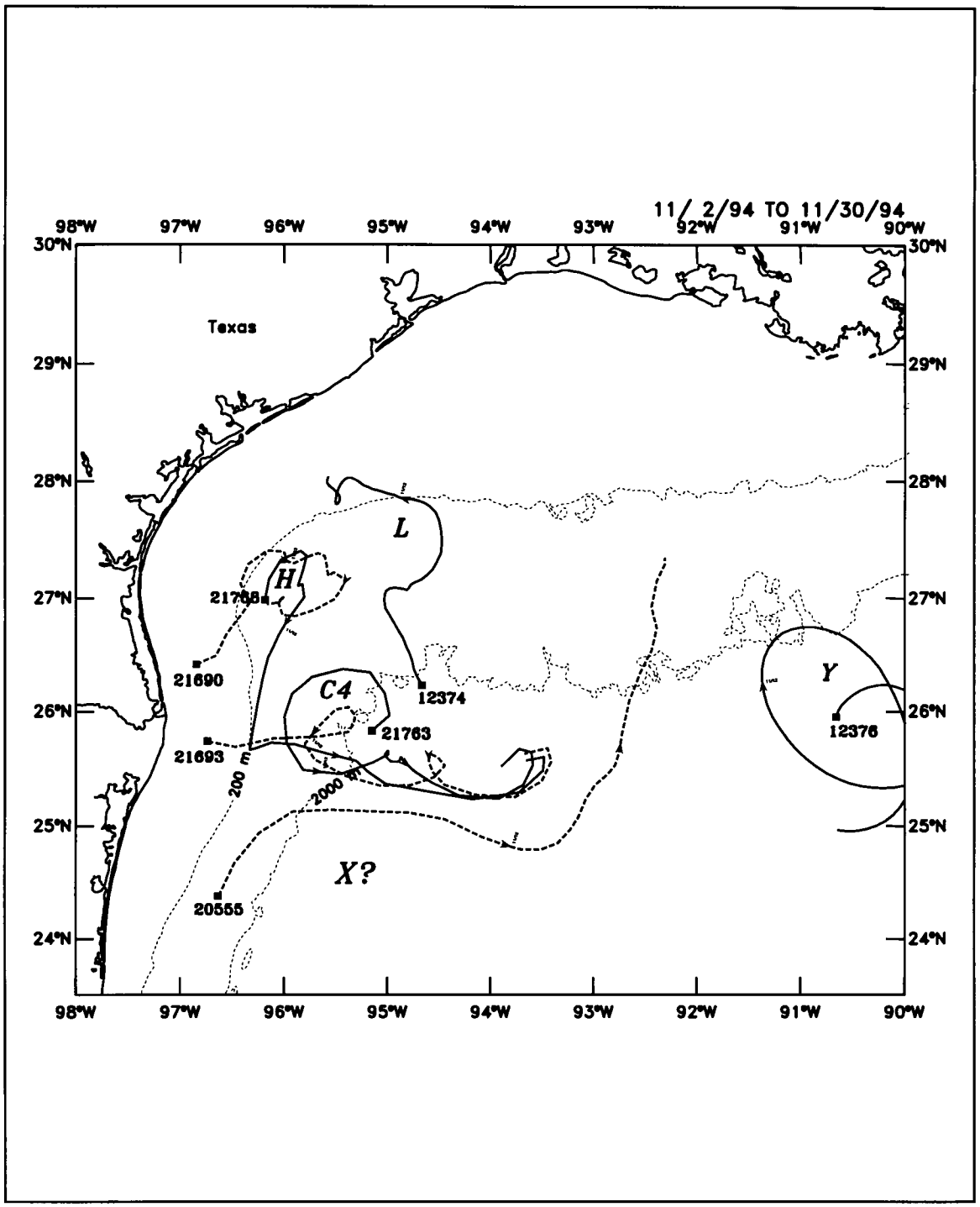

Figure 5.7-4b. Smoothed tracks from drifters 12374 and 12376, and daily-averaged positions from SCULP drifters 20555, 21690, 21693, 21763 and 21768 for the 26-day period beginning November 2, 1994. Small anticyclonic and cyclonic features are identified with an H or an L, respectively.

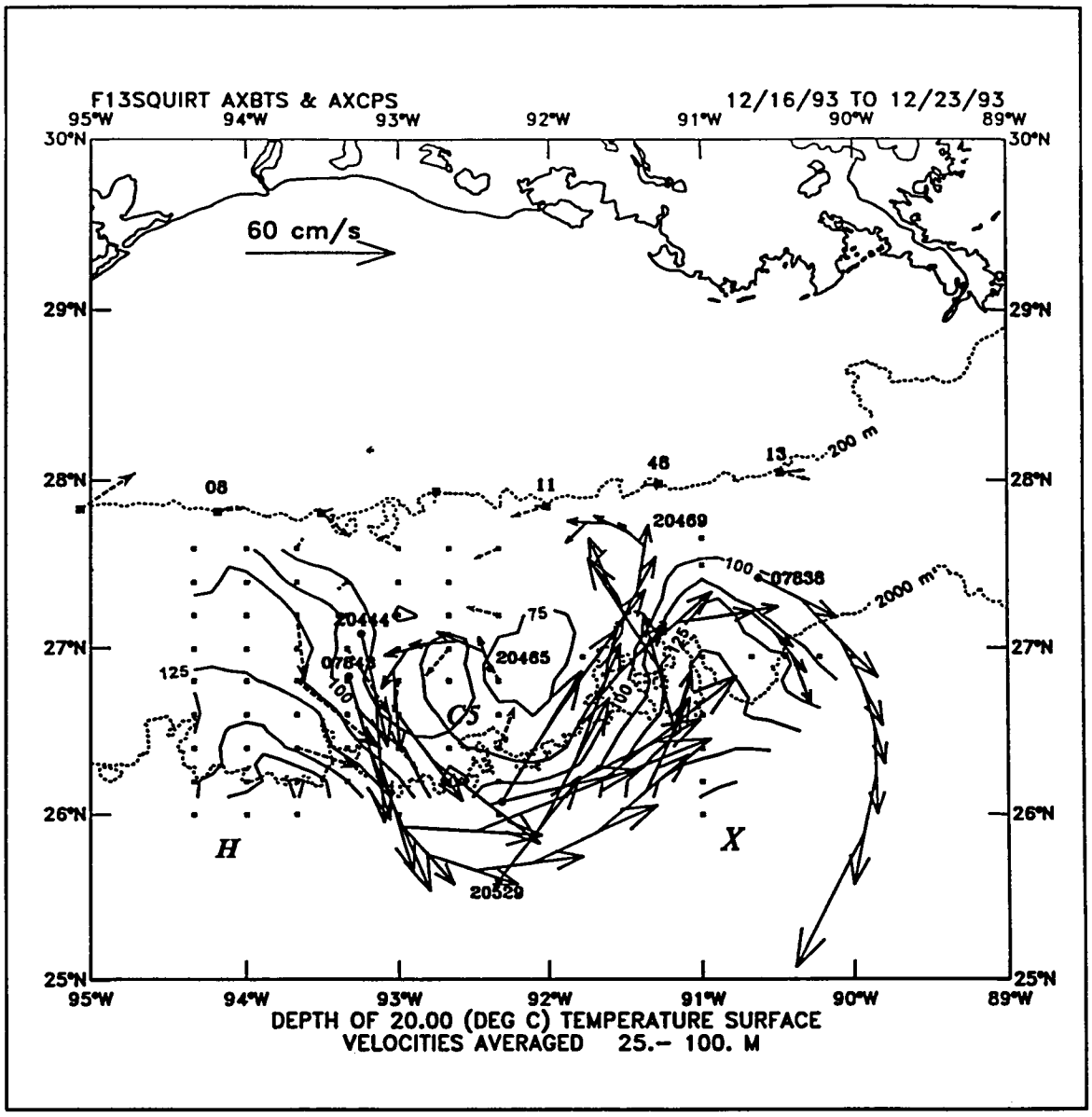

Figure 5.7-5a. Depth of the 20°C temperature surface from the F13SQUIRT and F14LEDDY surveys. Daily velocity vectors from SCULP drifters 20444, 20465, 20469 and 20529 are overlaid beginning December 15, 1993; and from LATEX drifters 07838 and 07843 beginning December 10 and December 20, 1993, respectively. Dashed arrows emanating from crosses are 25-100 m averaged-smoothed velocities from AXCP profiles. Dashed and solid arrows emanating from squares represent the 12-m and 100-m daily mean 40-HLP currents, respectively, from the LATEX A shelf-break moorings for December 21, 1993.

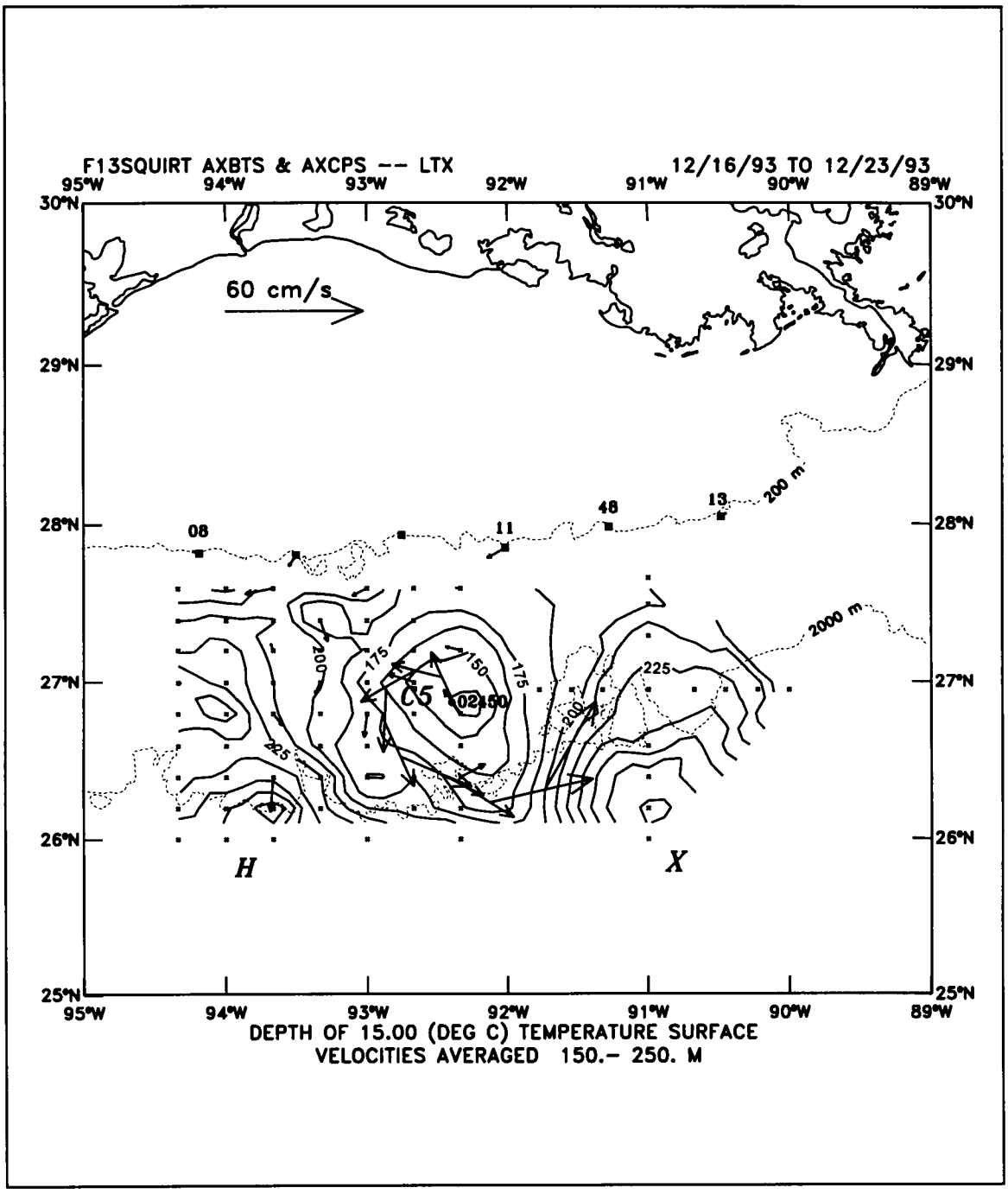

Figure 5.7-5b. Depth of the 15°C temperature surface from the F13SQUIRT and F14LEDDY surveys. Daily velocity vectors from drifter 02450 begin December 15, 1993. Dark arrows emanating from crosses are 150-250 m averaged-smoothed velocities from AXCP profiles. Arrows emanating from squares represent bottom level (~200 m) daily mean 40-HLP currents from the LATEX A shelf-break moorings for December 21, 1993.

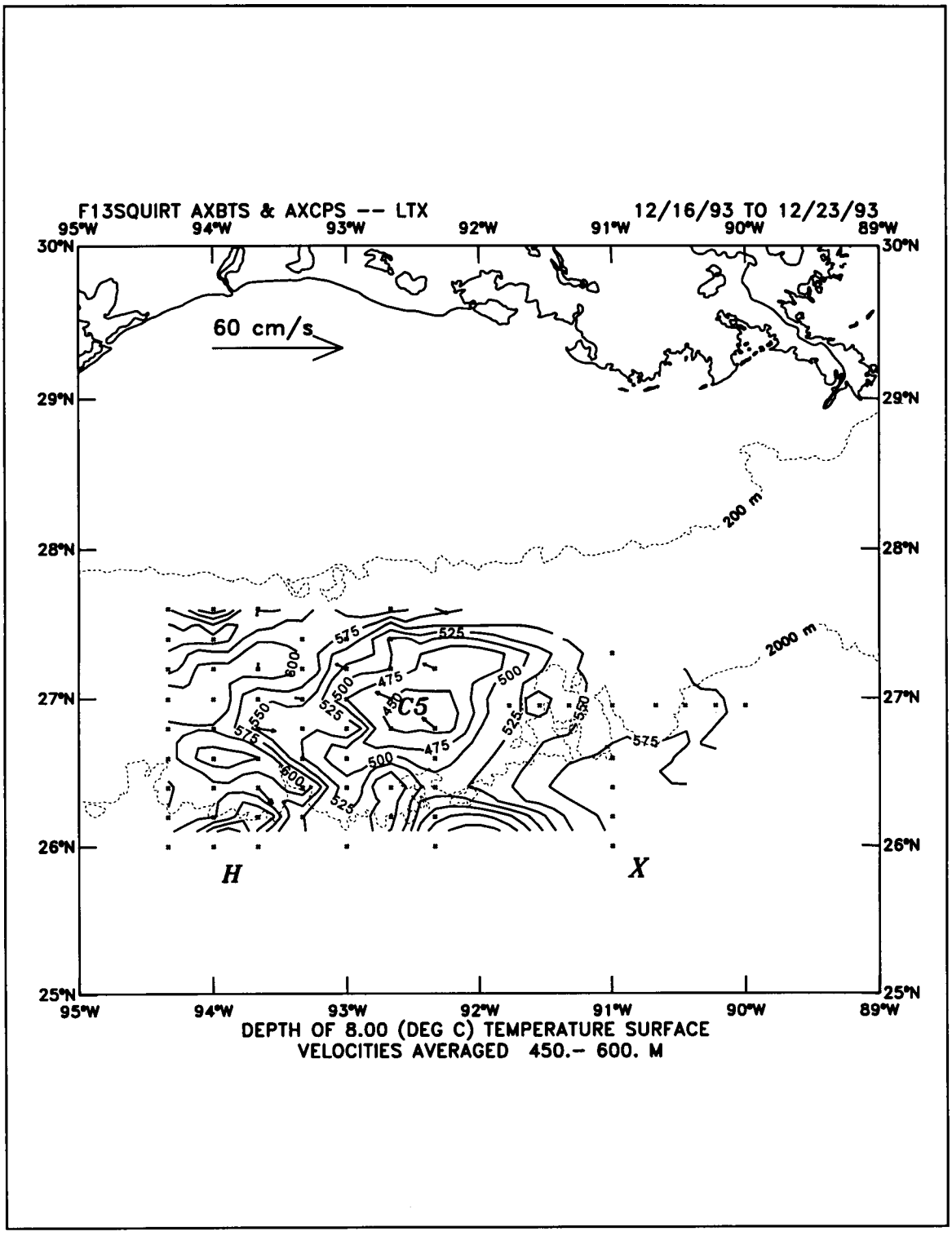

Figure 5.7-5c. Depth of the 8°C temperature surface from the F13SQUIRT and F14LEDDY surveys. Dark arrows emanating from crosses are 450-600 m averaged-smoothed velocities from AXCP profiles.

15°C surface reaching to about 275 m depth (compare with Figure 5.6-3b for eddy Y).

Unlike previous examples, there does not appear to have been any strong interaction between the cyclone and eddy X. There is no indication of the deep temperature structures of eddy X being advected northwards by the cyclone's velocity field, as with eddy W_N, or any indication that the cyclone was moving in the direction of the swirl velocities of the anticyclone. The GulfCet 07 cruise of December 5-12, 1993 showed eddy X and the cyclone in much the same position as in Figure 5.7-5. The center of the cyclone, as indicated by the temperature contours, does appear to be a little east of that indicated by the AXCP velocities, but this may be because of a lack of resolution around 92°W longitude between the two different surveys.

Figure 5.7-6 shows the December 1993 to March 1994 tracks from four SCULP drifters. Drifter 20465 remained in the cyclone (C5) around 92°W longitude until the beginning of March 1994. During the same time period, drifter 20469 moved around the cyclone and eventually into eddy X. Eddy X made a slow westward translation during February and March 1994 and apparently moved the cyclone a little eastward along the slope. Drifter 20396 showed two anticyclones, one along the western slope at ~24.5°N latitude, and the other corresponding to the anticyclone whose northwest corner was captured in the F13SQUIRT survey. Drifter 20440 moved through three cyclones. The two cold eddies located along 96°W longitude are indeed separate entities, as shown by tracks from drifter 20440 (and drifters 20457, 20461 and 20463, which are not shown) during the period of the mid-December 1993 survey. These two cold eddies are also in similar positions to the two western slope cyclones found in October and November 1994 (Figures 5.6-5a and 5.7-4). The small upper-slope cyclone that moved clockwise around the 94°W longitude anticyclone, and moved towards the 92°W longitude cyclone in February and March 1994 (Figure 5.7-6), was probably also separate from the other cyclones. This latter cyclone is one of the best examples of a cyclone propagating around a warm eddy in the drifter data set. Another drifter that appears to have stayed with a propagating cyclone on the slope is drifter 07837 (Figure 5.1-1), which translated westward after being seeded into a small cyclone near 94°W longitude. This cyclone was surveyed during the F02SLOPE and F03SEDDY surveys in August 1992 (see Section 5.7.4). In this case, also, a drifter (07493, Figure 5.1-1) showed that a large deep-water cyclone (C6) centered at about 25°N latitude, 94°W longitude is the probable cause of the rapid westward translation. Thus, this apparently-isolated

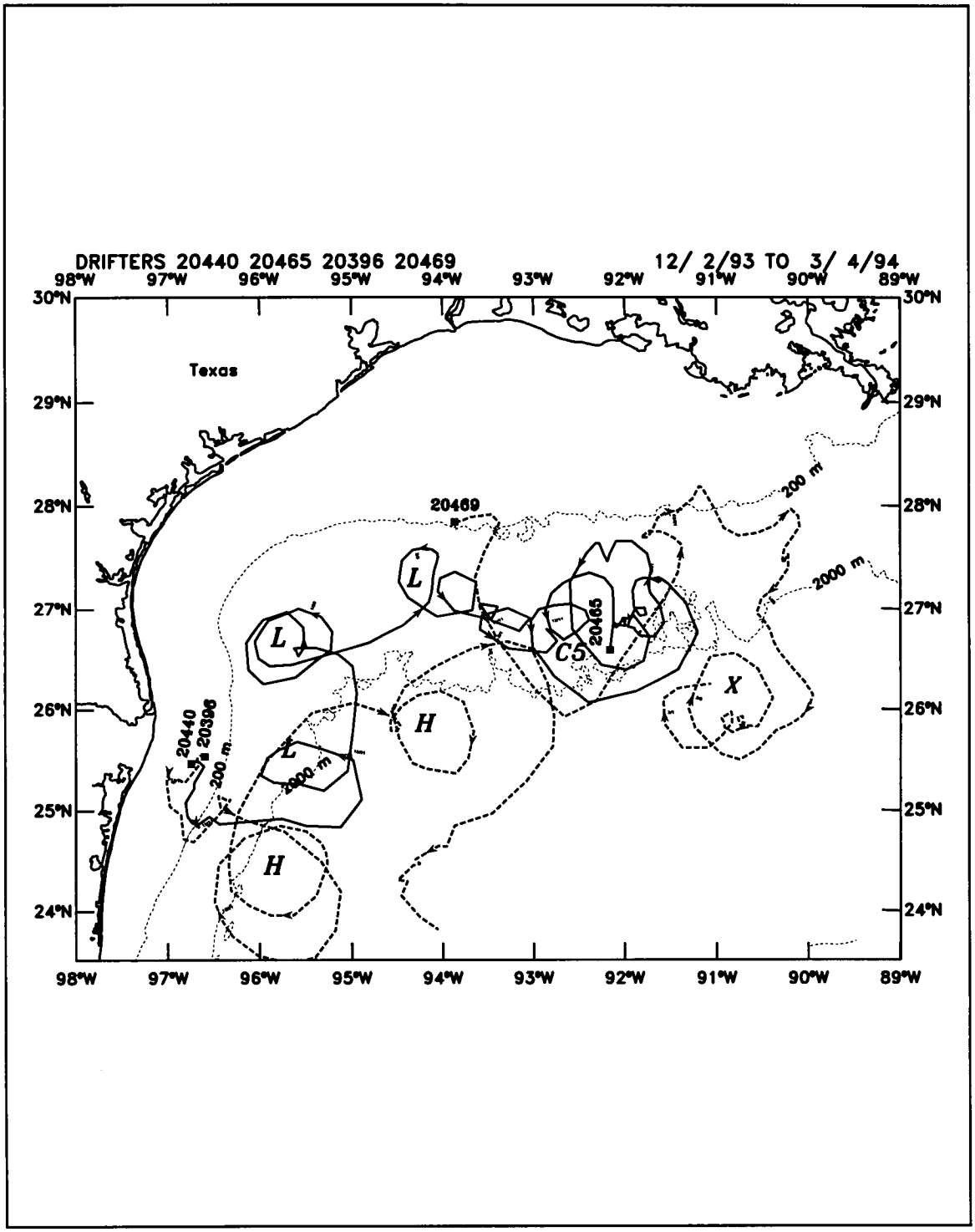

Figure 5.7-6. Daily averaged positions for SCULP drifters 20396, 20440, 20465 and 20469 for a three-month period beginning December 1, 1993. Arrow heads are every 10 days. Anticyclonic and cyclonic features are identified with an H or an L, respectively.

slope cyclone could also be regarded as a small peripheral eddy of the larger cyclone.

The presence of an almost stationary slope cyclone for three months around 93°W longitude caused a number of shelf drifters to exit the shelf and move southward, across slope from December 1993 through February 1994. The majority left the slope around 93.5°W to 94°W longitude in the vicinity of shelf-break mooring 09. Figures 5.7-5a and b show the one-day averaged velocities for December 21,1993 (the date of the AXCP survey) for the 40-HLP current meter records from the shelf-break moorings. The direction of flow corresponds to that of the slope eddies closest to the moorings. Thus, moorings 08 and 09 showed eastward flows corresponding to the warm eddy at 94°W longitude. Moorings 11 and 48 showed westward flows corresponding to the cyclone, and at mooring 13, flows were again eastward because of eddy X. The along-isobath convergence of flows produced a substantial offshore component at mooring 09, in just the region where drifters left the shelf to move around the cyclone and eddy X (Figure 5.7-5a).

The velocity time series from the moorings for the December 1993 to March 1994 period are given in Figure 5.7-7. The periods of the F13SQUIRT and F14LEDDY surveys are marked, and the directions of flow over the 10-day period were basically the same, as indicated in Figure 5.7-5a. In particular, the offshore component (the positive shaded part of the component plot; Figure 5.7-7b) was sustained at the 12-meter level of mooring 09. The general characteristics of the low frequency currents are that they were highly variable, with onshore-offshore flows comparable to along-isobath flows, except for major eastward-flowing events. Events can be quite long-lasting, with periods of up to one month, but there is little evidence of strong coherence between the moorings in the array. However, fluctuations in the currents were highly similar between the surface and mid-depth (100 m) levels (the bottom meters generally had very small current magnitudes). Eastward flowing events were generally highly sheared (e.g. moorings 08 and 09 in January and February 1994), and westward flowing events had weak vertical shears. This corresponds to the expected flow fields of the outer edges of warm (anticyclonic) and cold (cyclonic) eddies, respectively (Figures 5.6-7 and 5.6-4). Similar characteristics were observed from current meters deployed on the mid- and lower slope in an earlier study (Hamilton 1992).

After the December 1993 surveys, a sustained eastward event occurred, first at mooring 08, and then at mooring 09. This was presumably the effect of the anticyclone at 94°W longitude. Drifter 20440 showed a small cyclone north of the warm

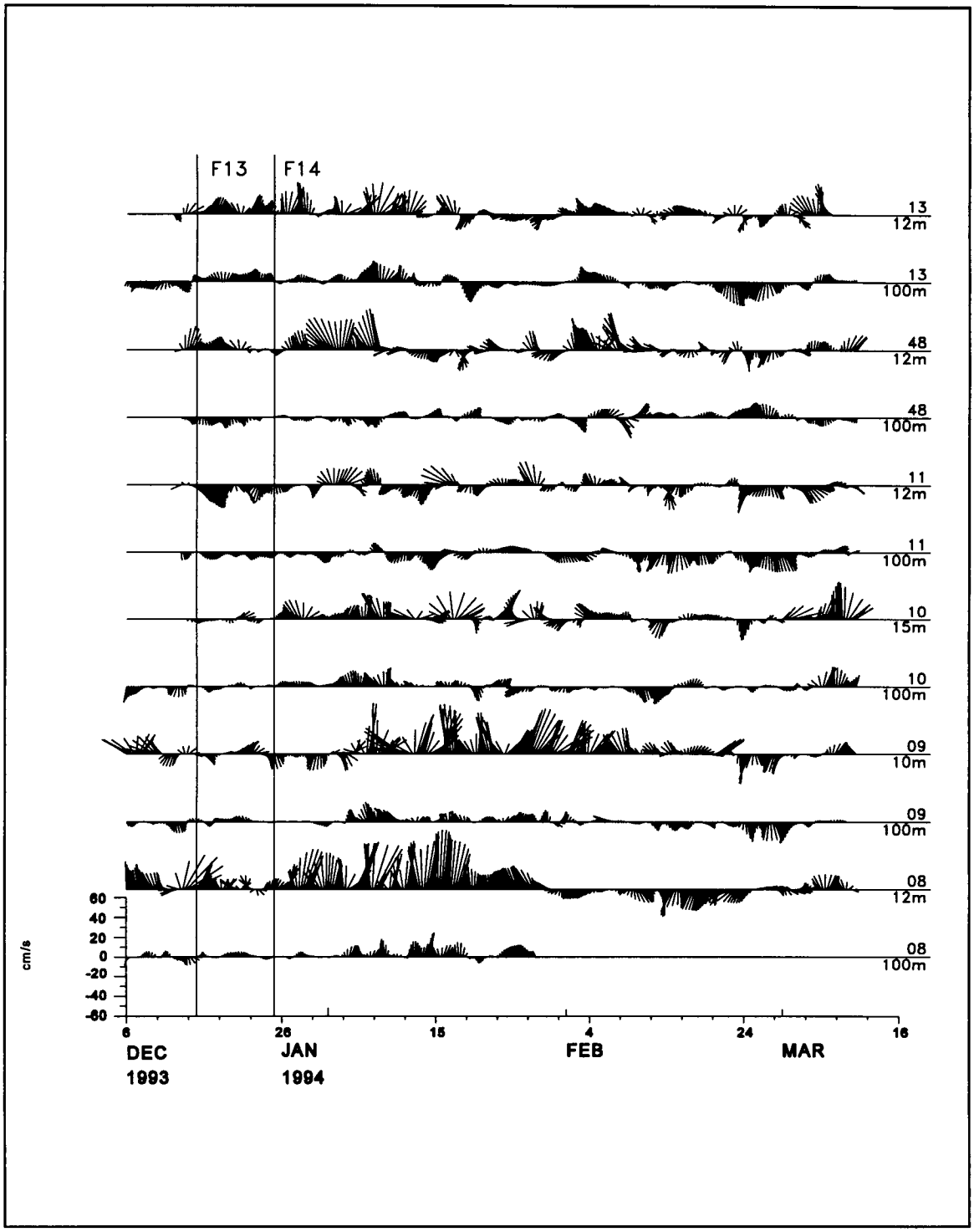

Figure 5.7-7a. Stick plots of rotated 40-HLP currents from the LATEX A shelf-break moorings for the period from December 6, 1993 to March 16, 1994. Up is the along-isobath direction towards the east. Vertical lines mark the time period covered in Figure 5.7-5.

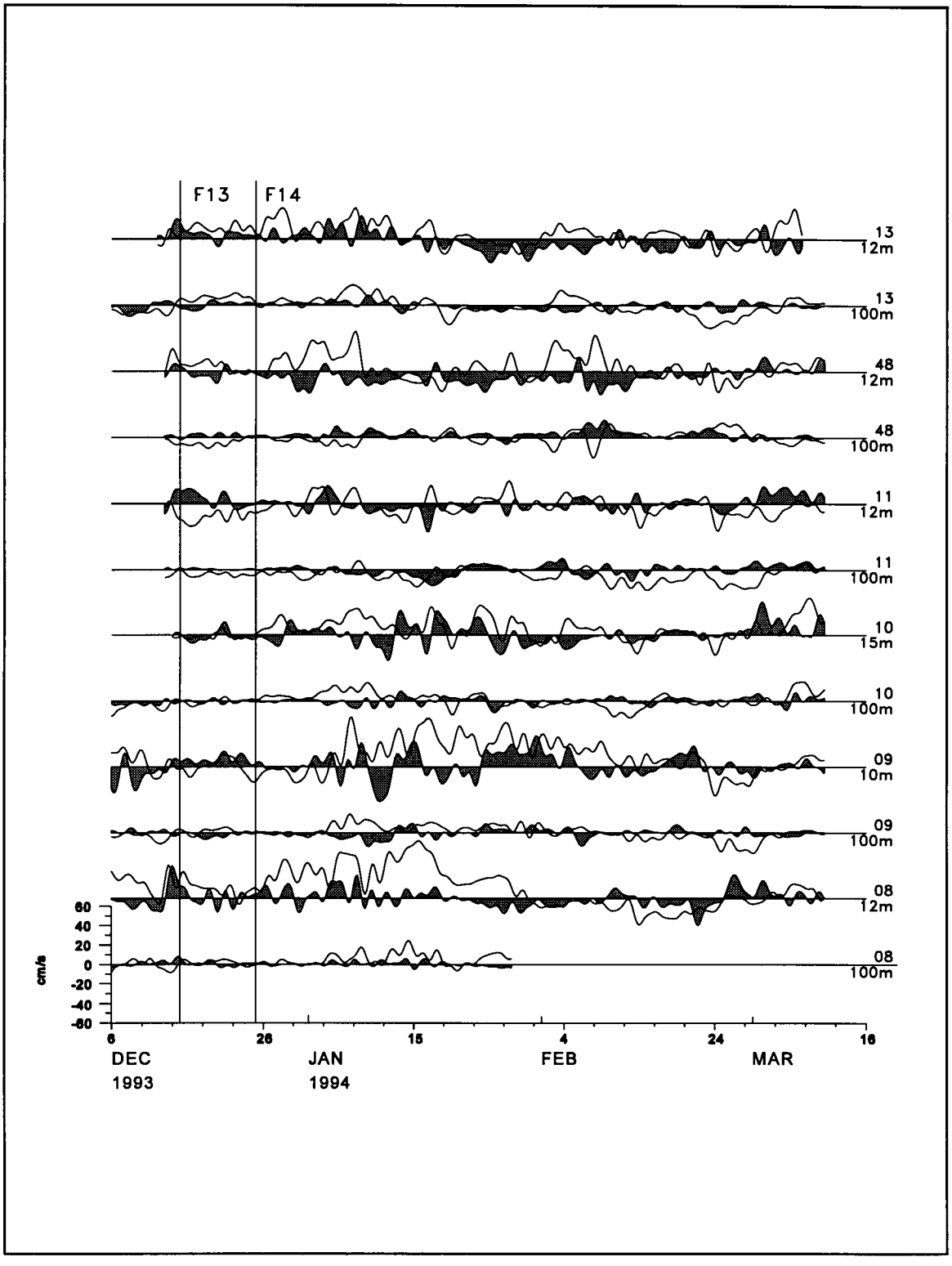

Figure 5.7-7b. U (shaded) and V (solid) components of the rotated 40-HLP currents from the LATEX A shelf-break moorings for the period from December 6, 1993 to March 16, 1994.

eddy at the beginning of February 1994 (Figure 5.7-6). Flows at mooring 08 reversed at this time. Shelf-break cur-rents at mooring 11, which was closest to the cyclone at ~92°W longitude, and drifter 20465, had mainly westward flows for the whole period. Moorings further east (moorings 48 and 13) also showed sustained westward flow events after eddy X ceased to be an influence around the middle of January 1994 (Figure 5.7-7). Mooring 09 had large onshore-offshore velocities, with offshore predominating. Surface speeds reached as much as 30 to 40 $cm \cdot s^{-1}$. At the 12-meter level of moorings 48 and 13, onshore flows predominated (Figure 5.7-7b), presumably because they were primarily influenced by the northeast quadrant of the cyclone near 92°W longitude (Figure 5.7-6).

5.7.4 August 1992 Small Slope Cyclone

The westward propagating cyclone tracked by drifter 07837 in Figure 5.1-1 has already been discussed as an example of a small peripheral eddy propagating around a large eddy; in this case another cyclone. However, it is worth examining this eddy in more detail because the initial hydrographic survey that located the cyclone on the shelf had about the best resolution for such a feature of any of the LATEX C AXBT surveys. The 15°C and 8°C surfaces from the combined F02SLOPE and F03SEDDY surveys are shown in Figures 5.7-8a, b. The northern edge of eddy U can be seen over the 2000 m isobath in the east. The cyclone is centered at about 26.8°N latitude, 93.5°W longitude, about 100 km west of the nearest edge of eddy U. There is very little expression in the 15°C surface of this cyclone, but in the 8°C surface there is strong doming within the eddy diameter of about 40 km. The shallowest depth of the 8°C surface is about 350 m which is the shallowest observed for any of the LATEX cyclones. Both the 15°C and 8°C surfaces suggest a weak anticyclone and another cyclone, north of eddy U, around 92°W longitude, and 90.5°W longitude, respectively (Figure 5.7-8a,b).

Drifter 07837 was drogued at 200 m and remained in the core of the cyclone as it moved west-northwestward. Swirl velocities ranged from 10 to 20 $cm \cdot s^{-1}$ and mean radii ranged from 10 to 15 km over the month-and-a-half lifetime of the drifter. The mean translation speed was about 3 $km \cdot day^{-1}$ and rotational periods were 5 to 7 days. The westward movement may be accounted for by a much larger cyclone to the south and not by the cleaving of eddy V from eddy U in early September 1992. Despite the small size of the cyclone at depth, there appears to be some influence of the shelf-break, near-surface, westward currents at moorings 09 and 10 (Figure 5.7-8a). Similarly, the other two slope eddies that are north of eddy U also appear to be influencing flows at the shelf-break moorings.

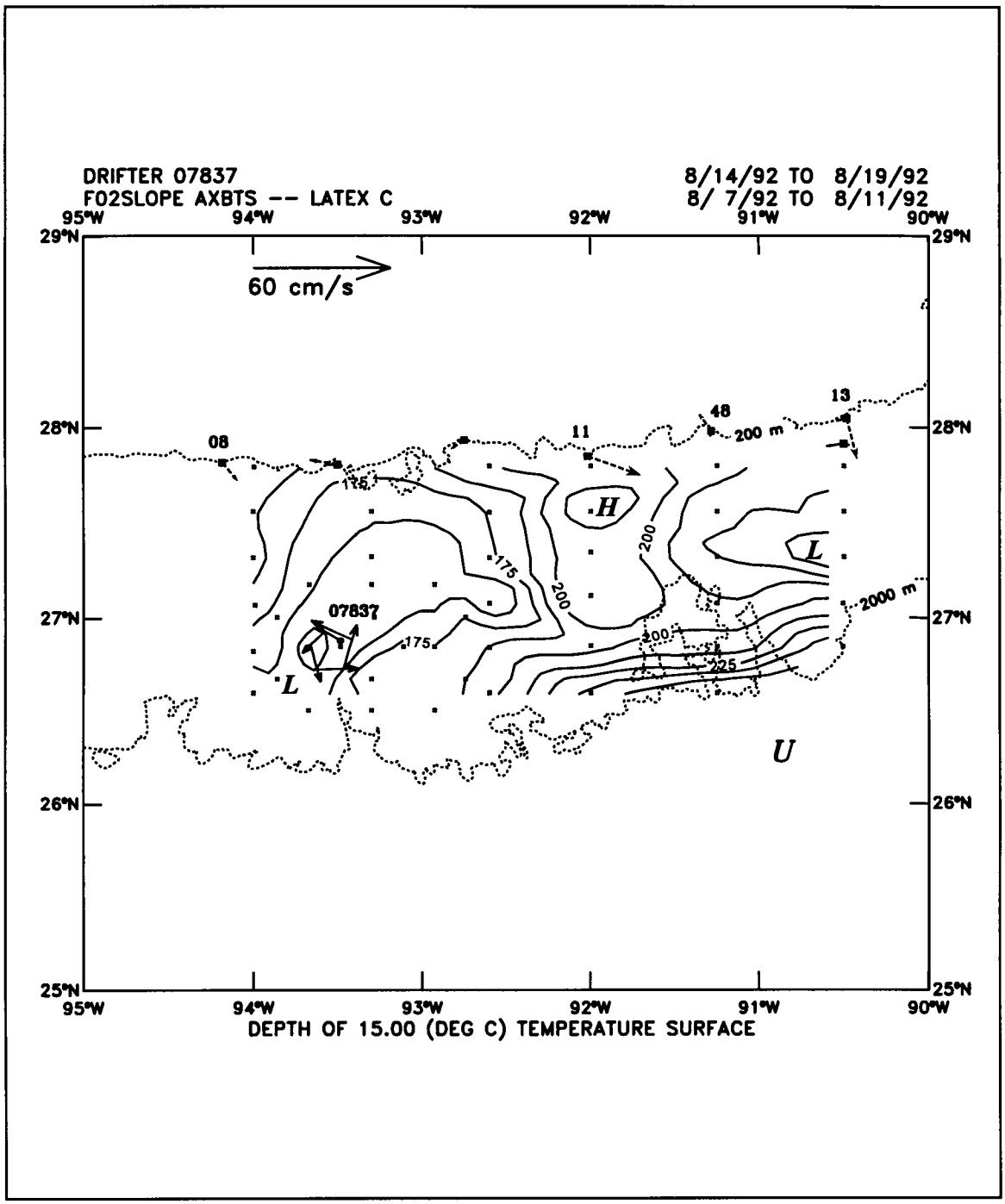

Figure 5.7-8a. Depth of the 15°C temperature surface from the F02SLOPE and F03SEDDY surveys. Dashed and solid arrows emanating from squares represent the 12-m and 100-m daily mean 40-HLP currents, respectively, from the LATEX A shelf-break moorings for AUGUST 10, 1992. Daily velocity vectors from drifter 07837 are overlaid beginning August 14, 1992.

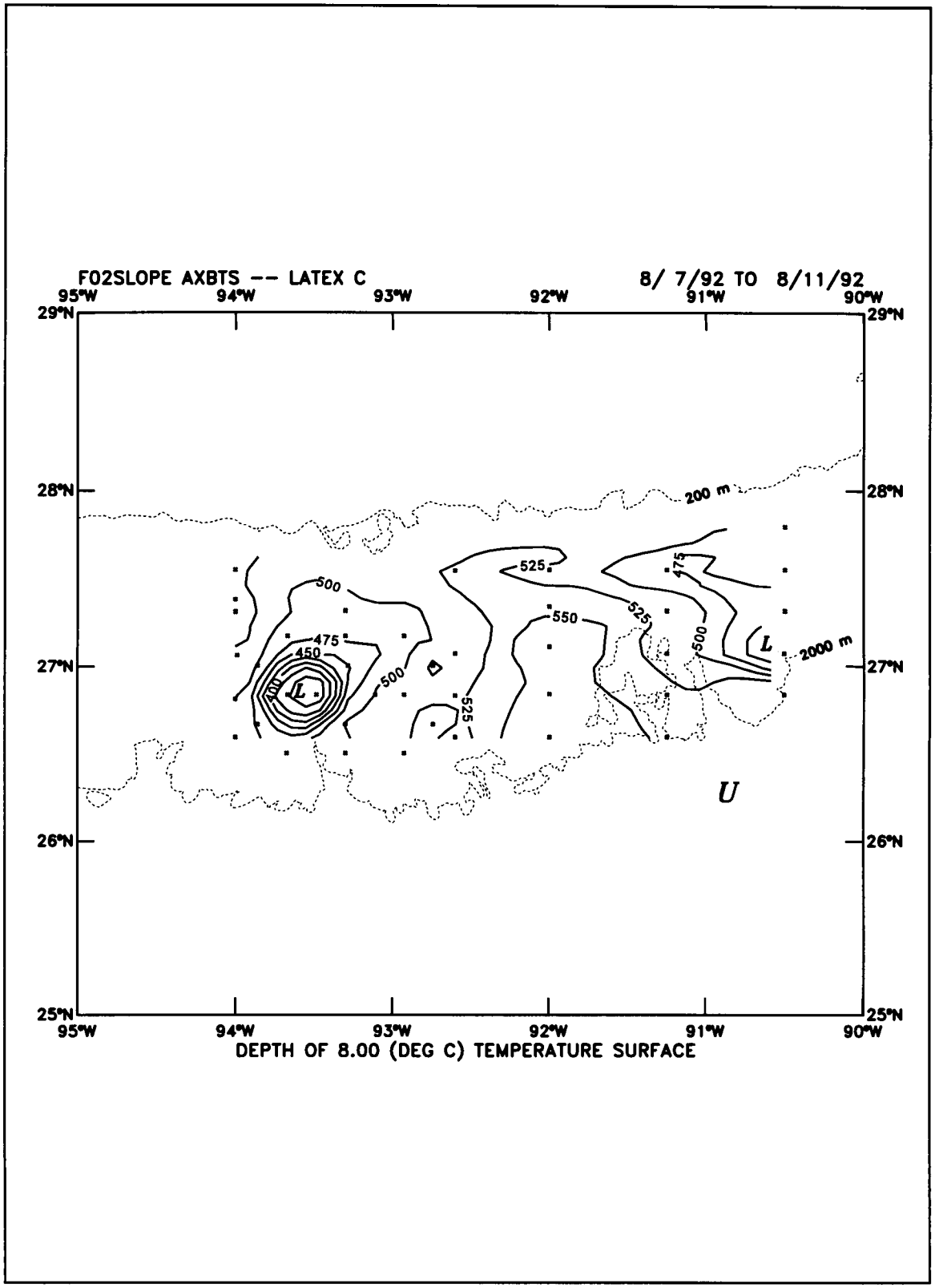

Figure 5.7-8b. Depth of the 8°C temperature surface from the F02SLOPE and F03SEDDY surveys.

This is another example of smaller weaker slope eddies masking any effects on shelf-break flows of a vigorous Loop Current eddy in the deep basin.

5.7.5 Discussion

Velocities at the shelf break appear to have been closely related to the eddy field on the slope. The eddies account for many of the characteristics of the velocity time series. The shorter-period fluctuations in Figure 5.7-7 often have a strong rotary component and suggest that there may be smaller eddies or instabilities present that are not resolved by the drifters or the detailed hydrographic surveys. There are examples from the August 1993 surveys (Section 5.4) that suggest that small upper-slope eddies can mask the influences of Loop Current eddies and mid- and lower-slope cyclones on shelf-break currents.

As discussed in regard to the May 1994 surveys (Figure 5.7-1), shelf-break flows were all eastward and it is less certain if they were caused by the small upper slope anticyclones (Figures 5.7-1 and 5.7-3). However, an examination of stick vectors and components (Figure 5.7-9) for the upper levels of the moorings in Figure 5.7-1, for the three-month period beginning in May 1994, shows a similar lack of coherence between moorings. Flows were predominantly eastward for most of the moorings during most of this three-month period. There is, however, evidence of a slowly clockwise-propagating signal from mooring 49 to mooring 09, beginning in the middle of June 1994. A survey (F17SLOPE) on August 13, 1994, showed the presence of a large slope anticyclone in the northwestern corner similar to the late stages (May 1993) of eddy V (see Figures 5.2-8 and 5.2-12). Many characteristics of the June through August 1994 parts of Figure 5.7-9 are similar to the propagating events observed around the periphery of eddy V between February and April 1993 (Figure 5.2-8). Thus, it appears that a large warm eddy moved into the northwest corner of the slope in June 1994 and displaced the eddies observed in Figure 5.7-1. A candidate for this warm eddy would be the large anticyclone (possibly eddy X) centered about 25°N latitude, 95°W longitude, shown by drifter 20500 in Figure 5.7-3.

5.8 Miscellaneous Slope Anticyclones

Two surveys, F12SLOPE and F17SLOPE, showed the existence of weak anticyclones in the northwestern corner of the slope that had some similarities to the late stages of eddy V's life. The latter survey follows on from the discussion of the May 1994 surveys, and indeed the most likely candidate for the origin of this eddy is the warm anticyclone shown by drifter

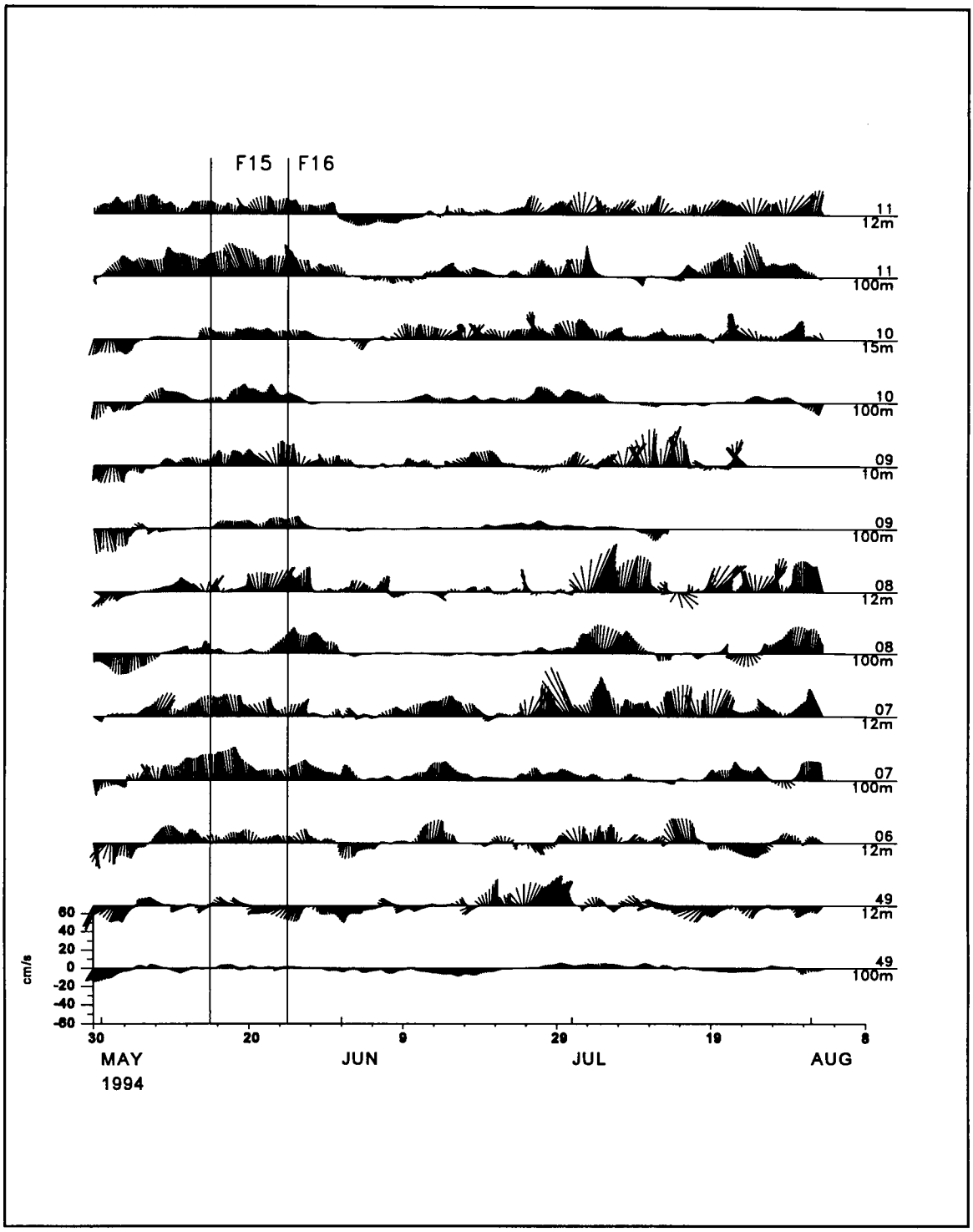

Figure 5.7-9a. Stick plots of rotated 40-HLP currents from the LATEX A shelf-break moorings for the period from April 30, 1994 to August 8, 1994. Up is the along-isobath direction towards the east. Vertical lines mark the time period covered in Figure 5.7-1.

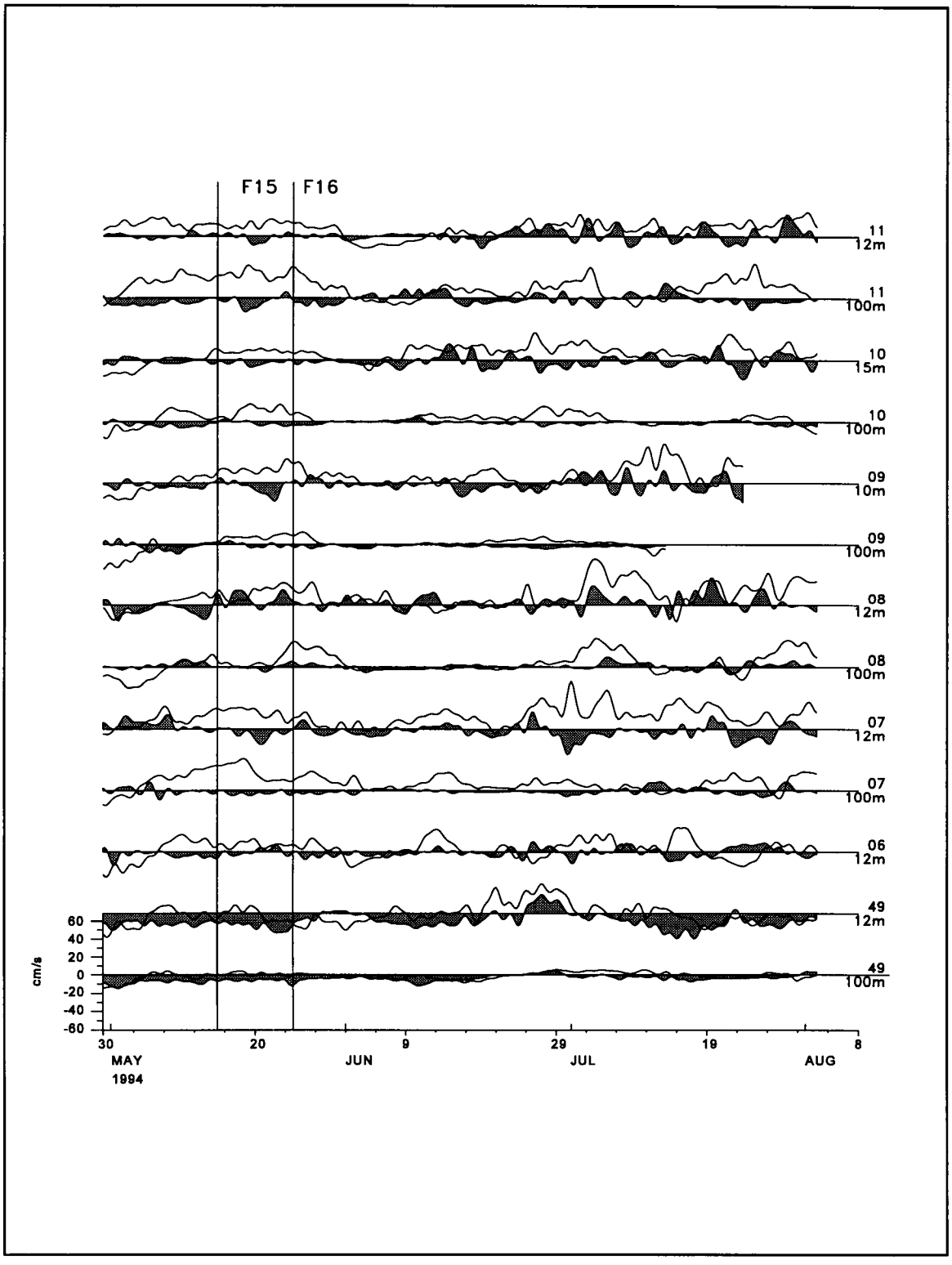

Figure 5.7-9b. U (shaded) and V (solid) components of the rotated 40-HLP currents from the LATEX A shelf-break moorings for the period from April 30, 1994 to August 8, 1994.

20500 (Figure 5.7-3) in May and June 1994. The depth of the 20°C, 15°C and 8°C isotherms for the August 1994 survey are given in Figure 5.8-1. The eddy is elongated in an east-west direction in the upper surfaces and there are indications that there are two small cyclones on the periphery at about 27°N latitude, 96°W longitude, and at 27.5°N latitude, 94°W longitude. The most westerly cyclone is clearly forcing the southwesterly flows at shelf-break moorings 04, 06 and 49. The other cyclone has a weaker effect on the adjacent shelf-break currents.

Unfortunately, no SCULP drifters entered this region of the slope in August 1994. Therefore, how this warm eddy and its associated cyclones evolved is uncertain. However, the anticyclone was weak, with the 15°C and 8°C isotherms depressed to about 250 m and 590 m, respectively (compare with eddy Y in Figure 5.6-3). Eddy V, at this stage in its evolution, apparently dissipated quite rapidly after the May 1993 surveys even though the swirl velocities on its outer edges were still on the order of 60 $cm \cdot s^{-1}$ (Figure 5.2-12a). The shelf-break currents (Figure 5.8-2, moorings 04, 49 and 06) indicate that the western peripheral cyclone remained in this vicinity until about August 20, 1994, when the flows reversed and became typical of an anticyclone. This may indicate that the dissipating anticyclone moved westward, similar to eddy V in May 1993 (Figure 5.1-2), so that its outer, higher-speed flows intruded over the shelf break. There is evidence from the phasing of the cyclonic-flow events between moorings 04, 06 and 07 that the western cyclone moved eastward, in the same direction as the swirl velocities of the warm eddy. Temperatures at 100 m at the moorings were cool when flows were cyclonic and warm when anticyclonic, which helps to confirm this interpretation of anticyclonic movement of the peripheral cyclone.

The last eddy to be discussed is an anticyclone that occupied much of the slope at 94°W longitude between the October 1993 (F12SLOPE) and December 1993 (GulfCet 06 and F13SQUIRT) surveys. The 20°C, 15°C, and 8°C temperature surfaces are given in Figure 5.8-3. There appear to be cyclones on either side. To the east, the structures appear complex, but the shelf-edge velocity suggests an upper slope cyclone around 93°W longitude. To the west, the deep 8°C temperature surfaces indicate a fairly large cyclone at about 95.5°W longitude. The westward upper layer currents at moorings 06 and 07 (Figure 5.8-3a) are consistent with a slope cyclone in this position.

The drifter track for drifter 20446 and the current vectors (Figure 5.8-3a) provide a nice example of across-shelf-break

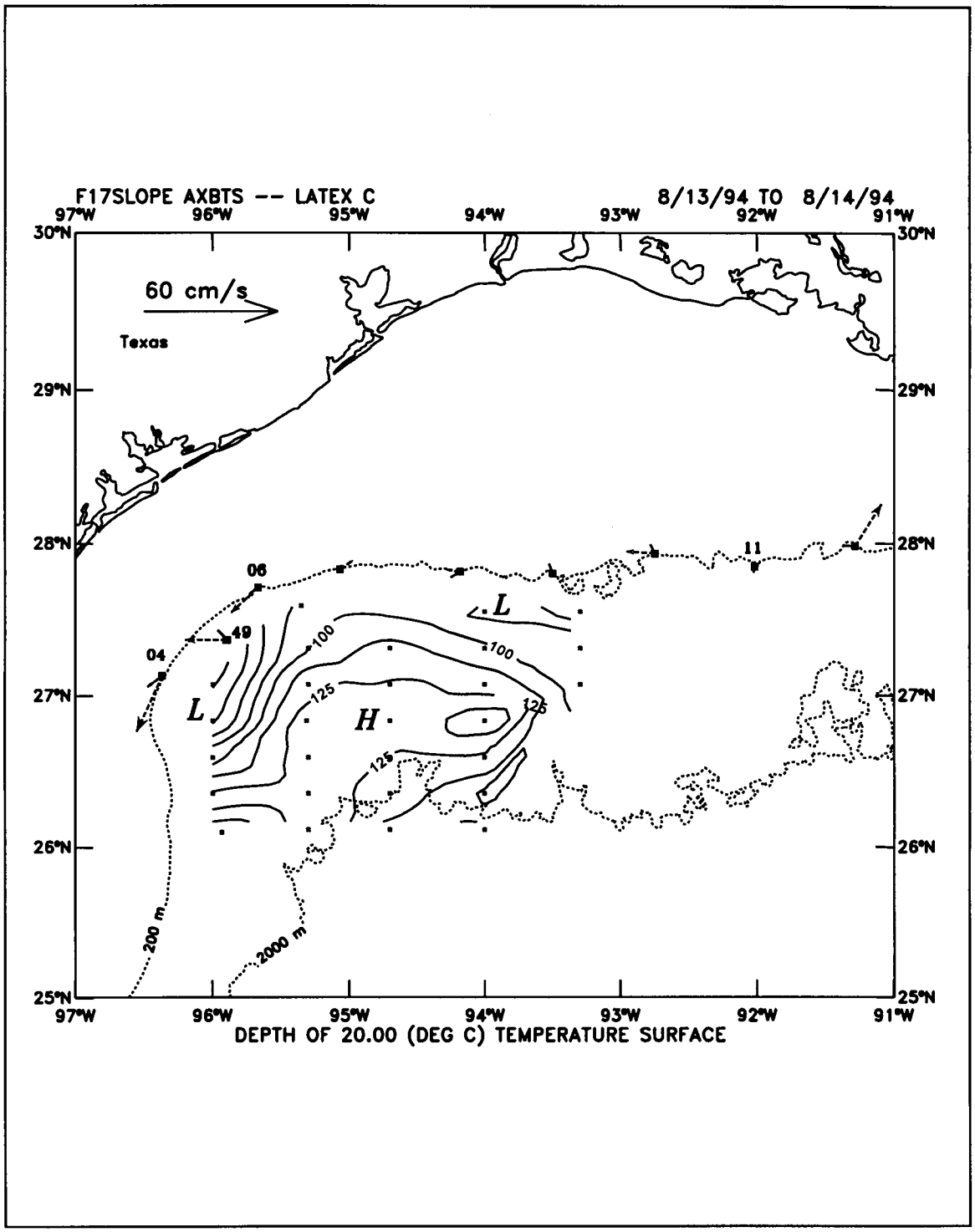

Figure 5.8-1a. Depth of the 20°C temperature surface from the F17SLOPE survey. Dashed and solid arrows emanating from squares represent the 12-m and 100-m daily mean 40-HLP currents, respectively, from the LATEX A shelf-break moorings for August 13, 1994.

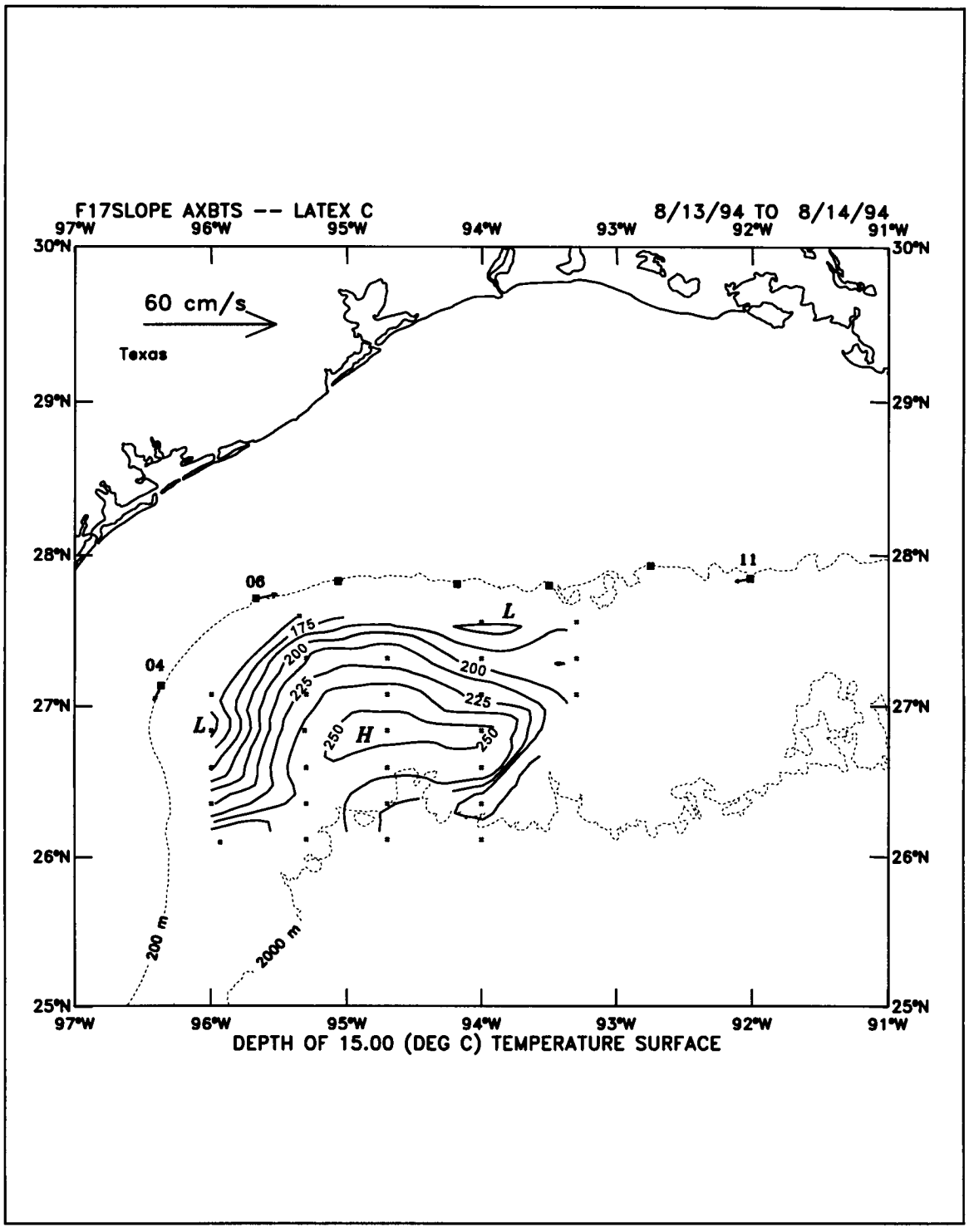

Figure 5.8-1b. Depth of the 15°C temperature surface from the F17SLOPE survey. Arrows emanating from squares represent bottom level (~200 m) daily mean 40-HLP currents from the LATEX A shelf-break moorings for August 13, 1994.

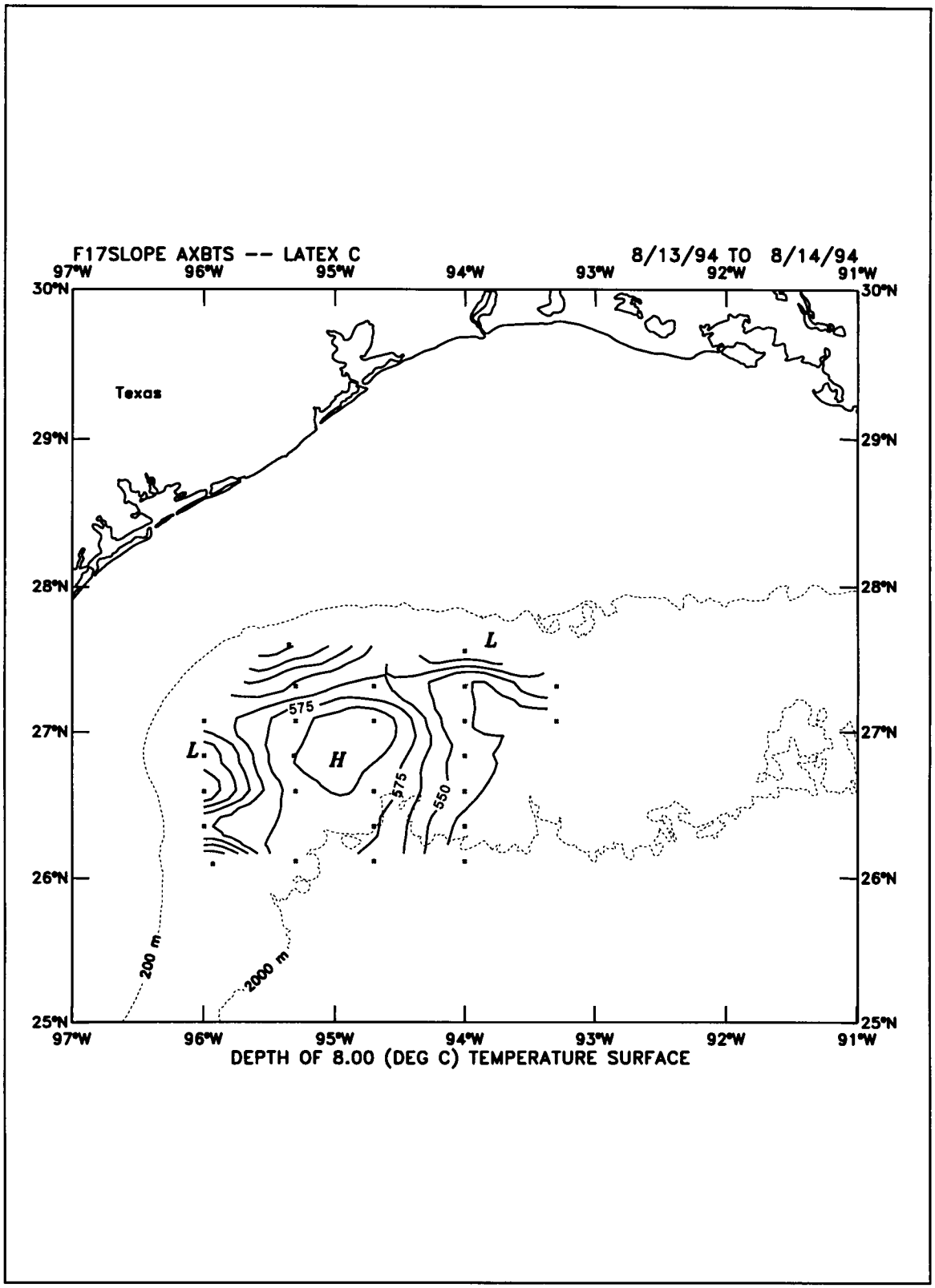

Figure 5.8-1c. Depth of the 8°C temperature surface from the F17SLOPE survey.

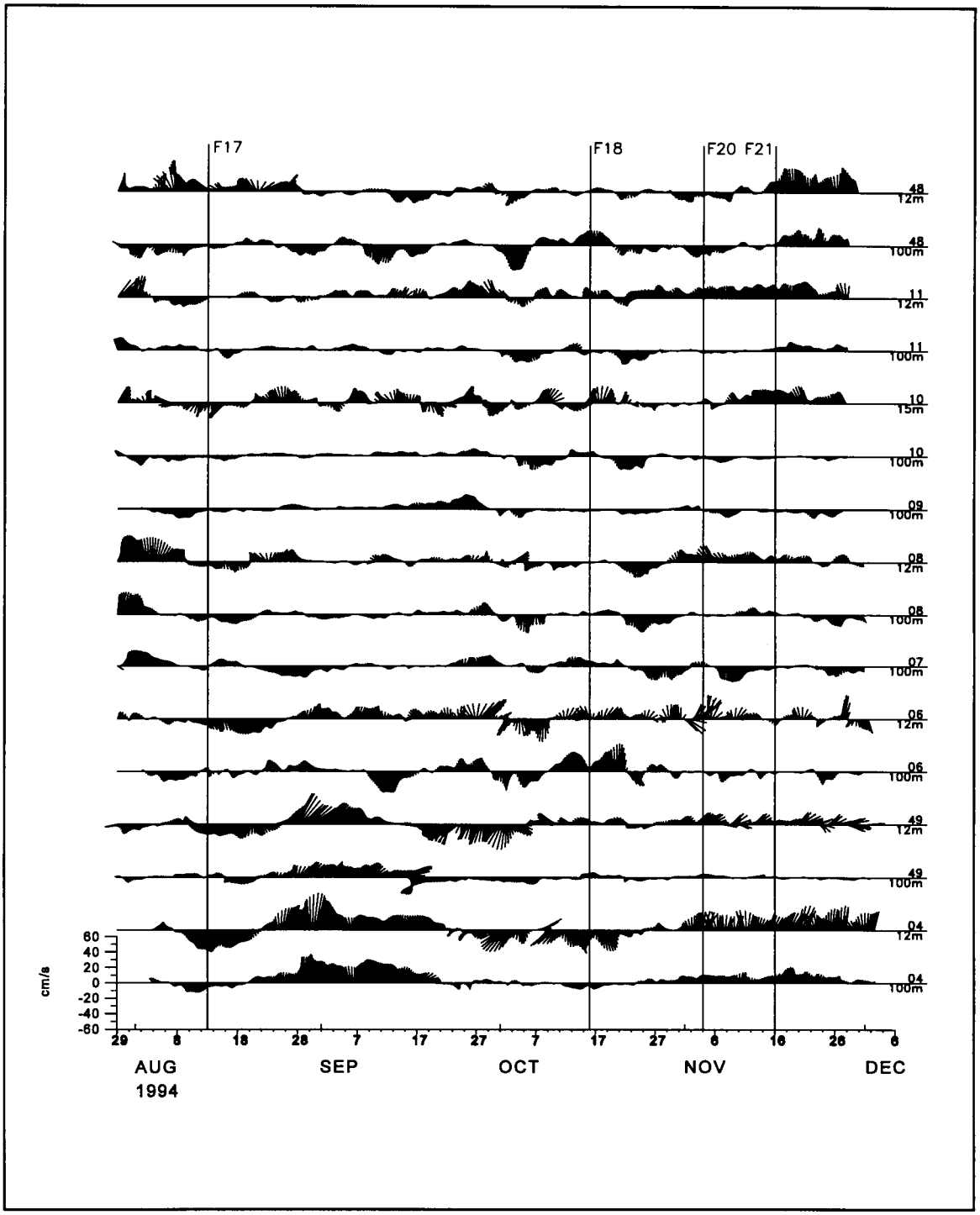

Figure 5.8-2. Stick plots of rotated 40-HLP currents from the LATEX A shelf-break moorings for the period from July 29, 1994 to December 6, 1994. Up is the along-isobath direction towards the east. Vertical lines mark (in order) the start of the F17SLOPE, F18LEDDY and F20SLOPE surveys, and the end of the F21SQUIRT survey.

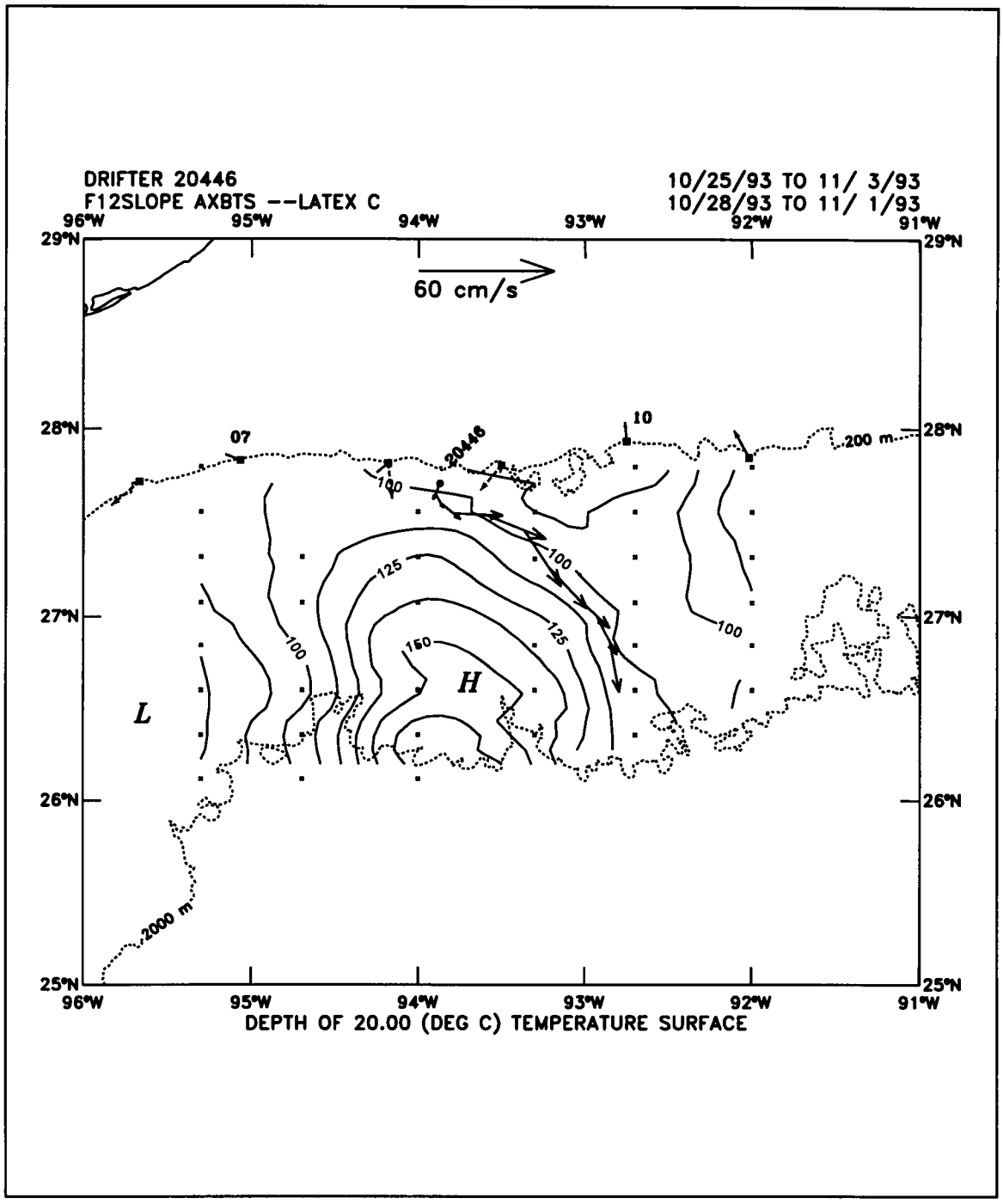

Figure 5.8-3a. Depth of the 20°C temperature surface from the F12SLOPE survey. Dashed and solid arrows emanating from squares represent the 12-m and 100-m daily mean 40-HLP currents, respectively, from the LATEX A shelf-break moorings for October 30, 1993. Daily velocity vectors from SCULP drifter 20446 are overlaid beginning October 25, 1993.

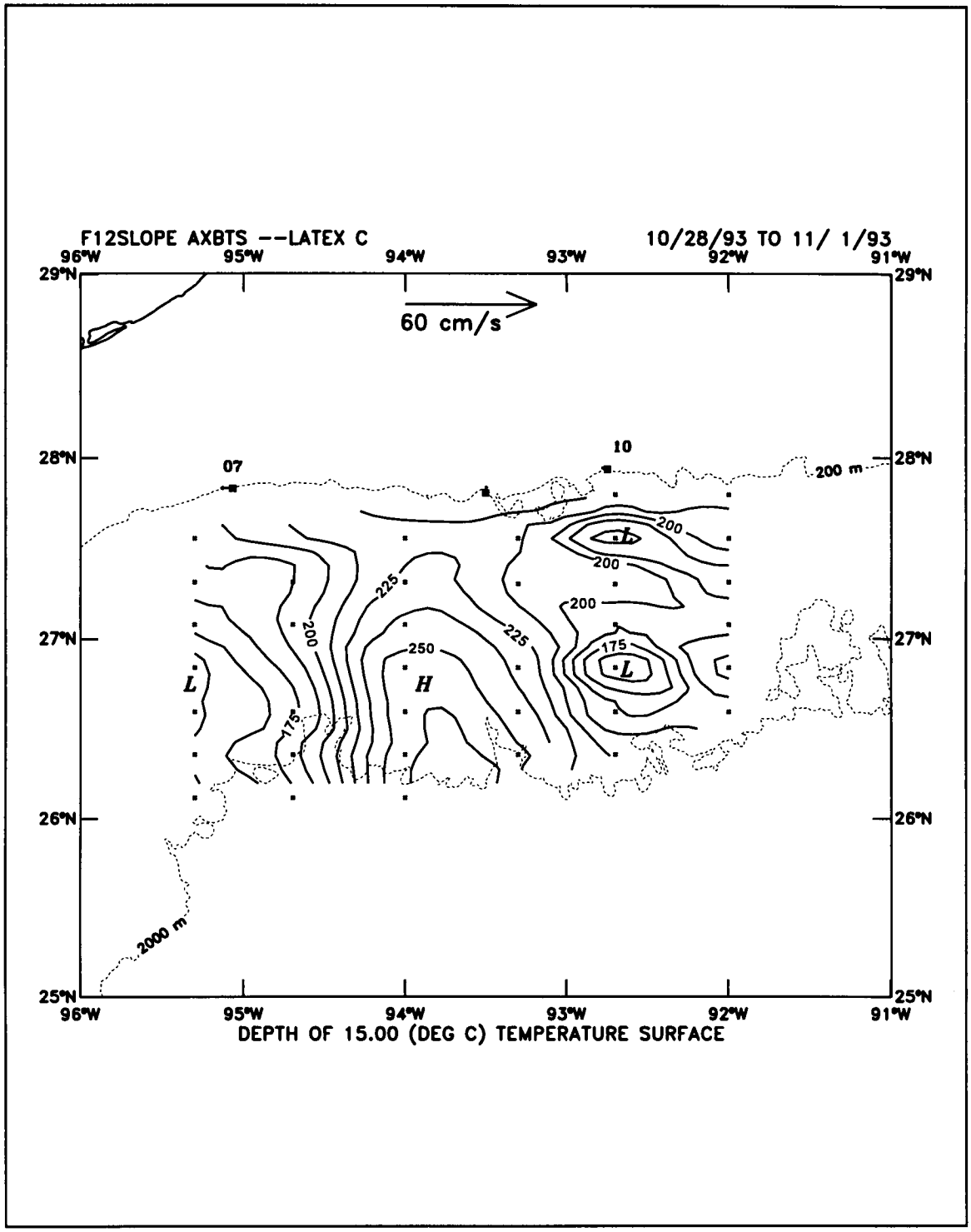

Figure 5.8-3b. Depth of the 15°C temperature surface from the F12SLOPE survey. Arrows emanating from squares represent bottom level (~200 m) daily mean 40-HLP currents from the LATEX A shelf-break moorings for October 30, 1993.

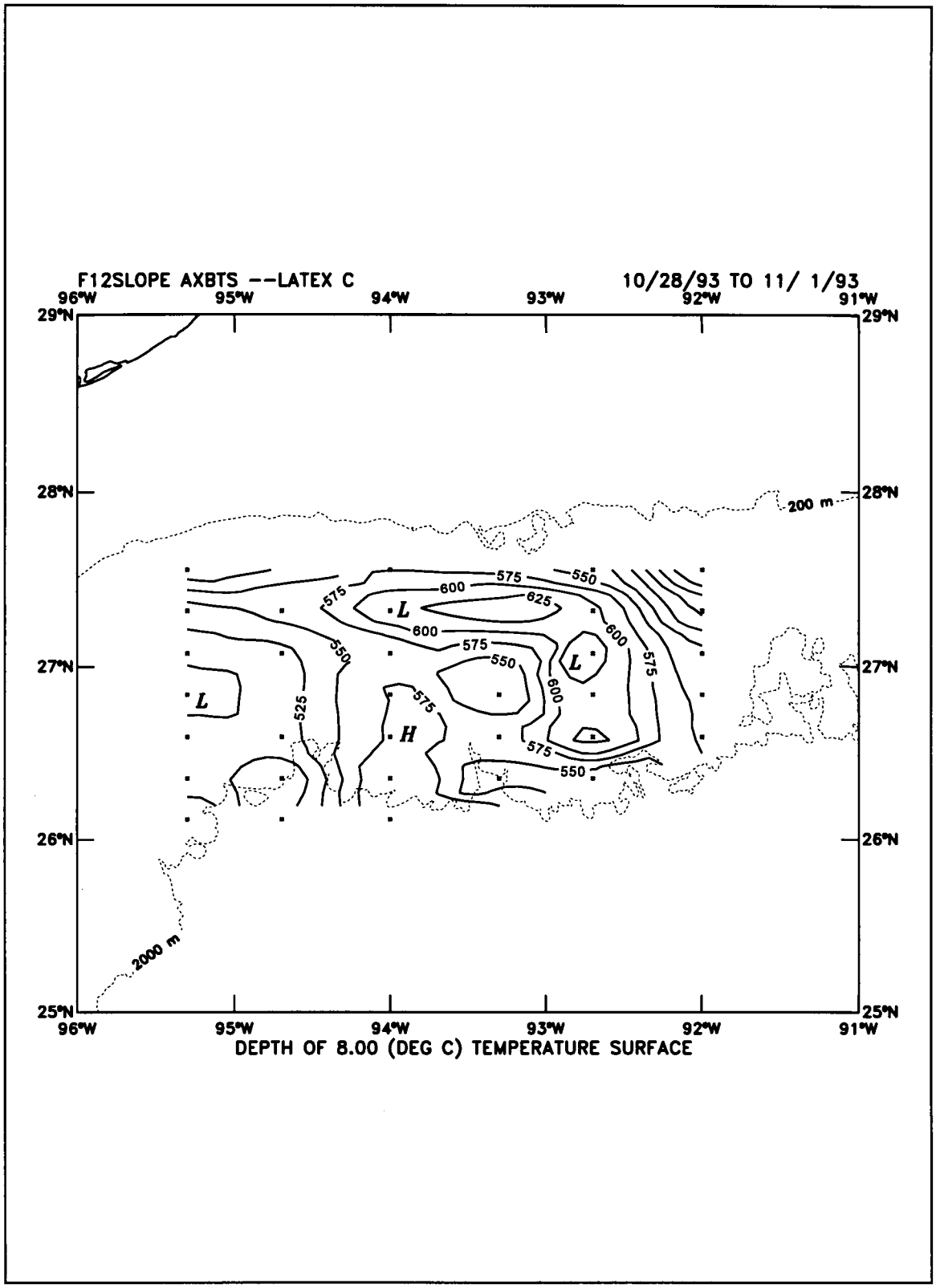

Figure 5.8-3c. Depth of the 8°C temperature surface from the F12SLOPE survey.

transports generated by counter-rotating slope-eddy flows. The interaction between the anticyclone and the smaller upper-slope cyclone to the east generated offshore currents around 94°W longitude (moorings 08 and 09). Drifter 20446 crossed the shelf break and moved rather slowly, at speeds of 20-30 $cm \cdot s^{-1}$ around the outer edge of the warm eddy.

The deep temperature surface (Figure 5.8-3c) shows the anticyclone breaking up into cells. The structure was particularly complex near 93°W longitude. The north-south section (Figure 5.8-4a) shows the small cyclone just south of the shelf break, but on the lower slope, at station 28. The isotherms above 11°C are raised, similar to the cyclone, and the deep isotherms are depressed. The east-west vertical section (Figure 5.8-4b) confirms this structure, and shows that the deep isotherms are depressed to greater depths than the adjacent warm eddy to the west (also see Figure 5.8-3c). The structure involves more than one AXBT drop in the north-south section, and therefore a faulty AXBT profile can be discounted. This kind of eddy, where the isotherms are raised and lowered above and below a subsurface level, has been observed quite frequently in the ocean, and has usually been classified as a sub-meso-scale coherent vortex (SCV) (McWilliams 1985). In particular, lenses of Mediterranean water (meddies) are observed at thermocline depths in the north Atlantic, and are thought to be an important part of heat and salt transport. Meddies are known to be long-lasting and individuals have been tracked for up to two years (Armi et al. 1989). Meddies rotate clockwise with maximum swirl velocities at the neutral level (e.g. at 11°C in Figure 5.8-4). A typical radius is about 10-20 km with 500 m to 1000 m depths. This scale is similar to a small cyclone observed in August 1992 (Figure 5.7-8). McWilliams (1985) argues that the most likely generation mechanism for SCVs is by mixing and subsequent geostrophic adjustment. This would not appear to be likely in this case, because the SCV is not isolated and there is no obvious source of anomalous water (such as Mediterranean water) to provide energy for the mixing. A more likely explanation in this case is from an instability of the eddy flows of the anticyclone. Circumstantial support for this comes from the GulfCet 07 survey, a month later, where there is no sign of a similar anomaly over the slope. Also, no other example of this kind of eddy has been observed in the many detailed slope surveys of the LATEX C and GulfCet programs, or in the many routine hydrographic transects of the northwest slope performed by Texas A&M University over the last decade (Biggs, personal communication). Therefore, it may be concluded, tentatively, that the particular "meddy-like" anomaly in F12SLOPE is a rather uncommon phenomenon involving eddy instabilities or interactions between eddies.

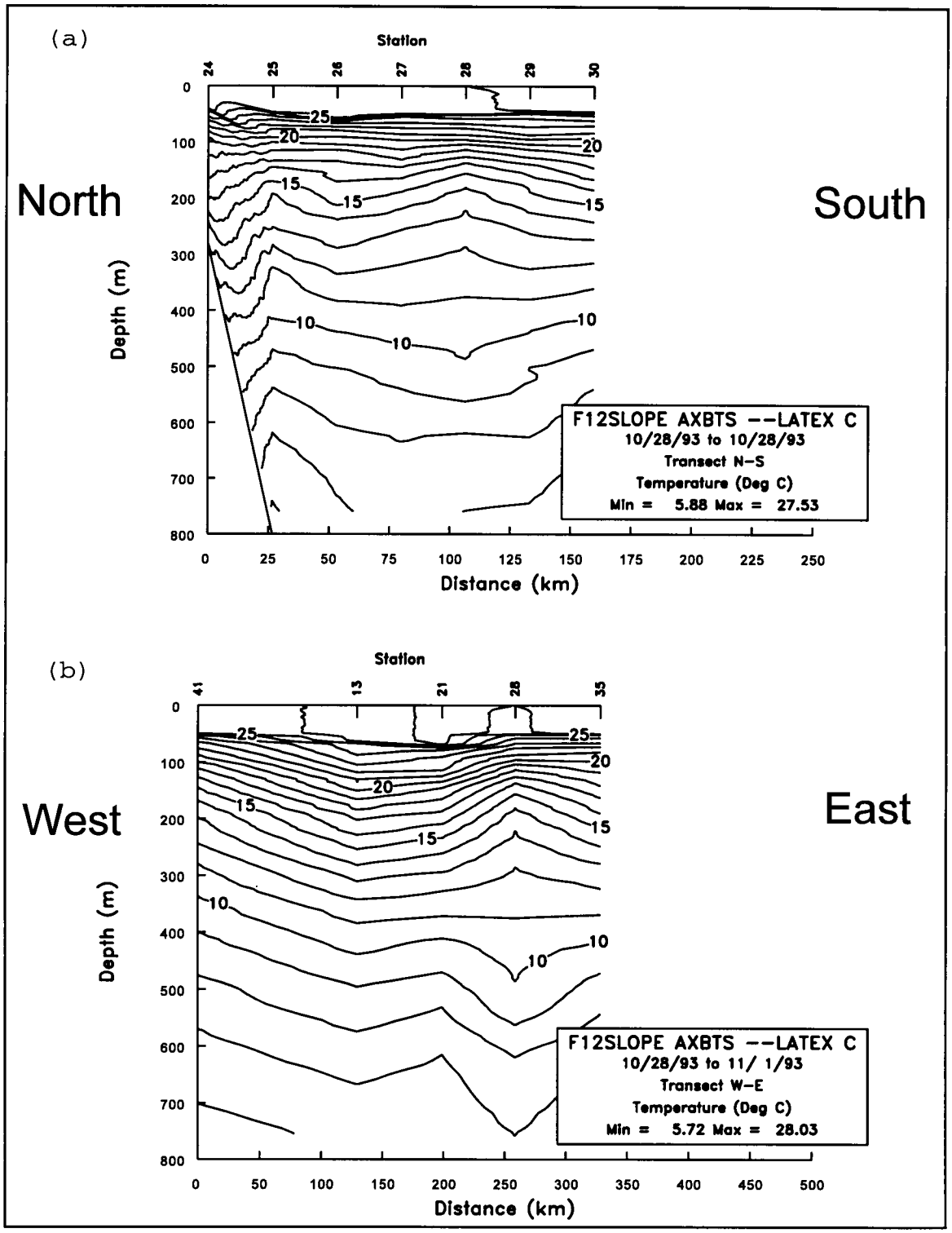

Figure 5.8-4. Vertical section of temperature from the F12SLOPE survey through the SLV for (a) the north-south section [stations 24 to 30] and (b) the west-east section [stations 41 to 35].

5.9 Summary

5.9.1 Loop Current Eddy Kinematics

The histories of four Loop Current anticyclones in the central and western Gulf of Mexico (U, V, W and Y) have been investigated using drifter track data, supplemented with data from hydrographic surveys and current meter moorings. All four eddies interacted to a greater or lesser degree with other cyclones and anticyclones and the topography of either the northern or western slope. Two of the eddies (U, and the main part of W) followed a southwestward path across the Gulf of Mexico, eventually interacting with the Mexican slope at about 23.5°N latitude. This southwestward path has been observed and described in previous drifter studies (Kirwan et al. 1984; Lewis and Kirwan 1985). However, the new information from drifter 02448 demonstrates that an eddy may stall against the Mexican slope and then move northward again, with little change in size or swirl velocities over a three-month period.

Both eddy U and eddy W separated from the Loop Current as very large anticyclones (diameters ~400 km), and both, shortly thereafter, reduced in size while still in the deep water of the central Gulf of Mexico by creating secondary anticyclonic eddies, V and W_N, before moving into the western Gulf. Both eddies V and W_N followed westward paths, and ended up in similar positions at the base of the northern slope at ~91°W longitude. Eddy V was vigorous, with a relatively short rotational period, and moved rapidly westward along the base of the slope until it reached the northwestern corner. The path of the center of this eddy was about 1° north of a previously observed eddy that propagated due west (Lewis et al. 1989; Hamilton 1990). After reaching the northwest corner, eddy V made an excursion up onto the slope and then returned seaward to the 2000 m isobath. Hydrography and the paths of drifters drogued at different depths indicate that the vertical central axis became tilted (near surface layers ~30 km northwest of the deeper layers) when it moved onto the slope. After this event in January 1993, the center of eddy V remained over the 2000 m isobath until April 1993. In addition, there are indications from altimetry (Jochens et al. 1996) that eddy V may have interacted with eddy U, which had coalesced with an earlier eddy, eddy T, to become located adjacent to the central Mexican slope at this same time. By May 1993, eddy V had weakened and moved north onto the middle slope of the northwest corner of the Gulf of Mexico with maximum surface velocities close to the shelf break. Eddy V then moved fairly quickly westward and probably dissipated in June or July 1993. The current meter records indicate that the anticyclonic circulation around eddy V influenced shelf-break flows in the

northwestern corner of the Gulf of Mexico from November 1992 through the summer of 1993. It is difficult to determine from the shelf-break current meter records, alone, whether eddy V dissipated and was replaced by another anticyclone, or continued to exist through the summer. By October 1993, a cyclone was in this position in the northwest corner of the Gulf of Mexico.

Eddy W_N was, from its origin, a much weaker anticyclone than eddy V. Initially, it followed a similar westward path along the base of the slope. In August 1993, it interacted with a cyclone on the lower slope. This event was captured by drifters in both features, and by AXBT surveys. The AXBT and AXCP data clearly show that the deeper layers of the cyclone advected the lower layers of eddy W_N northward over the slope, and caused the deeper sections of both eddies to be closer together than the near-surface circulations, thus tilting the central axes. Shortly after this event, eddy W_N moved rapidly away to the south-southwest, and removed with it all traces of the deeper warm anomalies that had been present over the middle and lower slope. The rapid translation into deeper water may, in part, have been caused by the anticyclonic flows of the trailing edge of the main part of eddy W, which had propagated across the Gulf of Mexico while eddy W_N was stalled at the base of the slope. One conclusion is that the paths and characteristics of anticyclones in the central and western Gulf of Mexico are often influenced by interactions with other warm and cold eddies, both over the lower slope and in the deep basin.

The last LATEX eddy, eddy Y, was large (~300 km in diameter) and vigorous. It behaved, in its central Gulf of Mexico phase, more conventionally, by moving west-southwestward, seaward of the lower slope, between September 1994 and February 1995. Hydrographic surveys showed at least two peripheral cyclones, one on the mid and upper slope due north of the center of eddy Y in October 1994 at about 89.5°W longitude, and one on its western edge in November 1994 at about 91°W longitude. Because of closely spaced surveys, about 10 days apart, the latter cyclone was shown to move northward onto the slope, in the same direction as eddy Y's swirl velocities, at a speed on the order of 5.18 $km \cdot day^{-1}$. Velocity data show a strong northward jet between the eddies and some evidence of tilting of the cyclone's axis towards the anticyclone. After the end of the field surveys, drifter tracks showed that eddy Y interacted with another large slope cyclone at 93.5°W longitude in March 1995, and then probably coalesced with an anticyclone against the western Mexican slope, at about 25°N latitude, in April and May 1995. The results of this study into Loop Current eddies and earlier

work (Hamilton, 1992) suggest that relatively large (100-150 km diameter) cyclones are quite often associated with Loop Current eddies.

An adaption of the translating ellipse model of Glenn et al. (1990) was used to parameterize the drifter tracks in terms of translation and swirl velocities, semi-major axis lengths, and inclination of the major axis from east. The results are summarized in Table 5.9-1 in terms of means over selected portions of the paths of eddies U, V, W_N, W and Y. There are a few general trends in these means. When an eddy approaches the Mexican slope, it seems to have a significantly longer rotational period than earlier in its life after it became separated from the Loop Current. This may be because these eddies (U and W) absorbed smaller, weaker anticyclones (T and W_N, respectively) in this region of the Gulf of Mexico. Eddies V and Y also showed increasing rotational periods with time. Second, when an anticyclone is in contact with the slope region, little decay or dissipation appears to occur over time scales on the order of one month. Third, an interaction with another eddy or with slope topography seems to decrease or stop the clockwise rotation rate of the semi-major axis of the ellipse. Fourth, larger more vigorous eddies (i.e., U and Y), in the central Gulf of Mexico, tend to have longer rotational periods and slower clockwise rotation rates than their smaller cousins (i.e., V and W_N).

It is noteworthy, in Table 5.9-1, that swirl velocities derived from drifters remain relatively constant. Simultaneous comparisons of drifter swirl velocities with the temperature fields show that, for a vigorous mature eddy, the drifter track tends to follow the 200 m contour of the 20° C isotherm. The resulting mean radii are generally about half the true radius of the region where the eddy is in approximate solid-body rotation. When the eddy begins to slow its rotation rate, the drifter tends to move to a larger radius, closer to the edge, thereby maintaining the swirl velocities calculated from the drifter track. Thus, swirl velocities alone may not be a good indication of the vigor of an anticyclone.

Long-term decreases in rotational periods are better indications of decreases in relative vorticity than swirl speeds because, if the drifter is in the region of near-solid body rotation, a decrease in swirl speed accompanied by a decrease in radius, and vice-versa, indicates no change in relative vorticity if the period remains the same. Interaction with topography may change the size and swirl velocities of the eddy by Taylor column stretching with no change in vorticity. Dissipation of eddy vorticity could occur from lateral friction and the radiation of planetary waves. The latter may

TABLE 5.9-1. Summary statistics of ellipse model parameters.

Eddy	Drifter	Dates	Mean				Mean Clockwise Rotation Rate of Major Axis ($deg \cdot day^{-1}$)	Comments
			Period (days)	Translation Speed ($cm \cdot s^{-1}$)	Swirl Speed ($cm \cdot s^{-1}$)	Radius (km)		
V	02447	09/20/92-11/11/92	7.3±0.6	6.8±2.7	55±11	55±9	8	Westward translation to 95°W
V	02447	11/11/92-01/21/93	8.3±1.0	4.4±2.7	48±7	55±8	4	Interaction with slope
V	06938	05/12/93-06/03/93	9.4±1.1	6.7±2.8	49±8	62±5	0	Final stages of decay on upper slope
U	02449	11/06/92-01/02/93	10.3±1.2	5.9±3.4	34±7	48±6	4	Southwestward translation across central Gulf of Mexico
U+T	02449	01/19/93-03/30/93	12.7±1.5	5.4±2.7	28±8	50±17	2.5	Approach to Mexican slope
W_N	02448	07/07/93-08/08/93	8.2±1.2	5.7±2.0	17±9	20±13	4.5	Interaction with slope cold eddy
W_N	02448	08/08/93-09/02/93	6.3±0.5	8.6±2.6	36±9	31±9	0	SSW translation into western Gulf of Mexico
W	02448	09/19/93-10/15/93	13.8±1.7	7.3±3.0	43±10	79±12	2	Approach to Mexican slope
W	02448	10/15/93-12/05/93	13.1±1.4	3.8±1.9	45±7	80±10	2	Stalled against Mexican slope
W	02448	12/05/93-01/12/94	12.4±0.9	5.6±2.7	47±6	80±11	0	Northward migration along the Mexican slope
Y	12376	09/22/94-01/10/95	10.4±2.5	5.8±3.0	48±9	69±20	2	WSW translation 89°W - 93°W
Y	12377	10/17/94-02/03/95	11.3±2.1	5.8±3.0	47±17	72±22	2	WSW translation 89°W - 93°W

occur in interaction with other eddies and slope topography. Friction is probably the principal mechanism for the slow decay of eddies as they cross the deep basin of the central Gulf. Section 4.6 estimates the decay of eddies from altimetric estimates of vorticity and, based on the exponential fit (Figure 4.6-1), it would be expected that the eddy rotation period would increase by about two days between 90°W and 95°W longitude. This is about the difference between the eastern and western parts of the eddy V and eddy U and U + T analyses. The difference between eddies W_N and W is larger, but these two features can be considered to be different eddies (Table 5.9-1).

5.9.2 Ensemble Statistics

The previous section summarizes the statistics of the individual Loop Current eddies studied during the LATEX program. Section 4.7 calculates the basic mean statistics using four eddies (B, C, D and F) tracked using altimeter data during the GEOSAT mission. This section calculates mean Lagrangian statistics for eddies that were tracked with drifters for more than one month between 1985 and 1995. The drifter paths prior to LATEX were obtained by the previous Gulf of Mexico Physical Oceanography Program, and their kinematic analyses are given in SAIC (1988, 1989), Lewis et al. (1989) and Biggs et al. (1996). For this analysis, these paths were smoothed and parameters calculated using the least-square ellipse model of Glenn et al. (1990), exactly the same as for the LATEX drifters discussed above. Table 5.9-2 gives the eddy names and the drifters that were analyzed. Figure 5.9-1 shows the paths of the centers of these eddies derived from the ellipse model calculations.

The ensemble of eddy paths in Figure 5.9-1 has a predominantly southwesterly trend and occupies a broad area of 2-3° latitude width in the center of the deep basin. The eddy centers occupy similar locations to those obtained from altimetry and given in Figure 4.5-1. In this context, the path of eddy V appears to be anomalous in that it moves from east to west (Figure 5.2-1) and is closer to the slope than any other observed eddy. There are substantial deviations from the southwesterly trend near the Mexican slope. Therefore, in the statistics, the paths have been divided into portions that are east and west of 94°W longitude (Table 5.9-2), so that eddies freely propagating through the deep basin are separated from those eddies being influenced by the topography of the Mexican slope.

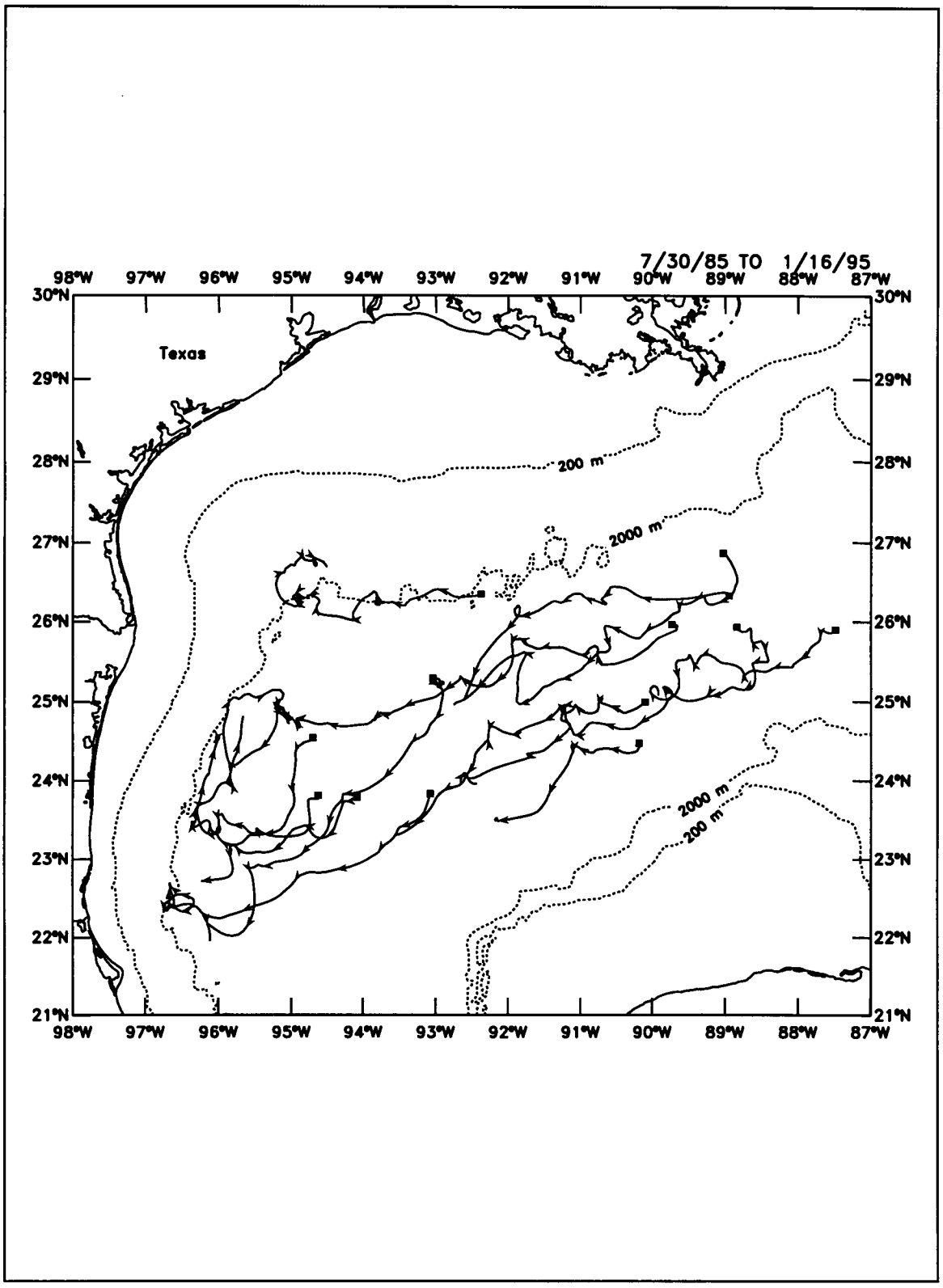

Figure 5.9-1. Paths of eddy centers used for ensemble statistics. Arrow heads are at 10 day intervals.

Table 5.9-2. Drifters in Loop Current Eddies.

Eddy	Drifter	Dates	
		East of 94°W	West of 94°W
A	05495	08/12/85-09/05/85	09/11/85-12/11/85
B	03378	07/29/85-11/16/85	11/17/85-03/08/86
C	03379	03/14/86-05/31/86	--
E	03344	11/21/87-02/14/88	--
E	03353	--	06/22/88-09/11/88
F	03345	05/27/88-11/30/88	--
T	07493	02/26/92-04/21/92	04/25/92-06/30/92
U	02449	11/06/92-01/02/93	--
U + T	02449	--	01/19/93-03/30/93
V	02447	09/20/92-10/20/92	10/29/92-01/21/93
W_N	02448	06/20/93-09/02/93	--
W	02448	--	09/19/93-01/12/94
Y	12376	09/22/94-01/16/95	--
Total Number of Days		**824**	**625**

Following Davis (1985), the Lagrangian auto- and cross-correlations of the U and V components of the center translation velocities are calculated for each path (or partial path) in Figure 5.9-1 that is east or west of 94°W longitude and then ensemble averaged. The results are given in Figure 5.9-2. In the deep basin the Lagrangian auto-correlation time scale is about five days for both components. This is about half the mean eddy period. West of 94°W longitude, the U and V component time scales are about 13 and seven to eight days, respectively, which are on the order of the eddy period. Auto-correlation time scales for the smoothed drifter velocities are about half the eddy period, as would be expected for strongly circular motions (not shown). The eddy center velocity ensemble mean cross-correlations are relatively weak in the basin, but significant near the slope. For the latter, V lags behind U by about seven days, and the symmetrical shape indicates a periodicity on the order of 20 days. Examination of the paths in Figure 5.9-1 shows many portions with anticyclonic curvature and periodicities on the order of 20 to

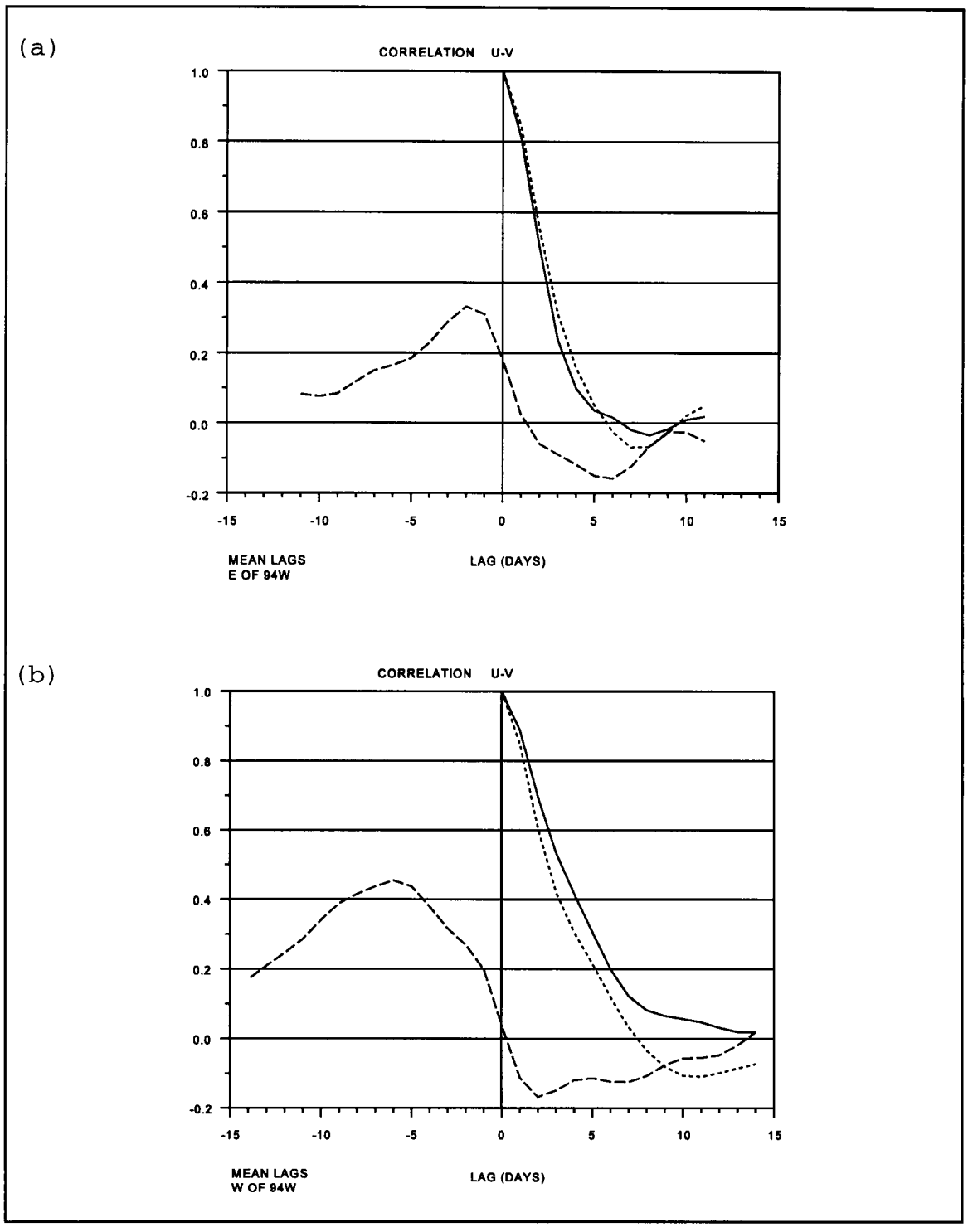

Figure 5.9-2. Lagrangian time-lagged correlations of eddy translation velocity components for (a) means for paths east of 94°W longitude and (b) means for paths west of 94°W longitude [<UU> (solid), <VV> (short dashed) and <UV> (long dashed)].

30 days in all parts of the Gulf of Mexico. This periodicity was also noted in the individual analyses of eddies V, U+T and W (see Figures 5.2-11, 5.3-2 and 5.4-1). Thus, Lagrangian time scales are relatively short compared to the ~100 day path length, but increase towards the slope and become less isotropic with the east-west (U) time scale, becoming longer as the east-west locations become more stationary adjacent to the slope.

Ensemble Lagrangian averages for the velocity components, mean eddy radius, swirl velocity and period are given in Table 5.9-3. In the basin, mean translation speed is 4.2 $cm \cdot s^{-1}$ at 243°T. The principal axis of the variability is very similar (35°) to the mean direction of the paths in Figure 5.9-1. Against the slope, the mean translation speed is less than half that east of 94°W longitude, and is approximately directed east-west. The small northward velocity (v) coupled with large northward variance, and the principal axis being directed more northerly along the trend of the slope, implies that eddies move equally in either direction (northward or southward) along the slope.

Table 5.9-3. Lagrangian Mean Statistics of Gulf of Mexico Loop Current Eddies.

Central Gulf of Mexico (east of 94°W Longitude)				
Variable	Units	Mean	Standard Deviation	Principal Axes*
East Translation U	$cm \cdot s^{-1}$	-3.76	3.93	35°
North Translation V	$cm \cdot s^{-1}$	-1.91	3.68	
Geometric Mean Radius	km	65.1	17.4	
Swirl Velocity	$cm \cdot s^{-1}$	46.8	12.8	
Eddy Period	days	10.2	1.6	
Western Gulf of Mexico (west of 94°W Longitude)				
East Translation U	$cm \cdot s^{-1}$	-1.96	3.81	69°
North Translation V	$cm \cdot s^{-1}$	-0.32	4.17	
Geometric Mean Radius	km	51.6	12.4	
Swirl Velocity	$cm \cdot s^{-1}$	36.0	8.1	
Eddy Period	days	10.8	1.9	

* Principal Axis direction is counterclockwise from the east.

There is no evidence, in this limited sample of seven eddies, that eddies prefer to move north after colliding with the slope. This is contrary to the analysis of eddy paths from imagery by Vukovich and Crissman (1986). They indicated that northward movement is characteristic of eddies colliding with the slope around 23°N to 24°N latitude.

Mean radii and swirl velocities decrease between east and west, but the period only increases by 0.6 days. This is less than observed for individual eddies, such as U, and may be the result of using a different set of eddy paths in each of the regions. However, these three parameters together indicate a weakening of the eddy circulation in the west.

5.9.3 Slope Eddies

Detailed surveys, combined with drifter tracks, particularly in the last year of the LATEX C field program, have shown that the Louisiana-Texas slope has frequent occurrences of warm and cold eddies with a wide range of scales. At large scales, westward propagating Loop Current eddies intrude over the lower and mid slope (e.g. eddies V, W_N, X and Y). Loop Current eddies can also move completely onto the slope, usually in the northwest corner of the Gulf of Mexico, apparently when these circulations are weakening and/or are moved northwards by eddy circulations further south against the Mexican slope. Eddy V is the prime example of this phenomenon in these data; however, the rather similar anticyclone, of unknown origin, found in the northwest corner of the Gulf of Mexico in August 1994 (F17SLOPE) seems to be another example. Warm eddies in the northwest corner of the slope can persist in approximately the same position for several months.

Vigorous cyclones on the order of 100 km to 150 km in diameter have been mapped and shown to move both on and off the slope, depending on the direction of the swirl velocities of adjacent anticyclones. The cyclone to the west of eddy Y moved northward over the lower slope at a speed of ~5 $km \cdot day^{-1}$. The cyclone over the 2000 m isobath in May 1994 (F15SLOPE and F16SQUIRT) moved southeastward into deeper water, apparently affected by the deep water anticyclone to its southwest. Other data show that a lower-slope cyclone can persist in approximately the same position for several months. For example, according to drifter data, the cyclone observed in December 1993 (F13SQUIRT/F14LEDDY) persisted until at least March 1994. In addition, persistent slope cyclones have been observed in previous studies (Hamilton 1992). However, it is not clear from present data whether they are always associated with a companion anticyclone as in the two examples cited above. Isolated cyclones can exist on the slope, perhaps as

the result of an earlier anticyclone-cyclone interaction, and then interact with other westward moving eddies, such as the case of the slope cyclone with eddy W_N. It is also noted that cyclones of these kinds of scales do not appear to have any preferred sites. They are found at all positions over the slope including the northwest corner of the Gulf of Mexico (see Figure 5.7-6). A theory of cyclone generation by topographic dispersion and vortex stretching for an isolated vigorous anticyclone interacting with a steep north-south slope was given by Smith (1986). However, if this were the only mechanism, cyclones would be found more frequently in the west, which does not seem to be the case. This theory does, however, explain the formation of a cyclone by eddy B's interaction with the Mexican slope in 1985 (Lewis et al. 1989).

The May and November 1994 cyclones were intensively surveyed and permitted a first look at their velocity and temperature structures. Both cyclones were similar, and though a cold central perturbation was detected to the limit of the measurements (1500 m depth), the most energetic velocities (>5 $cm \cdot s^{-1}$) were between the surface and 800 m to 1000 m levels. As expected for a cyclone where horizontal temperature gradients are very small in the upper 200 meters, vertical velocity shears were small. The radius of near-solid-body rotation was 30 to 50 km, and maximum speeds (~40 to 50 $cm \cdot s^{-1}$) occurred in a broad subsurface region between 100 m and 300 m depth on the outer edge of the rotating solid-body center. Both the May and November 1994 cyclones had a small warm central perturbation between the base of the mixed layer and about 200 m depth. This may have been the result of entrainment of water from the adjacent warm eddy, or that the cyclones' upper-layer swirl velocities converged and produced sinking in the middle of the eddies. There is also evidence from the temperature fields that the vertical central axes of the cyclones were tilted, with the surface waters closer to the adjacent anticyclone than the deeper waters. However, eddy W_N and its slope cyclone provide a counter-example; in this case the deeper waters of the cyclone were closer to the anticyclone than the surface waters. In all cases, there is some uncertainty in these conclusions due to the spacing of the AXBT and AXCP stations.

The surveys showed that there were even smaller eddies, on the order of 30 to 50 km diameter, that were quite common on the slope, and on the upper slope adjacent to the shelf break. Both cyclones and anticyclones were observed, and there were examples of anticyclones with differing depth distributions of their respective temperature fields. In the May 1994 survey, a mid-slope anticyclone had a signature in the 15°C surface but not in the 8°C surface; and an upper-slope anticyclone of

similar size was observed to have a stronger signal in the 8°C surface. In some cases, these eddies were observed to propagate around the periphery of the larger cyclones and anticyclones on the slope, in the direction of the swirl velocities of the larger eddies. The two eddies need not necessarily have opposite rotation directions. These phenomena have been observed in deep water, and suggest that the smaller eddies are related to instabilities or perturbations of the outer shear zones of the larger eddies. The instability mechanism may be related to the theory of the formation of Gulf Stream cold frontal eddies in the South Atlantic Bight by Luther and Bane (1985). This would require both a bottom slope and a velocity field with both horizontal and vertical shears similar to that of larger anticyclones. This type of small eddy motion can even occur when they are adjacent to the shelf break, and so can be a major part of the signal in the observed shelf-break current velocity time series. More than one of these perturbations, often with opposite rotational velocities, can occur on the periphery of larger slope eddies.

The occurrence of adjacent, counter-rotating, upper-slope eddies seems to be the principal method by which water is exchanged across the shelf break. The multitude of eddies, of differing scales and strengths over the slope, can produce regions of intense flow that can transport material across the general trend of the isobaths. Drifters are often moved from one eddy periphery to the next as they make their way from the outer shelf to the central basin, or vice-versa. The small upper-slope eddies also often mask the effect on the shelf-break currents of larger, more vigorous slope eddies. Thus, even though a vigorous cyclone may be on the lower slope, an intervening upper-slope eddy may prevent its flows from being directly measured by shelf-break current meters. In other cases, however, currents directly attributable to a larger slope eddy, or a Loop Current eddy that has intruded over the lower slope, are clearly detected by the shelf-break current meters.

This description of the slope eddy field characteristics provides a tentative explanation for the shelf-break current meter observations. A preliminary analysis of the subtidal currents with respect to the hydrographic survey and drifter tracks indicates that flows are not likely to be coherent, even between quite closely spaced stations. Currents can only occasionally be ascribed to major Loop Current eddies passing to the south. Events can be observed to propagate both eastward and westward, depending on the direction in which the small upper-slope eddies are moving, which is related to adjacent larger slope eddies' swirl velocities. The lower frequency events can be quite long lasting (weeks to months)

depending on the persistence of the nearby slope eddy (e.g. eddy V in the northwest corner of the Gulf of Mexico). This model also predicts that cross-isobath current fluctuations are likely to be as large as the along-isobath fluctuations, because of onshore-offshore flows forced by the eddies. At various times, the time series plots of shelf-break currents presented in this report exhibit all of these characteristics. Thus, shelf-break currents, excluding wind-forced or residual flows, appear to be closely related to the slope eddy field. Therefore, it may be difficult to quantify the dynamics of the observed flow fields in terms of more usual continental shelf theories.

In light of the influence of slope eddies on shelf break circulation, the eastward flows along the shelf break postulated by Cochrane and Kelly (1986), as part of a cyclonic shelf gyre, may not be a continuous flow. Cochrane and Kelly (1986) based their results on a limited number of seasonal shelf-wide hydrographic cruises. The slope eddy field was not sampled. Thus, eastward recirculation may have occurred fortuitiously because of the presence of a warm eddy in the northwest corner of the Gulf of Mexico. This occurred in the first part of the SCULP drifter program when eddy V was over the slope for several months; the drifters moved eastward but stalled east of 94°W longitude and then often jumped offshore (Niiler, pers. comm.). There is one example in the velocity maps where the flow is apparently eastward over most of the shelf break (Figure 5.7-1a), but even this can be attributed to a sequence of warm slope eddies, and such flows only lasted a few weeks (Figure 5.7-9). There are, however, many counter-examples of both eastward and westward flows along the shelf break (e.g., Figure 5.7-5a). Thus, any eastward recirculation of southward-flowing shelf waters along the shelf break is probably an intermittent phenomenon with time scales of weeks, rather than seasons.

VI. SUMMARY AND CONCLUSIONS

This report documents analysis of both satellite altimeter data from the Navy's GEOSAT mission, from April 1985 through December 1989, and the data collected over the slope and deep water of the northwestern Gulf of Mexico during this three-year physical oceanography program. Data from the LATEX A hydrographic cruises, shelf break current meters, and drifters originally deployed on the shelf; the SCULP drifter program; the GulfCet program; and Texas A&M Ship-of-Opportunity cruises have been used to enhance the analysis. Additionally, both the GulfCet and Texas A&M Ship-of-Opportunity cruises deployed drifters in various features on request.

The data collected during the field portion of this program consisted of 704 temperature and 71 velocity records from airborne expendable probes and 37 (including LATEX A drifters which left the shelf) Argos-tracked Lagrangian drifter tracks. The temperature and velocity data were collected during a series of 21 aerial surveys including nine Slope Surveys, five Loop Current Eddy Surveys, and seven surveys of small scale circulation features. The three Slope Surveys made during each year used a regular grid and were timed to generally coincide with LATEX A quarterly hydrographic surveys. The remaining surveys were designed to cover a particular feature in detail or, in the case of Loop Current eddies, to establish the major dimensions of the feature and locate the center for purposes of deploying a drifter. Thermal front analyses from AVHRR imagery were provided by LATEX B and used in real time to plan feature surveys. Altimetry data from the ERS-1 and TOPEX/Poseidon satellites were provided by the University of Colorado for the same purposes. Data were also available from the offshore industry to aid in Loop Current eddy detection.

GEOSAT data from the April 1985 through December 1989 time period were acquired from NOAA. These originally consisted of the along-track records from the ERM and cross-over points from the GM. Geodetic mission along track data (April 1985 through September 1986) were declassified by the Navy in the summer of 1995 and released to the public. Various mean surfaces were available during the program and culminated in the OSUMSS95 released in 1995. Declassification of the GM along-track data and release of the OSUMSS95 during the summer of 1995 meant that all the data and tools were finally available to produce accurate, satellite altimetry derived climatologies of sea surface height, wave height and wind speed for the Gulf of Mexico. These GEOSAT derived climatologies are to be found in Appendices A, B, and C, respectively.

Qualitative and quantitative evaluations of the mean surface were made using survey data and drifter data to determine the validity and accuracy of the mean surface. The standard deviation (~2 cm) of the mean sea surface height was less than the estimated along-track precision of the altimeter (~5 cm rms), which confirms the validity of the mean surface used.

Comparisons of drifter velocities and altimetry derived velocities had correlations greater than 0.70 during both the GM and the ERM, which confirms the consistency of the climatology during both the GM and the ERM. Comparison of sea surface height with either dynamic topography or the depth of the 8°C isotherm indicated the altimeter values were about 150% of the hydrography derived values. The difference could be accounted for by the barotropic signal to which the hydrography is insensitive and the baroclinic component below the depth of the hydrographic data. The conclusion is that the altimeter preserves the sea surface height signal and the slope of the sea surface.

The data have also been used to track a series of five Loop Current eddies (out of six detected during the GEOSAT period) in the Gulf of Mexico over their life span and to compare the statistics with similar measures derived from drifter tracks and from survey data. Comparisons of various dimensions and kinematic parameters derived from altimetry and from drifter tracks or cited in the literature are in excellent agreement. Observation of the life histories of individual eddies and their interactions with the Mexican slope, other Loop Current eddies and with smaller cyclones and anticyclones provide new insight into those interactions. For example, the merger of eddies B and C in May-July 1986 was well observed. The merger apparently conserved mass and circulation with the required energy input coming from an adjacent smaller cyclone. The data suggest that the historically observed southwestward Loop Current eddy path toward the western Gulf of Mexico is the normal path in the absence of external forcing. Deviations from that path are likely the result of eddy-eddy interactions.

The overall conclusion from analysis of the historical GEOSAT data is that satellite altimetry referenced to an accurate mean surface can provide an accurate, all-season, all-weather means of observing individual features and basin wide circulation, barring data outages.

Observations of Loop Current eddies during the field period and computation of various eddy dimensions and kinematic parameters were consistent with similar estimates from the GEOSAT period and with values cited in the literature. The availability of extensive drifter data and frequent survey

data allowed observation of some of these eddies in greater detail and over longer time periods than in the past, except for the GEOSAT period just discussed. Again, it was possible to observe the interaction of the Loop Current eddies with other features. The analysis suggests that Loop Current eddies have a longer rotational period as they approach the Mexican shelf than earlier in their lives; little decay occurs over scales of a month if the eddy is in contact with the slope; eddy-eddy or eddy-slope interactions seem to slow or stop the anticyclonic rotation of the major axis; and larger eddies in the central Gulf of Mexico have longer rotational periods and slower rotation rates than smaller eddies. Comparison of the temperature structure of an eddy with drifter derived swirl velocities indicate that swirl velocities by themselves may not be a good indication of eddy vigor since the drifters tend to move toward the edge of the eddy as the eddy rotation rate slows.

Cyclones on the order of 100-150 km diameter were detected in deep water and on the slope and monitored in various surveys. They could move rapidly or stay in one place for several months depending on the relative location of nearby anticyclones, including Loop Current eddies. Such eddies were often detected with a nearby anticyclone but were also detected alone on the slope. Interactions of these cyclones with nearby anticyclones resulted in tilting of the central axis, mostly toward the anticyclone, but in one case, away from the anticyclone.

Even smaller cyclones and anticyclones were detected near both cyclones and anticyclones, in deep water and on the slope. The smaller features sometimes were observed to propagate around the periphery of the larger eddy, both in deep water and on the slope. This type of eddy motion also occurred at the shelf break. The motions at the shelf break may be a primary means of shelf-water export or intrusion of slope water on the shelf. The presence of such eddy motions over the slope and shelf break may explain the lack of coherence among current meter records at the shelf break even over relatively short length scales. These eddies may also occasionally mask the effect of larger eddies on the shelf break currents. On other occasions the shelf break currents are clearly related to the larger cyclones and anticyclones on the slope.

The eddy field of the central and western Gulf of Mexico is shown to be complex, with eddies of many scales being detected. Interactions among these eddies can influence the paths of even the largest anticyclones, the Loop Current eddies. The interactions at the shelf break may also be a major mechanism for shelf-slope exchanges.

In conclusion, the major scientific results are the description of Loop Current eddy behavior using GEOSAT altimetry and validation by drifter data; documentation of the complexity of the eddy field including interactions among cyclones and anticyclones; and analyses which suggest that the eddy field could be responsible for the lack of coherence between LATEX A current meter records at the shelf break. The significant results on the complexity of the eddy field and its probable impact on shelf break currents validate the use of aerial surveys to collect detailed data over such a large area in a short period of time.

VII. REFERENCES

Anderson, O.B., P.L. Woodworth, and R.A. Flather. 1995. Intercomparison of recent ocean tide models. J. Geophys. Res. 100:25261-25282.

Armi, L., D. Hebert, N. Oakley, J.F. Price, P.L. Richardson, H.T. Rossby, and B. Ruddick. 1989. Two years in the life of a Mediterranean salt lens. J. Phys. Oceanogr. 19: 354-370.

Atkinson, L.P., T.N. Lee, J.O. Blanton, and G.-A.Paffenhöfer. 1987. Summer upwelling on the southeastern continental shelf of the U.S.A. Prog. Oceanogr. 19:231-266.

Biggs, D.C., G. Fargion, P. Hamilton, and R. Leben. 1996. Cleavage of a Gulf of Mexico Loop Current eddy by a deep water cyclone. (submitted to J. Geophys. Res.).

Boyd, J.D. 1987. Improved depth and temperature conversion equations for Sippican AXBTs. J. Atmos. Oceanic Technol. 4:545-551.

Boyd, J.D. and R.S. Linzell. 1993. Evaluation of the Sparton tight-tolerance AXBT. J. Atmos. Oceanic Technol. 10: 892-899.

Brooks, D.A. 1984. Current and hydrographic variability in the northwestern Gulf of Mexico. J. Geophys. Res. 89(C5):8022-8032.

Brooks, D.A., and R.V. Legeckis. 1982. A ship and satellite view of hydrographic features in the western Gulf of Mexico. J. Geophys. Res. 87(C6):4195-4206.

Carter, D.J.T., P.G. Challenor, and M.A. Srokosz. 1992. An assessment of GEOSAT wave height and wind speed measurements. J. Geophys. Res. 97:11383-11392.

Cartwright, D.E. and A.C. Edden. 1973. Corrected tables of tidal harmonics. Geophys. J. of the Roy. Soc. 23:253-264.

Cartwright, D.E. and R.J. Taylor. 1971. New computations of the tide generating potential. Geophys. J. of the Roy. Soc. 23:45-74.

Chelton, D.B. and F.J. Wentz. 1986. Further development of an improved altimeter wind speed algorithm. J. Geophys. Res. 91:14150-14260.

Cheney, R.E. and J.L. Lillibridge. 1992. ERS-1 fast delivery altimeter data for tropical ocean monitoring. EOS, Trans. Amer. Geophys. Un. 73:84.

Cheney, R.E., B.C. Douglas, and R.W. Agreen. 1991a. GEOSAT altimeter crossover difference handbook. NOAA Manual NOS NGS 6, Rockville, Md.

Cheney, R.E., N.S. Doyle, B.C. Douglas, R.W. Agreen, L. Miller, E.L. Timmerman, and D.C. McAdoo. 1991b. The complete GEOSAT altimeter GDR handbook. NOAA Manual NOS NGS 7, Rockville, Md.

Churchill, J.H., P.C. Cornillon, and G.W. Milkowski. 1986. Cyclonic eddy and shelf-slope water exchange associated with a Gulf Stream warm-core ring. J. Geophys. Res. 91(C8):9615-9623.

Cochrane, J.D., and F.J. Kelly. 1986. Low-frequency circulation on the Texas-Louisiana continental shelf. J. Geophys. Res. 91:10645-10659.

Cooper, C.K., G.Z. Forristall, and T.M. Joyce. 1990. Velocity and hydrographic structure of two Gulf of Mexico warm-core rings. J. Geophys. Res. 95:1663-1680.

Cressman, G.P. 1959. An operational objective analysis system. Mon. Weather Rev. 87:367-374.

Crosby, D.S., L.C. Breaker, and W.H. Gemmill. 1993. A proposed definition for vector correlation in geophysics: theory and application. J. Atmos. Oceanic Tech. 10:355-367.

Cushman-Roisin, B. 1989. On the role of filamentation in the merging of anticyclonic lenses. J. Phys. Oceanogr. 19: 253-258.

Cushman-Roisin, B., W.H. Heil, and D. Nof. 1985. Oscillations and rotations of elliptical warm-core rings. J. Geophys. Res. 90:11756-11764.

Davis, R.E. 1985. Drifter observations of coastal surface currents during CODE: The statistical and dynamical views. J. Geophys. Res. 90:4756-4772.

Didden, N. and F. Schott. 1993. Eddies in the North Brazil Current retroflection region observed by GEOSAT altimetry. J. Geophys. Res. 98:20121-20131.

Dobson, E.B., F. Monaldo, J. Goldhirsh, and J. Wilkerson. 1987. Validation of GEOSAT altimeter derived wind speeds and significant wave heights using buoy data. J. Geophys. Res. 92:10719-10731.

Elgin, R.H. 1994. An evaluation of XCTD performance with design improvements. Sippican, Inc. Marion, Mass., 6 pp.

Elliot, B.A. 1982. Anticyclonic rings in the Gulf of Mexico. J. Phys. Oceanogr. 12:1293-1309.

Emery, W.J., G.H. Born, D.C. Baldwin, and C.L. Norris. 1990. Satellite-derived water vapor corrections for GEOSAT altimetry. J. Geophys. Res. 95:2953-2964.

Etcheto, J. and L. Banege. 1992. Wide-scale validation of GEOSAT altimeter-derived wind speed. J. Geophys. Res. 97: 11393-11409.

Forristall, G.Z., K.J. Schaudt and C.K. Cooper. 1992. Evolution and kinematics of a Loop Current eddy in the Gulf of Mexico during 1985. J. Geophys. Res. 97:2173-2184.

Garvine, R.W., K-C Wong, G.G. Gawarkiewicz, R.K. McCarthy, R.W. Houghton, and F. Aikman III. 1988. The morphology of shelfbreak eddies. J. Geophys. Res. 93:15593-15608.

Gill, A.E. and R.W. Griffiths. 1981. Why should two anticyclonic eddies merge? Ocean Modelling. 41:10-16.

Glenn, S.M. and C.C. Ebbesmeyer. 1993. Drifting buoy observations of a Loop Current anticyclonic eddy. J. Geophys. Res. 98:20105-20119.

Glenn, S.M., G.Z. Forristall, P. Cornillon, and G. Milkowski. 1990. Observations of Gulf Stream ring 83-E and their interpretation using feature models. J. Geophys. Res. 95:13043-13064.

Griffiths, R.W. and E.J. Hopfinger. 1987. Coalescing of geostrophic vortices. J. Fluid Mech. 178:73-97.

Haines, B.J., G.H. Born, G.W. Rosborough, J.G. Marsh, and R.G. Williamson. 1990. Precise orbit computation for the GEOSAT exact repeat mission. J. Geophys. Res. 95:2871-2885.

Hamilton, P. 1987a. The structure of shelf and Gulf Stream motions in the Georgia Bight. Progr. Oceanogr. 19:329-351.

Hamilton, P. 1987b. Characterization of slope circulations in the northern Gulf of Mexico. Final Report to Joint Industry Program SAIC 87/1071. 240 pp. + Appendices.

Hamilton, P. 1990. Deep currents in the Gulf of Mexico. J. Phys. Oceanogr. 20:1087-1104.

Hamilton, P. 1992. Lower continental slope cyclonic eddies in the central Gulf of Mexico. J. Geophys. Res. 97:2185-2200.

Hanawa, K., P. Rual, R. Bailey, A. Sy, and M. Szabados. 1995. A new depth-time equation for Sippican or TSK T-7, T-6 and T-4 expendable bathythermographs (XBT). Deep Sea Res. 42(8):1423-1451.

Hendricks, J.R., R.R. Leben, G.H. Born, and C.J. Koblinsky. 1996. EOF analysis of global TOPEX/POSEIDON data and implications for detection of global sea level rise. J. Geophys. Res. 101:14131-14146.

Hofmann, E.E. and S.J. Worley. 1986. An investigation of the circulation of the Gulf of Mexico. J. Geophys. Res. 91:14221-14236.

Hooker, S.B. 1987. Mesoscale eddy dynamics by the method of point vortices. Ph.D. dissertation, Univ. of Miami, Coral Gables, Fla. 158 pp.

Houghton, R.W., F. Aikman III, and H.W. Ou. 1988. Shelf/slope frontal structure and cross-shelf exchange at the New England shelf break. Cont. Shelf Res. 8:687-710.

Hurlburt, H.E. and J.D. Thompson. 1982. The dynamics of the Loop Current and shed eddies in a numerical model of the Gulf of Mexico, pp. 243-298. In: J.C.J. Nihoul, ed. Hydrodynamics of Semi-enclosed Seas. Elsevier.

Jochens, A.E., R.R. Leben, and G.S. Fargion. 1996. Observations of Loop Current Eddy Vazquez in the Northwest Gulf of Mexico (submitted to J. Geophys. Res.).

Johnson, D.R., J.D. Thompson, and J.D. Hawkins. 1992. Circulation in the Gulf of Mexico from GEOSAT Altimetry during 1985-1986. J. Geophys. Res. 97:2201-2214.

Kennelly, M.A., R.H. Evans, and T.M. Joyce. 1985. Small-scale cyclones of the periphery of a Gulf Stream warm-core ring 82B. J. Geophys. Res. 90:8845-8857.

Kirwan, A.D., Jr., J.K. Lewis, A.W. Indest, P. Reinersman, and I. Quintero. 1988. Observed and simulated kinematic properties of Loop Current rings. J. Geophys. Res. 93: 1189-1198.

Kirwan, A.D., Jr., W.J. Merrell, Jr., J.K. Lewis, and R.E. Whitaker. 1984a. Lagrangian observations of an anti-cyclonic ring in the western Gulf of Mexico. J. Geophys. Res. 89(C3): 3417-3424.

Kirwan, A.D., Jr., W.J. Merrell, Jr., J.K. Lewis, R.E. Whitaker, and R. Legeckis. 1984b. A model for the analysis of drifter data with an application to a warm core ring in the Gulf of Mexico. J. Geophys. Res. 89:3425-3438.

Klobuchar,J.A. 1987. Ionospheric time-delay for single-frequency GPS users. IEEE Trans. Aersp. Electron. Syst. 23:325-331

Leben, R.R. and G.H. Born. 1993. Tracking Loop Current eddies with satellite altimetry. Adv. Space Res. 13:325-333.

Leben, R.R. and G.H. Born. 1994. TOPEX and ERS-1 altimeter observations of Loop Current eddies U, V, W and X and associated cyclones (abstract). EOS, Trans. Amer. Geophys. Un. 75:212.

Leben, R.R. and G.H. Born. 1995. An updated climatology of Loop Current eddies from GEOSAT altimetry. Proceedings: Fifteenth Gulf of Mexico Information Transfer Meeting.

Lewis, J.K., A.D. Kirwan, Jr., and G.Z. Forristall. 1989. Evolution of a warm-core ring in the Gulf of Mexico: Lagrangian observations. J. Geophys. Res. 94(C6):8163-8178.

Lewis, J.K. and A D. Kirwan, Jr. 1985. Some observations of ring topography and ring-ring interactions in the Gulf of Mexico. J. Geophys. Res. 90:9017-9028.

Lewis, J.K. and A.D. Kirwan, Jr. 1987. Genesis of a Gulf of Mexico ring as determined from kinematic analysis. J. Geophys. Res. 92:11727-11740.

Luther, M.E. and J.M. Bane. 1985. Mixed instabilities in the Gulf Stream over the continental slope. J. Phys. Oceanogr. 15:3-23.

McWilliams, J.C. 1985. Submesoscale coherent vortices in the ocean. Rev. Geophys. 23:165-182.

Merrell, W.J., and J.M. Morrison. 1981. On the circulation of the western Gulf of Mexico with observations from April 1978. J. Geophys. Res. 86(C5):4181-4185.

National Oceanic and Atmospheric Administration. 1986. ETOP05 digital relief of the surface of the earth. Data Announce. 86-MGG-07. Natl. Geophys. Data Cent. Washington, D.C.

Nof, D. 1988. The fusion of isolated nonlinear eddies. J. Phys. Oceanogr. 18:887-905.

Nowlin, W.D., Jr., A.E. Jochens, N.L. Guinasso, Jr., D.A. Wiesenburg, R.O. Reid, S.A. Hsu, and R.C. Hamilton. 1991. Louisiana/Texas Shelf Physical Oceanography Program Task A (A Technical Proposal). Texas A & M University, Dept. of Oceanography. Ref. No. 93-06-T. College Station, Tx. 196 pp.

Pedder, M.A. 1993. Interpolation and filtering of spatial observations using successive corrections and Gaussian filters. Mon. Weath. Rev. 121: 2889-2902.

Press, W.H., S.A. Tuekolsky, W.T. Vetterling, and B.P. Flannery. 1992. Numerical Recipes in Fortran, The Art of Scientific Computing. Cambridge University Press. 2nd Edition. 963 pp.

Rual, P., A. Sy, A. Dessier, and J.P. Rebert. 1995. New depth equation for Sparton XBT-7 expendable bathythermographs. Presented at IGOSS Third meeting of the Task Team on Quality Control Procedures for Automated Systems, 23-25 October 1995. Ottawa, Canada.

SAIC. 1986. Gulf of Mexico physical oceanography program, final report: years 1 and 2. Volume II: technical report. MMS Contract No. 14-12-0001-29158, SAIC report no. SAIC-86/1023. 378 pp.

SAIC. 1988. Gulf of Mexico physical oceanography program, final report: year 3. Volume II: technical report. MMS Contract No. 14-12-0001-29158, OCS Report/MMS 88-0046. 241 pp.

SAIC. 1989. Gulf of Mexico physical oceanography program, final report: year 5. Volume II: technical report. MMS Contract No. 14-12-0001-29158, OCS Report/MMS 89-0068. 333 pp.

SAIC. 1994. Louisiana/Texas Shelf Physical Oceanography Program: Eddy Circulation Study, Annual report: Year 1. OCS Study/MMS 94-0027. U.S. Department of the Interior, Minerals Management Service, Gulf of Mexico OCS Region, New Orleans, La. 53 pp.

SAIC. 1995. Louisiana/Texas Shelf Physical Oceanography Program: Eddy Circulation Study, Annual report: Year 2. OCS Study/MMS 95-0027. U.S. Department of the Interior, Minerals Management Service, Gulf of Mexico OCS Region, New Orleans, La. 63 pp.

Sanford, T.B., P.G. Black, J.R. Haustein, J.W. Feeney, G.Z. Forristall, and J.F. Price. 1987. Ocean response to a hurricane, I observations. J. Phys. Oceanogr. 17:2065-2083.

Schrama, E.J.O. and R.E. Ray. 1994. A preliminary tidal analysis of TOPEX/POSEIDON altimetry. J. Geophys. Res. 99:24799-24808.

Schwiderski, E.W. 1980. On charting global tides. Rev. of Geophys. Space Phys. 18:243-268.

Singer, J.J. 1990. On the error observed in electronically digitized T-7 XBT data. J. Atmos. Oceanic Technol. 7(4): 603-611.

Sippican, Inc. 1985. Operation and Maintenance Manual, MK9 Oceanographic Data System, R-1197/C, September 1985. Sippican, Inc. Marion, Mass.

Sippican, Inc. 1989. MK-12 Oceanographic Data Acquisition System, R-2626, December 1989. Sippican, Inc. Marion, Mass.

Sippican, Inc. 1995. R-3174 AXCTD Probe Data Analysis Report, March 14,1995. Sippican, Inc. Ocean Systems Division. Marion, Mass.

Smith, D.C. 1986. A numerical study of Loop Current eddy interaction with topography in the western Gulf of Mexico. J. Phys. Oceanogr. 16:1260-1272.

Smith, D.C. and J.J. O'Brien. 1983. The interaction of a two-layer isolated mesoscale eddy with bottom topography. J. Phys. Oceanogr. 13:1681-1697.

Sturges, W. 1992. The spectrum of Loop Current variability from gappy data. J. Phys. Oceanogr. 22:1245-1256.

Sturges, W. 1994. The frequency of ring separations from the Loop Current. J. Phys. Oceanogr. 24:1647-1651.

Sy, A. 1993. Field evaluation of XCTD performance. WOCE Newsletter, No. 14, pp. 33-37.

Sy, A. 1995. Modified MK-12/XCTD system finally passes the field test in the North Atlantic (unpublished manuscript).

Tai, C.K. 1989. Accuracy assessment of widely used orbit error approximations in satellite altimetry. J. Atmos. Oceanic Technol. 6:147-150.

Vidal, V.M.V., F.V. Vidal, and J.M. Pérez-Molero. 1992. Collision of a Loop Current anticyclonic ring against the continental slope of the western Gulf of Mexico. J. Geophys. Res. 97:2155-2172.

Vidal, V.M.V. , F.V. Vidal, A.F. Hernandez, E. Meza and J.M Pérez-Molero. 1994. Baroclinic flow, transports, and kinematic properties of a cyclonic-anticyclonic-cyclone ring triad in the Gulf of Mexico. J. Geophys. Res. 99:7571-7597.

Vukovich, F.M. 1995. An updated evaluation of the Loop Current's eddy-shedding frequency. J. Geophys. Res. 95:8655-8659.

Vukovich, F.M. and B.W. Crissman. 1986. Aspects of warm rings in the Gulf of Mexico. J. Geophys. Res. 91:2645-2660.

Walker, N.D., O.K. Huh, and L.J. Rouse, Jr. 1993. Recent Loop eddy separation in the Gulf of Mexico. EOS, Trans. Amer. Geophys. Un. 74:30.

Wentz, F. 1989. User's manual for the collocated SSM/I tape. Remote Sensing Systems, Santa Rosa, Ca.

Witter, D.L. and D.B. Chelton. 1991. A method for developing an altimeter wind speed algorithm, with application to GEOSAT. J. Geophys. Res. 96:8853-8860.

Yi, Y. 1995. Determination of Gridded Mean Sea Surface from Altimeter Data of TOPEX, ERS-1, and GEOSAT. Ph.D. Thesis. Department of Geodetic Science and Surveying, The Ohio State University, Columbus, Oh.

The Department of the Interior Mission

As the Nation's principal conservation agency, the Department of the Interior has responsibility for most of our nationally owned public lands and natural resources. This includes fostering sound use of our land and water resources; protecting our fish, wildlife, and biological diversity; preserving the environmental and cultural values of our national parks and historical places; and providing for the enjoyment of life through outdoor recreation. The Department assesses our energy and mineral resources and works to ensure that their development is in the best interests of all our people by encouraging stewardship and citizen participation in their care. The Department also has a major responsibility for American Indian reservation communities and for people who live in island territories under U.S. administration.

The Minerals Management Service Mission

As a bureau of the Department of the Interior, the Minerals Management Service's (MMS) primary responsibilities are to manage the mineral resources located on the Nation's Outer Continental Shelf (OCS), collect revenue from the Federal OCS and onshore Federal and Indian lands, and distribute those revenues.

Moreover, in working to meet its responsibilities, the **Offshore Minerals Management Program** administers the OCS competitive leasing program and oversees the safe and environmentally sound exploration and production of our Nation's offshore natural gas, oil and other mineral resources. The MMS **Royalty Management Program** meets its responsibilities by ensuring the efficient, timely and accurate collection and disbursement of revenue from mineral leasing and production due to Indian tribes and allottees, States and the U.S. Treasury.

The MMS strives to fulfill its responsibilities through the general guiding principles of: (1) being responsive to the public's concerns and interests by maintaining a dialogue with all potentially affected parties and (2) carrying out its programs with an emphasis on working to enhance the quality of life for all Americans by lending MMS assistance and expertise to economic development and environmental protection.